

*GEODYNAMIC EVOLUTION OF THE
SCOTIA SEA (ANTARCTICA),
PALEOCEANOGRAPHIC IMPLICATIONS
AND GLOBAL CHANGE*

YASMINA M. MARTOS MARTÍN

Ph.D. Thesis-Tesis Doctoral 2014



Editor: Editorial de la Universidad de Granada
Autor: Yasmina M. Martos Martín
D.L.: GR 1857-2014
ISBN: 978-84-9083-041-3



GEODYNAMIC EVOLUTION OF THE SCOTIA SEA (ANTARCTICA), PALEOCEANOGRAPHIC IMPLICATIONS AND GLOBAL CHANGE

YASMINA MAGDALENA MARTOS MARTÍN

Ph.D. Thesis-Tesis Doctoral

Instituto Andaluz de Ciencias de la Tierra
(Consejo Superior de Investigaciones Científicas-Universidad de Granada)

2014



GEODYNAMIC EVOLUTION OF THE SCOTIA SEA (ANTARCTICA), PALEOCEANOGRAPHIC IMPLICATIONS AND GLOBAL CHANGE

Memoria de Tesis Doctoral presentada por la Licenciada en Física Dña. Yasmina Magdalena Martos Martín para optar al Grado de Doctor por la Universidad de Granada

Granada, 11 de Febrero de 2014

Fdo. Yasmina Magdalena Martos Martín

VºBº del Director

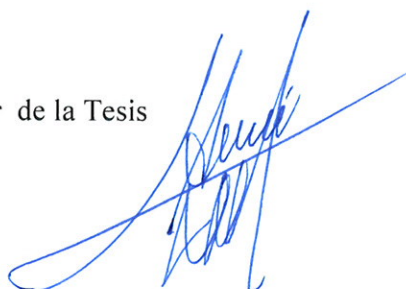
Fdo. Andrés Maldonado López

Programa de Doctorado de Ciencias de la Tierra (UGR)

La doctoranda Yasmina Magdalena Martos Martín y el director de la tesis Andrés Maldonado López garantizamos, al firmar esta tesis doctoral, que el trabajo ha sido realizado por la doctoranda bajo la dirección del director de la tesis y hasta donde nuestro conocimiento alcanza, en la realización del trabajo, se han respetado los derechos de otros autores a ser citados, cuando se han utilizado sus resultados o publicaciones.

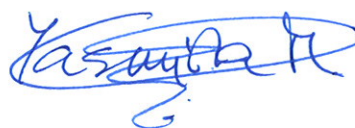
En Granada a 11 de Febrero de 2014

Director de la Tesis



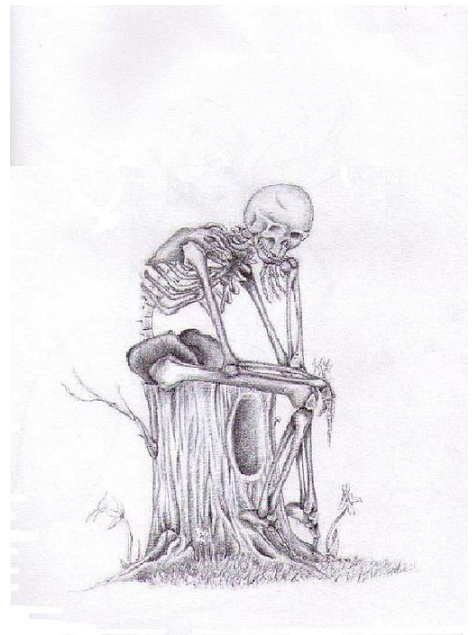
Fdo.: Andrés Maldonado López

Doctoranda



Fdo.: Yasmina M. Martos Martín

A mi Familia



*No nos atrevemos a muchas cosas porque son difíciles,
pero son difíciles porque nonos atrevemos a hacerlas.
Las cosas difíciles llevan mucho tiempo,
lo imposible puede tardar un poco más ...
(Lucio Anneo Séneca)*

Agradecimientos

Esta Tesis Doctoral ha sido llevada a cabo dentro de los proyectos antárticos GLOBANT (CTM2008-06386-C02/ANT), ConPACA (CTM2011-30241-CO2-01/02), MAREGEO y colaboración Hispano-Rusa (CSIC-Russian Academy of Sciences) financiados por el Gobierno de España. Asimismo, la Tesis ha sido desarrollada dentro del programa de Formación de Personal Investigador (BES-2009-026533) promovido por el Ministerio de Ciencia e Innovación, asociada al Instituto Andaluz de Ciencias de la Tierra (CSIC-UGR). A lo largo del disfrute de la beca predoctoral se han realizado 4 estancias breves en el extranjero con una duración total superior a 12 meses y financiadas por el Ministerio de Ciencia e Innovación. Los resultados obtenidos a lo largo del desarrollo de la Tesis han sido presentados en congresos de carácter internacional, y tanto la Association of Polar Early Career Scientists (APECS) como el Scientific Committee on Antarctic Research han colaborado económicamente para mi asistencia a dichos congresos.

Agradecer a la tripulación del BIO Hespérides y el BIO Las Palmas, así como al personal de la Unidad de Tecnología Marina por su dedicación y buena acogida durante las campañas antárticas.

Quisiera agradecer al Instituto Andaluz de Ciencias de la Tierra, a la Universidad de Granada (en especial al Departamento de Geodinámica) y al Programa de Doctorado de Ciencias de la Tierra por su acogida.

Mi más profundo agradecimiento a todas aquellas personas que directa o indirectamente han participado y me han apoyado a lo largo de estos años. Un gran agradecimiento a mi Director de Tesis, Andrés Maldonado, por la motivación continua y el apoyo recibido.

Además quiero dar las gracias al grupo SCAN, y en especial a esos que desde más cerca o más lejos (Fernando, Javier, Paco) me habéis apoyado.

Un agradecimiento especial para Jesús Galindo-Zaldívar y Manuel Catalán por sus largas horas de discusiones científicas fructíferas y su originalidad.

Agradecer a Anatoly A. Schreider (Russian Academy of Sciences, Moscow, Russia) esas discusiones sobre anomalías magnéticas y los métodos de obtención de las mismas.

Quiero agradecer a Karsten Gohl (Alfred Wegener Institute for Polar and Marine Research, Bremerhaven, Germany) su hospitalidad y su apoyo. Un agradecimiento también para Larry Lawver e Ian W. D. Dalziel (Institute for Geophysics The University of Texas at Austin, Austin, Texas, USA) por las productivas conversaciones científicas y su interés en mis estudios; y en especial a Ian por su gran hospitalidad.

Gracias a todos los que me habéis hecho sentir como en casa cuando he estado fuera de España: Alison, Gordon, Renas, María, Jah, Ansa, Mariana...

Agradecer a todos los que me apoyáis desde hace tantos años directa o indirectamente desde la tierra de Jaén: Cristina, Noelia, María, Ángel, Jordy, Mariano, Maribel, Luis A., M^o Carmen, y un largo etc., y a sus respectivas familias.

Mil gracias a todos aquellos con los que comparto los buenos y malos momentos prácticamente día a día, de cerca y desde la lejanía: Patricia, Edu, Manuel, Idaira, Irene, Pedro, Vicente, Enric...y especialmente a Xoán, Lara, Julia, Diana y Moha.

Un agradecimiento enorme a todos mis “madrileños” por su gran apoyo desde hace tantos años: Maca, Nacho, Dani, Hanfri, Clara, Iria, Roque, María, Gabi, y especialmente a Javi, pues eres un ejemplo a seguir en todos los aspectos...ya te has hecho mayor!

Por último infinitas gracias a TODA mi Familia, sin olvidar a nadie, por su gran paciencia y apoyo incondicional en todos los pasos de mi vida.

Muchas gracias a todos porque sin vosotros esto no sería posible.

Table of Contents

Abstract	1
Resumen	3
Extended Abstract	5
Resumen extendido	9
Chapter 1. Introduction	13
Chapter 2. Objectives and Thesis structure	25
Chapter 3. Regional setting and background	29
3.1. The Scotia Sea.....	31
3.1.1. Tectonic setting and evolution	33
3.1.2. Regional stratigraphy	39
3.1.3. Oceanographic setting.....	41
3.2. The Bransfield Strait region.....	43
Chapter 4. Data and Methodology	47
4.1. Data sources.....	49
4.2. Methodologies.....	52
Chapter 5. Asthenospheric Pacific-Atlantic flow barriers and the West Scotia Ridge extinction	57
1. Introduction.....	60
2. Methodology	62
3. Complete Bouguer anomaly maps	63
4. Gravity modeling	63
5. Discussion.....	71
6. Conclusions.....	73
Supporting Information.....	75
Chapter 6. Thermal behaviour and subsidence of small oceans: the West Scotia Sea	83
1. Introduction.....	86

2. Regional setting	87
3. Methodology	90
4. Thermal behaviour of small oceans: The West Scotia Sea thermal subsidence and heat flow.....	92
5. Discussion	94
6. Conclusions.....	97
Chapter 7. Insights about the structure and evolution of the Scotia Arc from a new magnetic data compilation.....	99
1. Introduction.....	103
2. Regional setting	104
3. Material and methods.....	106
4. Magnetic maps.....	108
4.1. New Magnetic Anomaly map	108
4.2. Analytic signal magnetic anomaly map	108
5. Magnetic anomaly profiles and modeling.....	111
6. Discussion	115
7. Conclusions.....	118
Chapter 8. Tectonics and palaeoceanographic evolution recorded by contourite features in southern Drake Passage (Antarctica).....	121
1. Introduction.....	124
2. Regional setting	126
2.1. Tectonic evolution.....	126
2.2. Regional stratigraphy	128
2.3. Oceanographic setting.....	129
3. Data and methodology	130
4. Seismic stratigraphy.....	131
4.1. Older units.....	132
4.2. Younger units.....	133
5. Geometry of drifts and erosional features.....	140
5.1. Scotia Plate.....	140
5.2. Phoenix Plate.....	140
6. Temporal evolution of channels and moats	141
7. Discussion.....	144
7.1. Drifts and erosional features	144
7.2. Tectonic evolution.....	147
7.3. Palaeoceanographic implications.....	148
7.4. Evolutionary stages	149
8. Conclusions.....	152
Chapter 9. Initial stages of oceanic spreading in the Bransfield Rift from magnetic and gravity data analysis.....	155

1. Introduction.....	158
2. Geological setting	159
3. Data compilation.....	162
3.1. Magnetic data.....	162
3.2. Gravity data.....	165
4. Magnetic and Gravity anomaly maps	165
4.1. Magnetic map.....	165
4.2. Bouguer gravity map.....	167
5. Characterization of the central linear magnetic anomaly	168
6. Forward gravity and magnetic modeling.....	171
7. Discussion.....	174
8. Conclusions.....	180
Chapter 10. Monitoring the evolution of Deception Island volcano from magnetic anomaly data (South Shetland Islands, Antarctica).....	183
1. Introduction.....	186
2. Regional setting	188
3. Material and methods.....	189
3.1. Error budget study.....	190
3.1.1. External contributions.....	192
3.1.2. Ship's position.....	193
3.1.3. Instrument errors	194
3.1.4. UAV flight	194
4. Comparison of anomaly maps and secular variation scenario.....	194
4.1. Regional magnetic anomaly map.....	195
4.2. Inner Bay magnetic study.....	196
4.2.1. Austral summer 1987/1988 vs. December 1999	197
4.2.2. December 1999 vs. December 2008	197
4.2.3. Secular Variation and Magnetic study off DI	197
4.3. Modeling and interpretation.....	201
4.3.1. Regional model	201
4.3.2. DI inner Bay area	205
4.3.3. DI outer area.....	207
5. Discussion	208
5.1. DI inner bay area.....	208
5.2. DI outer area.....	211
6. Conclusions.....	216
Chapter 11. General discussion	219
Chapter 12. Conclusions/Conclusiones	227
Conclusions.....	229
Conclusiones	235

Chapter 13. References.....	241
Appendix. Other SCI published articles of the study area as a coauthor	263
Deep-sea pre-glacial to glacial sedimentation in the Weddell Sea and southern Scotia Sea from a cross-basin seismic transect.....	265
Initial Phase of the West Scotia Mid-Oceanic Ridge Opening.....	289
Furrows in the southern Scan Basin, Antarctica: interplay between tectonic and oceanographic influences.....	295

Abstract

The opening of the Drake Passage marked the final break-up of Gondwana Supercontinent, with the creation of the Scotia Arc. The Scotia Sea, located between South America and Antarctica, is constituted at present by the Scotia and Sandwich plates. To the west of the Scotia Plate, the Shackleton Fracture Zone accommodates the Phoenix Plate and Scotia Plate movements. The development of the Scotia Sea is considered a key gateway for both asthenospheric and oceanic currents. The opening of the Drake Passage is evoked as the last Southern Ocean gateway, which led to the instauration of the Antarctic Circumpolar Current, isolating the Antarctic Continent and bearing a major influence on climatic and global changes.

In this Ph.D. Thesis it is shown that the opening of the passage meant a gateway for Pacific mantle outflow because of the absence of deep lithospheric roots in the passage (Chapter 5). The mantle material fed the West Scotia Ridge until the uplift of the Shackleton Fracture Zone in the middle Miocene (Chapter 8). The Shackleton Fracture Zone relief formed a lithospheric root in the Drake Passage, serving as a barrier for the asthenospheric flows, avoiding the mantle material fed the West Scotia Ridge properly. Simultaneous to this asthenospheric setting, the uplift of the Shackleton Fracture Zone together with the initial incursions of the Weddell Sea Deep Water in the Scotia Sea forced the Circumpolar Deep Water and the Polar Front to move even further from Antarctica. This had profound climatic implications, favoring the thermal isolation of Antarctica and the growing and permanent ice-sheets.

As the Scotia Arc is considered a small ocean formed as a back-arc, and fed mostly by the Pacific mantle, the small convection cells responsible for oceanic spreading lend the West Scotia Sea a very different thermal behavior than large oceans (Chapter 6). The mantle dynamics also control the tectonic distribution of the Scotia Arc and surrounding areas. The subduction of the Phoenix Plate in the western margin of the Antarctic Peninsula formed the batholithic body known as the Pacific Margin Anomaly, which is used to propose an initial distribution of the continental blocks in the Antarctic Peninsula and in the Scotia Arc, and an opening model of the Scotia Sea (Chapter 7). As a consequence of the

Phoenix Plate subduction, due to the roll-back of the South Shetland Islands Block, the Bransfield Strait developed as a back-arc basin. This basin is found to be in its final stages of continental extension in some areas, and in the early stages of oceanic spreading in others (Chapter 9). The Bransfield Strait is characterized by a central neovolcanic axis, the Deception Island active volcano being located in its southern part. The volcano is a consequence of the active extensional setting of the Bransfield Strait, analyzed here using a new methodology (Chapter 10) in order to assess its volcanic activity over a 20-year period.

In summary, an interdisciplinary analysis of the Scotia Arc and surrounding areas is accomplished in this Ph.D. Thesis in order to improve in the knowledge and understanding of the study area evolution and the implications in global scale.

Resumen

La apertura del Paso del Drake, situado entre Sudamérica y la Antártida, constituyó la última etapa de fragmentación del Supercontinente Gondwana, dando lugar al Arco de Scotia. Este arco bordea el Mar de Scotia, y está formado actualmente por las placas de Scotia y Sandwich. El límite oeste del Mar de Scotia lo forma la Zona de Fractura Shackleton que acomoda el movimiento entre la Placa Phoenix y la Placa Scotia. La formación del Paso del Drake y el Mar de Scotia se considera de gran importancia para la circulación oceánica, permitiendo la instauración de la Corriente Circumpolar Antártica que aisló al continente antártico, con fuertes implicaciones en cambios climáticos y globales.

A lo largo de esta Tesis Doctoral se muestra que la apertura del Paso del Drake supuso un portal para el manto procedente del Pacífico debido a la ausencia de las raíces litosféricas profundas (Capítulo 5). Este material mantélico alimentó la Dorsal Occidental de Scotia hasta que la Zona de Fractura Shackleton comenzó a elevarse en el Mioceno medio (Capítulo 8). La formación de este relieve conllevó el desarrollo de una raíz litosférica en el Paso del Drake, impidiendo el paso de los flujos astenosféricos y por tanto la adecuada alimentación de la Dorsal Occidental de Scotia. Simultáneamente, el levantamiento de la Zona de Fractura Shackleton, junto con las incursiones iniciales del Agua Profunda del Mar de Weddell en el Mar de Scotia forzaron a la Corriente Circumpolar Antártica y al Frente Polar a desplazarse hacia el norte en la zona de estudio, alejándose de la Antártida. Esto tuvo grandes implicaciones climáticas, favoreciendo el aislamiento térmico de la Antártida y el crecimiento y estabilidad de las capas de hielo.

Al considerarse el Arco de Scotia como un océano de pequeñas dimensiones formado como un barck-arc y alimentado principalmente por el manto procedente del Pacífico, las pequeñas células mantélicas responsables de la expansión oceánica hacen que el comportamiento térmico de Mar de Scotia Occidental sea diferente al de los océanos de grandes dimensiones (Capítulo 6). La dinámica del manto controla también la distribución tectónica del Arco de Scotia y las regiones circundantes. La subducción de la Placa Phoenix en el margen oeste de la Península Antártica dio lugar al cuerpo batolítico conocido como Anomalía del Margen Pacífico. Dicha anomalía ha sido utilizada para proponer la

distribución inicial de los bloques continentales en la Península Antártica y en el Arco de Scotia, así como un modelo de apertura del Mar de Scotia (Capítulo 7). Como consecuencia de la subducción de la Placa Phoenix, debido al roll-back del Bloque de las Islas Shetland del Sur, se desarrolló la cuenca de back-arc del Estrecho de Bransfield. Esta cuenca parece encontrarse en su etapa final de extensión continental en algunas áreas y en los comienzos de extensión oceánica en otras (Capítulo 9). El Estrecho de Bransfield se caracteriza por un eje neo-volcánico central, en el que se encuentra el volcán activo de Isla Decepción. Este volcán surge como consecuencia del régimen extensional que caracteriza la Cuenca Bransfield. La actividad volcánica de Isla Decepción ha sido analizada en un periodo de 20 años aplicando una nueva metodología que ha permitido detectar las crisis volcánicas ocurridas dentro de ese periodo (Capítulo 10).

En definitiva, en esta Tesis Doctoral se realiza un análisis multidisciplinar del Arco de Scotia y regiones circundantes con vistas a mejorar en el conocimiento y entendimiento de su evolución así como la comprensión de sus implicaciones a escala global.

Extended abstract

The opening of the Drake Passage involved the final break-up of Gondwana Supercontinent, and gave way to the development of the Scotia Arc. The Scotia Sea, located between South America and Antarctica, is constituted at present by the Scotia and Sandwich plates. The Scotia Arc is surrounded by the Former Phoenix and the Antarctic plates to the west, the Antarctic Plate to the South and the South American Plate in the remaining sites. The structure that accommodates the movements between the Scotia Plate and the Former Phoenix Plate is known as the Shackleton Fracture Zone. The development of the Scotia Sea is associated with the final gateway for the Southern Ocean, with implications for global ocean circulation and, in turn, for global changes on the Earth. Moreover, this break-up has been theoretically considered as the gateway for Pacific mantle outflow, since deep lithospheric roots are no longer present in the area.

In this Ph.D. Thesis, the Scotia Sea and surrounding areas are analyzed in order to improve our understanding of the asthenospheric and lithospheric dynamics of the study area, their effects on the growth pattern of oceanic basins—including paleoceanographic and depositional and tectonic processes—and how these processes may have influenced global changes. To reach these objectives, several kinds of geophysical data (multichannel seismic and gravity and magnetic data) and methodologies are applied. They are described and discussed in the six scientific articles that constitute the main body of this Ph.D. Thesis.

It is proposed that the Drake Passage is still a gateway for asthenospheric currents (Chapter 5) from the Pacific to the Atlantic Ocean and the Weddell Sea. However, they cannot flow freely due to the continental lithospheric roots of South America and Antarctica, and to the influence of the Shackleton Fracture Zone lithospheric root. The lithospheric root associated with this structure was most likely responsible for the extinction of oceanic spreading in the West Scotia Sea because the mantle material supply decreased. This lithospheric root developed when the structure started to uplift, forming the present relief.

Moreover, owing to the small size of the West Scotia Sea and this asthenospheric/lithospheric setting, the lithosphere presents an abnormal thermal behavior

in comparison with large oceans (Chapter 6). The small size of the mantle cells means relatively low heat flow and thinner lithosphere. These factors determine a faster evolution to reach thermal equilibrium of the lithosphere and the final depths. Based on this faster thermal evolution for small oceans, we propose a new depth-age relationship, $d(t) = 4480 - 19380\exp(-t/4)$. The heat flow was modeled indicating older apparent ages than in large oceans; and although the age cannot be determined for crusts over 15 Ma, heat flow is the best measure to obtain the maximum lithospheric thickness in small oceans. All these processes favored the oceanic deep water connection and affected continental and oceanic flora and faunal exchanges.

The magnetic studies of the Scotia Arc show that the varying intensity of the Pacific Margin Anomaly may be a consequence of the asymmetry of the trend of subduction of the Phoenix Plate, which is orthogonal to the Pacific Margin of the Antarctic Peninsula and oblique to South America (Chapter 7). The Pacific Margin Anomaly is well recognized in the Antarctic Peninsula and in the South Shetland Islands, extending along the South Scotia Ridge continental blocks —South Orkney Microcontinent and southern Discovery Bank— and it may occur in the northern part of Herdman Bank. However, some magnetic anomalies identified in the North Scotia Ridge may be associated with basic rocks emplaced in pull-apart basins formed along a broad transcurrent zone separating South America and Antarctica since the Cretaceous due to the South Atlantic oceanic spreading. This has brought to light a novel continental block reconstruction of the Arc before its development.

This asthenospheric and lithospheric setting influenced the tectonics and oceanic current distribution above the seafloor. The opening of the Drake Passage entailed the onset of the Antarctic Circumpolar Current. Evidence of bottom-current activity is observed throughout the entire sedimentary record (Chapter 8). The Circumpolar Deep Water influenced the oldest depositional units (until the Miocene); and the combined effect of this current and the Weddell Sea Deep Water affected the younger units developing drift deposits. Moreover, we found that the Shackleton Fracture Zone may have initiated as an oceanic ridge before the middle Miocene, diverting the Weddell Sea Deep Water into two branches, one northward and another westward to the Pacific Ocean. The Shackleton Fracture Zone relief, together with the initial incursions of the Weddell Sea Deep Water,

forced the Antarctic Circumpolar Current and the Polar Front to move even further from Antarctica. These events are coeval with the onset of the permanent East Antarctic Ice Sheet and with tundra landscape that persisted until at least 12.8 Ma in the Antarctic Peninsula.

In the Scotia Arc and the Phoenix Plate framework, the Bransfield Strait was studied in order to discuss its oceanic character (Chapter 9). The Bransfield Basin is located between the South Shetland Islands and the Antarctic Peninsula, and it is usually considered as a back-arc basin associated with the subduction of the Phoenix Plate. Many authors have discussed its oceanic character. In this Ph.D. Thesis we show that the integration of the potential field data and the modeling are compatible with the extensional character of the basin, which probably floored in the central sector by an oceanic crust above an anomalous mantle.

Additionally, the presence of an active volcanic axis and the thin crust support rifting in its latest stages, or the presence of an incipient oceanic crust formed by recent oceanic spreading in the central part of the Bransfield Basin. Relevant evidence of the volcanic activity of the basin can be observed in the Deception Island volcano (Chapter 10). After about a 20-year-long (from 1987 to 2008) magnetic study of this structure, we performed very detailed analysis of the error budget to ensure confidence in the results. Once this was done, based on the changes in the magnetic anomaly maps, the spatial distribution of ΔSV and the forward modeling, we found that: the changes in the inner bay of the island would have been caused by magma uplift (at some time between 1987 and 1999, towards the southeastern part of Deception Island) and the later spreading of its thermal effects, and the SE outer part of the island was also affected by the magma uplift. These developments can be associated with the 1992 and/or 1999 volcanic crises, and posterior progressive cooling of the smaller structures. The fast and simple magnetic technique carried out in this study allows the evolution of an active volcano to be monitored, which could complement other techniques.

In summary, this multidisciplinary analysis of the Scotia Arc integrating a variety of methodologies to an extensive data bank represents a significant step to improved knowledge and understanding of the development of the Scotia Arc and surrounding areas, and their implications for evolution at the global scale.

Resumen extendido

La apertura del Paso del Drake, el cual está localizado entre Sudamérica y la Antártida, supuso la ruptura final del Supercontinente Gondwana, dando lugar al Arco de Scotia. Los elementos geológicos que constituyen dicho arco se encuentran en la actualidad dispersos a lo largo del perímetro del Mar de Scotia, que está constituido actualmente por la Placa de Scotia y la Placa Sandwich. El Mar de Scotia está bordeado por la extinta Placa Phoenix y la Placa Antártica al oeste, la Placa Antártica hacia el sur y la Placa Sudamericana al norte y al este. La estructura que acomoda el movimiento entre la extinta Placa Phoenix y la Placa de Scotia es la Zona de Fractura Shackleton. El desarrollo del Mar de Scotia se considera como el último portal oceánico para el Océano Antártico con implicaciones en la circulación oceánica global, y por consiguiente, en cambios a nivel global en la Tierra. Aparte de las implicaciones en la distribución de las corrientes oceánicas, el Paso del Drake también ha sido considerado como un portal para el manto procedente del Pacífico ya que las raíces litosféricas profundas desaparecieron en el momento de la ruptura final de Gondwana.

En esta Tesis Doctoral se analizan el Mar de Scotia y las zonas circundantes con el fin de mejorar el conocimiento y entendimiento de la dinámica astenosférica y litosférica en el área y sus efectos en los patrones de crecimiento de las cuencas oceánicas, incluyendo procesos deposicionales, tectónicos y paleoceanográficos, así como la influencia de estos procesos en los cambios a escala global. Para alcanzar los objetivos planteados se han usado diferentes tipos de datos (fundamentalmente sísmica de reflexión multicanal, gravedad y magnetismo) y se han aplicado diversas técnicas geofísicas. Tanto los datos como los métodos aplicados son descritos y discutidos en detalle en el cuerpo principal de esta Tesis Doctoral.

En este estudio se propone la presencia actual de corrientes astenosféricas procedentes del Pacífico desplazándose hacia el Océano Atlántico y el Mar de Weddell a través del Paso del Drake (Capítulo 5). Sin embargo, el movimiento de estas corrientes astenosféricas está restringido por la presencia de las raíces litosféricas continentales de Sudamérica y la Antártida, así como de la raíz de la Zona de Fractura Shackleton. La raíz

litosférica asociada a esta estructura parece responsable de la extinción del eje de expansión del Mar de Scotia Occidental debido al descenso en el suministro del material mantélico. Dicha raíz litosférica se desarrolló cuando la Zona de Fractura Shackleton comenzó a elevarse hasta formar el relieve actual.

Debido al pequeño tamaño del Mar de Scotia Occidental y a su marco astenosférico/litosférico, la litosfera presenta un comportamiento térmico anómalo en comparación con el observado en los océanos de grandes dimensiones (Capítulo 6). El tamaño reducido de las células mantélicas determina los valores relativos bajos de flujo de calor y la litosfera más delgada en los océanos pequeños. A su vez, estos factores conllevan una evolución más rápida al alcanzar el equilibrio térmico de la litosfera y las profundidades finales de su zona superior. En base a esta evolución más rápida para la litosfera de océanos pequeños, se propone la siguiente relación profundidad-edad, $d(t) = 4480 - 19380\exp(-t/4)$. Se ha modelizado el flujo de calor, el cual indica edades aparentes superiores que en los océanos de gran tamaño; y aunque la edad de cortezas de edades superior a 15 Ma no puede ser determinada, el método de flujo de calor es el más apropiado para obtener el valor máximo de espesor de la litosfera en océanos pequeños. Todos estos procesos favorecieron la conexión de aguas profundas entre mares y océanos, y afectaron a los intercambios continentales y oceánicos de flora y fauna.

Por otro lado, los estudios magnéticos en el Arco de Scotia muestran que la variabilidad de la intensidad de la Anomalía del Margen Pacífico podría ser consecuencia de la subducción asimétrica de la Placa Phoenix, la cual es ortogonal en el Margen Pacífico de la Península Antártica y oblicua en Sudamérica (Capítulo 7). La Anomalía del Margen Pacífico se observa bien en la Península Antártica y en las Islas Shetland del Sur, extendiéndose a lo largo de los bloques continentales que se encuentran en la Dorsal de Scotia Meridional: el Microcontinente de las Orcadas del Sur y el Banco Discovery, y puede llegar a observarse en la parte norte del Banco Herdman. Sin embargo, algunas anomalías magnéticas identificadas en la Dorsal Norte de Scotia podrían estar asociadas a rocas básicas emplazadas en cuencas de pull-apart que se desarrollaron a lo largo de la zona transcurrente que separa Sudamérica y la Antártida a partir del Cretácico, debido a la expansión oceánica del Atlántico Sur. Esta información da lugar a una novedosa

reconstrucción de la posición de los bloques continentales del Arco de Scotia anterior a su desarrollo.

Este marco astenosférico y litosférico influenció la tectónica y la distribución de corrientes sobre del fondo oceánico. Es posible observar la actividad de corrientes oceánicas de fondo a lo largo de toda la secuencia sedimentaria (Capítulo 8). La apertura del Paso del Drake supuso el inicio de la Corriente Circumpolar Antártica de forma que los depósitos más antiguos fueron influenciados por el Agua Profunda Circumpolar y los más jóvenes por el efecto combinado de ésta y el Agua Profunda del Mar de Weddell. Además de este hecho, se propone que la Zona de Fractura Shackleton comenzó a ser un relieve oceánico al menos a partir del Mioceno medio y produce la desviación del Agua Profunda del Mar de Weddell en dos ramas, una con dirección norte y otra con dirección oeste, hacia el Pacífico. El relieve de esta zona de fractura junto con las incursiones iniciales del Agua Profunda del Mar de Weddell forzaron el desplazamiento hacia el norte de la Corriente Circumpolar Antártica y del Frente Polar en la región de estudio. Dichos eventos son coetáneos con el comienzo de la Capa de Hielo permanente de la Antártida Oriental y con el final del paisaje de tundra que estuvo presente en la Península Antártica hasta hace al menos 12.8 Ma.

La naturaleza oceánica del Estrecho de Bransfield también ha sido objeto de estudio de esta Tesis Doctoral dentro del contexto del Arco de Scotia y la Placa Phoenix (Capítulo 9). Esta cuenca se encuentra entre las Islas Shetland del Sur y la Península Antártica, y en general se considera una cuenca de back-arc asociada a la subducción de la Placa Phoenix. En base a la integración de datos de campo potencial y la modelización se ha encontrado que las observaciones son compatibles con el carácter extensional de la cuenca y que probablemente hay presencia de corteza oceánica en el sector central de la misma.

El Estrecho de Bransfield está caracterizado por un eje volcánico central y una corteza delgada, lo que apoyan un estado de extensión continental en sus últimas etapas o la presencia de corteza oceánica incipiente formada por la expansión oceánica del sector central de la Cuenca Bransfield. Una evidencia importante de la actividad volcánica de la cuenca se refleja en el volcán Isla Decepción (Capítulo 10). Se ha realizado un riguroso análisis de errores para ganar confianza en los resultados obtenidos a partir del estudio de datos magnéticos en un periodo de 20 años. Los cambios en los mapas de anomalías

magnéticas, la distribución espacial de ΔSV y los modelos directos realizados para Isla Decepción muestran que los cambios producidos parecen debidos a un ascenso de magma en la zona sureste, tanto interior como exterior de la isla, en algún momento entre 1987 y 1999, y a una posterior extensión de los efectos térmicos. Esto se asocia con las crisis volcánicas ocurridas en 1992 y/o 1999, y con un progresivo enfriamiento de las estructuras pequeñas. Esta técnica sencilla y rápida, que puede complementar a otras, permite monitorizar la evolución de un volcán activo.

En resumen, el análisis multidisciplinar del Arco de Scotia, el cual integra una gran variedad de metodologías y grandes bases de datos, representa un paso muy importante para la mejora en el conocimiento y entendimiento del desarrollo del Arco de Scotia y las zonas circundantes, así como sus implicaciones en la evolución a escala global.

Chapter 1

INTRODUCTION

The break-up of the continental fragments amalgamated in the Gondwana Supercontinent since the early middle Jurassic (~180 Ma) involved numerous geophysical, geological, chemical and biological events of the Earth's history. According to the theory of Plate Tectonics, proposed in the 1960s (Vine and Matthews, 1963), the origin of the seafloor is derived from the mantle dynamics, which determine continental drift. Convection cells in the upper mantle are responsible for the drifting of tectonic plates, which are composed by the lithosphere lying directly upon the asthenosphere. The lithosphere is formed by the crust and the lithospheric mantle. There are two main forces that influence plate motion: friction and gravity. The friction is due to the interaction between the major convection currents in the asthenosphere and the more rigid overlying lithosphere. The gravity forces, in contrast, are related to local convection currents that exert a downward frictional pull on plates in subduction zones at ocean trenches.

The mantle return flow was initially treated by several authors as a response to movements of the plates (Harper, 1978; Chase, 1979; Hager and O'Connell, 1979; Parmentier and Oliver, 1979; among others). More recently, shrinkage of the Pacific and the resulting mantle outflow suggest that motions of the continents may be the dominant control on return flow in the mantle. Alvarez (1982) proposed a possible driving mechanism in which the lower mantle (below the mid-mantle transition zone) undergoes a convective overturn. This convection drives the continents by viscous coupling to their roots. The return flow in the upper mantle provides a volumetric compensation for the motion of the continental masses without passing under them, and oceanic plates, underlain by weak asthenosphere, are mostly decoupled from the lower mantle and mainly driven by slab pull (Figure 1.1).

The upper mantle dynamics control the plate tectonic drift, but the dynamics change when shallow mantle gateways open. The shallow return flow and deep continental lithospheric roots place the strongest constraints on the geographical pattern of return flow and predict recognizable surface manifestations (Alvarez, 1982). Alvarez's hypothesis predicts an upper mantle Pacific outflow through the three continental gaps in this ocean (Figure 1.2) taking into account the progressive shrinkage of the Pacific over the last 180 Ma. The three gaps are the Caribbean, the Drake Passage and the Australian-Antarctic gap.

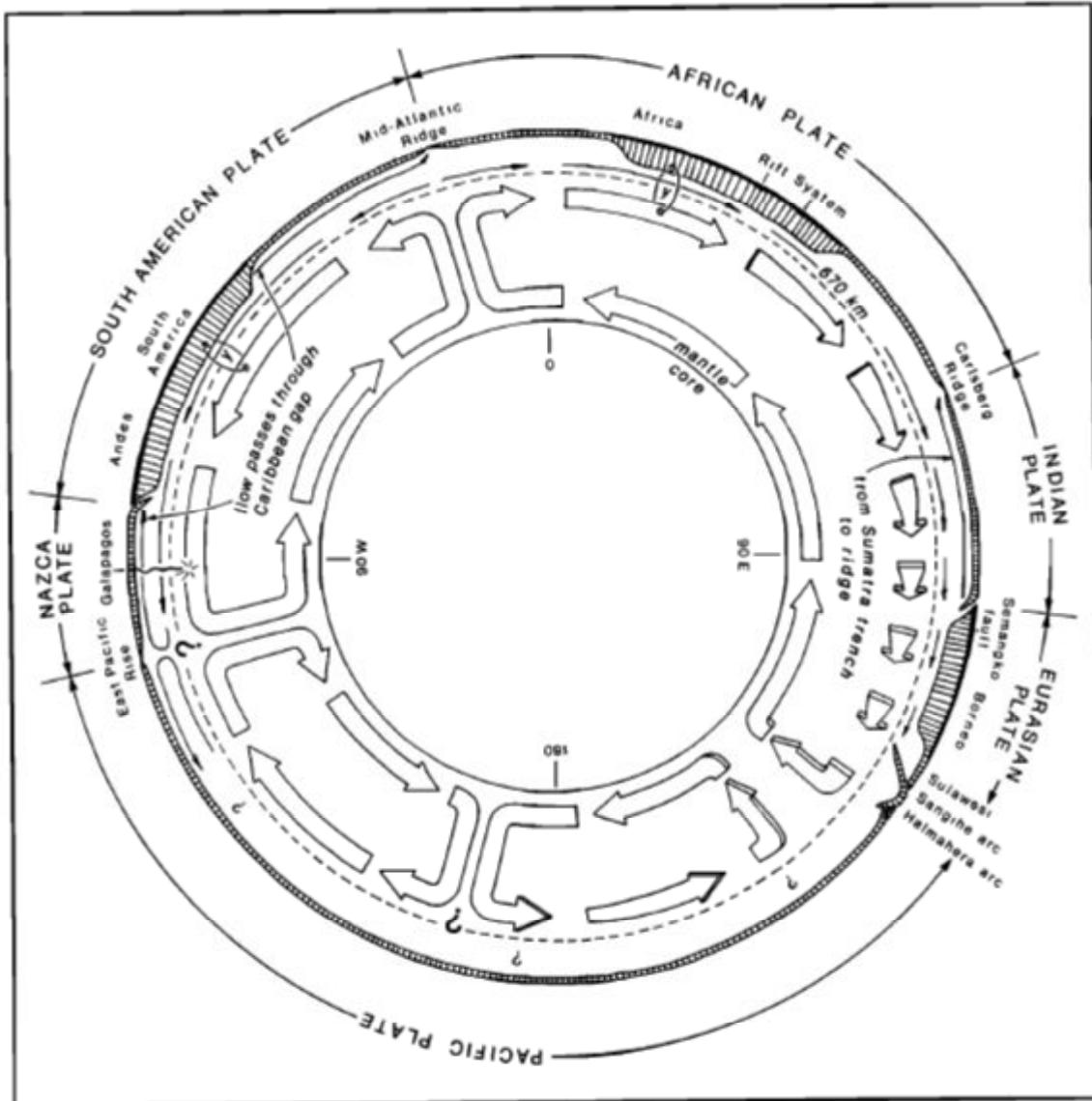


Figure 1.1. Equatorial section through the Earth, looking north, showing the mantle flow pattern and driving mechanism considered by Alvarez (1982). Arrows show movement direction (not rate) relative to the grid of axes of convergence and divergence at the top of the lower mantle; this grid should deform slowly compared to the other motions shown. In the mantle above 670 km, the lower arrows show the subasthenosphere upper mantle, entrained by movement of the uppermost lower mantle; the upper arrows show return flow in the asthenosphere. Black, continental crust; vertical lines, lithosphere. The links at 'y' indicate that South America and Africa move with the lower mantle flow. The model places stronger constraints on the lower mantle convective pattern in the continental hemisphere than in the Pacific hemisphere, where the pattern shown is extremely speculative.

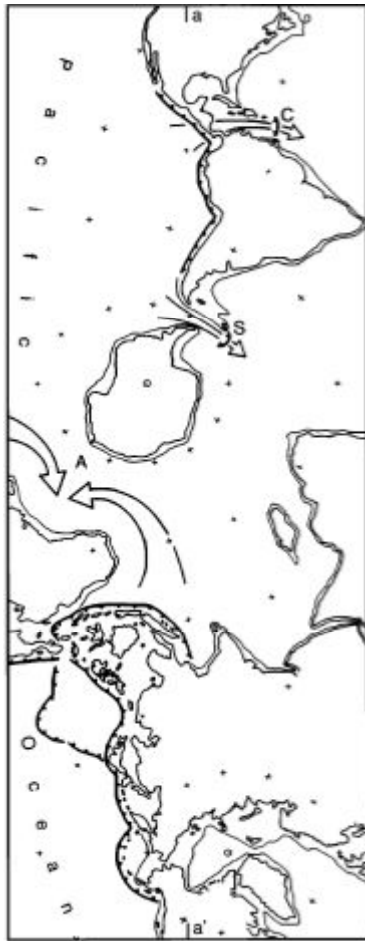


Figure 1.2. From Alvarez (1982). Oblique cylindrical projection tangent to the globe along a great circle (a-a') approximating the perimeter of the Pacific Ocean (pole at 15°N, 0°E). Large, open arrows show the suggested mantle return flow through gaps in the Pacific perimeter. C, Caribbean; S, Scotia Arc-Drake Passage region; A, Australia-Antarctica gap.

The eastward motion of the Caribbean and Drake Passage regions supports the shallow mantle flow movement from the Pacific to the Atlantic Ocean. Also assuming Alvarez's hypothesis (Alvarez, 1982), even the Atlantic ridge system is fed by material derived from the Pacific, which has escaped through either the Caribbean or the Scotia gap. The correspondence between the predicted Pacific mantle outflow and the geological and geophysical character of the Australian-Antarctic gap, the Caribbean, and the easternmost Scotia areas provides support for the model of shallow return flow with the presence of deep continental roots (Alvarez, 1982).

Mantle flow is detectable seismically through the anisotropic effects upon wave propagation by means of oriented mantle material that arises due to lattice-preferred orientation in olivine (Silver and Chan, 1991). Other authors interpret seismological data to evoke fast polarization patterns around South America, in the Caribbean and the Drake Passage Pacific gaps (Russo and Silver, 1994; Polet et al., 2000; Helffrich et al., 2002).

Meanwhile, convection cells transport materials and heat to the base of the lithosphere. The hottest lithosphere is located in oceanic ridge areas where mantle flows to the surface forming the oceanic crust. Heat is theoretically transported from the ridges to the ocean boundaries. Consequently, the older oceanic lithosphere is colder, with lower heat flow; it is therefore denser, and sinks into the asthenospheric mantle due to isostasy

equilibrium. This effect produces an increase in lithosphere thickness, since part of the asthenosphere becomes lithospheric mantle (Figure 1.3). This process is known as thermal subsidence. Two theoretical models, the half-space cooling model (Davis and Lister, 1974) and the plate model (Langseth et al., 1966; McKenzie, 1967), have been proposed since the 1960s. In brief, both stem from the heat equation in one dimension (equation 1.1), given that heat transport is driven by conduction and the internal heat generation is much smaller than the other terms of the heat equation. However, for solving the equation, the boundary and initial conditions are different for each model.

$$\frac{\partial T}{\partial t} = \kappa \frac{\partial^2 T}{\partial y^2} \quad \text{where } T \text{ is temperature, } t \text{ is time, } \kappa \text{ is the thermal diffusivity, and } y \text{ is the spreading direction.} \quad (1.1)$$

The half-space cooling model considers:

$$T = T_1 \quad \text{at } t = 0, \quad y > 0$$

$$T = T_0 \quad \text{at } y = 0, \quad t > 0$$

$$T \rightarrow T_1 \quad \text{as } y \rightarrow \infty, \quad t > 0$$

While the plate model considers:

$$T = T_1 \quad \text{at } t = 0, \quad 0 \leq y \leq y_{L_0}$$

$$T = T_0 \quad \text{at } y = 0, \quad t > 0$$

where T is temperature, T_1 is mantle temperature, T_0 is surface temperature and y_{L_0} is the depth of the base of the lithosphere.

After several mathematic operations (see for example Turcotte and Schubert (2002)) and applying the half-space cooling model conditions, we arrive at the relationships between heat flow and age, and between seafloor depth and age (equations 1.2 and 1.3 respectively):

$$q_0 = k(T_1 - T_0)(\pi\kappa t)^{-1/2} \quad \text{where } k \text{ is the thermal conductivity.} \quad (1.2)$$

$$d = \frac{2\rho_m\alpha_v(T_1-T_0)}{(\rho_m-\rho_w)} \left(\frac{\kappa}{\pi}t\right)^{1/2} \quad \text{where } d \text{ is depth of the oceanic seafloor, } \alpha_v \text{ is the thermal expansion coefficient, and } \rho_m \text{ and } \rho_w \text{ are the densities of the mantle and water, respectively.} \quad (1.3)$$

On the other side, applying the conditions for the plate model and considering approximations of the deviations of the surface heat flow from the half-space cooling result, the relationships take the following shape (equations 1.4 and 1.5):

$$q_0 = \frac{k(T_1-T_0)}{y_{L_0}} \left[1 + 2\exp\left(-\frac{\kappa\pi^2 t}{y_{L_0}^2}\right) + 2\exp\left(-\frac{4\kappa\pi^2 t}{y_{L_0}^2}\right) \right] \quad (1.4)$$

$$d = \frac{2\rho_m\alpha_v(T_1-T_0)y_{L_0}}{(\rho_m-\rho_w)} \left[\frac{1}{2} - \frac{4}{\pi^2} \exp\left(-\frac{\kappa\pi^2 t}{y_{L_0}^2}\right) \right] \quad \text{where } y_{L_0} \text{ is the lithospheric thickness when } t \rightarrow \infty. \quad (1.5)$$

Then, the heat flow and the depth of the seafloor depend on the age of the oceanic crust.

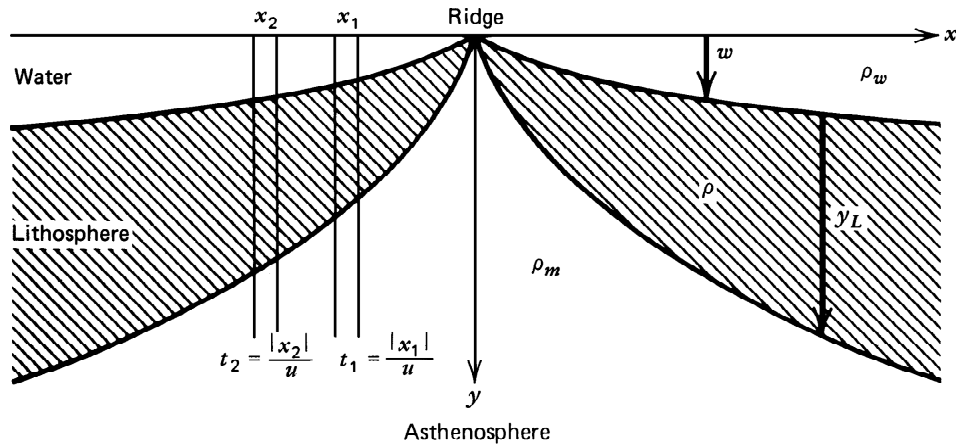


Figure 1.3. After Turcotte and Schubert (2002). Representation of the thermal contraction of the lithosphere with age. ρ_m and ρ_w are the densities of the mantle and water respectively, y_L is the thickness of the lithosphere, w is the seafloor depth, and u is the spreading rate.

Taking into account these models for lithosphere cooling, several authors (Parsons and Sclater, 1977; Stein and Stein, 1992, 1993; Hillier and Watts, 2005; Crosby et al., 2006; Korenaga and Korenaga, 2008; Crosby and McKenzie, 2009; Hasterok, 2013) have

proposed empirical laws for the thermal subsidence of large oceans since the 1970s. These models analyze the relationship between heat flow, ocean floor depth, and age. The empirical laws show that the half-space cooling model (Davis and Lister, 1974) fits thermal behavior for young oceanic crust (around < 60 Ma), whereas the plate model better describes the thermal behavior of old oceanic crust (about ≥ 60 Ma) (Langseth et al., 1966; McKenzie, 1967). Better fits between theoretical model and data are found for $y_{L_0} = 125$ km (Turcotte and Schubert, 2002). The most cited empirical models involve data mainly from the north Atlantic and Pacific oceans. The first empirical model was obtained by Parsons and Sclater (1977) (equation 1.6),

$$\begin{cases} d(t) = 2500 + 350\sqrt{t} & t \leq 70 \text{ Ma} \\ d(t) = 6400 - 3200\exp(-t/63) & t > 70 \text{ Ma} \end{cases} \quad \begin{array}{l} \text{where } d \text{ is depth in} \\ \text{meters and } t \text{ is time in} \\ \text{millions of years.} \end{array} \quad (1.6)$$

which has been compared by other authors such as Stein and Stein (1992) or Hasterok (2013). The Parsons and Sclater (1977) and Stein and Stein (1992) equations are widely used to obtain the age of oceanic crust when magnetic anomaly data related to the oceanic spreading are not available (e.g. Barker et al., 2013).

Major consequences of the mantle dynamics and the thermal behavior of the lithosphere are seen above the seafloor on the planet, where continental and oceanic geometries are altered, continental and oceanic flora and faunal exchanges take place, and global oceanographic and climate changes occur. The break-up of Gondwana Supercontinent entailed the formation of oceanic gateways with implications for global ocean circulation, as well as for the diversification of species. Gondwana was totally separated in the late Eocene-early Oligocene, and warm water flow characterized oceanic circulation (Perrin, 2002) by that time (Figure 1.4A). Later, when four equatorial gateways closed and three polar ones opened, the global oceanic circulation became a well-ventilated major surface current system, involving a cooler global ocean (Figure 1.4B). All the changes in the gateway systems —and possibly orbital forcing and catastrophic events— are related to global climate changes on the planet (Zachos et al., 2001). Based on IODP or ODP data, values of $\delta^{18}\text{O}$ and $\delta^{13}\text{C}$, and sedimentary, climatic, tectonic and biotic studies (Copeland, 1997; Lawver and Gahagan, 1998; Barker et al., 1999; Alroy et al., 2000;

Zachos et al., 2001, among others), changes in the global climate are identified (Figure 1.5). Major extinctions and diversification are associated with important climate changes, and these, in turn, with the closing or opening of oceanic gateways. These events are better known from 70 Ma to present.

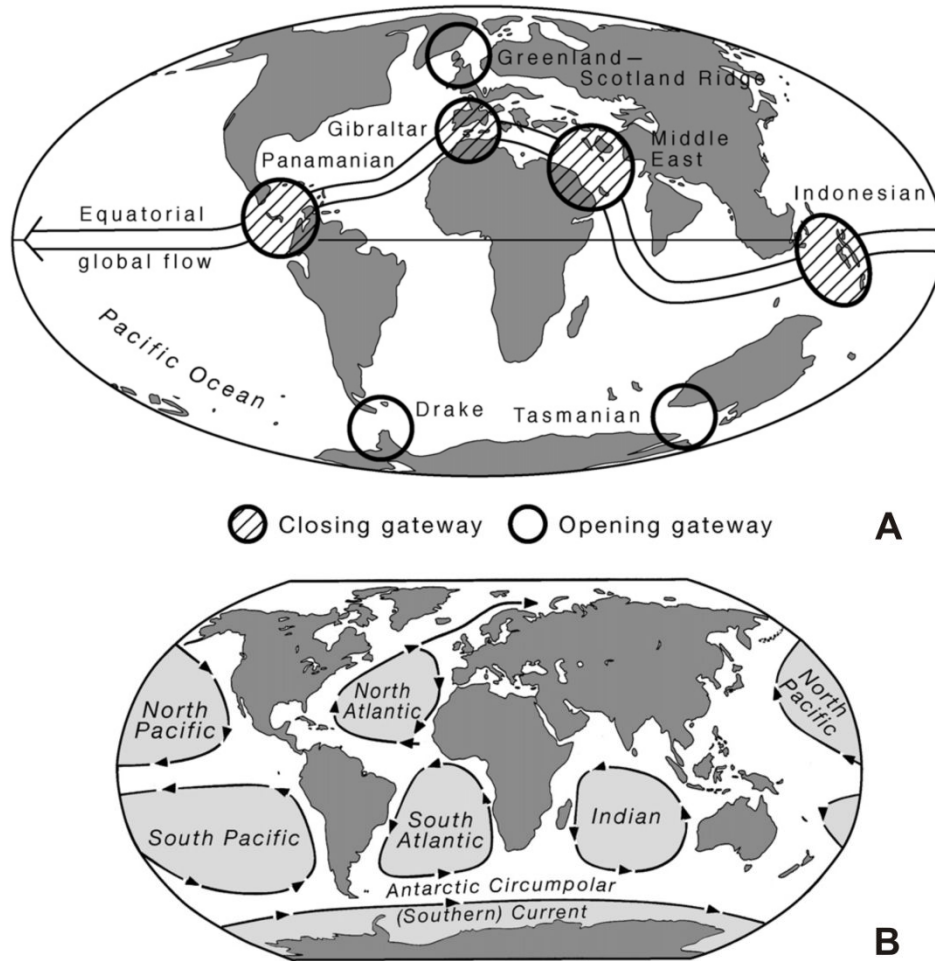


Figure 1.4. Oceanic current distribution on the Earth (after Potter and Szatmari, 2009). A) Late Eocene to Early Oligocene equatorial and warm water flow. B) Oceanic current distribution in recent days.

According to Figure 1.5, some of the most relevant events of the Cenozoic include: the opening of the Tasmania-Antarctic and Drake Passage gateways, the ice-sheet evolution in Antarctica, the closing of seaways producing mammal dispersion, and catastrophic events such as meteor impact and extensive volcanic activity. Together with gateway dynamics, these events produced major extinctions.

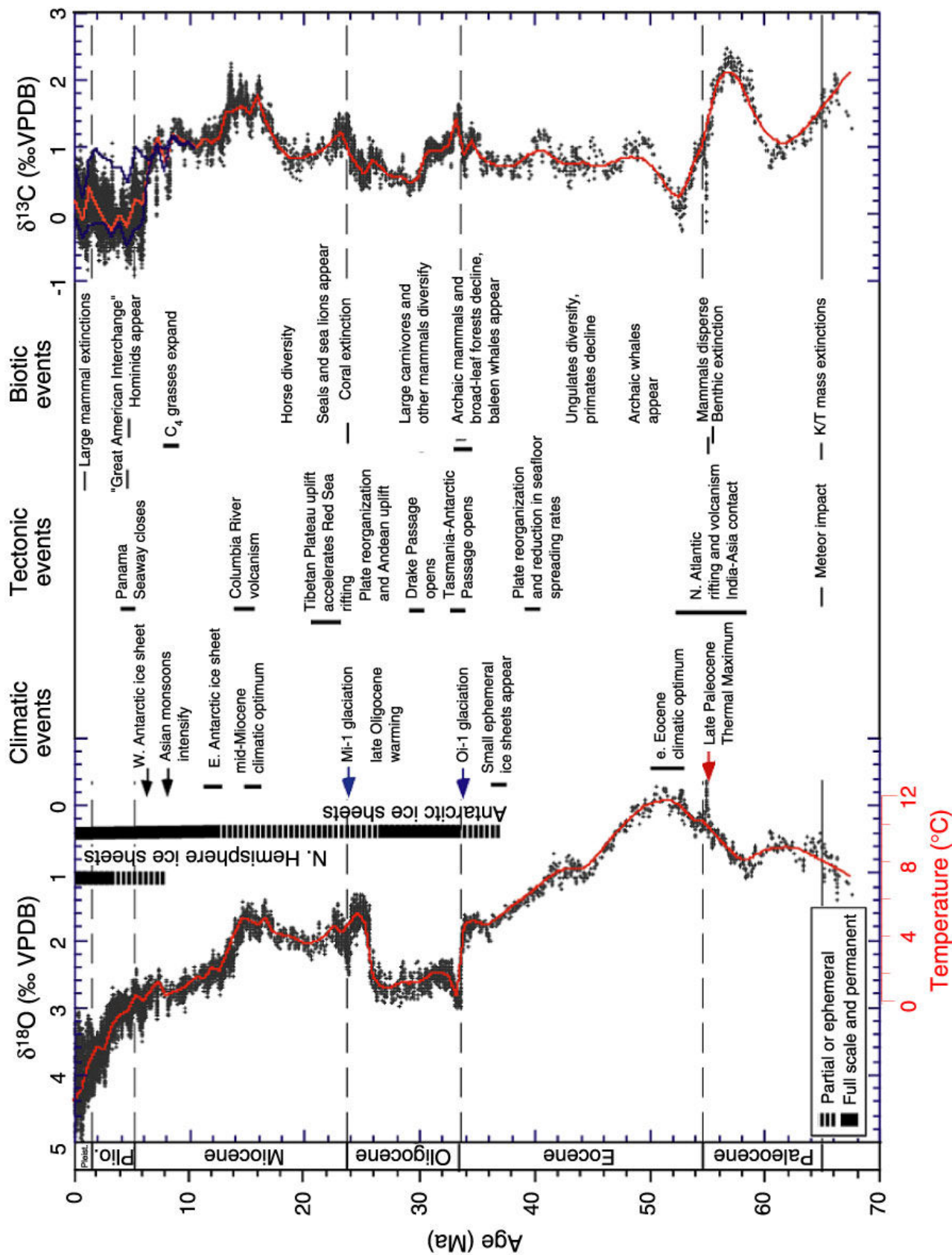


Figure 1.5. Cenozoic events in climate, tectonics, and biota vs. $\delta^{18}\text{O}$ and ^{13}C in benthic foraminiferal calcite (after Zachos et al., 2001). VPDB = Vienna Pee Dee belemnite.

In summary, the dynamics of the Drake Passage constitute a turning point that influenced global changes during the Cenozoic. The main objective of this Ph.D. Thesis is to analyze relevant aspects of the evolution of this key gateway and how its dynamics may have influenced global changes. The opening of the Drake Passage resulted in the creation of the Scotia Arc, which in turn led to a new pattern of asthenospheric flow and oceanic currents on the Earth. A detailed description of the objectives and the area of study are respectively explained in detail in Chapters 2 and 3.

Chapter 2

OBJECTIVES AND THESIS STRUCTURE

The opening of the Drake Passage is one of the most important events of the Cenozoic. It affected the planet on a global scale, as it entailed the final break-up of Gondwana Supercontinent. This implied the main aspects and consequences of the continental fragmentation described in Chapter 1. Hence, this Ph.D. Thesis focuses on the evolution of the opening of Drake Passage and surrounding areas, as well as its global-scale consequences. In this framework, in order to better understand the main implications of the opening of this gateway, along with the formation and dynamics of the Scotia Sea and surrounding areas, the objectives of the Ph.D. Thesis are:

- 1) To determine the main features of the young oceanic lithosphere of the Scotia Sea and provide new geophysical constraints that help to evaluate inferred changes in mantle flow patterns in the Scotia Sea region, improving our knowledge of the lithospheric structure and density variations in the lithosphere and the upper asthenosphere.
- 2) To characterize the thermal behavior of the lithosphere of the Scotia Sea, since it is a small ocean and an important gateway for deep oceanic circulation, and its faunal and floral exchanges have far-reaching implications for the history of the Earth.
- 3) To present a new magnetic data compilation of the Scotia Arc, which enables us to identify and characterize the main shallow and intermediate crustal geological features, while analyzing the tectonic structures, leading us to reconstruct their former relative position and to discuss the tectonic differences between the northern and southern branches of the arc.
- 4) To constrain the paleoceanography of this key region and shed light on the relationships between depositional processes, tectonic evolution and bottom-current circulation, as well as to understand the last important climate change in Antarctica, which in turn influenced the Eocene/Oligocene global climate change.
- 5) To constrain the deep structure of the Bransfield Strait, a young back-arc basin located to the southwest of Scotia Sea, and discuss its oceanic character.

6) To characterize the magnetic anomalies of Deception Island (South Shetland Islands) and their variation since 1987, as a support to new knowledge of its in-depth structure and the recent volcanic activity in the Bransfield Strait framework.

The results of this Thesis have been published or are under review by high impact journals. They constitute the main body of the study, and for that reason the style, numbering and reference formats requested by the journal where they are published are maintained. Thus, in addition to the English and Spanish Abstracts, the Thesis comprises the following chapters:

Chapter 1 offers a general introduction of the topic.

Chapter 2 includes the main objectives of the Thesis.

Chapter 3 presents the regional setting and evolution of the study area, including the tectonic, stratigraphy and paleoceanographic settings.

Chapter 4 provides a summary of the data sources and methodology used in this Thesis, since they are described in detail in each article.

Chapters 5 to 10 constitute the scientific articles that compile the complete Thesis. Detailed descriptions of the results of the Thesis are found in these chapters. They account for every main objective described above, in order.

Chapter 11 corresponds to the general discussion of the Thesis.

Chapter 12 compiles the main conclusions of this Thesis in English and Spanish.

Chapter 13 is the Reference section, which includes the bibliography used in the complete Thesis.

The **Appendix** closes the Thesis, including other published (co-authored) articles. While these articles are related to the study area and topic, they are not part of the main body of the Thesis. They are presented as additional works and collaborations done while the Thesis was underway.

Chapter 3

REGIONAL SETTING AND BACKGROUND

The development of the Drake Passage gave rise to the Scotia Sea, an ocean basin located between South America and the Antarctic Peninsula (Figure 3.1). It was formed by the tectonic development of the Scotia Arc since the Oligocene (Barker and Burrell, 1977; Barker, 2001) due to dispersion of the continental blocks that connected South America and Antarctica. The Arc propagated eastwards, forming oceanic back-arc basins inside the tectonic arc in several stages (Barker, 2001; Livermore et al., 2005, 2007; Dalziel et al., 2013; Eagles and Jokat, 2014; see Figure 3.2). The Scotia Sea is at present composed by two active plates, the Scotia and Sandwich plates. It is bounded by the Shackleton Fracture Zone, the former Phoenix and the Antarctic Plate to the west, and by the North Scotia Ridge, the South Scotia Ridge, the South Shetland Islands Block and South Sandwich Islands on the remaining sides (Figure 3.1). In this framework, and given the effect of subduction of the Phoenix Plate below the west margin of the Antarctic Peninsula, the Bransfield Strait basin developed (Dalziel, 1984; Gambôa and Maldonado, 1990). This basin is located between the South Shetland Islands and the Antarctic Peninsula, and it currently shows volcanic activity (Grácia et al., 1996; Ibáñez et al., 2003).

3.1. The Scotia Sea

The Drake Passage is a deep gateway. Although the age of the initial tectonic opening is not well constrained, it would have significant implications for global oceanic circulation and climate evolution in Antarctica, as it created the final gateway to allow the establishment of a full circum-Antarctic circulation and the thermal isolation of the Antarctic continent (cf., Kennett, 1977; Lawver et al., 1992; Barker, 2001; Barker and Thomas, 2004; Livermore et al., 2004; Maldonado et al., 2006; Scher and Martin, 2006), coeval with a global reduction in atmospheric CO₂ (Deconto and Pollard, 2003). However, the importance of the opening of the Drake Passage and the creation of the Scotia Sea, as triggers of Antarctic thermal isolation, are viewed as a subject of controversy. Some authors suggest that the heat anomalies caused by the opening and the initial circumpolar current were too weak to lead to the abrupt Cenozoic cooling (Huber and Sloan, 2001; Zhong-Shi et al., 2010). Moreover, the area has been described as a passage where eastward Pacific mantle outflow moves to the Atlantic Ocean (Figure 1.2) (Alvarez, 1982; Russo and Silver, 1994; Pearce et al., 2001; Helffrich et al., 2002; Dalziel et al., 2013). Once South

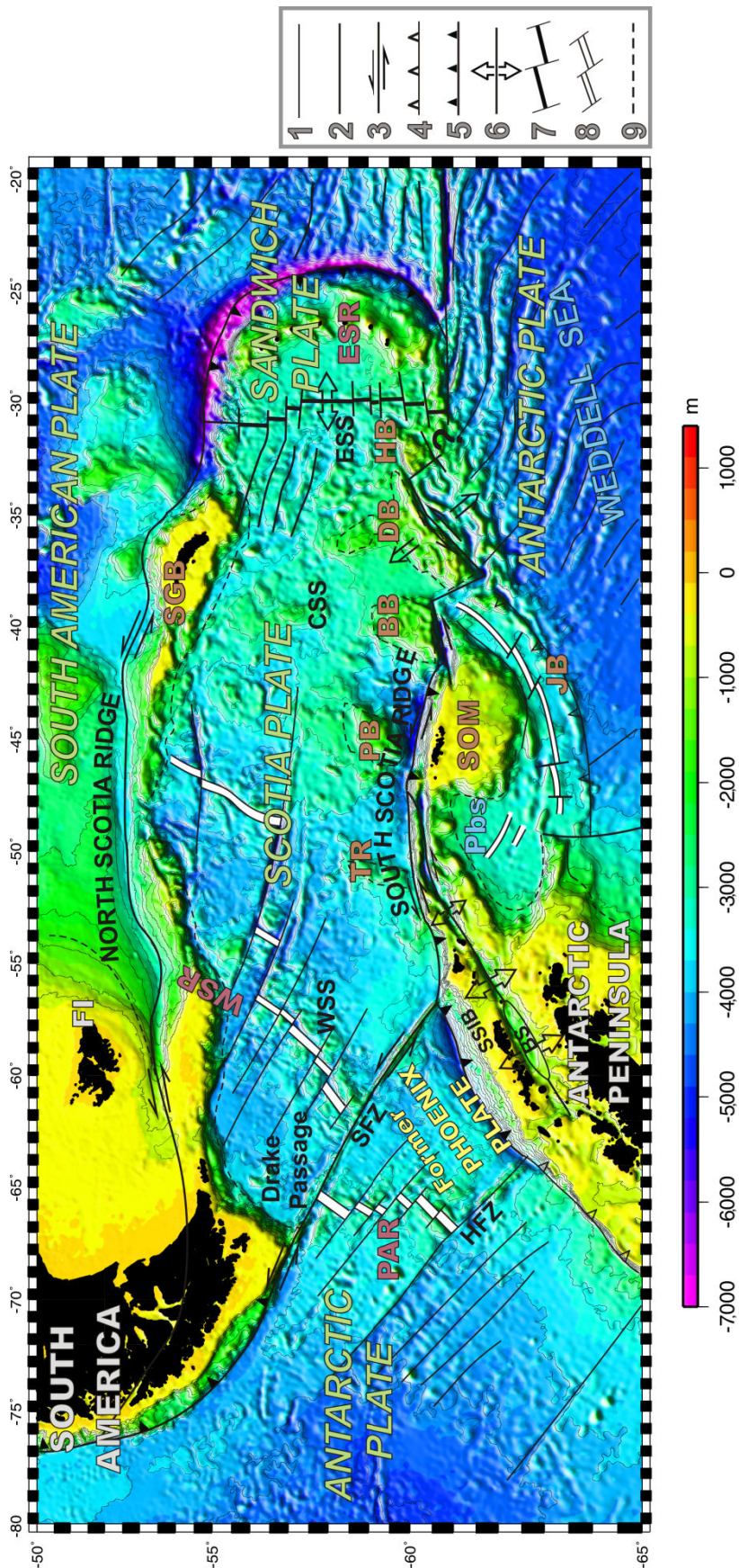


Figure 3.1. Geological setting of the Scotia Sea (according to Bohoyo et al., 2007). Scotia Arc bathymetry satellite map (Smith and Sandwell, 1997). Main tectonic features are shown in the figure. BB, Bruce Bank; BS, Bransfield Strait; DB, Discovery Bank; ESR, East Scotia Ridge; FI, Falkland Islands; HB, Herdman Bank; HFZ, Hero Fracture Zone; JB, Jane Bank; PAR, Phoenix-Antarctic Ridge; PB, Pirie Bank; Pbs, Powell Basin; SFZ, Shackleton Fracture Zone; SGB, South Georgia Bank; SOM, South Orkney Microcontinent; SSIB, South Shetland Islands Block; TR, Terror Rise; WSR, West Scotia Ridge. 1, Inactive subduction zone; 2, Active subduction zone; 3, Transcurrent fault; 4, Inactive subduction zone; 5, Active subduction zone; 6, Active extensional zone; 7, Active spreading center; 8, Inactive spreading center; 9, Continental-oceanic crust boundary.

America and Antarctica separated, the absence of deeper continental lithospheric roots and the rupture of the former subduction zone that extended from South America to the Antarctica allowed the Pacific mantle to flow into the Scotia Sea area, and afterward to the Atlantic mantle reservoir (Alvarez, 1982). Scarce geochemical data are consistent with this idea (Pearce et al., 2001).

3.1.1. Tectonic setting and evolution

The Scotia Sea contains at present two active plates, the Scotia Plate and the Sandwich Plate, which are bounded by the Shackleton Fracture Zone to the west and by the Scotia Arc on the three remaining sides. West of the Shackleton Fracture Zone, the Scotia Plate is bounded by the extinct Phoenix Plate, which is now part of the Antarctic Plate. The Scotia Arc is composed of the South Sandwich Arc, the North Scotia Ridge, and the deformed continental crustal blocks of the South Scotia Ridge and the South Shetland Islands Block (the continental block between the Antarctic Peninsula and the extinct Phoenix Plate). Along the South Scotia Ridge lies the sinistral transcurrent boundary between the Antarctic and Scotia plates, where restraining and releasing tectonic structures are well correlated with present stress (British Antarctic Survey, 1985; Pelayo and Wiens, 1989; Aldaya and Maldonado, 1996; Galindo-Zaldívar et al., 1996; Barker, 2001; Thomas et al., 2003; Geletti et al., 2005; Bohoyo et al., 2007; Smalley et al., 2007).

The Shackleton Fracture Zone is an active, transpressive fault zone that accommodates, in conjunction with the South Scotia Ridge, the relative motions between the Scotia and Antarctic plates (Barker et al., 1991; Livermore et al., 1994; Aldaya and Maldonado, 1996; Galindo-Zaldívar et al., 1996; Klepeis and Lawver, 1996; Kim et al., 1997; Maldonado et al., 2000). It is a significant structural relief with elevations of hundreds to thousands of meters above the surrounding ocean floor (Maldonado et al., 2000; Livermore et al., 2004), which crosses the entire length of the Drake Passage. This structure Zone is subducted below the northern tip of the South Shetland Islands Block, forming a triple junction (presently Antarctic-Scotia-South Shetland Islands Block) (Aldaya and Maldonado, 1996; Klepeis and Lawver, 1996). The evolution of this fracture zone, which constitutes part of the Antarctic-Scotia plate boundary, has been largely influenced by spreading of the Phoenix-Antarctic Ridge and of the West Scotia Ridge.

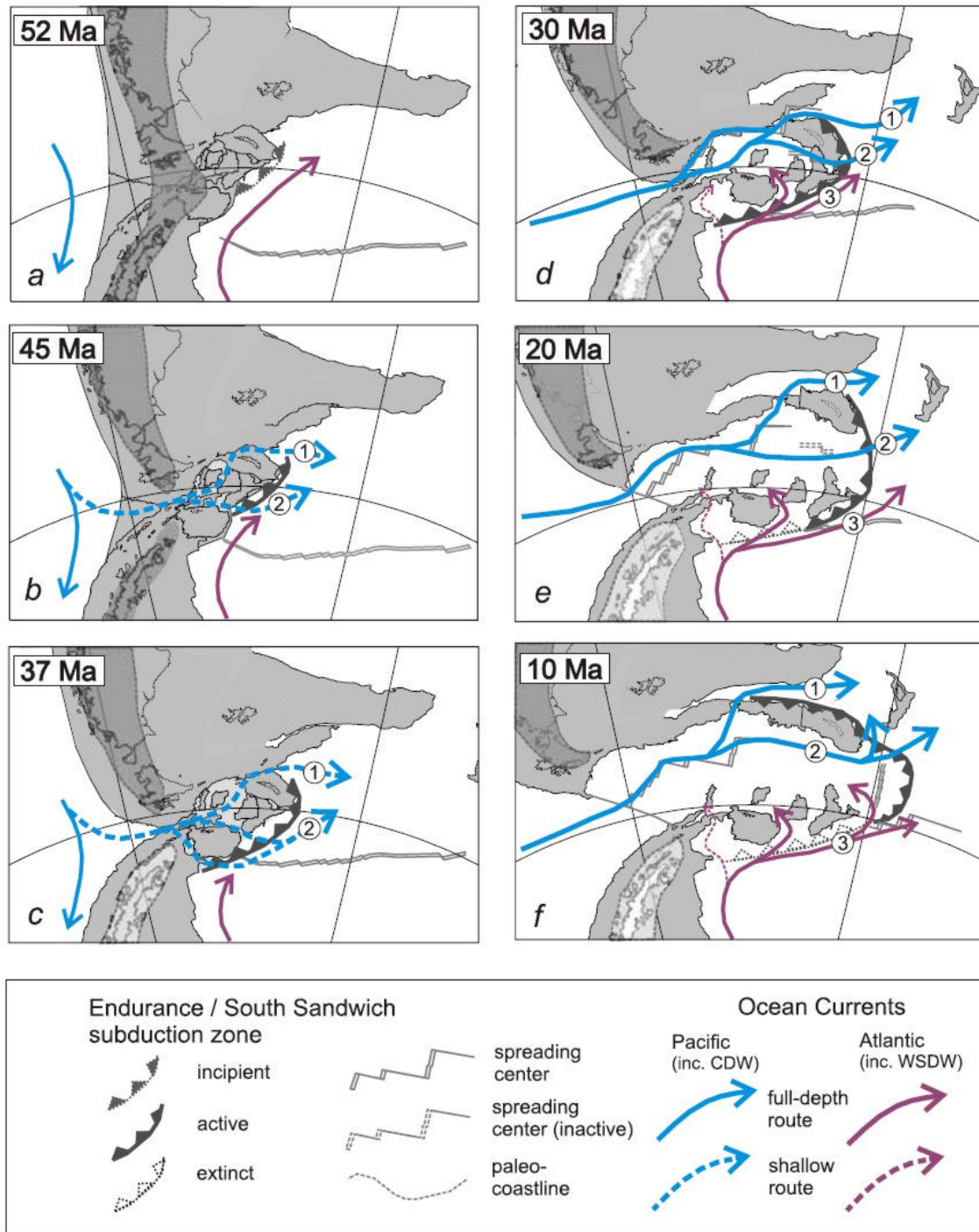


Figure 3.2. Livermore et al. (2007) reconstructions of Scotia Sea tectonic evolution at six times within the last 52 Ma. Reconstructions are made using the parameters of Livermore et al. (2005) for South America relative to a fixed Antarctic plate and Eagles et al. (2005) for Tierra del Fuego relative to the Antarctic Peninsula. Magnetic anomaly ages from Eagles et al. (2005, 2006). Numbers represent deep opened gateways for oceanic currents.

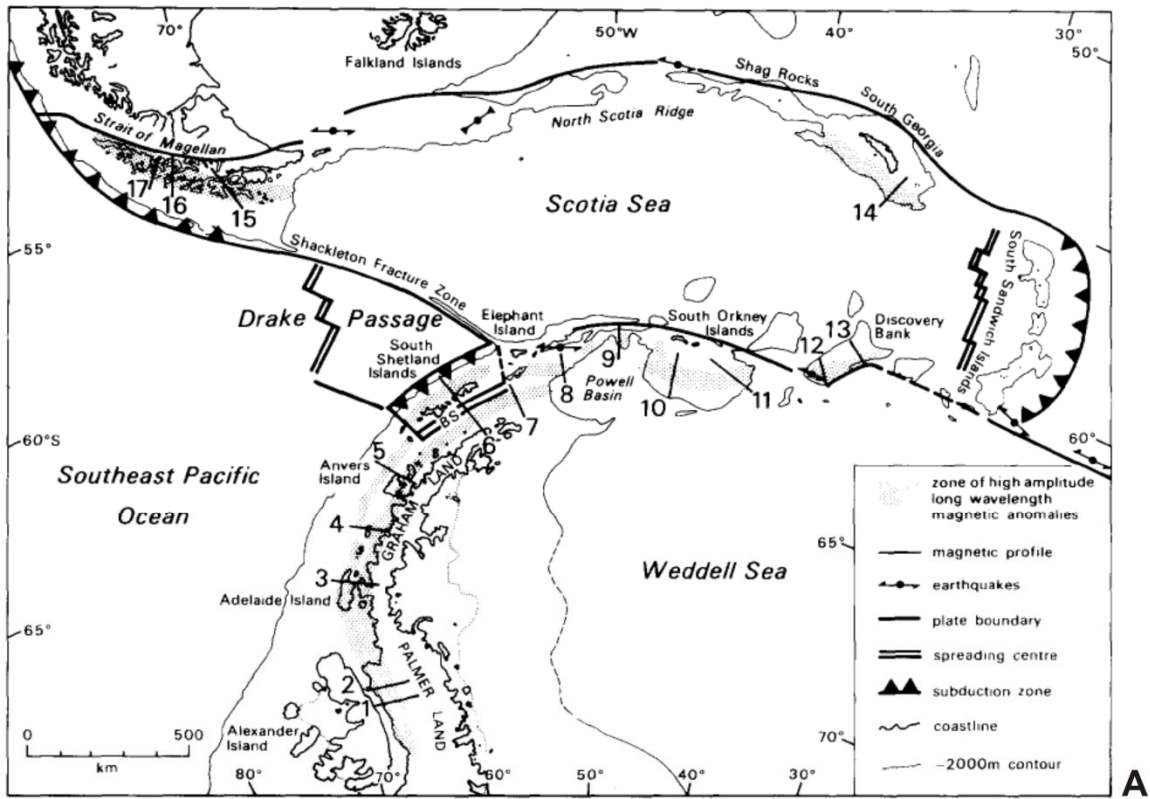
The Scotia Sea contains several spreading ridges that began to be active in the Oligocene and led to the opening of the Drake Passage (Barker, 2001; Eagles et al., 2005; Livermore et al., 2005, 2007; Lodolo et al., 2010). During the initial stages of continental rifting and oceanic spreading in the Scotia Sea, the south Scotia Sea was characterized by narrow NNE-SSW basins, which influenced the circulation of conspicuous water masses in the region (King and Barker, 1988; Galindo-Zaldívar et al., 1994; Lawver and Gahagan, 1998; Maldonado et al., 1998; Eagles and Livermore, 2002; Galindo-Zaldívar et al., 2002).

The Scotia Sea is generally divided in three regions: The West Scotia, the Central Scotia and the East Scotia Seas (Figure 3.1). The West Scotia Sea is the largest back-arc oceanic basin, around 1,500 x 1,000 km², formed by the West Scotia spreading center (Barker, 2001), with oceanic crust ages of around 30 to 6 Ma determined by well constrained oceanic spreading magnetic anomalies (Figure 3.3) (Lodolo et al., 1997; Maldonado et al., 2000; Eagles et al., 2005). The spreading center has a roughly NE-SW orientation and is divided by transform faults of NW-SE orientation in the West Scotia Sea up to E-W trends in the Central Scotia Sea. The opening of this oceanic basin was responsible for the last stages of separation of South America and the Antarctic Peninsula forming the Drake Passage. The southwestern Scotia Sea is a key region for constraining the time of opening because it contains the oceanic crust that developed during the initial phases of oceanic spreading (Aldaya and Maldonado, 1996; Lodolo et al., 2006, 2010; Martos-Martín et al., 2010). The oldest oceanic magnetic anomalies interpreted in the region suggest an early Oligocene opening age (ca. 32 Ma, Lodolo and Tassone, 2010; Maldonado et al., 2010; Martos-Martín et al., 2010; Schreider et al., 2012), and arguments based on plate tectonic reconstructions propose an opening during the middle Eocene (ca. 45 Ma, Livermore et al., 2007), the Oligocene (Lawver and Gahagan 2003; Geletti et al., 2005; Lodolo et al., 2010), or the Miocene (Barker, 2001). In addition to its influence during the initial evolutionary stages, the Shackleton Fracture Zone has been suggested as a significant barrier to the circumpolar deep flow since the late Miocene (8 Ma, Livermore et al., 2004). The deformed continental blocks of the South Scotia Ridge also influenced the bottom-current distribution in the area.

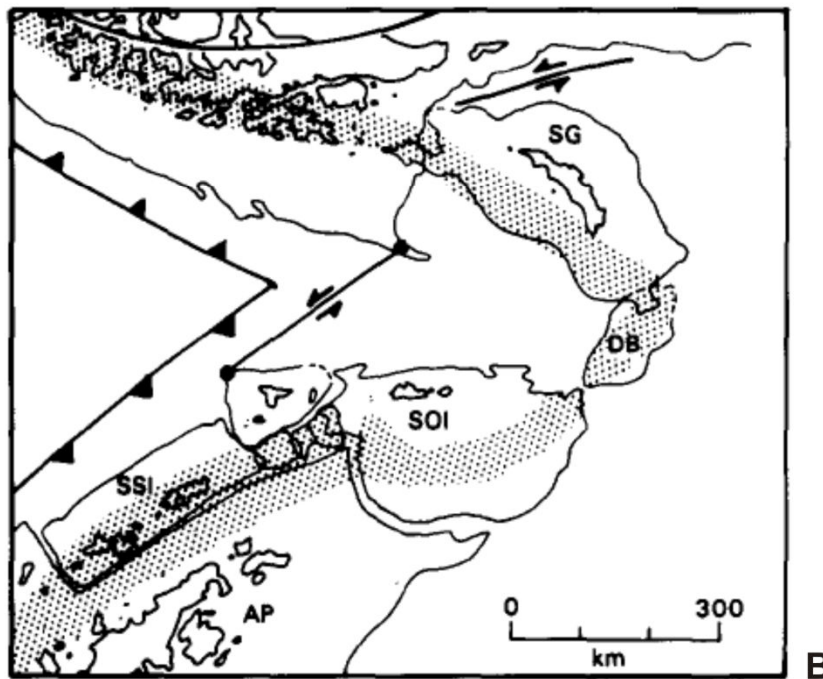
roll-back processes at the subduction hinge and active spreading in the Bransfield Strait (Maldonado et al., 1994; Livermore et al., 2000; Maurice et al., 2003).

Through several marine magnetic and aeromagnetic studies carried out in the Scotia Arc region, the main magnetic signature of the area and a magnetic anomaly belt known as the Pacific Margin Anomaly or West Coast Magnetic Anomaly have been revealed (Parra et al., 1984, 1988; Garret et al., 1986/87; Maslanyj et al., 1991). The southern part of the belt is located in the Pacific Margin of the Antarctic Peninsula. Northwards, the belt splits into two branches, whose widest separation is found in Bransfield Strait, due to back arc-tectonics (Garret and Storey, 1987; Garret, 1990; Barker, 2001). This feature extends along the southern continental fragments that lie in the margin of the Scotia Sea, along the South Scotia Ridge (Suriñach et al., 1997). The anomaly is caused by the emplacement of a linear basic to intermediate batholithic complex, related to a Cretaceous magmatic arc (Vaughan et al., 1998), resulting from crustal extensional episodes associated with the oceanic subduction of the Phoenix Plate along the Pacific margin (Garret et al., 1986/87; Garret, 1990, 1991). Some studies also suggest the extension of this magnetic anomaly belt into the South Scotia Ridge, South Orkney Microcontinent, Discovery Bank, South Georgia and South America (Figure 3.4) (Garret et al., 1986/87; Suriñach et al., 1997; Barker et al., 2001) and its connection to the Antarctic Peninsula, the South Shetland Islands and Bransfield Strait (Ghidella et al., 1991; 2011). Most studies of the magnetic anomaly distribution in the Scotia Sea, however, focus on the analysis of sea-floor spreading in order to constrain the tectonic evolution of the Scotia Arc (Eagles and Livermore, 2002; Kovacs et al., 2002; Eagles et al., 2006; Galindo-Zaldívar et al., 2006; Eagles, 2010).

Figure 3.4. Pacific Margin Anomaly distribution (after Garret et al. (1986/87)). A sketched map of the Scotia Arc. Shadow areas represent places where the Pacific Margin Anomaly is found. Numbers designate modeled profiles by Garret et al. (1986/87). BS, Bransfield Strait. B) Early Cenozoic reconstruction of the Scotia Arc (65 Ma) based on alignment of magnetic anomalies (shadow areas). AP, Antarctic Peninsula; DB, Discovery Bank; SG, South Georgia; SOI, South Orkney Islands; SSI South Shetland Islands. The solid circles mark the borders of the Shackleton Fracture Zone.



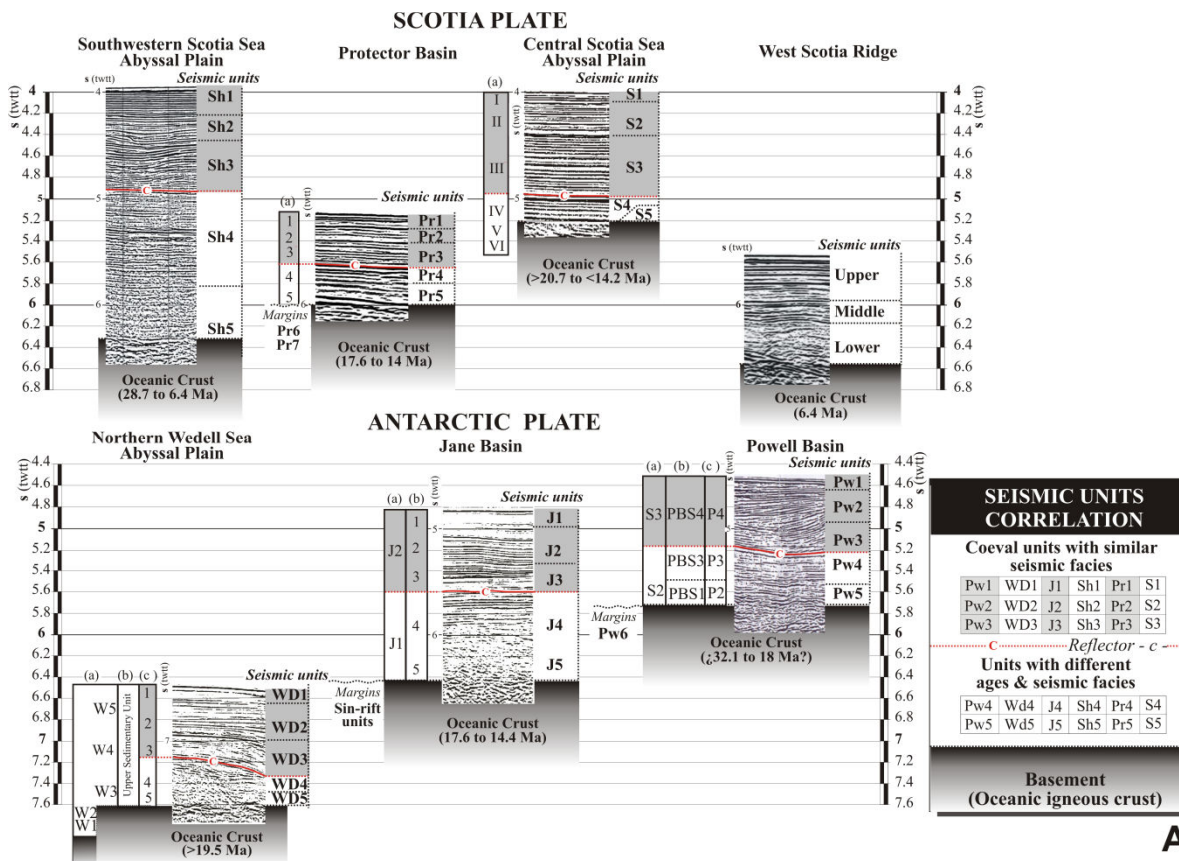
A



B

3.1.2. Regional stratigraphy

Five major seismic units (Units 5 to 1 from bottom to top) have been regionally correlated in the southern and central Scotia Sea by Maldonado et al. (2006) (see Figure 3.5). The discontinuities separating units are designated as d to a from bottom to top. Unit 5 fills basement depressions with an estimated Oligocene to early Miocene age. Unit 4 is sheet-like and considered to be early to middle Miocene in age. Unit 3 exhibits both mounded and sheet-like geometries and the suggested age is middle to late Miocene (Maldonado et al., 2003, 2005). Mounded and sheet-like shapes are dominant in Unit 2, which is attributed a late Miocene to early Pliocene age. Unit 1 is described as a relatively thin early Pliocene to Recent unit. Most recent studies (Lindeque et al., 2013, see their Figure 5) recognized six main units that are also in agreement with the previous studies.



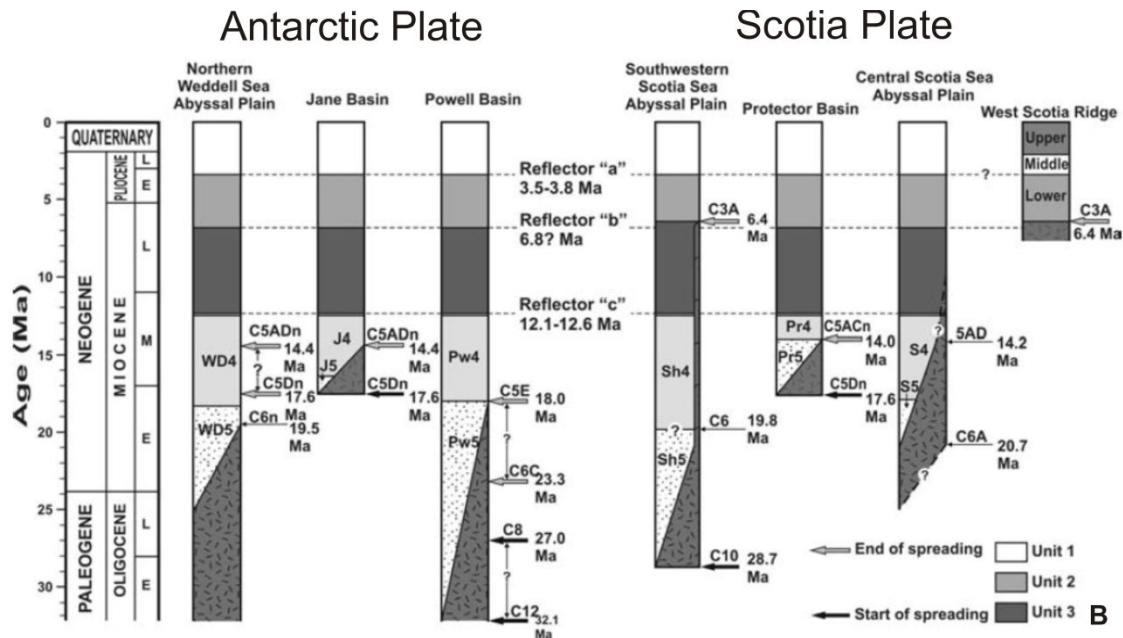


Figure 3.5. Correlation and ages of the main seismic units identified in the basins near the boundary between the Antarctic and Scotia plates (from Maldonado et al., 2006). A) Fragments of multichannel seismic reflection profiles illustrate representative sections of the basins. Depth in seconds two way travel time (twtt). The seismic units identified are shown in the vertical bar to the right of seismic reflection profiles. The seismic units described by previous authors are shown in vertical bars to the left of the seismic reflection profiles. The age of the oceanic basin floor is given according the identified magnetic anomalies. The major discontinuity is named Reflector c and is illustrated in the seismic records. The basins described in the Scotia Plate include: Southwestern Scotia Sea Abyssal Plain, Protector Basin; Central Scotia Sea Abyssal Plain: (previous studies: a, Maldonado et al., 2003, 2005), and the West Scotia Ridge. The basins identified in the Antarctic Plate include: Northern Weddell Sea Abyssal Plain: (previous studies: a, Maldonado et al. 1998; b, Rogenhagen and Jokat, 2000; c, Maldonado et al., 1998); Jane Basin: (previous studies: a, Maldonado et al., 1998; b, Bohoyo, 2004 and Maldonado et al., 2005). Powell Basin: (previous studies: a, Rodríguez-Fernández et al., 1997; b, Coren et al., 1997; c, Viseras and Maldonado, 1999). B) Stratigraphic correlation of seismic units and key reflectors identified in the basins of the area. The spreading time span of each basin is also shown.

Numerous types of drifts, such as mounded elongated, basement controlled, sheeted, patch, channel related and plastered drifts have been identified in the western continental margin of the Antarctic Peninsula, the Scotia and the Weddell seas (Howe et al., 1998; Howe and Pudsey, 1999; Michels et al. 2002; Pudsey, 2002; Rebesco et al. 2002; Stow et al., 2002; Maldonado et al., 2003; Hernández-Molina et al., 2004, 2006; Maldonado et al., 2005; Uenzelmann-Neben, 2006; Rebesco and Camerlenghi, 2008). Drift and contourite deposits in the southern and central Scotia Sea are mainly associated to the three youngest units above Reflector c (Maldonado et al., 2006).

3.1.3. Oceanographic setting

The full opening of the Drake Passage allowed the establishment of the Antarctic Circumpolar Current, which controls the transport of heat, salt, and nutrients around the Southern Ocean. This current is also the principal contributor to the boundary currents of the South Atlantic, South Pacific, and Indian oceans (Nowlin and Klinck, 1986; Naveira Garabato et al., 2002a). In addition, the Weddell Sea is one of the main engines of the global Thermohaline Circulation, being the source of deep and bottom waters due to enhanced atmosphere-ice-ocean interactions (Brennecke, 1921; Gill, 1973; Carmack, 1977; Fahrback et al., 1995; Foldvik and Gammelsrød, 1988; Rahmstorf, 2006).

Two important deep-water masses are distinguished in the region (Figure 3.6) (Orsi et al., 1999; Naveira Garabato et al., 2002b; Hernández-Molina et al., 2006, 2007; Hillenbrand et al., 2008): (a) the Circumpolar Deep Water, which flows mostly eastwards through the Scotia Sea as the deepest part of the Antarctic Circumpolar Current. This water mass is composed of lower (the Lower Circumpolar Deep Water) and upper (the Upper Circumpolar Deep Water) fractions, and (b) the Weddell Sea Deep Water, which flows within the Weddell Gyre, preferentially along the northwestern Weddell Sea above the slope of the Antarctic Peninsula. A branch of the Weddell Sea Deep Water enters the Scotia Sea through several narrow passages (Discovery, Bruce, Orkney, and Phillip passages) of the South Scotia Ridge (Naveira Garabato et al., 2002b; Schodlok et al., 2002; Naveira Garabato et al., 2003; Hernández-Molina et al., 2006; Bohoyo et al., 2007; Carter et al., 2008). Within the Scotia Sea, the Weddell Sea Deep Water is commonly subdivided into lower and upper components (Tarakanov, 2009). The Weddell Sea Deep Water flows westwards along the northern slopes of the South Scotia Ridge and reaches the Pacific margin of the Antarctic Peninsula (Locarnini et al., 1993; Orsi et al., 1995; Camerlenghi et al., 1997; Rebesco et al., 1997; Orsi et al., 1999; Naveira Garabato et al., 2002b). The initial incursions of the Weddell Sea Deep Water into the Scotia Sea through the Jane Basin are estimated to have occurred in the middle Miocene (Maldonado et al. 2003, 2006).

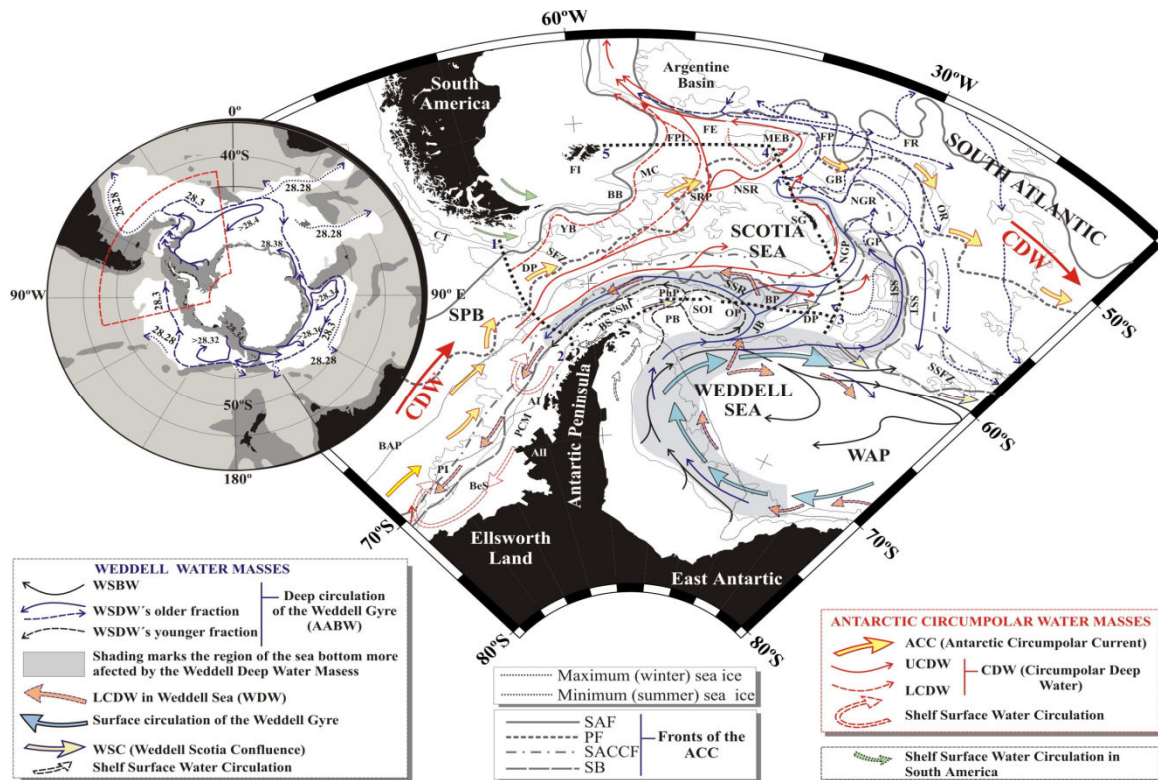


Figure 3.6. Summary of regional oceanographic framework and water mass dynamics (from Hernández-Molina et al., 2006; and references therein). Distribution of the flow pattern of Antarctic Bottom Water (AABW) with different density values (from Orsi et al., 1999). Schematic circulation patterns of the deep water masses in the Weddell Sea, Bellingshausen Sea and Scotia Sea overlain on regional bathymetry (Isobaths of 1500, 4000 and 6000 m). Also shown are Antarctic Circumpolar Current (ACC) fronts. Legends of the ACC fronts: SAF, Subantarctic Front; PF, Polar Front; SACCF, Southern ACC Front; SB, Southern Boundary of the ACC. Legend of the physiographic reference points, in alphabetical order: AI, Adelaide Island; All, Alexander Island; BAP, Bellingshausen Abyssal Plain; BB, Burdwood Bank; BP, Bruce Passage; BS, Bransfield Strait; BeS, Bellingshausen Sea; CT, Chile Trench; DP, Discovery Passage; FI, Falkland Island; FE, Falkland Escarpment; FP, Falkland Passage; FPL, Falkland Plateau; FR, Falkland Ridge; GB, Georgia Basin; GP, Georgia Passage; HFZ, Hero Fracture Zone; JB, Jane Basin; MEB, Maurice Ewing Bank; NGP, Northeast Georgia Passage; NGR, Northeast Georgia Ridge; NSR, North Scotia Ridge; OP, Orkney Passage; OR, Orcadas Ridge; PB, Powell Basin; PCM, Pacific Continental Margin of Antarctic Peninsula; PI, Peter Island; PhP, Philip Passage; SG, South Georgia; SFZ, Shackleton Fracture Zone; SOI, South Orkney Island; SPB, Southeastern Pacific Basin; SRP, Shag Rocks Passage; SSFZ, South Sandwich Fracture Zone; SShI, South Shetland Island; SSI, South Sandwich Island; SSR, South Scotia Ridge; SST, South Sandwich Ridge; WAP, Weddell Abyssal Plain; YT, Yaghan Basin. Legend of the water masses: ACC, Antarctic Circumpolar Current; CDW, Circumpolar Deep Water; SPDW, Southeast Pacific Deep Water; LCDW, Lower Circumpolar Deep Water; UCDW, Upper Circumpolar Deep Water; AABW, Antarctic Bottom Water; WSC, Weddell Scotia Confluence; WDW, Warm Deep Water; WSBW, Weddell Sea Bottom Water; WSDW, Weddell Sea Deep Water.

3.2. The Bransfield Strait region

The Bransfield Strait, located between the Antarctic Peninsula and the South Shetland Islands (Figure 3.7), is considered a back-arc basin related to the subduction of the former Phoenix Plate below the South Shetland Island Block (Barker et al., 1991; Dalziel, 1984; Gambôa and Maldonado, 1990; Maldonado et al., 1994, Figure 3.8). It is affected by the southwestward extensional end of the transtensional and transcurrent fault system that deforms the continental blocks of the South Scotia Ridge (Galindo-Zaldívar et al., 2004, 2006a). The Bransfield Strait has a NE–SW orientation and it has been developing since the Pliocene. It ends to the southwest, also coinciding with the southwest end of the South Shetland trench along the Pacific margin of the Antarctic Peninsula (Jabaloy et al., 2003). To the NE, the Bransfield Strait is connected with discontinuous depressions located

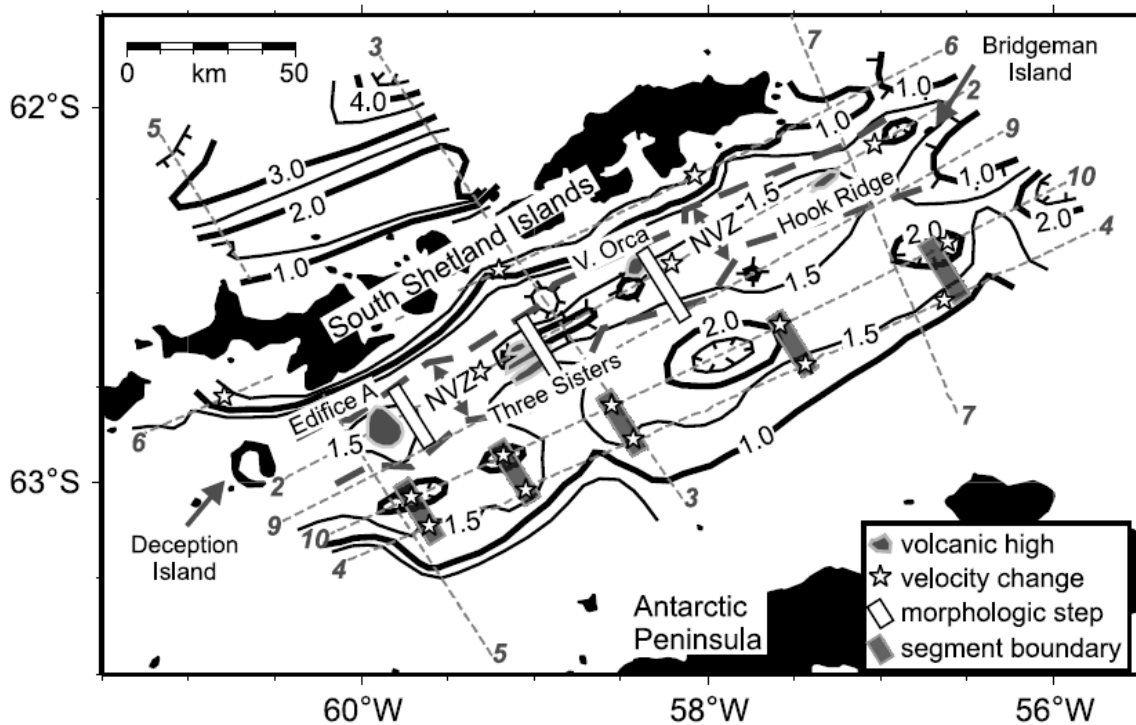


Figure 3.7. Depth to 4 km/s contour (a proxy for basement depth), hand-contoured from all two dimensional velocity profiles. Contour interval is 0.5 km. Neovolcanic zone, volcanic highs, velocity changes, morphologic steps, and interpreted segment boundaries are overlain. The volcanic highs and morphologic steps (from Grácia et al., 1996), and the velocity changes are from Christeson et al. (2003) velocity models. NVZ, neovolcanic zone.

along the South Scotia Ridge. This lens-shaped basin is usually divided into three sub-basins: Western, Central and Eastern (Gràcia et al., 1996; Christeson et al., 2003; Galindo-Zaldívar et al., 2004). Full swath-bathymetry data covering the central and eastern Bransfield Basin show a linear trend of volcanic features, roughly aligned along the basin (Canals et al., 1994; Gràcia et al., 1996). Galindo-Zaldívar et al. (2004) analyzed multichannel seismic profiles by studying the shallow structure of the Bransfield Basin and its eastward prolongation through the Scotia Sea. They proposed a tectonic picture where roll-back played a major role in the development of the Bransfield Basin, supporting the existence of incipient oceanic crust.

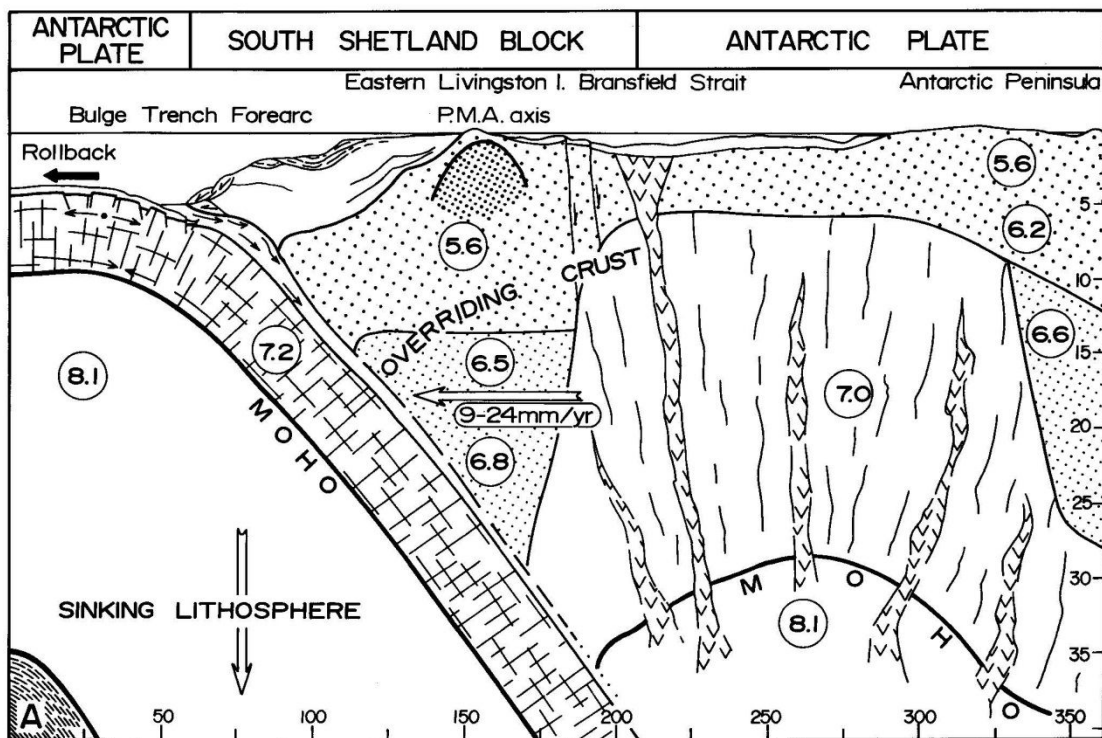


Figure 3.8. Interpretative cross section of the South Shetland active margin showing the main tectonic elements (from Maldonado et al., 1994). Generalized cross section through Livingston Island with NNW-SSE orientation. P.M.A., Pacific Margin Anomaly. Circled numbers indicate seismic velocities from Grad et al. (1993).

Parra et al. (1984), who modeled aeromagnetic data in the area, arrived at an age of the basin of 1.8 Ma, and an average velocity of 0.9 cm/yr full rate for the opening. On the basis of aeromagnetic data, González-Ferrán (1991) suggested an average full spreading rate of 0.25-0.75 cm/yr for the last 2 Ma. Magmatic activity is well established, but

according to Lawver et al. (1996) there is no strong evidence of normal seafloor spreading within the basin, probably due to its youth, which makes the magnetic patterns diffuse. More recently, Christeson et al. (2003) published results of a wide-angle seismic survey carried out in the region, consisting of a grid of five strikes and three dip profiles. They observed that the crustal thickness pattern was consistent with propagation of the extension from the NE towards the SW. In addition, from the upper mantle velocities, they suggest the occurrence of a small amount of partial melt or normal upper mantle anisotropy with the slow direction parallel to the rift axis, in order to justify velocities of 7.45 ± 0.2 km/s at depths of 14–17 km.

Moreover, Quaternary volcanism is recorded at Deception Island, located by the boundary faults between the South Shetland Block and the Bransfield Basin, and in several places among the South Shetland Islands. Deception Island constitutes the emergent part of a young active shield volcano (Figure 3.9) of basaltic-andesite composition and an external

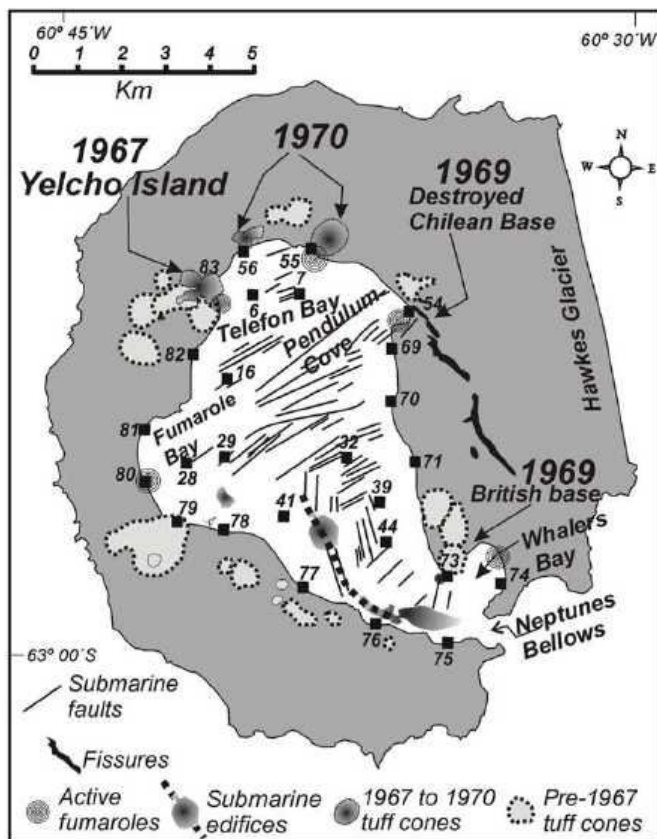


Figure 3.9. Map of Deception Island, including main fault system and submarine structures (modified from Rey et al. 1995, 2002; Somoza et al., 2004).

diameter of about 17 km. It is a horseshoe-shaped island, which is a collapsed and drowned volcanic crater, providing a natural harbor for shipping since it was discovered by sealers in 1820. This volcanic island has been very active during its entire evolution, and it is composed of basaltic to andesitic rocks that date from < 0.75 Ma to historical eruptions (1842, 1967, 1969 and 1970) (Smellie, 2001). Apart from these eruptions there were two additional periods of abnormal seismic activity in 1992 and 1999, described by Ortiz et al. (1997) and Ibañez et al. (2003). Nowadays, most of its activity is represented by vigorous hydrothermal circulation, a slight resurgence of the inner bay floor, and intense seismicity, with frequent volcano-tectonic and long period events (Zandomeneghi et al., 2009). Previous studies report seismic information in terms of refraction and P wave tomography (Grad et al., 1992, 1997; Ben-Zvi et al., 2009; Zandomeneghi et al., 2009) or potential field data (Vila et al., 1992; Muñoz-Martín et al., 2005) to draw a general picture of the crustal structure of Deception Island.

Chapter 4

DATA AND METHODOLOGY

A comprehensive dataset of swath bathymetry, gravity, magnetic, high resolution and multichannel seismic profiles acquired from 1953 to 2011 in Antarctica was compiled for this study. The component datasets were first analyzed using several methodologies involving software applications and personally developed computer programs. The most appropriate techniques were employed in order to attain the multiple objectives proposed for this study. This chapter summarizes the data sources and methodologies applied in view of the main objectives, while details are given in each corresponding section of the research chapters (Chapter 5 through Chapter 10).

4.1. Data sources

Gravity, magnetic and seismic reflection data are the main geophysical data used in this Ph.D. Thesis.

Gravity data

The GGM02S gravity model was used, derived from 363 days of Gravity Recovery and Climate Experiment (GRACE) gravity satellite in-flight data (Tapley et al., 2005). This model provides free-air gravity anomalies on the reference ellipsoid, which is approximately mean sea level. These values are defined as the difference between the gravity at a specific point on the reference ellipsoid and the normal gravity defined at the same point.

Marine free air gravity data from the Marine Trackline Geophysical Data System (GEODAS) (Metzger and Campagnoli, 2007) was also used. A total of 13 cruises were carried out in the period 1992-2000. Additional gravity data were obtained from a geophysical survey performed by the Royal Observatory of the Spanish Navy in January-February 2002 in the Bransfield Strait (Figure 4.1).

Magnetic data

The GEODAS DVD Version 5.0.10, available from the U.S. National Geophysical Data Center, was used as the magnetic data source (Figure 4.2, black lines). The resulting dataset consists of approximately 20 million records collected by about 2,400 cruises from 1953 to 2003. Further marine magnetic data were added to the GEODAS in 2008, as well

as data from seven Spanish cruises carried out on board the BIO Hespérides between 1992 and 2008 (Figure 4.2, blue lines), to update the dataset. Altogether, the final dataset comprised roughly 23 million records.

Aeromagnetic flight information was also incorporated into the magnetic dataset. One additional flight of reference in the area was by the U.S. Naval Research Lab. From 1951 through 1994, the Navy's Project Magnet program continuously collected vector aeromagnetic survey data to support the U.S. Geospatial-Intelligence Mapping Agency in world magnetic modeling and charting (Figure 4.2, red lines). These data had to be digitalized. Moreover, in 2011 an aeromagnetic flight at 4 km height (Figure 4.2, green lines) was performed under the National Geophysical Data Center's aeromagnetic program, focused on obtaining global data to support modeling of the Earth's magnetic field.

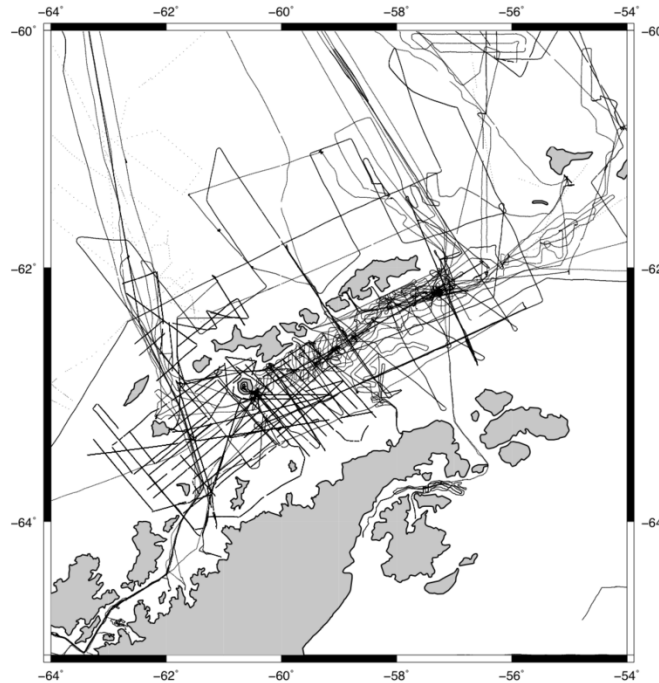


Figure 4.1. Marine gravity track line coverage from the Marine Trackline Geophysical Data System and the geophysical survey performed by the Royal Observatory of the Spanish Navy in January-February 2002.

During the past decade, several artificial magnetic satellites were put in operation (Oersted, CHAMP). The data from this additional source enabled us to “adjust” the long wavelengths of the different compilations used for the study area.

Additionally, it was possible to achieve a detailed compilation of magnetic data of Deception Island and surrounding areas for this Ph.D. Thesis. Altogether, geophysical cruises carried out by the Royal Observatory of the Spanish Navy in the austral summers of 1987, 1988-1989, 1990-1991, December 1999 (DECVOL cruise), January-February 2002 (GEODEC cruise), and December 2008 (MAREGEO cruise) provide a body of information spanning almost two decades. Also, on December 18th 2011 an aeromagnetic survey at 800 m was conducted using an unmanned aerial vehicle (UAV) over Deception Island, covering its northern half.

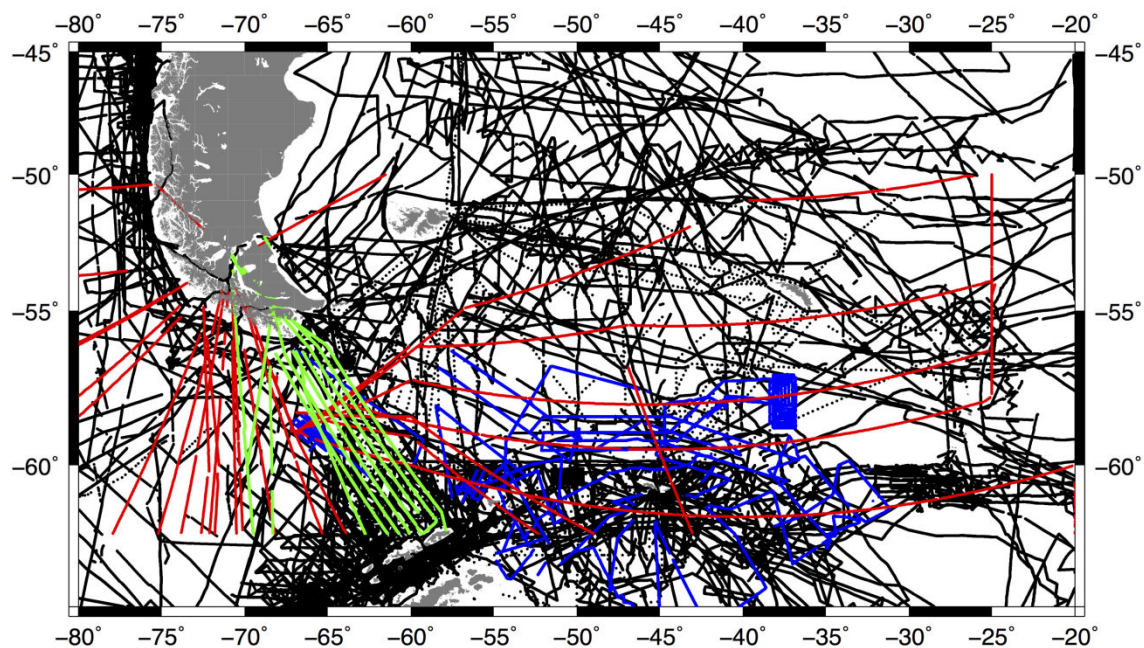


Figure 4.2. Magnetic trackline dataset in the Scotia Arc and surrounding areas. Black lines: GEODAS dataset corrected with CM4 model (Quesnel et al., 2009). Red lines: aeromagnetic survey data from the World Magnetic Modeling and Charting Program (carried out from 1951 to 1994). Green lines: Aeromagnetic flight at 4 km height performed in 2011 and under the National Geophysical Data Center's aeromagnetic program. Blue lines: seven Spanish cruises carried out on board the BIO Hespérides between 1992 and 2008.

Seismic reflection data

Multichannel seismic reflection profiles acquired in the West Scotia Sea from 1992 to 2008, on board the BIO Hespérides, were used in this Ph.D. Thesis (Figure 4.3). The first survey was carried out with a tuned array of seven Bolt air guns with a total volume of 16.3 l; the others were carried out with a tuned array of six Bolt air guns with a total volume of

15.26 1. All of them used a 96-channel streamer with an active length of 2.4 km and a shot interval of 50 m. Multichannel seismic data were recorded with a DFS V digital system and a sampling record interval of 2 ms and 10 s record lengths. Data were processed with a standard protocol, including time migration using a DISCO/FOCUS system.

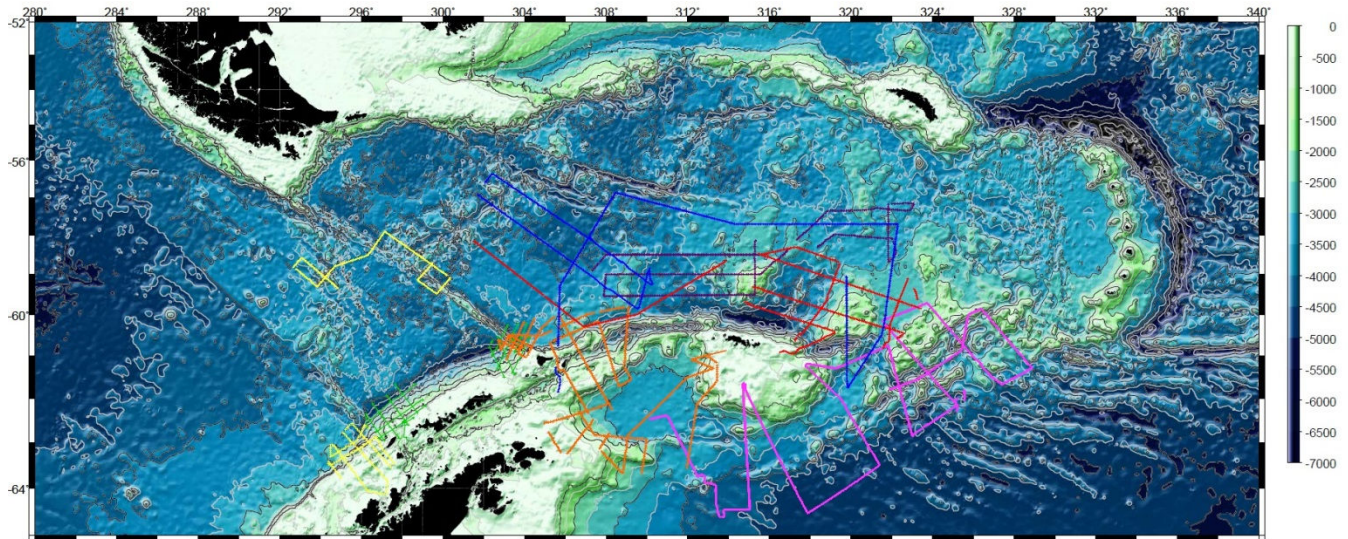


Figure 4.3. Bathymetry map of the Scotia Arc (Smith and Sandwell, 1997). Multichannel seismic profiles of the SCAN group are shown in the map. Green lines, ANT92 cruise; Orange lines, HESANT 92/93 survey; Yellow lines, ANTPAC 97/98 survey; Pink lines, SCAN 97 cruise; Purple lines, SCAN 2001 cruise; Red lines, SCAN 2004 cruise; Blue lines, SCAN 2008 survey.

4.2. Methodologies

The data sources described in the last section were used for different objectives:

Gravity data

The gravity data were used to determine the main features of the young oceanic lithosphere of the Scotia Sea and provide new geophysical constraints to evaluate inferred changes in mantle flow patterns in the Scotia Sea region, thereby gaining a better knowledge of the lithospheric structure and density variations in the lithosphere and the upper asthenosphere. Furthermore, the data helped constrain the deep structure of the Bransfield Strait and enrich discussion of its oceanic character.

Then, for the Scotia Sea, Complete Bouguer anomalies were calculated taking into account the Nettleton (1976) procedure. The water layer was corrected using a density of 1.03 g/cm^3 ; to apply Terrain corrections, the SRTM30PLUS4 grid was used as a local grid

(Smith and Sandwell, 1997). The same digital elevation model was applied as a regional grid, once undersampled at 13 km. A terrain density of 2.67 g/cm^3 was used, corresponding to the average density of the surrounding continental crust. The mean density value is close to the one considered, even though the area is occupied by oceanic crust with denser basements, given that the sedimentary infill has lower densities. The regional grid was used beyond 2 km. A Bouguer anomaly grid with a 13 km resolution was obtained, revealing the deep features. This Bouguer anomaly map at sea level was then continued upward to 50 km. As this was done in the Fourier domain, it helps attenuate short wavelength features related to shallow structures. It therefore enhanced the signal of mantle sources when shallower ones were present. Once the maps were obtained, important profiles were selected for gravity modeling across the main structures in the Scotia Sea. GRAVMAG software (Pedley et al., 1993) was used for this modeling. Densities used in the gravity modeling are in agreement with other works done in the area (Ferris et al., 2000, Galindo-Zaldívar et al., 2006; Bohoyo et al., 2007, among others).

For the Bransfield Strait the methodology was similar, applying the SRTM30PLUS4 grid as a regional grid for Terrain corrections (Smith and Sandwell, 1997), and data from a local full swath-bathymetry survey for local corrections (Gràcia et al., 1997). The regional grid was used beyond 10 km, and additionally in those areas where there was no local bathymetry data. Finally, a Bouguer anomaly grid with a 3 km resolution was obtained. Oasis Geosoft was used for modeling, and for constraint the initial density values were based on Christeson et al. (2003) (their figures 13a, b) and Galindo-Zaldívar et al. (2004) (southeastern segment of MCS profile BR30). A low-density value for the upper mantle, within the neovolcanic zone, was considered according to past seismic studies (Ashcroft, 1972; Christeson et al., 2003; Grad et al., 1997).

Magnetic data

The magnetic data served to present a new magnetic data compilation of the Scotia Arc, making it possible to identify and characterize the main geological features, while analyzing the tectonic structures. Hence, their former relative position could be reconstructed, shedding new light on: the tectonic differences between the northern and southern branches of the arc; the oceanic character of the Bransfield Strait; and the

magnetic anomalies of Deception Island and their variation since 1987, improving knowledge of its deep structure and the recent volcanic activity in the Bransfield Strait framework.

For the new compilation of the Scotia Arc, magnetic anomalies from the GEODAS dataset were recalculated taking advantage of the recently released comprehensive model CM4, which enabled us to correct total field marine data by a proper separation of spatial and temporal variations (Sabaka et al., 2004). Magnetic anomaly data from the updated GEODAS, the Spanish cruises and aeromagnetic flights were also calculated using the CM4 model. The CM4 model provides a means of precisely modeling and separating the core field and external fields, so that the former's secular variation behaves in a smooth and continuous way (Ravat et al., 2003). All the new information was cleaned by means of a careful check and removal of spurious data, and finally, a line leveling method was applied to reduce data misfits among cruises. To assess the improvement in quality and coherence of the cruise dataset, the root mean squares of the crossover differences were calculated, and were reduced from 179.6 nT (before leveling) to 35.9 nT (after leveling). Additionally, satellite data helped us complete the areas not covered by marine or aeromagnetic surveys. The short wavelength (< 320 km) anomalies from the marine and low-altitude flights were selected, while longer wavelengths (> 320 km) were filled using magnetic satellite information (Ravat and Purucker, 1999). GRAVMAG software (Pedley et al., 1993) was used to model main structures of the Scotia Arc. The initial depth values for Curie point were based on Garret et al. (1986/87), and the magnetic susceptibilities were based on data from the Antarctic Peninsula (Maslanyj et al., 1991).

To discuss the oceanic character of the Bransfield Strait, marine magnetic data from GEODAS were used along with magnetic data acquired by the Royal Observatory of the Spanish Navy during the austral summers of 1989-90, 1990-91, December 1999 (DECVOL), January-February 2002 (GEODEC), and December 2008 (MAREGEO). The core field contribution was subtracted using the best-reference geomagnetic field, which is the DGRF evaluated at the time period of the cruises. Data from DECVOL, GEODEC and MAREGEO were lag corrected, spike removed and diurnally corrected using data from the Livingston Island geomagnetic observatory. Data from an auxiliary reference station installed at Deception Island were also used. As the GEODAS cruises were not corrected

by external field contribution, the cruises DECVOL, GEODEC and MAREGEO were used as masters. Crossover analyses were used to estimate the quality of the geophysical surveys as well as to provide an effective technique for improving the internal consistency of the geophysical data grids (Wessel and Watts, 1988; Thakur et al., 1999). Since the local magnetic anomaly is time-invariant, if the anomaly crossover difference between two tracks is examined, the residual will reflect the error budget. This is mainly due to the geomagnetic field time-dependent components: secular variation and to the external field contribution, as well as navigation errors. Leveling techniques were also applied to data. All filtered offshore magnetic anomaly data were merged to derive a 3 km resolution map. To further aid in the interpretation of the magnetic anomaly data, reduction to the pole (Baranov and Naudy, 1964) was also applied. Reduction to the pole serves to transform data that are collected in areas where the magnetic inclination is not vertical to the way the data appear at the geomagnetic pole; that is, the anomalies are essentially de-skewed and positioned symmetrically over their sources. Inclination and declination average values of -55° and 11.5° were respectively considered for the whole area.

The detailed study of Deception Island was likewise performed using data from the geophysical cruises carried out by the Royal Observatory of the Spanish Navy in the austral summers of 1987, 1988-1989, 1990-1991, December 1999 (DECVOL), January-February 2002 (GEODEC), and December 2008 (MAREGEO), and data from an aeromagnetic survey. This body of information, spanning almost two decades, allowed us to detect temporal changes of magnetic anomalies in the volcano area by isolating signals of volcanic origin, and comparing magnetic grids obtained in different periods. The available data enhance our knowledge of the tectonics and volcanic evolution of the study area. Data from the different marine surveys were obtained by means of marine proton precession magnetometers, which were towed 200 m astern. Their sampling rate was fixed at 0.16 Hz. These data were corrected by means of lag corrections and spike removal. Only the most recent cruises were corrected by removal of external fields, relying on different options: the Livingston Island geomagnetic observatory, a local reference station at the island, the CM4 model's external field estimation (Sabaka et al., 2004.), or a combination of the above. Details about error budgets are amply explained in Chapter 10.

Seismic reflection data

This type of geophysical data served to: 1) help characterize the thermal behavior of the lithosphere of the Scotia Sea; and 2) constrain the paleoceanography of the West Scotia Sea and study the relationships between depositional processes, tectonic evolution and bottom-current circulation.

For 1), the multichannel seismic data were initially used to determine the oceanic basement depth and the sediment thickness. Later, the ages of the oceanic crust were determined in the region from the analysis of magnetic anomalies (Eagles et al., 2005), allowing us to study the depth-age, heat flow-age, and lithospheric thickness modeling. It was assumed that the ocean of study follows and depends on the same parameters as those comprising the subsidence equation for the plate model (see equations 1.4 and 1.5) (Turcotte and Schubert, 2002).

For 2), the seismic reflection data were used to correlate the main reflections in the sedimentary record from the southwestern Scotia Sea to the Pacific Ocean across the Shackleton Fracture Zone, based on the recognition of seismic facies and the acoustic characteristics of the underlying basement. Moreover, contourite drifts and erosional features such as channels are identified by means of seismic data. Using the channel shape information, we arrived at estimations of the minimum volumetric flow rate percentages of the Weddell Sea Deep Water branches in the southwestern Scotia Sea.

Chapter 5

ASTHENOSPHERIC PACIFIC-ATLANTIC FLOW BARRIERS AND THE WEST SCOTIA RIDGE EXTINCTION

Published in:
Geophysical Research Letters
Vol. 41, 1-7
doi:10.1002/2013GL058885

Received 28 November 2013
Accepted 4 December 2013

Asthenospheric Pacific-Atlantic flow barriers and the West Scotia Ridge extinction

Yasmina M. Martos^{1,*}, Jesús Galindo-Zaldívar^{1,2}, Manuel Catalán³, Fernando Bohoyo⁴,
Andrés Maldonado¹

¹ *Instituto Andaluz de Ciencias de la Tierra (Consejo Superior de Investigaciones Científicas/Universidad de Granada). Avda. de Las Palmeras nº 4, 18100. Armilla, Granada (Spain).*

² *Universidad de Granada. Avda. de la Fuente Nueva, s/n, 18071. Granada (Spain).*

³ *Real Instituto y Observatorio de la Armada. Cecilio Pujazón, s/n, 11100. San Fernando (Spain).*

⁴ *Instituto Geológico y Minero de España. Ríos Rosas, 23, 28003. Madrid (Spain).*

** Corresponding author
Tel. +34 958230000
E-mail address: yasmartos@ugr.es*

Key Points

- Pacific mantle outflow is still present through the Drake Passage
- The Shackleton Fracture Zone modified asthenospheric flow patterns
- A redistribution of mantle flow may have caused West Scotia Ridge extinction

Key words: Drake Passage, Bouguer anomaly, gravity modeling, asthenospheric currents, asthenospheric gateways

Abstract

The Drake Passage is considered a gateway for oceanic and asthenospheric flows since its opening, entailing widespread consequences for climate and plate tectonics, respectively. Both the surface and the 50 km upward continued Bouguer anomaly maps of the Scotia Sea and surrounding areas, based on Gravity Recovery and Climate Experiment gravity satellite data, improve our knowledge of deep lithospheric structures and the asthenosphere. We show that the West Scotia Sea is likely to be underlain by an

anomalously low-density upper mantle. Gravity data are compatible with variable lithospheric thicknesses related to asthenospheric currents. The new data suggest that the development of the Shackleton Fracture Zone since the middle Miocene was probably a main factor that determined the evolution of the eastward Pacific mantle flows and the extinction of the West Scotia Sea oceanic spreading around 6 Ma ago. Deep lithospheric roots are likely to divert asthenospheric currents around them, flowing eastward through Drake Passage.

Index Terms: 8120 Dynamics of lithosphere and mantle: general; 3010 Gravity and isostasy; 3040 Plate tectonics; 1635 Oceans

1. Introduction

The Drake Passage has been studied in detail because of its significance as the most recent gateway for the southern oceans. The opening of this passage produced a redistribution of oceanic currents around Antarctica with the onset of the Antarctic Circumpolar Current [Kennett, 1977; Barker, 2001], and influenced a global climate change on the Earth since the Oligocene. Moreover, the area has been considered as a passage where eastward Pacific mantle outflow moves to the Atlantic Ocean [Alvarez, 1982; Russo and Silver, 1994; Pearce et al., 2001; Helffrich et al., 2002; Dalziel et al., 2013]. Once South America and Antarctica separated, the absence of deeper continental lithospheric roots and the rupture of the former subduction zone that extended from South America to the Antarctica allowed the Pacific mantle to flow into the Scotia Sea area and afterward to the Atlantic mantle reservoir [Alvarez, 1982]. Also, scarce geochemical data are consistent with this idea [Pearce et al., 2001].

At present day, the Scotia Sea is located between the South American and Antarctic plates, comprising the Scotia and Sandwich plates, which are confined by the Scotia Arc (Figure 1). The Scotia Arc is bounded by the North Scotia Ridge to the north, by the South Scotia Ridge to the south, by the Shackleton Fracture Zone (SFZ) and Former Phoenix Plate to the west, and by the South Sandwich Arc to the east. Several continental banks and oceanic basins that influence the regional oceanic circulation are located in the southern part of the Scotia Sea.

The Scotia Sea contains several spreading ridges starting at the Oligocene that led to the opening of the Drake Passage [Barker, 2001; Eagles *et al.*, 2005]; whereas spreading in the West Scotia Ridge ended around 6 Ma ago [Maldonado *et al.*, 2000], the East Scotia Ridge is still active. On the other hand, the spreading axis between the Antarctic Plate and the Former Phoenix Plate ceased about 3 Ma [Livermore *et al.*, 2000]. The SFZ is an active, transpressive fault zone that accommodates, in conjunction with the South Scotia Ridge, the relative motion between the Scotia and Antarctic plates [Klepeis and Lawver, 1996; Maldonado *et al.*, 2000]. This tectonic element became a barrier for bottom oceanic currents since the middle Miocene [Martos *et al.*, 2013], when tectonic compression started to uplift this morphostructural feature.

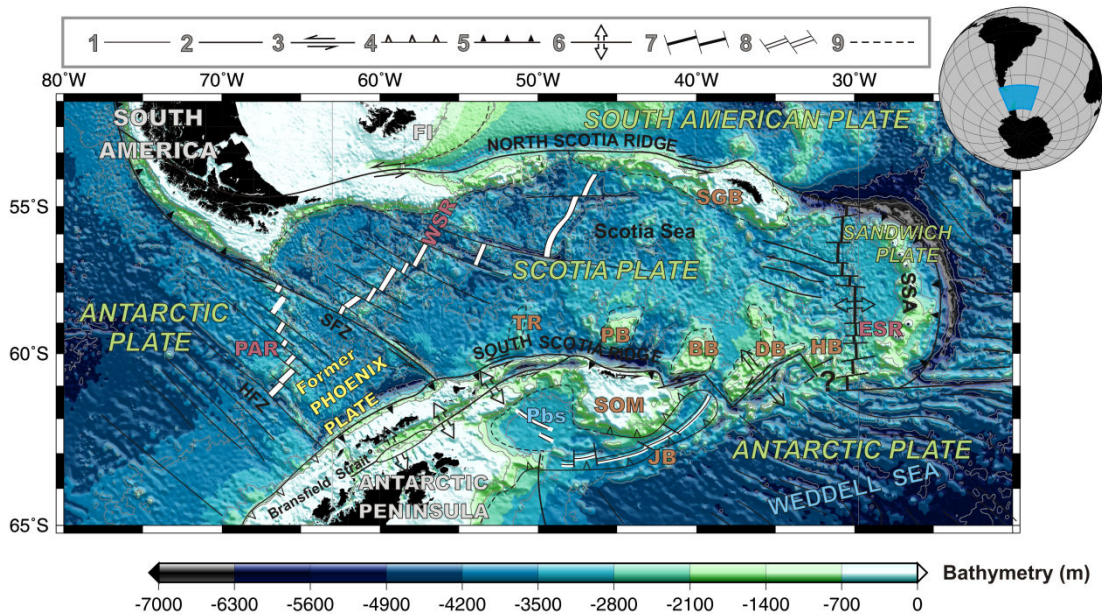


Figure 1. Geological setting of the Scotia Sea. Scotia Arc bathymetry satellite map [Smith and Sandwell, 1997]. Main tectonic features are shown in the figure. BB, Bruce Bank; DB, Discovery Bank; ESR, East Scotia Ridge; FI, Falkland Islands; HB, Herdman Bank; HFZ, Hero Fracture Zone; JB, Jane Bank; PAR, Phoenix-Antarctic Ridge; PB, Pirie Bank; Pbs, Powell Basin; SFZ, Shackleton Fracture Zone; SGB; South Georgia Bank; SOM, South Orkney Microcontinent; SSA, South Islands Arc; TR, Terror Rise; WSR, West Scotia Ridge. 1, Inactive fracture zone; 2, Active fracture zone; 3, Transcurrent fault; 4, Inactive subduction zone; 5, Active subduction zone; 6, Active extensional zone; 7, Active spreading centre; 8, Inactive spreading centre; 9, Continental-oceanic crust boundary.

This region is covered by global satellite data that reveal free air gravity anomalies from mean sea level data. The available Gravity Recovery and Climate Experiment

(GRACE) data [Tapley *et al.*, 2005] provide a new opportunity to determine Bouguer anomalies related to the large lithospheric structures of this remote but key region.

The main objective of our study is to determine the main features of the young oceanic lithosphere of the Scotia Sea based on analysis of a new compilation of gravity data. We moreover provide new geophysical constraints that help to evaluate inferred changes in mantle flow patterns in the Scotia Sea region improving the knowledge of the structure of the lithosphere and the density variations in the lithosphere and the upper asthenosphere. The impact of the development of the lithospheric roots of the SFZ on the asthenospheric circulation is revealed as a factor determining the end of oceanic spreading of the West Scotia Ridge.

2. Methodology

We used the GGM02S gravity model, derived from 363 days of GRACE satellite in-flight data [Tapley *et al.*, 2005]. This model provides free-air gravity anomalies on the reference ellipsoid, which is approximately mean sea level. These values are defined as the difference between the gravity at a point on the reference ellipsoid and the normal gravity defined at the same point.

Complete Bouguer anomalies were calculated taking into account the Nettleton [1976] procedure. Water layer was corrected using a density of 1.03 g/cm^3 ; to apply Terrain corrections, we used the SRTM30PLUS4 grid as a local grid [Smith and Sandwell, 1997]. The same digital elevation model was applied as a regional grid, once undersampled at 13 km. A terrain density of 2.67 g/cm^3 was used, corresponding to the average density of the surrounding continental crust. The mean density value is close to the one considered, even though the area is occupied by oceanic crust with denser basements, given that the sedimentary infill has lower densities. The regional grid was used beyond 2 km. A Bouguer anomaly grid with a 13 km resolution was obtained, which reveals the deep features.

The Bouguer anomaly map at sea level was then continued upward to 50 km. As this was done in the Fourier domain, it helps to attenuate short wavelength features related to shallow structures. Thus, it enhanced the signal of mantle sources when shallower ones were present. Once we obtained the 50 km height map, we selected three main profiles for gravity modeling across the main structures in the Scotia Sea. GRAVMAG software

[Pedley *et al.*, 1993] was used for this modeling. Densities used in the gravity modeling are in agreement with other works in the area [Ferris *et al.*, 2000, Galindo-Zaldívar *et al.*, 2006; Bohoyo *et al.*, 2007, among others].

3. Complete Bouguer Anomaly maps

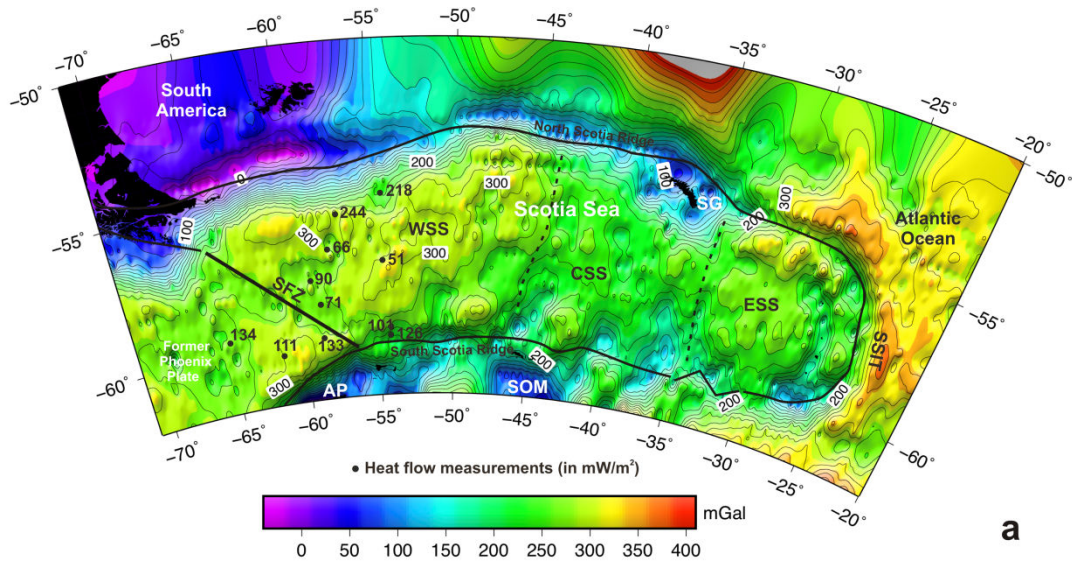
The Bouguer anomaly map at sea level (Figure 2a) shows different gravity signatures for each sector of the Scotia Arc and the surrounding areas. While high density oceanic areas are characterized by maxima, low density continental lithosphere —e.g., South American continent, Antarctic Peninsula, South Orkney microcontinent, South Georgia, and other banks along both the North and South Scotia ridges— reveals minima. Oceanic-continental plate boundaries are well marked by the high-to-low anomaly value transition. The Former Phoenix Plate and the Scotia Sea are characterized by a pattern of predominant high values alternating with intermediate values of Bouguer anomaly (Figure 2a). The Atlantic Ocean, in contrast, shows higher values. Although, the West Scotia Sea displays high Bouguer anomaly values, an area of local minimum is located in the transition between the Phoenix Plate and the West Scotia Sea corresponding to the SFZ. Relatively low local values are observed in the Central Scotia Sea, respect to the West Scotia Sea and the East Scotia Sea, increase slightly toward the east in the East Scotia Sea.

After the upward continuation to 50 km of the Complete Bouguer anomaly map, long wavelength signals are identified, while shallow structures are not perceptible. The main provinces of the study area are well identified (Figure 2b): the Former Phoenix Plate, the West Scotia Sea, the Central Scotia Sea, the East Scotia Sea, the Atlantic Ocean and continental regions of South America, and the South and North Scotia ridges. The West Scotia Sea has a wide local maximum in its middle part, while the Central Scotia Sea has relatively low values in comparison with the gravity signature of the surrounding oceanic areas of the Scotia Sea.

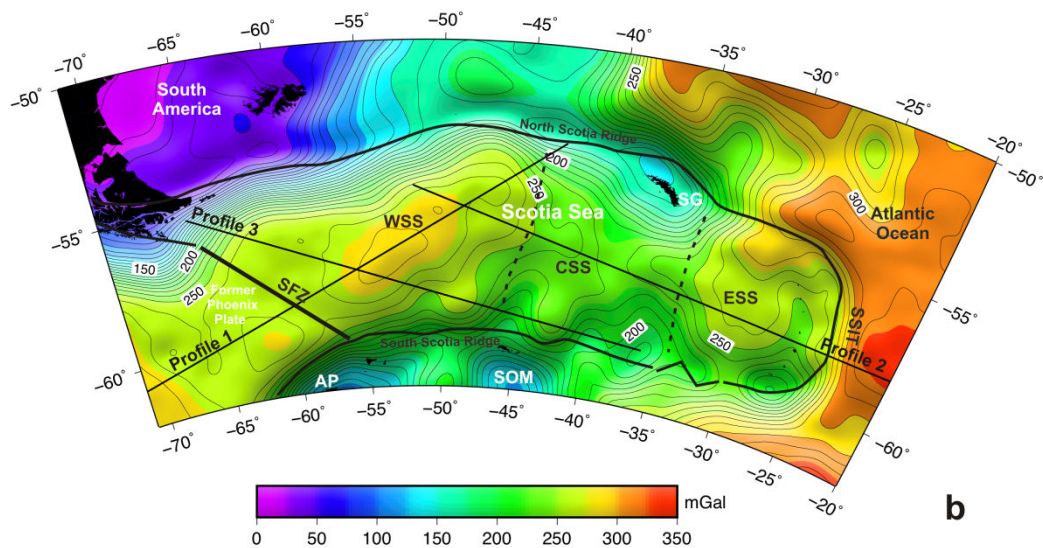
4. Gravity modeling

From the upward continued at an elevation of 50 km complete Bouguer anomaly map (Figure 2b) we selected three profiles for modeling in order to enhance knowledge about:

- The transition from the Former Phoenix Plate, crossing the SFZ, the West Scotia Sea, and the local gravity low of the North Scotia Ridge (Profile 1 with WSW-ENE orientation, Figure 2b).
- The transition from the West Scotia Sea, the Central Scotia Sea, the East Scotia Sea to the Atlantic oceanic crust, crossing the South Sandwich Island Trench (Profile 2 with NW-SE orientation, Figure 2b).
- The transition from the South American continent, the West Scotia Sea to the South Scotia Ridge, crossing all continental banks and small oceanic basins located in the southern part of the Scotia Arc (Profile 3 with WNW-ESE, Figure 2b).



a



b

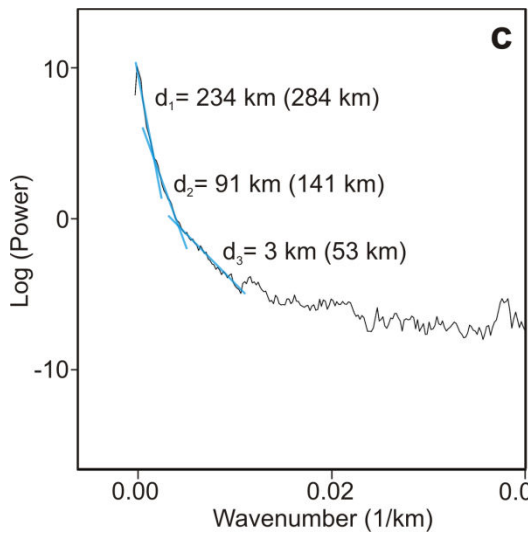


Figure 2. Complete Bouguer anomaly maps and spectrum. a) Complete Bouguer anomaly map at sea level. Main features are shown in the figure. Heat flow values of the West Scotia Sea are presented [<http://www.heatflow.und.edu>]. High values are located in the borders of the Scotia Sea while low values are found in inner parts. b) Bouguer Anomaly map at 50 km height. c) Spectrum of the 50 km Bouguer anomaly map. Main horizons are found at 284, 141 and 53 km, corresponding to depths below sea level of 234 km, 91 km and 3 km depth. Legend in A and B: Legend: AP, Antarctic Peninsula; CSS, Central Scotia Sea; ESS, East Scotia Sea; SFZ, Shackleton Fracture Zone; SG, South Georgia; SOM, South Orkney Microcontinent; SSIT, South Sandwich Islands Trench; WSS, West Scotia Sea.

The gravity modeling is complex in this remote region because of the scarce seismic data regarding the depth of the Moho discontinuity [Allen, 1966; Ewing *et al.*, 1971]. To aid gravity modeling, we applied the Spector and Grant [1970] method to the upward continued map. Identifying the depth of the top of the sources of the anomalies, it can also be used to reveal a body centroid's location. We selected a window size enough to contain the main gravity anomalies which are presented in the study area. Three main horizons were thus found (Figure 2c): horizon 1 as the deepest at (234 ± 18) km; horizon 2 at (91 ± 5) km, and horizon 3 at (3 ± 1) km. As spectral methods are not exact, we should interpret these depths in a generic way. We correlate the deepest contribution to the asthenosphere, horizon 2 to the lithosphere on oceans, and the shallowest would correspond to a crustal boundary. As it is difficult to constrain crustal thicknesses, we took Profile 1, with a WSW-ENE trend from the Antarctic Plate to the North Scotia Ridge, as a reference profile to discuss the main features of the deep structure of the area by gravity modeling. To this end we considered a wide range of densities (see supporting information) and we applied normal density values for sea-water, crust, lithospheric-mantle, and asthenosphere [Ferris *et al.*, 2000, Galindo-Zaldívar *et al.*, 2006; Tassara *et al.*, 2006; Cella *et al.*, 1998; Bohoyo *et al.*, 2007, among others].

As a first attempt, we modeled the Bouguer Anomaly data using a constant lithospheric-asthenospheric discontinuity depth (Figure 3a). The geometry suggests the oceanic crust would be thinner in the older areas, which is not congruent with the

geological evolution and geophysical information, such as that derived from multichannel seismic profiles [Maldonado *et al.*, 2000].

In addition, we modeled a constant Moho depth (Figure 3b), resulting in a model where the lithosphere would have to be thinner in older oceanic areas, which does not seem to be realistic.

Summarizing, although the fit between calculated and observed anomalies is acceptable for both models, they are not compatible from a geological or physical viewpoint, because in older oceans the crust and lithosphere should be thicker (see Eagles *et al.* [2005] and British Antarctic Survey [1985] for age details of the Scotia Arc). Accordingly, the only suitable models should consider the presence of a low-density mantle in the West Scotia Sea. Moreover, considering that the most important contribution of the complete Bouguer Anomaly map at 50 km mainly represents deep lithospheric structures, we tested another model using rather uniform crustal thickness, while different mantle densities and lithospheric thicknesses should accommodate gravity anomaly values (Figure 4a).

Lower mantle densities are located in the West Scotia Sea (3.300 g/cm^3), increasing toward the southwest and northeast (up to 3.360 g/cm^3). Greater lithospheric thicknesses are located in the North Scotia Ridge and the Antarctic Plate (almost 90 km), with an asthenospheric rising in the region next to the SFZ. The West Scotia Sea displays a thinner lithosphere, of about 70 km.

Profile 2 (Figure 4b) also shows a heterogeneous lithospheric mantle where the lower densities are located in the West Scotia Sea, which increases toward the Atlantic Ocean (from 3.300 g/cm^3 to 3.360 g/cm^3). The Atlantic oceanic crust is older [Livermore and Woollett, 1993] and denser (2.945 g/cm^3) than the crust in the Scotia Sea (2.85 g/cm^3). The deeper part of the Atlantic Oceanic subducting slab is modeled as a dense oceanic crust (3.194 g/cm^3), assuming the effect of the insertion of an eclogite body [Larter *et al.*, 2003]. The thickest lithosphere of the Scotia Sea is seen in the central region (about 70 km).

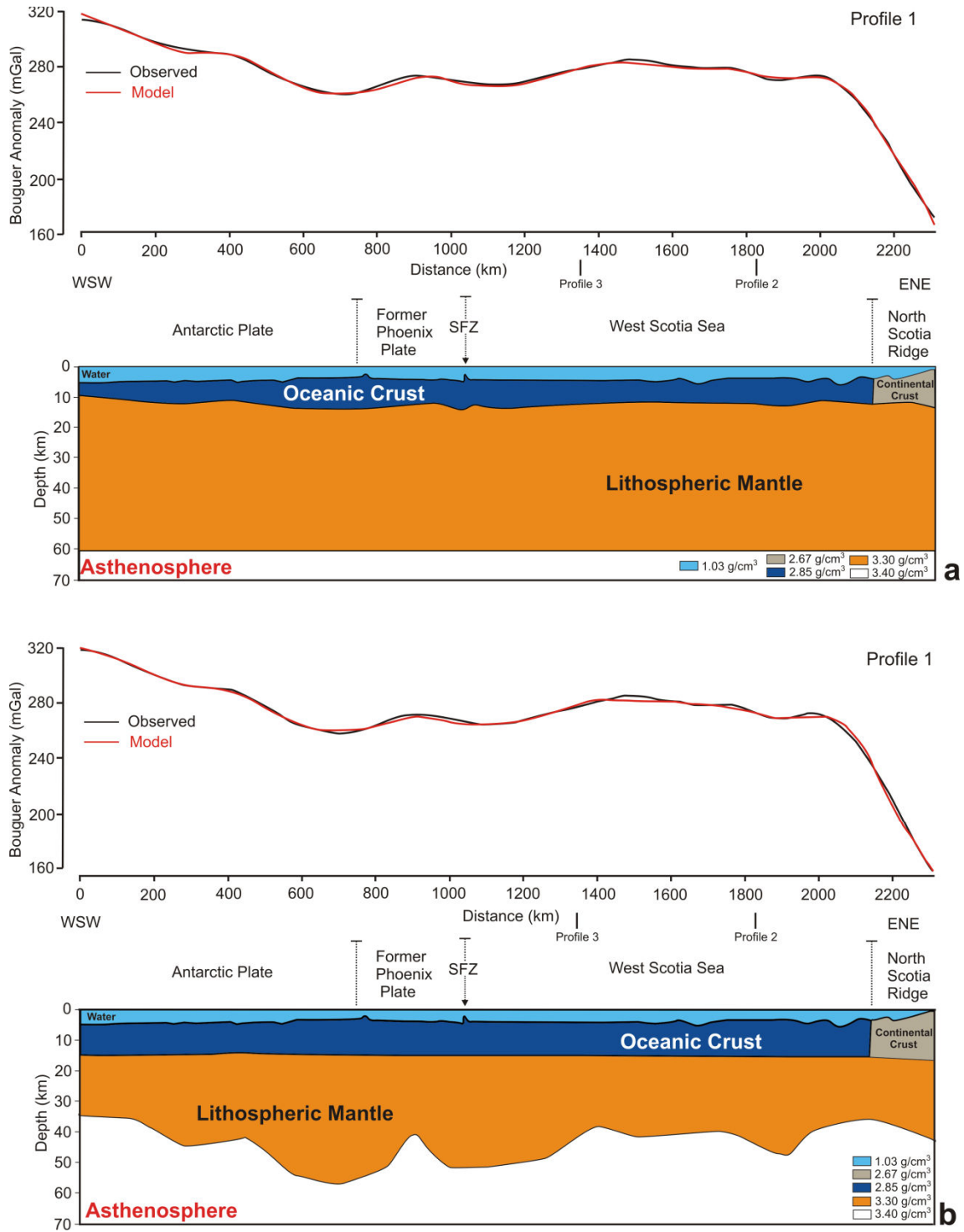


Figure 3. Tentative gravity models which fit the observed data but are not reasonable from the geological and physical point of views for this area. A) Gravity model of Profile 1 assuming a constant lithosphere depth. B) Gravity model of Profile 1 assuming a constant oceanic crust depth.

Figure 4. Gravity models of the three selected profiles.

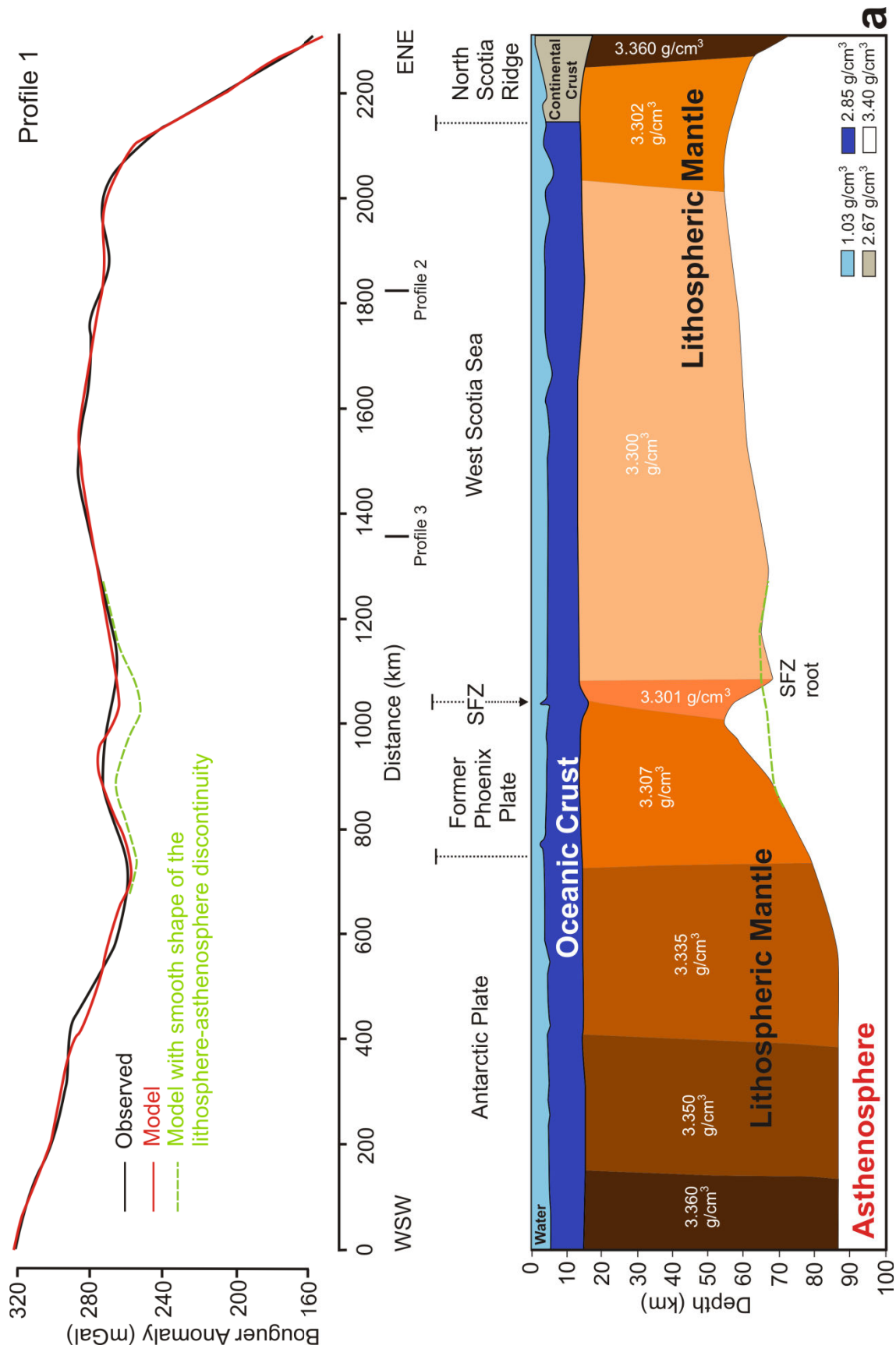


Figure 4a. Gravity model of Profile 1. Anomalous lithospheric mantle as well as a Shackleton Frature Zone root are identified. An alternative model with a smooth shape of the lithosphere-asthenosphere discontinuity, which does not fit the observed data, is presented. Dashed dotted line represents this model.

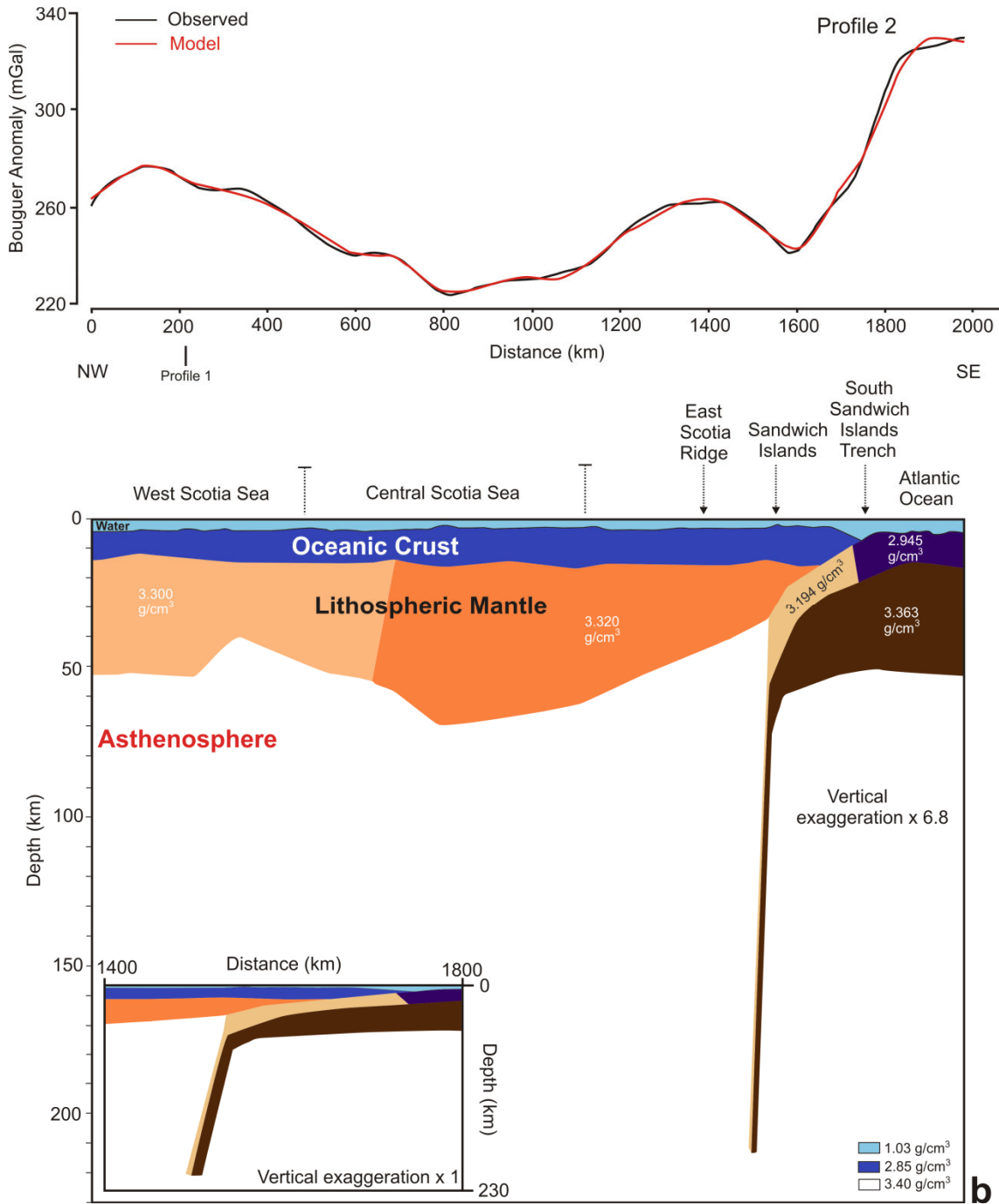


Figure 4b. Gravity model of Profile 2. The Central Scotia Sea is characterized by a thicker lithosphere than the rest of the Scotia Sea. The subduction slab of the Atlantic Ocean is modeled with a maximum depth of 215 km.

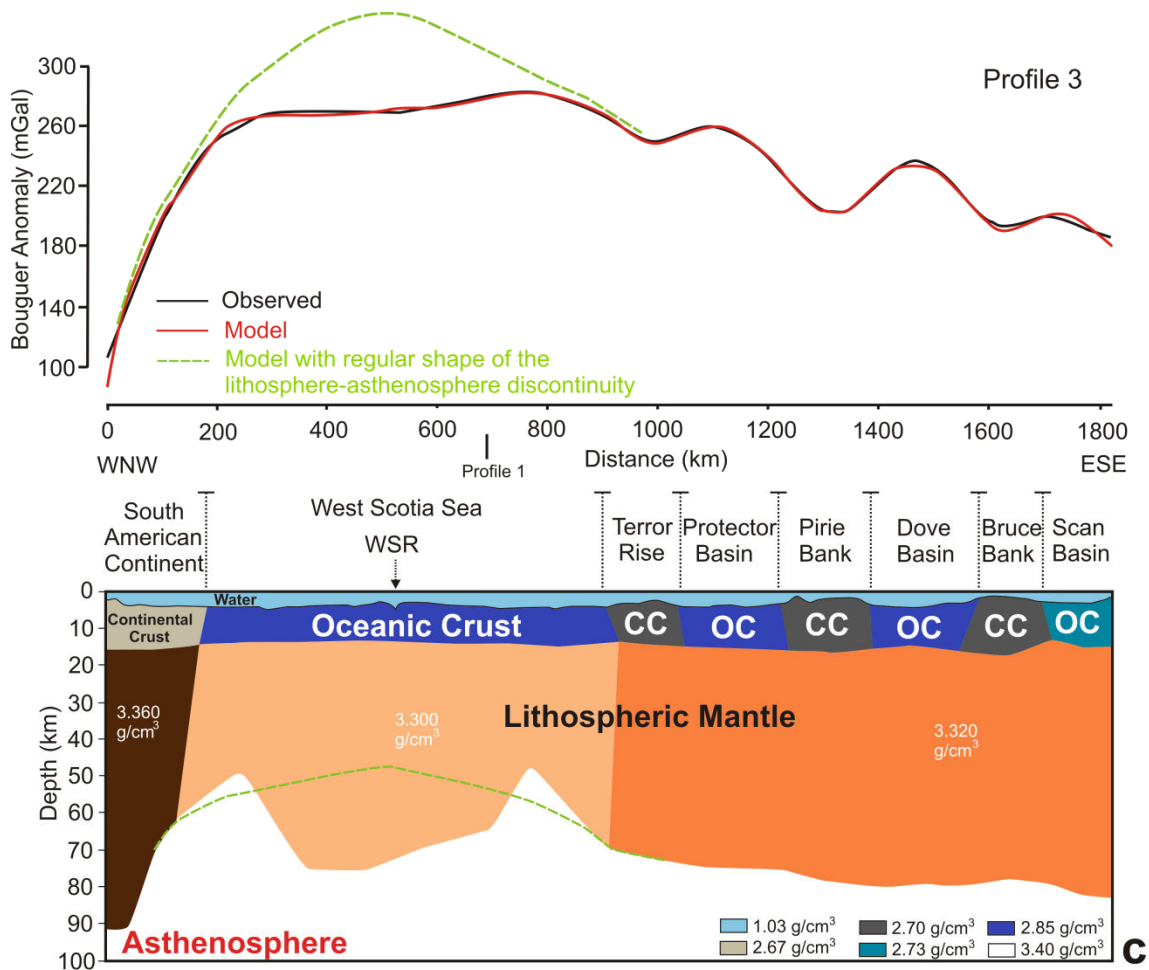


Figure 4c. Gravity model of Profile 3. The West Scotia Sea shows a lower density than the surrounding areas. An alternative model with regular shape of the lithosphere-asthenosphere discontinuity for the West Scotia Sea is shown in the figure (Dashed dotted line). CC, Continental Crust; OC, Oceanic Crust.

Profile 3 (Figure 4c), where short wavelengths appear in the Bouguer anomaly data, were modeled including lateral crustal density variations and allow for minor changes in the crustal bottom depth. The model also shows a heterogeneous lithospheric mantle, with higher densities in the South American continent (3.360 g/cm^3) and lower densities in the West Scotia Sea (3.300 g/cm^3). The density of the small banks of continental crust in the southern Scotia Sea is slightly higher than normal continental density, probably due to the presence of transitional crustal zones. In turn, the density of the oceanic crust of the Scan Basin is lower than in other basins, most likely because of thicker sedimentary infill or the presence of an intermediate basement [Lobo *et al.*, 2011]. The lithospheric thicknesses are greater in the area where the submarine banks and small oceanic basins are located (about

80 km) in the south part of the Scotia Sea and in the South American continent (90 km). The West Scotia Sea is characterized by two asthenospheric risings along the plate's borders and a maximum thickness of the lithosphere of about 75 km in its central part. The lithospheric mantle of the southern Atlantic Ocean, the Antarctic Plate, South America, and the North Scotia Ridge are characterized by the same density (3.360 g/cm³).

5. Discussion

The analysis of GRACE gravity data [Tapley *et al.*, 2005], complemented with bathymetric databases, leads us for the first time to present a complete Bouguer Anomaly map of the Scotia Arc, which reveals major density variations in the region (Figure 2a). The upward continuation to 50 km of the Bouguer Anomaly map highlights the deep lithospheric features (Figure 2b). The gravity modeling enabled us to identify a low-density anomalous lithospheric mantle in the West Scotia Sea region with respect to the surrounding areas (Figures 2 and 4). Our gravity models shows that the thicker lithosphere in the region is found in the continental areas and the Antarctic Plate (about 90 km), whereas the Scotia Plate has a thinner lithosphere (around 70 km). The West Scotia Sea lithosphere is the thinnest one, and a rising of the mantle is observed in the proximity of the SFZ together with a sharp lithospheric root (Figure 4). The northeastern part of the West Scotia Sea (close to the North Scotia Ridge), and the easternmost basin area, located in the South Scotia Sea, are characterized by thinner lithosphere (Figures 4a and 4b) in agreement with the high heat flow values in respect to the central part of the West Scotia Sea (<http://www.heatflow.und.edu>) (Figure 2a). We interpret these lithospheric variations as a consequence of asthenospheric current flows.

Based on our gravity modeling, the hypothesis of Alvarez [1982] and geochemical [Pearce *et al.*, 2001] and seismic anisotropy [Russo and Silver, 1994; Helffrich *et al.*, 2002] studies, we propose an evolution of asthenospheric flow models for the study area (Figure 5). Around 28 Ma, during the initial phases of the opening of the Drake Passage, a mantle gateway was created, since lithospheric continental roots related to South America, the Antarctic Peninsula and the subduction zones were broken in that area. The thinned lithosphere of the newly born Scotia Sea facilitated mantle flows between the Pacific and the Atlantic (Figure 5a). The SFZ started its uplift as an intraoceanic ridge during the

middle Miocene [Martos *et al.*, 2013] producing a root displaced eastward, probably owing to Pacific asthenospheric outflow. This feature, which became a barrier, influenced the distribution of the asthenospheric flows dispersed northward and southward from the ridge root (Figure 5b). Then, the main asthenospheric flow was deflected, flowing along the western side of the root of the SFZ, toward the north and south ends of this structure (Figure 5c).

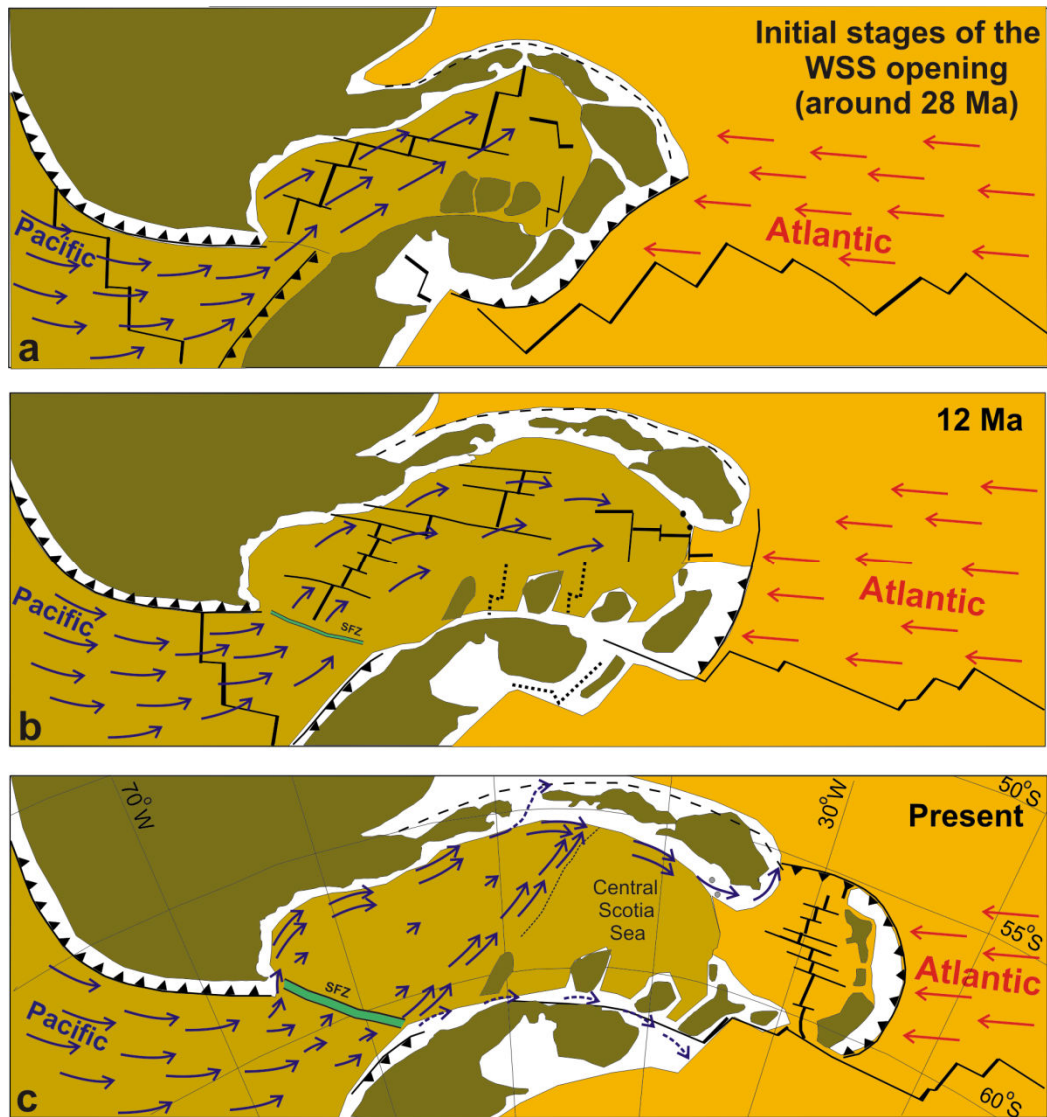


Figure 5. Sketch of the evolution model proposed for the Drake Passage as a mantle gateway (according to Barker [2001]; Pearce *et al.* [2001]; Eagles *et al.* [2005]). A) In the first stages of the passage opening the Pacific mantle flowed freely into the Scotia Sea due to the absence of lithospheric roots. B) In the Middle Miocene the Shackleton Fracture Zone started to uplift [Martos *et al.*, 2013], and this evolution created a lithospheric root related to this structure. Then, the root began to behave as a barrier for the Pacific asthenospheric currents. C) Asthenospheric current distribution at present times. The Shackleton Fracture Zone developed a deep lithospheric root and formed the barrier for the asthenosphere. SFZ, Shackleton Fracture Zone; WSS, West Scotia Sea.

In this framework, the West Scotia Ridge could not be fed properly by the Pacific mantle outflow; hence, the spreading activity began to decrease until its extinction around 6 Ma [Maldonado *et al.*, 2000]. In view of our asthenospheric flow model, we tentatively propose two main rims for the flux in the present (Figure 5c):

- One branch of the flow moves northward along the western margin of the SFZ up to the end of the structure, crosses the root gap formed by the SFZ and the South American continent, and continues moving along the North Scotia Ridge, which constitutes an important lithospheric root. The flow escapes through a narrow root gap located in the North Scotia Ridge and through the northern part of the East Scotia Sea, considering the subduction zone tip as a window for the asthenospheric flow.

- Another branch flows to the south along the western margin of the SFZ, crossing the root gap formed by this structure and the South Scotia Ridge. Once it reaches the thin continental blocks located in the southwestern part of the Scotia Sea, the asthenospheric flow follows these roots and the western margin of the Central Scotia Sea up to the North Scotia Ridge. The other possible flow is largely confined between the South Scotia Ridge and the continental blocks (Figure 5) escaping to the Weddell Sea.

6. Conclusions

The analysis of oceanic gateways is of global relevance, to further understand deep oceanic currents with climatic implications and the distribution of asthenospheric currents, with implications for plate tectonics. The Scotia Sea is a key region since represents the final gateway for the isolation of Antarctica.

We put forth a complete Bouguer anomaly map of the Scotia Sea and surrounding regions, revealing for the first time major lithospheric mantle density contrasts. The new gravity data support the presence of a thinner and low density lithospheric mantle in the West Scotia Sea area, thereby suggesting variable lithospheric thicknesses.

The SFZ is a major geological structure in the region since the middle Miocene. Our data suggest that the SFZ started to behave as an asthenospheric barrier for the Pacific mantle outflow since the middle Miocene, at the same time period as for oceanic currents. The decrease in Pacific mantle outflow toward the West Scotia Ridge in the Scotia Sea may be one main factor behind the extinction of the oceanic spreading. The Pacific mantle

outflow could still be present through the Drake Passage, at the northern and southern borders of continental lithosphere, supporting Alvarez's [1982] hypothesis.

Acknowledgements

We thank the constructive comments and suggestions of F. Ferraccioli and another anonymous reviewer which contribute to improve this research. The study was founded by the CTM2008-06386-C02/ANT and CTM2011-30241-CO2-01/02 projects and by a pre-doctoral fellowship from the "Ministerio de Ciencia e Innovación" of Spain (FPI). This work also benefited from a research stage abroad funded by the FPI program. Generic Mapping Tools software was used in this work.

The Editor thanks Fausto Ferraccioli and an anonymous reviewer for their assistance in evaluating this paper.

Supporting Information

Readme.txt

Supporting Information for

Asthenospheric Pacific-Atlantic flow barriers and the West Scotia Ridge extinction

Yasmina M. Martos^{1,*}, Jesús Galindo-Zaldívar^{1,2}, Manuel Catalán³, Fernando Bohoyo⁴,
Andrés Maldonado¹

¹ Instituto Andaluz de Ciencias de la Tierra (Consejo Superior de Investigaciones Científicas/Universidad de Granada). Avda. de Las Palmeras nº 4, 18100. Armilla, Granada (Spain).

² Universidad de Granada. Avda. de la Fuente Nueva, s/n, 18071. Granada (Spain).

³ Real Instituto y Observatorio de la Armada. Cecilio Pujazón, s/n, 11100. San Fernando, Cádiz (Spain).

⁴ Instituto Geológico y Minero de España. Ríos Rosas, 23, 28003. Madrid (Spain).

* Corresponding author

E-mail address: yasmartos@ugr.es

Geophysical Research Letters

Introduction

We included new gravity models considering a wide range for the density of the asthenosphere, which support the main results shown in the main text.

1. text01.doc This document contains tables with density values of the new models as well as the discussion of the different models.

2. fs01.tif (Figure 6) Gravity models of the three selected profiles. Three different models are presented for every profile. Blue, red and green lines represent models with densities for the asthenosphere of 3.3 g/cm³, 3.4 g/cm³ and 3.5 g/cm³ respectively. a) Gravity model of Profile 1. The lithospheric mantle is composed by seven bodies (see Table 1 in text01.doc). b) Gravity model of Profile 2. See Table 2 in text01.doc for density details. c) Gravity model of Profile 3. Three bodies compose the lithospheric mantle (see Table 3 in text01.doc). CC, Continental Crust; OC, Oceanic Crust.

Gravity modeling

We tried different gravity models for the selected profiles taking into account a wide range of asthenosphere densities. On the other hand we assumed a constant density of the crust in the models, just the lithospheric mantle was used to get the best fit. Once we determined the best fit for the shape of the lithosphere-asthenosphere discontinuity (see models in the main text) we modeled the profiles using new densities for the asthenospheric mantle.

Profile 1

Considering that densities for the water, oceanic and continental crust have values of 1.03 g/cm³, 2.85 g/cm³ and 2.67 g/cm³ respectively based on previous studies [Ferris et al., 2000, Galindo-Zaldívar et al., 2006; Bohoyo et al., 2007, among others] we tried some different models changing the density of the asthenosphere and the density of the mantle. See Table 1 and Auxiliary Materials (Figure 6a, fs01.tif).

Table 1

Model in function of the Asthenosphere's density (g/cm ³)	Densities (g/cm ³)								Observations
	Body 1	Body 2	Body 3	Body 4	Body 5	Body 6	Body 7	Body 8	
3.3	3.237	3.229	3.213	3.181	3.171	3.172	3.167	3.237	
3.4	3.360	3.350	3.335	3.307	3.301	3.300	3.302	3.360	Best fit
3.5	3.482	3.471	3.457	3.433	3.434	3.428	3.445	3.482	

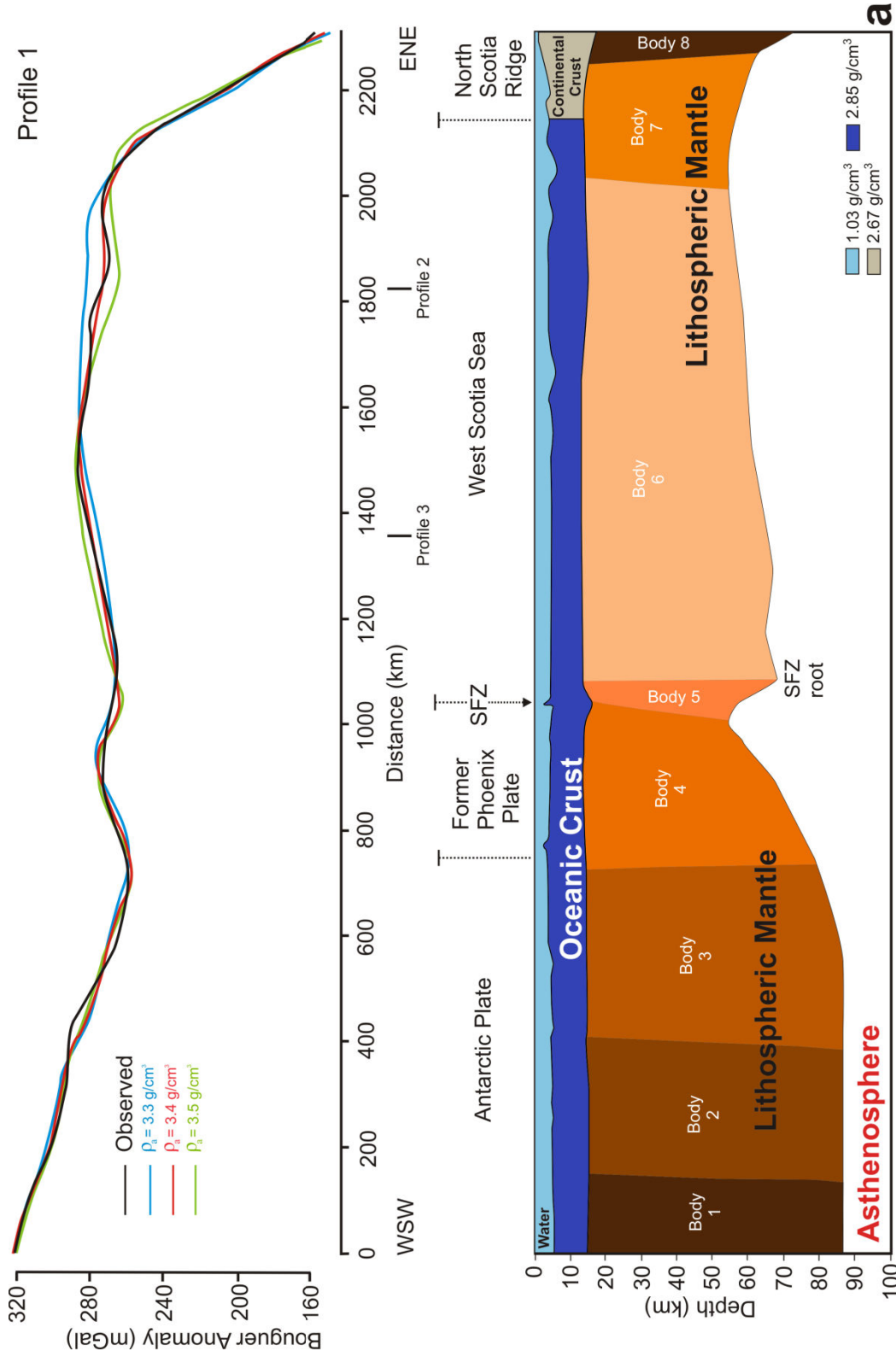


Figure 6a. Gravity model of Profile 1. Three different models are presented: Blue, red and green lines represent models with densities for the asthenosphere of 3.3 g/cm³, 3.4 g/cm³ and 3.5 g/cm³ respectively. The lithospheric mantle is composed by seven bodies (see Table 1 in text01.doc).

Profile 2

Considering that densities for the water and oceanic crust have values of 1.03 g/cm^3 and 2.85 g/cm^3 respectively based on previous studies [Galindo-Zaldívar *et al.*, 2006; Bohoyo *et al.*, 2007] we tried some different models changing the density of the asthenosphere and the density of the mantle below the crust. See Table 2 and Auxiliary Materials (Figure 6b, fs01.tif).

Table 2

Model in function of the Asthenosphere's density (g/cm^3)	Densities (g/cm^3)				Observations
	Body 1	Body 2	Body 3	Body 4	
3.3	3.172	3.185	3.057	3.217	
3.4	3.300	3.320	3.194	3.360	Best fit
3.5	3.428	3.458	3.356	3.500	

To get a good fit considering a density of the asthenosphere of 3.3 g/cm^3 or 3.5 g/cm^3 , the density of the lithospheric mantle of the West Scotia Sea should be heterogeneous. In the case we modify the shape of the West Scotia Sea, the geometry is in disagreement with the geology and the other profiles.

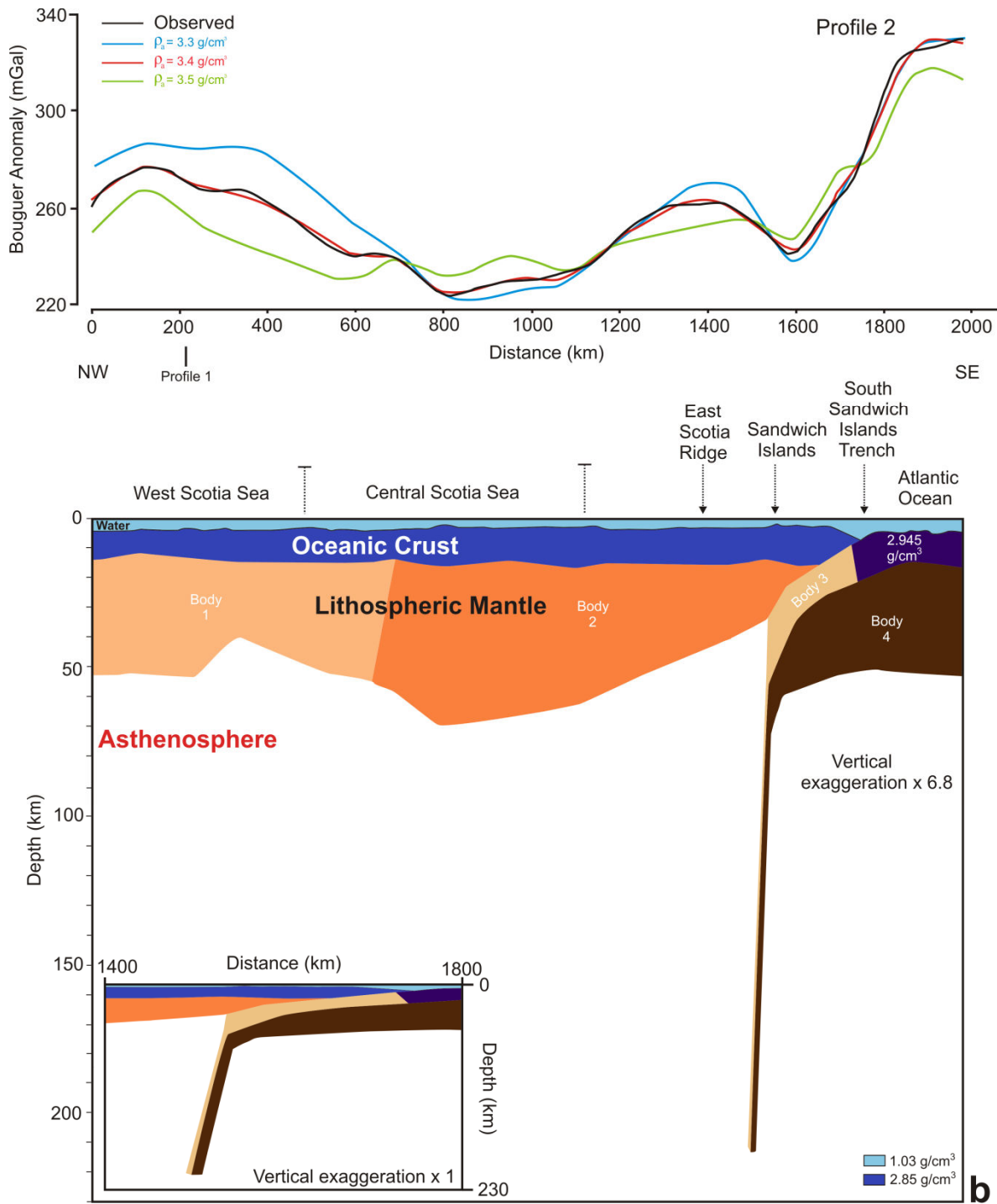


Figure 6b. Gravity model of Profile 2. Three different models are presented: Blue, red and green lines represent models with densities for the asthenosphere of 3.3 g/cm^3 , 3.4 g/cm^3 and 3.5 g/cm^3 respectively. See Table 2 in text01.doc for density details.

Profile 3

Considering that densities for the water, oceanic and continental crust have been based on previous studies (See Figure 6C for densities) [Ferris et al., 2000, Galindo-Zaldívar et al., 2006; Bohoyo et al., 2007; among others], we tried some different models changing the density of the asthenosphere and the density of the mantle below the crust. See Table 3 and Auxiliary Materials (Figure 6c, fs01.tif).

Table 3

Model in function of the Asthenosphere's density (g/cm ³)	Densities (g/cm ³)			Observations
	Body 1	Body 2	Body 3	
3.3	3.237	3.172	3.300	
3.4	3.360	3.300	3.320	Best fit
3.5	3.482	3.428	3.445	

Considering a density of the asthenosphere of 3.3 g/cm³ and fixed density of the oceanic and continental crustal blocks of the South Scotia Sea, is impossible to get a good fit.

Conclusions

In general, considering a density of 3.4 g/cm³ for the asthenosphere we get the best results for the models in agreement with other geological and geophysical data and it is the most realistic value for the Scotia Sea from the geological and physical point of view.

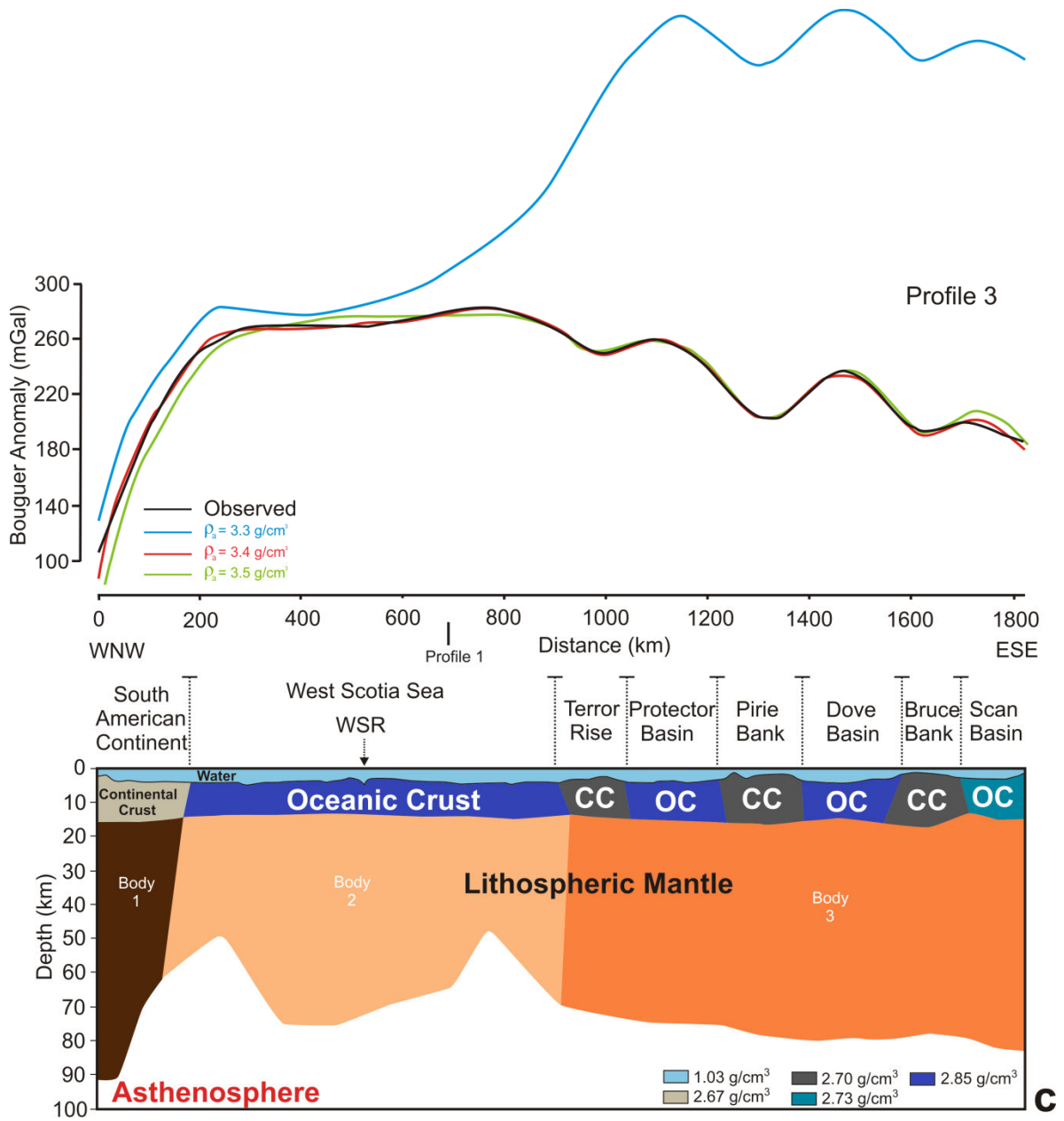


Figure 6c. Gravity model of Profile 3. Three different models are presented: Blue, red and green lines represent models with densities for the asthenosphere of 3.3 g/cm³, 3.4 g/cm³ and 3.5 g/cm³ respectively. Three bodies compose the lithospheric mantle (see Table 3 in text01.doc). CC, Continental Crust; OC, Oceanic Crust.

Chapter 6

THERMAL BEHAVIOUR AND SUBSIDENCE OF SMALL OCEANS: THE WEST SCOTIA SEA

*In revision for **Journal of Geodynamics***

Thermal behaviour and subsidence of small oceans: The West Scotia Sea

Yasmina M. Martos^{1,*}, Jesús Galindo-Zaldívar^{1,2}, Manuel Catalán³, Fernando Bohoyo⁴,
Andrés Maldonado¹

¹ *Instituto Andaluz de Ciencias de la Tierra (Consejo Superior de Investigaciones Científicas/Universidad de Granada). Avda. de Las Palmeras nº 4, 18100. Armilla, Granada (Spain).*

² *Universidad de Granada. Avda. de la Fuente Nueva, s/n, 18071. Granada (Spain).*

³ *Real Instituto y Observatorio de la Armada. Cecilio Pujazón, s/n, 11100. San Fernando, Cádiz (Spain).*

⁴ *Instituto Geológico y Minero de España. Ríos Rosas, 23, 28003. Madrid (Spain).*

* *Corresponding author*
Tel. +34 958230000
E-mail address: yasmartos@ugr.es

Abstract

The progressive sinking of the ocean seafloor is a consequence of lithospheric cooling. The process is controlled by lithospheric thermal behaviour, influenced, in turn, by the activity of mantle cells. Here we show that small oceans, such as the West Scotia Sea, reach thermal equilibrium more quickly than larger ones, following a different subsidence law ($d(t) = 4480 - 19380\exp(-t/4)$, where d and t are the depth in metres and time in millions of years, respectively). Heat flow data are often used to date oceanic crust, but we found that, for oceanic crust of the same age, the lower heat flow in small oceans implies older apparent ages than if plate model empirical relationships for large oceans are considered. In addition, the asymptotic heat flow values for oceanic crust older than 15 Ma in small oceans prevents their use as a suitable dating method. This circumstance is a consequence of the small size of the mantle cells, with low heat and energy transport. Our results demonstrate that small oceans have faster thermal evolution and behave like old oceanic crust in large oceans. The West Scotia Sea is a good example of small ocean affected by this process, which controlled global climate change and the thermal isolation of Antarctica because it constituted the last gateway during the inception of the Antarctic Circumpolar Current.

Highlights:

- Young small oceans behave as old large oceans from the thermal standpoint
- Standard oceanic crust heat flow dating methods cannot be used in small oceans
- Fast cooling occurs in small oceans by the small and low energy convection cells

Keywords: Thermal subsidence; heat flow; oceanic gateway; Scotia Sea; changes in global scale

1. Introduction

Oceans constitute more than 70% of the earth's surface and knowledge of their evolution is essential to understand global changes. Their relief influences the pattern of oceanic currents that constrain heat transfer and the present-day climate. Since the Plate Tectonic theory was proposed in the 1960s (Vine and Matthews, 1963), the origin of the seafloor has been known to be related to mantle dynamics, which determine continental drift. Partially melted materials rise from the deep mantle, become unstable, and generate convection cells, which transport materials and heat to the base of the lithosphere. The hottest lithosphere are located in oceanic ridge areas where mantle flows to the surface forming the oceanic crust. Heat is transported from ridges to the ocean boundaries. Consequently, the older oceanic lithosphere is colder, with lower heat flow; it is therefore denser, and sinks into the asthenospheric mantle due to isostasy equilibrium. This effect produces an increase in lithosphere thickness since part of the asthenosphere becomes lithospheric mantle. The process is known as thermal subsidence. Two theoretical models (the half-space cooling model (Davis and Lister, 1974) and the plate model (Langseth et al., 1966; McKenzie, 1967) and several empirical models (Crosby and McKenzie, 2009; Crosby et al., 2006; Hasterok, 2013; Hillier and Watts, 2005; Korenaga and Korenaga, 2008; Parsons and Sclater, 1977; Stein and Stein, 1992, 1993) have been proposed to account for it since the 1970s. These models analyse the relationship between heat flow, ocean floor depth, and age. The half-space cooling model (Davis and Lister, 1974) fits thermal behaviour for young (proportional to the square root of age) oceanic crust, whereas

the plate model better describes the thermal behaviour of old oceanic crust (proportional to an exponential decay of age) (Langseth et al., 1966; McKenzie, 1967). Both dependences are summarized at Parsons and Sclater (1977) (equation 1), based on the plate model (Langseth et al., 1966; McKenzie, 1967), that we consider as the most classic reference:

$$\begin{cases} d(t) = 2500 + 350\sqrt{t} & t \leq 70 \text{ Ma} \\ d(t) = 6400 - 3200\exp(-t/63) & t > 70 \text{ Ma} \end{cases} \quad (1)$$

where d represents positive depths of the seafloor in metres and t is age in millions of years.

However, up to now it has not been tested in small oceans, which generally occur in backarc tectonic settings. The main objective of this study is to characterize the thermal behaviour of this kind of oceans since they are important gateways for deep oceanic circulation and faunal and floral exchanges with global implication in the Earth history. We analyse the thermal behaviour of the West Scotia Sea in the framework of the Scotia Arc (Fig. 1) because is one of the best examples of small oceans on the planet, and constitutes the last oceanic gateway that isolates Antarctica. In addition, the determinations of the oceanic basement depth and heat flow are data used to estimate the age of the oceanic crust in remote regions where no other data are available. Anyway, although small oceans in active tectonics areas may be affected by flexural deformations, the presence of major faults in the borders of Scotia Sea contribute to uncouple the lithospheric boundaries and minimize the flexural effects. The West Scotia Sea is the best suitable area to check the thermal behaviour of small oceans instead of the Central Scotia Sea that includes continental banks, or the young East Scotia Sea. This area was poorly explored up to now due to the harsh weather predominating in the Drake Passage.

2. Regional Setting

The age of the initial tectonic opening of the Drake Passage is not well constrained, and has significant implications for global oceanic circulation and climate evolution in Antarctica as it created the final gateway to allow the establishment of a full circum-Antarctic circulation and the thermal isolation of the Antarctic continent (Barker, 2001;

Barker and Thomas, 2004; Kennett, 1977; Lawver et al., 1992; Livermore et al., 2004; Maldonado et al., 2006) coeval with global reduction in the atmospheric CO₂ (DeConto and Pollard, 2003).

The Scotia Sea has been formed by the tectonic development of the Scotia Arc since the Oligocene (Barker, 2001; Barker and Burrell, 1977) due to the dispersion of the continental blocks that connected South America and Antarctica. The Arc propagated eastwards, forming oceanic backarc basins inside the tectonic arc in several stages (Barker, 2001). At present, it is composed of the eastern Sandwich plate and the western Scotia plate in between the major South American and Antarctic plates (British Antarctic Survey, 1985). The Scotia Sea is bounded by the Weddell Sea to the south, by the Southern Atlantic Ocean to the north and east, and by the Pacific Ocean to the west. The West Scotia Sea is the largest backarc oceanic basin, around 1,500 x 1,000 km², formed by the West Scotia spreading centre (Barker, 2001), with oceanic crust ages of around 30 to 6 Ma determined by well constrained oceanic spreading magnetic anomalies (Eagles et al., 2005; Lodolo et al., 1997; Maldonado et al., 2000). The spreading centre has a roughly NE-SW orientation and is divided by transform faults of NW-SE orientation in the West Scotia Sea up to E-W trends in the Central Scotia Sea (Fig. 1). The opening of this oceanic basin was responsible for the last stages of separation of South America and the Antarctic Peninsula forming the Drake Passage. It has been proposed not only a gateway for deep oceanic flow but also a gateway for Pacific mantle outflow (Alvarez, 1982, 1990; Nerlich et al., 2013; Pearce et al., 2001).

Eastwards, the Central Scotia Sea is formed by a complex array of oceanic basins and thin continental banks, which constituted the continental connection between South America and the Antarctic Peninsula (Barker, 2001). The poor development of seafloor spreading magnetic anomalies and the absence of other suitable data for dating determine controversial proposals for spreading ages (Barker, 2001; Civile et al., 2012; Eagles et al., 2006).

Westwards, the Shackleton Fracture Zone (Geletti et al., 2005) is a sinistral tranpressive fault that separates the Scotia Plate and the Antarctic Plate, roughly parallel to the transform faults affecting West Scotia and Phoenix-Antarctic ridges. The former

Phoenix plate belongs to the Antarctic plate after the extinction of the Antarctic-Phoenix spreading axis 3.3 Ma ago (Livermore et al., 2000).

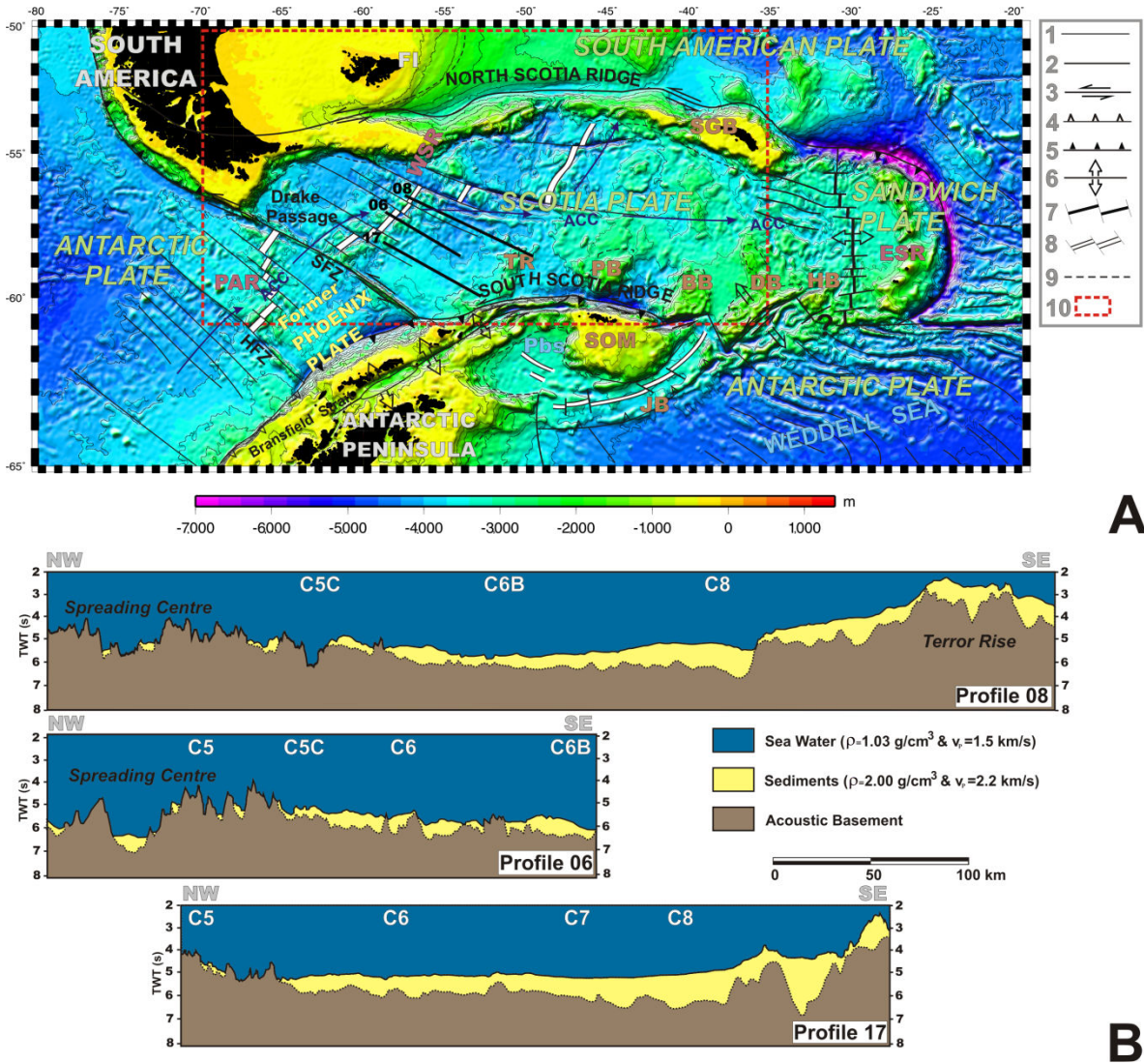


Figure 1. Geological setting of the Scotia Sea and interpretation of multichannel seismic profiles located in the West Scotia Sea. A: Scotia Arc bathymetry satellite map (Smith and Sandwell, 1997). Multichannel seismic profile tracks and main tectonic features are shown in the figure. ACC, Antarctic Circumpolar Current; BB, Bruce Bank; DB, Discovery Bank; ESR, East Scotia Ridge; FI, Falkland Islands; HB, Herdman Bank; HFZ, Hero Fracture Zone; JB, Jane Bank; PAR, Phoenix-Antarctic Ridge; PB, Pirie Bank; Pbs, Powell Basin; SFZ, Shackleton Fracture Zone; SGB; South Georgia Bank; SOM, South Orkney Microcontinent; TR, Terror Rise; WSR, West Scotia Ridge. 1, Inactive fracture zone; 2, Active fracture zone; 3, Transcurrent fault; 4, Inactive subduction zone; 5, Active subduction zone; 6, Active extensional zone; 7, Active spreading centre; 8, Inactive spreading centre; 9, Continental-oceanic crust boundary; 10, Study area. B: Sketch of the multichannel seismic profiles 17, 06, and 08, in two-way travel time. Chrons from the available compilation (Eagles et al., 2005) are shown in the profiles.

3. Methodology

We used several kinds of geophysical data in this study to discuss the suitability of the oceanic basement depth and age relationships for small oceanic basins. Multichannel seismic (MCS) allow us to determine the oceanic basement depth and the sediment thickness. The ages of the oceanic crust have been determined in the region from the analysis of magnetic anomalies (Eagles et al., 2005) and allow to study the depth-age, heat flow-age, and lithospheric thickness modelling. In the other hand, gravity data were considered to identify the signal of mantle sources.

Multichannel seismic profiles, basement and crustal age

We identify the seafloor and the seismic acoustic basement in MCS profiles obtained in the Drake Passage during SCAN2004 and DRAKE-SCAN 2008 cruises. MCS have been acquired by the R/V Hespérides and are located along spreading corridors orthogonal to the spreading centres. The surveys were carried out with a tuned array of six Bolt air guns with a total volume of 15.26 l. Both used a 96-channel streamer with an active length of 2.4 km and a shot interval of 50 m. MCS data were recorded with a DFS V digital system and a sampling record interval of 2 ms and 10 s record lengths. Data were processed with a standard protocol, including time migration using Promax software.

We determined the top of the igneous layers of the oceanic crust by identifying the large amplitude and chaotic reflections of the top of the oceanic basement. Moreover, the sedimentary infill has a different seismic signal characterized by the presence of well-defined reflectors. The ages of the oceanic crust of the West Scotia Sea have been considered after the available compilation (Eagles et al., 2005) obtained from the analysis of seafloor spreading magnetic anomalies.

Depth-age, heat flow-age, and lithospheric thickness modelling

We assume that our small ocean follows and depends on the same parameters as those comprising the subsidence equation for the plate model (Turcotte and Schubert, 2002):

$$d(t) = \frac{\rho_m \alpha_v (T_1 - T_0) y_{L0}}{\rho_m - \rho_w} \left[\frac{1}{2} - \frac{4}{\pi^2} \exp\left(-\frac{\kappa \pi^2 t}{y_{L0}^2}\right) \right] \quad (2)$$

where ρ_m and ρ_w are mantle and water density respectively, α_v is the volumetric coefficient of thermal expansion, $T_1 - T_0$ is the temperature gradient between the bottom and the top of the lithosphere, y_{L0} is the thickness of the lithosphere at large time scales, κ is thermal diffusivity, and t is age.

Also we analyse heat flow as a function of age based on the plate model (Turcotte and Schubert, 2002):

$$q_0 = \frac{k(T_1 - T_0)}{y_{L0}} \left[1 + 2 \exp\left(-\frac{\kappa \pi^2 t}{y_{L0}^2}\right) + 2 \exp\left(-\frac{4\kappa \pi^2 t}{y_{L0}^2}\right) \right] \quad (3)$$

where k is the thermal conductivity, $T_1 - T_0$ is the temperature gradient between the bottom and the top of the lithosphere, y_{L0} is the thickness of the lithosphere over large time scales, κ is the thermal diffusivity, and t is the age.

Gravity data analysis

In this study we used the GGM02S gravity model, derived purely from 363 days of GRACE satellite in-flight data (Tapley et al., 2005). This model provides free-air gravity anomalies, defined as the difference between the gravity at a point on the reference ellipsoid and the normal gravity defined at the same point. Therefore, these values are defined on the reference ellipsoid, which is approximately mean sea level.

The water slab was corrected using a density of 1.03 g/cm^3 . The complete Bouguer anomalies were calculated following the Nettleton procedure (Nettleton, 1976). To apply Terrain corrections, we used the SRTM30PLUS4 grid as a local grid (Smith and Sandwell, 1997), and as a regional grid we used the same Digital Elevation Model, once undersampled at 13 km. We have used 2.67 g/cm^3 as the terrain density corresponding to the average density of the surrounding continental crust. Even if the area is occupied by oceanic crust with denser basements and the sedimentary infill has lower densities, the mean value will be close to the considered one. The regional grid was used beyond 2 km.

Finally, we obtained a Bouguer anomaly grid with a 13 km resolution, which should provide a view to deep features.

The Bouguer anomaly map is also upward continued. It is done in the Fourier domain and helps to attenuate short wavelength features that have a shallow origin. We use it to enhance the signal of mantle sources when shallower ones are present.

4. Thermal behaviour of small oceans: The West Scotia Sea thermal subsidence and heat flow

To obtain the thermal subsidence for the West Scotia Sea we calculated the seafloor and basement depths from two-way travel time MCS profiles considering the water (1.5 km/s) and sediment (2.2 km/s) P wave velocities, obtained using the seismic refraction results for the closest Powell Basin area (King et al., 1997). In order to apply the correction for sediment loading (Steckler and Watts, 1978) and estimate the corrected basement depth by isostasy, we consider a 2 g/cm^3 mean density of the sedimentary layer using the Nafe-Drake curve (Ludwig et al., 1970). We used the constant value because sediment thickness is less than 1 km in our study area (Sykes, 1996).

We also identify the ages in the oceanic corridors from the Eagles et al. (2005)'s compilation. However, in the spreading corridors, where the last identified anomaly is far from the continental-oceanic boundary, the oldest oceanic spreading rates were considered in order to estimate the ages of the remaining oldest oceanic crust area. After estimation of corrected basement depth and the identification of oceanic crustal ages, we determined their relationships, rejecting areas proximate to the oceanic ridge due to their irregular behaviour.

Our result shows that the thermal subsidence for this young small ocean follows the $d(t) = 4480 - 19380\exp(-t/4)$ relationship between depth and age (Fig. 2), reaching thermal equilibrium quickly. We found a correlation factor higher than 0.80 between our data and this mathematical relation. When trying to fit our results to the classic empirical subsidence law (Parsons and Sclater, 1977) for young oceans, we obtained correlation factors lower than 0.40. Also, we found that oceanic crust of similar age is shallower southwest of the study area, with the same thermal behaviour but affected by a depth offset (Fig. 2A).

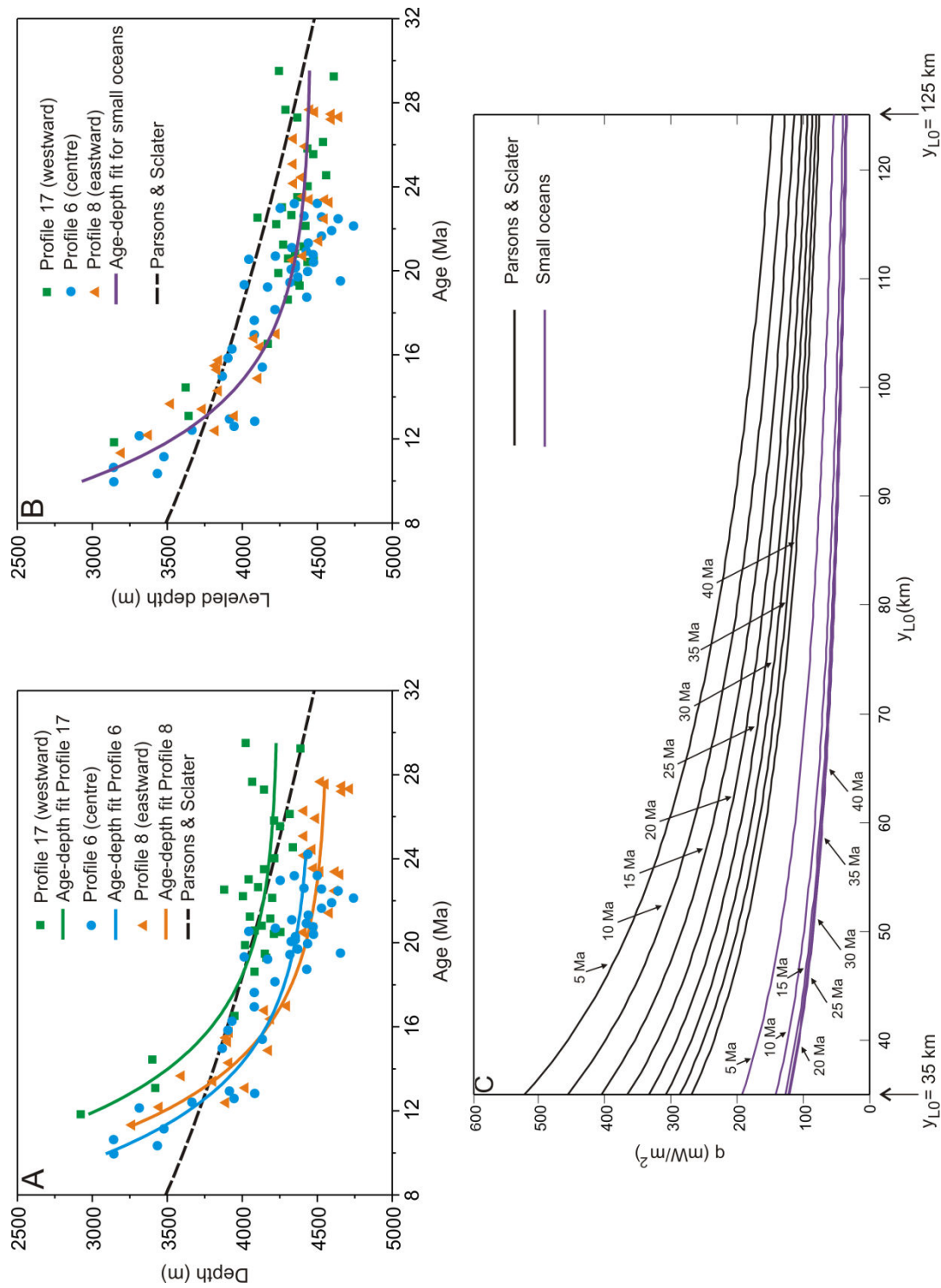


Figure 2. Age-depth and lithospheric thickness-heat flow relationships. See Fig. 1 for profile location. A) Comparison of age-depth relationship of every corridor and the classic empirical relationship (Parsons and Sclater, 1977). The thermal behaviour is the same for all of the corridors, but an offset level is observed. Corridors are more elevated westwards. The green squares and green curve represent data and the best fit equation for profile 17 respectively. The blue dots and blue curve are data and the best fit equation for profile 6, respectively. The orange triangles and orange curve represent data and the best fit equation for profile 8 respectively. Parsons and Sclater's law is represented by the black dashed line. B) Levelled profiles at the same level and general best fit for the small ocean (violet line). Parsons and Sclater's law is represented by the black dashed line. C) Heat flow versus maximum thickness of the lithosphere based on the plate model (equation 3, Methods). Violet lines represent the model for small oceans every 5 Ma, from 5 Ma to 40 Ma. Black lines represent heat flow versus maximum thickness of the lithosphere for the same range as our model, taking into account the classic empirical law (Parsons and Sclater, 1977). An average value of the lithosphere for the thermal conductivity of 3.138 W/mK , $T_1 - T_0 = 1350 \text{ K}$ and $\kappa = 1 \text{ mm}^2/\text{s}$ has been considered to compare the two models. We propose a model for a small ocean, which reaches asymptotic thermal behaviour from 15 Ma onwards. Maximum lithospheric thicknesses for our model (35 km) and the plate model (125 km) are indicated in the figure.

On other hand, assuming plate model solutions (equation 2), and a value of $1 \text{ mm}^2/\text{s}$ for the thermal diffusivity (Buck et al., 1988), we estimated 35 km of maximum lithosphere thickness from the value of the exponent ($e^{-t/4}$) which is an appropriate value for young small oceans.

Additionally, in order to test the accuracy of these results, we have modelled the heat flow that reaches the seafloor (Fig. 2C) based on the plate model solution (equation 3). For the modelling, we used the average mean values of $3.138 \text{ Wm}^{-1}\text{K}^{-1}$ for the thermal conductivity of the lithosphere, $T_1 - T_0 = 1350 \text{ K}$ and $\kappa = 1 \text{ mm}^2/\text{s}$. Finally, we obtained the thermal behaviour for the West Scotia Sea small ocean and compare the results with the classic empirical model (Fig. 2C). We display heat flow versus maximum thickness of the lithosphere every 5 Ma from 5 Ma to 40 Ma, which includes the age range of the oceanic crust for the study area (Fig. 2C). Heat flow values only depend on the lithospheric thickness for ages older than 15 Ma. Moreover, for the same lithospheric thickness, the heat flow values are lower for small than for large oceans (Fig. 2C).

5. Discussion

Classic half-space cooling and plate models (Davis and Lister, 1974; Langseth et al., 1966; McKenzie, 1967) are based on the assumption that seafloor bathymetry is driven by evolving thermal buoyancy of the underlying lithosphere, with other forces (such as mantle-flow-induced stress, flexural support from surrounding buoyancy structures, among others) negligible. This is generally valid for vast oceans basins like the Pacific and Atlantic. However, this assumption is not always valid for small pieces of seafloor surrounded by continental masses because of the strong mechanical coupling between continents and ocean floor across these margins. In the Scotia Sea, the oceanic boundaries may be considered uncoupled since most of them correspond to major faults (Barker, 2001; British Antarctic Survey, 1985). Indeed, in this study we obtained well fit age-depth relationship for oceanic areas without any disturbance related to flexural effects. The West Scotia Sea is the best area to develop this study since seafloor ages from magnetic anomalies are better identified than in other small seas like the Caribbean Sea.

The age-depth relationship proposed in this study (Fig. 2B) is different than that proposed by classic theoretical and empirical subsidence equations for young oceanic crust (Crosby and McKenzie, 2009; Crosby et al., 2006; Hasterok, 2013; Hillier and Watts, 2005; Korenaga and Korenaga, 2008; Parsons and Sclater, 1977; Stein and Stein, 1992, 1993). The West Scotia Sea behaves like an old oceanic crust, reaching thermal equilibrium quickly. The plate cooling model (equation 2) is in excellent agreement with data for 125 km of maximum lithosphere thickness (Parsons and Sclater, 1977) in large oceans (such as the North Pacific or North Atlantic oceans). However, assuming plate model solutions (equation 2), our estimated 35 km value of maximum lithosphere thickness is appropriate for young small oceans. We also modelled the heat flow that reaches the seafloor based on the plate model solution (equation 3).

The small size of the West Scotia Sea determines a different mantle thermal behaviour than those proposed to date for large oceans (Crosby and McKenzie, 2009; Crosby et al., 2006; Hasterok, 2013; Hillier and Watts, 2005; Korenaga and Korenaga, 2008; Parsons and Sclater, 1977; Stein and Stein, 1992, 1993). Thermal equilibrium is reached faster and, whereas in large oceans the heat flow decreases with increasing age, in small oceans like the Scotia Sea, heat flow values only depend on the lithospheric thickness for ages older than 15 Ma (Fig. 2C). Therefore, the present heat flow technique is not a suitable method to date small oceans since apparent older ages are obtained for the oceanic crust.

Also, a depth offset between oceanic crust of similar age in the study area is found, but with the same thermal behaviour (Fig. 2A). In order to analyse this feature, we studied mantle heterogeneity from the Bouguer Anomaly map of the West Scotia Sea. The Bouguer anomalies obtained from the upward continuation at 50 km (Fig. 3) mainly represent the upper mantle structures and have a regional maxima coinciding with the northeastern and eastern West Scotia Sea spreading centre. The relatively higher Bouguer anomalies represent denser mantle that corresponds to relatively colder materials. This scenario may be a consequence of residual slow small active mantle cells below the extinct West Scotia Ridge area (British Antarctic Survey, 1985). These mantle cells were bounded to the southeast by the subduction of the Weddell Sea in an initial stage when the West Scotia Sea was a backarc basin (Barker, 2001; Livermore, 2003). Later, the subduction migrated

eastwards and a new backarc basin and the Sandwich Arc developed in the East Scotia Sea (Livermore, 2003). The Central Scotia Sea represents an old piece of thinned continental and oceanic crust that separates the two main basins (Eagles, 2010). In this context, oceanic spreading progressively ceased in the West Scotia Sea, but some activity remains in the underlying mantle cells. These cells, developed in a backarc setting, are smaller than in large oceans, implying lower and slower heat transport. They continue to be infilled by the hottest westwards Pacific mantle (Alvarez, 1982, 1990; Pearce et al., 2001), and as a consequence the mantle becomes colder towards the northeast, causing greater sinking of the oceanic crust (Fig. 4).

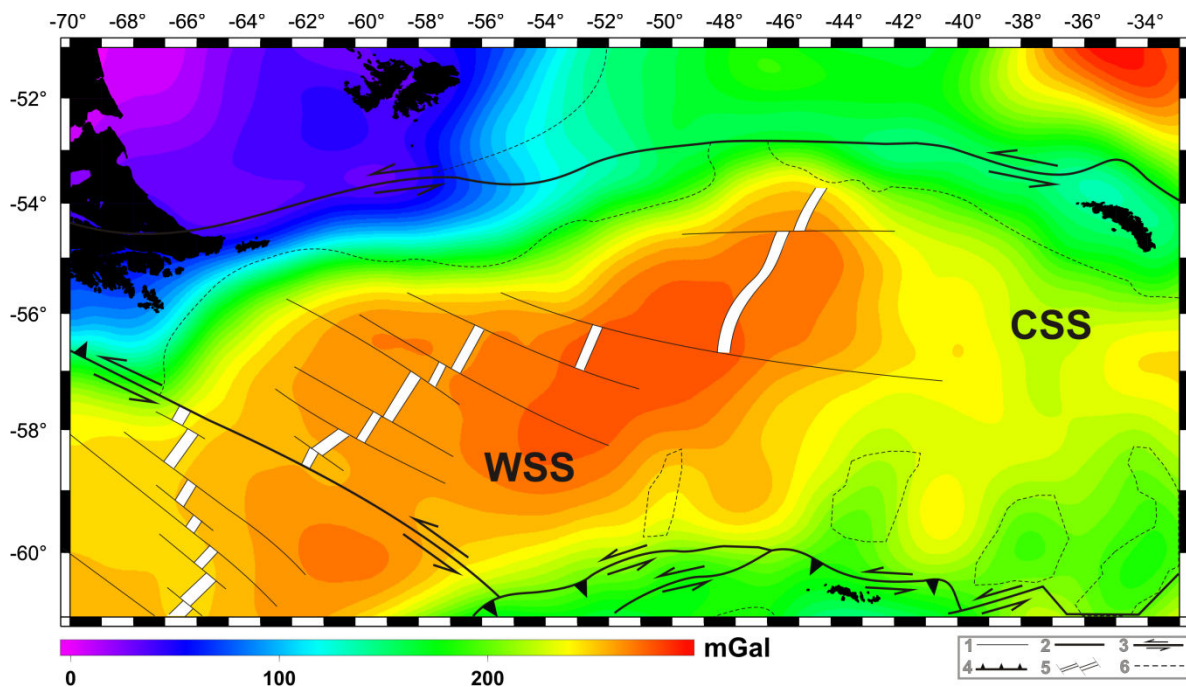


Figure 3. Bouguer anomaly map derived from GRACE satellite in-flight data and Geosat predicted satellite bathymetry (Smith and Sandwell, 1997). Values at 50 km from the upward-continued Bouguer anomaly map at surface. The main tectonic elements of the Scotia Sea are indicated. WSS, West Scotia Sea; CSS, Central Scotia Sea. 1, Inactive fracture zone; 2, Active fracture zone; 3, Transcurrent fault; 4, Active subduction zone; 5, Inactive spreading centre; 6, Continental-oceanic crust boundary.

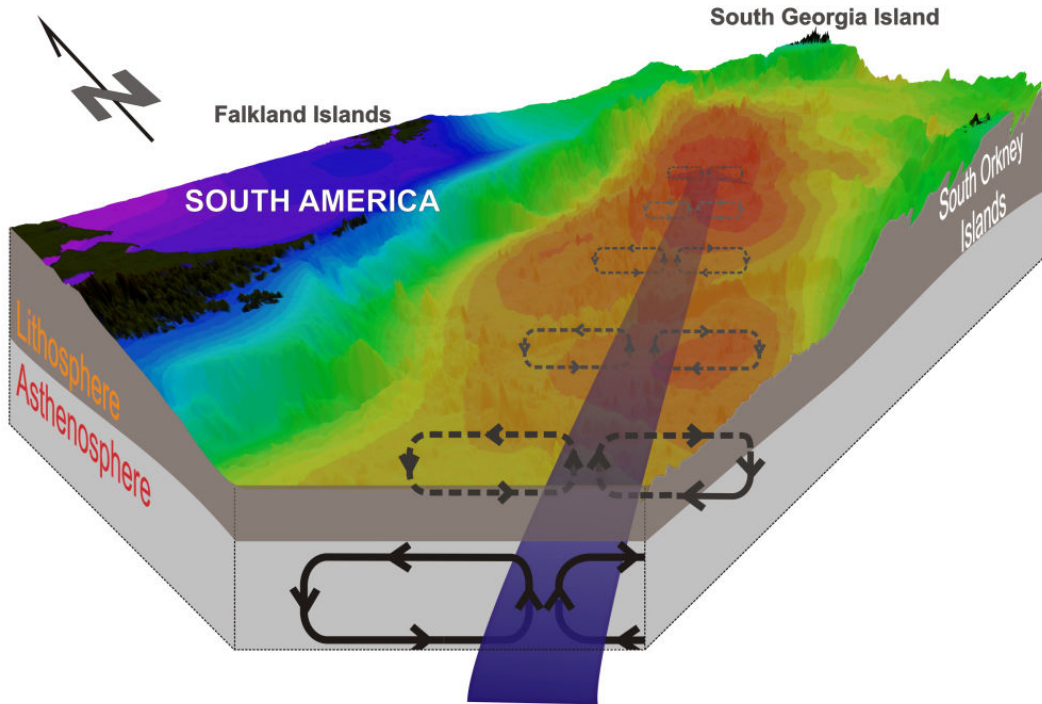


Figure 4. 3D view of the present setting below the western part of the Scotia Sea. The main tectonic features are shown in the figure. Black lines with arrows represent mantle convection. The wide blue arrow shows the northeastward decrease of the Pacific mantle outflow to the Scotia Sea.

6. Conclusions

We propose that small young oceans have a thinner lithosphere and relatively low heat flow due to the small size and low energy of the mantle cells. These factors determine a faster evolution to reach thermal equilibrium and final depths. Based on this faster thermal evolution for small oceans, we propose the depth-age relationship of $d(t) = 4480 - 19380\exp(-t/4)$ for that behaviour. As a consequence, the low heat flow values ($50\text{--}70 \text{ mW/m}^2$) (<http://www.heatflow.und.edu>) in small oceans such as the West Scotia Sea indicate older apparent ages than for large oceans. In addition, in small oceans, crustal ages older than 15 Ma cannot be discriminated, but heat flow is the best measure to obtain their maximum lithospheric thickness. Moreover, in the West Scotia Ridge area, the northeastward decrease in the activity of the mantle cells, mainly filled from the Pacific mantle (Alvarez, 1982, 1990; Pearce et al., 2001), determines progressive mantle cooling and deepening of the oceanic corridors, supported by MCS data and gravity anomalies.

These processes helped the extinction of spreading centres and the faster deep sea connection between the Pacific and Atlantic oceans through the Drake Passage, a key area for the inception of the Antarctic Circumpolar Current with global climate effects and oceanic and continental flora and faunal exchanges (Ghiglione et al., 2008; Mackensen, 2004; Lawver and Gahagan, 2003; Zachos et al., 2001).

Acknowledgements

We thank I. W. D. Dalziel and L. Lawver for critical discussions. The study was founded by the CTM2008-06386-C02/ANT and CTM2011-30241-CO2-01/02 projects and by a pre-doctoral fellowship from the "Ministerio de Ciencia e Innovación" of Spain (FPI). This work has also benefited from a research stage abroad funded by the FPI program. Generic Mapping Tools software has been used in this work.

Chapter 7

INSIGHTS ABOUT THE STRUCTURE AND EVOLUTION OF THE SCOTIA ARC FROM A NEW MAGNETIC DATA COMPILATION

*In revision for **Global and Planetary Change***

Insights about the structure and evolution of the Scotia Arc from a new magnetic data compilation

Yasmina M. Martos^{1,*}, Manuel Catalán², Jesús Galindo-Zaldívar^{1,3}, Andrés Maldonado¹, Fernando Bohoyo⁴

¹ *Instituto Andaluz de Ciencias de la Tierra (Consejo Superior de Investigaciones Científicas/Universidad de Granada). Avda. de Las Palmeras nº 4, 18100. Armilla, Granada (Spain).*

² *Real Instituto y Observatorio de la Armada. Cecilio Pujazón, s/n, 11100. San Fernando, Cádiz (Spain).*

³ *Departamento de Geodinámica. Universidad de Granada. Avda. de la Fuente Nueva, s/n, 18071. Granada (Spain).*

⁴ *Instituto Geológico y Minero de España. Ríos Rosas, 23, 28003. Madrid (Spain).*

** Corresponding author
Tel. +34 958230000
E-mail address: yasmartos@ugr.es*

Abstract

The analysis of a new regional compilation of magnetic anomalies from marine, aeromagnetic and satellite data reveals the main structural/tectonic elements of the Scotia Arc. The most relevant magnetic anomaly in the continental crust, the Pacific Margin Anomaly (PMA), is related to a basic to intermediate elongated batholith. It was emplaced by subduction processes along the Pacific continental margin of the Antarctic Peninsula and can be followed within the continental blocks of the South Scotia Ridge and South America. Four representative magnetic profiles also show the structure in depth, and allow us to characterize the main crustal elements of the region. The PMA is seen to have a roughly W-E orientation, decreasing in intensity eastwards from the Pacific Margin of the Antarctic Peninsula and extending towards the South Scotia Ridge to Discovery Bank and even to Herdman Bank. However, the identification of the PMA in the North Scotia Ridge is uncertain, since the magnetic anomalies and the modeled profiles do not support the presence of an important batholithic body. This setting can be attributed to the kinematics of subduction, almost orthogonal to the Pacific margin of the Antarctic Peninsula and

oblique along the South American margin. We propose a reconstruction of the initial distribution of the main continental blocks in the initial stages during the Cretaceous, taking into account the continuity of the PMA along the Antarctic Peninsula and South Scotia Ridge. The anomalies identified in the northern Scotia Sea are probably related to local basic rocks intruded in pull-apart basins that developed in the South America-Antarctica plate boundary deformation zone during the initial stages of South Atlantic Ocean spreading.

Highlights

- The most complete and accurate magnetic anomaly map of the Scotia Arc is presented
- Pacific Margin Anomaly extends along the South Scotia Ridge and Antarctic Peninsula
- The North Scotia Ridge includes basic rocks emplaced in pull-apart basins
- The subduction process of the Phoenix Plate is asymmetrical along the Pacific margin

Keywords: Magnetic anomalies; Analytic signal map; Magnetic models; Pacific Margin Anomaly; Tectonic reconstruction; Antarctica.

Abbreviations

PMA, Pacific Margin Anomaly

1. Introduction

Several marine magnetic and aeromagnetic studies carried out in the Scotia Arc region reveal the main magnetic signature of the area and recognize a magnetic anomaly belt called the Pacific Margin Anomaly (PMA) or West Coast Magnetic Anomaly (Parra et al., 1984, 1988; Garret et al., 1986/87; Maslanyj et al., 1991). The southern part of the belt is located in the Pacific Margin of the Antarctic Peninsula. Northwards, the belt splits into two branches whose widest separation is found in Bransfield Strait, due to back arc-tectonics (Garret and Storey, 1987; Garret, 1990; Barker, 2001; Catalán et al., 2013). This feature extends along the southern continental fragments that lie in the margin of the Scotia Sea, along the South Scotia Ridge (Suriñach et al., 1997). The anomaly is caused by the emplacement of a linear basic to intermediate batholithic complex, related to a Cretaceous magmatic arc (Vaughan et al., 1998), resulting from crustal extensional episodes associated to the oceanic subduction of the Phoenix Plate along the Pacific margin (Garret et al., 1986/87; Garret, 1990, 1991). Some studies also suggest the extension of this magnetic anomaly belt into the South Scotia Ridge, South Orkney Microcontinent, Discovery Bank, South Georgia and South America (Garret et al., 1986/87; Suriñach et al., 1997; Barker et al., 2001) and its connection to the Antarctic Peninsula, the South Shetland Islands and Bransfield Strait (Ghidella et al., 1991, 2011). Most studies of the magnetic anomaly distribution in the Scotia Sea, however, focus on the analysis of sea-floor spreading in order to constrain the tectonic evolution of the Scotia Arc (Eagles and Livermore, 2002; Kovacs et al., 2002; Eagles et al., 2006; Galindo-Zaldívar et al., 2006; Eagles, 2010).

This study presents a new magnetic data compilation of the Scotia Arc, which enables us to identify and characterize the main geological features, while analyzing the tectonic structures. The data provide new insights regarding the features of the PMA along the continental blocks distributed around the Scotia Arc, leading us to reconstruct their former relative position and to discuss the tectonic differences between the northern and southern branches of the arc.

2. Regional Setting

The Scotia Sea is an ocean basin located between South America and the Antarctic Peninsula; it is bounded by the Shackleton Fracture Zone to the west and by the Scotia Arc on the three remaining sides (Fig. 1). The Scotia Arc, which contains the Scotia and Sandwich plates, is now limited by the Former Phoenix Plate to the West, at present part of the Antarctic Plate. The Arc comprises oceanic crust, volcanic arcs and continental crustal blocks, including the North and South Scotia Ridges, and the South Shetland Islands Block (the continental block between the Antarctic Peninsula and the extinct Phoenix Plate). Along the South Scotia Ridge lies the sinistral transcurrent boundary between the Antarctic and Scotia plates, where restraining and releasing tectonic structures are well correlated with present stress (British Antarctic Survey, 1985; Pelayo and Wiens, 1989; Aldaya and Maldonado, 1996; Galindo-Zaldívar et al., 1996; Barker, 2001; Thomas et al., 2003; Geletti et al., 2005; Bohoyo et al., 2007; Smalley et al., 2007). The Shackleton Fracture Zone is an active, transpressive fault zone that accommodates, in conjunction with the South Scotia Ridge, the relative motions between the Scotia and Antarctic plates (Barker et al., 1991; Livermore et al., 1994; Aldaya and Maldonado, 1996; Galindo-Zaldívar et al., 1996; Klepeis and Lawver, 1996; Kim et al., 1997; Maldonado et al., 2000). The Shackleton Fracture Zone is subducted below the northern tip of the South Shetland Islands Block, forming a triple junction (presently Antarctic-Scotia-South Shetland Islands Block) (Aldaya and Maldonado, 1996; Klepeis and Lawver, 1996). The evolution of this fracture zone, which constitutes part of the Antarctic-Scotia plate boundary, has been largely influenced by spreading of the Phoenix-Antarctic Ridge and of the West Scotia Ridge, the beginning of its uplift being dated in the middle Miocene (Martos et al., 2013).

The Scotia Sea contains several spreading ridges that began to be active at least in the Oligocene (Barker, 2001; Bohoyo, 2004; Eagles et al., 2005; Livermore et al., 2005; Galindo-Zaldívar et al., 2006; Lodolo et al., 2010). During the initial stages of continental rifting and oceanic spreading in the Scotia Sea, the south Scotia Sea was characterized by narrow NNE-SSW basins influencing the circulation of conspicuous water masses in the region (King and Barker, 1988; Lawver and Gahagan, 1998; Maldonado et al., 1998; Eagles and Livermore, 2002). The Phoenix Plate underwent subduction below the Antarctic Plate during the late Mesozoic and Cenozoic (Dalziel, 1984; Barker et al., 1991; Eagles et

al., 2004, 2009). The subduction continued at the South Shetland Trench due to roll-back processes at the subduction hinge and produced active spreading in Bransfield Strait (Maldonado et al., 1994; Livermore et al., 2000; Maurice et al., 2003).

The age of the initial tectonic opening of the Drake Passage, between South America and the Antarctic Peninsula, is not well constrained yet, but has significant implications for global oceanic circulation and climate evolution in Antarctica. It formed the final gateway allowing the establishment of a full circum-Antarctic circulation, thereby favoring a global climate change (cf., Kennett, 1977; Lawver et al., 1992; Barker, 2001; Barker and Thomas, 2004; Livermore et al., 2004; Maldonado et al., 2006) coeval with global reduction in atmospheric CO₂ (Deconto and Pollard, 2003).

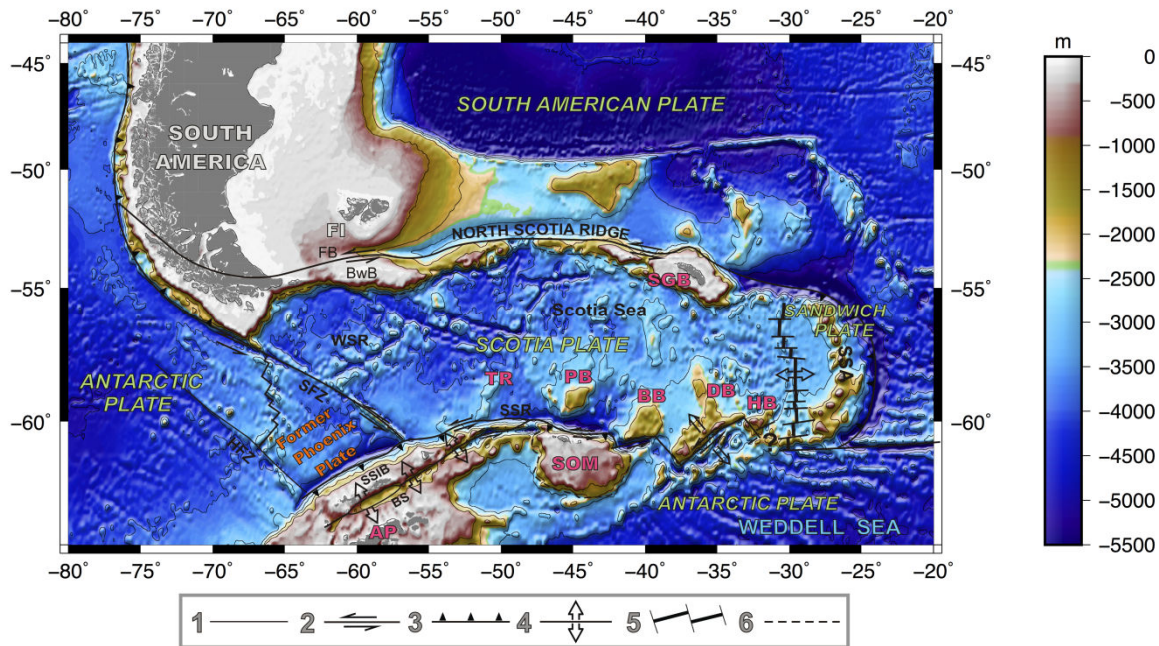


Figure 1. Geological setting of the Scotia Sea. Scotia Arc bathymetry satellite map (Smith and Sandwell, 1997). AP, Antarctic Peninsula; BB, Bruce Bank; BS, Bransfield Strait; BwB, Burdwood Bank; DB, Discovery Bank; FB, Falkland Basin; FI, Falkland Islands; HB, Herdman Bank; HFZ, Hero Fracture Zone; PB, Pirie Bank; SFZ, Shackleton Fracture Zone; SGB; South Georgia Bank; SOM, South Orkney Microcontinent; SSA, South Sandwich Arc; SSIB, South Shetland Islands Block; SSR; South Scotia Ridge; TR, Terror Rise; WSR, West Scotia Ridge. 1, Fracture zone; 2, Transcurrent fault; 3, Subduction zone; 4, Active extensional zone; 5, Active spreading centre; 6, Continent-oceanic crust boundary.

3. Material and methods

The World Digital Magnetic Anomaly Map's Task aims to produce a world map reflecting lithospheric magnetic field anomalies at 5 km of altitude. Priority was given to near-surface data, and particularly to marine information. A new global marine magnetic data set was created by Quesnel et al. (2009). The GEODAS DVD Version 5.0.10, available from the U.S. National Geophysical Data Center, was used as the data source (Fig. 2, black lines). Magnetic anomalies were recalculated taking advantage of the released comprehensive model CM4, which enabled us to correct total field marine data by a proper separation of spatial and temporal variations (Sabaka et al., 2004). All the new information was cleaned by means of a careful check and removal of spurious data, and finally, a line leveling method was applied to reduce data misfits among various cruises. The resulting data set consists of about 20 million records collected by about 2400 cruises from 1953 to 2003. Further marine magnetic data which were added to the GEODAS in 2008, as well as seven Spanish cruises carried out on board the BIO Hespérides between 1992 and 2008 (Fig 2. blue lines), allowed us to update the dataset. Altogether, there are about 23 million records in the new set of data. To assess the improvement in quality and coherence of the data set, we calculated the root mean square of the crossover differences, which were reduced from 179.6 nT (before leveling) to 35.9 nT (after leveling).

Marine coverage is not very dense in the Southern Hemisphere, and improving it calls for including other sources such as aeromagnetic flights. The first of these additional flights in the area comes from the U.S. Naval Research Lab. From 1951 through 1994, the Navy's Project Magnet program continuously collected vector aeromagnetic survey data to support the U.S. Geospatial-Intelligence Mapping Agency in world magnetic modeling and charting (Fig. 2, red lines). Moreover, in 2011 an aeromagnetic flight at 4 km height (Fig. 2, green lines) was performed under the National Geophysical Data Center's aeromagnetic program, focused on obtaining global data to support modeling of the Earth's magnetic field. Some of the previous studies on magnetic anomalies (Lodolo et al., 1997; Barker, 2001; Eagles et al., 2005) were not corrected by external fields, or the core field contribution. The use of IGRF/DGRF are generally adequate for removing the main magnetic field effects from surveys carried out in short time spans. However, because the IGRF/DGRF models are not continuous from one epoch to another, any imprecision in

correctly modeling temporal variations of the Earth's magnetic field can be aliased on the first-order derivative as a bias. When a number of surveys (carried out at very different periods of time) and their associated inaccuracies are adjacent to one another, the error surface may be complex. The CM4 model provides a means of precisely modeling and separating the core field and external fields, so that the former's secular variation behaves in a smooth and continuous way (Ravat et al., 2003). Additionally, during the past decade, several artificial magnetic satellites were put in operation (Oersted, CHAMP). They enabled us to "adjust" the long wavelengths of the different compilations used for the study area. We selected the short-wavelength (< 320 km) anomalies from the marine and low-altitude flights, while longer wavelengths (> 320 km) were filled using magnetic satellite information (Ravat and Purucker, 1999).

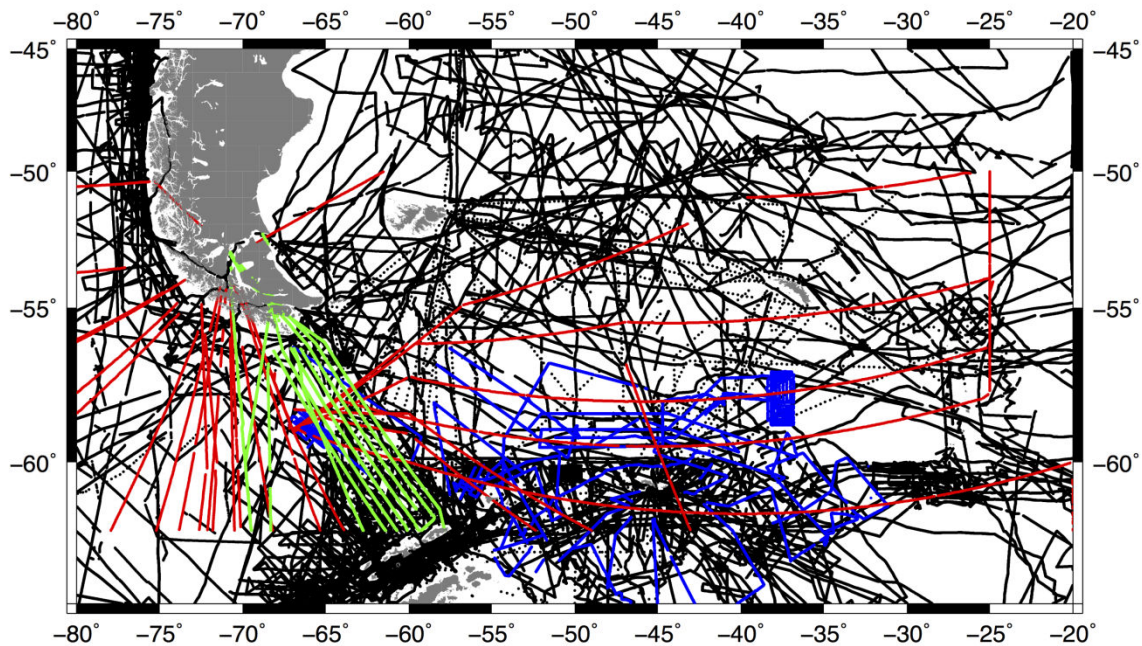


Figure 2. Magnetic trackline dataset in the Scotia Arc and surrounding areas. Black lines: GEODAS dataset corrected with CM4 model (Quesnel et al., 2009). Red lines: aeromagnetic survey data from the World Magnetic Modeling and Charting Program (carried out from 1951 to 1994). Green lines: Aeromagnetic flight at 4 km height performed in 2011 and under the National Geophysical Data Center's aeromagnetic program. Blue lines: 7 Spanish cruises carried out on board the BIO Hespérides between 1992 and 2008.

4. Magnetic maps

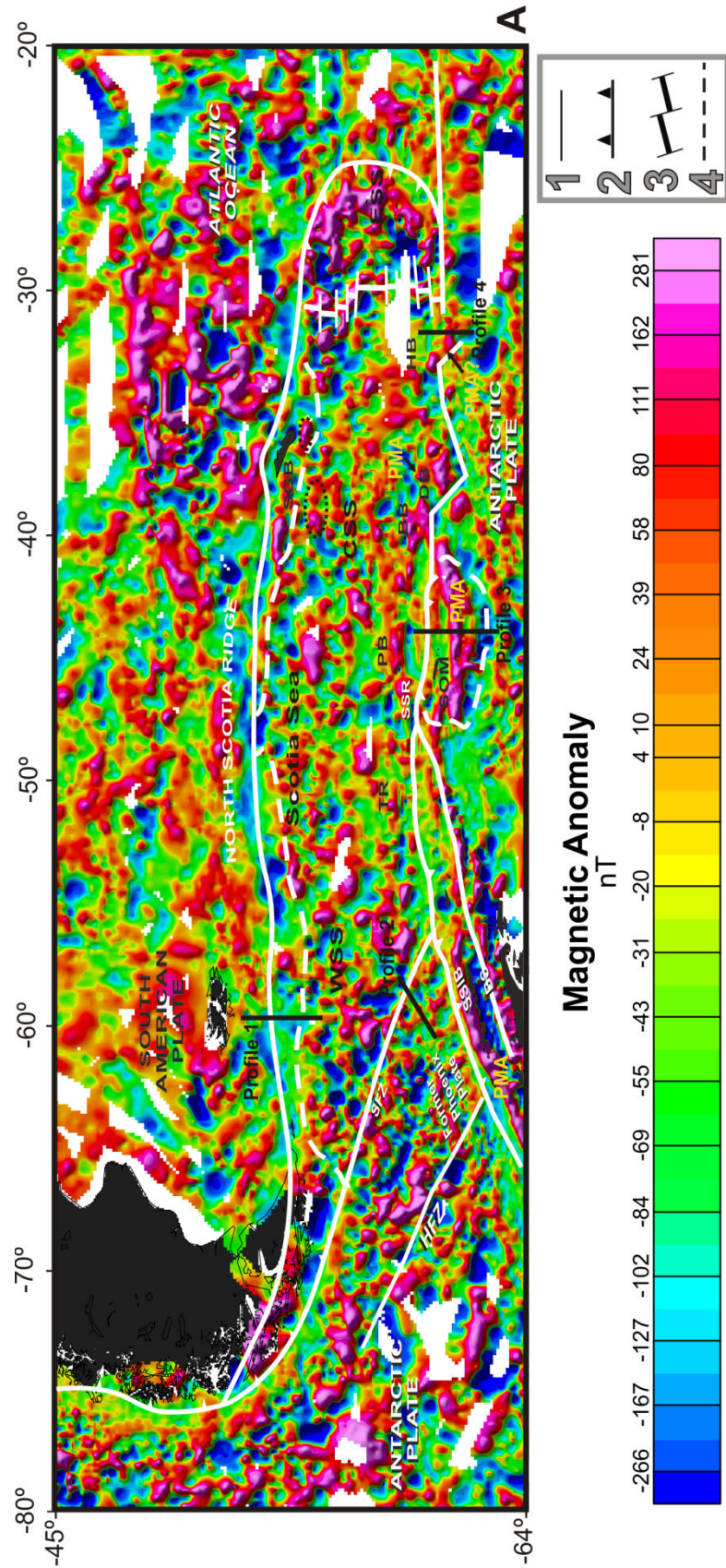
Using the data compilation described above, we created a new magnetic anomaly map (Fig. 3A) and an analytic signal magnetic anomaly map (Fig. 3B) in order to identify the main tectonic structures in the Scotia Arc.

4.1. New Magnetic Anomaly map

The new magnetic anomaly map was created using a 0.13° cell size. The map shows specific magnetic signatures for different provinces (Fig. 3A). The oceanic areas of Antarctica, the Former Phoenix Plate, the East Scotia Sea, and the Atlantic Ocean northeastwards of South Georgia Bank are characterized by wide amplitude anomalies. The Central Scotia Sea generally displays low amplitudes extending towards the West Scotia Sea, with a well-marked boundary to the north, in the North Scotia Ridge. Bransfield Strait is confined by two large magnetic maxima, while the South Orkney Microcontinent shows a wide positive anomaly. The southern and northern boundaries of the Scotia Arc are well represented in the magnetic anomaly map as a maximum-minimum transition. Dipole anomalies in the oceanic regions of the West Scotia Sea and Former Phoenix Plate, with marked maxima located on the north side, are well recognized.

4.2. Analytic signal magnetic anomaly map

The analytic signal map (Fig. 3B) was created in the Fourier domain in order to localize main magnetic sources in the study area, with a 0.13° cell size resolution. Several magnetic signature provinces are identified in oceanic areas. The Antarctic (including the Former Phoenix Plate), the East Scotia Sea and the Atlantic Ocean sector located northeast of the South Georgia Bank are characterized by intense maxima, while the eastern part of the West Scotia Sea, the Central Scotia Sea and most of the Atlantic Ocean present intermediate and low values. The Shackleton Fracture Zone is well identified in the Drake Passage as a linear feature. The sources of the PMA southwards of Scotia Sea are well observed, particularly in Bransfield Strait, the South Orkney Microcontinent and Discovery Bank.



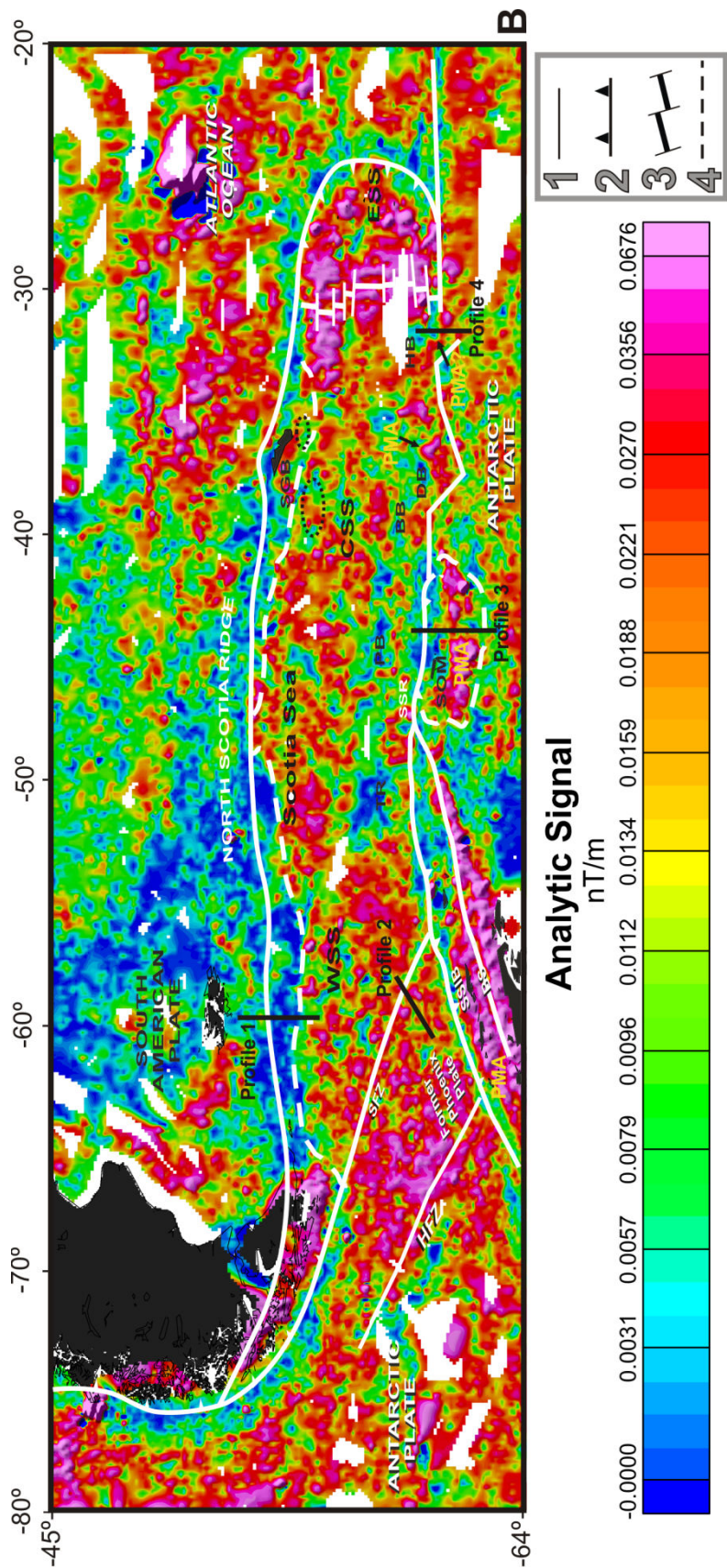


Figure 3. Magnetic anomaly maps. A) New magnetic anomalies map. B) Analytic signal map. The four selected profiles for modeling are shown in the figure.

BB, Bruce Bank; BS, Bransfield Strait; CSS, Central Scotia Sea; DB, Discovery Bank; ESS, East Scotia Sea, HB, Herdman Bank; HFZ, Hero Fracture Zone; PB, Pirie Bank; PMA, Pacific Margin Anomaly; SFZ, Shackleton Fracture Zone; SGB, South Georgia Bank; SOM, South Orkney Microcontinent; SSIB, South Shetland Islands Block; SSR, South Scotia Ridge; TR, Terror Rise; WSS, West Scotia Sea. 1, Fracture zone; 2, Subduction zone; 3, Active spreading centre; 4, Continent-oceanic crust boundary.

5. Magnetic anomaly profiles and modeling

Four representative profiles (Fig. 3-7) were selected taking into account the magnetic anomaly map and the analytic signal map in order to study and characterize the main structures of the Scotia Arc from the magnetic point of view, and in particular, the PMA. We chose the best developed dipoles, W-E elongated and with maxima to the north, from areas having good trackline coverage (Fig. 2). For the purpose of magnetic modeling, the sediment layer was considered to have null total magnetization. In addition, rocks were understood to have magnetic properties above a specific depth within the crust due to thermal gradient effects (Curie temperature) and thereafter, the initial depth values were based on Garret et al. (1986/87). The PMA, related to the emplacement of basic and intermediate igneous rocks, was studied in outcropping areas of the Antarctic Peninsula (Maslanyj et al., 1991), where magnetic susceptibilities ranging from 0.033 SI to 0.274 SI were determined, and Königsberger ratios close to or greater than 1.

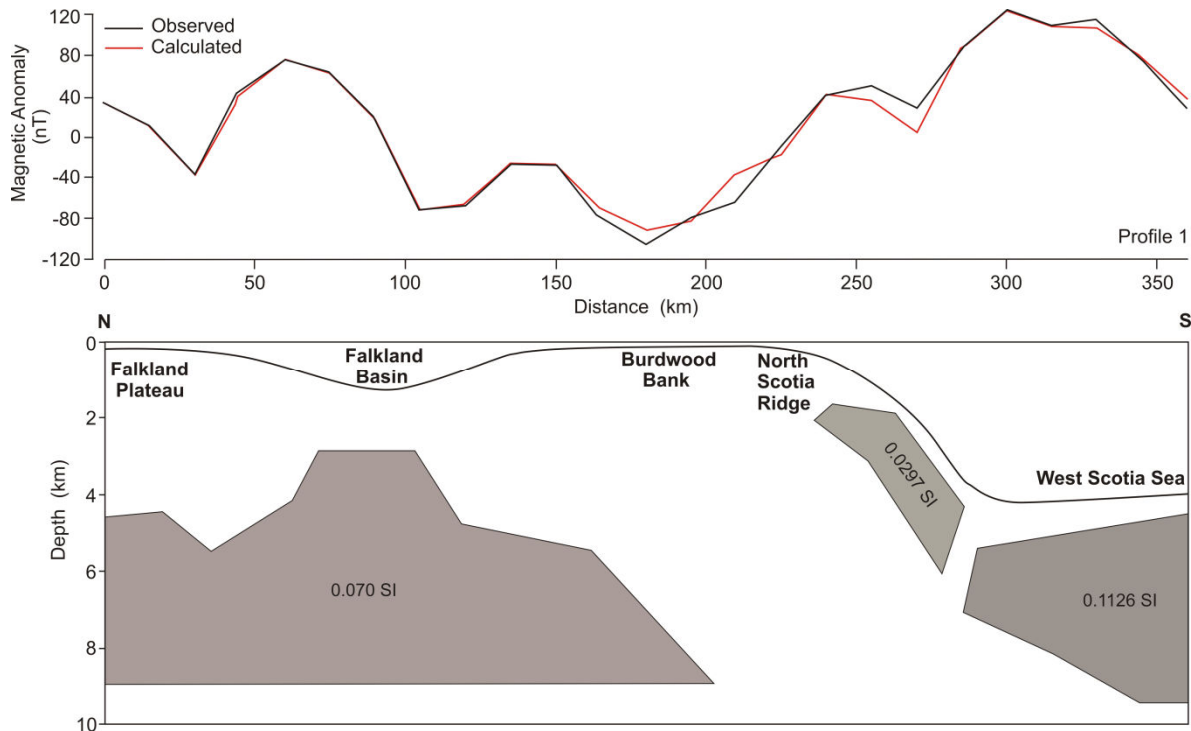


Figure 4. Magnetic model of Profile 1. See Figure 3 for location. Magnetic field parameters used for modeling: $F = 30357$ nT, $D = 6.22^\circ$ and $I = -50.81^\circ$.

Profiles 1, 3 and 4 were used to model the magnetic anomaly bodies located in continental banks to identify and study the PMA along the Scotia Arc. The models extend up to depths comprised between 8 and 11 km, where magnetic properties are probably lost due to high crustal temperatures. Moreover, Profile 2 was used to describe the transition between the Former Phoenix Plate and the Scotia Plate through the Shackleton Fracture Zone.

Profile 1 (Fig. 4), which crosses the South American continent and the North Scotia Ridge with north-south orientation, shows a magnetic signal range between 120 and -100 nT, composed by four maxima. Three main magnetic bodies are needed to fit the observed data. The largest one, with a susceptibility of 0.070 SI, is located in the Falkland Plateau, Falkland Basin and Burdwood Bank. Its shallowest area is found around 3 km depth and the deepest part at 9 km depth. The magnetic structure with the highest susceptibility (0.1126 SI) is in the West Scotia Sea, modeled from 5 km to 9 km depth. The body with the lowest susceptibility, 0.0297 SI, is also the shallowest one (between 1.5 km and 6 km) and it is situated at the continental border of the continent-ocean boundary in the North Scotia Ridge.

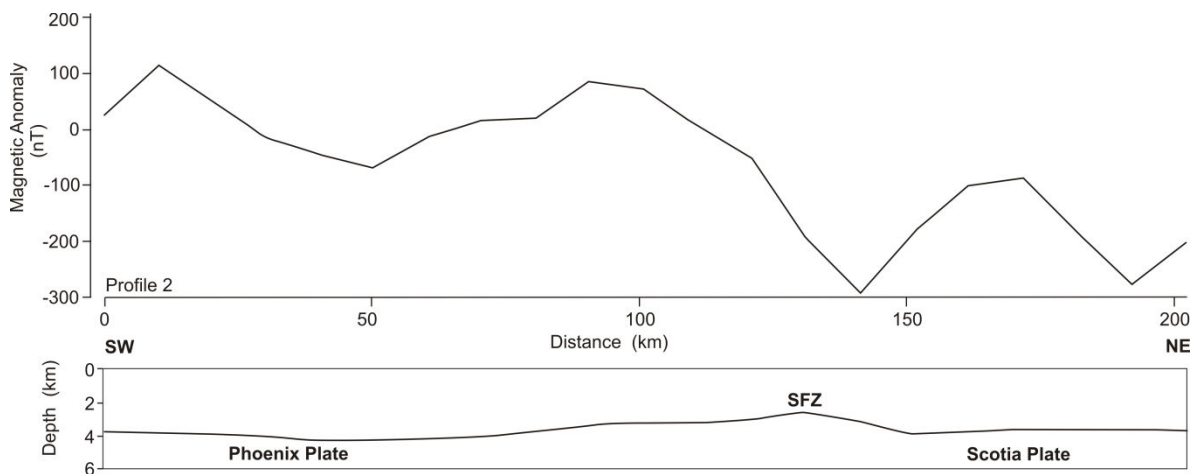


Figure 5. Magnetic anomaly of Profile 2. See Figure 3 for location. SFZ, Shackleton Fracture Zone.

Profile 2 (Fig. 5) crosses the Shackleton Fracture Zone from the Former Phoenix Plate to the West Scotia Sea with SW-NE orientation. We used it as a sample profile to present the differences in the main magnetic signatures between the plates, since this fracture constitutes a main border of the structure of the oceanic crust. In this profile, the magnetic signal of the Former Phoenix Plate is higher (maximum around 100 nT) and wider (about 90 km) than the signal in the West Scotia Sea. Modeling this profile from the magnetic standpoint of view is no easy task, given the high remanent magnetization due to oceanic spreading.

Profile 3 (Fig. 6), with north-south orientation, lies between the Scotia Sea and the South Orkney Microcontinent. The magnetic signal of this profile ranged between 400 nT and -250 nT, exhibiting a large maximum located in the center. Two magnetic structures are necessary to fit the observed signal. The greatest body (150 km width x 9 km thick) is also the one with the highest susceptibility, 0.8530 SI, while we consider a susceptibility of 0.0194 SI for the smallest one (about 50 km width x 5 km maximum thickness). Both are situated in the South Orkney Microcontinent, but the smaller body is closer to the continent-ocean boundary between the Microcontinent and the Scotia Plate.

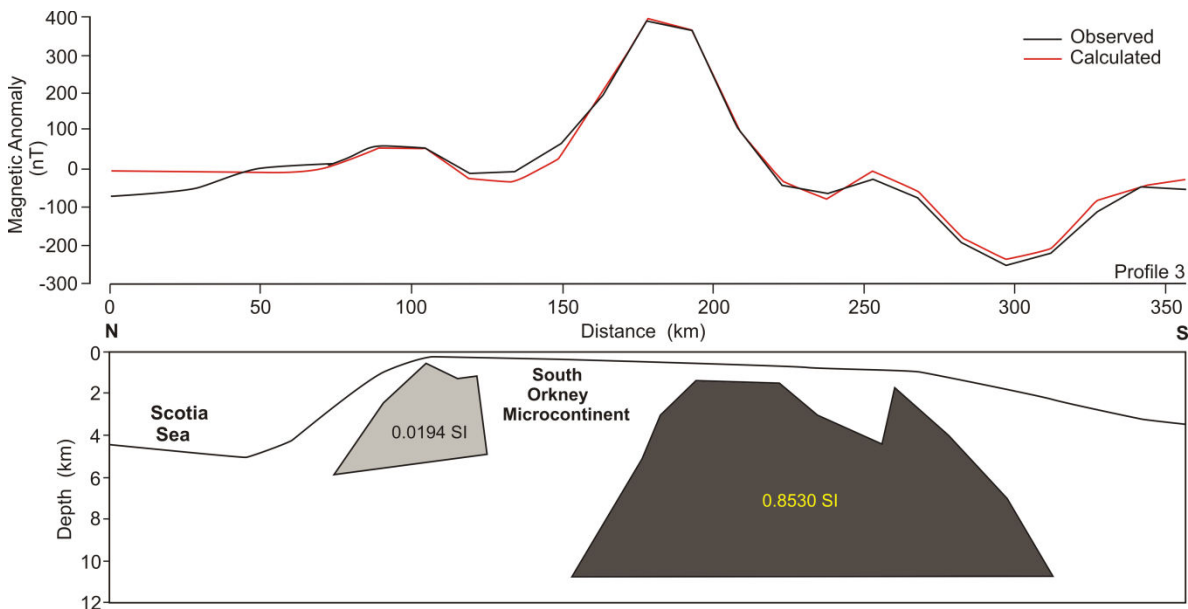


Figure 6. Magnetic model of Profile 3. See Figure 3 for location. Magnetic field parameters used for modeling: $F = 33111$ nT, $D = 1.91^\circ$ and $I = -56.18^\circ$.

Profile 4 (Fig. 7), the easternmost profile modeled, crosses the eastern tip of the South Scotia Ridge to the Weddell Sea with north-south orientation. Two wide (around 100 km width) and high maxima and a minimum characterize the magnetic signal of the profile. The signal amplitude varies between 200 nT and -200 nT. Two main magnetic structures are found to fit the observed data, the magnetic susceptibility and size decreasing to the south. The smallest body is located between 4 km and 8 km depth with a susceptibility of 0.0673 SI. An elongated structure (around 100 km long) with similar thickness but higher susceptibility (0.1047 SI) than the previous one is found in Herdman Bank, in the northern part of the profile.

In sum, the largest and most magnetized structures are located in the southern part of the Scotia Sea, specifically in the continental blocks of the South Scotia Ridge. Most relevant on the northern side is the elongated anomaly located nearby the continent-ocean boundary.

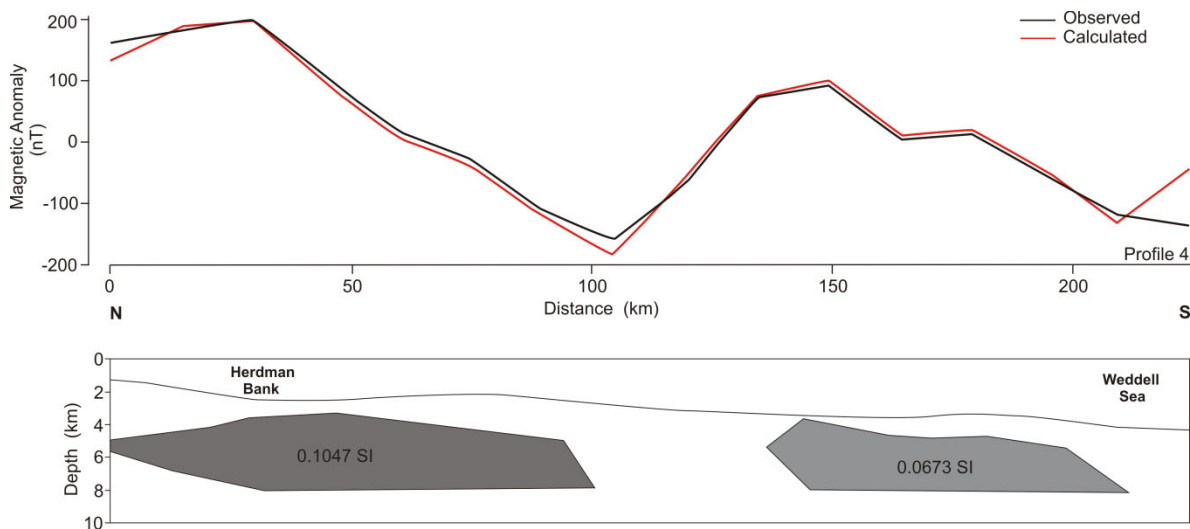


Figure 7. Magnetic model of Profile 4. See Figure 3 for location. Magnetic field parameters used for modeling: $F = 31760$ nT, $D = -4.26^\circ$ and $I = -57.36^\circ$.

6. Discussion

The magnetic data compilation provides insights about the Scotia Arc main features and tectonics. However, this study based on the most recent magnetic anomaly dataset focuses on the magnetic signatures and subsurface magnetic structures, rather than magnetic anomalies related to oceanic spreading that are addressed in other detailed research (British Antarctic Survey, 1985; Barker, 2001; Eagles et al., 2005). The wide amplitude magnetic anomalies located in the Antarctic, Former Phoenix and Sandwich plates are related to oceanic spreading in these three plates (Fig. 3). The Shackleton Fracture Zone, corresponding to a main oceanic boundary between the Former Phoenix and Scotia plates, is also characterized by a change in magnetic signal (Figs. 3A and 5). The Central Scotia and the eastern part of the West Scotia Sea show medium values of magnetic amplitudes related to the presence of a more conspicuous setting of small oceanic basins and continental banks.

The PMA, with W-E orientation, is well identified along the southern Scotia Arc in several of the continental blocks, including the South Orkney Microcontinent and Discovery Bank, and could also be recognized in the northern part of Herdman Bank (Fig. 3). However, Bruce and Pirie Banks do not reflect the well elongated W-E magnetic anomalies that could be attributed to the PMA.

The susceptibilities used to model the selected profiles (Figs. 3, 4, 6, 7) generally fall in the range of the measurements observed in the Antarctic Peninsula (Maslanyj et al., 1991). Due to the presence of remanent magnetism parallel to the induced one, confirmed by the high Königsberger ratios, in some cases we considered the susceptibility values higher than the field measurements because remanent and induced magnetizations were parallel. The highest magnetization is found in the South Scotia Ridge and the largest body in the area (with 0.8530 SI), located in the South Orkney Microcontinent (Fig. 6), is interpreted as a part of the PMA, in coincidence with other authors (Garret et al., 1986/87). At any rate, a partial origin of these magnetic anomalies might be related to the subduction of the Weddell Sea oceanic crust below the South Orkney Microcontinent and Discovery Bank (Bohoyo, 2004). Garret et al. (1986/87) identified the PMA in Discovery Bank, in the easternmost part of the south Scotia Arc. Moreover, Profile 4 shows a magnetic body (0.1047 SI) located in the northern part of Herdman Bank that can be interpreted as part of

the PMA (Fig. 7). Although its origin may be linked to the South Sandwich volcanic arc (Hamilton, 1989; Barker, 2001), part of this bank could derive from dispersed continental fragments such as Discovery Bank (Barker, 2001). This profile was modeled using two main magnetic bodies with different susceptibilities (0.1047 SI and 0.06730 SI).

The modeling of the North Scotia Ridge profile, in contrast, depicts anomalous magnetic bodies different than those of the PMA located along the South Scotia Ridge. A large body is found under the Falkland Basin (Profile 1, Fig. 4), which we interpret as an intrusive dyke due to the thinning of the continental crust along this W-E linear basin. The oceanic crust is well identified and is represented by a large magnetic body reaching the continent-ocean boundary.

The PMA was identified by Garrett et al. (1986/87) in the southeastern South Georgia Bank, where we also observed a lineated W-E magnetic anomaly (Fig. 3A, black dashed circle). Yet in the analytic signal map it is not well recognized as a main magnetic source (Fig. 3B, black dashed circle), in contrast to the PMA bodies along the South Scotia Ridge. Another possible anomaly that may be related to the PMA is observed in the northern part of the Central Scotia Sea, southwest of South Georgia (Fig. 3A, black dashed circle). This anomaly is located in an area of complex crustal nature that may correspond to very thin continental banks or oceanic crust with unclear spreading (British Antarctic Survey, 1985; Eagles, 2010), producing a low magnetic signal; it is likewise not well identified in the analytic signal map (Fig. 3). If we interpreted these anomalies as part of the northern branch of the PMA, only a few blocks with low magnetization are seen to have similar PMA features as in the South Scotia Ridge. We therefore suggest that the PMA does not occur along the North Scotia Ridge. The continent-ocean boundary in the North Scotia Ridge is characterized by maxima values related to the contact with the continental crust, because of its transcurrent character.

We propose a model for the initial distribution of the continental blocks in the Scotia Arc (Fig. 8). The basic to intermediate batholithic body that is responsible for the PMA signal is larger in the western part of Antarctic Peninsula and Shetland Islands, where it is composed by two branches separated by the Bransfield Strait (Garrett et al., 1986/87; Maslanyj et al., 1991; Ghidella et al., 2011, Catalán et al., 2013).

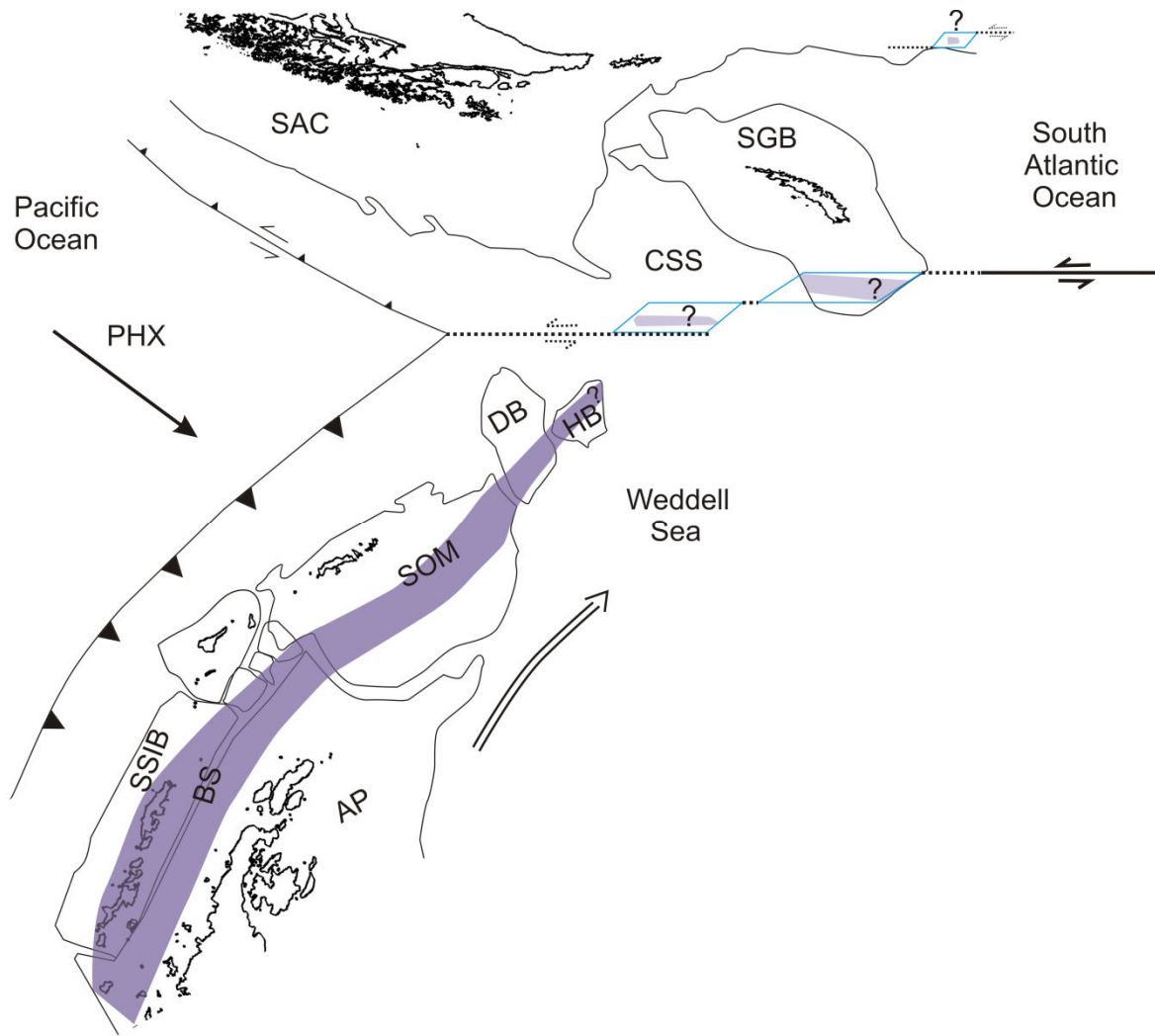


Figure 8. Tectonic sketch of main structures during the development of the linear batholith related to the PMA in the Cretaceous. The subduction process is orthogonal in the Antarctic margin and oblique in the South American margin. Dark violet areas show the PMA magnetic signal, namely the basic to intermediate batholithic body due to the subduction process. Light violet areas are those which could be related to basic bodies associated with pull-apart basins. AP, Antarctic Peninsula; BS, Bransfield Strait; CSS, Central Scotia Sea; DB, Discovery Bank; HB, Herdman Bank; PHX, Phoenix Plate; SGB, South Georgia Bank; SOM, South Orkney Microcontinent; SAC, South American Continent; SSIB, South Shetland Islands Block.

The asymmetry between the northern and southern Scotia Arc can be related to the asymmetrical subduction process of the Phoenix Plate since the Cretaceous in the western part of Antarctica and South America (Fig. 8) (Dickson et al., 1968; Larson, 1976; British Antarctic Survey, 1985; Cande et al., 1988; Renking and Sclater, 1988; Dalziel et al., 2013). The subduction process was directed southeastwards, mainly affecting the western

part of Antarctica (Larson, 1976; Renking and Sclater, 1988) while South America was affected obliquely. Thereafter, the development of the basic to intermediate batholithic body along the southernmost American continental margin is smaller than in the Antarctic margin, where it decreases in size towards the NE. Assuming this setting, a major part of the continental elements of the North Scotia Ridge that constituted the original continental South America-Antarctica bridge, like the South Georgia Bank, would be located east of the subduction zone and were probably not directly affected by this process. In this context, the relevant anomalies along the North Scotia Ridge may be related to basic rocks most likely emplaced in pull-apart basins developed along a broad transcurrent fault zone that separated the South American and Antarctic plates during the initial stages of development of the South Atlantic Ocean (Fig. 8, blue areas).

7. Conclusions

We present the most complete compilation to date of the magnetic anomalies of the Scotia Arc from marine, aeromagnetic and satellite data. While high intensity anomalies are identified in the oceanic areas of the Former Phoenix Plate, and western part of the West Scotia Sea, East Scotia Sea, and northeast of the South Georgia Islands, low intensity anomalies occur in the Central Scotia Sea and eastern part of West Scotia Sea.

A linear anomaly identified north of the North Scotia Ridge coincides with the Falkland Basin, probably evidencing the intrusion of an E-W elongated dyke in an episode of crustal thinning. In addition, a long linear maximum is observed along the continent-ocean boundary, south of the North Scotia Ridge.

The PMA is well recognized in the Antarctic Peninsula and in the South Shetland Islands, extending along the South Scotia Ridge continental blocks: South Orkney Microcontinent and southern Discovery Bank and it may occur in the northern part of Herdman Bank. The magnetic models show that the PMA is the consequence of linear basic to intermediate batholiths, in turn related to a subduction of the oceanic Former Phoenix Plate below the Pacific continental margin. The variability in the intensity of the PMA, which decreases eastwards from the Antarctic Peninsula along the South Scotia Ridge, may be a consequence of the asymmetry of the trend of subduction (Fig. 8): orthogonal to the Pacific Margin of the Antarctic Peninsula and oblique to South America.

However, the PMA appears to be absent in the North Scotia Ridge, where the main recognized anomalies (South Georgia Bank, and other minor anomalies) may be associated with basic rocks emplaced in pull-apart basins formed along a broad transcurrent zone that separates South America and Antarctica since the Cretaceous due to the South Atlantic oceanic spreading (Fig. 8). These data provide new insight into the South America-Antarctica continental bridge reconstruction, prior to the development of the Scotia Arc (Fig. 8).

Acknowledgments

The study was founded by the CTM2008-06386-C02/ANT and CTM2011-30241-CO2-01/02 projects and by a pre-doctoral fellowship from the “Ministerio de Ciencia e Innovación” of Spain (FPI). This work has also benefited from research stages abroad funded by the FPI program. Generic Mapping Tools software was used in this work.

Chapter 8

TECTONICS AND PALAEOCEANOGRAPHIC EVOLUTION RECORDED BY CONTOURITE FEATURES IN SOUTHERN DRAKE PASSAGE (ANTARCTICA)

Published in:
Marine Geology
Vol. 343, 76-91

Received 26 November 2012
Received in revised form 19 June 2013
Accepted 20 June 2013

Tectonics and palaeoceanographic evolution recorded by contourite features in southern Drake Passage (Antarctica)

Yasmina M. Martos ^{a,*}, Andrés Maldonado ^a, Francisco J. Lobo ^a, F^o Javier Hernández-Molina^b and Lara F. Pérez ^a

^a *Instituto Andaluz de Ciencias de la Tierra (CSIC/UGR), Avda. de las Palmeras, 4, 18100 Armilla, Granada, Spain. E-mail address: yasmartos@ugr.es*, amaldona@ugr.es, pacolobo@iact.ugr-csic.es, lfperez@iact.ugr-csic.es*

^b *Department of Earth Sciences, Royal Holloway University of London, Egham, Surrey TW20 0EX, United Kingdom. E-mail address: fjhernan@uvigo.es*

** Corresponding author.
Tlf: +34 958 23 00 00 / Fax: +34 958 55 26 20*

Abstract

The sedimentary record in the vicinity of the triple junction at the southern Drake Passage is analyzed in order to decode the palaeoceanographic evolution and the influence of tectonic events. The break-up of the last connection between South America and Antarctica led to the circulation of important oceanographic bottom flows, including the Antarctic Circumpolar Current (ACC) and the Weddell Sea Deep Water (WSDW). The Shackleton Fracture Zone (SFZ), a ridge crossing the central Drake Passage, has been proposed as a major barrier that constrained the free circulation of bottom flows in the area, but whose timing and importance is poorly established. Also, the South Scotia Ridge (SSR), a prominent relief composing the southern part of the Scotia Arc, has controlled oceanographic exchanges between the Weddell and Scotia seas, as bottom flows from the Weddell Sea to the Scotia Sea have been conducted across narrow gateways along the SSR. On the basis of a network of multichannel seismic profiles, we interpret the uplift dynamics of the SFZ in the southern Drake Passage and its influence on the evolution of the bottom-current circulation and by extension on contourite processes.

Six main seismic units, identified and correlated between the Scotia and the Former Phoenix plates, depict a south-west-directed tilting of the deposits above a mid-Miocene

reflector (Reflector c) on the Phoenix Plate. The regional correlation of the main reflections and contourite features indicates that the deepest fraction of the ACC, the Lower Circumpolar Deep Water (LCDW as the lower part of the Circumpolar Deep Water, CDW), flowed freely from the latest Eocene to the middle Miocene, and that these palaeoflows have been active until the present in the abyssal plain of the central-western Scotia Sea. SFZ uplift was initiated, at the latest, during the middle Miocene (about 12 Ma), when the SFZ began to be an effective barrier to bottom flows in the southern Drake Passage. The ridge forced the ACC and the Polar Front to shift northward contributing to the thermal isolation of Antarctica and more polar conditions. The northward displacement of the LCDW and the opening of passages along the SSR favoured the insertion of WSDW flows along the southern part of the Drake Passage, westward into the Pacific Ocean and northward into the abyssal plain of the southwestern Scotia Sea. Based on the morphology and evolution of the main erosional features, we also calculate a ratio between two volumetric flow rates related to the two major branches of the WSDW in the southwestern Scotia Sea area. The highest ratio is found for the age of Reflector b and is probably related with the strongest incursions of the WSDW in the area, as well as with SFZ uplift. This work demonstrates the common occurrence of large depositional and erosional features in deep marine environments related to bottom-current activity and their important implications on decoding palaeoceanographic, climatic and tectonic events.

Keywords: Shackleton Fracture Zone, South Scotia Ridge, contourite features, Antarctic Circumpolar Current, Weddell Sea Deep Water, tectonic evolution

1. Introduction

The Drake Passage is a deep gateway the entire length of which is crossed by the Shackleton Fracture Zone (SFZ), a significant structural relief with elevations of hundreds to thousands of meters above the surrounding ocean floor (Maldonado et al., 2000; Livermore et al., 2004). The age of the initial tectonic opening of the Drake Passage is not well constrained, but likely has significant implications for global oceanic circulation and climate evolution in Antarctica as it created the final gateway to allow the establishment of a full circum-Antarctic circulation and the thermal isolation of the Antarctic continent (cf.,

Kennett, 1977; Lawver et al., 1992; Barker, 2001; Barker and Thomas, 2004; Livermore et al., 2004; Maldonado et al., 2006) coeval with global reduction in the atmospheric CO₂ (Deconto and Pollard, 2003). However, the importance of the opening of the Drake Passage as trigger of the Antarctic thermal isolation is a subject of controversy as some authors suggest that the heat anomalies caused by the opening and the initial circumpolar current were weak to lead to the abrupt Cenozoic cooling (Huber and Sloan, 2001; Zhong-Shi et al., 2010).

The southwestern Scotia Sea is a key region for constraining the time of opening because it contains the oceanic crust that developed during the initial phases of oceanic spreading (Aldaya and Maldonado, 1996; Lodolo et al., 2006, 2010). The oldest oceanic magnetic anomalies interpreted in the region suggest an early Oligocene opening age (ca. 32 Ma, Lodolo and Tassone, 2010), and arguments based on plate tectonic reconstructions propose an opening during the middle Eocene (ca. 45 Ma, Livermore et al., 2007), the Oligocene (Lawver and Gahagan 2003; Geletti et al., 2005; Lodolo et al., 2010), or the Miocene (Barker, 2001). In addition to its influence during the initial evolutionary stages, the SFZ has been suggested as a significant barrier to the circumpolar deep flow since the late Miocene (8 Ma, Livermore et al., 2004). In addition, the deformed continental blocks of the South Scotia Ridge (SSR) have also influenced the bottom-current distribution in the area. Therefore, the complex tectonic evolution of this region has influenced bottom-current circulation, which in turn has controlled the growth patterns of contourite drifts (Fig. 1).

We analyze the triple junction region in the southwestern Scotia Sea, where the extinct Phoenix, Antarctic, and Scotia plates meet (Aldaya and Maldonado, 1996). The study area is located where the SFZ intersects the SSR and where the Weddell Sea Deep Water (WSDW) enters the Pacific Ocean from the Scotia Sea. Above the WSDW is flowing east the Circumpolar Deep Water (CDW), specially its lower fraction, the Lower Circumpolar Deep Water (LCDW) (the deeper fraction of the Antarctic Circumpolar Current (ACC)) (Carter et al. 2008) (Fig. 1). In this context, we focus on two main objectives:

(1) To characterize the type, distribution, and development of deposits that resulted from the interaction between the sea-bottom reliefs, caused by active tectonics, such as SFZ

uplift and the SSR development, and the circulation of the main water masses. In order to achieve this goal, we combine these observations with the information about the opening of the Drake Passage, the history of the SFZ as a bottom-current barrier and the SSR gateway development.

(2) To understand how the palaeo-bathymetry of the region has influenced bottom-current flows over time and the global climate. To achieve this objective, we discuss the age of the initial ACC incursion into the Scotia Sea and the insertion of WSDW towards the Pacific Ocean. Thereby, we describe the evolution of main branches of bottom currents and how they could have influenced the global climate.

The results presented in this study help to constrain the palaeoceanography of this key region and understand how the relationships between depositional processes, tectonic evolution and bottom-current circulation are, as well as, to understand the last important climate change in Antarctica which, in turns, influenced the Eocene/Oligocene global climate change.

2. Regional setting

2.1 Tectonic evolution

The Scotia Sea is an ocean basin located between South America and the Antarctic Peninsula (Fig. 1) containing at present two active plates, the Scotia Plate and the Sandwich Plate, which are bounded by the SFZ to the west and by the Scotia Arc on the three remaining sides. West of the SFZ, the Scotia Plate is bounded by the extinct Phoenix Plate, which is now part of the Antarctic Plate. The Scotia Arc is composed of the South Sandwich Arc, the North Scotia Ridge, and the deformed continental crustal blocks of the SSR and the South Shetland Islands Block (the continental block between the Antarctic Peninsula and the extinct Phoenix Plate). Transpressional tectonics occurs in the western part of the SSR, while the central and eastern parts of the SSR are affected by transtensional tectonics (British Antarctic Survey, 1985; Pelayo and Wiens, 1989; Aldaya and Maldonado, 1996; Galindo-Zaldívar et al., 1996; Lodolo et al., 1997; Barker, 2001; Thomas et al., 2003; Geletti et al., 2005; Smalley et al., 2007).

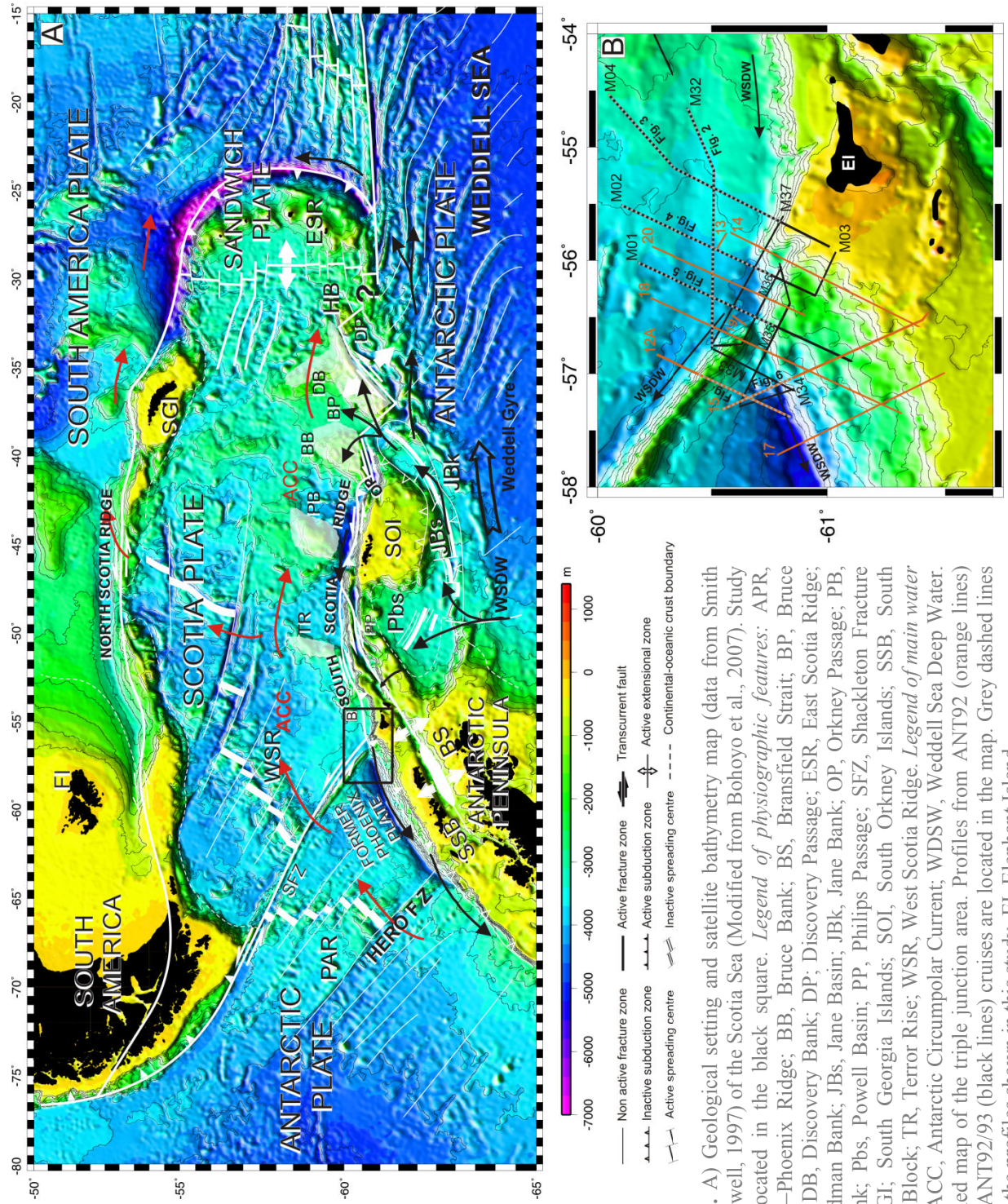


Figure 1. A) Geological setting and satellite bathymetry map (data from Smith and Sandwell, 1997) of the Scotia Sea (Modified from Bohoyo et al., 2007). Study area is located in the black square. *Legend of physiographic features:* APR, Antarctic–Phoenix Ridge; BB, Bruce Bank; BS, Bransfield Strait; BP, Bruce Passage; DB, Discovery Bank; DP, Discovery Passage; ESR, East Scotia Ridge; HB, Herdman Bank; JBs, Jane Basin; JBk, Jane Bank; OP, Orkney Passage; PB, Pirie Bank; Pbs, Powell Basin; PP, Phillips Passage; SFZ, Shackleton Fracture Zone; SGI, South Georgia Islands; SOI, South Orkney Islands; SSB, South Shetland Block; TR, Terror Rise; WSR, West Scotia Ridge. *Legend of main water masses:* ACC, Antarctic Circumpolar Current; WDSW, Weddell Sea Deep Water. B) Detailed map of the triple junction area. Profiles from ANT92 (orange lines) and HESANT92/93 (black lines) cruises are located in the map. Grey dashed lines represent the profiles shown in this study. EI, Elephant Island.

The Scotia Sea contains several spreading ridges that began to be simultaneously active in the Oligocene and led to the opening of the Drake Passage (Barker, 2001; Eagles et al., 2005; Livermore et al., 2005; Lodolo et al., 2010). During the initial stages of continental rifting and oceanic spreading in the Scotia Sea, the south Scotia Sea was characterized by narrow NNE-SSW basins, which influenced the circulation of conspicuous water masses in the region (King and Barker, 1988; Galindo-Zaldívar et al., 1994; Lawver and Gahagan, 1998; Maldonado et al., 1998; Eagles and Livermore, 2002; Galindo-Zaldívar et al., 2002).

The Phoenix Plate underwent subduction below the Antarctic Plate during the late Mesozoic and Cenozoic (Dalziel, 1984; Barker et al., 1991; Eagles et al. 2004; Eagles et al., 2009). The Phoenix-Antarctic Ridge, the spreading axis of the extinct Phoenix Plate, ceased spreading at Chron C2A (2.6–3.6 Ma), and the Phoenix Plate became part of the Antarctic Plate (Larter and Barker, 1991; Livermore et al., 2000). The subduction continued at the South Shetland Trench due to roll-back processes at the subduction hinge and active spreading in the Bransfield Strait (Maldonado et al., 1994; Livermore et al., 2000; Maurice et al., 2003).

The SFZ is an active, transpressive fault zone that accommodates, in conjunction with the SSR, the relative motions between the Scotia and Antarctic plates (Barker et al., 1991; Livermore et al., 1994; Aldaya and Maldonado, 1996; Galindo-Zaldívar et al., 1996; Klepeis and Lawver, 1996; Kim et al., 1997; Maldonado et al., 2000). The SFZ is subducted below the South Shetland Islands Block, forming a triple junction (presently Antarctic-Scotia-South Shetland Islands Block) (Aldaya and Maldonado, 1996; Klepeis and Lawver, 1996), and its evolution has been largely influenced by the spreading on the Phoenix-Antarctic Ridge and on the West Scotia Ridge.

2.2 Regional stratigraphy

Five major seismic units (Units 5 to 1 from bottom to top) have been regionally correlated in the southern and central Scotia Sea (Maldonado et al. 2006). The discontinuities separating units are designated as d to a from bottom to top. Unit 5 fills basement depressions with an estimated Oligocene to early Miocene age. Unit 4 is sheet-like and considered to be early to middle Miocene in age. Unit 3 exhibits both mounded

and sheet-like geometries and the suggested age is middle to late Miocene (Maldonado et al., 2003, 2005). Mounded and sheet-like shapes are dominant in Unit 2, which is attributed as late Miocene to early Pliocene age. Unit 1 is described as a relatively thin early Pliocene to Recent unit.

Numerous types of drifts such as mounded elongated, basement controlled, sheeted, patch, channel related and plastered drifts have been identified in the western continental margin of the Antarctic Peninsula, the Scotia and the Weddell seas (Howe et al., 1998; Howe and Pudsey, 1999; Michels et al. 2002; Pudsey, 2002; Rebesco et al. 2002; Stow et al., 2002; Maldonado et al., 2003; Hernández-Molina et al., 2004; Maldonado et al., 2005; Hernández-Molina et al., 2006; Uenzelmann-Neben, 2006; Rebesco and Camerlenghi, 2008). Drift and contourite deposits in the southern and central Scotia Sea are mainly associated to the three youngest units above Reflector c (Maldonado et al., 2006).

2.3 Oceanographic setting

The full opening of the Drake Passage allowed the establishment of the ACC, which controls the transport of heat, salt, and nutrients around the Southern Ocean. This current is also the principal contributor to the boundary currents of the South Atlantic, South Pacific, and Indian oceans (Nowlin and Klinck, 1986; Naveira Garabato et al., 2002a). In addition, the Weddell Sea is one of the main engines of the global Thermohaline Circulation as it is the source of deep and bottom waters due to enhanced atmosphere-ice-ocean interactions (Brennecke, 1921; Gill, 1973; Carmack, 1977; Fahrback et al., 1995; Foldvik and Gammelsrød, 1988; Rahmstorf, 2006).

Two important deep-water masses are distinguished in the region (Orsi et al., 1999; Naveira Garabato et al., 2002b; Hernández-Molina et al., 2006; 2007; Hillenbrand et al., 2008) (Fig. 1B): (a) the CDW, which flows mostly eastwards through the Scotia Sea as the deepest part of the ACC. This water mass is composed of a lower (LCDW) and upper (UCDW) fractions, and (b) the WSDW which flows within the Weddell Gyre, preferentially along the northwestern Weddell Sea above the slope of the Antarctic Peninsula. A branch of the WSDW enters the Scotia Sea through several narrow passages (Discovery, Bruce, Orkney, and Phillip passages) of the SSR (Naveira Garabato et al., 2002b; Schodlok et al., 2002; Naveira Garabato et al., 2003; Hernández-Molina et al.,

2006; Bohoyo et al., 2007; Carter et al., 2008) (Fig. 1). Within the Scotia Sea, the WSDW is commonly subdivided in lower and upper components (Tarakanov, 2009). The WSDW flows westwards along the northern slopes of the SSR and reaches the Pacific margin of the Antarctic Peninsula (Locarnini et al., 1993; Orsi et al., 1995; Camerlenghi et al., 1997; Rebesco et al., 1997; Orsi et al., 1999; Naveira Garabato et al., 2002b). The initial incursions of the WSDW into the Scotia Sea through the Jane Basin are estimated to have occurred in the middle Miocene (Maldonado et al. 2003, 2006).

In the study area, the LCDW flows eastwards (Orsi et al., 1995; Moore et al., 1997) above and farther north than the WSDW, which flows to the west (Fig. 1).

3. Data and methodology

Multichannel seismic reflection profiles (MCS) were acquired during two cruises (Fig. 1B) in the southwestern Scotia Sea on board the BIO Hespérides. The first survey obtained 1525 km of MCS profiles and the second gathered a total of 3560 km of MCS data. The first survey was carried out with a tuned array of seven Bolt air guns with a total volume of 16.3 l, and the second survey was carried out with a tuned array of six Bolt air guns with a total volume of 15.26 l. Both of them used a 96-channel streamer with an active length of 1.2 km and a shot interval of 50 m. MCS data were recorded with a DFS V digital system and a sampling record interval of 2 ms and 10 s record lengths. Data were processed with a standard protocol, including time migration using a DISCO/FOCUS system. We have focused on the seismic profiles located near the boundary between the Scotia and Antarctic plates and the extinct Phoenix Plate (Fig. 1B).

Basin-to-basin jump correlations including the correlation of the main reflections in the sedimentary record from the southwestern Scotia Sea to the Pacific Ocean across the SFZ have been based on the recognition of seismic facies and the acoustic characteristics of the underlying basement. Additionally, we have considered previous regional studies where the five younger units are correlated between the Weddell Sea and the southwestern Scotia Sea (Maldonado et al., 2003, 2005, 2006). The tentative age attributions of the main seismic discontinuities made by these authors considered: (a) the correlation of the ODP site 697 located in the Jane Basin with the western Scotia Sea for the younger main reflectors; and (b) the age of magnetic anomalies of the oceanic crust to estimate the ages of

the older discontinuities taking into account the stratigraphic sequence thickness observed at selected sites. In order to estimate the age of each reflector, Maldonado et al. (2003) defined a sedimentation rate curve for each stratigraphic section constrained by sedimentation rates of nearby surface sediment cores and of ODP boreholes located in the Antarctic Peninsula, the Jane Basin and the northern Weddell Sea.

In this paper, we describe the drifts around the triple junction region of the southern Drake Passage. We use the following classification criteria and terminology regarding contourite sedimentation: Contourites are defined as sediments deposited or substantially reworked by the persistent action of bottom currents. Bottom currents are capable of building thick and extensive accumulations of sediments. These sediment bodies are considered as “contourite drifts” or simply “drifts” (Faugères et al., 1999; Rebesco, 2005; Faugères and Stow, 2008; Rebesco and Camerlenghi, 2008; Rebesco et al., 2008). Erosional features, such as channels and moats, are identified throughout the study area. Contourite channels are erosional features trending parallel or oblique to the margin that are mainly formed by the action of bottom currents. Moats are channels trending parallel to the strike of the slope and are genetically associated with mounded, elongated, and separated drifts (Hernández-Molina et al., 2008). Sediment waves are a type of bedforms generated by the current activity that can be buried or on the modern seafloor superimposed on drifts (Faugères et al., 1999; Wynn and Masson, 2008).

We also estimate the minimum volumetric flow rate percentages of the WSDW through the two major branches, one flowing north along the eastern slope of the SFZ and another flowing towards the Pacific Ocean. The volumetric flow rate in both branches is given by the equation $Q = A \cdot v$, where A is the area of the flow's vertical section and v is the average flow velocity. Then we calculate $Q_{2,i}/Q_{1,i}$ for every main reflector from Reflector c upwards, with 1 and 2 being the main branches and i a specific reflector (see section 6).

4. Seismic stratigraphy

The MCS profiles show a succession of sedimentary units above the acoustic basement. The abyssal plain basement is characterized by high-amplitude discontinuous reflections and irregular diffractions above sparse, weak reflections, mainly attributed to igneous rocks. The basement is also identified in the continental margins and at some

locations of elevated seafloor, where it exhibits chaotic seismic facies. The abyssal plain basement is located at variable depths ranging from 0 s to 2.0 s (twtt) below the seafloor mainly due to irregularities in the basement surface.

Five main reflectors (e to a from bottom to top) constitute major discontinuities in the deep-water sedimentary record of the southwestern Scotia Sea. These reflectors delimit six seismic units (Unit 6 to Unit 1 from bottom to top). The unit boundaries are conformable or slightly erosional and are overlain by reflections which are either conformable or display downlap terminations.

The three oldest seismic units exhibit seismic facies that are distinctively different from the facies of the three younger units (Figs. 2 to 7). These younger units decrease in thickness to the south on both the Scotia and Phoenix plates, but are thinner on the Phoenix Plate. The younger units are deformed and affected by faults next to and over the SFZ in the Phoenix plate (Fig. 7). These deposits prograde southwards on the Phoenix Plate, whereas they exhibit east- and northeast-directed progradations on the Scotia Plate. The triple junction region is characterized by a morphological depression and a reduced or absent sediment cover.

4.1 Older units

Unit 6 is confined within deep basement depressions (Figs. 2). The unit shows an infilling geometry and its thickness varies from 0.05 s to 0.30 s (twtt) on the southwestern Scotia Plate (Fig. 2B) and from 0.03 s to 0.22 s (twtt) on the southeastern Phoenix Plate (Figs. 6B). Unit 6 exhibits low reflectivity and an aggradational configuration (Figs. 2A, 2C) with scarce, discontinuous internal reflections deformed by faults (Fig. 5B). The top boundary (Reflector e) is an irregular, laterally discontinuous erosional surface (Fig. 2B).

Unit 5 overlies either the igneous basement or Unit 6 and its distribution is more widespread than the underlying Unit 6 (Figs. 3). Overall, Unit 5 also shows infilling geometries (Figs. 2B) and thickness ranging from 0.05 s to 0.45 s (twtt) on the southwestern Scotia Plate (Fig. 3B) and between 0.07 s and 0.26 s (twtt) on the Phoenix Plate (Figs. 6B). The unit shows low reflectivity and an aggradational configuration (Fig. 3C), with parallel and discontinuous internal reflections that are disrupted by faults (Fig. 3A). Several well-identified sub-units with infilling geometries can be identified within the

unit on the study area of the Scotia Plate (Fig. 2A). Reflector d is an erosional surface that marks the top of Unit 5 and displays laterally variable amplitudes with low lateral continuity due to disruptions by basement highs and faults (Fig. 2).

Unit 4 overlies either Unit 5 or the basement (Figs. 5B). In general, its geometry is controlled by the basement morphology. Unit 4 shows infilling geometries with marked thickening towards the southwest on the Scotia Plate study area close to the boundary with the SSR and the SFZ (Fig. 2B). Unit thickness varies from 0.1 s to 0.7 s (twtt) on the southwestern Scotia Plate (Fig. 3B) and from 0.03 s to 0.32 s (twtt) on the southeastern Phoenix Plate (Fig. 6B). The unit locally progrades towards the south on the Phoenix Plate (Fig. 6). Toplap terminations and erosional truncations are locally observed (Fig. 5D). The unit increases in reflectivity and continuity towards the northeast of the study area, evolving laterally into chaotic seismic facies, whereas towards the west and southwest it shows erosional features (Fig. 4A). The deposits are deformed by tectonic features on the extreme southwestern Scotia Plate (Fig. 5B) and on the southeastern Phoenix Plate, where the unit displays erosional features (Fig. 6). The top boundary (Reflector c) is a high-amplitude regional reflector with erosional features and undulating relief due to tectonic influence (Fig. 4A).

4.2 Younger units

The three younger units (3, 2, and 1) are distinctive on the southwestern Scotia Plate, where they tend to show high lateral continuity, although there are also abundant internal erosional features and thickness variations (Fig. 3B). In contrast, on the southeastern Phoenix Plate, the main discontinuities above Reflector c are not clearly imaged due to the occurrence of landslides and tectonic disruptions in the proximity of the SFZ (Figs. 7).

Unit 3 lies above Reflector c on the Phoenix Plate or locally on top of basement highs on the southwestern Scotia Plate. It is wedge-shaped, thickening towards the west and southwest on the Scotia Plate (Figs. 2B). Unit thickness ranges between 0.05 s and 0.55 s (twtt), but generally increases to the east of the study area of the Scotia Sea (Fig. 2B) and is between 0.06 s and 0.35 s (twtt) on the Phoenix Plate, disappearing towards the South Shetland Trench (Fig. 6B). Internal reflections show high reflectivity (decreasing upwards)

on the eastern and northeastern studied area of the Scotia Plate (Fig. 4) and the unit is commonly sheet-like (Figs. 5E, 6). The internal configuration is characterized by parallel reflections on the Scotia Plate and by wavy to sub-parallel and discontinuous reflections with south-directed progradations or by erosional features on the Phoenix Plate. A prominent reflection is also identified within Unit 3, deformed by tectonic features (Fig. 3) in the Scotia Sea (Fig. 2A), where lateral continuity decreases towards the northeast and west of the study area of the Scotia Plate. The top boundary (Reflector b) is laterally continuous on the Scotia Plate and shows an undulatory pattern (Fig. 3C).

Unit 2 is located above Reflector b and is locally absent, particularly in the proximity of the continental margin, where moats are well developed (Figs. 4C, 6B). The deposits of Unit 2 are thicker on the western and southwestern Scotia Plate study area, and there is also a significant variation in thickness, from 0.05 s to 0.4 s (twtt), from the east to the west in both plates (Figs 3, 6). On the SFZ, this unit is not easily identified since the boundary with the youngest Unit 1 is not evident. Overall, Unit 2 shows infilling external shapes (Figs. 5B), but sheet-like geometries are dominant in the east and northeast (Fig. 3A). This unit exhibits onlap terminations (Fig. 3C) and an increase in abundance of high-amplitude sub-parallel internal reflections to the northeast (Figs. 3A, 4A). Erosional features are observed in the shallower reflections and the top boundary (Reflector a) is a laterally discontinuous, high-amplitude reflection.

Unit 1 is the youngest deposit above Reflector a and is relatively thin and continuous (Figs. 3B, 5B), becoming thinner to the east (Fig. 3B). The maximum thickness in the study area is 0.3 s (twtt) on the Scotia Plate and 0.16 s (twtt) on the Phoenix Plate (Figs. 5B, 6B). Its geometry is sheet-like (Fig. 5), with a reflective acoustic response at the base and more transparent upwards. The unit exhibits sub-parallel, high-amplitude, and high-continuity reflections (Fig. 4).

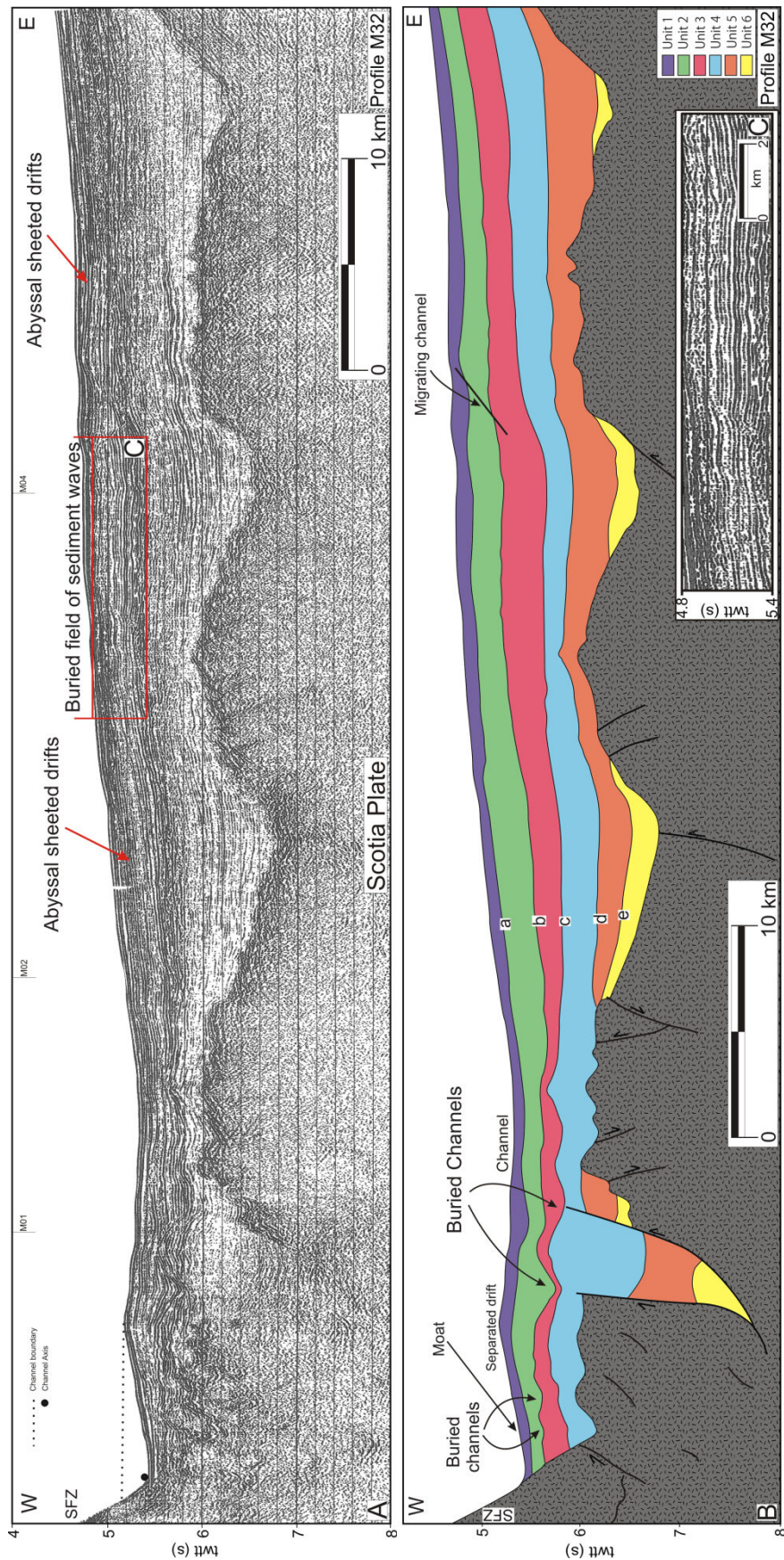


Figure 2. A) MCS of Profile M32 (see Fig. 1 B for location), SFZ, Shackleton Fracture Zone. B) Main seismic units and Reflectors a to e are represented, as well as main sedimentary features. C) Detail of seismic signal of the sediment wave field. See Sections 4 and 5 for details. Vertical scales are expanded in B and C.

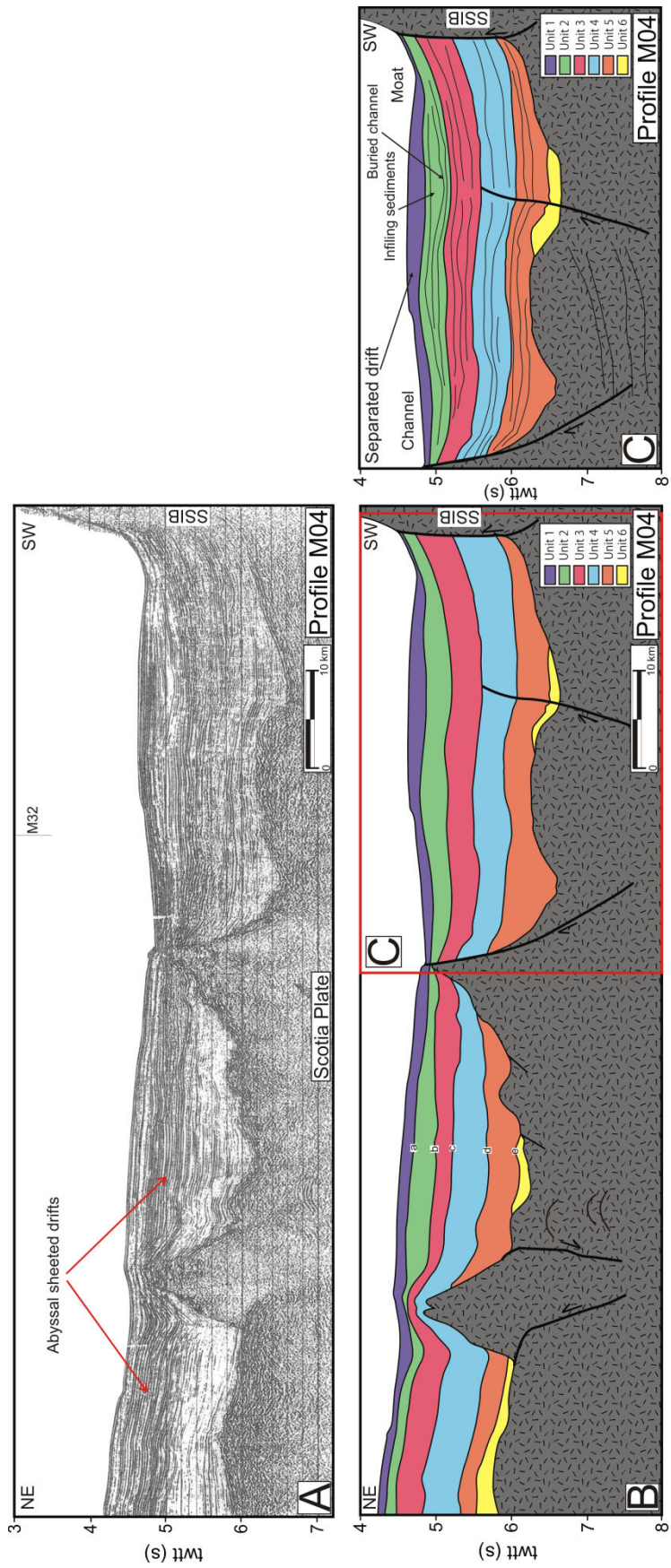


Figure 3. A) MCS of Profile M04 (see Fig. 1 B for location). SSIB, South Shetland Island Block. B) Interpretation with main seismic units and Reflectors a to e (see Sections 4 and 5 for details). C) Description of main seismic features (vertical scale is expanded).

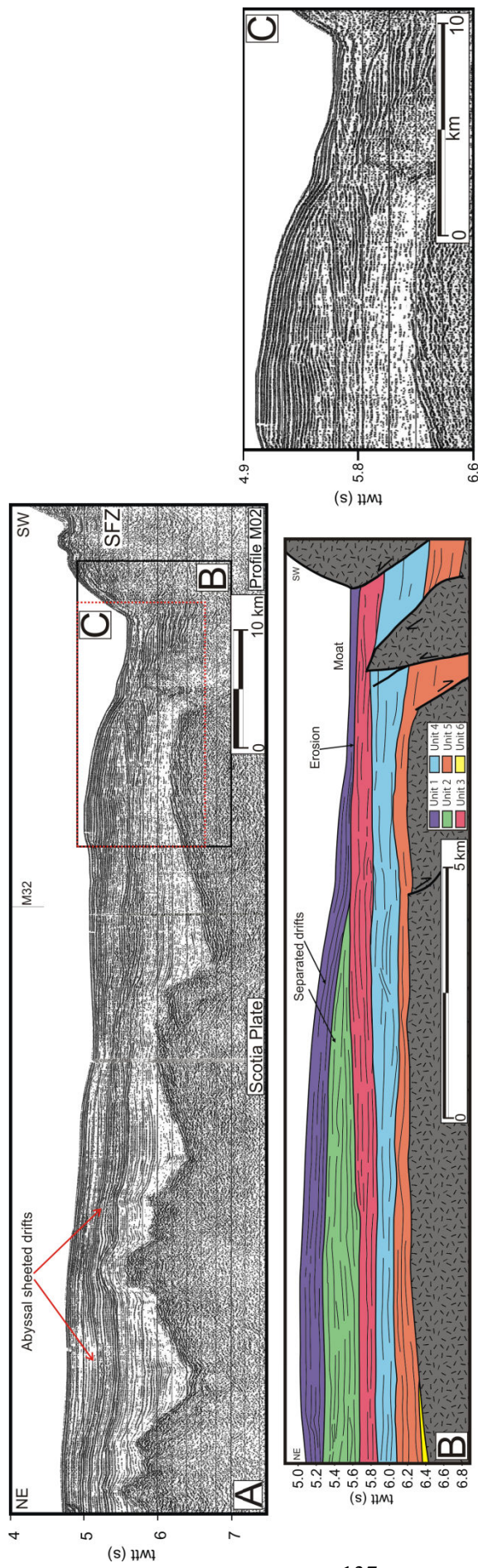


Figure 4. Reinterpretation of Profile M02, from Maldonado et al. (2006) (their figure 7B). A) MCS of Profile M02 (see Fig. 1 B for location). SFZ, Shackleton Fracture Zone. B) A detailed interpretation of the seismic profile with main Reflectors (a to e) and units. C) Detail of the seismic signal of the mounded elongated and separated drift.

See Sections 4 and 5 for details. Vertical scales are expanded in B and C.

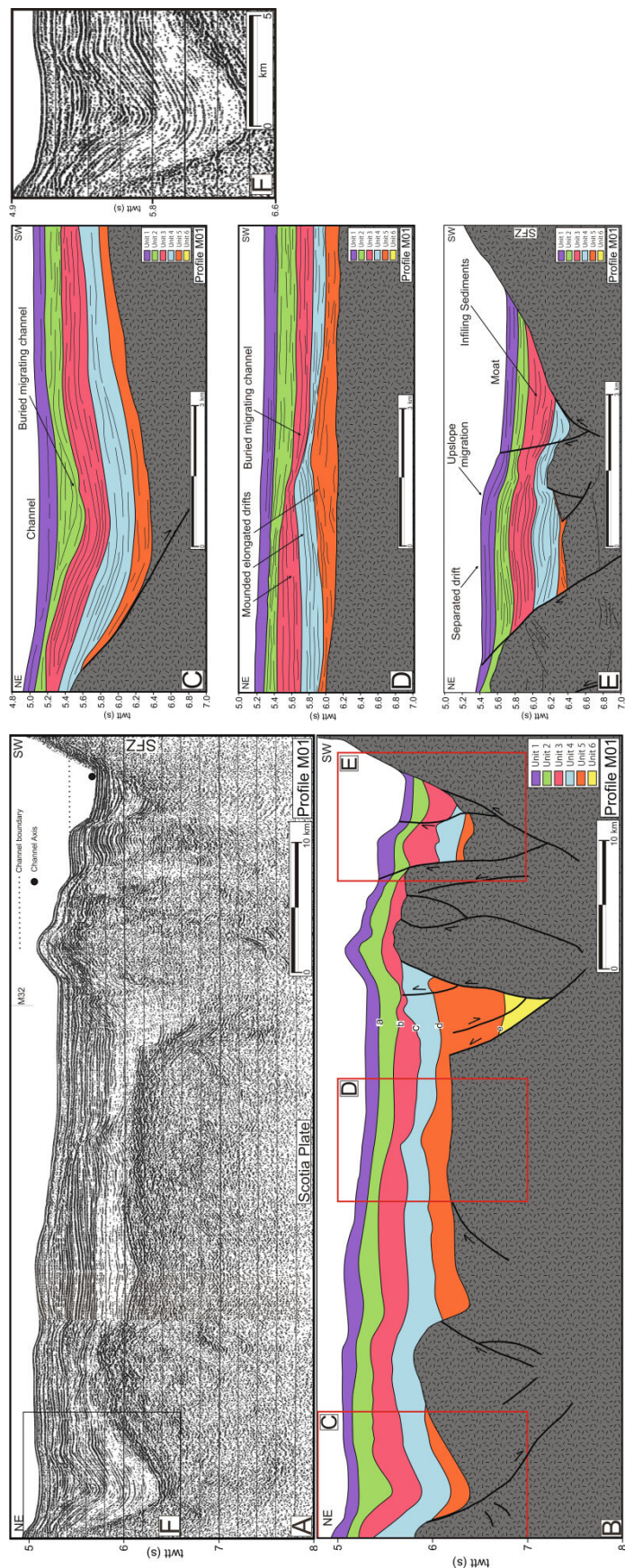


Figure 5. A) Seismic Profile M01 (see Fig. 1 B for location). SFZ, Shackleton Fracture Zone. B) Main seismic units and Reflectors a to e are shown here. C), D) and E) are detailed interpretations of three interesting parts of the profile (see Sections 4 and 5 for details). F) Detail of the seismic signal of the buried migrating channel. The vertical scale is expanded in C, D, E and F.

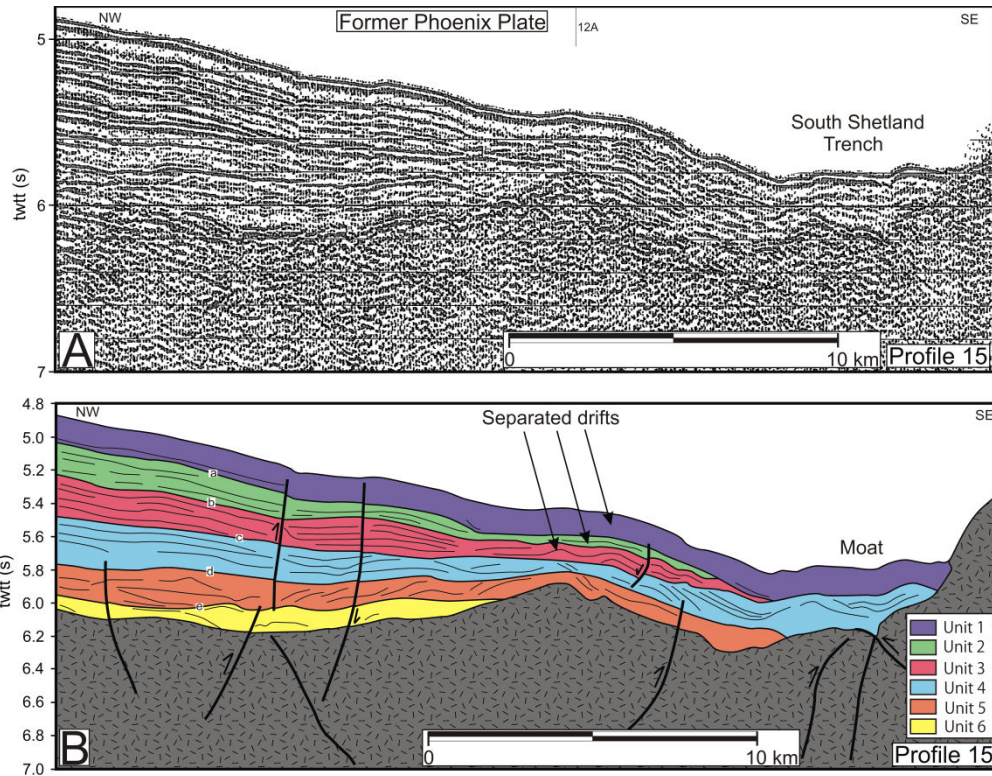


Figure 6. A) MCS of Profile 15 (see Fig. 1 B for location). B) Detailed interpretation of the seismic profile. Main seismic units and Reflectors a to e are marked, as well as the main seismic features (see Sections 4 and 5 for details).

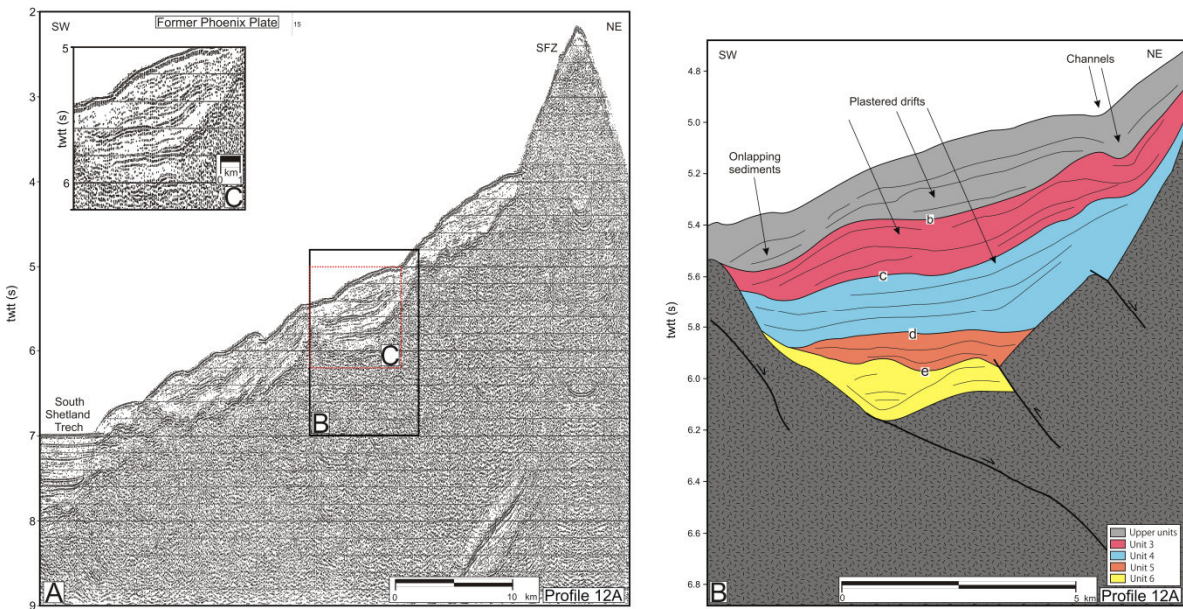


Figure 7. A) Seismic signal of Profile 12A (see Fig. 1 B for location). SFZ, Shackleton Fracture Zone. B) Detailed interpretation of a part of the profile. It has not been possible to delimit Units 1 and 2. C) Detail of the seismic signal of the plastered drifts. See Sections 4 and 5 for details. Vertical scales are expanded.

5. Geometry of drifts and erosional features

5.1 Scotia Plate

Two main types of drifts are identified in the southwestern region of the Scotia Sea: mounded elongated drifts and abyssal-sheeted drifts (Figs. 8A, C). Mounded elongated drifts are characterized by aggrading to prograding continuous convex-upward seismic reflectors (Figs. 2, 5D). Mounded elongated and separated drifts (hereafter separated drift for simplicity) occur at the base of steep slopes adjacent to the SFZ and the South Shetland Island Block (Figs. 2B, 3C, 4B, 5E, 8) and are characterized by convex-up lenticular reflections with upslope migration trends. Separated drifts are larger above Reflector b (Fig. 4C), although in the proximity of the SFZ they are observed in the four youngest units (Figs. 5E). These mounded drifts have high relief (200–450 m above the surrounding seafloor) and widths of 4.5 to 20 km. Abyssal-sheeted drifts are more extensive towards the northeast part of the study area, where they cover large areas of the abyssal plain (Figs. 8B, 8C) and are characterized by flat-lying, continuous sub-parallel reflections. Down section, the reflections become less continuous and less abundant.

Buried channels and moats are frequently observed in the sedimentary record (Figs. 3C, 5C, F). Some of these channels display significant vertical and lateral migrations (Figs. 3A 5C, D, F). Profile M01 (Fig. 5), for example, shows a channel migrating northeastwards from Reflector c to Reflector b (Fig. 5D), whereas another channel migrates southwestwards from Reflector b to Reflector a (Fig. 5C, F). The seafloor also reveals a host of moats and channels that were active during the deposition of Units 1 and 2 (Figs. 2B, 3C, 4B, 5C, E).

A buried field of sediment waves with a wavelength of 1-4 km (Fig. 2A, C) has been identified within Unit 2.

5.2 Phoenix Plate

The identification of sedimentary deposits is difficult on the Phoenix Plate because the units are largely deformed by tectonic features and mass gravity processes induced by the plate subduction and SFZ uplift (Fig. 7). However, several separated and plastered drifts can be identified in this region.

Separated drifts are attached to the SFZ from Units 4 to 1 (Fig. 6B) and show high

relief (about 200 m) with upslope migration (Fig. 6B). The drifts are 5 to 6.5 km wide and are characterized by convex-up mounded reflectors. Plastered drifts are best developed in the western slope of the SFZ where they infill small depressions (Fig. 7B). These drifts contain reflections parallel to the basement topography.

Contourite channels and moats are common on the Phoenix Plate, where they are more developed than on the southwestern Scotia Plate. Moats are identified from Reflector d upwards (and locally throughout the stratigraphic section) (Fig. 6B, 9).

6. Temporal evolution of channels and moats

The evolution and distribution of contourite erosional features (channels and moats) in the sedimentary record are described herein (Fig. 9). Channels show a general southward migration from the basement to Reflector d (Fig. 9B, 9C) and a northward migration above this reflector (Fig. 9D, 9E). Channels and moats in the South Shetland Trench are observed throughout the entire sedimentary sequence. Channels are generally stable through time in the Scotia Sea abyssal plain. Channels are observed above Reflector d close to the SSR (Fig. 9C) and above Reflector c close to the SFZ (Fig. 9D).

Channels and moats are more developed close to the bases of ridges. Taking into account the information from sections 4 and 5 we consider that erosional features observed upwards from Reflector c are due to bottom-current activity while depressions or channels observed downwards from Reflector c have been mainly controlled by the tectonic features. It is also evident that the influence of bottom currents close to the SFZ and to the SSR increases from Reflector c upwards. The bottom current that flows westwards along the SSR base-of-slope is intersected by the SFZ and it forces a branch diversion towards the northwest (Branch 1) and a southwestward branch diversion aided by the Coriolis force (Branch 2), entering the Pacific Ocean (Fig. 8, 9). Branch 2 flows between the two major bottom reliefs of the SFZ and the South Shetland Islands Block through a narrow, confined passage where the flows intensify (Nowlin and Zenk, 1988).

We have estimated the minimum percentage of the volumetric flow rate in these two major branches from Reflector c age to the present. The calculation indicates the main core of the flow generated by the water masses due to the relief, but not the total associated water mass. The volumetric flow rate in both branches can be described by the equation

$Q=A \cdot v$, where Q represents the discharge, A is the area of the moat and v is the velocity of the current. Taking into account the sections of the moats we can deduce that the flow velocity in Branch 2 has been higher than in Branch 1 (see Fig. 9) since the moat is more developed in Branch 2 (Figs. 5E, 2B). Using the information derived from the MCS profiles (Figs. 2, 5), we have been able to calculate the cross-sectional areas of the moats and channels. Given the discharge that reaches the SFZ, namely Q_i , and considering that it is divided into two branches, $Q_{1,i}$ and $Q_{2,i}$ (where they are related by $Q_i = Q_{1,i} + Q_{2,i}$ and i represents the reflector under study), it is possible to estimate the proportion of the total core flow that is diverted through each branch.

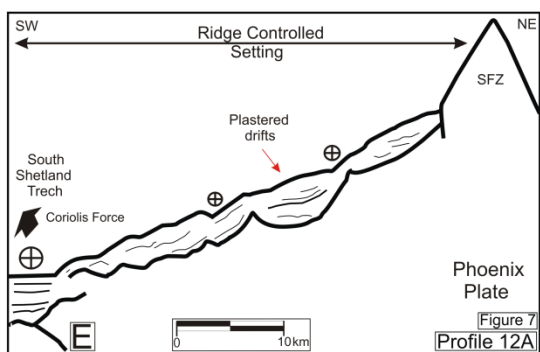
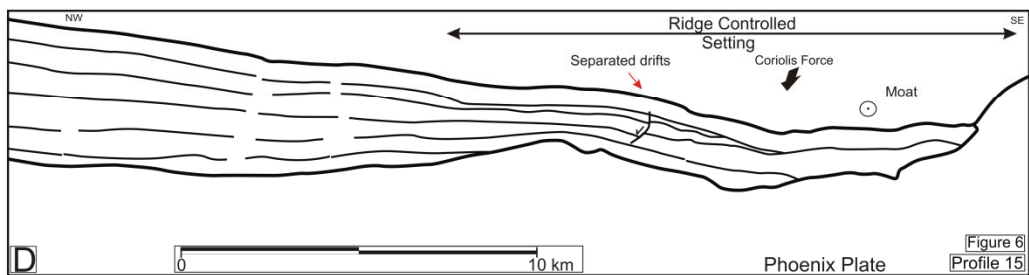
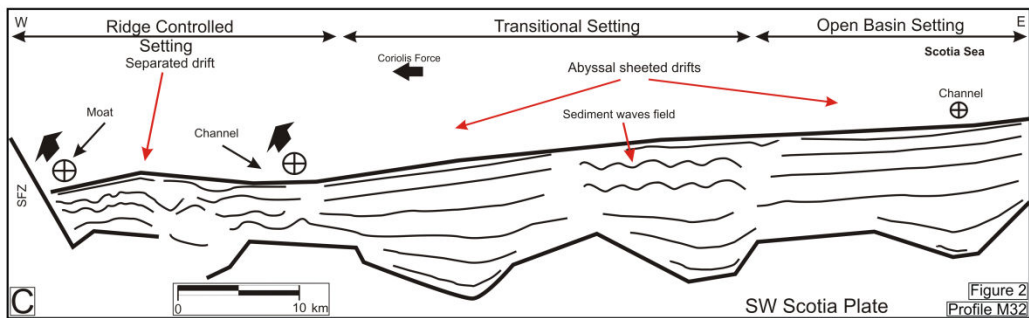
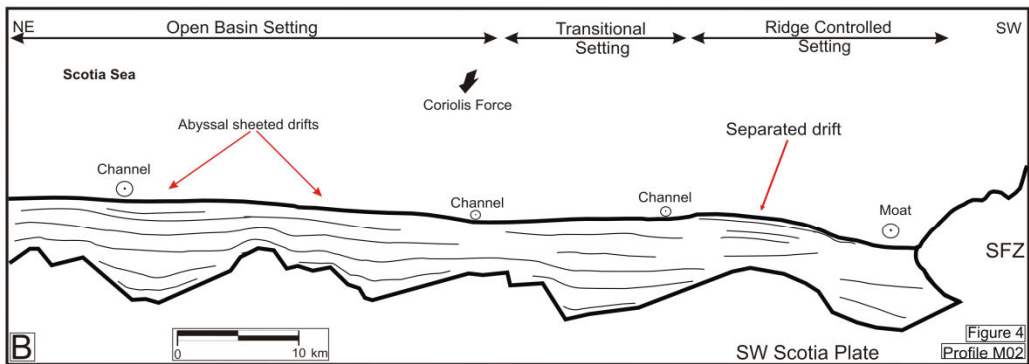
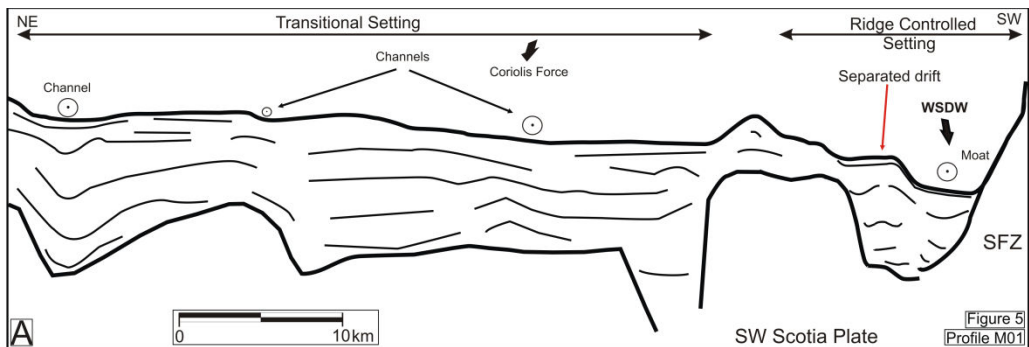
We have estimated the cross-sectional areas of the moats for every major discontinuity, from Reflector c to the seafloor. A straightforward calculation shows that, in the limit where the flow velocities in each branch are equal ($v_1 = v_2$), we can evaluate the quotients $Q_{1,i}/Q_i$ and $Q_{2,i}/Q_i$:

$$\frac{Q_{1,i}}{Q_i} = \frac{v_{1,i} \cdot A_{1,i}}{v_{1,i} \cdot A_{1,i} + v_{2,i} \cdot A_{2,i}} \xrightarrow{v_{1,i}=v_{2,i}} \frac{Q_{1,i}}{Q_i} = \frac{A_{1,i}}{A_{1,i} + A_{2,i}} \quad (1)$$

$$\frac{Q_{2,i}}{Q_i} = \frac{v_{2,i} \cdot A_{2,i}}{v_{1,i} \cdot A_{1,i} + v_{2,i} \cdot A_{2,i}} \xrightarrow{v_{1,i}=v_{2,i}} \frac{Q_{2,i}}{Q_i} = \frac{A_{2,i}}{A_{1,i} + A_{2,i}}$$

Afterwards, taking into account the assumption (i.e., the real situation), $v_1 < v_2$, we have calculated the inequalities $Q_{1,i}/Q_i < 1$ and $Q_{2,i}/Q_i < 1$. Then, we can obtain the relationship between $Q_{2,i}$ and $Q_{1,i}$ as a quotient, $Q_{2,i}/Q_{1,i}$. This quotient is totally independent of the absolute velocity or the initial transport in the limit where $v_1 = v_2$ (and the same can be applied to the quotients $Q_{1,i}/Q_i$ and $Q_{2,i}/Q_i$). This calculation depicts the

Figure 8. Generalized schematic drawings (not to scale) based on MCS profile cross-sections of the southwestern Scotia Sea and the southeastern Phoenix Plate. Open basin, transitional, and ridge-controlled depositional environmental settings are indicated in the figure. The open basin setting corresponds to the abyssal plain, whereas the ridge-controlled setting is represented by the base of slope of the SSR and the slopes of the SFZ; a transitional setting is identified in between both of them. A) Section across southwestern Scotia Sea from the SFZ that shows an extensive control of basement topography on the development of drifts. B) Section across the southwestern Scotia Sea from the SFZ. C) Section parallel to the SSR that shows the main contourite drifts. D) Section across the southeastern Phoenix Plate reaching the South Shetland Trench. E) Section crossing the Shackleton Fracture Zone. See Figure 1 B for location and Figures 2, 3, 4, and 5 for details.



relationship that the volumetric flow rate must satisfy in this area taking into account the observations and results obtained from the analysis of the MCS profiles, as well as the assumption $v_1 < v_2$. Calculated values for Reflector c ($Q_{2,c}/Q_{1,c} > 0.22$, where A_1 is 2.46 km^2 and A_2 is 0.55 km^2), Reflector a ($Q_{2,a}/Q_{1,a} > 0.27$, where A_1 is 3.05 km^2 and A_2 is 0.83 km^2), and the seafloor ($Q_{2,s}/Q_{1,s} > 0.38$, where A_1 is 2.38 km^2 and A_2 is 0.9 km^2) are similar. However, the quotient is very high for Reflector b ($Q_{2,b}/Q_{1,b} > 0.78$, where A_1 is 1.11 km^2 and A_2 is 0.87 km^2).

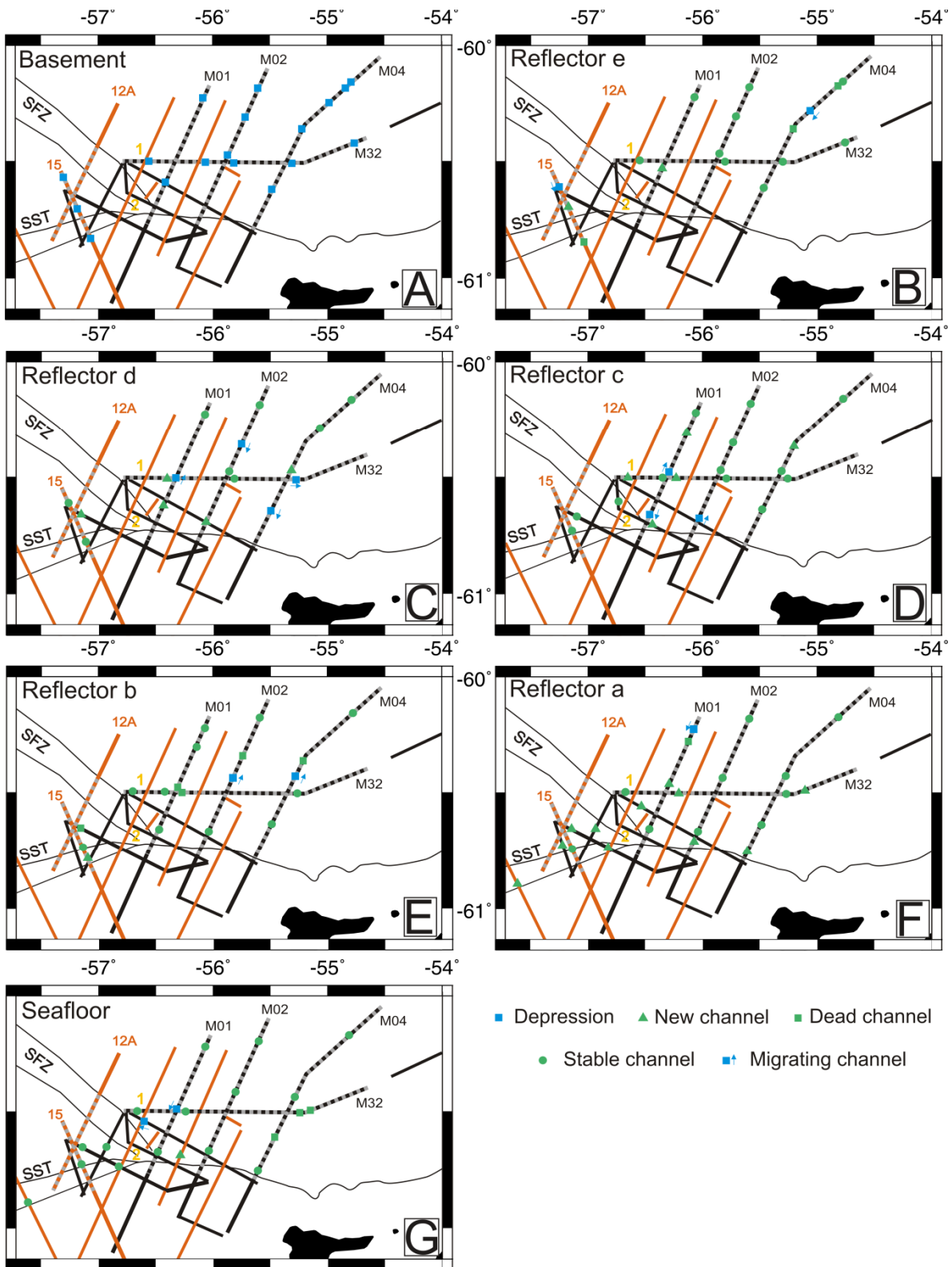
7. Discussion

The morphological and tectonic evolution of the southern Drake Passage has influenced the circulation of the main deep-water masses throughout the area. The interaction between the eastward flows of the LCDW and the westward flows of the WSDW resulted in a host of depositional and erosional bottom features that attest to the action of the bottom currents on the seafloor, which in turn was continuously conditioned by active regional tectonics.

7.1 Drifts and erosional features

Most of the sediments above the igneous oceanic crust in the southern Drake Passage record a significant influence of bottom currents on both sides of the SFZ, and the major stratigraphic discontinuities can be traced across the region. The distribution of the oldest deposits below seismic Reflector c is largely related to the location of depressions in the igneous basement controlled by the tectonic activity of the area. In contrast, bottom relief was less influential in controlling the distribution of the younger deposits. Instead the distribution and characteristics of bottom currents became progressively more influential in the growth patterns of those deposits as observed in other nearby areas (Maldonado et al., 2006).

Figure 9. Channel and moat evolution in the study area. Profiles from ANT92 (orange lines) and HESANT92/93 (black lines) cruises and the two main branches of bottom-current flow from the Weddell Sea reaching the Shackleton Fracture Zone. Branches 1 and 2 are represented by 1 and 2 in the figure. Grey dashed lines represent the profiles shown in this study. A) Depression distribution at basement time. We consider basement time as the start time. B) Channel evolution and distribution at Reflector e time. C) Channel evolution and distribution at Reflector d time. D) Channel evolution and distribution at Reflector c time. E) Channel evolution and distribution at Reflector b time. F) Channel evolution and distribution at Reflector a time. G) Channel evolution and distribution in the present. SFZ, Shackleton Fracture Zone. SST, South Shetland Trench. Elephant Island is shown on the map.



Three physiographic settings have been identified based on the bathymetric control (Fig. 8): open basin, transitional, and ridge-controlled. The open basin setting is located in areas with subdued relief, such as the abyssal plains of the Scotia and Phoenix plates (Figs. 8B, 8C), where sheeted drifts occur throughout the entire sedimentary sequence. The transitional setting is located in the transition between the continental margin or ridges and the abyssal plains (Figs. 8, 9) and is characterized by an abundance of drift deposits crossed by buried contourite channels and with local superimposed sediment waves. The ridge-controlled setting is defined by areas where the flows are more restricted by tectonics and seafloor relief, and separated drifts prevail (Fig. 8).

The ridge-controlled setting evolved over time due to tectonic and bottom-current influence. The SSR has been a prominent relief throughout the depositional history, although its influence as a ridge-controlled setting in the older deposits does not seem to be significant as these deposits do not show extensive occurrence of moats or separated drifts, but rather sheeted or wedge geometries (Figs. 2B, 3B). A major change is observed at Reflector c, when moats and separated drifts indicative of the ridge-controlled setting became more abundant (Figs. 4C, 5E, 9). The onset of the ridge-controlled setting after Reflector c was also favoured by SFZ uplift, which instigated the formation of mounded drifts and moats around that relief (Fig. 9D).

Conspicuous evidence of bottom current activity in the study area is observed within the sedimentary record. The tectonic activity during the deposition of the older units constrained the bottom flow circulation and the evolution of depositional processes, as recorded by large depressions, moats and channels associated to those units (eg. South Shetland Trench formed a moat). This was caused by the initiation of deep gateways and passages along the SSR (Schodlok et al., 2002; Maldonado et al., 2003; Galindo-Zaldívar et al., 2006; Maldonado et al., 2006; Bohoyo et al., 2007; Carter et al., 2008) that allowed the flow of the Weddell water masses into the Scotia Sea and eventually into the Pacific Ocean (Hernández-Molina et al., 2006). However, the most significant intensification and widest distribution of bottom currents occurred above Reflector c in Unit 3. Units 3, 2, and 1 show evidence of intense flow activity as revealed by the extensive occurrence of moats, channels, and contourite deposits.

The initial incursions of the WSDW into the Scotia Sea, through the Jane Basin, and into the Pacific margin of the Antarctic Peninsula occurred around the middle Miocene (Maldonado et al., 2003; Hernández-Molina et al., 2004, 2006). Therefore, the older deposits in the study area are considered to have been affected by the LCDW, whereas the younger deposits were mainly affected by the WSDW (Fig. 10). The LCDW flowed eastwards in the southern Drake Passage through the initial corridors and basins opening between the continental blocks (Fig. 10A), whereas the WSDW entered the Scotia Sea later thanks to the opening of new passages through the SSR (Fig. 10B). The regional channel migration between Reflectors c and b (Fig. 9D, 9E) is attributed to the emplacement of the westward WSDW flows coeval with the uplift of the SFZ (see Section 7.2), which displaced the CDW to the north (Figs. 10B, 10C).

7.2 Tectonic evolution

Earlier studies suggested that deep-water flows were inhibited in the Drake Passage by overlapping continental slivers along the SFZ until about 23.5 Ma (Barker and Burrell, 1977; Barker, 2001). In contrast, more recent interpretations have proposed that the SFZ is a recent feature that began to behave as a barrier only after 8 Ma (late Miocene) (Livermore et al., 2004). These authors inferred a small change in the pole of rotation that led to the clockwise realignment of the ridge in the west Scotia Plate, which became oblique to the older fabric after circa 8 Ma.

The structure, geometry, and distribution of the seismic units in the study area indicate a progressive tilting of the sedimentary units on the margins of the SFZ. The tilting is marked above Reflector c and the units are deformed and affected by faults (Fig. 7). The deposits are prograding to the south on the Phoenix Plate, whereas they exhibit east- and northeast-directed progradations on the Scotia Plate. Assuming that the estimated age of Reflector c is middle Miocene (~12 Ma) (Maldonado et al., 2003, 2005, 2006), the SFZ initiated as an oceanic ridge in the middle Miocene, coinciding with the onset of the permanent East Antarctic Ice Sheet (Vincent and Berger, 1985; Flower and Kennett, 1994; Zachos et al., 2001) and with tundra landscape that persisted until at least 12.8 Ma in the Antarctic Peninsula (Anderson et al., 2011). During this initial phase, the ridge modified the water masses flow across the Drake Passage (Fig. 10B), but the deposits composing the

older units indicate that the SFZ was ineffective at inhibiting the connection between the Pacific Ocean and the Scotia Sea. The change in the Euler pole 8 Ma ago, proposed by Livermore et al. (2004), probably subsequently augmented the uplift. Compression in the southern SFZ can be linked to the changing plate motion and rotation poles likely due to the higher activity of the Pacific and African superplumes during the middle and late Miocene (Potter and Szatmari, 2009), including the development of new oceanic basins during the Miocene east of the southwestern Scotia Sea along the SSR (Galindo-Zaldívar et al., 2006). At 8 Ma, the LCDW moved farther north because of SFZ uplift (Fig. 10C), coeval with the northward expansion of the Antarctic Peninsula and the grounding cycles of the East Antarctic and West Antarctic ice sheets (Maldonado et al., 2000; Bart et al., 2005; Anderson, 2006; Anderson and Wellner, 2011; Smith and Anderson, 2011).

7.3 Palaeoceanographic implications

The Eocene-Oligocene transition is known as one of the most significant changes in the Earth's climate (Miller and Mabin, 1998; Zachos et al., 2001). During the earliest Oligocene, a major change in water temperature in the southern oceans was apparently related to the opening of deepwater seaways (Kennett and Stott, 1990; Mead et al., 1993). It is widely accepted that the Scotia Sea region was the location of the final barrier to a complete circum-Antarctic deep-water flow, although its timing, consequences, and significance for the evolution of global climate are still a subject of debate (Lawver et al., 1992; Barrett, 1996; Barker, 2001).

The opening of the Drake Passage allowed the onset of the ACC flow, and the consequent thermal isolation of the Antarctic continent (Kennett, 1977). The initial incursions of the WSDW are proposed to have occurred during the middle Miocene (Maldonado et al., 2003), but nowadays the WSDW escapes towards the Scotia Sea through several other passages located in the SSR region, such as the Bruce, Orkney, and Discovery passages for the lower fraction of the WSDW, and the Philips Passage for the upper fraction of the WSDW (Fig. 1) (Naveira Garabato et al., 2002b; Schodlok et al., 2002). Although several authors have studied how and where the WSDW escapes from the Weddell Sea into the southern Scotia Sea (Fahrbach et al., 1991; Gordon et al., 2001; Visbeck et al., 2001; Schodlok et al., 2002; Naveira Garabato et al., 2003), the analysis of

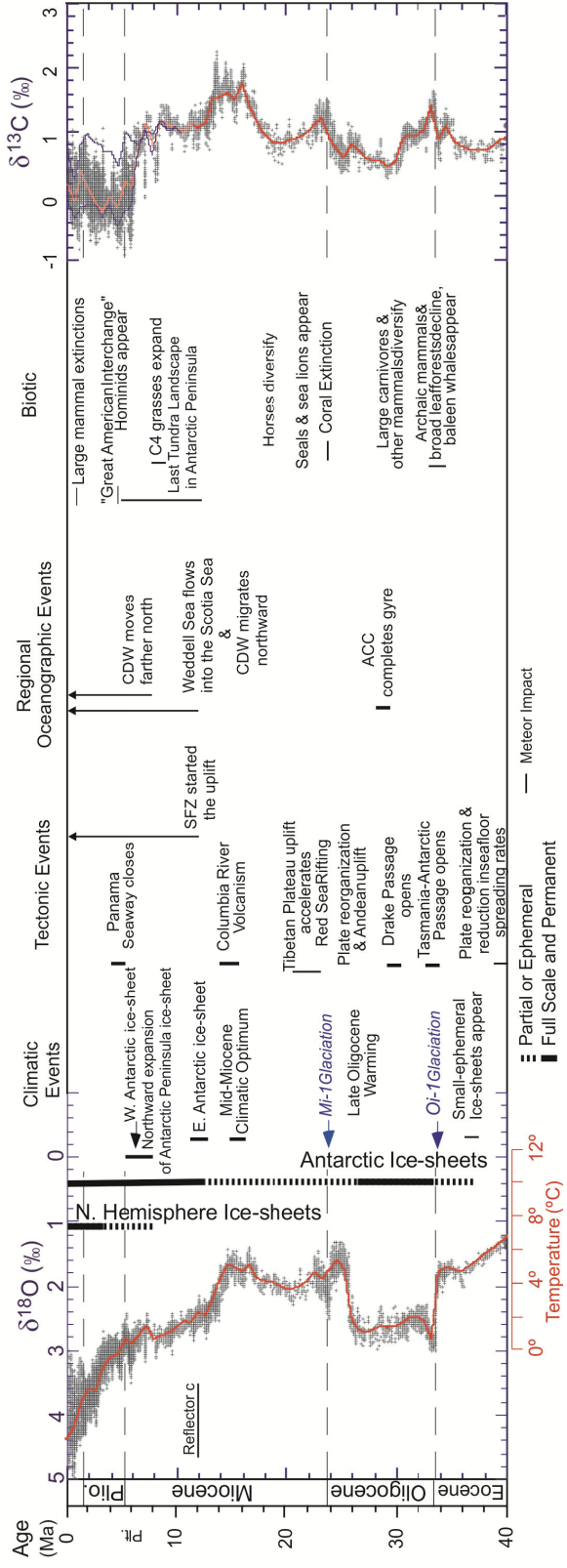
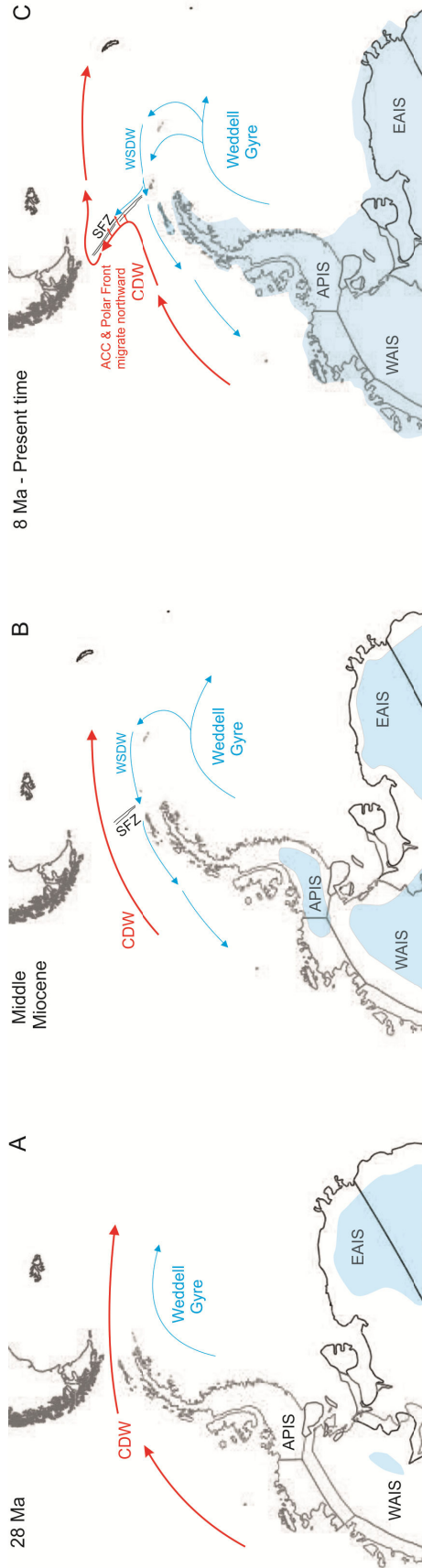
these flows in the area of the triple junction of the southern Drake Passage is still poorly constrained.

Erosional features are most highly developed next to ridges, suggesting an intensification of bottom-current activity along the flanks of these topographic highs. The tectonic influence of the SSR can be detected from Reflector d upwards (Fig. 9C) and is still active at present. Erosional features next to the SFZ have been forming since the middle Miocene (Fig. 9D), and WSDW effects are identified close to the SSR since the formation of Reflector c. In addition, migrating channels are widespread (Figs. 2, 5), and they record the evolution of bottom currents through time (Fig. 9). Taking into account the evolution of the channels and moats (Fig. 9), it can be observed that the LCDW has influenced the seafloor far from the SSR since the basement formation to the present day. Besides, channel generation through the stratigraphic column occur at the same locations in the northeastern study area.

SFZ uplift has influenced the distribution of nearby channels and moats (Fig. 9D) since channels formed and migrated around the structure. The high value of the $Q_{2,i}/Q_{1,i}$ quotient at Reflector b is probably related to the stronger incursions of the WSDW into the area, as well as to SFZ uplift. In addition, some channels that were active until Reflector c generation are not observed afterwards, and the influence of the LCDW is not observed in the southwestern part of the study area (Fig. 9D,E). The value of the $Q_{2,i}/Q_{1,i}$ quotient decreased at Reflector a, when Branch 1 became more important and the water masses approached new conditions after the significant WSDW incursion. Although the bottom-current distribution and the tectonic setting are very similar in this area for the Reflector a and for the present, the water mass flow through Branch 2 is proportionately a little higher nowadays (Fig. 9F, 9G). Once the flow crosses the narrow corridor between the SFZ and the South Shetland Islands Block, it splits into additional minor branches, influenced by the bathymetric highs in the southeastern corner of the Phoenix Plate (Fig. 9). Most of the flow, however, continues southwestwards confined by the South Shetland Trench.

7.4 Evolutionary stages

The oceanographic, climate and tectonic evolution can be summarized as follow:



a. Tectonic and water masses distribution around 28 Ma

The CDW flows eastwards through the small opening between South America and Antarctica (Fig. 10A). Deep-water masses that circulated into the Weddell Gyre could not flow into the Scotia Sea by that time. Some small ice sheets start to grow on the continent.

b. Tectonic and water masses distribution during the middle Miocene

The SFZ begins the uplift and water masses from the Weddell Sea start to enter the Scotia Sea. The LCDW migrates northwards, allowing the WSDW to flow to the Pacific Ocean (Fig. 10B). The EAIS becomes permanent and isolated ice sheets grow in the West Antarctica and in the Antarctic Peninsula (Vincent and Berger, 1985; Flower and Kennett, 1994; Zachos et al., 2001) (see summary table of figure 10). The ice-sheet formation in this step of the thermal isolation evolution is also based on the studies of Miller et al. (2008), who propose about an 80 m sea-level fall for the middle Miocene and a greater decrease up to nowadays.

c. Tectonic and water masses distribution over the last 8 Ma

The uplift of the SFZ forced the LCDW to move northward farther from Antarctica (Fig. 10C), favouring the thermal isolation of the area and in coincidence with the ice-sheet grounding cycle in the East Antarctica, Antarctic Peninsula, and West Antarctica (Maldonado et al., 2000; Livermore et al., 2004; Bart et al., 2005; Anderson and Wellner, 2011; Smith and Anderson, 2011) (see summary table of figure 10). The WDSW enters the Scotia Sea through several passages and it is divided into two main branches when the current is intersected by the SFZ.

Figure 10. Idealized sketch of bottom-current evolution and thermal isolation of Antarctica as a result of the opening of the Drake Passage and the start of the Circumpolar Deep Water (CDW), the uplift of the Shackleton Fracture Zone, and the incursions of water masses from the Weddell Sea. The tectonic reconstruction has been made using GPlates software (Boyden et al, 2011). Blue areas represent the general ice-sheet distribution for each period. CDW, Circumpolar Deep Water; WSDW, Weddell Sea Deep Water; SFZ, Shackleton Fracture Zone; APIS, Antarctic Peninsula Ice Sheet; WAIS, West Antarctic Ice Sheet; EAIS, East Antarctic Ice Sheet. A) Tectonic and water masses distribution around 28 Ma. B) Tectonic and water masses distribution during the middle Miocene. C) Tectonic and water masses distribution over the last 8 Ma. Summary table of $\delta^{18}\text{O}$ and $\delta^{13}\text{C}$ records, key climatic, tectonic, regional oceanographic and biotic events from 40 Ma to present (based and modified of Zachos et al. (2001)). Global deep-sea $\delta^{18}\text{O}$ record based on data compiled from DSDP and ODP sites by Zachos et al. (2001). Key climatic events and the development of Antarctic ice-sheets are shown by vertical bars that provide a rough qualitative indication of ice volume (Zachos et al. 2001). The time spans of key tectonic events are represented by vertical bars or arrows, as well as the regional oceanographic events and main biotic events. Reflector c is shown in the table.

8. Conclusions

Sedimentary evolution, tectonics, mantle dynamics, palaeoceanographic and climate-change processes are linked in the study of the triple junction region in the southern Drake Passage. The main contributions of this work are summarized in the following points:

1. Evidence of bottom-current activity in the southern Drake Passage is observed throughout the entire sedimentary record. The features observed in the older units seem to be the result of the influence of the initial CDW flows whose trajectories were controlled by tectonic depressions. In contrast, the sediment bodies composing the younger units are interpreted as drift deposits that evolved under the combined effects of WSDW and CDW flows.

2. The SFZ may have initiated as an oceanic ridge before the middle Miocene. The SFZ proto-relief, together with the initial incursions of the WSDW, forced the ACC and the Polar Front to move northwards, away from Antarctica, favouring the thermal isolation of the Antarctic region (Fig. 10B) and, coeval with the onset of the permanent East Antarctic Ice Sheet and with tundra landscape that persisted until at least 12.8 Ma in the Antarctic Peninsula (see summary table of figure 10). Subsequently, around 8 Ma, the LCDW was displaced even farther north because of SFZ uplift (Fig. 10C). This process caused an additional impact on the thermal isolation of Antarctica and on global climate change, as the Antarctic Peninsula, East Antarctic, and West Antarctic ice sheets grounded.

3. The influence of bottom currents became the controlling factor above Reflector c. Erosional features were more conspicuous and larger, occurring in distinctive patterns that contrast with the underlying strata. These erosional features are more conspicuous adjacent to ridges, suggesting an intensification of bottom-current activity due to the opening of deep gateways located along the SSR and to the deflection of the flows. Since the age of Reflector c, the WSDW has escaped from the Weddell Sea through these small passages, and flowed westwards along the SSR until intersecting with the SFZ. As a consequence, a part of the current is diverted northwards, whereas the remaining flow continues southwestwards into the Pacific Ocean, aided by the Coriolis force.

Acknowledgements

This work was supported by CGL2004-05646/ANT, CTM2008-06386-C02/ANT, CTM2011-30241-CO2-01, CTM 2008-06399-C04/MAR and CTM 2012-39599-C03, IGCP 619 and INQUA 1204 projects and by a predoctoral fellowship of the "Ministerio de Ciencia e Innovación" of Spain (FPI). This work also has been benefited for two research stages abroad funded by the FPI program. F.J. Hernández-Molina contributed to this work throughout a research stage at Heriot-Watt University (UK) during his sabbatical year in 2013. L.F.P. thanks the JAE-predoc grant of the CSIC. Generic Mapping Tools and GPlates software have been used in this work. The English style of the manuscript was thoroughly reviewed by Christine Laurin. We thank the positive comments and suggestions from Dr. Robert Later and Dr. John Anderson as reviewers who helped us to improve the final version of this manuscript.

Chapter 9

INITIAL STAGES OF OCEANIC SPREADING IN THE BRANSFIELD RIFT FROM MAGNETIC AND GRAVITY DATA ANALYSIS

Published in:
Tectonophysics
Vol. 585,102-112

Received 14 July 2011
Received in revised form 16 July 2012
Accepted 13 September 2012

Initial stages of oceanic spreading in the Bransfield Rift from magnetic and gravity data analysis

Manuel Catalán^{1*}, Jesús Galindo-Zaldivar^{2,3}, José Martín Davila¹, Yasmina M. Martos², Andrés Maldonado², L. Gambôa⁴ and A.A. Schreider⁵

1 Real instituto y Observatorio de la Armada. San Fernando, 11100, Cádiz (Spain).

2 Instituto Andaluz de Ciencias de la Tierra (CSIC/UGR). Avda. de Las Palmeras n° 4, 18100. Armilla (Spain).

3 Departamento de Geodinámica, Universidad de Granada. Campus Fuentenueva, s/n 18002 Granada (Spain).

4 Universidad Fluminense. Rua Miguel de Frias 9, Niteroi 24220-900 Rio de Janeiro (Brazil).

5 Institute of Oceanology. Russian academic of sciences. Nahimovski prospect 36, 117997 Moscow (Russia).

*Corresponding author:
E-mail: mcatalan@roa.es
Fax: 34 956 - 599366*

Abstract

Bransfield Basin, a 500 km long and 100 km wide extensional structure with a well-marked NE-SW orientation, is considered a back-arc basin developed since the Pliocene and associated with subduction of the former Phoenix Plate below the South Shetland Islands Block. Extension also occurs in this area as a consequence of the end of the sinistral fault zone that deforms the South Scotia Ridge. On the basis of potential field data from marine cruises, we provide new magnetic and Bouguer gravity maps of the area at sea level. We have characterized the central magnetic anomaly by using Euler deconvolution method, spectral analysis and forward modeling obtaining a thin (1.5 km) and shallow (4 km b.s.l.) layer, and a low total magnetization (2.6 A/m). The forward modeling was constrained on basis of previous seismic refraction studies. Our models show two situations. The first presents a uniform density values along the entire crust in the basin. This would be compatible with rifting in a more advanced stage, or even an oceanic crust in its earliest stages, while the second would support the existence of a stretched, thinned and altered crust through the injection of volcanic material. In the light of these models,

analysis of the new potential field maps presented in this work and information from previous studies we consider that the Central Bransfield Basin is in a rifting in its latest stages or presents an incipient oceanic crust formed by recent oceanic spreading.

Key words/phrases: Back-arc basin, potential fields, crustal structure, Pacific margin anomaly, northern Antarctic Peninsula.

1. Introduction

The process that leads to the formation of an ocean can be studied in different areas in the world. North of Africa and Arabia shows three rifts systems which represent different stages of a evolutionary sequence: (a) a continental rift system in East Africa, (b) at the Red Sea where the transition from a continental rift to oceanic rift is taking place right now, and (c) the Gulf of Aden which has already evolved to oceanic rift (Bonatti, 1987; Cochran and Martinez, 1988). This evolutionary process could seem simple.

Taylor et al. (1995) study the western Woodlark Basin/Papuan Peninsula region of New Guinea. They showed the manner in which seafloor spreading is initiated at continental margins, and what conditions are necessary to cause them, are more complex than it might first appear. Some assumptions should be reconsidered: (a) that continental rifting ceases when sea-floor spreading begins, or (b) that oceanic fracture zones develop from transfer or transform faults within continental rifts.

Marginal basins are extensional structures developed along active continental margins in different tectonic contexts. They may be formed during continental rifting as occur in Afar Depression related to the development of the triple junction between Nubian, Arabian and Somalian plates (Beyene and Abdelsalam, 2005). However, they are generally related to oceanic subduction, forming arc and back-arc systems (Taylor, 1995 and references herein). Back-arc basins are especially well developed around the Pacific and Indian oceans (New Zealand, Japan, New Hebrides, and Kuril) and also in the Scotia Sea area. Arc and back-arc systems parallel to continental margins allows to the development of narrow and elongated basins that determined the development of marginal areas of restricted oceanic circulation. These regions have related active magmatism with differentiated geochemical features (Taylor, 1995).

The Antarctic Peninsula and the South Scotia Ridge provides two examples of inactive and active back-arc basins parallel to continental margins: The Jane Bank and Jane Basin (Bohoyo et al., 2002) and the South Shetland Islands and Bransfield Strait (Gamboa and Maldonado, 1990; González-Casado et al., 2000). The Jane Basin is an oceanic basin formed between the Weddell Sea margin of the South Orkney microcontinent and the Jane Arc. The seismic profiles and magnetic anomalies demonstrate that it was formed during the Miocene and is inactive at Present. However, the Bransfield Basin is a more recent structure and continues to be under debate its active opening and its crustal nature (Galindo-Zaldivar et al., 2004; Gamboa and Maldonado, 1990; González-Casado et al., 2000; Lavwer et al., 1996, among others).

The aim of this contribution is to constrain the deep structure of the Bransfield Basin, discussing its oceanic or non-oceanic character, from the study of a new compilation of available gravity and magnetic data.

2. Geological Setting

The study area lies between the Antarctic Peninsula and the South Shetland Islands (SSI) (Fig. 1). This area (Bransfield Strait) is considered a back-arc basin related to the subduction of the former Phoenix Plate below the SSI block (Barker et al., 1991; Dalziel et al., 1984; Gamboa and Maldonado, 1990). Moreover it is affected by the southwestward extensional end of the transtensional and transcurrent fault system that deforms the continental blocks of the South Scotia Ridge (Galindo-Zaldivar et al., 2004, 2006a). The Bransfield Strait is a 500 km long and 100 km wide extensional structure with a well-marked NE-SW orientation that has been developing since the Pliocene. It ends to the southwest, also coinciding with the southwest end of the South Shetland trench along the Pacific margin of the Antarctic Peninsula (Jabaloy et al., 2003). To the NE, the Bransfield Strait is connected with discontinuous depressions located along the South Scotia Ridge. This lens-shaped basin is usually divided into three sub-basins: Western, Central and Eastern (Christeson et al., 2003; Galindo-Zaldivar et al., 2004; Gràcia et al., 1996). The Smith and Low islands, located at the southeastward prolongation of the Hero Fracture Zone (HFZ), mark the southwestern boundary between the Western and Central basins (González-Casado et al., 2000). The HFZ is an ancient transform fault that behaves as a

limit between the former Phoenix Plate and the Antarctic Plate (Fig. 1). This feature presents a clear bathymetric relief in the oceanic crust, but there is no clear evidence of its continuation through the South Shetland Block (Galindo-Zaldivar et al., 2004; Jabaloy et al., 2003; Maldonado et al., 1994). In the hanging wall, however, the subduction of the positive reliefs of the HFZ along the Pacific margin of the South Shetland block determines local deformation and uplifts as well as the occurrence of HP/LT (high pressure-low temperature) metamorphic rocks at Smith Island. The boundary between the Central and Eastern Bransfield basin is located at the Bridgeman Island volcano (Fig. 1).

Full swath-bathymetry data covering the central and eastern Bransfield Basin show a linear trend of volcanic features, roughly aligned along the basin (Canals et al., 1994; Gràcia et al., 1996). Moreover, Quaternary volcanism is recorded at Deception Island, located by the boundary faults between the South Shetland Block and the Bransfield Basin, and in several places among the South Shetland Islands. Galindo-Zaldivar et al. (2004) analyzed multichannel seismic profiles by studying the shallow structure of the Bransfield Basin and its eastward prolongation through the Scotia Sea. They proposed a tectonic picture where roll-back played a major role in the development of the Bransfield Basin, supporting the existence of incipient oceanic crust.

Parra et al. (1984), who modeled aeromagnetic data in the area, arrived at an age of the basin of 1.8 Ma, and an average velocity of 0.9 cm/yr full rate for the opening. On the basis of aeromagnetic data, González-Ferrán (1991) suggested an average full spreading rate of 0.25-0.75 cm/yr for the last 2 Ma. Magmatic activity is well-established, but according to Lawver et al. (1996) there is no strong evidence of normal seafloor spreading within the basin, probably due to its youth, which makes the magnetic patterns diffuse. Kim et al. (1992) modeled eight marine profiles across the strait based on dyke bodies. This dyke model suggested that the amount of extension was higher in the eastern basin than in the western basin.

More recently, Christeson et al. (2003) have published results of a wide-angle seismic survey carried out in the region, consisting of a grid of five strike and three dip profiles. They observed that the crustal thickness pattern was consistent with propagation of the extension from the NE towards the SW. In addition, from the upper mantle velocities, they suggest the occurrence of a small amount of partial melt or normal upper mantle

anisotropy with the slow direction parallel to the rift axis, in order to justify velocities of 7.45 ± 0.2 km/s at depths of 14-17 km.

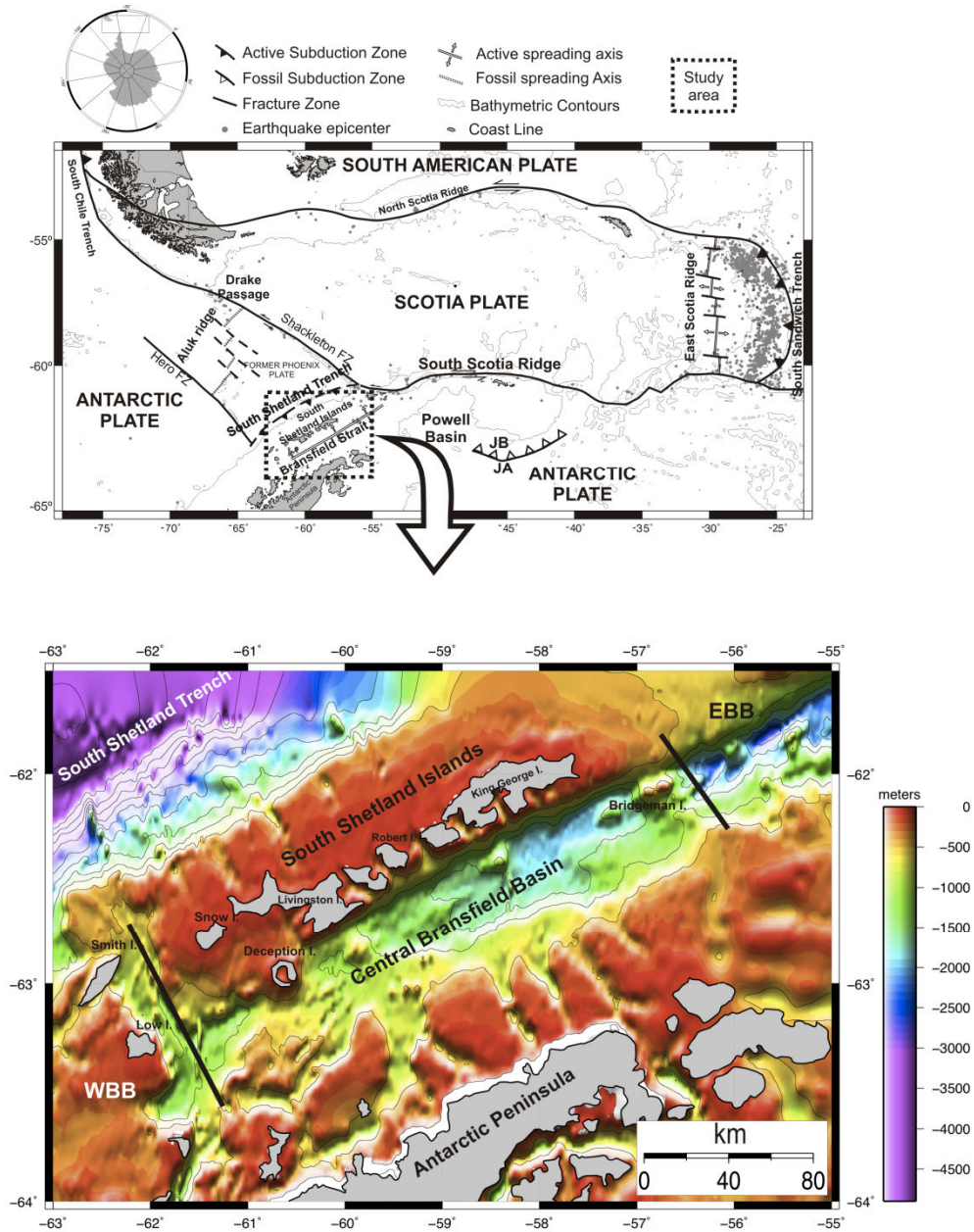


Figure 1. a) Regional geotectonic framework of the region and location of the study area. Main geological features are included. b) Regional satellite bathymetry of the work area (Smith and Sandwell, 1997). JB : Jane Basin. JA: Jane Arc. EBB: Eastern Bransfield Basin. WBB: Western Bransfield Basin. Boundaries between basins are represented by black solid lines.

3. Data compilation

The available data on the region include marine gravity and magnetic measurements (Fig. 2). This area has a dense coverage due to the presence of numerous seasonal and permanent Antarctic stations of different countries, relatively good sea conditions and low summer ice cover.

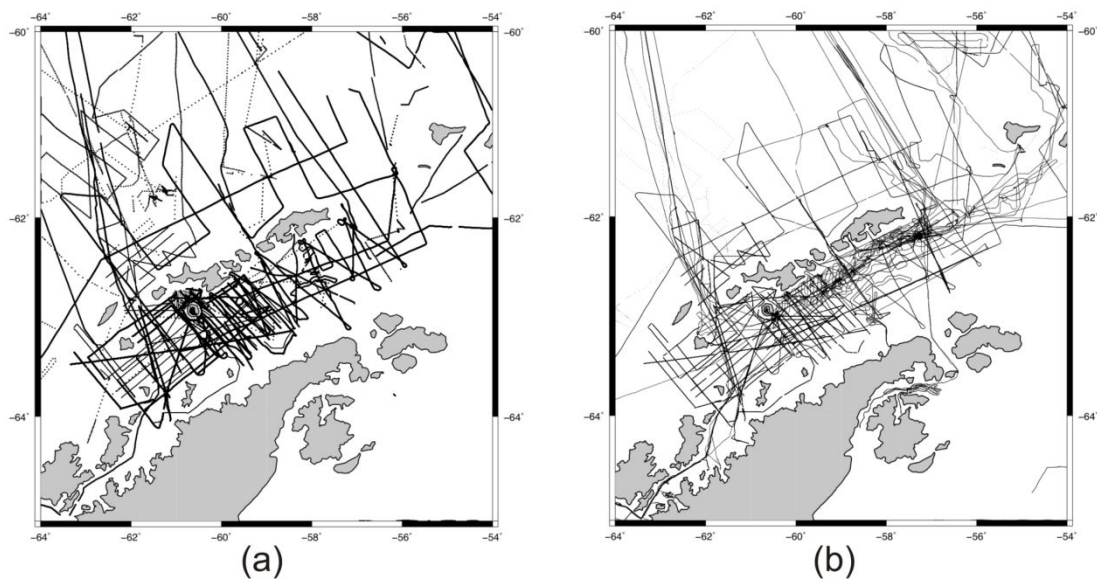


Figure 2. Marine track coverage. (a) Marine magnetic track line coverage. (b) Marine gravity track line coverage.

3.1 Magnetic data

We used marine magnetic data from the Marine Trackline Geophysical Data System (GEODAS) (Metzger and Campagnoli, 2007) in this work. A total of 21 cruises were carried out in the period 1961-2000. In addition, further geophysical expeditions were performed by the Royal Observatory of the Spanish Navy (ROA) during several austral summers: 1989-90, 1990-91, December 1999 (DECVOL-99), January-February 2002 (GEODEC-MAR), and December 2008 (MAREGEO) (Fig. 2a). We subtracted the core field contribution using the best-reference geomagnetic field, which is the DGRF evaluated at the time period of the cruises.

Data from DECVOL-99, GEODEC-MAR and MAREGEO were lag corrected, spike removed and diurnally corrected using data from the Livingston Island geomagnetic observatory. Data from an auxiliary reference station installed at Deception Island was also used. As the GEODAS cruises were not corrected by external field contribution, the ROA cruises DECVOL-99, GEODEC-MAR and MAREGEO were used as masters.

Crossover analyses are used to estimate the quality of the geophysical surveys as well as to provide an effective technique for improving the internal consistency of the geophysical data grids (Thakur et al., 1999; Wessel and Watts, 1988). Since the local magnetic anomaly is time-invariant, if we examine the anomaly crossover difference between two tracks, the residual will reflect the error budget. This is mainly due to the geomagnetic field time-dependent components: secular variation (SV) and to the external field contribution, as well as navigation errors.

A careful and detailed analysis of every crossover was performed; discarding those cruises where residuals were systematically high (we arbitrarily selected 300 nT as a threshold). We carried out a previous leveling on GEODEC-MAR, DECVOL-99 and MAREGEO track lines using a statistical tie line leveling technique, which corrects for intersection errors that follow a specific pattern or trend. The algorithm calculates a least-squares trend line through an error signal to derive a trend error curve, which is then added, as a correction, to the signal to be leveled. Subsequently, and using the ROA cruises as masters (DECVOL-99, GEODEC-MAR and MAREGEO), we leveled those complementary surveys (GEODAS data) using crossover residuals. All filtered offshore magnetic anomaly data were merged to derive a 3 km resolution map (Fig. 3a). To further aid in the interpretation of the magnetic anomaly data, reduction to the pole (Baranov and Naudy, 1964) was also applied. Reduction to the pole serves to transform data that are collected in areas where magnetic inclination is not vertical to the way the data appear at the geomagnetic pole; that is, the anomalies are essentially deskewed and positioned symmetrically over their sources. We used -55° and 11.5° as average values for inclination and declination, respectively, for the whole area (Fig. 3b).

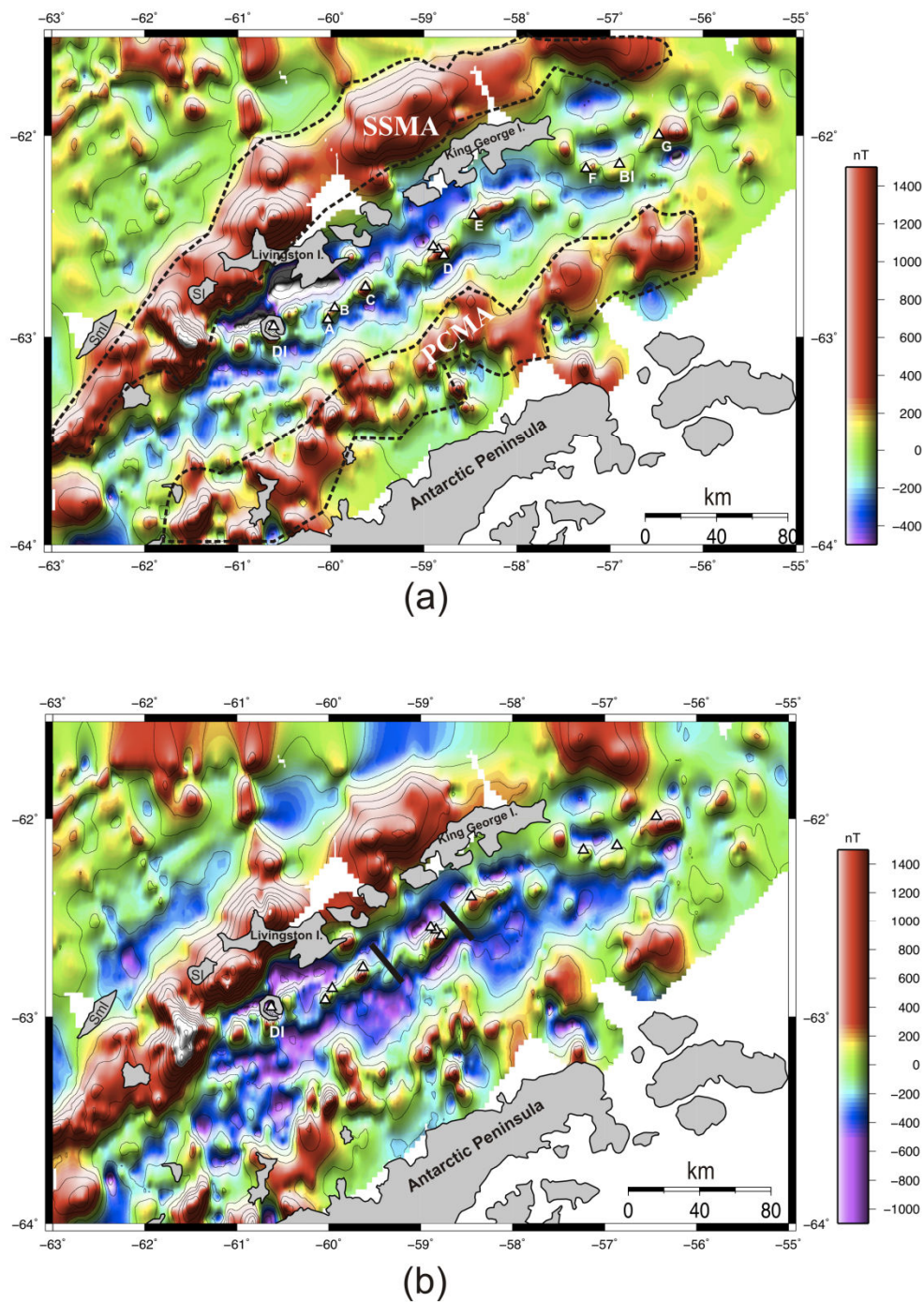


Figure 3. Magnetic anomaly maps. (a) 3 km resolution magnetic anomaly map, obtained after leveling of marine magnetic lines, with white labels highlighting sub-aerial and submarine volcanoes. Label “C” corresponds to the so-called “Orca Volcano”. Label “D” (also called “Three Sisters” in Christeson et al. (2003)) corresponds to three parallel features. DI: Deception Island. BI: Bridgeman Island. Two black dashed polygons give an approximate representation of the local Pacific Margin Anomaly coverage over the study area. SSMA: South Shetlands Magnetic Anomaly. PCMA: Pacific Coast Magnetic Anomaly. SI: Snow Island. SmI: Smith Island. (b) Final magnetic map reduced to the pole. Both maps: Colour palette in nT. Contour interval: 200 nT. Two NW-SE thick black lines show where the linear magnetic anomaly associated with the neovolcanic axis appears disrupted by offsets. White triangles highlight subaerial and submarine volcanoes.

3.2 Gravity data

In this work we used marine free air gravity data from the Marine Trackline Geophysical Data System (GEODAS) (Metzger and Campagnoli, 2007). A total of 13 cruises were carried out in the period 1992-2000. In addition, a geophysical survey was performed by the ROA in January-February 2002 (GEODEC-MAR) in the area (Fig. 2b).

Water slab was corrected using a density of 1.03 g/cm^3 . Complete Bouguer anomalies were calculated following the Nettleton (1976) procedure. To apply Terrain corrections, we used the SRTM30PLUS4 grid as a regional grid (Smith and Sandwell, 1997) and data from a local full swath-bathymetry survey for local corrections (Gràcia et al., 1997). We have used 2.67 g/cm^3 as the terrain density, considering that most of the surrounding areas have a continental character. Regional grid was used beyond 10 km, and additionally in those areas where there was no local bathymetry data. Finally, we obtained a Bouguer anomaly grid with a 3 km resolution that can be compared on an equal basis with the marine magnetic grid (Fig. 4a).

4. Magnetic and Gravity anomaly maps

4.1 Magnetic map

The Central Bransfield Basin (CBB) is enclosed by two long wavelength positive anomalies (Fig. 3). The first one (South Shetlands Magnetic Anomaly: SSMA) runs SW-NE along the South Shetland block, while the second (Pacific Coast Magnetic Anomaly: PCMA) runs roughly sub-parallel along the Antarctic Peninsula margin (Garret, 1990; Ghidella et al., 2002; Suriñach et al., 1997). The maximum value of magnetic anomaly identified in the SSMA (higher than 1300 nT) is reached between Smith and Snow islands. There are other maximum, located northern Livingston Island (900 nT) and northwest of King George Island (700 nT). Generally speaking this block shows a progressive decrease in amplitude of anomaly as we progress northeastward.

The CBB is characterized by long wavelength negative values, showing an average of -400 nT in the scalar magnetic anomaly (Fig. 3a) and also in the reduction to the pole map (Fig. 3b).

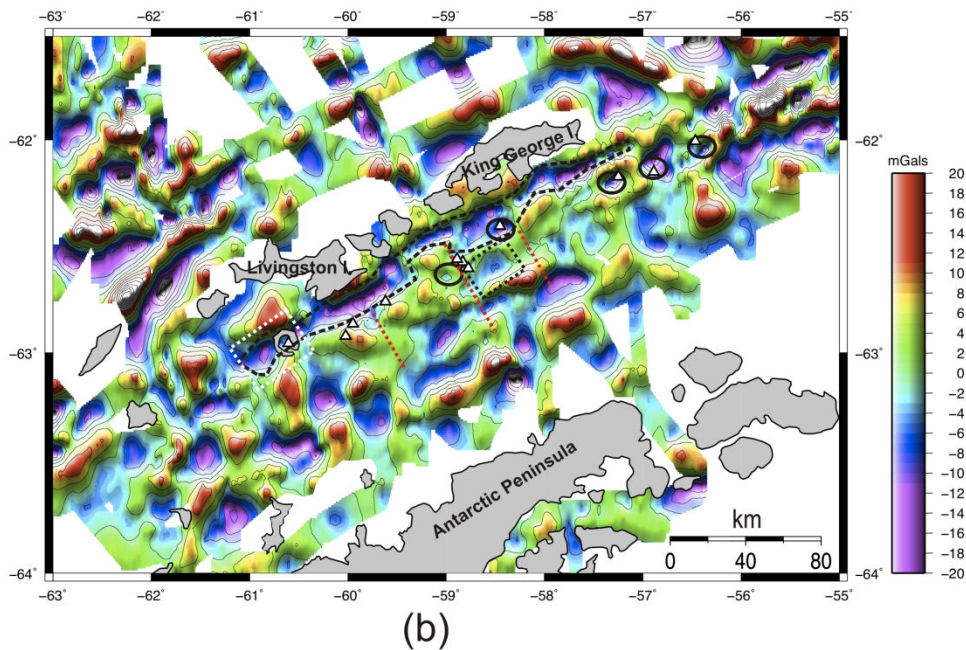
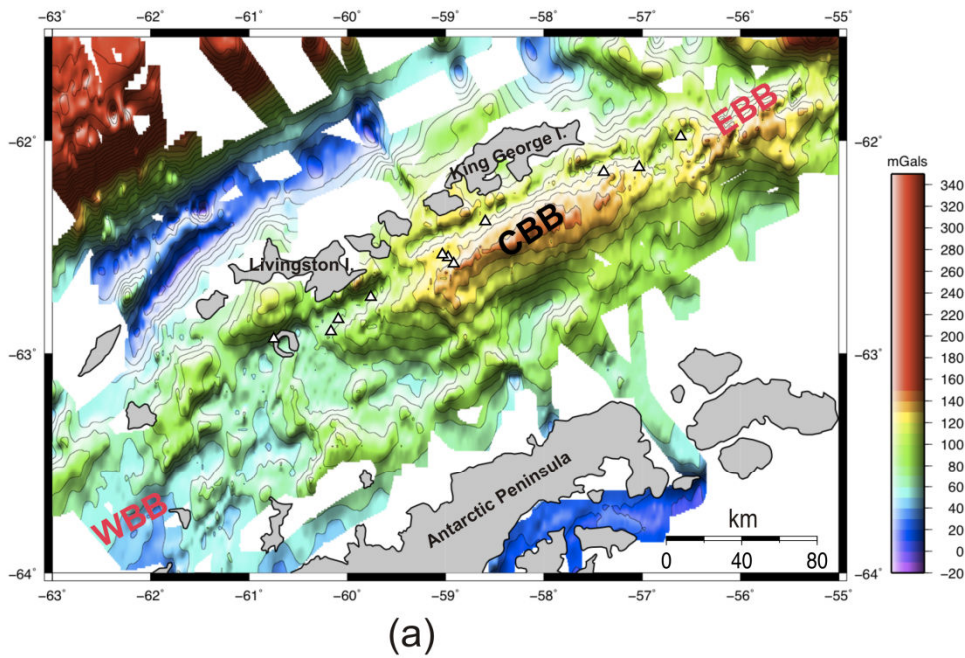


Figure 4. Gravity anomaly maps. (a) Bouguer anomaly map at sea surface and 3 km resolution. Contour interval: 10 mGal. WBB: Western Bransfield Basin. CBB: Central Bransfield Basin. EBB: Eastern Bransfield Basin. (b) Bouguer anomaly map high pass filtered, cut-off wavelength: 50 km. Red dotted lines show morphologic steps from Gràcia et al. (1996). A Bouguer gravity anomaly low is highlighted inside a black dashed rectangle. A large linear low surrounds the southern part of South Shetland Archipelago (inside a dashed black polygon, see text for comments). Black circles delimit short wavelength gravity lows, which appear associated with volcanic edifices. A white dashed rectangle delimits a proposed magma chamber at DI. Both maps: White triangles highlight subaerial and submarine volcanoes.

Throughout the CBB, a series of short wavelength positive anomalies can be picked out. Some of them correspond to submarine volcanoes as their position coincide with those volcanic edifices, 'A' to 'G', described by Gràcia et al. (1996) (Fig. 3a). Labels 'DI' and 'BI' (same figure) correspond to sub-aerial volcanoes, such as those of Deception and Bridgeman Islands, respectively. Although some anomalies are rounded, they are generally elongated in a NE-SW trend parallel to the Bransfield basin axis. Volcanoes present values of magnetic anomaly of 300 nT on average, reaching its highest (450 nT) and lowest amplitude (135 nT) in edifice 'G' and 'F' respectively. The PCMA's magnetic anomaly amplitude keeps roughly uniform (400 nT) along the whole block reaching a maximum value of 800 nT in its southwestern part.

The reduced-to-the-pole magnetic map (Fig. 3b) shows, in general, a similar picture but with a general southward translation of the anomalies. Furthermore, positive short wavelength signals are slightly better resolved. This is not obvious along the neovolcanic line, but it is quite evident along the southern part of the CBB, where peaks related with SSMA blocks have a reduced magnetic footprint, and so are better resolved.

4.2 Bouguer gravity map

The map shows terrains in the northwestern part where high values occur (higher than 200 mGals) (Fig. 4a). These values correspond to well-developed oceanic domains, in this case the extinct Phoenix Plate in the Drake Passage. In a matter of just 50 km, the high values descend to 10 mGals due to the presence of the South Shetland trench. Southeast of the trench there lies the South Shetland Block, followed by the Bransfield Basin. Inside the CBB, Bouguer gravity anomalies show an average of 100 mGals and 140 mGals for the local maxima. Bouguer anomaly values become progressively lower towards the south.

All these features within the CBB provide a first approach to the spatial variation of crustal thickness in the area. According to past seismic studies (Grad et al., 1997; Christeson et al., 2003), the thinnest values are located along the neovolcanic zone. These studies indicate that thickness increases asymmetrically away from the neovolcanic zone, reaching 20-26 km along the South Shetland forearc, but only 14-20 km along the Antarctic Peninsula margin at similar distances from the neovolcanic zone (Christeson et al., 2003; their figure 13b).

Nevertheless, details are not possible to be observed in the gravity map because of the gravity high. Additionally, as magnetic properties are constrained to middle crust (MC) and upper crust (UC) depths due to thermal gradients, it is difficult to compare the two maps (Bouguer gravity and magnetic). Taking into account that deeper sources dominate the long wavelength part of the spectrum, we applied a high-pass filter to the Bouguer gravity map, selecting a 50 km cut-off for wavelength coinciding with the width of the large gravity high, to remove it from the map. This new map (Fig. 4b) shows intra-crustal anomalous bodies that depict equivalent patterns to the reduced-to-the-pole magnetic map (Fig. 3b).

5. Characterization of the central linear magnetic anomaly

To derive information concerning a possible spreading process in the Bransfield Strait, one key is to characterize the central linear magnetic anomaly. This was accomplished by means of the following scheme: a) estimation of the depth to the top, b) estimation of the depth to the bottom, and c) estimation of its total magnetization.

a) Depth to the top

We applied three-dimensional (3-D) located Euler deconvolution to the magnetic dataset, used to evaluate the depth and location of causative bodies of potential field anomalies. For a complete discussion of Euler deconvolution, see Thomson (1982), Reid et al. (1990) and Ravat (1996), who provide the mathematical background of the technique as well as its relevant applications. We should underline that we are interested in potential sources (neovolcanic axis) that could be limited in width according with the central magnetic anomaly width, which is inferred from the reduce to the pole map (Fig. 3b). Its depth was limited too, according to the volcanic origin of these sources, which we expect it to be at sub-cortical Curie depth, while their length extends all along the CBB. We therefore selected a structural index equal to 1, which would represent an ideal body with one infinite dimension (Reid et al., 1990).

The located Euler deconvolution modifies classical approaches by first locating only those windows which encompass peak-like structures in the data. A peak-finding routine is first run to locate peaks and estimate a window size using the locations of adjacent

inflection points. These locations and window sizes can then be used to define the solution using the standard Euler deconvolution method.

This method is widely used in terrestrial and marine applications to model the source depths of discrete gravity and magnetic anomalies. Ferris et al. (2000) performed an interpretation of an airborne magnetic data compilation to reveal a series of anomalies that were interpreted as a sequence of rifts. They determine spatial relationship between anomalies combining gravity and magnetic Euler solutions. Salem et al. (2007) performed a study of structural mapping using Euler method on high-resolution aeromagnetic data collected in the northern Red Sea. They delineated a set of fault systems, and a long and wide magnetic body, which they interpreted as related to the Red Sea rift. Russell and Whitmarsh (2003) applied Euler technique to estimate the contribution of basement relief to the observed magnetic anomalies at the west Iberia margin.

Figure 5 displays the set of Euler depth solutions. Along the CBB we obtained nearly 4 km depth sources. If we take into account that the water layer is approximately 1.5 km thick and the sediment layer is 2.5 km thick (Christeson et al., 2003), we infer that the source(s) generating the linear positive magnetic anomaly along the CBB axis is (are) shallow.

b) Depth to the bottom

Several authors (Blakely, 1988, 1995; Shuey et al., 1977) have used the shape of the radially average spectra to estimate the depth extent of magnetic sources. In particular, the position k_{\max} of the maximum along the $|k|$ axis is related to the depth to the bottom of the layer according to the following equation:

$$k_{\max} = \frac{\log z_b - \log z_t}{z_b - z_t} \quad (1)$$

where z_b and z_t are the depths to the bottom, and to the top of the layer, respectively, measured from the survey height, and k_{\max} is expressed in radians per unit of distance. Although spectrum analysis provides depth estimates with simple assumptions, we must highlight that these methods have fundamental limitations. Following Blakely (1995), we

note that the determination of the depth to the bottom of the source (z_b) cannot be known without knowledge of the depth to its top (z_t). Secondly, this estimation of the depth to the bottom focuses on the lowest wave number parts of the Fourier domain, which is quite sensitive to poorly known regional fields, and, to be able to discriminate with accuracy the peak in the spectrum, the magnetic survey must have a minimum dimension, L , which fulfils the equation:

$$L \geq \frac{4\pi(z_b - z_t)}{\log z_b - \log z_t} \quad (2)$$

Blanco-Montenegro et al. (2003) applied the method based on the k_{\max} estimation to a grid centered in Gran Canaria Island, suggesting the presence of rocks located at mantle-like depths, which could behave as magnetic sources.

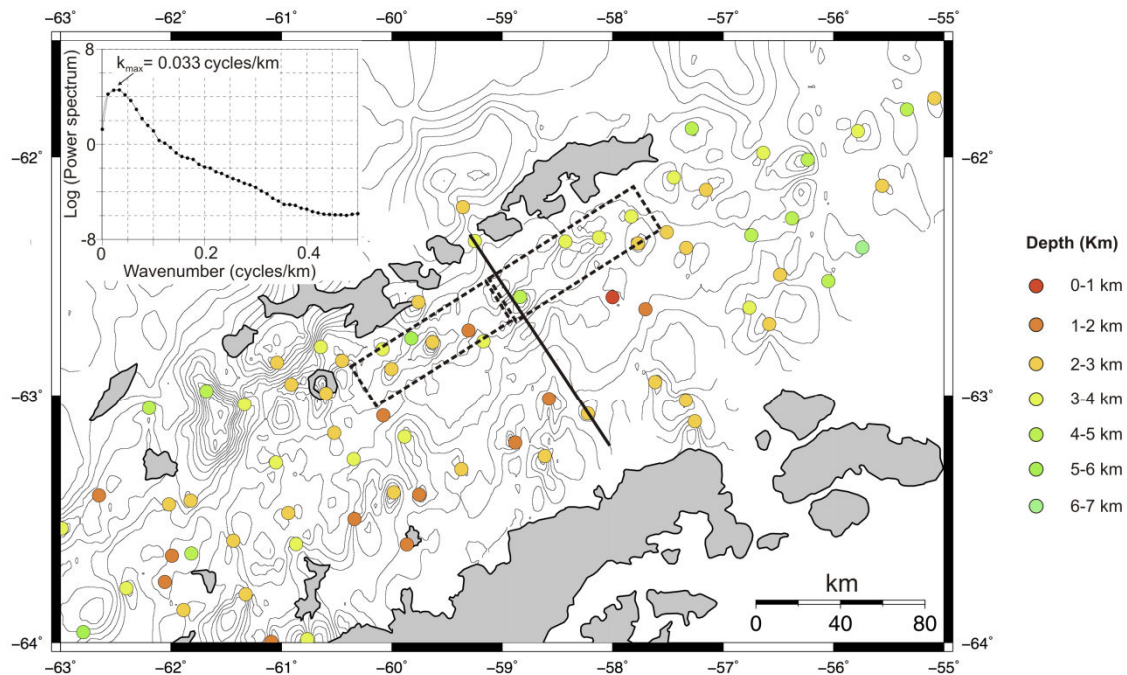


Figure 5. Euler solutions for a structural index of 1 and a depth tolerance of 15%. Contour interval: 200 nT. Inserted graph shows a radial average power spectrum from two different 80 km length windows in the SW-NE direction (in black dashed lines, windows used for the depth to the bottom spectral calculus). See text for comments. Thick black line shows the profile selected for the forward modelling of the CBB crustal structure.

We followed a similar technique to Blanco-Montenegro et al. (2003). In order to solve the peak in the spectrum, taking into account equation (2) and using 10 km as z_b , we selected an 80 km size for the window (following Kim et al., 1992) we considered 10 km as Curie depth). Thus, we extracted two different 80 km NW-SE windows from the magnetic anomaly map (Figure 5), and we have obtained a k_{\max} of 0.033 cycles/km.

To obtain z_b values we must solve equation (1). We assumed $z_t = 4$ km in view of our results after the Euler deconvolution analysis. The result shows that the depth to the bottom of this magnetic source lies at 5.5 km b.s.l., which provides a 1.5 km thick magnetic source.

6. Forward gravity and magnetic modeling

To accomplish the gravimetric and magnetic modeling we defined a 5-layer structure on the basis of a simplification of velocity models derived from wide-angle seismic data from Christeson et al. (2003) (their figure 5, profiles 2 and 9).

A first layer behaves as sedimentary rocks, another as upper crust (UC), the third as middle crust (MC), the fourth one as lower crust (LC) and finally the mantle. We adopted a simplified assumption (small number of bodies), since a greater number would introduce complexities and a probable non-realistic approximation of the real picture.

This 5-layer structure allows us to account for different facts: a) sediments were considered to have null total magnetization, b) rocks are believed to have magnetic properties above a specific depth within the crust due to thermal gradient effects (Curie temperature), and c) it helps us control short gravity and magnetic wavelengths that characterize these profiles.

The initial density values used for our models were based on those from the previously cited bibliography, and they were modeled as horizontal layers. To constrain surface features, particularly sediment layer thickness, we used Christeson et al. (2003) (their figure 13a, b) and Galindo-Zaldívar et al. (2004) (southeastern segment of MCS profile BR30). We considered a low-density value for the upper mantle, within the neovolcanic zone, according to past seismic studies (Ashcroft, 1972; Christeson et al., 2003; Grad et al., 1997).

In particular the last reference constrains velocities of 7.45 ± 0.20 km/s within the upper mantle in the area, which corresponds to the Bouguer gravity high. This means that 7.25 km/s and 7.65 km/s could be considered as lower and upper mantle velocity boundaries, respectively. Their preferred model has a mantle velocity of 7.45 km/s, so we used this value to estimate the crustal thickness. Our model suggests a value of 10.2 km. To use of 7.25 km/s or 7.65 km/s changes this estimation by ± 2 km, in close agreement with the resulting uncertainty on Moho depth from seismic data (Christeson et al., 2003).

Parra et al. (1984) and Kim et al. (1992) used 10 km for crustal thickness in their models in the Bransfield Strait. This threshold is considered in our study as well, since deeper crust (below 10 km) yields an insignificant contribution. Having established a value of 10 km for crustal thickness, we checked two different models for the NW-SE profile. The first (Model 1) considers an upper mantle density of 3030 kg/m^3 ($V_p = 7.25$ km/s – upper boundary), whereas the second (Model 2), which is exactly the same in terms of geometry, uses an upper mantle density equal to 3160 kg/m^3 ($V_p = 7.45$ km/s – lower boundary). Finally, Figure 6 represents the models that best fit our gravity and magnetic data. Final layer composition (density and bulk susceptibility) is shown in Table I.

Although the fit to observed gravity is excellent, we did not attempt to fit the details of the composite magnetic profile except to model appropriate wavelengths and amplitudes. Throughout the study, only induced magnetization was considered. Other authors (Garret, 1990; Suriñach et al., 1997) support this assumption, as previous analysis of igneous rock samples from Antarctic Peninsula shows a Koenigsberger ratio close to unity and stable remanence directions, which additionally are close to the present-day theoretical axial dipolar field. This means that the total magnetization vector is in the same direction as the ambient field.

Initially we fit the magnetic model by only modifying the bulk susceptibility and thickness of UC and MC. The best fit was obtained by providing a positive susceptibility contrast for MC of 0.02 (SI), and an almost non-magnetic UC (0.005 SI).

The gravity in this profile shows three different behaviors (Fig. 6): a) a first segment goes from km 0 to km 18 and corresponds to the block of islands, b) from 18 km to 54 km there is a transitional area, and c) from 54 km until the end of the profile, a Moho deepening marks the transition to the Antarctic Peninsula.

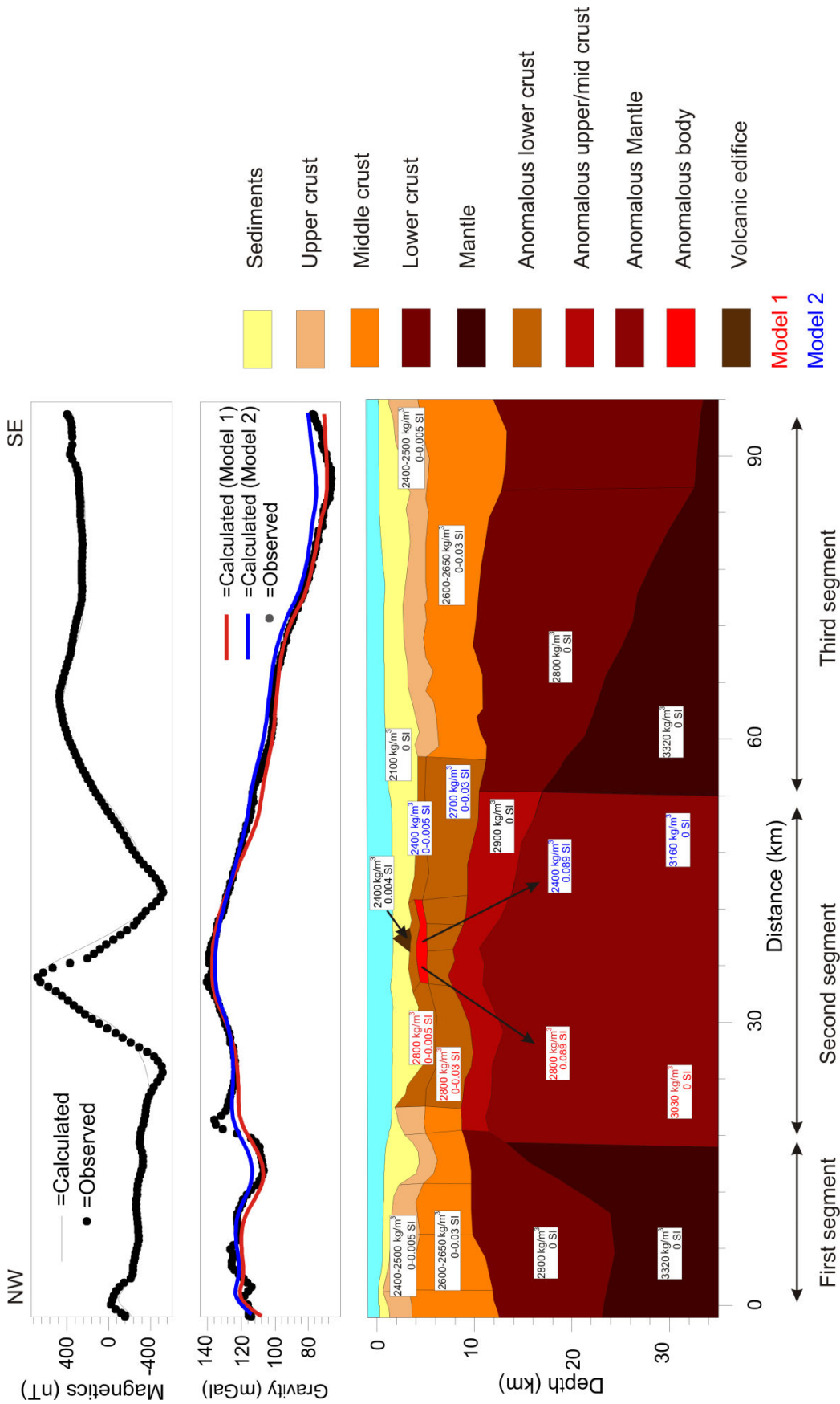


Figure 6. Magnetic and Gravity models for NW-SE profile. Magnetic units: mGals. Susceptibility units: S.I. Density units: kg/m³. Profile location shown at Figure 5 (Thick black line). Gravity shows three parts in this profile: a) a first segment which goes from km 0 to km 18, corresponding to the block of islands, b) from 18 km to 54 km, a transitional area, and c) from 54 km until the end of the profile, where the Moho deepening marks the transition to the Antarctic Peninsula. Two different models were checked for the NW-SW profile. Final layer composition (density and bulk susceptibility) is shown in the plot and in Table I. Red line shows the gravity response of Model 1 and a blue line shows the gravity response of Model 2. Density and susceptibility values in red for Model 1 and in blue for Model 2, whereas Density and Susceptibility values were the same for Model 1 and 2 we have written them in black.

This profile shows a broad gravity high, which we fit by a crustal thinning. By doing this, the Moho reaches its shallowest depth at 12.2 km. A gravity low is located between km 12 to km 18, which is southwardly bounded by a strong gravity gradient (13 mGal/km). We have modeled it by including a thick local sediment layer.

A deepening in Moho depth as we progress southeastwardly (to the Antarctic Peninsula) makes the gravity anomaly decrease smoothly. The magnetic profile is mainly conditioned by the central positive high, which was modeled as a 1.5 km thick layer at 4 km depth. The best fit was obtained with 2.6 A/m (0.089 SI).

Units	First segment		Second segment				Third segment	
	ρ (kg/m ³)	χ (SI)	Model 1		Model 2		ρ (kg/m ³)	χ (SI)
			ρ (kg/m ³)	χ (SI)	ρ (kg/m ³)	χ (SI)		
Sea water	1640	0	1640	0	1640	0	1640	0
Sedimentary layer	2100	0	2100	0	2100	0	2100	0
Upper Crust (UC)	2400-	0-	2800	0-	2400	0-	2400-	0-
	2500	0.005					2500	0.005
Middle Crust (MC)	2600-	0-0.03	2800	0-0.03	2700	0-0.03	2600-	0-0.03
	2650						2650	
Lower Crust (LC)	2800	0	2900	0	2900	0	2800	0
Mantle	3320	0	3030	0	3160	0	3320	0
Anomalous body	-	-	2800	0.089	2400	0.089	-	-
Volcanic edifice	-	-	2400	0.004	2400	0.004	-	-

Table I. Physical properties used in gravity and magnetic models.

7. Discussion

The compilation of available gravity and magnetic data provide new insights regarding its crustal and upper mantle structure and contribute to discussion of its continental or oceanic character.

Crustal structure and volcanic features

Along the axis of the CBB there is a neovolcanic lineation, which depicts a direct correlation between magnetic and gravity responses (Figs. 3b, 4b). Several short wavelength gravity lows appear associated with volcanic edifices (Fig. 4b: inside black circles). This is most likely due to overcompensation of the gravity response, given a density lower than 2.67 g/cm^3 (Fig. 6, volcanic edifice).

Two more features can be highlighted: a) a long linear gravity low starting at Deception Island (DI) and running through the southern South Shetland margin (Fig. 4b: black dashed polygon), and b) a gravity low slightly south of the neovolcanic axis (Fig. 4b: dotted black rectangle). The former negative gravity anomaly probably has to do with the transition between the SSI block and the CBB. This negative gravity anomaly is displayed in Figure 6 between km 12 and km 18, and it was model by increasing the thickness of the sedimentary layer. This may be a consequence of the Bransfield Strait Current circulation, which is confined to shelf break of the SSI (Zhou et al., 2002) or to the presence of a small narrow basin delimited by a crustal block detached from the South Shetland Block margin. Although this anomaly seems to extend as far as DI, it may not be real, and ends at the southwestern tip of Livingston Island. We propose that its continuation to DI (Fig. 4b: inside a white dashed rectangle) is related with a magma chamber. To support this, we should consider some previous studies performed in the region of DI. Muñoz-Martín et al. (2005) detected a wide Bouguer gravity and magnetic low at the same geographical location (NW part of DI). They forward-modeled it as a partially melted intrusive body at a depth of approximately 2 km by using Euler Deconvolution techniques. Moreover, the January 2005 seismic tomography experiment (Zandomeneghi et al., 2009) localized an area of V_p anomalies (low values) at a depth of 2 km in the NW part of DI, and it was interpreted as a magma chamber.

Concerning the latter (localized gravity low south of neovolcanic axis) Christeson et al. (2003) recognizes a primary feature in a velocity difference plot, between the Three Sisters and Orca volcanoes (labels “C” and “D” in Figure 3a). This velocity anomaly area is located around the widest part of the CBB, and they held it to be related with the presence of shallow magmatic material. This zone was quite well constrained and does not extend to either the north or south. In fact, these authors detected a low seismic velocity in the

aforementioned area (between Three Sisters and Orca volcanoes) in coincidence with the gravity low south of the neovolcanic axis (Fig. 4b: dotted black rectangle). As the magnetic map shows negative values, we propose a high thermal gradient area.

Rifting and initial stages of oceanic spreading

CBB shows segments of rifting and/or nascent spreading that are supported by the gravity and magnetic data, in addition to other geophysical and geodetical research. Typical rifting involves volcanic activity and extensional deformation. The first one can be easily identified in the CBB (Fig. 3), while the second is supported by geodesy, seismic and seismology studies.

Recent GPS measurements show a NW differential extensional component between the SSI block and the Antarctic Peninsula that reaches a maximum in the central Bransfield Basin (Taylor et al., 2008), and active normal faulting is observed in seismic profiles (Galindo-Zaldívar et al., 2006a; Gràcia et al., 1996). An earthquake focal mechanism determined from shallow and intermediate seismicity indicates NW-SE extensional stresses compatible with the opening of the CBB (Galindo-Zaldívar et al., 2006a; Pelayo and Wiens, 1989). Aschcroft (1972) indicated the existence of steep normal faults at the South Shetland margin, having as much as 4 km of downthrow to the southeast.

The large Bouguer gravity anomaly high (Fig. 4a) suggests thin crust in the area, which is supported by Christeson et al. (2003) and by our gravity/magnetic forward models (Fig. 6).

Gràcia et al. (1996) recognized four different bathymetric terraces bounded by morphologic steps trending N145°, which could be indicative of faults, as they disrupt the Bouguer gravity highs in the 50 km high-pass filtered map (red dotted lines, Fig. 4b). A similar feature appears in the magnetic anomaly map (Fig. 3), where the linear magnetic anomaly associated with the neovolcanic axis appears disrupted by two NW-SE offsets.

Total magnetization obtained at the central magnetic anomaly, located in association with the neovolcanic axis, is seen by spectral analyses and forward modeling to have a normal polarity, and not too high total magnetization value (2.6 A/m) for mid-ocean ridges, especially if we take into account that it would be the most recent and hottest extrusion into a plausible ocean floor (Klitgord, 1976).

Figure 4b shows a Bouguer gravity low (black dotted rectangle). This feature falls inside the large Bouguer gravity high and corresponds to a magnetic anomaly low (Fig. 3b). Christeson et al. (2003) detected a negative velocity difference with respect to the average velocity structure in this area, extending from sea floor to 8 km depth. This feature would be coherent with a high-temperature magmatic intrusion. These arguments (gravity, magnetic and velocity anomaly low) are compatible with a nascent spreading process. The difficulties arise from the low total magnetization value observed for the linear magnetic anomaly, which could be attributed to its recent age and slow cooling, although the highest one comes from the crustal thickness of the area. Christeson et al. (2003) locate the shallowest Moho (depth < 15 km) under the large Bouguer gravity high (Fig. 4a). It seems difficult to reconcile 12.5 km thickness with a limited or partial accretion of oceanic crust, although it is also difficult to explain as an extremely thin continental crust. An additional drawback comes from the crustal velocities obtained by Christeson et al. (2003), which were too low for a normal oceanic crust.

Our gravity model considers a low density value (on average 3100 kg/m³) for the upper mantle, within the neovolcanic zone, as described above (Fig. 6). The existence of low upper mantle velocities is well recognized from previous seismic studies (Ashcroft, 1972; Christeson et al., 2003; Grad et al., 1997). This anomalous mantle may be consequence of the southeastward-directed subduction of the former oceanic Phoenix Plate below the South Shetland Block. Once this low density of upper mantle is considered, our models suggest a lesser crustal thickness (10.2 km) below the large Bouguer gravity high than the value suggested by seismic studies (12.5 km).

Roots et al. (1979) justified an oceanic crust of shallow spreading ridges in young oceans, which thickens exponentially toward the continental margin from a seaward value of 6 km to values higher than 10 km. Such a large thickness for an oceanic crust was justified by the chilling effect caused by the two newly formed continental margins against the newborn oceanic crust. This feature may continue for the first 5.5 Ma after breakup while the thick oceanic crust continues to accrete, but with exponential decrease in thickness until a slow-chilling stage is reached and the thickness of the oceanic layer approaches the average value. This could be in favor of a nascent spreading process in the Bransfield Strait.

Christeson et al. (2003) checked several mantle velocities and concluded (after an analysis of uncertainty in velocity in the upper mantle) that the optimum velocity value was 7.45 km/s. Nevertheless, they suggest that velocities between 7.25 and 7.65 km/s produce acceptable RMS errors, and therefore estimated the uncertainty in upper mantle velocity at ± 0.2 km/s.

Our models reveal two situations. The first (Model 1) considers an upper mantle density of the second segment of 3030 kg/m^3 ($V_p = 7.25$ km/s). In Model 2 we used an upper mantle density of 3160 kg/m^3 ($V_p = 7.65$ km/s) for the so-called second segment (Fig. 6).

More specifically, Figure 6 shows a situation where: a) According with Model 1: LC, MC and UC densities in the second segment (km 18 to km 54) are similar, and are systematically higher than those in the first (km 0 to km 18) and third (km 54 until end of the profile). b) According with Model 2: LC, MC and UC densities in the second segment (km 18 to km 54) are different, and are systematically higher than those of the first (km 0 to km 18) and third (km 54 until end of the profile). This possibility would support the existence of a stretched, thinned and altered crust through the injection of volcanic material. This implies that rifting at the Bransfield Strait is ongoing and has not yet progressed to the formation of oceanic crust (cf., Christeson et al., 2003).

However, Figure 6 points to another possibility. According with Model 1 the use of 3030 kg/m^3 for the upper mantle not only increases the density of deeper layers (LC and MC), but also modifies (increasing) the UC density. It is important to highlight that we have tested different possibilities for the second segment UC densities, and all of them make the error increases; i.e., if we use the same UC density as we used in Model 1, the error of our model would reach values of almost 17 mGals (when in fact our final models show gravity errors equal to 3 mGals).

In short, Model 1 means that every layer (UC, MC and LC) features: a) a clear contrast in density between the second segment and the first and third one, b) UC and MC are difficult to be differentiated. This would be compatible with rifting in a more advanced stage, or even an oceanic crust in its earliest stages. The seismic reflection data from the central Bransfield Strait (Galindo-Zaldivar et al., 2004; Gamboa and Maldonado, 1990) tend to support the creation of an initial oceanic crust. The MCS profiles reveal typically

intense reflectors located at the top of the igneous layers of the oceanic crust below the sedimentary layer. In addition, the linear volcanic structure is uncovered by sediments supporting a very recent age compatible with active spreading processes.

The combined study (spectral analysis/Euler deconvolution), performed in two different but consecutive areas, shows a similar solution for the layer responsible for the magnetic response. Our solution shows a thin (1.5 km) and shallow layer (4 km b.s.l.), meaning that this process/alteration would have reached at least the UC bottom.

Supporting the extension and rifting	Supporting the creation of a nascent oceanic crust	References
LC, MC and UC show different densities (Model 2)	LC, MC and UC show similar densities (Model 1)	Our forward model
GPS studies		Taylor et al. (2008)
Volcanic activity		Gràcia et al. (1996); This study
	MCS data reveal intense reflectors at the top of the basement	Gamboa and Maldonado (1990); Galindo-Zaldívar et al. (2004)
Normal faulting		Aschcroft (1972); Gràcia et al. (1996); Galindo-Zaldívar et al. (2006)
Earthquake focal mechanism		Pelayo and Wiens (1989); Galindo-Zaldívar et al. (2006)
	Lineal magnetization pattern of the neovolcanic axis	This study
Not too high magnetization value		Klitgord (1976); Our forward model
Large crustal thickness (refraction studies)		Christeson et al. (2003)
	Large crustal thickness justify by chilling effect	Roots et al. (1979)
Too low crustal velocities		Christeson et al. (2003)

Table II. Summary of supporting ideas in favour of the extension and rifting or in favour of creation of oceanic crust.

The magnetization pattern of the neovolcanic axis resembles an almost continuous lineation only disrupted by two NW-SE offsets (Fig. 3b) compatible with the opening direction of the Basin and that may represent oceanic transform faults or rotating spreading segments. This suggests that the origin of the linear magnetic anomaly is a constructive

process reaching the UC bottom (at least), while intrusives (through alteration) would have produced an amorphous-like body. It could be compatible with rifting in its latest stages, or the beginning of formation of a newborn oceanic crust. The ideas and interpretations described in this section have been summarized in Table II.

8. Conclusions

The Bransfield Strait is an active back-arc basin located along the Pacific margin of the Antarctic Peninsula. It was formed by the northwestward separation of the South Shetland Block from the Antarctic Peninsula, driven by subduction of the oceanic crust of the former Phoenix Plate at the South Shetland trench and also by the western end of the sinistral fault zone located at the South Scotia Ridge. The integration of available marine gravity and magnetic data allow us to calculate newly detailed complete Bouguer and magnetic anomaly maps that further constrain crustal and upper mantle features.

The Bouguer anomaly map shows two long wavelength positive anomalies parallel to the basin margins. The former is related to a sharp separation between the basin and the South Shetland Block, while the second is located within the basin and displaced northwestwards along its symmetry axis. The latter one includes small positive anomalies related to a NE-SW volcanic axis. Bouguer anomalies reveal the asymmetry of the Bransfield Basin, with a smooth Antarctic Peninsula boundary and a sharp boundary with the South Shetland block. Moreover, the Bouguer anomaly models suggest that crustal thickness may reach down to 8.5 km along the volcanic axis and that the upper mantle has an anomalous low density in this area.

Magnetic anomalies of the area are characterized by the Pacific Margin Anomaly. It splits into two branches in the Bransfield Strait region by the opening of the basin: the northwestern margin of the Antarctic Peninsula (PCMA) and the South Shetland Islands (SSMA). Moreover, a narrow NE-SW elongated maxima corresponding to volcanic edifices surrounded by minima is located along the NW part of the CBB, further supporting the asymmetry of the Basin.

Integration of gravity and magnetic data supports volcanic activity along the central volcanic axis of the basin: local Bouguer anomaly minima correspond with areas of low

relative magnetic anomalies and susceptibility, thereby supporting the presence of active magmatic chambers in the CBB.

Gravity and magnetic data are compatible with the extensional character of the basin, probably floored in the central sector by an oceanic crust above an anomalous mantle. Moreover, the presence of an active volcanic axis and the thin crust support, as do other available geophysical data (MSC profiles), a rifting in its latest stages or the presence of an incipient oceanic crust formed by recent oceanic spreading in the CBB.

Acknowledgements

All figures were elaborated using GMT software (Wessel and Smith, 1998). We thank Dr. Miquel Canals for providing us the full swath bathymetry corresponding to the Central and Eastern Bransfield Basin. This research was supported by projects CSD2006-0041, P09-RNM-5388, 2010RU0037, CGL2010-21048, CTM2011-30241-C02-02, and RNM 148, and by a predoctoral fellowship of the "Ministerio de Ciencia e Innovación" of Spain (FPI).

Chapter 10

MONITORING THE EVOLUTION OF DECEPTION ISLAND VOLCANO FROM MAGNETIC ANOMALY DATA (SOUTH SHETLAND ISLANDS, ANTARCTICA)

*Under review in:
Global and Planetary Change*

Monitoring the evolution of Deception Island volcano from magnetic anomaly data (South Shetland Islands, Antarctica)

Manuel Catalán^{1*}, Yasmina M. Martos², Jesús Galindo-Zaldívar^{2,3}, Minoru Funaki⁴

¹ *Real Instituto y Observatorio de la Armada, 11000, San Fernando, Cádiz, Spain.*

² *Instituto Andaluz de Ciencias de la Tierra, CSIC-UGR, 18002 Granada, Spain.*

³ *Departamento de Geodinámica, Universidad de Granada, Campus Fuentenueva, s/n 18002 Granada, Spain.*

⁴ *National Institute of Polar Research, 9-10 Kaga 1, Itabashi, Tokyo 173-8515, Japan,
funakiminoru@gmail.com.*

*Corresponding author
E-mail: mcatalan@roa.es

Abstract

Deception Island is a young and active volcano located in the south-western part of Bransfield Basin backarc. During the last twenty years the Royal Observatory of the Spanish Navy has carried out geophysical surveys in the area. In addition, an UAV flight was conducted in 2011 at 800 m height on the northern half of Deception Island. Analysing and comparing magnetic grids obtained in different periods and tie point readings allows us to detect temporal changes, isolating signals of volcanic origin and. Magnetic cruises performed at Deception Island's inner bay (1988, 1999 and 2008), and the study of its outer magnetic anomaly changes, point to a period of high variations concentrated between December 1989 and December 1999 that may be related to the two main recent periods of seismic activity (1992 and January 1999). From December 1999 to December 2008, there were no significant changes in seismic activity; nevertheless, our data show some magnetic alterations, which might signal the slow progress of a volcanic environment towards equilibrium. Interpreting these magnetic changes called for the construction of several forward models. Additionally, we put forth this kind of study as a suitable, economical and easy method for monitoring an active volcanic system whenever it is possible to measure

the magnetic field with accurate positioning, and if the external field components are removed correctly.

Key words: Marine magnetics, Unmanned aerial vehicle, Secular variation, Volcano monitoring, Antarctica.

Abbreviations:

DI: Deception Island; BS: Bransfield Strait; SSI: South Shetlands Islands; PMA: Pacific Margin Anomaly; UAV: Unmanned Aerial Vehicle; CM4: Comprehensive Model 4; SV: Secular Variation; ARC: Arctowski Observatory; LIV: Livingston Island Observatory; ARM: Antarctic Reference Model; Δ SV: Delta Secular Variation; TRM: Thermo-remanent magnetization; SST: South Shetland Trench.

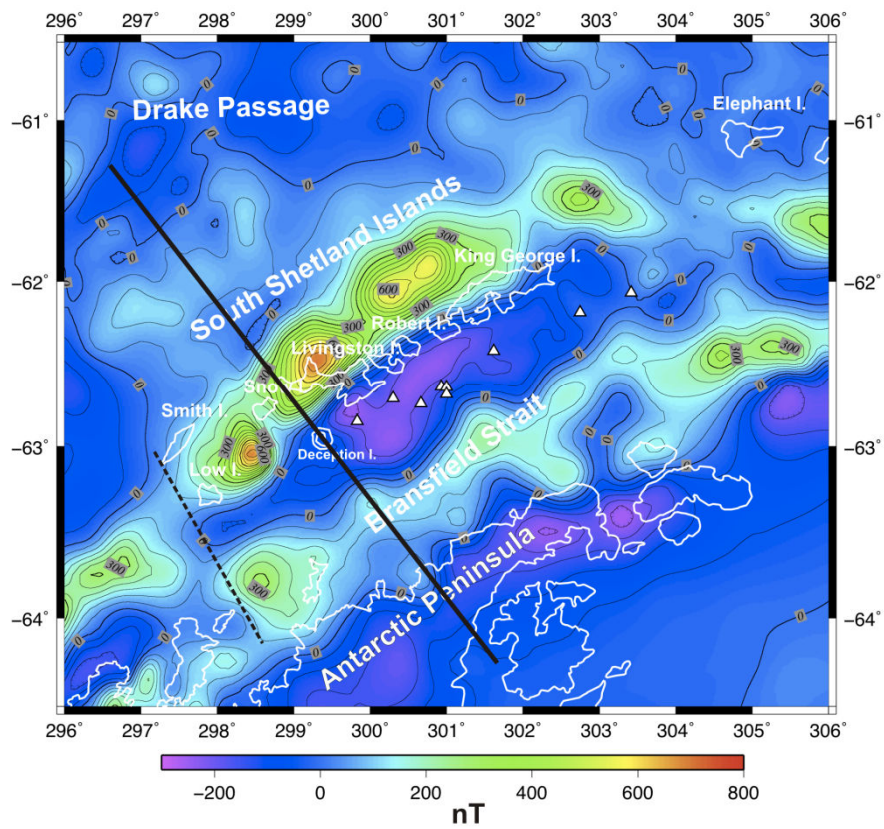
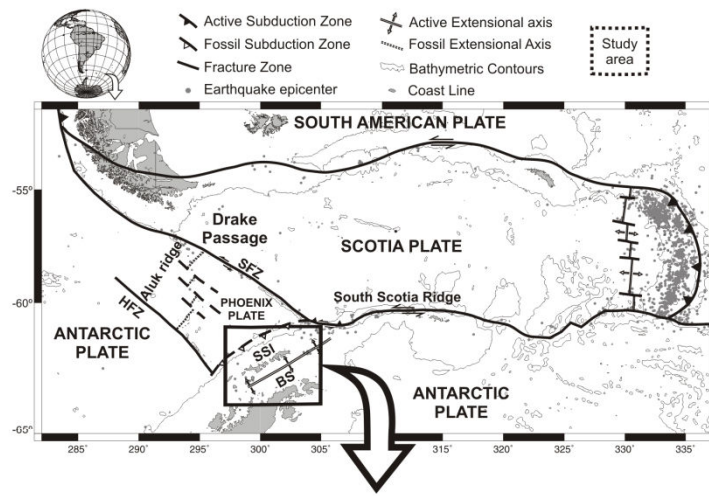
1. Introduction

The study of magnetic anomalies is one of the oldest methods used in geophysics to investigate subsurface geology. This method is based on anomalies of the magnetic field of the Earth, resulting from the magnetic properties of the underlying rocks and their sensitivity to changes in thermodynamic conditions.

Volcanic environments including intermediate and basic igneous rocks show a characteristic magnetic response. These volcanic rocks are generally characterized by high magnetic susceptibility values (Telford et al., 1990) and produced magnetic anomalies when cooled below the Curie Point temperature, becoming an excellent tool to determine the magma migration. Large values and high gradient areas are relatively common. Generally, the remnant contribution is significant and can potentially show high variability.

Figure 1. Geological setting.(a) Regional geotectonic framework of the area and location of the South Shetland Islands. Main geological features are included. (b) Magnetic map obtained from ADMAP database (Golynsky et al., 2001, 2002). This map refers to an average levelling surface of 1500 m. White triangles mark the presence of sub-aerial and submarine volcanoes. Thick black line represents geographical location of profile modelled in Figure 7. Contour interval: 50 nT. Colour palette in nT. SFZ: Shackleton Fracture Zone, BS: Bransfield Strait, HFZ : Hero Fracture Zone, SSI: South Shetland Islands. SST: South Shetland Trench at Figure 1(a) an arrow marks the presence of Deception Island (DI).

(a)



(b)

Deception Island (DI) constitutes the emergent part of a young active shield volcano (less than 1 Ma in age) of basaltic-andesite composition. It lies in the south-western part of the Bransfield Strait (BS), that is a backarc basin located between the Antarctic Peninsula and the South Shetland Archipelago (Fig. 1(a)) related to the oceanic subduction at the South Shetland Trench. It is a horseshoe-shaped island, which is a collapsed and drowned volcanic crater, providing a natural harbour for shipping since it was discovered by sealers in 1820. Its last eruptions took place in 1967, 1969 and 1970, destroying the British and Chilean scientific bases. There have been two additional periods of abnormal seismic activity in 1992 and 1999, described by Ortiz et al. (1997) and Ibañez et al. (2003).

The main aim of this research is to characterize the magnetic anomalies of Deception Island and their variation since 1987, as a support to improve the knowledge of its depth structure and the recent volcanic activity. The present study describes and interprets all magnetic data available from different scientific surveys carried out around and within the DI volcano by the Royal Observatory of the Spanish Navy between 1987 and 2008. In addition magnetic data obtained from UAV flight conducted in 2011 at 800 m height on the northern half of Deception Island are integrated.

2. Regional Setting

Bransfield basin is a 500 km long extensional basin, with a well-marked NE–SW orientation that developed during the Late Cenozoic. The Hero fracture zone and DI mark the abrupt ending towards the southwest (Fig. 1(a)), whereas the northeast limit is more gradual towards the South Scotia Ridge (González-Casado et al., 2000, Fig. 1(a)).

Bransfield Strait is considered a backarc basin of the oceanic subduction along the South Shetland Trench (SST) and below the South Shetland Islands (SSI) volcanic arc (Fig. 1). The origin of this archipelago is related to magmatism and deformation induced by the former Phoenix plate subduction under the Antarctic plate during the Upper Mesozoic–Cenozoic interval (Dalziel, 1984; Barker et al., 1991). This convergence ceased 3.3 Ma ago, when the Phoenix plate's spreading became inactive (Aluk Ridge, Fig. 1(a)) (Lawver et al., 1995; Livermore et al., 2000).

Bransfield Basin is enclosed by two long wavelength positive magnetic anomalies (Fig. 1(b)). The first one runs north-eastward along the South Shetland Islands, while the second runs roughly sub-parallel along the Antarctic Peninsula margin.

Several authors have studied these intense positive magnetic anomaly branches (Garrett, 1990; Suriñach et al., 1997; Ghidella et al., 2002). They are part of a magnetic anomaly belt known as the Pacific Margin Anomaly (PMA), which is interpreted as being caused by a mafic-intermediate batholith of varied age and composition (Garrett, 1990). This sigmoidal magnetic anomaly belt extends without interruption along the western Antarctic Peninsula as far as Adelaide Island (67°S-68°W), while in Bransfield Strait it is divided into the two previously mentioned branches. One branch is located along the SSI, and the other follows the margin of the Peninsula (Suriñach et al., 1997; Ghidella et al., 2002).

Throughout the BS, a series of submarine and sub-aerial seamounts can be found (Fig. 1(b): white triangles), some of them corresponding to sub-aerial volcanoes, such as Deception Island. DI is a complex strato-volcano with an external diameter of about 17 km. This volcanic island has been very active during its entire evolution, and it is composed of basaltic to andesitic rocks that date from < 0.75 Ma to historical eruptions (1842, 1967, 1969 and 1970) (Smellie, 2001). Nowadays, most of its activity is represented by vigorous hydrothermal circulation, slight resurgence of the inner bay floor and intense seismicity, with frequent volcano-tectonic and long period events (Zandomeneghi et al., 2009).

Previous studies have reported seismic information in terms of refraction and P wave tomography (Grad et al., 1992, 1997; Ben-Zvi et al., 2009; Zandomeneghi et al., 2009) or potential field data (Vila et al., 1992; Muñoz-Martín et al., 2005) to draw a general picture of the crustal structure of DI.

3. Material and Methods

Geophysical cruises carried out by the Royal Observatory of the Spanish Navy in the austral summers of 1987, 1988-1989, 1990-1991, December 1999 (DECVOL cruise), January-February 2002 (GEODEC cruise), and December 2008 (MAREGEO cruise) (Fig. 2) provide a body of information spanning almost two decades, allowing us to detect temporal changes of magnetic anomalies in the volcano area by isolating signals of

volcanic origin, and comparing magnetic grids obtained in different periods. Also, on December 18th 2011 an aeromagnetic survey at 800 m was conducted using an unmanned aerial vehicle (UAV) on Deception Island covering its northern half (Fig. 2). The available data enhance our knowledge of tectonics and volcanic evolution of the study area.

Data from the different marine surveys were obtained by means of marine proton precession magnetometers, which were towed 200 m astern. Their sampling rate was fixed at 0.16 Hz. These data were corrected by means of lag corrections and spike removal. Only the most recent cruises were corrected by removal of external fields, relying on different options: the Livingston Island geomagnetic observatory, a local reference station at DI, the CM4 model's external field estimation (CM4: Comprehensive model 4) (Sabaka et al., 2004.), or a combination of the above (see 3.1.1 for details). Table 1 summarizes the acronym that will be used in the text for every cruise, and the different corrections applied.

Moreover, on December 18th 2011 an UAV flight was conducted at 800 m height on the northern half of DI. This flight consisted in 12 km-length East-West lines with a 1 km as across-track distance. Two of them were repeat tracklines flown in the same course but in the opposite direction. Technical details regarding this technique could be found at Funaki et al. (2008).

3.1 Error Budget Study

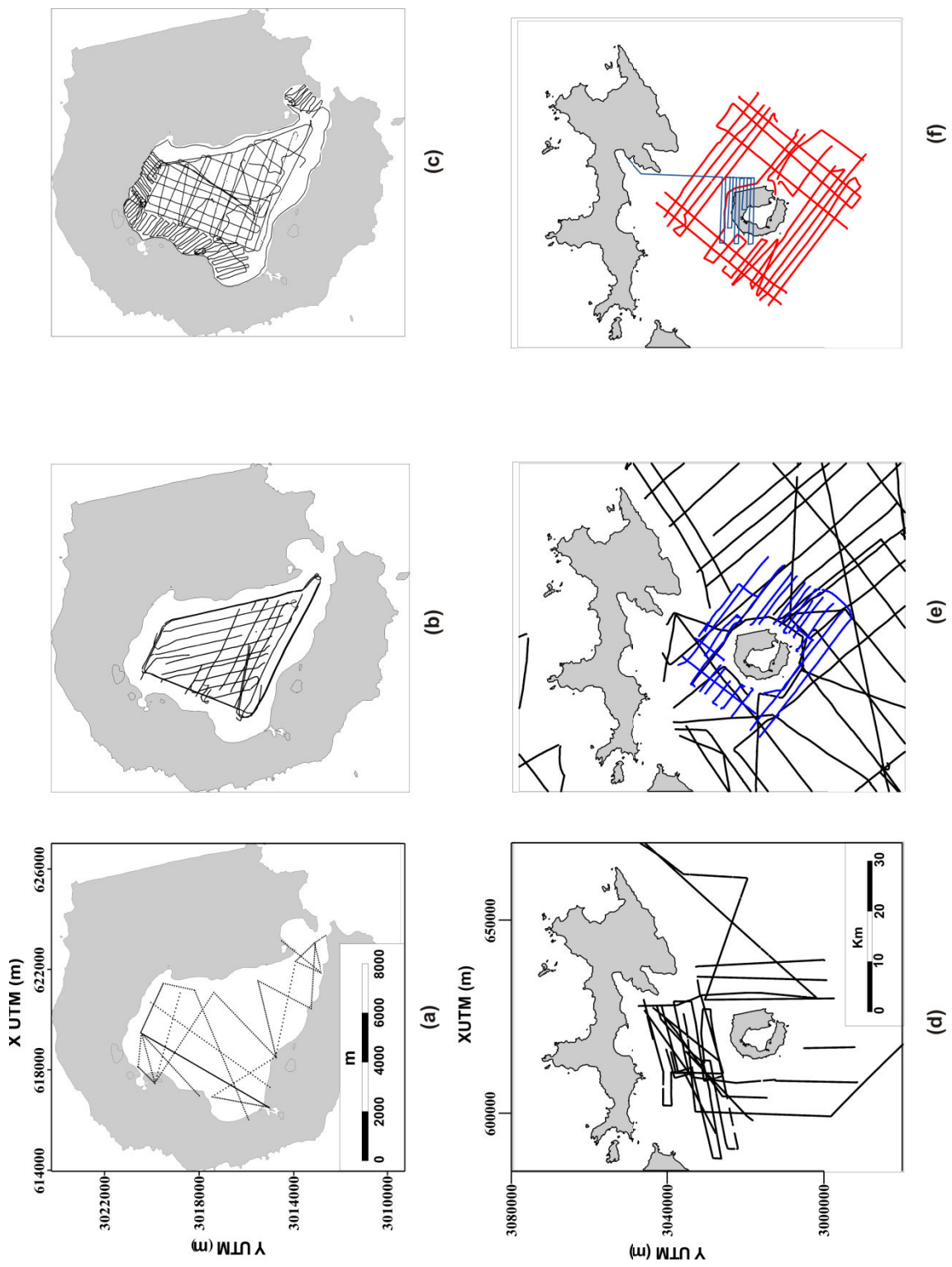
Marine magnetic readings are affected by three different error sources:

1. An incomplete cancellation of external field contributions.
2. An indirect effect produced by a possible lack of precision in the ship's position.

This fact, considering the local magnetic field gradient, could generate differences in crossover readings near the coast where the spatial gradient is maximized.

3. Instrumental errors.

Figure 2. Marine magnetic track line coverage in the area. Inside Deception Island: a) Austral summer 1987-1988, b) December 1999, and c) December 2008. Outside of Deception island: d) Austral summer 1989-90, e) December 1999 (blue lines), and January-February 2002 (black lines), and f) December 2008 (red lines) and unmanned aerial vehicle flight (blue lines). Coordinates in Universal Transverse Mercator (meters).



3.1.1 External contributions

External field contributions are usually extracted by using reference magnetic stations. Our records were corrected for this effect, except the oldest cruises (1987-1990) (Table 1) as these records do not show the time of acquisition —only the day of navigation is known. We should underline that the situation for the 1987/1988 inner bay survey was different, as it was corrected by using an on-land control point.

Cruise Acronym	Time period	Corrections			
		Shift to sensor's position	External field's		Core field
			Using local reference station	Using CM4 Model	
1987/1988	1987/1988 austral summer	YES	NO	NO	IGRF - 10
Las Palmas-89	01 dec. 1989 - 28 mar. 1990	YES	NO	NO	IGRF - 10
DECVOL	29 nov 1999 - 08 dec. 1999	YES	YES	YES (*)	IGRF - 10
GEODEC	14 jan. 2002 - 21 feb. 2002	YES	YES	NO	IGRF - 10
MAREGEO	03 dec. 2008 - 24 dec. 2008	YES	YES	NO	IGRF - 10

Table 1. Geophysical surveys and corrections applied. * See paragraph 3.1.1 for details.

Additionally, due to technical problems, one day during the DECVOL cruise data was not corrected by this contribution, as we did not have any reference station available. This issue was overcome by using the CM4 model's external field estimation.

Though one must be cautious when applying magnetic models in Polar Regions, where the Solar-Earth interaction is strongest, the DECVOL marine survey was carried out during the night-time. Thus, the regular magnetic daily variation impact was minimal. The Kp indexes were systematically low during this period (75% of the time characterized by Kp 3), and particularly low during the night (92% of the time characterized by Kp 3).

We calculated differences between the external field variation based on Livingston observatory data and the values provided by the CM4 model, obtaining a value of nT.

The older cruises (not corrected by external fields), with the exception of the 1987/1988 survey, took place close to a period of maximum solar activity. We analysed Livingston observatory data from December 2001 to March 2002, an ordinary austral summer research-working period, under solar activity conditions similar to those of the older cruises. Accordingly, the external magnetic field shows an average maximum amplitude of 50 nT for this period of time.

3.1.2 Ship's position

Nakatsuka et al. (2009) considered the effect of positioning errors as the crucial problem in areas of high magnetic anomaly gradients. Positioning was based on satellite Doppler techniques during the 80's. From the late 80's onward it came to be based on the Global Positioning System (GPS). The former satellite-based system provided an accuracy of roughly 200 m, whereas the latter shows an error in position just under 100 m. However, on 1st May 2000, the 'Selective Availability' code was turned off, allowing all users (military and civilian) to enjoy nearly the same level of access, with a precision of less than 20 m.

Although GPS did not provide full-time coverage at earlier dates (late 80's), the first surveys (1987–1990) were always performed taking advantage of windows of time where a GPS signal was available, except the 1987/1988 inner bay survey. The pneumatic boat's positioning was performed by visual bearings in this case. It is therefore not easy to

quantify its contribution to the error budget, a conditioning factor that will be further discussed in the section 5.

The analytical signal grid provides a good representation of the magnetic gradient distribution for the whole marine area of interest. A detailed analytical signal grid for the DI outer area, derived from MAREGEO and GEODEC data, shows an average gradient of 0.01 nT/m, while 0.12 nT/m (maximum value) may be considered as an upper limit. Considering, once again, that 100 m may represent the position error for the older surveys, this would justify an anticipated upper limit error contribution for uncertainty in navigation of about 12 nT (worst situation), and 1 nT on the average. The situation was completely different for later cruises (DECVOL, GEODEC and MAREGEO), as the error in position was less than 20 m.

3.1.3 Instrument errors

In relation to instrument errors, our experience with proton precession magnetometers (Catalán et al., 2006; Quesnel et al., 2009) leads us to assert that any error would be less than a few units of nT (we considered 5 nT as the worst situation). Therefore, its influence on the secular variation (SV) calculus would come to less than 0.5 nT/yr (when we compare cruises separated by a ten-year gap), and would moreover be attenuated as we merge different instruments.

3.1.4 UAV flight

We removed noisy measurements, and used data where the course was fixed. The difference in anomaly values between repeated track lines flown in opposite direction has been obtained. Its value was nT. It reflects the net effect of magnetization of the plane, the external fields' contribution, and positioning errors.

4. Comparison of anomaly maps and secular variation scenario

Two procedures were used to identify volcanic signals: a) identifying anomalous secular variation areas estimated from tie point readings, and b) comparing magnetic grids obtained in different periods.

We applied the first method offshore, away from DI; it was not possible to compare grids from various periods because of their different spatial coverage. In the central part of the inner bay of DI, spatial coverage of the three different surveys (Austral summer 1987/1988, December 1999 and December 2008) were denser and allowed us to compare grids from different periods (second method). Interpretation of these magnetic changes benefits from a general overview of the study area from the magnetic point of view.

4.1. Regional magnetic anomaly map

The maps in Figure 3 show the 1 km resolution scalar magnetic anomalies map upward continued up to 800 m (Fig. 3(a)) and 2 km (Fig. 3(b)) derived using marine and UAV data, applying a Kriging interpolation algorithm.

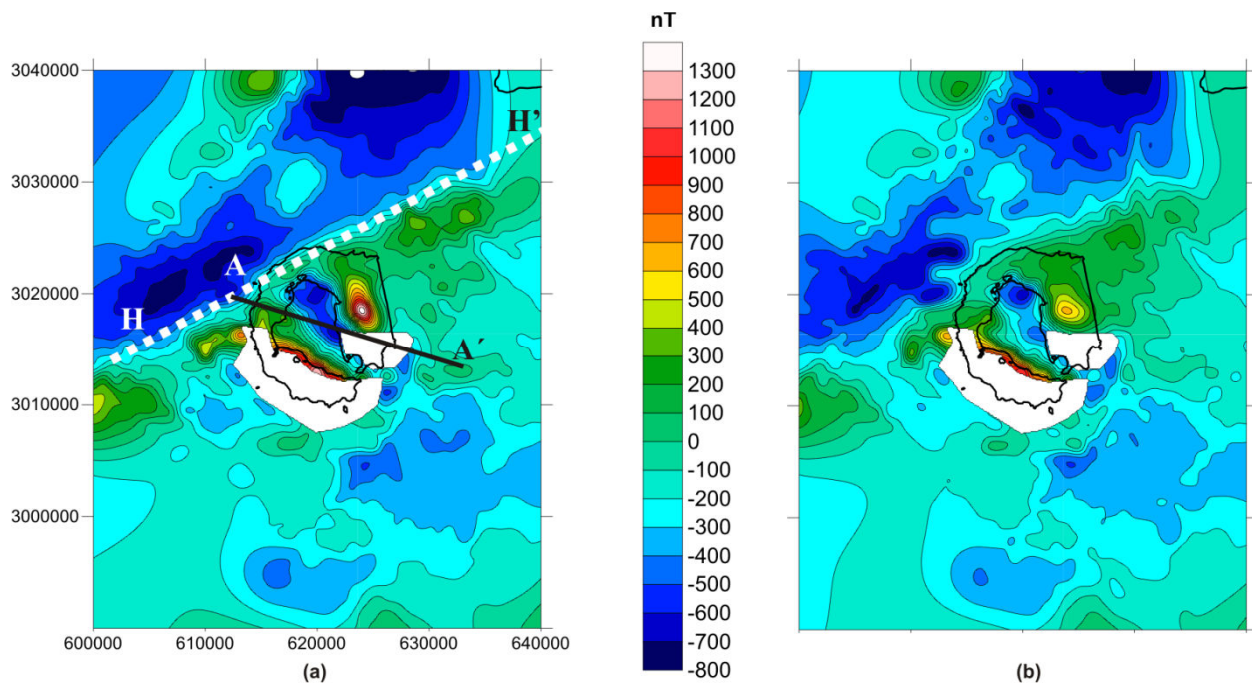


Figure 3. Upward continued magnetic anomaly map (1 km resolution) of Deception Island from marine and unmanned aerial vehicle survey data. a) up to 800 m, and b) up to 2 km. Coordinates in Universal Transverse Mercator (meters). Black solid line (A-A') represents geographical location of profile modelled in Figure 10. Contour interval: 100 nT.

The main feature observed on the magnetic anomaly map is a local dipolar trending NE-SW (H-H', Fig. 3(a)), which runs about 15 km northward of the rest of the volcanic

edifices that lie along the Bransfield Basin (Fig. 1(b): white triangles) (Gràcia et al., 1996). It was interpreted by Muñoz-Martín et al. (2005) as a consequence of the existence of two crusts with different magnetic properties. Previous seismic refraction research (Grad et al. 1992) supports the existence of two tectonic units on either side of DI: a crystalline basement to the northwest that may correspond to the continental South Shetland Block intruded by igneous rocks, and an altered different one, located at the southern part of DI corresponding to thinned continental or even initial oceanic crust (Catalán et al., 2013). Similar conclusions were achieved by Zandomeneghi et al. (2009) from a seismic tomography experiment. A local positive magnetic anomaly, embedded in a wider negative one, is observed in the north-western part of the map (Fig. 3(a) and (b)).

A positive local high appears on the eastern onshore part of DI, while a NW-SE negative linear anomaly occupies most of DI inner bay. Although we have no onshore data on the western part of DI we can observe positive anomaly values along its western shoreline. To attenuate the shallow-source anomalies due to near-surface rocks and to emphasize deeper sources this anomaly map was upward continued up to 2 km (Fig. 3(b)). This map provides a simpler magnetic anomaly picture. The linear gradient (Fig. 3(a): $H-H'$) still remains. The positive local high on the eastern onshore part of DI is associated to a negative anomaly with similar wavelength, which is located in the DI's inner bay.

The large negative anomaly which covers a great extension of DI inner bay seems to be embedded inside a general positive anomaly which covers the onshore part of DI. Values higher than 1000 nT are reached in the south-western onshore part of DI (Fig. 3(a) and (b)).

4.2. Inner Bay magnetic study

During the 1987/1988 austral summer, and in December 1999 and December 2008, DI's inner bay was surveyed using a marine magnetometer (Fig. 2 (a), (b) and (c)). We gridded this marine data and obtained three 300 m resolution scalar magnetic anomaly maps (Fig. 4 (a), (b) and (c)). This figure displays the location of the central linear gradient area (austral summer 1987/1988: black dashed line; December 1999: grey dashed line; December 2008: red dashed line). This feature marks the transition between positive (to the southwest) and negative (to the northeast) magnetic anomaly values in the inner bay of DI.

Certain differences in the location and position of the magnetic anomalies are shown, mainly affecting the amplitude of the NW-SE linear low that run through the inner bay, and the location of the high magnetic gradient area. To facilitate the interpretation we have subtracted the 1987/1988 magnetic anomaly grid (Fig. 4(a)) from the 1999 survey (Fig. 4(b)). A similar procedure has been followed to the 1999 and 2008 surveys. Fig. 4 (d) and (e) are respectively the result of these simple subtractions. Next we describe the location and position of magnetic anomalies from these three different time periods.

4.2.1. Austral summer 1987/1988 vs. December 1999

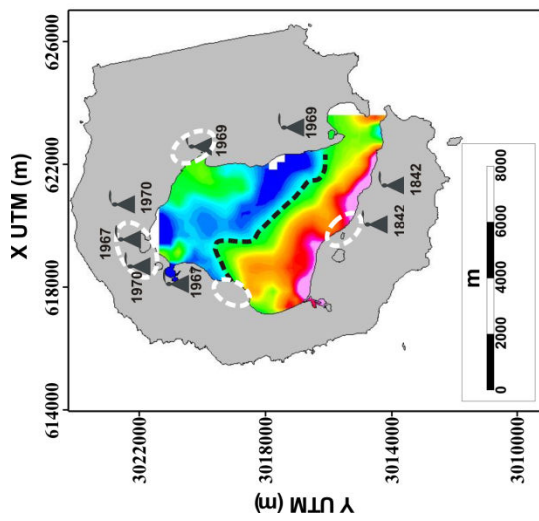
By comparing Fig. 4(a) and (b) we detected the disappearance of some local negative magnetic sources in the NW part of the bay. Additionally, the central part of the NW-SE linear gradient area is distorted and displaced by about 300 or 400 m to the NE (Fig. 4(b): black dashed line to grey dashed line). Fig. 4(d) shows that a general positive variation in the magnetic anomaly map (greater than 200 nT) represents most of DI inner bay. A dashed black polygon limits an area where negative values are obtained.

4.2.2. December 1999 vs. December 2008

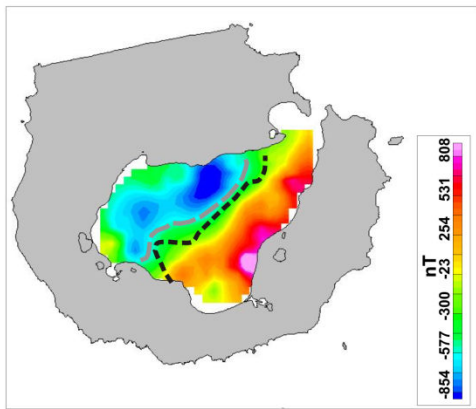
The magnetic anomaly values do not show significant variations (Fig. 4 (b) and (c)) between these two periods. The map of magnetic anomaly differences between both epochs (Fig. 4(e)) confirms this. The location of the positive differences area and negative differences area keep roughly the same with the previous period (Fig. 4(d)), but it shows an attenuation on the amplitude of these residuals (Fig. 4 (d) and (e)). The NW-SE trending gradient area shows practically no distortion, though it is displaced 500 m to the northeast (Fig. 4(c): grey dashed line to red dashed line).

4.2.3. Secular Variation and Magnetic study off DI

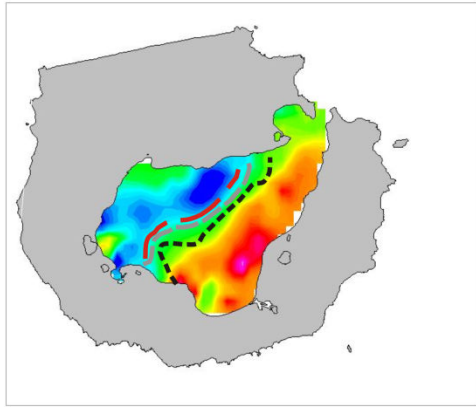
Crossover analyses are used to estimate the quality of a geophysical survey and are also an effective technique for improving the internal coherency of geophysical data grids (Wessel and Watts, 1988; Thakur et al., 1999; Quesnel et al., 2009). Since, in general, the local magnetic anomaly is time-invariant, if we examine the crossover difference between



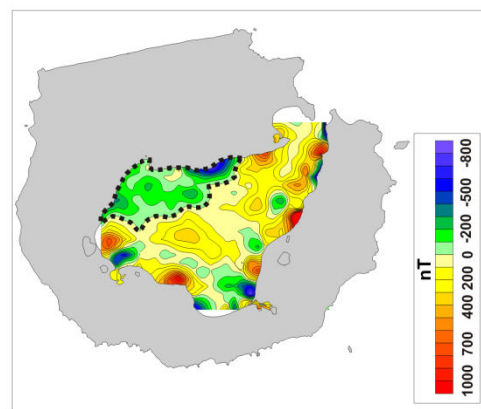
(a)



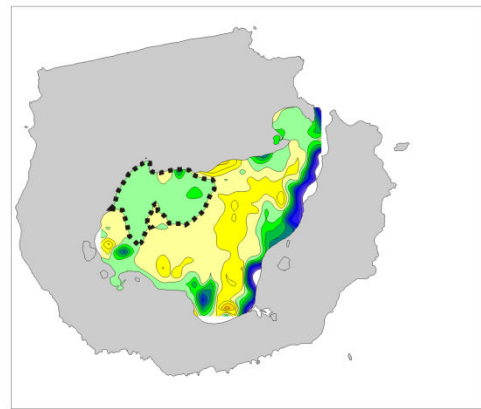
(b)



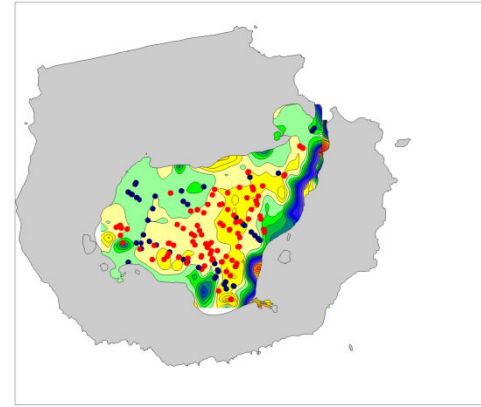
(c)



(d)



(e)



(f)

two tracks, the residue will contain information related to time-dependent geomagnetic field components, that is, SV and external field contributions.

We obtain the SV by means of finite differences between readings at tie points, and using the differences of acquisition time. For example, two measurements (39754 nT and 38800 nT) taken at a tie point, at two different times, respectively January 1, 1989 (1989.0000) and February 12, 1999 (1999.1178), allow us to infer the SV $(38800-39754)/(1999.1178-1989.0000)$, which means -94.3 nT/yr.

Geomagnetic observatories traditionally monitor local SV. Temporal monitoring in the BS was performed by Arctowski Observatory (ARC), established in 1978, at the Polish Base of the same name on King George Island (Fig. 1). This observatory ceased operations in December 1995, and the Livingston Island Observatory (LIV) started operations in December 1996.

Generally speaking, the SV has a global morphology. Thus, the differences in secular changes between sites some tens of kilometers apart are usually negligible. We compiled a synthetic temporal SV series using both ARC and LIV data (Fig.5: LIV in red dots, and ARC in red diamonds).

Secular variation varies smoothly over time, as can be observed in the ARC series. Yet we see fluctuations in LIV data that can hardly be justified (especially in 2003) as a result of the core geomagnetic field variation. Such alterations are most probably associated with data gaps, particularly during 2003, which make it difficult to assess the real SV. This

Figure 4. Magnetic map of the Deception Island's inner bay at three different periods: a) 1987-1988 (b), December 1999, (c) December 2008. The location of the linear central gradient area is depicted using a dashed line (black for austral summer 1987-1988, grey for December 1999, and red for December 2008). Figure 4 (a) shows historical eruptions and thermal and fumarolic fields (inside white dashed ellipse) (modified from Ibañez et al. 2000). d) This magnetic map shows the difference between Deception Island's inner bay at 1999 (Fig. 4(b)) and at 1987-1988 austral summer (Fig. 4(a)). e) It shows the magnetic anomaly change between Deception Island's inner bay at 2008 (Fig. 4(c)) and at 1999 (Fig. 4(b)). f) It shows the tie-point magnetic anomaly residua from every combination of cruises (Fig. 4(e)): MAREGEO vs. DECVOL, MAREGEO vs. 1987/1988 cruise, DECVOL vs. 1987/88 cruise. In red: a positive change in the magnetic anomaly at tie-point reading. In blue: a negative change in the magnetic anomaly at tie-point reading. Map of differences in the magnetic anomaly map for MAREGEO and DECVOL cruises is shown as background to facilitate interpretation. Figures 4(a), 4(b) and 4(c) share the same colour palette (inside Figure 4(b)). Figures 4(d) and 4(e) share the same colour palette (inside Figure 4(d)). Coordinates in Universal Transverse Mercator (meters). At Fig. 4(d) and (e) a dashed black polygon limits an area where negative values are obtained.

fact is confirmed by the yearbooks published on the Ebre Observatory website (http://www.obsebre.es/php/geomagnetisme/boletin_livingston.php).

In order to compare this data on equal terms with the Antarctic Reference Model (ARM), we filtered the ARC+LIV data series to attenuate the impact of data gap periods. This made it possible to represent a moving average of the ARC + LIV series (Fig.5: blue dots).

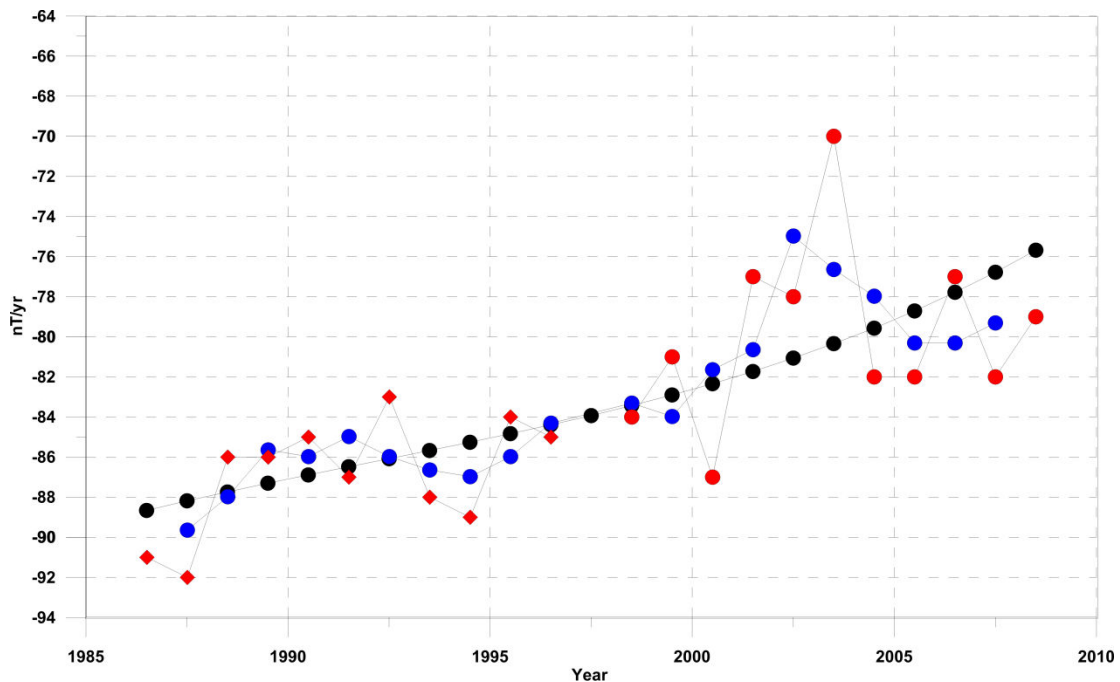


Figure 5. Secular variation of the area inferred from the Antarctic Reference Model (black dots), from Livingston observatory (LIV) (red dots) and from Arctowski observatory (ARC) (red diamonds). Blue dots indicate a running average of the raw observatory series (ARC+LIV).

There is a reasonable correlation between the two series. The mean of the differences between them is zero, supporting the values provided by the secular variation from the ARM model as a realistic representation of the real SV.

Using the SV derived from the ARM model (Fig. 5: black dots), we calculated a theoretical approach to the SV value. The difference between observed SV at tie points and the theoretical average value between tie points epochs calculated from ARM model, called Δ SV, mainly contains information related to local crustal processes.

The impact of the different error sources (external fields, positioning and instrumentals) on the final Δ SV error budget gives us a total budget of nearly 6 nT/yr for

the 1989-1999 period (external contribution: 5 (50/10)nT/yr, positioning error: 1.2 (12/10) nT/yr and instrumental errors: 0.5 nT/yr). The “10” that divides the external contribution (50 nT) and positioning error (12 nT) corresponds to the length of the time gap between 1989 and 1999. The external error contribution estimation based on Livingston observatory magnetic records is detailed in 3.1.1. The positioning and instrumental contribution estimations are respectively based on data given under 3.1.2 and 3.1.3.

This threshold value for the error (6 nT/yr) considers a situation where we lack magnetic reference station data and GPS precision, so that it may be considered the worst possible case.

Figure 6(a) describes the first period (DECVOL–“Las Palmas-89”). The main ΔSV anomaly is a wide low southeast of DI. In the same area, GEODEC-DECVOL period (Fig. 6(b)) shows positive ΔSV values, and isolated positive and negative values are also displayed during this period. The MAREGEO-GEODEC (Fig. 6(c)) period does not show significant changes.

4.3. Modelling and interpretation

4.3.1. Regional model

As a general approach to the area, and to facilitate the modelling of DI inner bay area (see 4.3.2 section), we performed 3D magnetic model delineation of its main features—BS, PMA (Southern and Northern branches), and DI— using prisms. We used the PRISM3D Fortran programme (Mendonça and Meguid, 2008) to calculate magnetic responses. The input of a particular geophysical model involves basic information such as observation height, local geomagnetic field parameters (intensity, declination and inclination), and geometric features of the different prisms in use (depth to the top and to the bottom, thickness, and horizontal dimensions). Additionally, information concerning the magnetic properties of every prism is needed (magnetisation intensity, inclination and declination) to describe plausible remnant effects.

Our model was built using eight main blocks (Fig. 7, Table 2). They consisted of a) two deep bodies (first and second block), accounting for the northern and southern branches of the PMA, and separated by a marginal basin within BS (the third block, or “BS lower crust” at Fig. 7). Magnetisations of the first two bodies were constrained using values

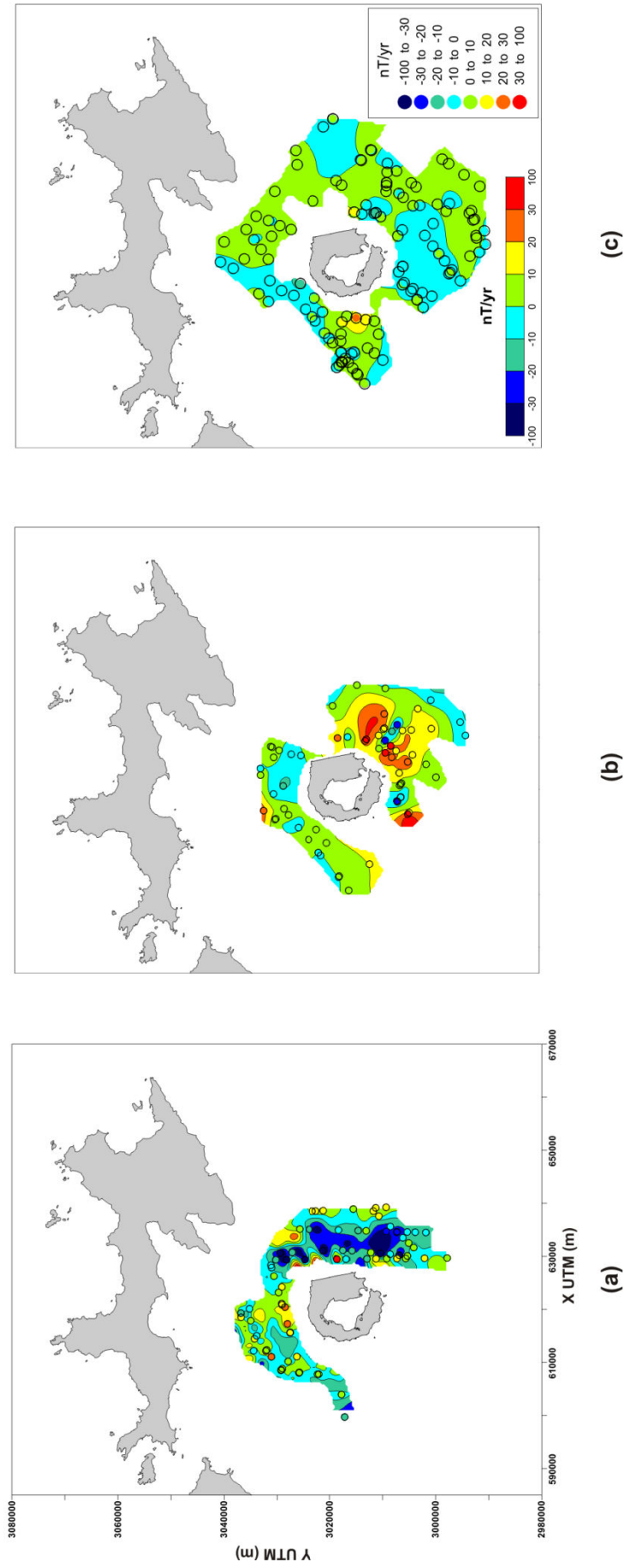


Figure 6. Magnetic anomaly variation outside of Deception Island. a) Colour map shows a grid obtained after subtracting the corresponding scalar anomaly maps for “Las Palmas-89” and DECVOL cruises, dividing the residuals by the period of time between the averages of their occurrence. Overlay are coloured dots plotted to show the (see text for comments) calculated at tie points. b) The same for DECVOL and GEODEC cruises. c) The same for GEODEC and MAREGEO cruises. Contour interval: every 10 nT/yr. Coordinates in Universal Transverse Mercator (meters).

provided by Garrett (1990). Their depths to the bottom were fixed at 15 km, which is in agreement with depths to the Moho values in DI surroundings (Christeson et al., 2003). b) Two more blocks (fourth and fifth) represent the upper crust: north of DI (“North DI upper crust” at Fig. 7) and south of DI (“BS upper crust” in Fig. 7). Their magnetisations were fixed by keeping an almost double net contrast of magnetisation between the northern and southern DI crust, as reported by Muñoz-Martín et al. (2005). Their depths to the top and to the bottom were fixed in accordance with Grad et al. (1992, 1997). c) Deception Island (sixth block, labelled as “DI magnetic basement” in Fig. 7).d) One block (seventh block) was needed to model DI magnetic response. It was labelled as “DI non-magnetic body”. It represents a magma reservoir. e) One more block (eighth block) was needed to reproduce the changes in DI magnetic anomaly picture throughout these last twenty years. It was labelled as “DI intrusive body”.

Body	Horizontal dimension (km ²)	Magnetization Intensity (A/m)	Declination(°)	Inclination (°)	Depth to the Top (km)	Depth to the bottom (km)
Northern PMA	80 x 130	3.5	10	-50	5	15
Southern PMA	80 x 130	3.5	10	-50	5	15
BS lower crust	100 x 130	0.5	10	-50	5	15
Northern DI upper crust	80 x 130	1	10	-50	0.5	5
BS upper crust	100 x 130	2	10	-50	1.5	5
DI magnetic basement	15 x 14	3.5	10	-50	1.5	5
DI non-magnetic body	5x5	0	-	-	3.5	5
DI intrusive body	4x2	0	-	-	2	5

Table 2. Physical and geometrical parameter of the regional model.

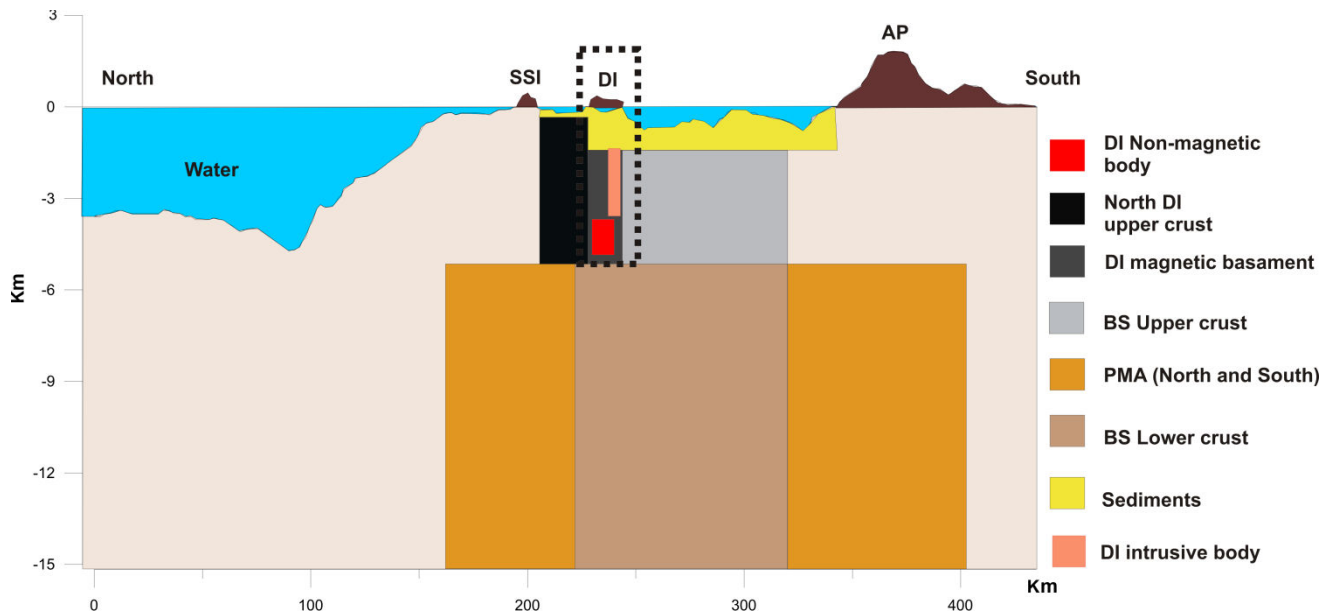


Figure 7. Distribution of blocks, along the profile (Figure 1: lower plot, thick black line) used for the 3D forward modelling of Deception Island area. SSI: South Shetland Islands. DI: Deception Island. AP: Antarctic Peninsula. BS: Bransfield Strait. PMA: Pacific Margin Anomaly.

Depth to the top and thickness values for BS crust, sediment layer, magnetic basement and the non-magnetic body inside DI were determined using information from Muñoz-Martín et al. (2005), Ben-Zvi et al. (2009) and Zandomenighi et al. (2009). Table 2 includes all the parameters used to characterize every prism. The model aims to reproduce the magnetic anomaly map in a qualitative way (Fig. 8 (a) and (b)). We used normal polarity magnetisation for all blocks. The sediment layer was considered as non-magnetic.

The NW part reflects the magnetic effect of the northern PMA influence (Fig.8 (a) and (b): inside a thick dashed green line). The high magnetic anomaly gradient area between northern DI and BS crusts is also depicted (Fig.8 (a) and (b): a thick black dash polygon inside). We should point out that we did not attempt to exactly reproduce two linear positive anomalies that represent local effects and correspond to intrusive bodies. Our model (Fig.8 (b)) reproduces the magnetic anomaly map at 2 km caused by magnetic bodies, which are below sea level. That is why the colour palette covers a narrower interval (-500 nT to 600 nT), while the real one, which includes sub-aerial masses, reflects a broader interval (-800 nT to 1000 nT).

Bransfield Basin is characterized by long wavelength negative values (Fig. 8, inside a black closed dotted polygon) as it represents the magnetic contrast between PMA long wavelength positive anomalies (northern and southern branches).

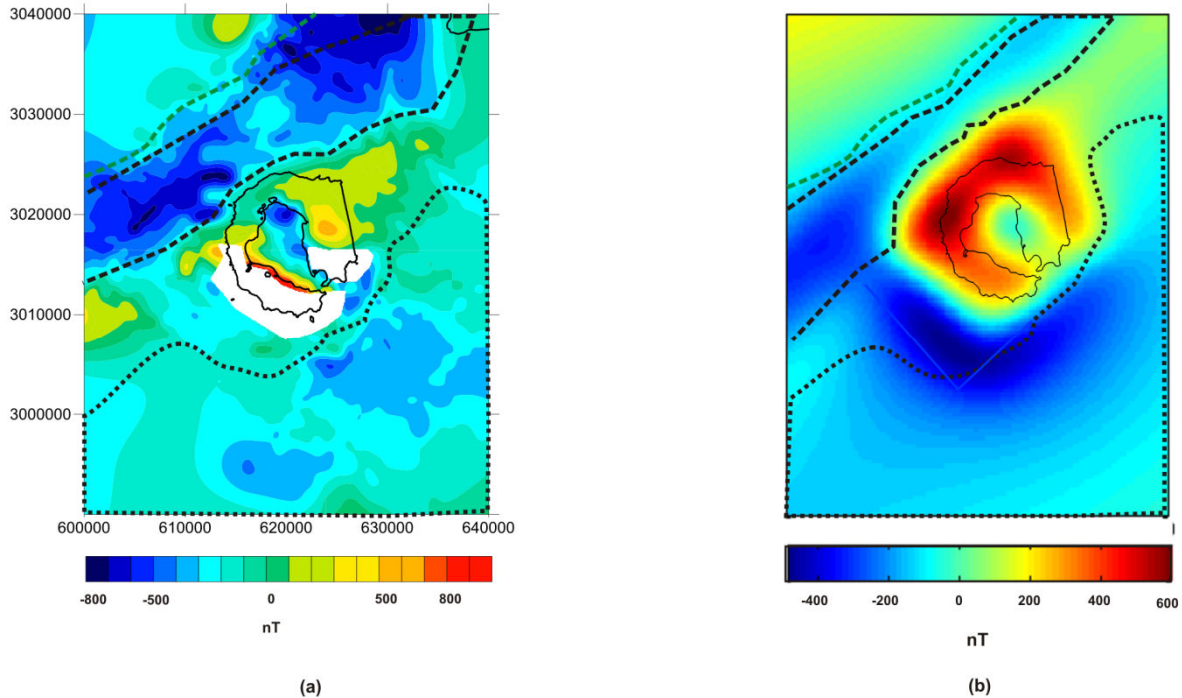


Figure 8. Observed magnetic anomalies from marine and unmanned aerial vehicle survey data at 2 km, and calculated anomalies from 3D modelling. (a) Scalar magnetic anomaly map from marine and unmanned surveys. (b) Forward regional model of the same area. Deception Island was modelled as a cube-like body (represented in this figure as a red square-like body). To facilitate the interpretation we overlaid a plot of Deception Island coastline in black. In a thick dashed green line, a positive magnetic anomaly shows the Northern Pacific Margin Anomaly (PMA). Additionally, a linear gradient represents the contact between a block formed by the Northern PMA and North Deception Island upper crust, and another block formed by the Southern PMA and Bransfield Strait. The magnetic anomaly produced by this contact is highlighted by a thick dashed black polygon. Bransfield Strait magnetic anomaly is limited by a black closed dotted polygon. Coordinates in Universal Transverse Mercator (meters).

4.3.2. DI inner Bay area

Figure 4 ((a), (b) and (c)) shows the DI inner bay anomaly maps; they serve as snapshots of its situation from a magnetic point of view in austral summer 1987/1988, December 1999, and December 2008.

We summarize the features of magnetic variations in each period (1987-1999, 1999-2008) (see 4.2):

(a) 1987-1999:

a. A general positive variation in the magnetic anomaly grid (greater than 200 nT) characterizes most of DI inner bay. A broad area located in the middle eastern offshore sector of the island shows negative values (Fig. 4 (d)).

b. There was an average 500 m north-eastward displacement of the NW trending gradient area (Fig. 4 (b): black thick dashed line and (c): grey thick dashed line).

(b) 1999-2008:

a. Previous pattern is repeated but it shows attenuation on the amplitude of positive and negative residuals (Fig. 4 (e)).

b. The NW trending gradient area shows practically no distortion, though it is displaced 500 m to the northeast (Fig. 4(c): grey dashed line to red dashed line).

To reproduce these features, which characterize the temporal evolution of the inner part of the island over the two decades we propose a forward model as reference of DI which should represent DI situation at 1987/1988 austral summer (Fig. 9(a)).

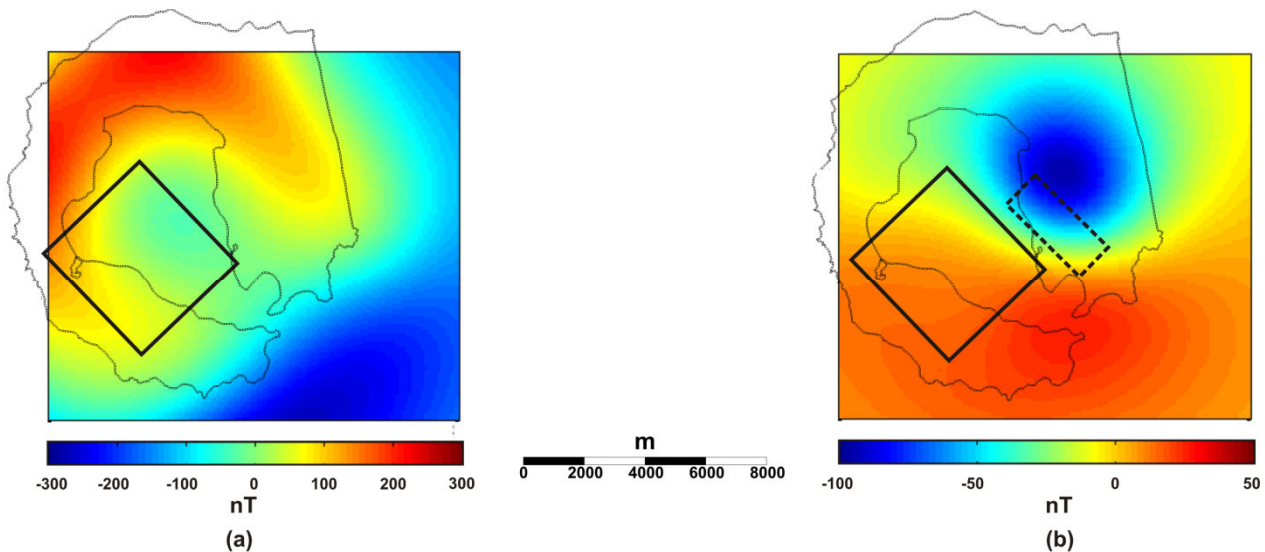


Figure 9. Magnetic anomalies obtained from 3D modelling. a) This map shows a magnetic forward model of Deception Island using Table 2. b) Simple difference between the magnetic anomaly at Deception Island after including a non-magnetic body in the eastern onshore part of the island and magnetic anomaly map displayed at Figure 9(a). A thin black rectangle shows the location of the non-magnetic body inside Deception Island's inner bay. A black dashed rectangle at Figure 9(b) designates the location of a new intrusive body proposed as origin of the magnetic anomaly changes at Deception Island.

The January 2005 seismic tomography experiment (Zandomeneghi et al., 2009) localized an area of V_p anomalies (low values) beneath the DI inner bay (north-western part). It extends to a depth of 5.5 km, and reaches its maximum velocity perturbation between 1 km and 2 km in depth. It was interpreted as a magma chamber. Muñoz-Martín et al. (2005) detected a wide Bouguer gravity and magnetic minimum at the same geographical location (toward the north-western part of DI). They forward modelled it as a partially melted intrusive body at a depth of approximately 2 km by using Euler Deconvolution techniques. A thin black rectangle shows the location of this non-magnetic body inside DI inner bay (Fig. 9(a) and (b)).

We should highlight some restrictions to our models: the PRISM3D Fortran programme only works with rectangular prisms. Additionally, we assumed isotropic physical parameters and constant magnetic properties (intensity of magnetisation, declination and inclination) (see Table 2). Magnetisation intensity for DI magnetic basement was determined by forward modelling, and selecting a 3.5 A/m value, as it provides the best fit to real observed anomalies (Fig. 9(a)). For particular details concerning physical and geometrical parameters of every block, see Table 2.

Taking into account the main differences between the austral summer 1987/1988 anomaly map and the situation in December 1999, we included a non-magnetic body in the eastern part of the island (a black dashed rectangle in Figure 9(b)).

Fig. 9(b) shows a simple difference between the magnetic anomaly at DI after including this non-magnetic body in the eastern part of the island and the magnetic anomaly map of Fig. 9(a) used as reference. The aforementioned inclusion of a new non-magnetic body in the eastern part of DI (Fig. 9(b)) is able to reproduce positive changes in the magnetic anomaly map in most of the inner bay, while producing negative changes in its eastern part. This features characterize the magnetic anomaly changes at the inner bay of DI from 1987 to 1999 (Fig. 4(d)), and from 1999 to 2008 (Fig. 4(e)).

4.3.3. DI outer area

The variation in the crustal magnetic anomalies for the period December 1989-December 1999 is shown in Fig. 6 (a) using tie point readings, supported with a residual grid. This provides a more complete estimation, obtained after subtracting the scalar

magnetic anomaly maps, then dividing the residuals by the period of time between both campaigns (see 5.2). The main feature observed is a wide low southeast of DI.

5. Discussion

Compilation of magnetic data in DI allows to constrain the deep structure and the variation of magnetic anomalies related to volcanic activity.

5.1. DI inner bay area

As previously described, in general, there were some differences between the first and the second (1987-1999) cruises (Fig. 4(a) and (b)). Analyzing all the possible sources of discrepancies observed between each pair of magnetic grids, we stress that regarding the DECVOL cruise (performed in 1999) neither external fields nor error on position could have had a significant impact on the error budget, as it was corrected by the use of a reference station and differential GPS (<20m).

The displacement could be attributed to wrong positioning and to a less dense and sparse distribution of lines during the 1987-1988 survey. As we explained before, the position was controlled by visual bearings. Therefore its impact on the error budget would be averaged out as it has a random character and cannot explain a 400m-shift displacement of the NW-SE high linear gradient area all along its 8 km in length. To support this notion, and to analyse the effect of a less dense and irregular distribution of tracklines, we carried out several simulations.

We introduced unbiased synthetic noises of 100 m RMS and 150 m RMS in the MAREGEO survey (selected as reference because there was no external field impact, as we used a reference station and a very accurate position using differential GPS).

A second test consisted of extracting data profiles from MAREGEO survey map by digitizing it, following the same trackline distribution as the 1987-1988 survey.

A third test was performed combining simultaneously the noise impact and the 1987-1988 trackline distribution, adding synthetic noises of 100 m RMS and 150 m RMS to those profiles extracted from MAREGEO survey. Finally we obtained new magnetic anomaly maps (taking into account the synthetic noise or the sparse trackline distribution, or both

factors simultaneously) that were compared with the original magnetic anomaly map (from MAREGEO survey) for DI inner bay.

In every case, we observed the following: a) the short wavelength magnetic anomalies slightly distorted both their shape and their amplitude, and sources with amplitude similar to the noise amplitude were the most altered; b) long wavelength features did not show any alteration, in either shape or amplitude, of particular interest in the NW-SE high linear gradient area.

By comparing Fig. 4(a) and (b) we detected the disappearance of some local negative magnetic sources in the NW part of the bay, coinciding with the area of historic fumarolic thermal fields, located near the last eruption centres (1967, 1970). Nevertheless, this is debatable, as it was poorly covered during the DECVOL cruise.

The main difference between the two grids affects a general positive variation in the magnetic anomaly grid (greater than 200 nT) which represents most of DI inner bay, and a broad area located in the middle eastern of DI's inner bay, which shows negative values. Both features are more clearly displayed at Fig. 4 (d). This was interpreted as a new magmatic intrusion at the eastern on shore part of DI (Fig. 9(b)). It is important to highlight that this area concentrates 1969-1970 eruptions (Ibañez et al., 2000).

As this procedure (simple differences between grids) could be debatable as this image could be distorted, i.e.: spatial aliasing effect (Nakatsuka et al., 2009), we have obtained the tie-point magnetic anomaly residua from this combination of cruises: MAREGEO vs DECVOL, MAREGEO vs 1987-1988 survey, DECVOL vs 1987-1988 survey. These differences do not contain any mathematical manipulation and nakedly express the evolution of the magnetic anomaly map between two epochs: 1999 vs. 1987-1988, 2008 vs. 1987-1988, survey 2008 vs. 1999. Fig 4(f) displayed our results. We have selected only two colours: red for a positive change in the magnetic anomaly at tie-point reading, and blue for a negative change. We have plotted in the background the map of differences in the magnetic anomaly map for MAREGEO and DECVOL cruises (Fig. 4(e)). We see a clear correlation between zones where, according with the map of differences, the magnetic anomaly has strengthened (the largest part of the map) and an area where the magnetic anomaly field is weakened (located in the mid-eastern area). We conclude that this simple difference between magnetic anomalies maps (Fig. 4(d) and (e)) could serve as

an estimation of magnetic anomaly change for the 1987-1999 period, or for the 1999-2008 period, respectively.

The uplift of a hot magmatic injection in the eastern part of the island, evidenced by the presence of a non-magnetised body, because its temperature is higher than Curie Point, would generate a positive change in the map of anomalies to the West and a negative change to the East (Fig. 9).

The observation of the NW-SE trend of the isolines for the difference map (Fig. 4 (d)) denotes the need to locate this new source in the mid-eastern coast of the island. This alteration would also produce the observed eastward shift of the long linear gradient area (Fig. 4 (b)). A black dashed rectangle at Figure 9(b) designates the location of a new intrusive body proposed as origin of those magnetic anomaly changes.

Comparison of the second (December 1999) and the third grid (December 2008), shows a similar pattern than the previous described for 1987-1999 period. It shows attenuation on the amplitude of positive and negative residuals (Fig. 4 (e)), and an average 500 m north-eastward displacement of the NW trending gradient area (Fig. 4 (b): grey thick dashed line and (c): red thick dashed line). This setting confirms the stand by existence of this hot magmatic intrusion.

We can discuss that this 500 m north-eastern displacement, which was detected between December 1999 (Fig. 4(b)) and December 2008 (Fig. 4(c)), could be attributed to the error budget. It is difficult to support this as both cruises were corrected by means of local reference stations and positioning error was always under 20 m (see 3.13).

The presence of an intrusive body in the same area (Fig. 4(f)) could justify the changes displayed in Figure 4(e). The physical interpretation would raise two possibilities: a) a smaller intrusion during the period 1999-2008, or b) the thermal inertia of the previous magmatic injection which would have a smaller demagnetizing effect during this period of time by heat transmission to the host rocks.

This event (previous magmatic injection) would have occurred between 1987 and 1999, in view of the two abnormal seismic periods in 1992 and 1999. This lead us to consider b) as a more realistic option.

Three main mechanisms could account for the observed magnetic variations: (a) thermal magnetisation related to magma cooling below its Curie temperature, (b)

piezomagnetic effects and (c) streaming potentials (Zlotnicki and Le Mouel, 1988; Tanaka, 1993; Del Negro et al., 2000).

The first mechanism is related to the fact that when magma cools below its Curie temperature it acquires a thermo-remanent magnetisation (TRM), conditioned by the intensity and direction of the Earth's magnetic field and by the composition of the magma. TRM is the primary natural remanent magnetisation of igneous rocks. The duration of such changes may range from weeks to years, closely conditioned by the size of the body and the cooling rate (Del Negro and Ferrucci, 1998).

The other two mechanisms, (b) and (c), are related to stress variations. This effect is exclusively reflected in (b), and its duration is that of the stress field (Zlotnicki and Le Mouel, 1988). The last one, (c), is the result of suddenly varying interstitial pressure on the distribution and/or circulation of iron-rich underground waters in a highly fractured rock media (Zlotnicki and Le Mouel, 1988; Del Negro et al., 2000). In relation to thermo-magnetic changes, mechanisms (b) and (c) are faster.

All these sources differ not only in the magnitude of the magnetic anomaly that they are able to produce but also in their time constants. Although we lack information concerning the timescale of all these signals, and the way the variation progressed over the periods 1987/1988 to December 1999, and December 1999 to December 2008. It is difficult to explain a progressive yearly rated change by short time effects, such as those that (b) and (c) would justify. We therefore propose TRM origin as the most plausible source for this volcano-magnetic signal.

This possibility is consistent with Ben-Zvi et al. (2009) and Robool (1980). They support the existence of a large magma chamber beneath the caldera, but also justified the existence of small-differentiated magma bodies that rise up to a high level and extend across the whole caldera. The latter adequately accounts for two features: a) historical eruptions have occurred all around the caldera, and b) at least three eruptive events have included simultaneous eruptions of chemically distinct lavas from multiple vents.

5.2. DI outer area

The study in this area was undertaken using ΔSV . In order to check whether ΔSV values derived from tie-point readings are greatly affected by noise (error budget), we

compared the corresponding grids in the following way: we subtracted the magnetic total field anomaly grids obtained for every period and we divide the residual grid by the period of time between them, using the average of their time of occurrence.

For instance, to obtain an average ΔSV estimation for the DECVOL (December 1 1999: 1999.91) and GEODEC (February 1 2002: 2002.083), we subtracted the scalar magnetic anomaly map for DECVOL from the corresponding one for GEODEC, and divided the result by 2.173 years (2002.083–1999.91). This affords an average SV estimation through the low-pass filtering effect induced by the 2D interpolation.

We represent these grids in Fig. 6(a), (b), and (c), and overlaid the corresponding tie-point readings, using an identical colour scale. Results are reasonably coherent, supporting the view that error sources had little impact on our ΔSV dataset (“Las Palmas-89” and DECVOL can be considered as the worst situation, the first taking place when GPS precision was about 100 m).

The evolution of anomalous bodies surrounding DI from the magnetic point of view led us to detect a wide minimum southeast of DI (December 1989–December 1999) (Fig. 6(a)). A total of 20 tie points out of 31 show a decrease in the magnetic signal, ΔSV , during this period of time (DECVOL-“Las Palmas 89”) higher than the noise threshold (absolute value, 6 nT/yr, see paragraph 4.2.3). It can be explained by means of major changes in magnetic properties, caused by thermal effects under the seafloor during this period, which causes a local weakening of the anomaly.

Zandomeneghi et al. (2009) and Pedrera et al. (2012) detected in this area (southeast of DI) the presence of a wide low V_p region that covers the whole island and is more pronounced at a depth of 2 km. It could serve as evidence for the existence of partial melt volume, given the two seismic crises that took place around this time (January 1992, and January 1999). Ibañez et al. (2003) interpreted the latter one as caused by the uplift of deep magmatic injection below the Port Foster area. We propose that this minimum of ΔSV (Fig. 6(a)) could be linked with the 1992 and/or 1999 volcanic crises and caused by a secondary magmatic uplift located southeast of DI.

Figure 6 (b) describes the variations of the crustal magnetic anomaly field during the period December 1999-February 2002, southeast of DI. This picture does not show any bias, and positive values alternate with negative ones.

Rey et al. (1995) located fracture systems, volcanic cones and fumarolic areas inside DI. They verified the confluence of two orthogonal fracture systems (NNW-SSE and NE-SW trends) southeast of DI and the prolongation of a submarine volcanic cone axis. All these facts would point to the existence of intrusive bodies in this area.

What we measured between December 1999 and January-February 2002 were isolated values of magnetic readings, which, when compared through the ΔSV , show variations in magnitude with a dipole-like appearance. We hold them to be caused by the magnetisation of small structures according to thermo-magnetic mechanisms. Although we lack information concerning the timescale of this signal, and how this variation progressed over the 2-yr period (December 1999–February 2002), a progressive yearly rated change by short time effects (stress and piezomagnetic origins) is not plausible. Instead, we propose TRM as the most likely origin for this volcano-magnetic signal.

To study cooling processes on a magma block from melt temperature to lesser values would serve to model its thermal magnetization curve. We came to an approximate solution based on several simplifying assumptions (i.e. disregarding latent heat, assuming that heat is transferred by conduction only). Additionally, we took the thermal diffusivity $\kappa = 0.005 \text{ cm}^{-1} \text{ s}^{-1}$, which is a good average for this type of magma (Büttner et al., 1998; Del Negro and Ferrucci, 1998), and applied Laplace's solution (Turcotte and Schubert, 2002).

Following Del Negro and Ferrucci (1998), its resolution shows that the temperature T at a certain time t and distance x from the symmetry plane of the magma layer, which is supposed to be perfectly horizontal, is given by (Carslaw and Jaeger, 1959):

$$\frac{T}{T_0} = \phi(\xi, \tau) = \frac{1}{2} \left\{ \text{erf} \frac{\xi + 1}{2\tau^{1/2}} - \text{erf} \frac{\xi - 1}{2\tau^{1/2}} \right\} \quad (1)$$

Where $\xi = x/a$ and $\tau = \kappa t/a^2$ are two dimensionless parameters, erf is the error function, a is the half-thickness of the magma layer and T_0 its initial temperature.

The intrusion temperature was assumed to be 1100°C, appropriate for basaltic magma. Eq. (1) was solved for different values of the half-thickness of the layer (parameter 'a'). We observed that this parameter was critical for the cooling process. The cooling

mechanism was only efficient when the half-thickness remained less than 5 m; otherwise, the temperature remained over Curie Temperature for years.

Therefore, nearly 2 yr (between 1999 and 2002) of progressive cooling of the magma reservoir led us to consider limited thickness for the solidified source (i.e. 5 m). The cooling process, which affected small size bodies, would have started after the end of the last volcanic crisis, enhanced by the existence of a fracture system near Neptune Bellows (Muñoz-Martín et al., 2005), which favours the intrusion of seawater.

Figure 6 (c) describes variations of the crustal magnetic anomaly field during the period February 2002-December 2008. The map does not show significant signals, with 121 out of 131 below the noise threshold level. It implies that no-magnetisation changes are appreciable in the area, meaning that stable conditions characterize the period in this area.

We propose the following temporal evolution for DI: sometime between 1987 and 1999, magma uplift took place in the eastern onshore and offshore parts of DI, with posterior spreading of its thermal effects (Fig. 10(a) and (b)) causing the variation in the magnetic anomaly distribution in DI inner bay and southeast of this island. This process could be related with the 1992 and/or 1999 volcanic crises. This thermal perturbation has continued during the second period (December 1999-January 2002). Small structures acquired magnetisation through thermo-magnetic effects enhanced as a consequence of the fracture system, facilitating water percolation (Fig. 10(b) and (c)).

The last study period (January/February 2002- December 2008) does not show significant changes in ΔSV (Fig. 6(c)). Nevertheless the magnetic anomaly maps at DI shows differences, which display a similar pattern (Fig 4(e)) than the distribution of anomaly differences obtained for 1987-1999 period (Fig 4(e)), although it shows smaller amplitudes. The cooling and related magnetisation may have been fully developed on the smallest structures, yet still would continue in opposite sense for larger structures and bodies but at much slower rate than during the first period of time (1987-1999). This hypothesis is coherent with our results as it would produce a slight modification on the magnetic anomaly map which falls below our noise threshold level (Fig. 6(c)).

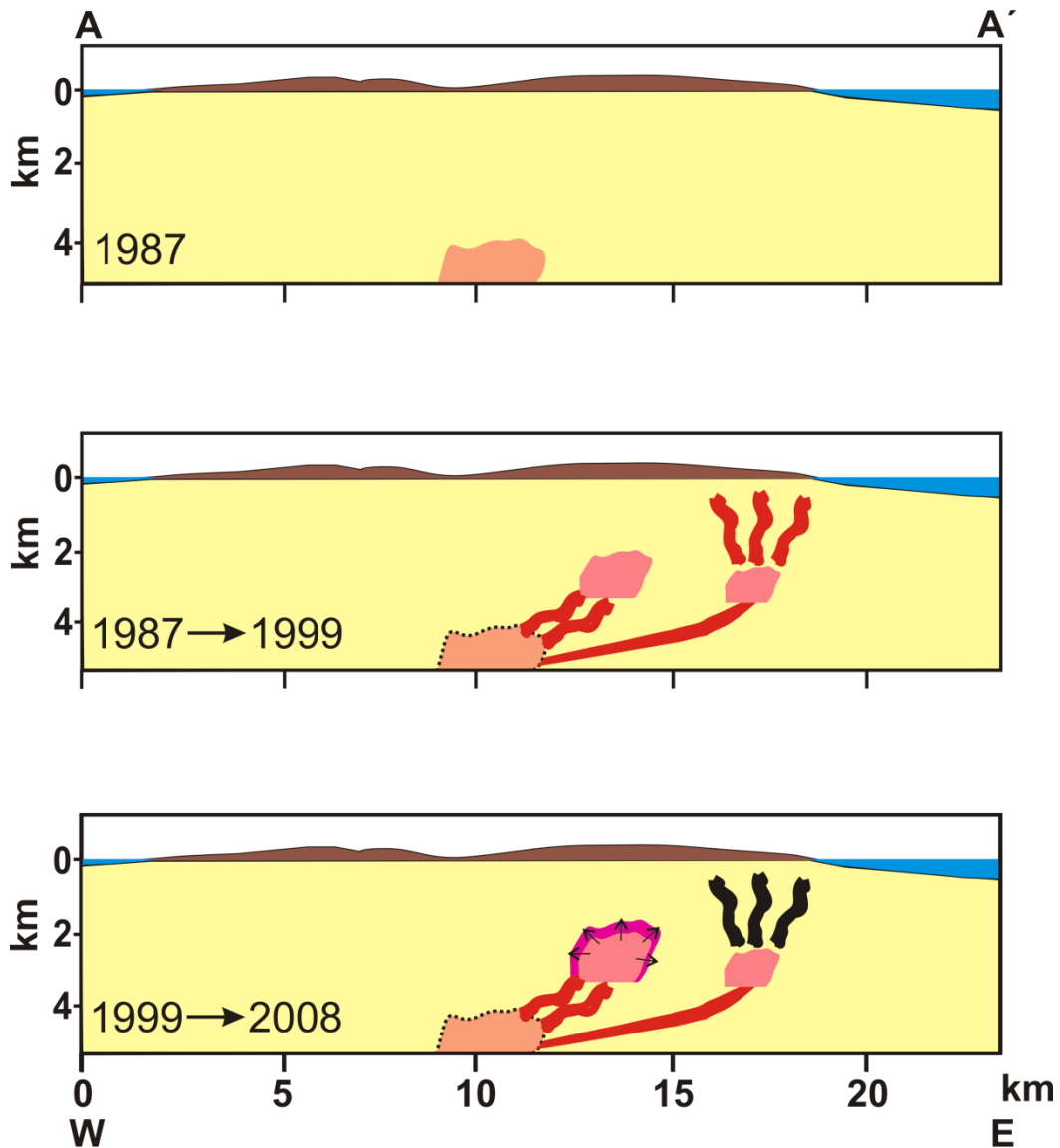


Figure 10. Snapshots of volcanic evolution of Deception Island (see figure 3a for the transect location). a) Initial situation in year 1987: one non-magnetic body is located under the inner bay of the island, according to Zandomenegi et al. (2009). b) Evolution of the system from 1987 to 1999. Shallow dyke injection intrusions are represented by orange fingers and two major magmatic intrusions whose horizontal projections fall on the mid-eastern Deception Island's inner bay and south-eastern offshore part of Deception Island. (See section 5 for comments and details). c) Evolution of the two non-magnetic bodies system from 1999 to 2008. Former shallow dyke injection intrusions, magnetized after cooling, are represented by black fingers (See section 5 for comments and details). Transmission of thermal effects during last period is represented by arrows and purple color. Labels W and E on top mark the orientation of the profile.

6. Conclusions

We analysed data from eight Antarctic cruises over the last 20 years, paying particular attention to five of them, which cover the following periods: 1987-1988 and 1989-1990 austral summers, December 1999, January-February 2002 and December 2008. In addition we consider aeromagnetic anomalies obtained in 2011 by an UAV flight in the northern half of DI. This allowed us to reconstruct the magnetic evolution of DI over a 20-year period.

In particular, because the earliest inner bay survey has been done in such a different fashion than the latest ones, with a very different line network, and different location techniques, we have performed an analysis that pursue to gain confidence in our results.

In reaching that conclusion, we performed a detailed study of errors on the inner bay surveys (paying a special emphasis on the first one). It consisted on three tests. We concluded that we could be confident in our results while they show a long wavelength character. It is important to highlight that we have not pay attention in our analysis to the numeric values but to the sign of these variations, that is: a large area with positive variations and an area with negatives variations.

According to the above, we detected variations in three scalar magnetic anomaly maps of DI inner bay performed in the 1987-1988 austral summer, December 1999 and December 2008 (Fig.4). These changes are proposed to be caused by magma uplift (at sometime between 1987 and 1999 towards the SE part of DI) and the later spreading of its thermal effects.

By studying the spatial distribution of ΔSV (Fig. 6), we found evidence supporting that the movement of magma also affected at least the immediate SE outer part of the island.

Analysis of the temporal and the spatial distribution of these differences (ΔSV) revealed variation in these values from 1989 to December 1999, which is coherent with the uplift of a deep magmatic injection below the eastern part of Port Foster area. This could be linked with the 1992 and/or 1999 volcanic crises (Ibañez et al., 2003). During the period 1999-2002, short wavelength alterations were detected, in turn coherent with a progressive cooling of the smaller structures. However, the period 2002-2008 showed no significant alterations at least above a threshold level, while the magnetic anomaly map inside DI

shows a pattern of alterations (Fig. 4(e)) which suggests a continuation of the same heating process but in a more gradual way, affecting larger structures. Both results would be coherent as ΔSV , for this last period, fall within the noise-threshold level do not allowing us to infer any conclusions strictly from them only.

This fast and simple magnetic technique, acquired periodically, allows the evolution of a volcano formed by intermediate and basic rocks to be monitored, which could complement other techniques. Such information is especially useful in remote locations, and does not require a continuous deployment of equipment. To take full advantage of this method it is important to place special emphasis on a) using precise positioning (GPS or DGPS), and b) removing the external field contribution through the use of a reference station located in the survey area. Neither of these two requirements is particularly difficult to accomplish in a geophysical survey nowadays.

Acknowledgments

Some of the figures were drawn with the aid of Generic Mapping Tools software (Wessel and Smith, 1998). The authors thank Dra. Roberta Tozzi and Dr. Angelo De Santis for providing the ARM model data for Deception Island. Projects CTM2011-30241-C02-01/02.

Chapter 11

GENERAL DISCUSSION

This study of the evolution of Scotia Arc and surrounding areas, from the processes in the asthenosphere to the oceanographic flows across Drake Passage, reveals the significance of this key gateway of the Earth. The newly contributed knowledge of this region sheds light on the mantle flows in the upper asthenosphere, the dynamics and structure of the lithosphere, the nature of the crust and paleoceanography across the southern Scotia Sea, as well as their influences regionally and globally.

The hypothesis of Alvarez (1982), which holds the Drake Passage to be a mantle gateway, has been tested by other authors (Russo and Silver, 1994; Polet et al., 2000; Pearce et al., 2001; Helffrich et al., 2002; Nerlich et al., 2013) on the basis of geochemical, seismic, and seismological data. Some support the notion of Pacific mantle outflow to the Atlantic through the Scotia Sea at the beginning of the continental break-up, and perhaps continue later. In this Ph.D. Thesis, the asthenospheric flow from the Pacific to the Scotia Sea has been positively tested using gravity data (see Chapter 5, Martos et al., 2014). Moreover, the continental lithospheric roots and thicker lithosphere found in the region provide clues as to the flow pathways. It is remarkable that the root of the Shackleton Fracture Zone deflected the asthenospheric flows since its uplift (Figure 5 in Chapter 5). This produced a decrease in the asthenospheric material supply in the West Scotia Ridge, affecting its activity until its final extinction around 6 Ma (Maldonado et al., 2000).

The mantle dynamics control both tectonics and lithospheric thermal behavior. For this reason, the West Scotia Sea back-arc, as the best example of a small oceanic basin on the Earth, is studied in order to understand its thermal behavior (Martos et al., 2012; see Chapter 6, Martos et al., *in revision (a)*). The results (see Figure 2 in Chapter 6) show that this sea does not fulfill the heat flow-age-depth_theoretical and empirical relationships established for large oceans (Parsons and Sclater, 1977; Stein and Stein, 1992, 1993; Hillier and Watts, 2005; Crosby et al., 2006; Korenaga and Korenaga, 2008; Crosby and McKenzie, 2009; Hasterok, 2013). The lithosphere of the Scotia Sea behaves like an old oceanic crust, reaching thermal equilibrium quickly, with an estimated maximum lithospheric thickness of 35 km. When heat flow values were modeled, the results obtained were very low for such a young ocean, and considering the heat flow measurements in the study area (50–70 mW/m²) (<http://www.heatflow.und.edu>). For this reason, we concluded

that the heat flow technique is not a suitable method to date the oceanic crust in small oceans. This lithospheric thermal behavior can be attributed to the small convection cells involved in the back-arc development —smaller than in large oceans, implying lower and slower heat transport. Additionally, the Pacific mantle outflow, which properly fed the West Scotia Ridge in the time period between the Drake Passage opening up to the Shackleton Fracture Zone uplift (see Chapter 5, Martos et al., 2014), then continued crossing the Drake Passage along the deep continental roots, providing the borders of the West Scotia Sea with a continuous hot material.

The most updated magnetic compilation of the entire Scotia Sea is presented in this Ph.D. Thesis (see Chapter 7, Martos et al., *in revision (b)*). The magnetic signatures of the Pacific and Atlantic Oceans, and West, Central and East Scotia Sea are well differentiated, showing the different magnetic characteristics in the Scotia Arc and in the surrounding areas. The new magnetic map compilation as well as the magnetic modelling in selected profiles reveals the W-E orientation of the Pacific Margin Anomaly in the southern Scotia Arc. Some authors identified this anomaly in the Bransfield Strait, in the continental blocks of the southern Scotia Arc, including the South Orkney Microcontinent and Discovery Bank, and even in the South Georgia Bank (Garret et al., 1986/87; Suriñach et al., 1997; Ghidella et al., 2011). Here, the magnetic signal and the Pacific Margin Anomaly were analyzed in order to propose a model for the initial distribution of the continental blocks in the Scotia Arc (see Figure 8 in Chapter 7) that is novel with respect to previous proposals (e.g. Barker, 2001; Livermore et al., 2005; Dalziel et al., 2013; Eagles and Jokat, 2014). The magnetic signal asymmetry between the northern and southern branches of the Scotia Arc is related to the asymmetry of the subduction process of the Phoenix Plate, which was directed southeastwards, mainly affecting the western part of Antarctica (Larson, 1976; Renking and Sclater, 1988), while South America was affected obliquely. In this context, the relevant anomalies along the North Scotia Ridge may be associated with basic rocks most likely emplaced in pull-apart basins developed along a broad transcurrent fault zone that separated the South American and Antarctic plates during the initial stages of development of the South Atlantic Ocean. Meanwhile, the southern branch was affected directly by the subduction, forming the batholith that produced the Pacific Margin Anomaly

observed in the south continental banks located in the Scotia Arc, possibly including the Herdman Bank.

The effects of mantle dynamics in the lithosphere and in the tectonic evolution (Martos et al., 2014 (Chapter 5); *in revision (a)* (Chapter 6); *in revision (b)* (Chapter 7)) of the area bore a high impact on the dynamics and growth patterns of the ocean floor, and hence in paleoceanography. For example, the faster sinking of the oceanic crust due to the abnormal thermal behavior of the West Scotia Sea influenced the development of new gateways and faster deep water interactions. Several geological studies have been carried out in the Scotia Arc (Schodlok et al., 2002; Maldonado et al., 2003, 2005, 2006; Livermore et al., 2004; Hernández-Molina et al., 2006; Carter et al., 2008; among others) in order to identify changes in oceanic currents, which are considered to influence global climate change around the Eocene/Oligocene boundary, when the opening of the Drake Passage may have occurred. Most of them focus on studying the main units in the sedimentary sequence, which may be interpreted as different stages in the oceanic current evolution. These studies identified a Reflector c (attributed to an age of 12.1 Ma) that recorded a major environmental change, possibly related to the initial incursions of the opening of new gateway across the South Scotia Sea or the dynamics of the ice-sheets (Galindo-Zaldívar et al., 2006; Maldonado et al., 2006; Lindeque et al., 2013). In this Ph.D. Thesis, the sedimentary sequence analyzed in the southwestern Scotia Sea using multichannel seismic data (see Chapter 8, Martos et al., 2013) reveals contourite drifts and erosional features. The sedimentary deposits and the study of the flow rate quotients point to the influence of the initial incursion of Circumpolar Deep Water on the older units, whereas younger units are influenced by a combination of Circumpolar Deep Water and Weddell Sea Deep Water. Furthermore, the deposits evidence the uplift of the Shackleton Fracture Zone at least in the middle Miocene, and the pole migration proposed by Livermore et al. (2004) at 8 Ma aided this uplifting. That is, this structure began to be a barrier for oceanic currents in the middle Miocene. The Initial incursion of the Weddell Sea Deep Water into the Scotia Sea, together with the Shackleton Fracture Zone proto-relief, forced the Circumpolar Deep Water and the Polar Front to move even further from Antarctica (see Figure 10 in Chapter 8). This fact favored the thermal isolation of Antarctica and it is considered coeval with the onset of the permanent East Antarctic Ice

Sheet and with the tundra landscape that persisted until at least 12.8 Ma in the Antarctic Peninsula (Anderson et al., 2011).

The tectonic evolution of the Scotia Arc, together with the subduction of the Phoenix Plate under the west margin of the Antarctic Peninsula, influenced the formation of the Bransfield Strait back-arc basin a few million years ago. The oceanic or continental character of the basin is still a subject of controversy among the geophysical and geological communities. GPS studies (Taylor et al., 2008), the volcanic activity (Gracia et al., 1996), the normal faulting (Aschcroft, 1972; Gràcia et al., 1996; Galindo-Zaldívar et al., 2006a), the earthquake focal mechanisms (Pelayo and Wiens, 1989; Galindo-Zaldívar et al., 2006a), the relatively low magnetization values (Klitgord, 1976) and refraction studies (Christeson et al, 2003) in the area support the extension and rifting processes of the Bransfield Strait. Additionally, multichannel seismic information (Gambôa and Maldonado, 1990; Galindo-Zaldívar et al., 2004) and the large crustal thickness explained by the chilling effect (Roots et al., 1979) would support the creation of a nascent oceanic crust. In this Ph.D. Thesis, the oceanic or continental character of the Bransfield Strait is discussed in view of previous research and recent study of potential fields in the area (see Chapter 9, Catalán et al., 2013). The new magnetic and gravity maps reveal different natures among the basin and the boundaries, the South Shetland Islands Block and the Antarctic Peninsula. The linear magnetization pattern of the neovolcanic axis of the Bransfield basin axis, displayed in the magnetic map (Figure 3 in Chapter 9), and the volcanic activity support the creation of nascent oceanic crust. Moreover, a main profile crossing the basin with NW-SE orientation was modeled from the magnetic and density properties, considering both the rifting and extensional setting, and the nascent oceanic spreading setting (Figure 6 in Chapter 9). The integration of the magnetic and gravity information together with the forward modeling are compatible with the extensional regime of the basin, and with the probable floored oceanic crust in its central area.

As mentioned earlier, the Bransfield Strait is characterized by a neovolcanic axis in its central part, due to the back-arc setting. Several submarine volcanoes are located in the axis, as well as some subaerial ones. The most representative subaerial volcano within the Bransfield basin is Deception Island. Historical eruptions of this active volcano occurred in 1842, 1967, 1969 and 1970. On the basis of petrological (Smellie, 2001), seismic (Grad et

al., 1992, 1997; Ben-Zvi et al., 2009; Zandomenighi et al., 2009) and potential field data (Vila et al., 1992; Muñoz-Martín et al., 2005), the crustal structure of Deception Island has been described. Here, eight Antarctic cruises and aeromagnetic data in the northern half of the island allowed us to reconstruct the magnetic evolution of the volcano in a 20-year period (Martos, 2010; see Chapter 10, Catalán et al., *under review*). The inner and outer areas of the island were studied using different methodologies. Additionally, an exhaustive error study was carried out to ensure the reliability of our results, given that accuracy is essential in this kind of study. For the inner bay, the 20-year span was divided into three periods. The forward modeling and the data compilation show that the magnetic signal was reached, considering changes of magma uplift, at some point between 1987 and 1999 in the SE part of Deception Island, with a later spreading of its thermal effects (see Figures 9 and 10 in Chapter 10). For the outer part of the island, study of the spatial distribution of differences of secular variation showed that the magma movement affected the immediate SE part of the volcano. These results are coherent with the volcanic crises taking place in the past 25 years (Ibáñez et al., 2003). Use of this fast and simple technique allows for monitoring an active volcano, if accuracy in positioning and in removing the external field components are possible.

In summary, the different geophysical and geological aspects of the Scotia Arc analyzed in this Ph.D. Thesis contribute to a better understanding of the geodynamics of the region, while also pointing to broader regional and global implications. The opening of the Drake Passage marked the final break-up between South America and Antarctica during the early Cenozoic. This entailed the opening of the last gateway of the Southern Ocean, which had a profound impact on the geodynamics of the Earth and the global climate.

Future Perspectives

The complete study done in this Ph.D. Thesis contributes to opening new research endeavors:

- In order to continue investigating the lithospheric roots and their effects on asthenospheric flows, and in turn on plate tectonics, it would be important to analyze the dynamics of the main gateways opened on the Earth. Once this is

complete, it may be possible to evaluate the present upper asthenospheric flows on the Earth, and gain further knowledge of global plate tectonics.

- The study of the thermal behavior of small oceans and the analysis of the heat flow-depth-age relationship, applying the same methodology to other small oceans on the Earth, is relevant to assess crustal dynamics in small ocean basins, as opposed to large oceanic basins, more often analyzed. This will help provide valid age results in small oceanic basins when magnetic spreading anomalies are not available or difficult to identify.
- The structure of the crust in the Scotia Sea is not fully defined at present. An extensive wide-angle refraction seismic experiment could help resolve some of the still outstanding and controversial aspects of the crustal nature in the Scotia Arc region.
- The analysis of additional conjugate margins in the Scotia Sea and surrounding areas will help to more precisely establish the timing of break-up, which is still a subject of controversy, and will help to assess and quantify the extensional regimes.

Chapter 12

**CONCLUSIONS
CONCLUSIONES**

Conclusions

The analysis of the geodynamic evolution of the Scotia Arc presented in this Ph.D. Thesis integrated a large data bank from the region, collected since 1950s, to which several methodologies were applied in order to assess the regional growth patterns. The component studies focus on diverse aspects of regional development, from asthenosphere flows to the evolution of oceanographic flows. The main body of the Thesis comprises six articles either published or under revision in high impact international journals. Detailed discussions corresponding to the different aspects addressed are therefore presented in each individual Chapter, whereas a general discussion is presented in Chapter 11. The most relevant conclusions can be summed up as follows:

1. A complete Bouguer anomaly map of the Scotia Sea and surrounding regions was created using satellite gravity data, revealing for the first time the major lithospheric mantle density contrasts.

- The new gravity data support the presence of a thinner and low density lithospheric mantle in the West Scotia Sea area, thereby suggesting variable lithospheric thicknesses.

- The data suggest that the Shackleton Fracture Zone started to behave as an asthenospheric barrier for the Pacific mantle outflow in the middle Miocene, simultaneously as for oceanic currents.

- The decrease in Pacific mantle outflow toward the West Scotia Ridge in the Scotia Sea may be a predominating factor responsible for the extinction of the oceanic spreading.

- The Pacific mantle outflow could still be present through Drake Passage, at the northern and southern borders of continental lithosphere, where the asthenospheric highs and high heat flow values are found, supporting Alvarez's (1982) hypothesis.

2. The lithospheric thermal behavior of the Scotia Sea was studied for the first time using multichannel seismic and gravity data, ages, and the plate cooling model.

- Small young oceans have a thinner lithosphere and relatively low heat flow due to the small size and low energy of the mantle cells.

- These factors determine a faster evolution in reaching thermal equilibrium and final depths. Based on this faster thermal evolution for small oceans, a new depth-age relationship is proposed

$$d(t) = 4480 - 19380\exp(-t/4).$$

- The heat flow was also modeled for small oceans, indicating older apparent ages than for large oceans. Although crustal ages older than 15 Ma cannot be discriminated, but heat flow is the best measure to obtain their maximum lithospheric thickness.

- In the northeastern part of the West Scotia Ridge, the activity of the mantle cells, mainly filled from the Pacific mantle, decreases; this determines the progressive mantle cooling and deepening of the oceanic corridors.

- All these processes contributed to the extinction of spreading centers and the relatively accelerated deep sea connection between the Pacific and Atlantic oceans through the Drake Passage, a key area for the inception of the Antarctic Circumpolar Current, associated with global climate effects, and oceanic and continental flora and faunal exchanges.

3. The most complete compilation of the magnetic anomalies of the Scotia Arc to date is presented, based on marine, aeromagnetic and satellite data. These data provide new insights into the South America-Antarctica continental bridge reconstruction, prior to the development of the Scotia Arc.

- High intensity anomalies are identified in the oceanic areas of the Former Phoenix Plate, in the western part of the West Scotia Sea, in the East Scotia Sea, and northeast of the South Georgia Islands. Low intensity anomalies occur in the Central Scotia Sea and the eastern part of West Scotia Sea.

- The linear anomaly identified north of the North Scotia Ridge coincides with the Falkland Basin, probably evidencing the intrusion of an E-W elongated dyke in an episode of crustal thinning.

- The continent-ocean boundary is characterized by a long linear maximum, which is observed along the southern part of the North Scotia Ridge.

- The Pacific Margin Anomaly is well recognized in the Antarctic Peninsula and in the South Shetland Islands, extending along the South Scotia Ridge continental blocks — the South Orkney Microcontinent and southern Discovery Bank— and it may also occur in the northern part of Herdman Bank.

- The variability in the intensity of the Pacific Margin Anomaly may be a consequence of the asymmetry of the trend of subduction, which is orthogonal to the Pacific Margin of the Antarctic Peninsula and oblique to South America.

- The main magnetic signal identified in the North Scotia Ridge (South Georgia Bank, and other minor anomalies) may be associated with basic rocks emplaced in pull-apart basins formed along a broad transcurrent zone that separates South America and Antarctica since the Cretaceous due to the South Atlantic oceanic spreading.

4. Sedimentary evolution, tectonics, paleoceanographic and climate-change processes of the triple junction region in the southern Drake Passage have been linked in this Thesis, on the basis of multichannel seismic data.

- Evidence of bottom-current activity is observed throughout the entire sedimentary record. The features observed in the older units seem to be the result of the influence of the initial Circumpolar Deep Water flows, whose trajectories were controlled by tectonic depressions. In contrast, the sediment bodies composing the younger units are interpreted as drift deposits that evolved under the combined effects of the Weddell Sea Deep Water and Circumpolar Deep Water flows.

- The Shackleton Fracture Zone may have initiated as an oceanic ridge before the middle Miocene. The relief, together with the initial incursions of the Weddell Sea Deep Water, forced the Antarctic Circumpolar Current and the Polar Front to move northwards, away from Antarctica; this favored the thermal isolation of the Antarctic region, which would have been coeval with the onset of the permanent East Antarctic Ice Sheet and with the tundra landscape that persisted until at least 12.8 Ma in the Antarctic Peninsula.

- The influence of bottom currents became the controlling factor above Reflector c. These erosional features are more conspicuous adjacent to ridges, suggesting an intensification of bottom-current activity due to the opening of deep gateways located along the South Scotia Ridge and to the deflection of the flows. Since the age of Reflector c, the

Weddell Sea Deep Water has escaped from the Weddell Sea through these small passages, and flowed westwards along the South Scotia Ridge until intersecting with the Shackleton Fracture Zone. As a consequence, a part of the current is diverted northwards, whereas the remaining flow continues southwestwards into the Pacific Ocean, aided by the Coriolis force.

5. The nature of the young back-arc basin, the Bransfield Strait, born as a consequence of the Scotia Sea and Phoenix Plate tectonic setting, are discussed in this Thesis in view of a new potential field data compilation.

- Bouguer anomalies reveal the asymmetry of the Bransfield Basin, with a smooth Antarctic Peninsula boundary and a sharp boundary with the South Shetland block. Moreover, the Bouguer anomaly models suggest that crustal thickness may reach down to 8.5 km along the volcanic axis located in the basin, and that the upper mantle has an anomalous low density in this area.

- Magnetic anomalies of the area are characterized by the Pacific Margin Anomaly. It splits into two branches in the Bransfield Strait region because of the opening of the basin. Moreover, a narrow NE-SW elongated maximum corresponding to volcanic edifices surrounded by minima is located along the northwestern part of the Central Bransfield Basin, further supporting the asymmetry of the basin.

- Integration of the data support volcanic activity along the central volcanic axis of the basin: local Bouguer anomaly minima correspond with areas of low relative magnetic anomalies and susceptibility, thereby supporting the presence of active magmatic chambers in the Central Bransfield Basin.

- Potential field data and modeling are compatible with the extensional character of the basin, probably floored in the central sector by an oceanic crust above an anomalous mantle. Moreover, the presence of an active volcanic axis and the thin crust, together with other available geophysical data (multichannel seismic profiles), support rifting in its latest stages or the presence of an incipient oceanic crust formed by recent oceanic spreading in the Central Bransfield Basin.

6. Within the framework of the active back-arc of Bransfield Strait, Deception Island volcano was analyzed for a 20-year period, from the magnetic standpoint.

- A very detailed error budget study was performed to gain reliability in the results. It is important to highlight that the magnetic study was not focused on the numerical values, but rather on the sign of the variations.

- Variations in three scalar magnetic anomaly maps of Deception Island inner bay—performed in the 1987-1988 austral summer, in December 1999 and December 2008—were detected. These changes are proposed to be caused by magma uplift at some time between 1987 and 1999 around the southeastern part of Deception Island, and the later spreading of its thermal effects.

- By studying the spatial distribution of ΔSV , we arrived at evidence supporting that the movement of magma also affected, at least, the immediate SE outer part of the island. Analysis of the temporal and the spatial distribution of these differences (ΔSV) revealed variations in these values from 1989 to December 1999, which is coherent with the uplift of a deep magmatic injection below the eastern part of Port Foster area. This could be linked with the 1992 and/or 1999 volcanic crises. During the period 1999-2002, short wavelength alterations were detected, in turn coherent with a progressive cooling of the smaller structures. Yet the period 2002-2008 showed no significant alterations above a threshold level, whereas the magnetic anomaly map inside Deception Island shows a pattern of alterations, which suggests a continuation of the same heating process but in a more gradual way, affecting larger structures.

- This fast and simple magnetic technique allows the evolution of an active volcano to be monitored periodically, and can be considered a useful complement to other techniques. The information obtained is especially useful when dealing with remote locations, and the continuous deployment of equipment is not possible. To take full advantage of this method, it is important to place special emphasis on using precise positioning and removing the external field contribution through the use of a reference station located in the survey area.

Conclusiones

Diferentes tipos de datos y metodologías han sido integradas en esta Tesis Doctoral con la finalidad de conseguir un mejor entendimiento de la evolución y dinámica del Arco de Scotia y las áreas circundantes, desde la astenosfera hasta sus implicaciones sobre el fondo oceánico. La Tesis consiste en seis artículos que o bien están publicados o en revisión en revistas de alto impacto internacional. Las discusiones detalladas se han presentado en cada artículo, así como una discusión general en el Capítulo 11. Por tanto, las conclusiones principales de esta Tesis Doctoral pueden resumirse en los siguientes puntos:

1. Se ha calculado el mapa de la anomalía de Bouguer Completa del Mar de Scotia y las áreas circundantes mediante datos de gravedad de satélite. El mapa revela los contrastes de densidad principales de la litosfera por primera vez en esta zona.

- Los datos de gravedad apoyan la presencia de un manto litosférico delgado y de baja densidad en el Mar de Scotia Occidental, sugiriendo así variabilidad en el espesor de la litosfera.

- Los datos sugieren que la Zona de Fractura Shackleton comenzó a comportarse como una barrera para los flujos astenosféricos procedentes del Pacífico en el Mioceno medio, al mismo tiempo que se convirtió en barrera para las corrientes oceánicas.

- El descenso en la salida del manto del Pacífico hacia la Dorsal Oeste de Scotia, en el Mar de Scotia, podría ser el principal responsable de la extinción de la dorsal oceánica del Mar de Scotia Occidental.

- La salida del manto del Pacífico a través del Paso del Drake podría ocurrir aún en la actualidad, en los bordes litosféricos del norte y del sur, donde se localizan los altos astenosféricos y los altos valores de flujo de calor, lo que apoya la hipótesis de Alvarez (1982).

2. El comportamiento térmico de la litosfera del Mar de Scotia ha sido estudiado por primera vez, a través de datos de gravedad y sísmica multicanal, así como de edades y del modelo de enfriamiento de placa.

- Océanos pequeños y jóvenes tienen un espesor litosférico más delgado y valores de flujo de calor bajos debido al pequeño tamaño y menor energía de las células mantélicas.

- Estos factores determinan una mayor velocidad a la hora de alcanzar el equilibrio térmico y las profundidades finales por la subsidencia. Debido a esta evolución térmica más rápida de los océanos pequeños, se propone la siguiente relación profundidad-edad

$$d(t) = 4480 - 19380\exp(-t/4).$$

- El flujo de calor ha sido modelizado para océanos pequeños e indica edades aparentes mayores que para océanos grandes. No es posible discriminar edades de la corteza superiores a 15 Ma en océanos pequeños. Sin embargo, el método del flujo de calor es la mejor medida para obtener el máximo espesor litosférico.

- En la zona noreste de la Dorsal Oeste de Scotia, la actividad de las células del manto, principalmente alimentadas por el manto del Pacífico, disminuye determinando el progresivo enfriamiento del manto y el hundimiento de los pasillos oceánicos.

- Todos estos procesos ayudaron a la extinción de los centros de expansión y a una más rápida conexión profunda entre los océanos Pacífico y Atlántico a través del Paso del Drake, el cuál es un área clave relacionada con el comienzo de la Corriente Circumpolar Antártica, con efectos climáticos globales e intercambios de flora y fauna marinos y terrestres.

3. Se ha presentado en esta Tesis Doctoral la compilación más completa de anomalías magnéticas del Arco de Scotia realizada a partir de datos marinos, aeromagnéticos y de satélite. Estos datos proporcionan una nueva visión sobre la reconstrucción del puente continental entre Sudamérica y la Antártida, anterior al desarrollo del Arco de Scotia.

- Anomalías de alta intensidad se identifican en las zonas oceánicas de la antigua Placa Phoenix y las zonas del oeste del Mar de Scotia Occidental, el Mar de Scotia Oriental y el área al noreste de las Islas Georgia del Sur. En cambio, anomalías de baja intensidad se observan en el Mar de Scotia Central y la parte este del Mar de Scotia Occidental.

- Las anomalías lineales identificadas al norte de la Dorsal Norte de Scotia coinciden con la Cuenca Falkland, lo que probablemente aporta evidencias de la intrusión un dique alargado en dirección E-O en un episodio de adelgazamiento continental.

- El límite continente-océano está caracterizado por un máximo lineal alargado, el cual se observa a lo largo del margen meridional de la Dorsal Norte de Scotia.

- La Anomalía del Margen del Pacífico se reconoce con claridad en la Península

Antártica y las Islas Shetlands del Sur, extendiéndose a lo largo de los bloques continentales de la Dorsal Sur de Scotia: Microcontinente de las Orcadas del Sur y el Banco Discovery, y podría identificarse en la parte norte del Banco Herdman.

- La variabilidad en la intensidad de la Anomalía del Margen del Pacífico podría ser consecuencia de la tendencia asimétrica de la subducción de la Placa Phoenix, la cual es ortogonal al Margen Pacífico de la Península Antártica y oblicua a Sudamérica.

- La principal señal magnética identificada en la Dorsal Norte de Scotia (Banco de las Georgia del Sur y otras anomalías menores) podría estar asociada a rocas básicas emplazadas en cuencas de pull-apart formadas a lo largo de la zona transcurrente que separa Sudamérica y la Antártida desde el Cretácico debida a la expansión oceánica del Atlántico Sur.

4. Procesos tectónicos, de evolución sedimentaria, paleoceanográficos y de cambio climático han sido relacionados en esta Tesis Doctoral haciendo uso de datos de sismica multicanal de la región del punto triple al sur del Paso del Drake.

- Se han observado evidencias de actividad de corrientes profundas a lo largo de toda la secuencia sedimentaria. Las características identificadas en las unidades más antiguas parecen estar relacionadas con la influencia de los flujos del Agua Profunda Circumpolar inicial, cuya trayectoria fue controlada por depresiones tectónicas. Por otra parte, las unidades más jóvenes se han interpretado como depósitos de drifts desarrollados bajo el efecto combinado de los flujos de las Aguas Profunda Circumpolar y la Profunda del Mar de Weddell.

- La Zona de Fractura Shackleton podría haber comenzado a formarse como relieve oceánico antes del Mioceno medio. Este relieve, junto con las incursiones iniciales del Agua Profunda del Mar de Weddell, forzaron a la Corriente Circumpolar Antártica y al Frente Polar a desplazarse hacia el norte, lejos de la Antártida, favoreciendo el aislamiento térmico de la región antártica, coetáneo al comienzo de la de la Capa de Hielo permanente de la Antártida Oriental y con el paisaje de tundra que persistió en la Península Antártica hasta hace al menos 12.8 Ma.

- La influencia de las corrientes de fondo fueron el factor controlador por encima del Reflector c. Las características erosivas están más marcadas cerca de las crestas

sugiriendo una intensificación de la actividad de las corrientes de fondo debida a la apertura de los portales oceánicos a lo largo de la Dorsal Sur de Scotia y de la desviación de los flujos. Desde la edad del Reflector c, el Agua Profunda del Mar de Weddell ha salido del Mar de Weddell a través de pequeños pasillos, y fluido hacia el oeste a lo largo de la Dorsal Sur de Scotia hasta intersectar la Zona de Fractura Shackleton. Como consecuencia, una parte de la corriente es desviada hacia el norte, mientras que el resto del flujo continúa hacia el suroeste en dirección al Océano Pacífico, ayudado por la fuerza de Coriolis.

5. En esta Tesis Doctoral se ha discutido la naturaleza del back-arc joven de la Cuenca del Bransfield, creado como consecuencia de la tectónica del Mar de Scotia y la Placa Phoenix. Para ello se ha usado una nueva compilación de datos de campo potencial.

- El estudio de las anomalías de Bouguer revelan la asimetría de la Cuenca del Bransfield, con un suave límite en la Península Antártica y un límite brusco con el bloque de las Islas Shetlands del Sur. Además, los modelos gravimétricos sugieren que el espesor cortical puede alcanzar los 8.5 km a lo largo del eje volcánico de la cuenca y que el manto superficial posee un valor de densidad bajo y anómalo en este área.

- Las anomalías magnéticas están caracterizadas por la Anomalía del Margen Pacífico. Ésta se divide en dos ramas en el Estrecho de Bransfield debido a su apertura. El máximo alargado en dirección NE-SW corresponde a edificios volcánicos rodeados por mínimos, que están localizados a lo largo de la parte noroeste de la parte Central de la Cuenca del Bransfield, apoyando la asimetría de la cuenca.

- La integración de los datos confirma la actividad volcánica del eje volcánico central de la cuenca. Los mínimos locales de anomalía de Bouguer corresponden con áreas de mínimos relativos de anomalías magnéticas y susceptibilidades, de este modo se apoya la presencia de cámaras magmáticas en la parte Central de la Cuenca Bransfield.

- Los datos de campo potencial y la modelización son compatibles con el carácter extensional de la cuenca, que probablemente presenta corteza oceánica sobre un manto anómalo en la parte central. Además, la presencia del eje volcánico activo y la corteza delgada apoyan, así como otros datos geofísicos (perfiles de sísmica multicanal), un proceso de extensión continental en sus etapas finales o la presencia de corteza oceánica incipiente formada por la extensión de la parte Central de la Cuenca Branfield.

6. Dentro del marco del back-arc activo del Estrecho de Bransfield, ha sido analizado el volcán Isla Decepción, desde el punto de vista magnético, durante un periodo de 20 años.

- Se ha realizado un análisis muy detallado de errores para confirmar la calidad de los resultados. Es importante señalar que el estudio magnético de la isla no se centra en valores numéricos concretos sino en variaciones de las anomalías.

- Se han detectado variaciones en tres mapas de anomalías magnéticas de la bahía interior de Isla Decepción: las campañas de 1987/1988, la de Diciembre de 1999 y la de Diciembre de 2008. Estos cambios parecen causados por un ascenso de magma (en algún momento entre 1987 y 1999 en el sureste de la isla) y por una expansión de los efectos termales más tarde.

- Se han encontrado, mediante el estudio de la distribución espacial de ΔSV , evidencias del movimiento del magma que afectan a la zona exterior sureste de la isla. El análisis de la distribución temporal y espacial de ΔSV revela variaciones de estos valores desde 1989 hasta Diciembre de 1999, lo que es coherente con el ascenso de una inyección magmática profunda bajo la parte este de Puerto Foster. Esto podría estar relacionado con las crisis volcánicas de los años 1992 y/o 1999. Durante el periodo 1999-2002, se detectan alteraciones de pequeña longitud de onda, que a su vez son coherentes con un progresivo enfriamiento de pequeñas estructuras. Sin embargo, el periodo 2002-2008 no muestra alteraciones significativas (al menos por encima del umbral), lo que sugiere una continuación en el proceso de calentamiento pero de una manera gradual que afecta a estructuras de gran tamaño.

- Esta técnica simple y rápida, con medidas magnéticas adquiridas periódicamente, permite monitorizar la evolución de la actividad de un volcán, y puede complementar a otras técnicas. Este tipo de información es especialmente útil en lugares remotos y no requiere un despliegue continuo de equipos. Sin embargo, para llevar a cabo esta técnica de manera fiable es necesario hacer énfasis en: usar un sistema de posicionamiento preciso y eliminar la contribución de campos magnéticos externos mediante el uso de una estación de referencia instalada en la zona de muestreo.

Chapter 13

REFERENCES

- Aldaya, F., Maldonado, A., 1996. Tectonics of the triple junction at the southern end of the Shackleton Fracture Zone (Antarctic Peninsula). *Geo-Marine Letters*. 16, 279-286.
- Allen, A., 1966. Seismic Refraction Investigations in the Scotia Sea. British Antarctic Survey Scientific Reports, London. British Antarctic Survey. 55, 44 pp.
- Alvarez, W., 1982. Geological evidence for the geographical pattern of mantle return flow and the driving mechanism of plate tectonics. *Journal of Geophysical Research*. 87, 6697-6710.
- Alvarez, W., 1990. Geologic evidence for the plate-driving mechanism: The continental undertow hypothesis and the Australian-Antarctic discordance. *Tectonics*. 9, 1213-1220.
- Alroy, J., Koch, P. L., Zachos, J. C., 2000. Global climate change and North American mammalian evolution. *Paleobiology*, 26 (sp4), 259-288.
- Anderson, J. B. (Ed.), 2006. SHALDRIL II Cruise Report (<http://shaldril.rice.edu/>, 369 pp.).
- Anderson, J. B., Warny, S., Askin, R., Wellner, J., Bohaty, S., Smith, T., 2011. Cenozoic Cryosphere Expansion and the Demise of Antarctica's Last Refugium. *Proceedings of the National Academy of Science*. 108, 11299-11726.
- Anderson, J. B., Wellner, J.S. (Eds.) 2011. Tectonic, Climatic, and Cryospheric Evolution of the Antarctic Peninsula. Geopress, American Geophysical Union, Washington DC, USA, 218pp. doi:10.1029/SP063.
- Ashcroft, W. A., 1972. Crustal structure of the South Shetland Islands and Bransfield Strait. *Scientific Reports-British Antarctic Survey*. 66, 1-43.
- Baranov, V., Naudy, H., 1964. Numerical calculation of the formula of reduction to the magnetic pole. *Geophysics*, 29, 67-79.
- Barker, P. F., 2001. Evolution of the Scotia Sea region: Relevance to broad-band seismology. *Terra Antarctica*. 8, 67-70.
- Barker, P. F., Barrett, P. J., Cooper, A. K., Huybrechts, P., 1999. Antarctic glacial history from numerical models and continental margin sediments. *Palaeogeography, Palaeoclimatology, Palaeoecology*, 150(3), 247-267.
- Barker, P. F., Burrell, J., 1977. The opening of Drake Passage. *Marine Geology*. 25, 15-34.
- Barker, P. F., Thomas, E., 2004. Origin, signature and palaeoclimatic influence of the Antarctic Circumpolar Current. *Earth Science Review*. 66, 143-162.
- Barker, P. F., Dalziel, I. W. D., Storey, B. C., 1991. Tectonic development of the Scotia Arc region. In: Tingey, R.J., (Eds.), *Antarctic Geology*. Oxford, Oxford University Press. 215-248.
- Barker, P. F., Lawver, L. A., Larter, R. D., 2013. Heat-flow determinations of basement age in small oceanic basins of the southern central Scotia Sea. Geological Society, London, Special Publications, 381.
- Barrett, P. J., 1996. Antarctic palaeoenvironment through Cenozoic times—A review. *Terra Antarctica Reports*. 3, 103-119.
- Bart, P. J., Egan, D., Warny, S. A., 2005. Direct constraints on Antarctic

- Peninsula Ice Sheet grounding events between 5.12 and 7.94 Ma. *Journal of Geophysical Research* 110, F04008. doi:10.1029/2004JF000254.
- Ben-Zvi, T., Willcock, W. S. D., Barclay, A.H., Zandomenighi, D., Ibáñez, J. M., Almendros, J. and T. W. Group, 2009. The P-wave velocity structure of Deception Island, Antarctica, from two-dimensional seismic tomography. In *Antarctica: a keystone in a changing world*-online Proceeding for the 10th international symposium on Antarctic Earth Sciences, Edited by A. cooper, C. Raymond and the 10th ISAES editorial team, U.S. Geol. Surv. Open file rep. 2007-1047, EA 078.
- Beyene, A., Abdelsalam, M. G., 2005. Tectonics of the Afar Depression: A review and synthesis, *Journal of African Earth Sciences*. 41, 41–59.
- Blakely, R. J., 1988. Curie Temperature isotherm analysis and tectonic implications of aeromagnetic data from Nevada. *Journal of Geophysical Research*, 93 (B10), 11817-11832.
- Blakely, R. J., 1995. *Potential theory in gravity and magnetic applications*. Cambridge University Press, New York. 441 pp.
- Blanco-Montenegro, I., Torta, J. M., García, A., Araña, V., 2003. Analysis and modelling of the aeromagnetic anomalies of Gran Canaria (Canary Islands), *Earth and Planetary Science Letters*, 206, 601-616.
- Bohoyo, F., 2004. Fragmentación continental y desarrollo de cuencas oceánicas en el sector meridional del Arco de Scotia, Antártida. Ph.D. Thesis, University of Granada, Granada. 252 pp.
- Bohoyo, F., Galindo-Zaldívar, J., Jabaloy, A., Maldonado, A., Rodríguez-Fernández, J., Schreider, A., Suriñach, E., 2007. Extensional deformation and development of deep basins associated with the sinistral transcurrent fault zone of the Scotia-Antarctic plate boundary. In: Cunningham, W. D., and Mann, P., (Eds.), *Geological Society Special Publication*. 203–217.
- Bohoyo, F., Galindo-Zaldívar, J., Maldonado, A., Schreider, A.A., Suriñach, E., 2002. Basin development subsequent to ridge-trench collision: the Jane Basin, Antarctica, *Marine Geophysical Research*, 23, 413-421.
- Bonatti, E., 1987. The rifting of continents, *Scientific American*. 261, 68-75.
- Boyden, J., Müller, R., Gurnis, M., Torsvik, T., Clark, J., Turner, M., Ivey-Law, H., Watson, R., Cannon, J., 2011. Next-generation plate-tectonic reconstructions using GPlates. In: Keller, G. and Baru, C. (Eds.), *Geoinformatics: Cyberinfrastructure for the Solid Earth Sciences*. Cambridge University Press. 95–114.
- Brennecke, W., 1921. Die ozeanographischen Arbeiten der deutschen antarktischen Expedition 1911-1912: Tech. rep. Arch. Deutsche Seewarter.
- British Antarctic Survey, 1985. Tectonic map of the Scotia Arc. In: British Antarctic Survey, C., (Eds.), *Sheet (Misc) 3*, p. Scale 1:3.000.000.
- Buck, W. R., Martínez, F., Steckler, M. S., Cochran, J. R., 1988. Thermal consequences of lithospheric extension: Pure and simple. *Tectonics*. 7, 213-234.
- Büttner, R., Zimanowski, B., Blumm, J., Hagemann, L., 1998. Thermal conductivity of a volcanic rock

- material (olivine-melilitite) in the temperature range between 288 and 1470 K. *Journal of Volcanology and Geothermal Research*. 80, 293–302.
- Camerlenghi, A., Crise, A., Pudsey, C. J., Accerbonm, E., Laterza, R., Rebesco, M., 1997. Ten-month observation of the bottom current regime across a sediment drift of the Pacific margin of the Antarctic Peninsula. *Antarctic Science*. 9, 426–433.
- Canals, M., Acosta, J., Baraza, J., Bart, P., Calafat, A., Casamor, J. L., De Batist, M., Ercilla, G., Farrán, M., Francés, G., Graciá, E., Ramos-Guerrero, E., Sanz, J. L., Sorribas, J., Tassone, A., 1994. La Cuenca Central de Bransfield (NW de la Península Antártica): Primeros resultados de la Campaña Gebra 93. *Geogaceta*. 16, 132-135.
- Cande, S. C., LaBrecque, J. L., Haxby, W. F., 1988. Plate kinematics of the South Atlantic: Chron C34 to Present. *Journal of Geophysical Research*. 93, 479-492.
- Carmack, E. C., 1977. Water characteristics of the Southern Ocean south of the Polar Front, A voyage of Discovery. London, Pergamon. 15–41.
- Carslaw, H. S., Jaeger, J. C., 1959. *Conduction of Heat in Solids*, 2nd edn, Oxford University Press, Oxford.
- Carter, L., McCave, I. N., Williams, M. J. M., 2008. Circulation and water masses of the Southern Ocean: A review. In: Florindo, F., and Siegert, M., (Eds.), *Antarctic Climate Evolution, Volume Developments in Earth and Environmental Sciences* 8. Amsterdam, Elsevier. 85–114.
- Catalán, M., Agudo, M. L., Muñoz, A., 2006. Bransfield Strait (Western Antarctica) from analysis of marine cross over data. *Geophysical Journal International*, 165-73-86.
- Catalán, M., Galindo-Zaldívar, J., Davila, J. M., Martos, Y. M., Maldonado, A., Gamböa, L., Schreider, A. A., 2013. Initial stages of oceanic spreading in the Bransfield Rift from magnetic and gravity data analysis. *Tectonophysics*. 585, 102-112.
- Catalán, M., Martos, Y. M., Galindo-Zaldívar, J., Funaki, M., under review. Monitoring the evolution of Deception island volcano from magnetic anomaly data (South Shetland Islands, Antarctica). *Global and Planetary Change*.
- Cella, F., Fedi, M., Florio, G., Rapolla, A., 1998. Gravity modelling of the litho-asthenosphere system in the Central Mediterranean. *Tectonophysics*., 287, 117-138.
- Chase, C. G., 1979. Subduction, the geoid, and lower mantle convection. *Nature*, 282, 464-468.
- Christeson, G.L., Barker, D.H.N., Austin, J.A., Dalziel, I.W.D., 2003. Deep crustal structure of Bransfield Strait: Initiation of a back arc basin by rift reactivation and propagation, *Journal of Geophysical Research*, 108 (B10), 2492, doi: 10.1029/2003JB002468.
- Civile, D., Lodolo, E., Vuan, A., Loreto, M. F., 2012. Tectonics of the Scotia–Antarctica plate boundary constrained from seismic and seismological data. *Tectonophysics*. 550, 17-34.
- Cochran, J.R., Martinez, F., 1988. Evidences from the northern Red Sea on the transition from continental to oceanic rifting. *Tectonophysics*. 153, 25-53.

- Copeland, P., 1997. The when and where of the growth of the Himalaya and the Tibetan Plateau. *Tectonic Uplift and Climate Change*, Plenum, New York, 19-40.
- Coren, F., Geccone, G., Lodolo, E., Zanolla, C., Zitellini, N., Bonazzi, C., Centonze, J., 1997. Morphology, seismic structure and tectonic development of the Powell Basin, Antarctica. *Journal Geological Society*. 154, 849–862.
- Crosby, A., McKenzie, D., 2009. An analysis of young ocean depth, gravity and global residual topography. *Geophys. J. Int.* 178, 1198–1219.
- Crosby, A., McKenzie, D., Sclater, J., 2006. The relations between depth, age and gravity in the oceans. *Geophysical Journal International*. 166, 553–573.
- Dalziel, I. W. D., 1984. The Scotia arc: An international geological laboratory: Episodes. 7, 7–13.
- Dalziel, I. W. D., Lawver, L. A., Norton, I. O., Gahagan, L. M., 2013. The Scotia Arc: Genesis, Evolution, Global Significance. *Annual Review of Earth and Planetary Sciences*. 41:767–93.
- Davis, E. E., Lister, C. R. B., 1974. Fundamentals of ridge crest topography. *Earth and Planetary Science Letters*. 21, 405-413.
- DeConto, R. M., Pollard, D., 2003. Rapid Cenozoic glaciation of Antarctica induced by declining atmospheric CO₂. *Nature*. 421, 245–249.
- Del Negro, C., Ferrucci, F., 1998. Magnetic history of a dyke on Mount Etna (Sicily). *Geophysical Journal International*. 133, 451-458.
- Del Negro, C., Ferrucci, F., Napoli, R., 2000. A review of the volcano-magnetic effects observed between 1981 and 1995 on Mount Etna (Italy). *Physics and Chemistry of the Earth (A)*. 25, 9-11, 725-730.
- Dickson, G. O., Pitman, W. C., Heirtzler, J. R., 1968. Magnetic Anomalies in the South Atlantic and Ocean Floor Spreading. *Journal of Geophysical Research*. 73, 2087-2100.
- Eagles, G., 2010. The age and origin of the Central Scotia Sea. *Geophysical Journal International*. 183, 587-600.
- Eagles, G., Jokat, W., 2014. Tectonic reconstructions for paleobathymetry in Drake Passage. *Tectonophysics*. 611, 28-50.
- Eagles, G., Livermore, R. A., 2002. Opening history of Powell Basin, Antarctic Peninsula. *Marine Geology*. 185, 195–205.
- Eagles, G., Gohl, K., Larter, R. D., 2004. High-resolution animated tectonic reconstruction of the south Pacific and West Antarctic margin. *Geochemistry, Geophysics, Geosystems*. 5, Q07002. doi: 10.1029/2003GC000657.
- Eagles, G., Gohl, K., Larter, R. D., 2009. Animated tectonic reconstruction of the Southern Pacific and alkaline volcanism at its convergent margins since Eocene times. *Tectonophysics*. 464, 21-29.
- Eagles, G., Livermore, R. A., Fairhead, J. D., Morris, P., 2005. Tectonic evolution of the West Scotia Sea. *Journal of Geophysical Research B: Solid Earth*. 110, 1–19.
- Eagles, G., Livermore, R., Morris, P., 2006. Small basins in the Scotia Sea: the Eocene Drake passage gateway. *Earth Planetary Science Letters*. 242, 343-353.

- Ewing, J. I., W. J. Ludwig, M. Ewing, and S. L. Eittreim, 1971. Structure of the Scotia Sea and Falkland Plateau, *Journal of Geophysical Research* 96, 7118-7137.
- Fahrbach, E., Knoche, M., Rohardt, G., 1991. An estimate of water mass transformation in the southern Weddell Sea. *Marine Chemistry*. 35, 25-44.
- Fahrbach, E., Rohardt, G., Scheele, N., Schroder, M., Strass, V., Wisotzki, A., 1995. Formation and discharge of deep and bottom water in the northwestern Weddell Sea. *Journal of Marine Research*. 53, 515-538.
- Faugères, J. C., Stow, D. A. V., Imbert, P., and Viana, A., 1999. Seismic features diagnostic of contourite drifts. *Marine Geology*. 162, 1-38.
- Faugères, J. C., Stow, D. A. V., 2008. Contourite Drifts. *Nature, Evolution and Controls*. In: Rebescio, M., and Camerlenghi, A., (Eds.), *Developments in Sedimentology*. Vol. 60. 257, 259-288.
- Ferris, J. K., Vaughan, A. P. M., Storey, B. C., 2000. Relics of a complex triple junction in the Weddell Sea embayment, Antarctica. *Earth and Planetary Science Letters*. 178, 215-230.
- Flower, B. P., Kennett, J. P., 1994. The middle Miocene climatic transition: East Antarctic ice sheet development, deep ocean circulation and global carbon cycling. *Palaeogeography, Palaeoclimatology, Palaeoecology*. 108, 537-555.
- Foldvik, A., Gammelsrød, T. P. P., 1988. Notes on Southern Ocean hydrography, sea-ice and bottom water formation. *Palaeogeography, Palaeoclimatology, Palaeoecology*. 67, 3-17.
- Funaki, M., Hirasawa, N., and the Ant-Plane Group, 2008. Outline of a small unmanned aerial vehicle (Ant-Plane) designed for Antarctic research. *Polar Science*, 2, 129-142.
- Galindo-Zaldívar, J., Balanyá, J. C., Bohoyo, F., Jabaloy, A., Maldonado, A., Martínez-Martínez, J. M., Rodríguez-Fernández, J., Suriach, E., 2002. Active crustal fragmentation along the Scotia-Antarctic plate boundary east of the South Orkney Microcontinent (Antarctica). *Earth and Planetary Science Letters*. 204, 33-46.
- Galindo-Zaldívar, J., Bohoyo, F., Maldonado, A., Schreider, A., Suriñach, E., Vázquez, J. T., 2006. Propagating rift during the opening of a small oceanic basin: the Protector Basin (Scotia Arc, Antarctica). *Earth Planetary Science Letters*. 241, 398-412.
- Galindo-Zaldívar, J., Gamboa, L., Maldonado, A., Nakao, S., Bochu, Y., 2006. Bransfield basin tectonic evolution. In: *Contributions to global earth sciences*, Fütterer DK, Damaske, D., Kleinschmidt G., Miller, H., Tessensohn, F. (eds.). Springer-Verlag, Berlin Heidelberg New York. 243-248.
- Galindo-Zaldívar, J., Gamboa, L., Maldonado, A., Nakao, S., Bochu, Y., 2004. Tectonic development of the Bransfield Basin and its prolongation to the South Scotia Ridge, northern Antarctic Peninsula. *Marine Geology*. 206, 267-282.
- Galindo-Zaldívar, J., Jabaloy, A., Maldonado, A., Sanz de Galdeano, C., 1996. Continental fragmentation along the SSR transcurrent plate boundary (NE

- Antarctic Peninsula). *Tectonophysics*. 258, 275–301.
- Galindo-Zaldivar, J., Jabaloy, A., Maldonado, A., Sanz de Galdeano, P., 1994. Transtensional deformation and internal basin evolution in the SSR. *Terra Antarctica*. 1, 303–306.
- Gamboa, L. A. P., Maldonado, P. R., 1990. Geophysical investigations in the Bransfield Strait and in the Bellingshausen Sea, Antarctica. In: B. St. John (ed.), *Antarctica as an Exploration Frontier-Hydrocarbon Potential, Geology and Hazards*. Am. Assoc. Petr. Geology. 31: 127-141.
- Garret, S. W., 1990. Interpretation of reconnaissance gravity and aeromagnetic surveys of the Antarctic Peninsula. *Journal of Geophysical Research*. 95/B5, 6759-6777.
- Garrett, S. W., 1991. Aeromagnetic Studies of Crustal Blocks and Basins in West Antarctica: A Review. In: Thomson, M. R. A., Crame, J. A. and Thomson, J. W. (eds.), *Geological Evolution of Antarctica*. Cambridge University Press, Cambridge 251–256.
- Garrett, S. W., Storey, B. C., 1987, Lithospheric Extension on the Antarctic Peninsula During Cenozoic Subduction. In Coward, M. P., Dewey, J. F. and Hancock, P. L. (eds.), *Continental Extension Tectonics*. Geological Society, Special Publication. 28, 419–431.
- Garrett, S. W., Renner, R. G. B., Jones, J. A., McGibbon, K. J., 1986/87. Continental Magnetic Anomalies and the Evolution of the Scotia Arc. *Earth Planetary Science Letters*. 81, 273–281.
- Geletti, R., Lodolo, E., Schreider, A.A., Polonia, A., 2005. Seismic structure and tectonics of the Shackleton Fracture Zone (Drake Passage, Scotia Sea). *Marine Geophysical Researches*. 26, 17–28.
- Ghidella, M. E., Forsberg, R., Greenbaum, J. S., Olesen, A. V., Zakrajsek, A. F., Blankenship, D. D., 2011. Magnetic anomaly data from a regional survey: from Tierra del Fuego to northern Palmer Land, Antarctic Peninsula. *Latinmag Letter, Proceedings Tandil*, A19, 1, 1-7.
- Ghidella, M. E., Raymond, C. A., Labrecque, J. L., 1991. Verification of Crustal Sources for Satellite Elevation Magnetic Anomalies in West Antarctica and the Weddell Sea and their Regional Tectonics Implications. In: Thomson, M. R. A., Crame, J. A., Thomson, J. W. (eds.), *Geological Evolution of Antarctica*. Cambridge University Press, Cambridge. 243–250.
- Ghidella, M. E., Yáñez, G., LaBrecque, J. L., 2002. Revised tectonic implications for the magnetic anomalies of the western Weddell Sea. *Tectonophysics*. 347, 65-86.
- Ghiglione, M. C., Yagupsky, D., Ghidella, M., Ramos, V. A., 2008. Continental stretching preceding the opening of the Drake Passage: Evidence from Tierra del Fuego. *Geology*. 36, 643-646.
- Gill, A. E. D.-S. R., 1973. Circulation and bottom water production in the Weddell Sea. *Deep Sea Research*. 20, 111–140.
- Golynsky, A.V., Chiappini, M., Damaske, D., Ferraccioli, F., Ferris, J., Finn, C., Ghidella, M, Ishihara, T., Johnson, A., Kim, H. R., Kovacs, L., LaBrecque, J., Masolov, V., Nogi, Y., Purucker, M., Taylor, P., Torta, M., 2001. "ADMAP - Magnetic Anomaly Map of the Antarctic,

- 1:10.000.000 scale map. In: Morris, P. and Von Frese R., eds. BAS (Misc.) 10, Cambridge, British Antarctic Survey.
- Golynsky, A.V., Morris, P., Kovacs, L.C., Ferris, J.K., 2002. A new magnetic map of the Weddell Sea and the Antarctic Peninsula, *Tectonophysics*, 347, 3-11.
- González-Casado, J.M., Giner-Robles, J.L., López-Martínez, J., 2000. Bransfield Basin, Antarctic Peninsula; not a normal back-arc basin. *Geology* 28, 1043-1046.
- González-Ferrán, O., 1991. The Bransfield Rift and its active volcanism. In: *Geological Evolution of Antarctica*, (eds.) Thomson, R.A., Crame, J.A., Thomson, J.W., Cambridge University Press, Cambridge, 505-509.
- Gordon, A. L., Visbeck, M., Huber, B., 2001. Export of Weddell Sea Deep and Bottom Water. *Journal of Geophysical Research*. 106, 9005–9017.
- Gràcia, E., Canals, M., Li Farrán, M., Prieto, M. J., Sorribas, J., Team, G., Baraza, J., Bart, P., Calafat, A. M., Casamor, M., De Bastist, M., Ercilla, G., Ramos, E., Sanz, J. L., Tassone, A., 1996. Morphostructure and evolution of the Central and Eastern Bransfield Basins (NW Antarctic Peninsula), *Marine Geophysical Researches*. 18, 429-448.
- Gràcia, E., Canals, M., Farrán, M., Sorribas, J., Pallàs, R., 1997. Central and eastern Bransfield basins (Antarctica) from high-resolution swath-bathymetry data. *Antarctic Science* 9 (2), 168-180.
- Grad, M., Guterch, A., Janik, T., 1993. Seismic structure of the lithosphere across the zone of subducted Drake plate under the Antarctic plate, West Antarctica. *Geophysical Journal international*. 115, 586-600.
- Grad, M., Guterch, A., Sroda, P., 1992. Upper crustal structure of Deception Island area, Bransfield Strait, West Antarctica. *Antarctic Science*. 4, 469-476.
- Grad, M., Shiobara, H., Janik, T., Guterch, A., Shimamura, H., 1997. Crustal model of the Bransfield Rift, West Antarctica, from detailed OBS refraction experiments. *Geophysical Journal International*. 130, 506-518.
- Hager, B. H., O'Connell, R. J., 1979). Kinematic models of large-scale flow in the Earth's mantle. *Journal of Geophysical Research*. 84(B3), 1031-1048.
- Hamilton, I. W., 1989. Geophysical investigations of subduction-related processes in the Scotia Sea. Unpublished PhD Thesis, Birmingham University, UK. pp. 328.
- Harper, J. F., 1978. Asthenosphere flow and plate motions. *Geophysical Journal of the Royal Astronomical Society*. 55(1), 87-110.
- Hasterok, D., 2013. A heat flow based cooling model for tectonic plates. *Earth and Planetary Science Letters*. 361, 34-43.
- Helffrich, G., Wiens, D. A., Vera, E., Barrientos, S., Shore, P., Robertson, S., Adaros, R., 2002. A teleseismic shear-wave splitting study to investigate mantle flow around South America and implications for plate-driving forces. *Geophysical Journal International*. 149, F1-F7.
- Hernández-Molina, F. J., Bohoyo, F., Naveira Garabato, A., Galindo-Zaldívar, J.,

- Lobo, F. J., Maldonado, A., Rodríguez-Fernández, J., Somoza, L., Stow, D. A. V., Vázquez, J. T., 2007. The Scan Basin evolution: Oceanographic consequences of the deep connection between the Weddell and Scotia Seas (Antarctica), in SCAR, ed. 1st International Symposium on Marine Sciences - ISMS07. Volume EA086, U.S. Geological Survey and The National Academies. SCAR. 1–4.
- Hernández-Molina, F. J., Larter, R. D., Rebesco, M., Maldonado, A., 2004. Miocene changes in bottom current regime recorded in continental rise sediments on the Pacific margin of the Antarctic Peninsula. *Geophysical Research Letters*. 31, 1–5.
- Hernández-Molina, F. J., Larter, R. D., Rebesco, M., Maldonado, A., 2006. Miocene reversal of bottom water flow along the Pacific Margin of the Antarctic Peninsula: Stratigraphic evidence from a contourite sedimentary tail. *Marine Geology*. 228, 93–116.
- Hernández-Molina F. J., Llave E., Stow D.A.V., 2008. Continental slope contourites. In: Rebesco M, Camerlenghi A (eds.) *Contourites. Developments in Sedimentology*. Elsevier, Amsterdam. Vol. 60., 379–407.
- Hillier, J., Watts, A., 2005. Relationship between depth and age in the North Pacific Ocean. *Journal of Geophysical Research*. 110, B02405.
- Hillenbrand, C. D., Camerlenghi, A., Cowan, E. A., Hernández-Molina, F. J., Lucchi, R. G., Rebesco, M., Uenzelmann-Neben, G., 2008. The present and past bottom-current flow regime around the sediment drifts on the continental rise west of the Antarctic Peninsula. *Marine Geology*. 255, 55–63.
- Howe, J. A., Livermore, R. A., Maldonado, A., 1998. Mudwave activity and current-controlled sedimentation in Powell Basin, northern Weddell Sea, Antarctica. *Marine Geology*. 149, 229–241.
- Howe, J. A., Pudsey, C. J., 1999. Antarctic circumpolar deep water: A Quaternary paleoflow record from the northern Scotia Sea, South Atlantic ocean. *Journal of Sedimentary Research*. 69, 847–861.
- Huber, M., Sloan, L. C., 2001. Heat transport, deep waters, and thermal gradients: Coupled simulation of an Eocene greenhouse climate. *Geophysical Research Letters*. 28, 3481–3484.
- Ibáñez, J. M., Carmona, E., Almendros, J., Saccorotti, G., Del Pezzo E., Abril, M., Ortiz, R., 2003. The 1998-1999 seismic series at Deception Island volcano, Antarctica. *Journal of Volcanology and Geothermal Research*. 128, 65-88.
- Ibáñez, J. M., Del Pezzo, E., Almendros, J., Larocca, M., Alguacil, G., Ortiz, R., García, A., 2000. Seismovolcanic signals at Deception Island volcano, Antarctica: wave field analysis and source modelling. *Journal of Geophysical Research*. 105, 13905-13931.
- Jabaloy, A., Balanyá, J.C., Barnolas, A., Galindo-Zaldívar, J., Hernández-Molina, F.J., Maldonado, A., Martínez-Martínez, J. M., Rodríguez-Fernández, J., Saenz de Galdeano, C., Somoza, L., Suriñach, E., Vazquez, J.T., 2003. The transition from an active to a passive margin (SW end of the South Shetland Trench, Antarctic Peninsula). *Tectonophysics*. 366, 55-81.

- Kennett, B. L. N., 1977. Towards a more detailed seismic picture of the oceanic crust and mantle. *Marine Geophysical Researches*. 3, 7–42.
- Kennett, J. P., Stott, L. D., 1990. Proteus and Proto-oceanus: ancestral Paleogene oceans as revealed from Antarctic stable isotope results. In: Barker, P.F., (Eds.), *Proceedings of the Ocean Drilling Program. Scientific Results*. College Station, TX. 113, 865–880.
- Kim, Y., Chung, T.W., Nam, S.H., 1992. Marine magnetic anomalies in Bransfield Strait, Antarctica. *Recent progress in Antarctic Earth Science: edited by Y. Yoshida et al.* 431–437.
- Kim, Y., Jin, Y.K., Nam, S.H., 1997. Crustal structure of the Shackleton Fracture Zone in the southern Drake Passage, Antarctica. In: Ricci, C.A., (eds.) *The Antarctic region: Geological evolution and processes*. Siena. Terra Antarctica Publications. 661–667.
- King, E. C., Barker, P. F., 1988. The margins of the South Orkney microcontinent. *Journal - Geological Society*, London. 145, 317–331.
- King, E., Leitchenkov, G., Galindo-Zaldívar, J., Maldonado, A., Lodolo, E., 1997. Crustal structure and sedimentation in Powell Basin. In: *Geology and Seismic Stratigraphy of the Antarctic Margin*, (eds.) Barker, P.F. and Cooper, A. AGU. Vol. 71, 75–93.
- Klepeis, K. A., Lawver, L. A., 1996. Tectonics of the Antarctic-Scotia plate boundary near Elephant and Clarence Islands, West Antarctica. *Journal of Geophysical Research B: Solid Earth*. 101, 20211–20231.
- Klitgord, K. D., 1976. Sea-floor spreading: The central anomaly magnetization high. *Earth and Planetary Science Letters*, 29, 201–209.
- Korenaga, T., Korenaga, J., 2008. Subsidence of normal oceanic lithosphere, apparent thermal expansivity, and seafloor flattening. *Earth and Planetary Science Letters*. 268, 41–51.
- Kovacs, L. C., Morris, P., Brozena, J., Tikku, A., 2002. Seafloor spreading in the Weddell Sea from magnetic and gravity data. *Tectonophysics*. 347, 343–64.
- Larson, R. L., 1976. Late Jurassic and Early Cretaceous Evolution of the Western Central Pacific Ocean. *Journal of Geomagnetism and Geoelectricity*. 28, 219–236.
- Langseth, M. G., LePichon, X., Ewing, M., 1966. Crustal structure of mid-ocean ridges: 5. Heat flow through the Atlantic Ocean floor and convection currents. *Journal of Geophysical Research*. 71, 5321–5355.
- Larter, R. D., Barker, P.F., 1991. Effects of ridge-crest trench interaction on Antarctic-Phoenix spreading: forces on a young subducting plate. *Journal of Geophysical Research*. 96:19583–19607.
- Larter, R. D., L. E. Vanneste, P. Morris, and D. K. Smythe, 2003. Structure and tectonic evolution of the South Sandwich Arc. In: Larter, R.D., and P. T. Leat (eds.), *Intra-oceanic subduction systems: tectonic and magmatic processes*, London, Geological Society of London. 255–284.
- Lawver, L. A., Gahagan, L. M., 1998. Opening of Drake Passage and its impact on Cenozoic ocean circulation. In: Crowley, T.J., and Burke, K.C., (Eds.), *Tectonic*

- Boundary Conditions for Climate Reconstructions. Oxford, Oxford University Press. 212–223.
- Lawver, L. A., Gahagan, L. M., 2003. Evolution of cenozoic seaways in the circum-Antarctic region. *Palaeogeogr. Palaeoclimatol. Palaeoecol.* 198, 11–37.
- Lawver, L. A., Gahagan, L. M., Coffin, M. F., 1992. The development of paleoseaways around Antarctica. *Antarctic Research Series – AGU*. 56, 7–30.
- Lawver, L. A., Keller, R. A., Fisk, M. R., Strelin, J. A., 1995. Bransfield Basin, Antarctic Peninsula: active extension behind a dead arc. In: Taylor, B. (ed.), *Back arc basins: tectonic and magmatism*. Amsterdam, Plenum Press. 315–342.
- Lawver, L. A., Sloan, B. J., Barker, D. H. N., Ghidella, M., Von Herzen, R. P., Keller, R. A., Klinkhammer, G. P., Chin, C. S., 1996. Distributed, active extension. In: *Bransfield Basin, Antarctic Peninsula: Evidence from Multibeam Bathymetry*. *GSA Today*. 6 (11), 1–6.
- Lindeque, A., Martos, Y. M., Gohl, K., Maldonado, A., 2013. Deep-sea pre-glacial to glacial sedimentation in the Weddell Sea and southern Scotia Sea from a cross-basin seismic transect. *Marine Geology*. 336, 61–83.
- Livermore, R. A., 2003. Back-arc spreading and mantle flow in the East Scotia Sea. In: Larter, R.D. and Leat, P.T. (eds.), *Intra-Oceanic Subduction Systems: Tectonic and Magmatic Processes*. Geological Society, London. Vol. 219. 255–284.
- Livermore, R. A., Woollett, R. W., 1993. Seafloor spreading in the Weddell Sea and southwest Atlantic since the Late Cretaceous. *Earth and Planetary Science Letters*. 117, 475–495.
- Livermore, R., Balanyá, J. C., Maldonado, A., Martínez, J. M., Rodríguez-Fernández, J., Sanz de Galdeano, C., Zaldívar, J. G., Jabaloy, A., Barnolas, A., Somoza, L., Hernández-Molina, J., Suriñach, E., Viseras, C., 2000. Autopsy on a dead spreading center: The Phoenix Ridge, Drake Passage, Antarctica. *Geology*. 28, 607–610.
- Livermore, R., Eagles, G., Morris, P., Maldonado, A., 2004. Shackleton Fracture Zone: No barrier to early circumpolar ocean circulation. *Geology*. 32, 797–800.
- Livermore, R., Hillenbrand, C. D., Meredith, M., Eagles, G., 2007. Drake Passage and Cenozoic climate: An open and shut case? *Geochemistry, Geophysics, Geosystems*. 8.
- Livermore, R., McAdoo, D., Marks, K., 1994. Scotia Sea tectonics from high-resolution satellite gravity. *Earth and Planetary Science Letters*. 123, 255–268.
- Livermore, R., Nankivell, A., Eagles, G., Morris, P., 2005. Paleogene opening of Drake Passage. *Earth and Planetary Science Letters*. 236, 459–470.
- Lobo, F. J., Hernández-Molina, F. J., Bohoyo, F., Galindo-Zaldívar, J., Maldonado, A., Martos, Y. M., Rodríguez-Fernández, J., Somoza, L., Vázquez, J. T., 2011. Furrows in the southeastern Scan Basin, Antarctica: interplay between tectonic and oceanographic influences. *Geo-Marine Letters*. 31 (5–6), 451–464.
- Locarnini, R. A., Whitworth III, T., Nowlin Jr., W. D., 1993. The importance of the Scotia Sea on the outflow of

- Weddell Sea Deep Water. *Journal of Marine Research*. 51, 135–153.
- Lodolo, E., Tassone, A., 2010. Gateways and climate: The Drake Passage opening. *Bollettino di Geofisica Teorica ed Applicata*. 51, 77–88.
- Lodolo, E., Civile, D., Vuan, A., Tassone, A., Geletti, R., 2010. The Scotia-Antarctica plate boundary from 35°W to 45°W. *Earth and Planetary Science Letters*. 293, 200–215.
- Lodolo, E., Coren, F., Schreider, A. A., Ceccone, G., 1997. Geophysical evidence of a relict oceanic crust in the southwestern Scotia Sea. *Marine Geophysical Researches*. 19, 439–450.
- Lodolo, E., Donda, F., Tassone, A., 2006. Western Scotia Sea margins: Improved constraints on the opening of the Drake Passage. *Journal of Geophysical Research B: Solid Earth* (1978–2012). 111 (B6), doi:10.1029/2006JB004361.
- Ludwig, W. J., Nafe, J. E., Drake, C. L., 1970. Seismic refraction, In *The Sea* (ed. Maxwell, A.E.) Wiley-Interscience, New York. 53-84.
- Mackensen, A., 2004. Changing Southern Ocean paleocirculation and effects on global climate. *Antarctic Science*. 16, 369-386.
- Maldonado, A., Balanyá, J. C., Barnolas, A., Galindo-Zaldívar, J., Hernández-Molina, J., Jabaloy, A., Livermore, R., Martínez-Martínez, J. M., Rodríguez-Fernández, J., De Galdeano, C. S., Somoza, L., Suriñach, E., Viseras, C., 2000. Tectonics of an extinct ridge-transform intersection, Drake Passage (Antarctica). *Marine Geophysical Researches*. 21, 43–67.
- Maldonado, A., Barnolas, A., Bohoyo, F., Galindo-Zaldívar, J., Hernández-Molina, J., Lobo, F., Rodríguez-Fernández, J., Somoza, L., Vázquez, J.T., 2003. Contourite deposits in the central Scotia Sea: The importance of the Antarctic Circumpolar Current and the Weddell Gyre flows. *Palaeogeography, Palaeoclimatology, Palaeoecology*. 198, 187–221.
- Maldonado, A., Barnolas, A., Bohoyo, F., Escutia, C., Galindo-Zaldívar, J., Hernández-Molina, J., Jabaloy, A., Lobo, F.J., Nelson, C. H., Rodríguez-Fernández, J., Somoza, L., Vázquez, J.T., 2005. Miocene to Recent contourite drifts development in the northern Weddell Sea (Antarctica). *Global and Planetary Change*. 45, 99–129.
- Maldonado, A., Bohoyo, F., Galindo-Zaldívar, J., Hernández-Molina, F. J., Jabaloy, A., Lobo, F. J., Rodríguez-Fernández, J., Suriñach, E., Vázquez, J. T., 2006. Ocean basins near the Scotia-Antarctic plate boundary: Influence of tectonics and paleoceanography on the Cenozoic deposits. *Marine Geophysical Researches*. 27, 83–107.
- Maldonado, A., Bohoyo, F., Galindo-Zaldívar, J., Hernández-Molina, F.J., Lobo, F.J., Martos-Martín, Y., Schreider, A., 2010. Small oceanic basins in the southwestern Scotia Sea reveal initial opening of Drake Passage (Antarctica). *International Polar Year. Oslo Science Conference*. Oslo (Norway).
- Maldonado, A., Larter, R. D., Aldaya, F., 1994. Forearc tectonic evolution of the South Shetland margin, Antarctic Peninsula. *Tectonics*. 13, 1345–1370.
- Maldonado, A., Zitellini, N., Leitchenkov, G., Balanyá, J. C., Coren, F., Galindo-Zaldívar, J., Lodolo, E., Jabaloy, A.,

- Zanolla, C., Rodríguez-Fernández, J., Vinnikovskaya, O., 1998. Small ocean basin development along the Scotia-Antarctica plate boundary and in the northern Weddell Sea. *Tectonophysics*. 296, 371–402.
- Martos, Y. M., 2010. Estudio geofísico y geodinámico de la Isla Decepción (Antártida) y su entorno próximo. *Boletín ROA 2/2010*. Nipo 076-10-146-9. ISSN 1131-5040, Dep leg CA 469-78.
- Martos, Y. M., Bohoyo, F., Galindo-Zaldívar, J., Maldonado, A., 2012. Age-depth relationship and lithosphere behaviour in the western and central Scotia Sea (Antarctica). XXXII SCAR Science Week, 5th Open Science Conference. Portland (USA).
- Martos, Y. M., Catalán, M., Galindo-Zaldívar, J., Maldonado, A., Bohoyo, F., in revision (b). Insights about the structure and evolution of the Scotia Arc from a new magnetic data compilation. *Global and Planetary Change*.
- Martos, Y. M., Galindo-Zaldívar, J., Catalán, M., Bohoyo, F., Maldonado, A., 2014. Asthenospheric Pacific-Atlantic flow barriers and the West Scotia Ridge extinction. *Geophysical Research Letters*. 41, 1-7. doi:10.1002/2013GL058885.
- Martos, Y. M., Galindo-Zaldívar, J., Catalán, M., Bohoyo, F., Maldonado, A., in revision (a). Thermal behaviour and subsidence of small oceans: The West Scotia Sea. In revision for *Journal of Geodynamics*.
- Martos, Y. M., Maldonado, A., Lobo, F. J., Hernández-Molina, F. J., Pérez, L. F., 2013. Tectonics and palaeoceanographic evolution recorded by contourite features in southern Drake Passage (Antarctica). *Marine Geology*. 343, 76-91.
- Martos-Martín, Y., Bohoyo, F., Galindo-Zaldívar, J., Lobo, F. J., Maldonado, A., Schreider, A., 2010. Crustal structure and age of the southwestern Scotia Plate sector (Scotia Arc, Western Antarctica). *International Polar Year. Oslo Science Conference*. Oslo (Norway).
- Maslanyj, M. P., Garret, S. W., Johnson, A. C., Renner, R. G., Smith, A. M., 1991. Aeromagnetic anomaly map of western Antarctica (Weddell Sea sector). *British Antarctic Survey*, Scale 1:2 500,000.
- Maurice, S. D. R., Wiens, D. A., Shore, P.J., Vera, E., Dorman, L. M., 2003. Seismicity and tectonics of the South Shetland Islands and Bransfield Strait from a regional broadband seismograph deployment. *Journal of Geophysical Research-Solid Earth*. 108, doi:10.1029/2003JB002416.
- McKenzie, D., 1967. Some remarks on heat flow and gravity anomalies. *Journal of Geophysical Research*. 72, 6261–6273.
- Mead, G. A., Hodell, D. A., Ciesielski, P. F., 1993. Late Eocene to Oligocene vertical oxygen isotopic gradients in the South Atlantic: Implications for Warm Saline Deep Water. In: Kennett, J.P., and Warnke, D.A. (eds.), *The Antarctic Paleoenvironment: A Perspective on Global Change*. AGU Antarctic Research Series. 60, 27–48.
- Mendonça C. A., Meguid A. M. A., 2008. Program to compute magnetization to density ratio and the magnetization inclination from 3-D gravity and magnetic anomalies. *Geophysics*. 34, 603-610.

- Metzger, D., Campagnoli, J., 2007. Marine Trackline Geophysics Data on DVD, Version 5.0.10, National Geophysical Data Center. Boulder, Colorado.
- Michels, K. H., Rogenhagen, J., Kuhn, G., 2002. Recognition of contour-current influence in mixed contourite-turbidite sequences of the western Weddell Sea, Antarctica. *Marine Geophysical Research*. 22, 465–485.
- Miller, M. F., Mabin, M. C. G., 1998. Antarctic Neogene landscapes—In the refrigerator or in the deep freeze? *GSA Today*. 8, 1–3.
- Miller, K. G., Wright, J. D., Katz, M. E., Browning, J. V., Cramer, B. S., Wade, B. S., Mizintseva, S. F., 2008. A view of Antarctic ice-sheet evolution from sea-level and deep-sea isotope changes during the Late Cretaceous–Cenozoic. In: Cooper, A.K., Barrett, P.J., Stagg, H., Storey, B., Stump, E., Wise, W., and the 10th International Symposium on Antarctic Earth Sciences team, (Eds.), *Antarctica: A Keystone in the Changing World. Proceedings of the 10th International Symposium on Antarctic Earth Sciences*. Washington, D. C. National Academy of Sciences Press. 55–70.
- Moore, J. K., Abbott, M. R., Richman, J. G., 1997. Variability in the location of the Antarctic Polar Front (90°–20° W) from satellite sea surface temperature data. *Journal of Geophysical Research*. 102, 27825–27833.
- Muñoz-Martín, A., Catalán, M., Martín, J., Carbó, A., 2005. Upper crustal structure of Deception Island area (Bransfield Strait, Antarctica) from gravity and magnetic modelling. *Antarctic Science*. 17 (2), 213–224.
- Nakatsuka, T., Utsugi, M., Okuma, S., Tanaka, Y., Hashimoto, T., 2009. Detection of aeromagnetic anomaly change associated with volcanic activity: an application of the generalized mis-tie control method. *Tectonophysics*, 478. 1-2, 3-18.
- Naveira Garabato, A. C., Heywood, K. J., Stevens, D.P., 2002a. Modification and pathways of Southern Ocean Deep Waters in the Scotia Sea. *Deep-Sea Research Part I: Oceanographic Research Papers*. 49, 681–705.
- Naveira Garabato, A. C., McDonagh, E. L., Stevens, D. P., Heywood, K. J., Sanders, R. J., 2002b. On the export of Antarctic Bottom Water from the Weddell Sea. *Deep-Sea Research Part II: Topical Studies in Oceanography*. 49, 4715–4742.
- Naveira Garabato, A. C., Stevens, D. P., Heywood, K. J., 2003. Water mass conversion, fluxes, and mixing in the Scotia Sea diagnosed by an inverse model. *Journal of Physical Oceanography*. 33, 2565–2587.
- Nettleton, L. L., 1976. *Gravity and magnetic in oil exploration*. New York, Mac Graw-Hill.
- Nerlich, R., Clark, S. R., Bunge, H. P., 2013. The Scotia Sea gateway: No outlet for Pacific mantle. *Tectonophysics*. 604, 41-50.
- Nowlin Jr., W.D., Klinck, J.M., 1986. The physics of the Antarctic Circumpolar Current. *Reviews of Geophysics*. 24, 469–491.
- Nowlin, Jr., W.D., W. Zenk, 1988. Westward bottom currents along the margin of the South Shetland Island Arc. *Deep Sea Research*. 35, 269-301.
- Orsi, A. H., Johnson, G. C., Bullister, J. L., 1999. Circulation, mixing, and production of Antarctic Bottom

- Water: Progress in Oceanography. 43, 55-109.
- Orsi, A. H., Whitworth III, T., Nowlin Jr., W. D., 1995. On the meridional extent and fronts of the Antarctic Circumpolar Current. Deep-Sea Research Part I. 42, 641–673.
- Ortiz, R., 1997. Monitoring of the volcanic activity of Deception Island, South Shetland Islands, Antarctica (1986-1995). In: Antarctic Region: geological Evolution and Processes, edited by C. A. Ricci. Terra Antarctica Publication, Siena. 1071-1076.
- Parmentier, E. M., Oliver, J. E., 1979. A study of shallow global mantle flow due to the accretion and subduction of lithospheric plates. Geophysical Journal of the Royal Astronomical Society. 57(1), 1-21.
- Parra, J. C., González-Ferrán, O., Bannister, J., 1984. Aeromagnetic Survey Over the South Shetland Islands, Bransfield Strait and Part of the Antarctic Peninsula. Revista Geológica de Chile. 23, 3–20.
- Parra, J. C., Yañez, G., USAC-Group., 1988. Aeromagnetic Survey on the Antarctic Peninsula and Surrounding Seas: Integration of the Data Obtained at Different Altitudes, Ser. Cient. INACH. 38, 117–131.
- Parsons, B., Sclater, J., 1977. An analysis of the variation of ocean floor bathymetry and heat flow with age. J. Geophys. Res. 82, 803–827.
- Pearce, J., Leat, P. T., Barker, P. F., Millar, I. L., 2001. Geochemical tracing of Pacific-to-atlantic upper-mantle flow through Drake Passage. Nature. 410, 457–461.
- Pedley, R. C., Bubsby, J. P., Dabek, Z. K., 1993. GRAVMAG 1.7. (2.5 D), version 1.5.
- Pelayo, A. M., Wiens, D. A., 1989. Seismotectonics and relative plate motions in the Scotia Sea region. Journal of Geophysical Research. 94, 7293–7320.
- Pedreira, A., Ruiz-Constán, A., Heredia, N., Galindo-Zaldívar, J., Bohoyo, F., Marín-Lechado, C., Ruano, P., Somoza, L., 2012. The fracture system and the melt emplacement beneath the Deception Island active volcano, South Shetland Islands, Antarctica. Antarctic Science. 24(02), 173-182.
- Perrin, C., 2002. Tertiary: the emergence of modern reef ecosystems. In: Kiessling, W., Flügel, E., Goloka, J. (Eds.), Phanerozoic Reef Patterns: Society for Sedimentary Geology Special Publication. Vol. 72, 587–621.
- Polet, J., Silver, P. G., Beck, S., Wallace, T., Zandt, G., Ruppert, S., Kind, R., Rudloff, A., 2000. Shear wave anisotropy beneath the Andes from the BANJO, SEDA, and PISCO experiments. Journal of geophysical research. 105(B3), 6287-6304.
- Potter, P. E., Szatmari P., 2009. Global Miocene tectonics and the modern world. Earth-Science Reviews. 96, 279–295.
- Pudsey, C.J., 2002. The Weddell Sea: Contourites and hemipelagites at the northern margin of the Weddell Gyre. Geological Society Memoir. 22, 289–303.
- Quesnel, Y., Catalán, M., Ishihara, T., 2009. A new global marine magnetic anomaly data set. Journal of

- Geophysical Research. 114, B04106.
doi:10.1029/2008JB006144.
- Rahmstorf, S., 2006. Thermohaline ocean circulation in: Elias SA (Eds.) Encyclopedia of Quaternary Sciences. Elsevier. Amsterdam, pp. 1–10.
- Ravat, D., 1996. Analysis of the Euler method and its applicability in environmental magnetic investigations. *Journal of Environmental and Engineering Geophysics*. 229-238.
- Ravat, D., Purucker, M., 1999. The future of satellite magnetic anomaly studies is bright!. *The Leading Edge*. 18, 326-329.
- Ravat, D., Hildebrand, T. G., Roest, W., 2003. New way of processing near-surface magnetic data: The utility of the Comprehensive Magnetic Field Model. *The Leading Edge*. 22, 784-785.
- Rebesco, M., 2005. Contourites. In: Selley, R. C., Cocks, L. R. M., and Plimer, I. R. (Eds.) *Encyclopedia of Geology*, Volume 4: Oxford, Elsevier. 513-527.
- Rebesco, M., Camerlenghi, A., 2008. Late Pliocene margin development and mega debris flow deposits on the Antarctic continental margins: Evidence of the onset of the modern Antarctic Ice Sheet? *Palaeogeography, Palaeoclimatology, Palaeoecology*. 260, 149–167.
- Rebesco, M., Camerlenghi, A., Van Loon, A. J., 2008. Contourite research: A field in full development. In: Rebesco, M., and Camerlenghi, A. (Eds.), *Contourites, Volume Developments in Sedimentology* 60, Elsevier. 3-10.
- Rebesco, M., Larter, R. D., Barker, P. F., Camerlenghi, A., Vanneste, L. E., 1997. The history of sedimentation on the continental rise west of the Antarctic Peninsula, in: Barker, P.F., and Cooper, A.K., (Eds.) *Geology and Seismic Stratigraphy of the Antarctic Margin, Part 2*. AGU. 71, 29–49.
- Rebesco, M., Pudsey, C. J., Canals, M., Camerlenghi, A., Barker, P. F., Estrada, F., Giorgetti, A., 2002. Sediment drifts and deep-sea channel systems, Antarctic Peninsula Pacific Margin. In Stow, D. A. V., Pudsey, C. J., Howe, J. A., Faugères, J.-C., and Viana, A. R. (eds.), *Deep-Water Contourite Systems: Modern Drifts and Ancient Series*, Seismic and Sedimentary Characteristics, Geological Society, London, *Memoirs*. 22, 353-371.
- Reid, A. B., Allsop, J. M., Granser, H., Millet, A. J., Somerton, I. W., 1990. Magnetic interpretation in three dimensions using Euler Deconvolution. *Geophysics*. 55 (1), 80-91.
- Renkin, M. L., Sclater, J. G., 1988. Depth and age in the North Pacific. *Journal of Geophysical Research*. 93, 2919-2935.
- Rey, J., Maestro, A., Somoza, L., Smellie, J. L., 2002. Submarine morphology and seismic stratigraphy of Port Foster. In: *Geology and Geomorphology of Deception Island*, edited by J. L. Smellie and J. López-Martínez. British Antarctic Survey, Cambridge, U. K. 40-46.
- Rey, J., Somoza, L., Martínez-Frías, J., 1995. Tectonic volcanic and hydrothermal event sequence on Deception Island (Antarctica). *Geo-Mar. Lett.* 15, 1-8.
- Rodríguez-Fernández, J., Balanyá, J. C., Galindo-Zaldívar, J., Maldonado, A., 1997. Tectonic evolution and growth

- patterns of a restricted ocean basin: the Powell Basin (northeastern Antarctic Peninsula). *Geodinamica Acta*. 10, 159–174.
- Rogenhagen, J., Jokat, W., 2000. The sedimentary structure in the western Weddell Sea. *Marine Geology*. 168, 5–60.
- Roobol, M. J., 1980. A model for the eruptive mechanism of Deception Island from 1820 to 1970. *British Antarctic Survey Bulletin*. 49, 137-156.
- Roots, W. D., Veevers, J. J., Clowes, D. F., 1979. Lithospheric model with thick oceanic crust at the continental boundary: a mechanism for shallow spreading ridges in young oceans. *Earth and Planetary Science Letters*. 43, 417–433.
- Russell, S. M., Whitmarsh, R. B., 2003. Magmatism at the west Iberia non-volcanic rifted continental margin: evidence from analyses of magnetic anomalies. *Geophysical Journal International*, 154, 706-730.
- Russo, R. M., Silver, P.G., 1994. Trench-Parallel flow beneath the Nazca Plate from seismic anisotropy. *Science*. 263, 1105-1111.
- Sabaka, T., Olsen, N., Purucker, M., 2004. Extending comprehensive models of the Earth's magnetic field with Oersted and CHAMP data. *Geophysical Journal International*. 159, 521-547.
- Salem, A., Aboud, E., Elsirafy, A., Ushijima, K., 2007. Structural mapping of Quseir area, northern red Sea, Egypt, using high-resolution aeromagnetic data. *Earth, Planets and Space*, 57, 761-765.
- Scher, H. D., Martin, E. E., 2006. Timing and climatic consequences of the opening of Drake Passage. *Science*, 312(5772), 428-430.
- Schodlok, M. P., Hellmer, H. H., Beckmann, A., 2002. On the transport, variability and origin of dense water masses crossing the SSR. *Deep Sea Research II*. 49, 4807–4825.
- Schreider, Al. A., Schreider, A. A., Galindo-Zaldívar, J., Maldonado, A., Martos-Martín, Y., 2012. Initial phase of the West Scotia Mid-Oceanic Ridge opening. *Oceanology*. 52, 540-544.
- Shuey, R. T., Schellinger, D. K., Tripp, A. C., Alley, L. B., 1977. Curie depth determination from aeromagnetic spectra, *Geophys. J.R. Astron. Soc.*, 50, 75-101.
- Silver, P. G., Chan, W. W., 1991. Shear wave splitting and subcontinental mantle deformation. *Journal of Geophysical Research: Solid Earth (1978–2012)*, 96(B10), 16429-16454.
- Smalley, R. Jr., Dalziel, I. W. D., Bevis, M. G., Kendrick, E., Stamps, D.S., King, E.C., Taylor, F. W., Lauria, E., Zakrajsek, A., Parra, H., 2007. Scotia arc kinematics from GPS geodesy. *Geophysical Research Letters*. 34, L21308, doi:10.1029/2007GL031699.
- Smellie, J. L., 2001. Lithostratigraphy and volcanic evolution of Deception Island, South Shetland Islands. *Antarctic Science*. 13 (2), 188-209.
- Smith, R. T., Anderson, J. B., 2011. Seismic Stratigraphy of the Joinville Plateau: Implications for Regional Climate Evolution. In: Anderson, J. B. and Wellner, J.S. (Eds.), *Tectonic, Climatic, and Cryospheric Evolution of the Antarctic Peninsula*. Geopress, AGU, Washington DC, USA. 51–61. doi:10.1029/2010SP000980.

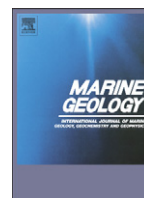
- Smith, W. H. F., Sandwell, D. T., 1997. Global seafloor topography from satellite altimetry and ship depth soundings. *Science*. 277, 1957–1962.
- Somoza, L., Martinez-Frias, J., Smellie, J. L., Rey, J., Maestro, A., 2004. Evidence for hydrothermal venting and sediment volcanism discharged after recent short-lived volcanic eruptions at Deception Island, Bransfield Strait, Antarctica. *Marine Geology*. 203, 119–140, doi:10.1016/S0025-3227(03)00285-8.
- Spector, A., Grant, F. S., 1970. Statistical models for interpreting aeromagnetic data. *Geophysics*. 35, 293-302.
- Steckler, M. S., Watts, A. B., 1978. Subsidence of the Atlantic-type continental margin off New York. *Earth and Planetary Science Letters*. 41, 1-13.
- Stein, C., Stein, S., 1992. A model for the global variation in oceanic depth and heat flow with lithospheric age. *Nature*. 359, 123–129.
- Stein, C., Stein, S., 1993. Constraints on Pacific midplate swells from global depth–age and heat flow–age models. In: *The Mesozoic Pacific: Geology, Tectonics, and Volcanism*. Geophysical Monograph Vol. 77 (eds. Pringle, M., Sager, W., Sliter, W., Stein, S.). AGU, Washington, DC. 53–76.
- Stow, D. A. V., Faugeres, J. C., Howe, J. A., Pudsey, C. J., Viana, A. R., 2002. Bottom currents, contourites and deep sea sediment drifts: Current state-of-the-art. *Geological Society of London Memories*. 7–20.
- Suriñach, E., Galindo-Zaldívar, J., Maldonado, A., Livermore, R. A., 1997. Large amplitude magnetic anomalies in the northern sector of the Powell Basin, NE Antarctica Peninsula. *Marine Geophysical Research*. 19, 65-80.
- Sykes, T. J. S., 1996. A correction for sediment load upon the ocean floor: Uniform versus varying sediment density estimation-implications for isostatic correction. *Marine Geology*. 133, 35-49.
- Tanaka, Y., 1993. Eruption mechanism as inferred from geomagnetic changes with special attention to the 1989-90 activity of Aso Volcano. *Journal of Volcanology and Geothermal Research*. 56, 319-338.
- Tapley, B., Ries, J., Bettadpur, S., Chambers, D., Cheng, M., Condi, F., Gunter, B., Kang, Z., Nagel, P., Pastor, R., Pekker, T., Poole, S., Wang, F., 2005. GGM02—An improved Earth gravity field model from GRACE. *Journal of Geodesy*. 79(8), 467-478.
- Tarakanov, R. Y., 2009. Antarctic bottom water in the Scotia Sea and the Drake Passage. *Oceanology*. 49, 607-621.
- Tassara, A., Götze, H., Schmidt, S., Hackney, R., 2006. Three-dimensional density model of the Nazca plate and the Andean continental margin. *Journal of Geophysical Research*. 111, B09404, doi:10.1029/2005JB003976.
- Taylor, B. 1995. Backarc basins : tectonics and magmatism. Springer.
- Taylor, B., Goodliffe, A., Martinez, F., Hey, R., 1995. Continental rifting and initial seafloor spreading in the Woodlark Basin. *Nature*. 374, 534-537.
- Taylor, F. W., Bevis, M. G., Dalziel, I. W. D., Smalley, Jr. R., Frohlich C., Kendrick E., Foster J., Phillips D., Gudipati K., 2008. Kinematics and segmentation of the South Shetland

- Islands-Bransfield basin system, northern Antarctic Peninsula, Geochemistry, Geophysics, Geosystems. 9, Q04035, doi:10.1029/2007GC001873.
- Telford, G., Geldart, L. P. Sheriff, 1990. Applied Geophysics, 2nd Edition, Cambridge University Press, Cambridge.
- Thakur, N. K., Gangadhara Rao, T., Subrahmanyam, C., Khanna, R., 1999. Crossover analysis of geophysical data in Bay of Bengal. *Geo-Marine Letters*. 19, 262-269.
- Thomas, C., Livermore, R., Fred Pollitz, 2003. Motion of the Scotia Sea plates. *Geophysical Journal International*. 155, 789-804.
- Thomson, D.T., 1982. EULDPH: A new technique for making computer-assisted depth estimates from magnetic data. *Geophysics*. 55, 80-91.
- Turcotte, D. L., Schubert, G., 2002. *Geodynamics*. Cambridge University Press, New York.
- Uenzelmann-Neben, G., 2006. Depositional patterns at Drift 7, Antarctic Peninsula: Along-slope versus down-slope sediment transport as indicators for oceanic currents and climatic conditions. *Marine Geology*. 233, 49-62.
- Vaughan, A. P. M., Wareham, C. D., Johnson, A. C., Kelley, S. P. A., 1998. Lower Cretaceous, syn-extensional magmatic source for a linear belt of positive magnetic anomalies: the Pacific Margin Anomaly (PMA), western Palmer Land, Antarctica. *Earth and Planetary Science Letters*. 158, 143-155.
- Vila, J., Marti, J., Ortiz, R., Garcia, A., Correig A. M., 1992. Volcanic tremors at Deception Island (South Shetland Islands, Antarctica). *Journal of Volcanology and Geothermal Research*. 53, 89-102.
- Vincent, E., Berger, W. H., 1985. Carbon dioxide and polar cooling in the Miocene: The Monterey hypothesis. In: Sundquist, E.T., and Broecker, W.S., (Eds.), *The Carbon Cycle and Atmospheric CO₂: natural Variations Archean to Present*. AGU Monogr. 32.
- Vine, F. J., Matthews, D. H., 1963. Magnetic Anomalies Over Oceanic Ridges. *Nature*. 199, 974-949.
- Visbeck, M., Gordon, A., Smethie, B., Schlosser, P., Toole, J., Huber, B., Krahnemann, G., 2001. The CORC/ARCHES Observing System for Weddell Sea Deep and Bottom Water Variability. *CLIVAR Exchanges*. 6, 4.
- Viseras, C., Maldonado, A., 1999. Facies architecture, seismic stratigraphy and development of a high-latitude basin: the Powell Basin (Antarctica). *Marine Geology*. 157, 69-87.
- Wessel, P., Smith, W. H. F., 1998. New, improved version of Generic Mapping Tools, released, *Eos Trans. AGU*. 79, 579.
- Wessel, P., Watts, A. B., 1988. On the accuracy of marine gravity measurements. *Journal of Geophysical Research*. 93, 393-413.
- Wynn, R. B., Masson, D. G., 2008. Sediment Waves and Bedforms. In: Rebesco, M., and Camerlenghi, A. (Eds.) *Contourites. Volume Developments in Sedimentology* 60, Elsevier. 289-300.

- Zachos, J., Pagani, H., Sloan, L., Thomas, E., Billups, K., 2001. Trends, rhythms, and aberrations in global climate 65 Ma to present. *Science*. 292, 686–693.
- Zandomeneghi, D. A., Barclay, A., Almendros, J., Ibañez, J., Wilcock, W. S. D., Ben-Zvi, T., 2009. Crustal structure of Deception Island volcano from P wave seismic tomography: Tectonic and volcanic implications. *Journal of Geophysical Research*. 114, B06310, doi:10.1029/2008JB006119.
- Zhong-Shi, Z., Qing, Y., Hui-Jun, W., 2010. Has the Drake Passage Played an Essential Role in the Cenozoic Cooling? *Atmospheric and Oceanic Science Letters*. 3, 288-292.
- Zhou, M., Niiler, P. P., Hu, J.-H., 2002. Surface currents in the Bransfield and Gerlache Straits, Antarctica, *Deep-Sea Research I*, 49, 267-280.
- Zlotnicki, J., Le Mouel, J.-L., 1988. Volcanomagnetic effects observed on Piton de la Fournaise volcano (Reunion Island): 1985-87, *Journal of Geophysical Research*. 93, 9157- 9171.

Appendix

OTHER SCI PUBLISHED ARTICLES OF THE STUDY AREA AS A COAUTHOR



Deep-sea pre-glacial to glacial sedimentation in the Weddell Sea and southern Scotia Sea from a cross-basin seismic transect

Ansa Lindeque^{a,*}, Yasmina M. Martos^b, Karsten Gohl^c, Andrés Maldonado^b

^a Alfred Wegener Institute for Polar and Marine Research, Am Alten Hafen 26, 27568 Bremerhaven, Germany. Now at TGS, Millbank House, 171–185 Ewell Road, Surbiton, Surrey, KT6 6AP, UK

^b Instituto Andaluz de Ciencias de la Tierra, CSIC/Universidad Granada, 18100 Armilla, Granada, Spain

^c Alfred Wegener Institute for Polar and Marine Research, Am Alten Hafen 26, 27568 Bremerhaven, Germany

ARTICLE INFO

Article history:

Received 3 March 2012

Received in revised form 22 October 2012

Accepted 4 November 2012

Available online 27 November 2012

Communicated by D.J.W. Piper

Keywords:

Antarctica
Weddell Gyre
Ice sheet expansion
Seismic reflection data
Seismic stratigraphy

ABSTRACT

Identification of the pre-glacial, transitional and full glacial components in the deep-sea sedimentary record is necessary to understand the ice sheet development of Antarctica and to build circum-Antarctic sediment thickness grids for palaeotopography/bathymetry reconstructions, which constrain palaeoclimate models. A ~3300 km long Weddell Sea to Scotia Sea multichannel seismic reflection data transect was constructed to define the first basin-wide seismostratigraphy and to identify the pre-glacial to glacial components. Seven main seismic units were mapped: Of these, WS-S1, WS-S2 and WS-S3 comprise the inferred Cretaceous–Palaeocene pre-glacial regime (>27 Ma in our age model), WS-S4 the Eocene–Oligocene transitional regime (27–11 Ma) and WS-S5, WS-S6, WS-S7 the Miocene–Pleistocene full glacial climate regime (11–1 Ma). Sparse borehole data from ODP Leg 113 and SHALDRIL constrain the ages of the upper three seismic units and seafloor spreading magnetic anomalies compiled from literature constrain the basement ages in the presented age model. The new horizons and stratigraphy often contradict local studies and show an increase in age from southeast to the northwest. The up to 1130 m thick pre-glacial seismic units form a mound in the central Weddell Sea basin and in conjunction with the eroded flank geometry, allow the interpretation of a Cretaceous proto-Weddell Gyre bottom current. The base reflector of the transitional seismic unit has a model age of 26.6–15.5 Ma from southeast to northwest, suggesting similar southeast to northwest initial ice sheet propagation to the outer shelf. We interpret an Eocene East Antarctic Ice Sheet expansion, Oligocene grounding of the West Antarctic Ice Sheet and Early Miocene grounding of the Antarctic Peninsula Ice Sheet. The transitional regime sedimentation rates in the central and northwestern Weddell Sea (6–10 cm/ky) are higher than in the pre-glacial (1–3 cm/ky) and full glacial regimes (4–8 cm/ky). The pre-glacial to glacial rates are highest in the Jane- and Powell Basins (10–12 cm/ky). Total sediment volume in the Weddell Sea deep-sea basin is estimated at $3.3\text{--}3.9 \times 10^6 \text{ km}^3$.

© 2012 Elsevier B.V. All rights reserved.

1. Introduction

Deep-sea sediment thicknesses, distribution patterns and deposition characteristics reveal the erosional, transport and deposition processes that were active during Antarctica's transition from a warm, pre-glacial to a cold, glacial climate. The geometry, distribution and thickness of sediment sequences produced by these processes can provide insight into the ice sheet development and palaeocirculation of the Weddell Sea. Additionally, sediment thickness grids are needed for palaeotopography (Lythe et al., 2001; Le Brocq et al., 2010; Wilson et al., 2011) and palaeobathymetry (Brown et al., 2006; Hayes et al., 2009) reconstructions at epochs with similar or higher atmospheric

pCO₂ than today, like the Eocene, Miocene, Pliocene and Pleistocene (Pagani et al., 2005; Tripathi et al., 2009, 2011). These palaeo-surface reconstructions provide boundary conditions for palaeoclimate models (e.g. Pollard and DeConto, 2009), which focus on predicting ice sheet behaviour under continued increase of pCO₂ levels.

Identification of these pre-glacial to glacial components in the deep-sea seismic sedimentary records is largely unresolved for the Weddell Sea basin and cross-regional stratigraphic grids for the West Antarctic margin are still absent. As a result, sediment thickness is largely omitted in palaeobathymetry reconstructions (e.g. Brown et al., 2006), or if considered, contain data from the 1970's (Hayes and La Brecque, 1991; Hayes et al., 2009) and few data points (Laske and Masters, 1997), which distort the grids. Tracing continuous horizons over large (>500 km) distances in seamless seismic data are thus needed to develop a basin-wide stratigraphy, identify the pre-glacial to glacial components in the deep-sea sedimentary record and estimate sediment thickness and volume.

* Corresponding author. Tel.: +447443833836.

E-mail addresses: ansa.lindeque@tgs.com (A. Lindeque), yasmartos@ugr.es (Y.M. Martos), karsten.gohl@awi.de (K. Gohl), amaldona@ugr.es (A. Maldonado).

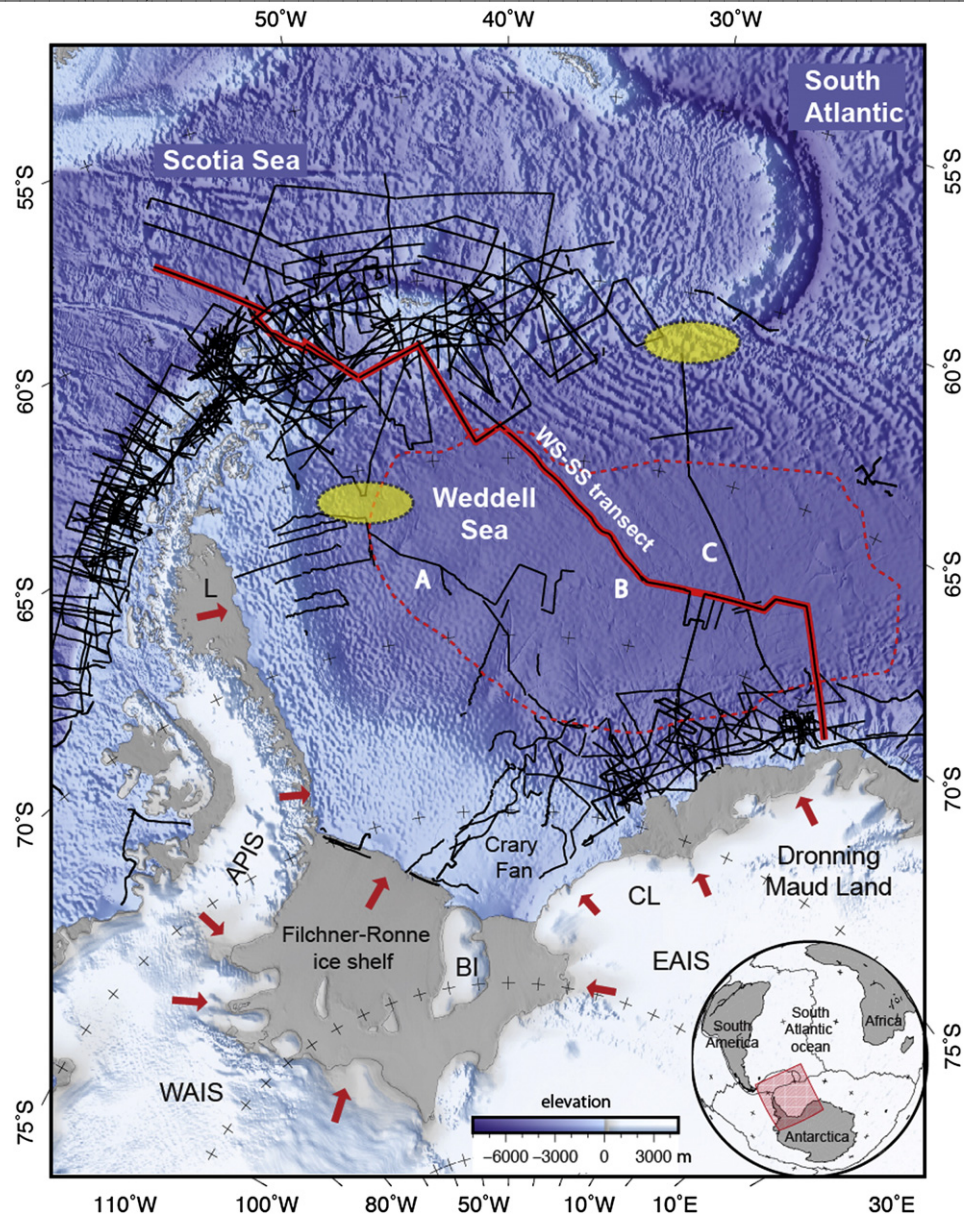


Fig. 1. Overview map of the Weddell Sea basin (WSB, red dotted outline) study area with all seismic profiles from the Seismic Data Library (black lines) and the WS-SS seismic transect (thick red line, marked B). Yellow ovals demarcate seismic data gaps in two alternative cross-basin transects A and C. Background image: global seafloor topography grid, version 13.1, Smith and Sandwell (1997) and for land the ETOPO1 Global Relief Model (Amante and Eakins, 2009). Red arrows indicate general ice flow drainage directions of the Antarctic Peninsula Ice Sheet (APIS), West Antarctic Ice Sheet (WAIS) and East Antarctic Ice Sheet (EAIS) after (Rignot et al., 2008; Pritchard et al., 2009; Bentley et al., 2010; Jamieson et al., 2010). L—Larsen ice shelf, BI—Berkner Island, CL—Coats Land. Globe insert: plate boundaries and study area (red square).

Notes to Table 1

Abbreviations: Epoch: Pleist. = Pleistocene, Paleo. = Paleocene, L = late, M = middle, E = early; *Chronos: Gradstein et al., 2004 appended with m (middle), y (young), see Table 3 for chrons along the WS-SS transect; APIS = Antarctic Peninsula Ice Sheet, WAIS = West Antarctic Ice Sheet, EAIS = East Antarctic Ice Sheet, WSBW = Weddell Sea Bottom Water. Sediment unit prefixes: S = Scotia Sea, Pr = Protector Basin, Sh = near Shackleton Ridge, Pw = Powell Basin, SOM = South Orkney Microcontinent, J = Jane Basin, SH = SHALDRIL II James Ross Basin, WD = northwestern Weddell Sea, W = southeastern Weddell Sea; pCO₂ ppm = partial pressure atmospheric CO₂ in parts per million.

References: ¹Anderson, 2006; ²Smith & Anderson, 2010; ³Busetti et al., 2000; ⁴Maldonado et al., 2000; ⁵Larter & Barker, 1989; ⁶Larter & Cunningham, 1993; ⁷Barker et al., 1988; ⁸Rogenhagen et al., 2004; ⁹Miller et al., 1990; ¹⁰BAS, 1985; ¹¹Maldonado et al., 2000; ¹²Livermore et al., 2000; ¹³Haq & Schutter, 2008; ¹⁴Bart et al., 2005; ¹⁵Tripati et al., 2009, 2011; ¹⁶Pagani et al., 2005; ¹⁷Bart et al., 2005; ¹⁸Zachos et al., 2001; ¹⁹Maldonado et al., 2007; ²⁰Eagles et al., 2005; ²¹Bohoyo et al., 2002; ²²Bohoyo, 2004; ²³Eagles & Livermore, 2002; ²⁴Anderson, 1999; ²⁵König and Jokat, 2006; ²⁶Zachos & Kump, 2005; ²⁷Lear et al., 2008; ²⁸Dingle & Lavelle, 1998; ²⁹Barker et al., 1991; ³⁰Oszko, 1997; ³¹Kennett et al., 1975; ³²Lawver & Gahagan, 1998, 2003; ³³Pollard & DeConto, 2009; ³⁴Barker, 2001; ³⁵Maldonado et al., 2003; ³⁶DeConto & Pollard, 2003; ³⁷Coxall et al., 2005; ³⁸Barker & Thomas, 2004; ³⁹Livermore et al., 2005; ⁴⁰Eagles et al., 2006; ⁴¹LaBrecque et al., 1986; ⁴²Bohoyo et al., 2007; ⁴³Scher & Martin, 2006; ⁴⁴Berner & Kothavala, 2001; ⁴⁵Livermore & Hunter, 1996; ⁴⁶Rogenhagen & Jokat, 2000; ⁴⁷Ghidella et al., 2002; ⁴⁸Jokat et al., 2003; ⁴⁹Jokat et al., 1996; ⁵⁰Hinz & Kristoffersen, 1987; ⁵¹Kristoffersen & Haugland, 1986; ⁵²LaBrecque & Ghidella, 1997; ⁵³Ferris et al., 2000; ⁵⁴Rogenhagen & Jokat, 2002; ⁵⁵Hunter et al., 1996; ⁵⁶Hinz & Krause, 1982; ⁵⁷Hinz, 1981; ⁵⁸Ghidella & La Brecque, 1997; ⁵⁹Livermore et al., 2007; ⁶⁰Surinäch et al., 1997; ⁶¹Galindo-Zaldívar et al., 2006.

Table 1

Deposition of seismic stratigraphic units in the Weddell and Scotia Seas during changes in tectonics, glaciation, climate and ocean circulation.

Epoch	Age (Ma)	Chron*	Seismic stratigraphic units, prefix indicates basin	Changes in tectonics, glaciation, sea level, climate and ocean circulation from literature		
Pleist.	0.0	C1y	SH1 (2.4–1.6 Ma) ^{1,2} SOM-A (ODP695,6,7) ³	Multiple grounding and retreat cycles of the APIS, WAIS and EAIS ^{1,2,4,5,6} Spreading in eastern Scotia Sea ends (C2o, 1.96 Ma) ¹⁰		
Pliocene	L	2.6	C2Ay	S1,Pr1,Sh1,Pw1,J1,WD1 ⁴ reflector a(3.8–3.5 Ma) ⁴	Intensified deep-water production, sheeted facies and contourite deposits ^{2,4,11} Spreading in central Scotia Sea ends (C2A, 3.3 Ma) ^{10,12}	
	E	3.6	C2Ary	S1–S3 progradation ^{5,6} SH2 (5.5–2.4 Ma) ^{1,2}	Major sea level decrease (Za2) ^{4,13} Grounding cycles of APIS on the continental shelf more frequent ^{2,5,7,14}	
Miocene	L	5.3	C3ry	SOM-B (ODP695,6,7, Hz2) ^{3,7} S4–S6 (6 Ma) ⁵	pCO ₂ fluctuates (200–400ppm, 12–0.01 Ma) ^{15,16} Peninsula Pacific margin ridge-trench collisions ^{5,6} sea level increase (6.3 Ma, Tor3/Me1) ¹³ Spreading in eastern Scotia sea starts (C4n.1o, 7.6 Ma) ¹⁰ Uplift at South Scotia Fracture Zone and Antarctic Peninsula ~8 Ma ago ⁵⁹	
	M	11.6	C5r.3ry	S2,Pr2,Sh2,Pw2,J2,WD2 ⁴ SH3 (8.2–5.5 Ma) ^{1,2} reflector c (6.8–6.4 Ma) ^{4,7}	High WSBW activity, expanding WAIS4,11 APIS grounding cycles (7.94–5.12 Ma) ¹⁷ Northward expansion of APIS (S4, S3), relatively thin sheet or small ice caps ^{1,2} Grounding cycles of EAIS and WAIS on the continental shelf ^{2,4,18} Spreading in western Scotia Sea ends (C5n.2m, 10.5 Ma) ¹⁹ Spreading in central Scotia Sea ends (C5n.2o, 10.95 Ma) ²⁰ Initial incursions of Weddell Sea Bottom Water (WSBW) into Scotia Sea ⁴ Permanent WAIS, bringing terrigenous sediments to margin ^{1,2}	eastern SS
				W5 (12 Ma, ODP692,3) ^{8,9} S3,Pr3,Sh3,Pw3,J3,WD3 ⁴ reflector b (12.6–12.1 Ma) ^{7,4} SH4 (13.8–8.2 Ma) ^{1,2} Pr4,J4 (14.1–12.1 Ma) ⁴ S4 (17.6–12.6 Ma) ⁴	Mid–Miocene glaciation (Mi4), a lowering of sea level (Ser3) and permanent EAIS ^{4,13,18} Mid–Miocene climate optimum (16–15 Ma) and global temperature decrease ~8°C ^{13,18} Spreading in Jane Basin ends (C5ADm, 14.4 Ma) ^{21,22} Early expansions of APIS onto the continental shelf in the south ² Bottom water circulation between Scotia Sea and Weddell Sea, WD4 drifts ⁴	uplift
	E	16.0	C5Cn.1ny	Pr5,J5 (17.6–12.6 Ma) ⁴ Pw4,WD4 (18.5–12.6 Ma) ⁴ Sh4 (19.8–12.6 Ma) ⁴ S5 (20.7–17.6 Ma) ⁴	Spreading in Scan Basin ends (C5Cn.3m, 16.6 Ma) ²¹ Spreading in Jane Basin and Scan basin starts (C5Dm, 17.6 Ma) ^{21,22} pCO ₂ fluctuates (300 to 400ppm, 20–12 Ma) ¹⁵ Spreading in Weddell Sea (C6m, 19.2 Ma) ²¹ and Powell Basin ends (C6AAo, 21.1 Ma) ²³	western & central Scotia Sea (SS) opening
Oligocene	L	23.0	C6Cn.2ry	WD5 (20.5–18.5 Ma) ⁴ Sh5 (28.0–19.0 Ma) ⁴ SOM-C (ODP695,6,7, Hz1) ^{3,7}	EAIS fully developed to shelf edge ^{2,24–28} Mi-1 Glaciation, warming 5–6°C ¹⁸ pCO ₂ increase (~400–930ppm, 28–25 Ma) rapid decrease (~930–400ppm, 25–23 Ma) ¹⁶ Central Scotia Sea spreading starts (C8n.2o, 26.1 Ma) ²⁰	
	E	28.4	C10n.1ry	 Pw5 (32.0–18.0 Ma) ⁴	pCO ₂ decrease (1800–400ppm, 33–28 Ma) ¹⁶ sealevel decrease by ~100m ¹³ Earliest observed glacial event on the Antarctic Peninsula (29.8 Ma) ²⁸ Opening of the Powell Basin starts (C11n.1o, 29.7 Ma) ^{22,25,60} Opening of the Protector Basin (33.7–30.2 Ma) ^{20,21,23} or (17.4–13.8 Ma) ⁶¹ Seafloor spreading in western Scotia Sea starts (C12m, 30.9 Ma) ^{19,20,29} EAIS & WAIS formation (33–31 Ma) ^{9,30,31,32} Onset of the Antarctic Circumpolar Current (ACC) ^{4,29,32,33} Abrupt Eocene–Oligocene (ca. 33 Ma) cooling ^{18,33,34} clockwise gyre in Scotia Sea ³⁵	ACC onset EAIS & WAIS expands
				W4 (35 Ma, ODP692,3) ^{8,9} SH5 (37–32 Ma) ^{1,2}	pCO ₂ decline (1750–700ppm, 38–33 Ma), temp ~4°C lower, orbital cycle changes ^{33,36–39} Spreading in Dove Basin ends (C15y, 34.7 Ma) ⁴⁰ pCO ₂ increase (750–1800 ppm, 35–33 Ma) ¹⁶ Initial continental/alpine glaciation on the Peninsula (49–32 Ma) ² Oi-1 glaciation ¹⁸ small ephemeral ice sheets in west Antarctica, EAIS expansion ^{7,34,41} Drake Passage fully open, SAM - Antarctic Peninsula separation complete ^{29,39,42} Penetration of Pacific water through Drake Passage ⁴³ Opening of Dove Basin starts (C18n.2o, 39.4 Ma) ⁴⁰ pCO ₂ increase (800 to 1800 ppm, 55–42 Ma) ⁴⁴ Complete change in deep ocean circulation, Antarctic Bottom Water forms (AABW) ⁴ Ridge-trench collisions on pacific margin of Peninsula starts (50 Ma) ⁵	Drake Passage opening paleo Scotia gyre epimeral ice
Eocene	L	33.8	C13ry			
	M	37.2	C17n.1ry			
Eocene	E	48.6	C22ny			
Paleo.	L	55.8	C24rm		Drake Passage and Weddell Sea continues to open ^{32,39,40}	
	E	61.7	C27ny		Shallow gateways, watermass exchange between Weddell and Scotia Seas ^{32,39,40}	
Cretaceous	L	65.5	C29rm		Falkland Plateau clearing the tip of Africa, opening of Drake Passage starts ²⁵ Herringbone pattern anomalies form ^{45,46,47} Spreading in Weddell Sea changes to WNW–ESE ^{45,46,47}	Weddell Sea opening
	E	84.0	C34ny		pCO ₂ decrease (>1800 to 800 ppm, 145–56 Ma) ⁴⁴	
		99.6	C34nm	W3 (114 Ma, ODP692,3) ⁸ W2 (118 Ma, ODP692,3) ⁸	Opening of South Atlantic Ocean complete, (AFR–ANT separated) ⁴⁸ Andenes Plateau ⁴⁹ Weddell Sea rift ⁵⁰ Polarstern Bank ⁹ Orion magnetic anomaly ^{41,51,52,53} Spreading in Weddell Sea now NNE–SSW and Anomaly-T forms ^{52,54}	
		124.6	M0ry	W1.5 (136 Ma, ODP692,3) ⁸ W3 (138–125 Ma) ⁹	Indian and South Atlantic oceans broaden, but gateways still closed ²⁵ Shear margin becomes transpressional ⁴⁵ First oceanic crust in Weddell Sea (M17, 142 Ma) ²⁵	
Jurassic	L	145.9	M19ry	W1 (160–145 Ma) ^{8,9}	Explora Escarpment, Explora wedge and Explora Anomaly form ^{25,50,55,56,57} N–S extension and stretching in front Dronning Maud Land, no seafloor yet ^{25,48,58}	
		154.9	M25Ary		South America (SAM) - southern Africa (AFR) separates from Antarctica (ANT) ^{25,48,49}	

Previous seismic reflection studies presented seismostratigraphy models for the southern Scotia Sea (e.g. Maldonado et al., 1998, 2003, 2005; Fig. 1), the Antarctic Peninsula (e.g. Larter and Barker, 1989; Rebesco and Camerlenghi, 2008; Smith and Anderson, 2010), the Jane and Powell Basins in the northwestern Weddell Sea (e.g. Coren et al., 1997; Bohoyo et al., 2002; Bohoyo, 2004; Fig. 1), and the southeastern Weddell Sea basin (Hinz and Kristoffersen, 1987; Miller et al., 1990; Rogenhagen and Jokat, 2000; Rogenhagen et al., 2004; Fig. 1). These identified three pre-glacial seismic stratigraphic units in the Weddell Sea and one in the Scotia Sea (Pw5, SH5, Sh5, SOM-C, fourth column in Table 1 and references in footnote) span the Jurassic to the end of the Oligocene. Three glacial regime units in the Weddell Sea and four in the Scotia Sea, Jane and Powell Basins were also identified. In contrast to the pre-glacial units, the glacial units were deposited over a comparatively short period of time (~21 Ma) during the Miocene to late Pleistocene. These studies are however local scaled, stratigraphically disconnected and use different nomenclatures, making it difficult to construct regional and cross-regional sediment thickness grids.

Rooted in a ~3300 km long transect, hereafter referred to as the Weddell Sea–Scotia Sea (WS–SS) seismic transect, this study aims to: (i) define a basin-wide seismic stratigraphic model for the Weddell Sea that is correlated to the southern Scotia Sea stratigraphy and tested against local studies and sparse boreholes; (ii) identify the pre-glacial (PG), transitional (T) and full glacial (FG) components in the deep-sea sediment record; (iii) quantify the sediment thicknesses, lateral age variation and tentative sedimentation rates of these components; (iv) consider the implications the findings might have for understanding the pre-glacial to glacial development of Antarctica amidst changes in climate, tectonics, and ocean circulation.

We define the pre-glacial regime as warm, predominantly ice sheet free conditions and open-ocean. The transitional regime describes a colder alpine-type climate and periods of ephemeral continental scale ice sheets that initially grounded on the outer shelf after multiple cycles of advance and retreat. The full glacial regime denotes a cold polar climate and the expansion of the ice sheets to the coast that permanently grounded on the outer shelf. Smaller advance and retreat cycles occurred, but the ice sheets remain grounded.

The WS–SS seismic transect focuses on the deep-sea sedimentary record because there the reflections are less disturbed or influenced by changes in sea level and glacial processes, making it easier to trace horizons over long distances. The thickness and geometry of the seismic sequences can give an indication of high sediment influx to the deep-sea, triggered for example by expanding ice sheets pushing sediments off the outer shelf, onto the slope and rise. The proposed age model provides a working hypothesis for further unravelling of the past ice-sheet dynamics and ocean circulation in the Weddell Sea that can be tested by future deep-sea drilling.

2. Tectonic, palaeoceanographic and palaeoclimate setting

The Weddell Sea basin experienced approximately 150 Ma of tectonic, palaeoceanographic and palaeoclimate history that spans the Mesozoic Gondwana break-up to the present (Table 1). Tectonic sea-floor spreading in the Weddell Sea started at ~147 Ma and continued into the Eocene. Sedimentation initially started in the Weddell Sea from ~138 Ma onwards (Miller et al., 1990; Rogenhagen et al., 2004), as Africa and Antarctica separated (e.g. Rogenhagen and Jokat, 2002; König and Jokat, 2006; Table 1). During the Early Eocene, Antarctica had a warm climate with high pCO₂ concentrations (>1800 ppm) and sea level was about 150 m higher than today (e.g. Zachos et al., 2001; Miller et al., 2008). Sediment deposits formed in the Antarctic Peninsula indicate shallow water gateways (seismic lithology unit SH5 at ~37 Ma onwards in Table 1; Anderson, 2006; Smith and Anderson, 2010; Anderson et al., 2011). This was followed by Oligocene sedimentation in the Powell Basin and western Scotia Sea (e.g. seismic stratigraphic units Pw5, Sh5, Maldonado et al., 2006) during the completion of the

Weddell Sea opening (e.g. Bohoyo et al., 2002; König and Jokat, 2006; Table 1; Fig. 1).

The Eocene–Oligocene transition at ~33 Ma signifies a period of several major changes: Antarctica's climate changed from warm and relatively ice-sheet free to cold and ice-covered, as temperatures decreased by about 4 °C; pCO₂ declined rapidly from 1750 to 700 ppm and orbital cycles changed (Barker, 2001; Zachos et al., 2001; DeConto and Pollard, 2003; Barker and Thomas, 2004; Coxall et al., 2005; Livermore et al., 2005; Pollard and DeConto, 2009); the Antarctic Circumpolar Current (ACC) developed (Lawver and Gahagan, 1998, 2003; Miller et al., 2008) as the Weddell Sea and Drake Passage opened and western Scotia Sea started to open (Bohoyo et al., 2002; Ghidella et al., 2002; König and Jokat, 2006; Maldonado et al., 2006); ephemeral ice sheets formed the initial East Antarctic Ice Sheet (EAIS) and West Antarctic Ice Sheet (WAIS) on higher elevations (LaBrecque et al., 1986; Barker et al., 1988; Miller et al., 1990; Oszko, 1997; Barker, 2001) as well as small ice-caps on the northern Antarctic Peninsula (Dingle and Lavelle, 1998; Smith and Anderson, 2010; Anderson et al., 2011).

In the Miocene (23.0–5.3 Ma), the EAIS, WAIS and Antarctic Peninsula Ice Sheet (APIS) growth accelerated and these ice sheets expanded to the outer shelf (dark grey bar on the right in Table 1, after e.g. Barker et al., 1988; Larter and Barker, 1989; Dingle and Lavelle, 1998; Barker, 2001; Zachos et al., 2001; Maldonado et al., 2006; Miller et al., 2008; Smith and Anderson, 2010; Davies et al., 2012). Atmospheric pCO₂ levels decreased further and more rapidly from ~930 to 400 ppm during 25–23 Ma (Zachos et al., 2001; Pagani et al., 2005; Zachos and Kump, 2005; Tripati et al., 2009, 2011). Sea level decreased by ~100 m (e.g. Haq and Schutter, 2008) and ocean bottom water circulation intensified between the Weddell and Scotia Seas as the ACC system developed fully (e.g. Maldonado et al., 2006).

From the Pliocene–Pleistocene, after ~5.3 Ma, smaller glacial and interglacial, climate and sea-level cycles occurred in the Quaternary but the EAIS, WAIS and APIS repeatedly extended to the outer shelf in a tectonic and ocean circulation setting similar than today (Table 1).

3. Datasets and methods

The WS–SS seismic transect is a first approach to identify the pre-glacial (PG), transitional (T) and full glacial (FG) components of the deep-sea sediment record in the Weddell Sea and southern Scotia Sea (Fig. 1). All three Antarctic ice sheets, the WAIS, EAIS and APIS, drain into the Weddell Sea (red arrows, Fig. 1) making this basin a unique area to study deep-sea sediment transport and depositional processes related to ice sheet growth and demise. Magnetic seafloor spreading anomalies, seismic reflection data and ODP boreholes (Fig. 2) were used to construct an age model and estimate sedimentation rates in the following manner:

3.1. Magnetic anomaly isochron compilation

To constrain basement ages, obtain a spreading age range for each basin that the WS–SS seismic transect crosses and to deduct the ages of the oldest sediments that lie on the basement, we compiled a cross-basin and cross regional seafloor spreading magnetic anomaly isochron map (Fig. 2; Table 2; online Supplement 1) for the Weddell Sea and Scotia Sea from published literature (BAS, 1985; LaBrecque and Ghidella, 1997; Nankivell, 1997; Surináč et al., 1997; Lodolo et al., 1998, 2010; Bohoyo et al., 2002, 2007; Eagles and Livermore, 2002; Ghidella et al., 2002; Kovacs et al., 2002; Eagles et al., 2005, 2006; Galindo-Zaldívar et al., 2006; König and Jokat, 2006; Maldonado et al., 2007; Eagles, 2010). This map compilation has not been published before and is available in the PANGAEA database (Lindeque et al., 2012).

Where available, magnetic anomaly picks were sourced from authors and imported into GIS ArcMap 10 (e.g. König and Jokat,

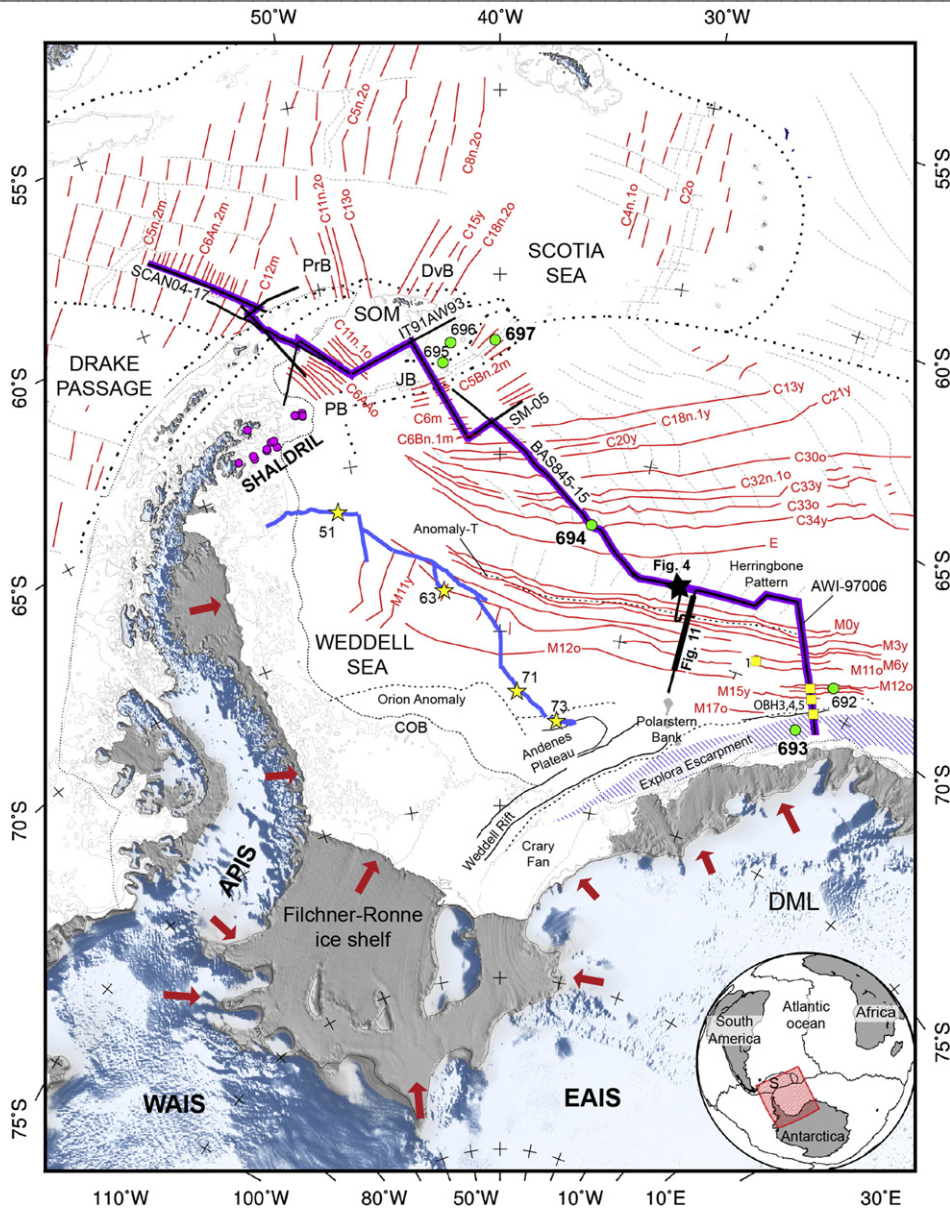


Fig. 2. Magnetic anomaly map compilation for the Weddell Sea and Scotia Sea region and the WS-SS seismic transect (purple line), simplified tectonic features, boreholes and velocity stations, in a polar stereographic projection. Red arrows and background image for land are the same as for Fig. 1. Datasets: red lines = Isochrons of magnetic spreading anomalies compiled from literature, labelled with our standardized chron nomenclature (Table 2); green circles = ODP leg 113 boreholes, bold numbers = boreholes in Fig. 3 used for the stratigraphic correlation; purple circles = SHALDRIL boreholes; stars and blue line = seismic recording stations and seismic reflection profiles from Rogenhagen and Jokat (2000); yellow squares = archive sonobuoy data (Hinz and Krause, 1982) and Ocean Bottom Hydrophone (OBH) stations after Ritzmann (1998). Tectonic features: thick dotted black lines = plate boundaries; grey dashed lines = transform faults and flow lines; double dotted lines = spreading ridges. Geographic features: COB = Continent Ocean Boundary, DML = Dronning Maud Land, DvB = Dove Basin, JB = Jane Basin, PB = Powell Basin, PrB = Protector Basin, SOM = South Orkney Micro continent.

2006). In regions where actual magnetic data picks were unavailable, published anomaly and isochron maps (e.g. Bohoyo et al., 2002; Maldonado et al., 2007) were georeferenced and the isochrons precisely digitized. Conflicting opinions do exist between studies in the same basin e.g. in the Powell Basin between Eagles and Livermore (2002) and Surináčh et al. (1997) due to ambiguous data and allow for alternative age interpretations. In such cases, the most recent publication or best fit with the regional trend was favoured. The digitized isochrons were combined with the isochrons from the data picks and exported as an ESRI shapefile that was geospatially superimposed on the transect (thin red lines in Fig. 2; online Supplement 1). All data picks and maps were used as published.

Chron nomenclature and ages in literature (Chron-L, Age-L in Table 2) often varied between authors who applied different time scales (e.g. Cande and Kent, 1995 versus Gradstein et al., 1994). We thus standardized the nomenclature of the final selected isochrons to the Gradstein et al. (2004) timescale. Chrons were appended with o = old, m = middle, y = young, to indicate which part of the modelled magnetic anomaly was picked in the original literature before assigning the updated chron nomenclature (respectively named Chron and Age in Table 2). The ages of the C-chron series slightly changed between the Gradstein et al. (2004) scale (used in this study) and the Cande and Kent (1995) scale. More significant age changes occurred in the M-series (Table 2) for example: chron M0y

Table 2
Isochrons of magnetic spreading anomalies crossing the Weddell Sea–Scotia Sea (WS–SS) seismic transect, see Fig. 2.

This study		Literature		Profile number	This study		Literature		Profile number
Chron	Age	Chron-L	Age-L		Chron	Age	Chron-L	Age-L	
Scotia Sea					Northeastern Weddell Sea				
C5n.2m	10.5	C5n	9.8	SCAN04–17 ¹	C6m	19.2	C6n	19.5	SM04 ²
C5An.2m	12.3	C5An	12.3	SCAN04–17 ¹	C6An.1m	20.1	C6An.1n	20.0	SM04 ²
C5Bn.2m	15.1	C5Bn.2n	15.1	SCAN04–17 ¹	C6An.2m	20.5	C6An.2n	20.4	SM04 ²
C5Cn.2m	16.4	C5Cn	16.4	SCAN04–17 ¹	C6Bn.1m	22.6	C6Bn	22.0	SM04 ²
C5Dm	17.4	C5Dn	17.3	SCAN04–17 ¹	C6Cn.3m	23.3	C6Cn	24.0	SM04 ²
C5Em	18.3	C5En	18.2	SCAN04–17 ¹	C7n.2m	24.4	C7n	25.0	SM04 ²
C6m	19.2	C6n	19.2	SCAN04–17 ¹	Central Weddell Sea				
C6An.2m	20.5	C6An.2n	20.0	SCAN04–17 ¹	C13y	33.3	C13	33.1	BAS845–15 ⁵
C6Bn.2m	22.1	C6Bn	21.9	SCAN04–17 ¹	C18n.1y	38.0	C18	38.4	BAS845–15 ⁵
C6Cn.2m	23.0	C6Cn	23.0	SCAN04–17 ¹	C20y	41.6	C20	42.5	BAS845–15 ⁵
C7n.2m	24.4	C7n	24.1	SCAN04–17 ¹	C21y	45.3	C21	46.2, 47.9	BAS845–15 ^{5, 6}
C7Am	25.4	C7An	25.0	SCAN04–17 ¹	C30o	67.7	C30	67.6	BAS845–15 ⁶
C8n.2m	25.8	C8n	25.4	SCAN04–17 ¹	C32n.1o	71.2	C32n.1	71.3	BAS845–15 ⁷
C9m	27.3	C9n, C9	27.2, 27.7	SCAN04–17 ^{1, 4}	C33y	73.6	C33	73.6	BAS845–15 ⁷
C10n.1y	28.1	C10	28.0	M05 ⁴	C33o	79.5	C33r	79.0	BAS845–15 ⁷
C10n.2y	28.5	C10n	28.5	SCAN04–17 ¹	C34y	84.0	C34	83.0	BAS845–15 ⁸
C11n.1m	29.6	C11n	29.5	SCAN04–17 ¹	E	93.0	E	93.0	BAS845–15 ⁵
C12m	30.9	C12n	30.9	SCAN04–17 ¹	Southwestern Weddell Sea				
Powell Basin					M0y	124.6	M0	118, 121	97006 ⁹ , 10 ⁹ , 30 ⁹
C6AAo	21.1	C6AA	21.8	IT89AW41 ³	M1o	127.2	M1n	122.0	97006 ⁹ , 10 ⁹ , 30 ⁹
C6Cn.3o	23.4	C6C	24.1	IT91AW90 ³	M3y	127.6	M3	123.0	97006 ⁹ , 10 ⁹ , 28 ⁹ , 30 ⁹
C7n.2o	24.5	C7	24.7	IT91AW92 ³	M5y	129.8	M4	125.4	97006 ⁹ , 10 ⁹ , 29 ⁹
C8n.2o	26.1	C8	26.5	IT91AW93 ³	M6y	131.2	M5	127.0	97006 ⁹
C9o	27.8	C9	27.9	IT91AW93 ³	M10y	133.5	M10	130.2	97006 ⁵ , 10 ⁵
C10n.1o	28.4	C10	28.5	IT91AW93 ³	M11y	135.7	M10Nr	131.5	97006 ⁸ , 10 ⁸
C11n.1o	29.7	C11	29.7	IT91AW93 ³	M12o	137.8	M11, M12	133, 134	97006 ^{8, 9} , 10 ^{8, 9}
Jane Basin					M12r.1y	138.6	M12.1N	135.6	97006 ⁹
C5ADm	14.4	C5ADn	14.4	SM04 ²	M13o	139.3	M13	136.6	97006 ⁹
C5Bn.2m	15.1	C5Bn.2n	15.1	SM04 ²	M15y	140.4	M15n	138.3	97006 ⁹
C5Cn.3m	16.6	C5Cn	16.6	SM04 ²	M17o	142.8	M17	142.3	96110 ⁹
C5Dm	17.4	C5Dn	17.6	SM04 ²					

Timescale: Chron and Age (this study) taken from Gradstein et al., 2004. Ages appended with old (o), middle (m) and young (y); Chron-L and Age-L (literature) from: C5n to C33r, Cande and Kent, 1995; C34 to E, Barker, 2001, 1994; M0 to M17, Kent and Gradstein 1986; Gradstein et al., 1994.

References: ¹Maldonado et al., 2007; ²Bohoyo et al., 2002; ³Eagles and Livermore, 2002; ⁴Lodolo et al., 1998; ⁵Kovacs et al., 2002; ⁶Ghidella et al., 2002; ⁷Nankivell, 1997; ⁸LaBrecque and Ghidella, 1997; ⁹König and Jokat, 2006. All ages are in Ma.

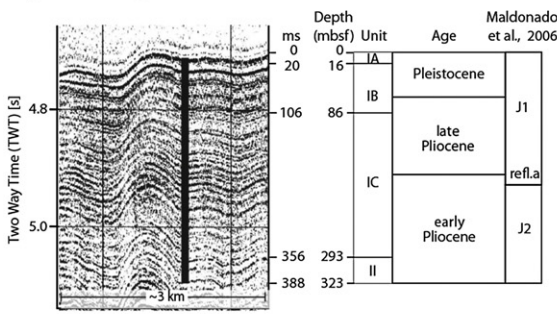
is now 124.6 Ma according to the Gradstein et al. (2004) scale, but was previously 118–121 Ma in the Cande and Kent (1995) scale used in Rogenhagen et al. (2004).

3.2. Borehole stratigraphy

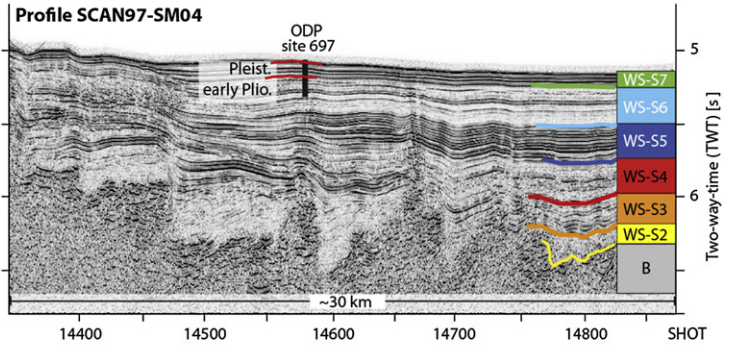
We projected Ocean Drilling Program (ODP) leg 113 borehole sites 693, 694 and 697 (Barker et al., 1988) into the WS–SS seismic transect (Figs. 2 and 3). The projection path was chosen parallel to the contour

or bathymetric feature (e.g. shelf edge, basin or ridge) in order to ensure the most accurate correlation. Site 693 lies ~65 km to the west of the transect, site 694 is line coincident and site 967 lies ~200 km to the east of the transect (Fig. 2). To compensate for these large offsets, the borehole horizons were matched to horizons in coincident seismic lines and traced along a series of crossing seismic tie lines until the horizon could be matched to equivalent reflectors in the WS–SS seismic transect data in order to obtain a stratigraphic age constrain for the upper 300 m (Fig. 3). The following seismic tie lines were

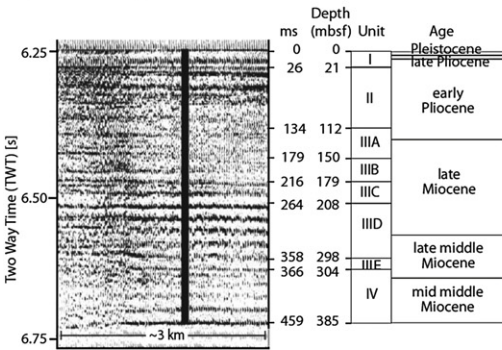
A) ODP leg 113 site 697



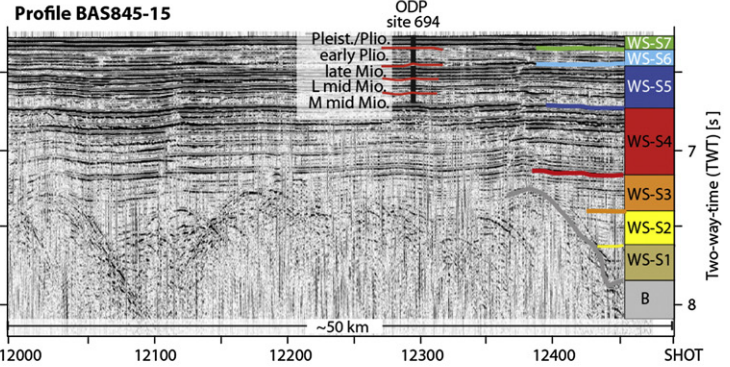
Profile SCAN97-SM04



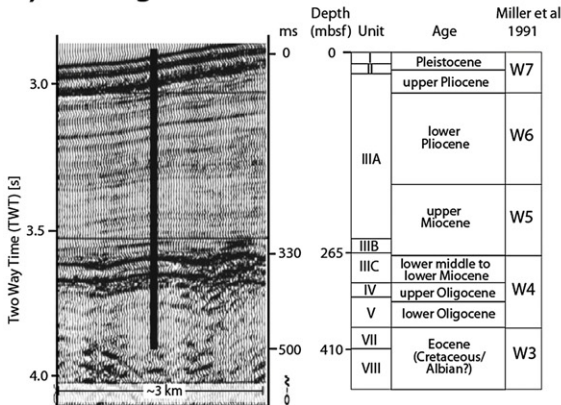
B) ODP leg 113 site 694



Profile BAS845-15



C) ODP leg 113 site 693



Profile AWI-96110

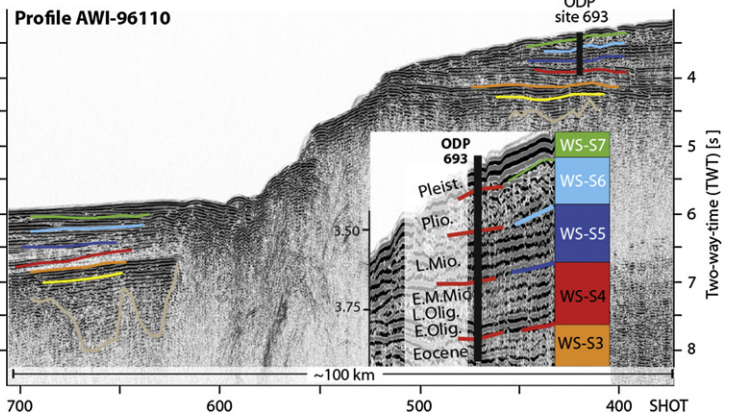


Fig. 3. Integration of nearby relevant borehole data. A, B, C: Left and middle images= stratigraphy of ODP leg 113 drill sites 697, 694 and 693 (Barker et al., 1988; for location see Fig. 2) with time scale and depth of main horizons as well as horizons interpreted in literature. Images on the right: extracts of WS–SS transect seismic data at the projected borehole position with our proposed Weddell Sea stratigraphy annotated. Units interpreted to represent glacial processes, are labelled in white. Plio. = Pliocene, Pleist. = Pleistocene, Mio. = Miocene, Olig. = Oligocene.

used: for site 697, lines IT91AW93, SM04 and SM05; none for site 694 as it lies directly on the transect; and for site 693, lines BGR78018, BGR78019, BGR86006 and BGR87097. Most of the seismic lines used are available in the Seismic Data Library System (SDLS; Wardell et al., 2007). Recent SHALDRIL boreholes on the Antarctic Peninsula (Smith and Anderson, 2011) were also incorporated and connected to the transect via tie lines IT91AW90, M08, BAS84-154 to cruise NBPO602A.

3.3. Seismic characterization

A transect of continuous seismic data through the central Weddell Sea basin and parallel to the margin was required to ensure the most representative deep-sea data for interpretation. Multichannel seismic

(MCS) reflection profiles collected on several expeditions of various organisations in the SDLS databank (Wardell et al., 2007), collectively form three transects across the central Weddell Sea (A, B, C in Fig. 1). Transects A and C provide seismic reflection data from the southeastern to northwestern Weddell Sea, but do not connect to or cross any seismic profiles at the Antarctic Peninsula, and hence were considered unsuitable for the objectives of this work (yellow ovals in Fig. 1 mark data gaps). The middle transect (B) was chosen for tracing the horizons because there are no data gaps between profiles and the transect is most representative of the deep-sea sedimentary archive, because it runs more or less through the middle of the Weddell Sea basin (red dashed outline in Fig. 1). Typical seismic characteristics defined in other studies through drilling and seismic reflection data (e.g. Bellingshausen Sea: Scheuer et al., 2006; Cosmonaut Sea: Leitchenkov et al., 2007, 2008;

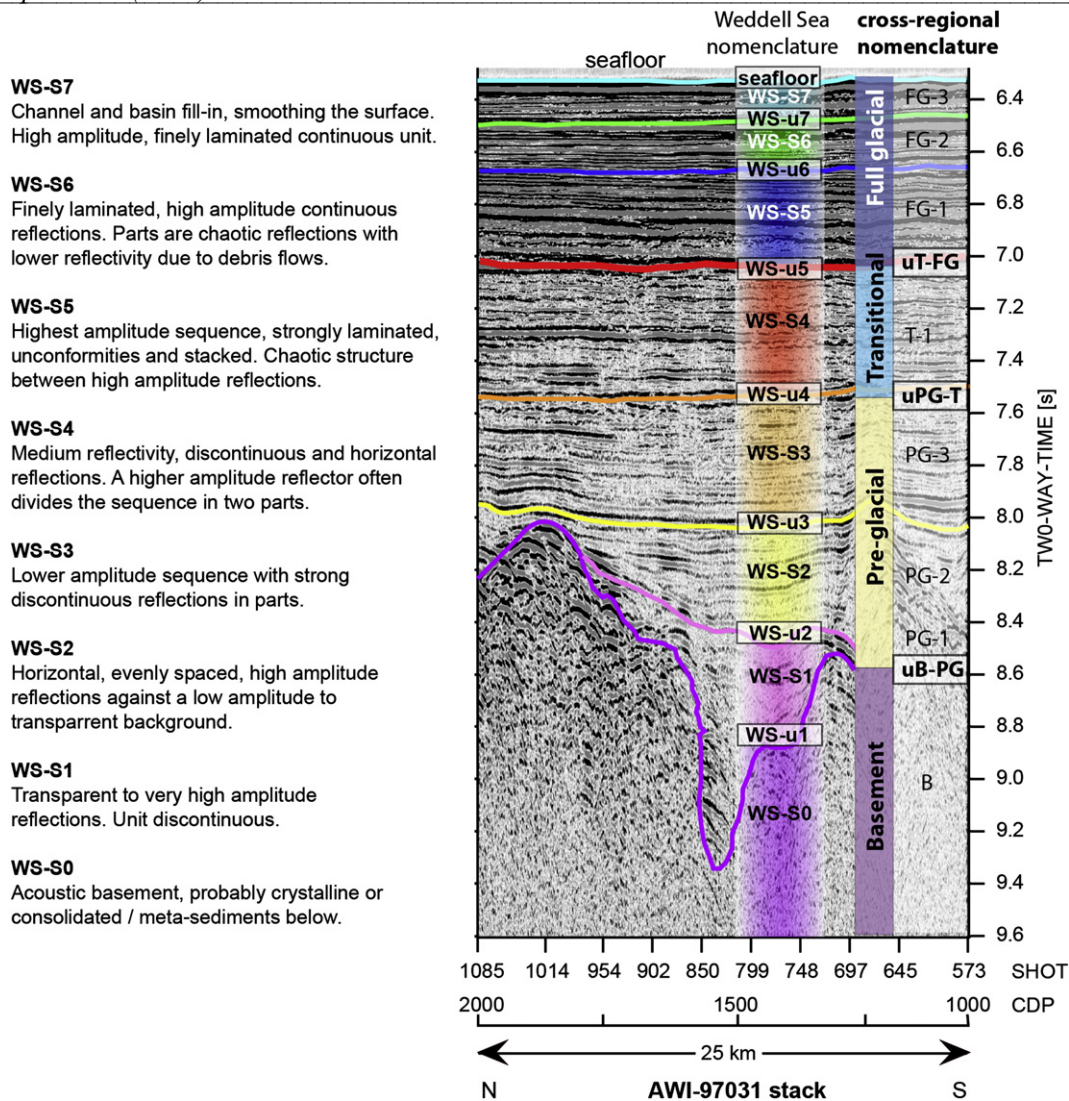


Fig. 4. Reference section, with the proposed Weddell Sea and circum-Antarctic stratigraphy superimposed on a typical seismic reflection image from the WS-SS transect. For location see Fig. 2. Vertical exaggeration is $\sim 6\times$. The seismic characteristics of each unit are listed on the left. Sediment units for the Weddell Sea stratigraphy are numbered WS-S1 to WS-S7 from bottom to top and separated by base reflectors or unconformities (WS-u1 to WS-u7). The simplified circum-Antarctic stratigraphy defines sequences interpreted to represent acoustic basement (B), pre-glacial (PG), transitional (T) and full glacial (FG) processes, separated by the associated base reflector discontinuities or unconformities (uB-PG, uPG-T and uT-FG).

Wilkes Land: DeSantis et al., 2003; Escutia et al., 2011) were used as a guide to identify the pre-glacial to glacial units; briefly summarised as follows:

The pre-glacial seismic facies are usually the first layers above basement. They show diagnostic low amplitude to transparent reflectivity and stronger discontinuous reflectors therein, appearing light grey to almost white in the seismic image. The transitional regime depicts a change in the deposition processes since reflectors are now closer spaced, horizontal and mostly continuous with medium amplitude. These characteristics often result in a medium grey appearance in seismic sections without gain adjustment on display. The continuous, high amplitude reflectors represent the full glacial sequence. Deposits from sporadic down-slope sediment transport generally result in complex internal structures and form turbidite channel-levee systems, or chaotic bodies in the case of debris-flow processes. Persistent bottom-currents that flow along-slope or oblique to the contours develop various types of contourites of which the sheeted and mounded drifts are the most prominent in this case. This sequence typically appears dark grey to black in seismic images and is the first layers below the seafloor.

Using these characteristic seismic facies changes, borehole correlation (Figs. 2 and 3) and other seismic stratigraphy models in the southeastern (Miller et al., 1990) and the northwestern Weddell Sea (Maldonado et al., 2006) as guidelines, we compiled a type section for the WS-SS seismic transect data (Fig. 4). A part of profile AWI-97030 was chosen from several other good example sections because: (1) it lies in the deeper part of the basin, (2) is close enough for correlations to the slope, (3) is a good representation of the changes in seismic facies, and (4) all the seismic units are present. See location of the type section in Fig. 2. We assigned a new bottom-to-top stratigraphy nomenclature for the Weddell Sea and proposed circum-Antarctic units (Fig. 4). The resulting model seismic stratigraphy was used as a template to interpret, or re-interpret the rest of the WS-SS seismic transect data.

Twenty-three MCS profiles were used to construct the ~ 3300 km long WS-SS seismic transect (Fig. 1; Table 3). All navigation data and some of the seismic reflection data (IT91 and BAS845 cruises) are public domain legacy data in the SDLS. Seismic data of profiles AWI-970x were in-house at AWI, and SEG-Y data of the Spanish lines (cruises SCAN-2004, HESANT-92/93, and SCAN-97) were provided for this

Table 3
Seismic reflection profiles used to construct the Weddell Sea–Scotia Sea (WS–SS) seismic transect.

Profile	Cruise	CDP spacing [m]	Source (# airguns × volume [L])	Streamer (channels/ length [m])	Profile length [km]	Processing stage of seismic data used	Area	Institute, References
SCAN04–17	SCAN–2004	25	7 × 16.40	96/2400	390	migrated	Scotia sea	a, 1
M31	HESANT–92/93	6.25	6 × 15.26	96/1200	197	migrated	Scotia sea	a, 2, 3
M05	HESANT–92/93	6.25	6 × 15.26	96/1200	304	migrated	Powell basin	a, 2, 3
IT89AW41	IT90AP	12.5	18 × 2.51	120/2975	206	stack	Powell basin	b, 4
IT91AW90	IT91AP	25	18 × 2.68	120/2975	208	stack	Powell basin	b, 4
IT91AW91	IT91AP	25	18 × 2.68	120/2975	147	stack	Powell basin	b, 4
IT91AW92	IT91AP	25	18 × 2.68	120/2975	56	stack	Jane basin	b, 4
IT91AW93	IT91AP	25	18 × 2.68	120/2975	374	stack	Jane basin	b, 5
SM04	SCAN–97	12.5	5 × 22.4	96/2400	362	migrated	Jane basin	a, 2, 6, 7, 8
SM05	SCAN–97	12.5	5 × 22.4	96/2400	231	migrated	Jane basin	a, 2, 6, 7
BAS845–15	BAS–84	25	4 × 8.5	48/2400	832	stack	central weddell sea	c, 9
AWI–97032	ANT–XIV/3	25	6 × 18	96/2400	27	stack	eastern weddell sea	d, 10, 11, 12
AWI–97031	ANT–XIV/3	25	6 × 18	96/2400	138	stack	eastern weddell sea	d, 10, 11, 12
AWI–97030	ANT–XIV/3	25	7 × 3 / 6 × 3	96/2400	109	stack	eastern weddell sea	d, 10, 11, 12
AWI–97029	ANT–XIV/3	25	7 × 21	96/2400	14	stack	eastern weddell sea	d, 10, 11, 12
AWI–97028	ANT–XIV/3	25	7 × 21	96/2400	16	stack	eastern weddell sea	d, 10, 11, 12
AWI–97027	ANT–XIV/3	25	7 × 21	96/2400	43	stack	eastern weddell sea	d, 10, 11, 12
AWI–97010	ANT–XIV/3	25	6 × 18	96/2400	335	stack	eastern weddell sea	d, 10, 11, 12
AWI–97009	ANT–XIV/3	25	6 × 18	96/2400	194	stack	eastern weddell sea	d, 10, 11, 12
AWI–97008	ANT–XIV/3	25	6 × 18	96/2400	49	stack	eastern weddell sea	d, 10, 11, 12
AWI–97007	ANT–XIV/3	25	6 × 18	96/2400	99	stack	eastern weddell sea	d, 10, 11, 12
AWI–97006	ANT–XIV/3	25	7 × 3 / 6 × 3	96/2400	312	stack	eastern weddell sea	d, 10, 11, 12
AWI–96110	ANT–XIII/3	50	1 × 32.6 & 60	96/2400	224	stack	eastern weddell sea	d, 13
Total km					4867			

Institutes: ^aInstituto Andaluz de Ciencias de la Tierra (IACT) and Consejo Superior de Investigaciones Científicas (CSIC), Spain; ^bIstituto Nazionale di Oceanografia e di Geofisica Sperimentale (OGS), Spain; ^cBritish Antarctic Survey (BAS), United Kingdom; ^dAlfred Wegener Institute for Polar and Marine Research (AWI), Germany. Profile names as in SDLS database (Wardell et al., 2007).

References: in order of appearance along the transect: ¹Maldonado et al., 2007; ²Maldonado et al., 2003; ³Maldonado et al., 1993; ⁴Coren et al., 1997; ⁵Busetti et al., 2000; ⁶Bohoyo, 2004; ⁷Maldonado et al., 2003; ⁸Maldonado et al., 2005; ⁹Larter and Cunningham, 1993; ¹⁰Rogenhagen and Jokat, 2000; ¹¹Rogenhagen and Jokat, 2000; ¹²Rogenhagen et al., 2004; ¹³Ritzmann, 1998.

study from the cooperating Institute (Table 3). The MCS data are unmigrated or migrated stacked time sections and used as received without additional processing or conversion into a depth section. The 23 profiles were joined at the exact line intersections from northwest to southeast, resulting in a basin-wide seamless seismic reflection profile (Figs. 5A and 6A, online Supplements 2 and 3). No time and phase shifts were necessary to match the profiles. The magnetic spreading anomaly isochrons (Fig. 2) and nearby ODP leg 113 boreholes (Fig. 3) were projected into the transect seismic image (red dashed lines and black arrows in Figs. 5A and 6A) to constrain the interpretation and basement age. The interpretation of the upper units was tested against borehole stratigraphic correlations (Fig. 3) and type section (Fig. 4). Thereafter we traced the strongest, undisturbed and most prominent seismic reflections and discontinuities, which define the basal boundaries of the sequences in the reference section, for the full transect length and present a basin-wide stratigraphy (Figs. 5B and 6B, online Supplements 2 and 3).

3.4. Sediment thickness estimates

Sediment thickness–depth sections were constructed from 13 points along the WS–SS seismic profile (Figs. 5–7). These particular

points were chosen so as to represent the major changes in the seismic facies and basin geometry, and are therefore not equidistant. Interval velocities from wide-angle seismic refraction data provide the nearest velocity information (Rogenhagen and Jokat, 2000, yellow stars Fig. 1) and were supplemented by velocity data deduced from sonobuoy (station 1, Hinz and Krause, 1982) and ocean bottom hydrophones (OBH3, 4, 5, Ritzmann, 1998) experiment observations. The velocity model from station 1 divided the sediments into two units and the velocity model at OBH 3, 4 and 5, divided deep-sea sediments into three or four units. This was problematic because an average velocity for each seismic unit was needed. To resolve it, the data from these four stations were combined into one velocity function and applied to points 11, 12 and 13 (Fig. 7C). The sediment layer division of Rogenhagen et al. (2004) often varied from our interpreted WS–SS stratigraphy and an interpolated velocity was calculated for each sedimentary unit in proportion to the thickness. The full velocity model is available as online Supplement 4.

Uncertainties in the sediment thickness of up to 70 m occur since the two-way-time picks can differ by one or two reflections (~30 ms) depending on visual interpretation. The uncertainty in interval velocities from refraction data is qualitatively estimated at ~0.1 km/s. Interval velocity in the same seismic unit change over distance due to increased

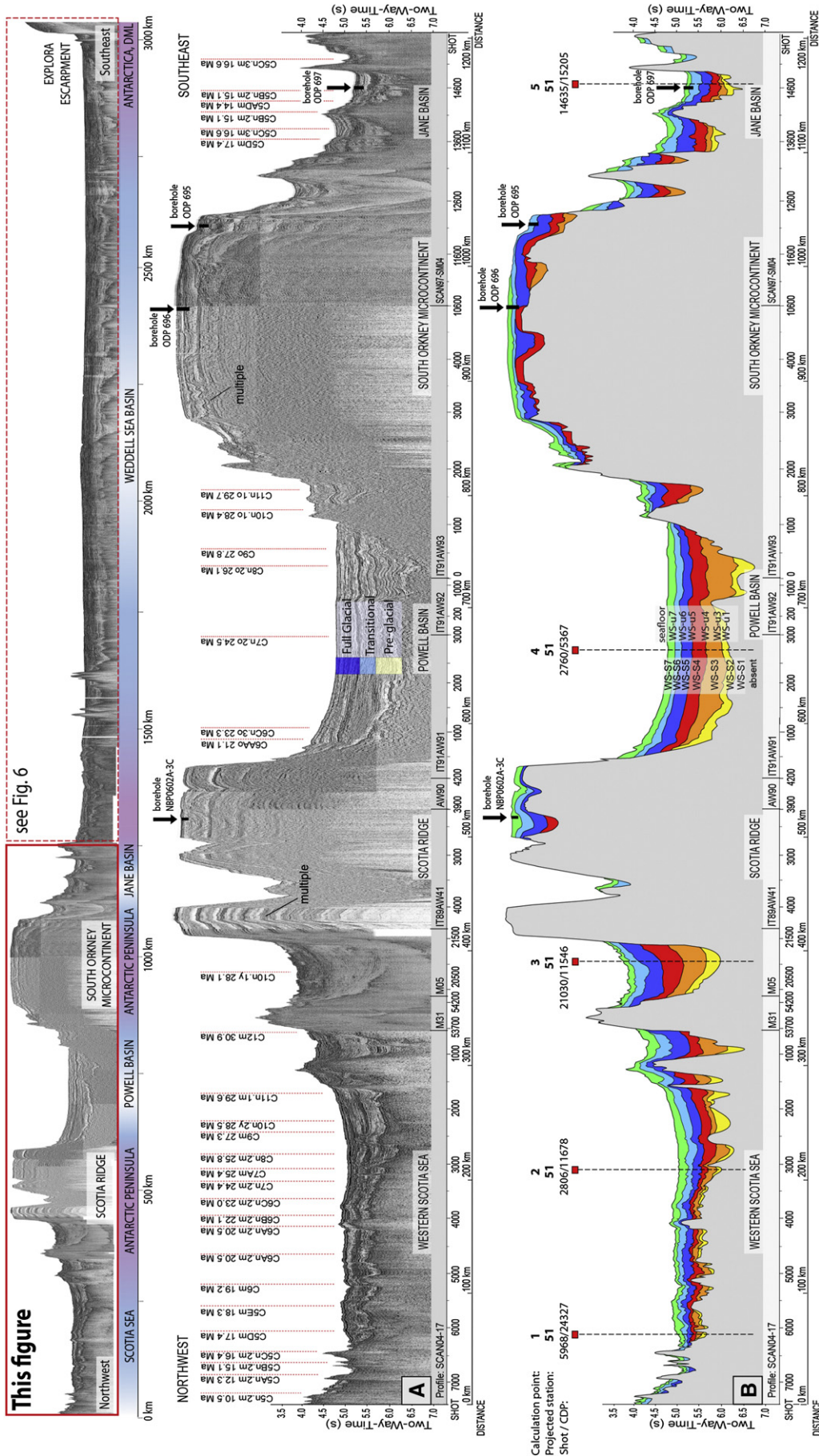


Fig. 5. Multichannel seismic acoustic image and interpretive line drawing of the deep-sea sedimentary archive along the WS-SS transect. Top: Overview of the entire transect with the part illustrated in (A) and (B) below, marked with the solid line red box. (A) Seamless multichannel seismic acoustic image of the Southern Scotia Sea–Jane Basin segment represented in a time section. Profiles and shot numbers are listed in the bar below. Red dashed drop-down lines represent magnetic anomalies crossing the WS-SS transect (see Fig. 2 and Table 2). (B) Interpretive line drawing of the seismic image in (A) and the sequences identified according to the reference section (see Fig. 4). Profiles and shot numbers are listed in the bar below. Red squares and dashed drop-down lines represent points selected for sediment thickness and sedimentation rate calculations.

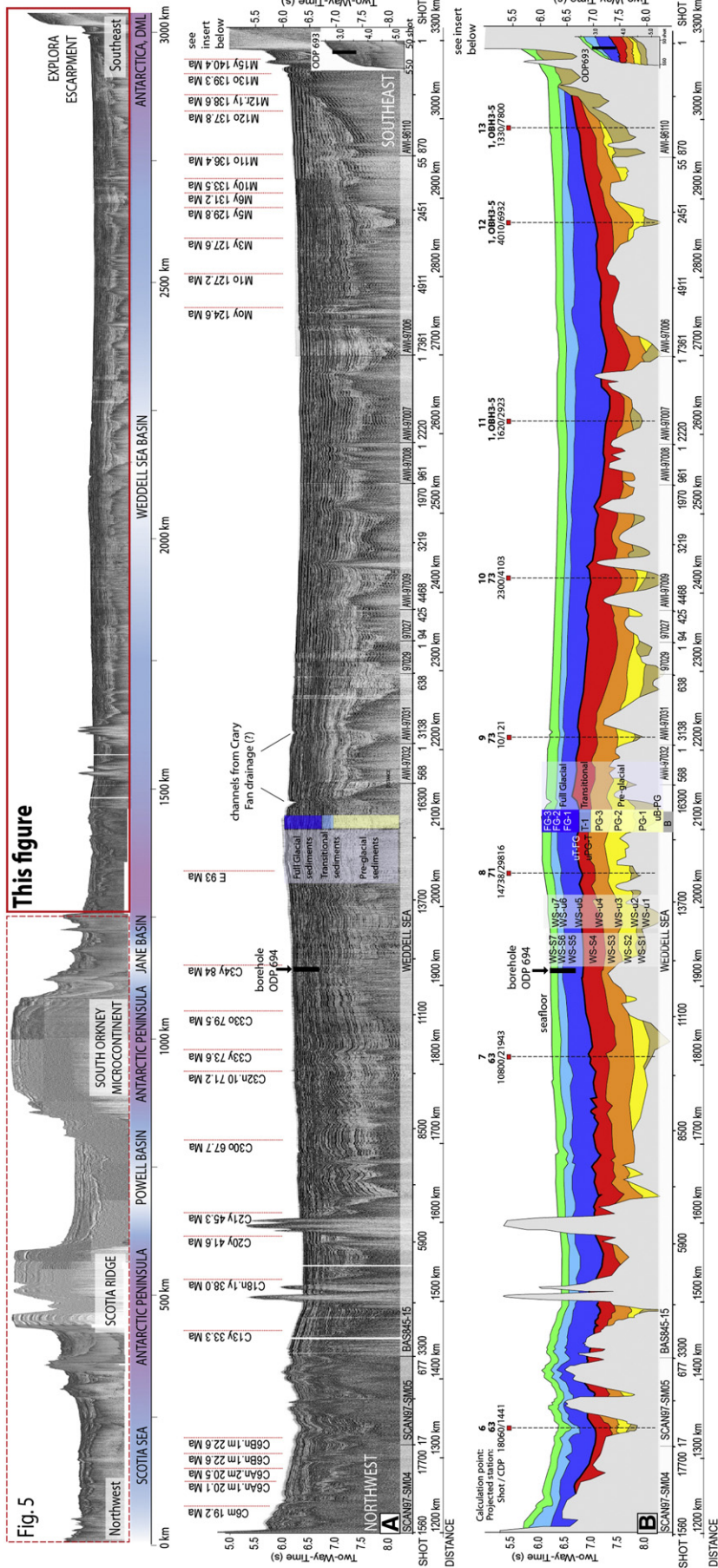


Fig. 5. Multichannel seismic acoustic image and interpretative line drawing of the deep-sea sedimentary archive along the WS–SS seismic transect continued. Top: Overview of the entire transect with the part illustrated in (A) and (B) below, marked with the solid line red box. (A) Seamless multichannel seismic acoustic image of the northwestern, central and southeastern Weddell Sea segments, represented in a time section. Individual profiles and shot numbers used are listed in the bar below. Red dashed drop-down lines represent magnetic anomalies crossing the WS–SS transect (see Fig. 2 and Table 2). (B) Interpretative line drawing of the seismic image in (a) and the sequences identified according to the reference section (see Fig. 4). The profiles and shot numbers are listed in the bar below. Red squares and dashed drop-down lines represent points selected for sediment thickness and sedimentation rate calculations. Black arrows between points 8 and 9 indicate channel-levee geomorphology, possibly related to the Cray Fan drainage channel-system (Michels et al., 2001, 2002) or bottom current activity.

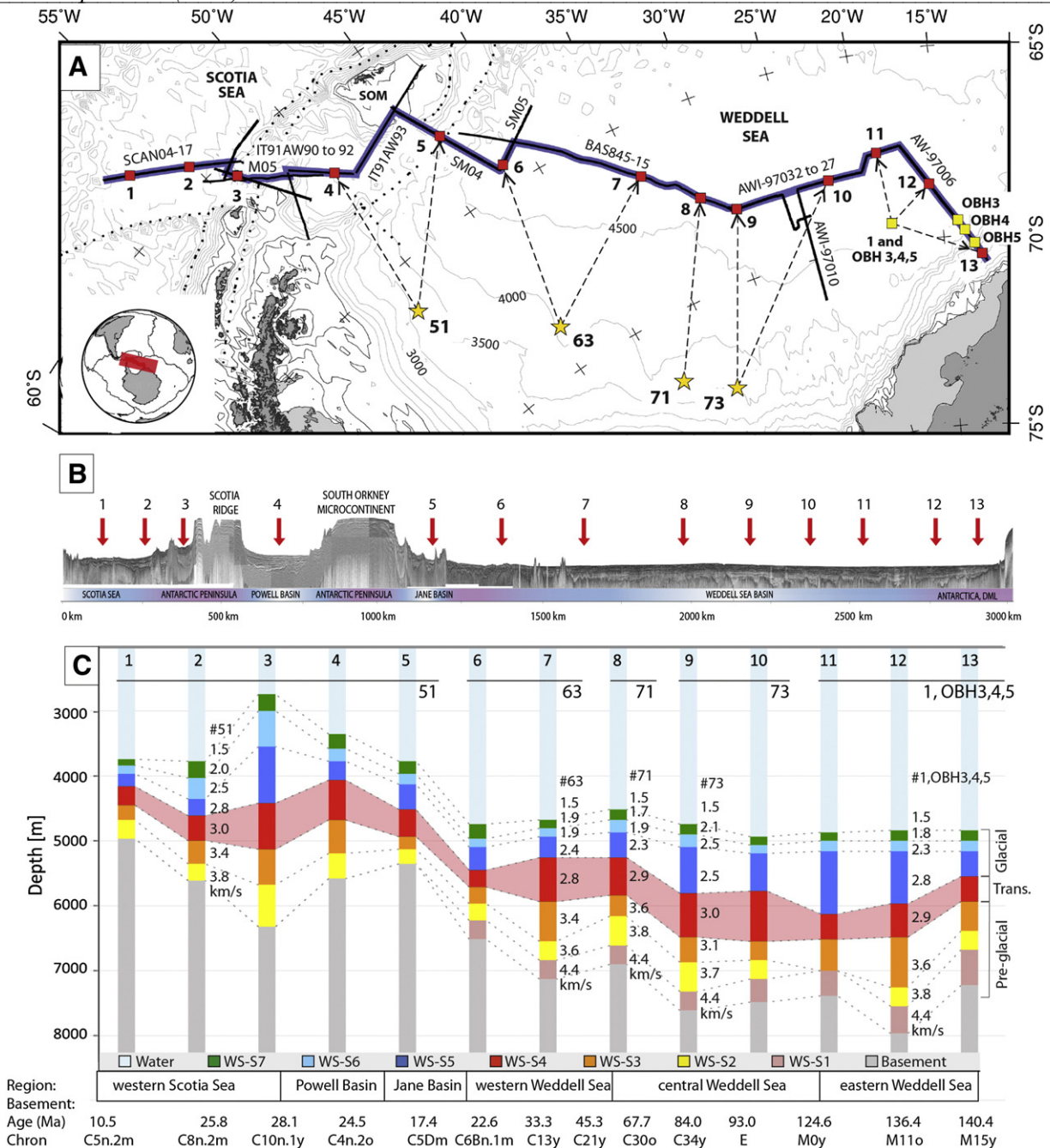


Fig. 7. Sediment thickness calculations for selected points on the WS-SS seismic transect. (A) Overview map showing the projection of each interval velocity station (yellow stars and squares) into the transect and matched to the 13 representative points (marked with red squares and numbered). (B) Overview of the seamless seismic reflection image of the WS-SS transect and the 13 selected points (red drop-down arrows). (C) Diagram of the sediment thickness (m) calculated at each point and the velocity data used, see text. Sediment units are listed below and identical to those identified in Figs. 5 and 6. The regional location of each point and the nearest magnetic chrons (Fig. 2 and Table 2) are annotated below.

compaction from more overburden and therefore using velocity data ~500 km from the transect introduce further uncertainties. Even so, the interval velocity model used was compiled from all available data nearest to the transect and in the Weddell Sea basin.

We minimize these uncertainties by assigning similar velocities to units with the same seismic facies characteristics. Velocity information from station 51 was used to calculate sediment thickness at points 1 to 5; station 63 for points 6 and 7; station 71 for point 8; and station 73 for points 9 and 10 (Fig. 7B and C). The resulting depth-sediment thickness diagram is shown in Fig. 7C and the sediment thickness for the pre-glacial to glacial units at each point are summarised in Table 4 and online Supplement 5.

3.5. Age model and sedimentation rate estimates

Our study is of basin-wide scale and since boreholes are few and far between, we constructed a hypothetical working age model as follows: a simplified Gradstein et al. (2004) geological time scale was re-drawn to a measurable vertical scale (Fig. 8, far left). The spreading age-range for each basin on the WS-SS seismic transect was taken from the magnetic anomaly compilation (Fig. 2 and Table 2) and drawn against the time scale (Fig. 8, black bars labelled sw SS, JB, PB and WS). The nearest isochron was taken at each of the 13 points used for the sediment thickness calculation, or linearly interpolated between the two closest anomalies, and matched to the time scale.

Table 4

Sediment thickness and sedimentation rate estimates at selected points on the WS–SS seismic transect, derived from the data in Figs. 1, 2 and 6 to 10.

Point	Region	Sedimentation thickness (m)				Sedimentation rate (cm/ky)		
		Total	Pre-glacial	Transitional	Glacial	Pre-glacial	Transitional	Glacial
1		1221	498	295	428	8.7	12.8	4.4
2	Scotia sea	1827	626	378	824	7.4	6.9	7.0
3		3582	1172	726	1684	10.7	11.2	16.0
4	Powell basin	2227	918	625	683	10.4	10.8	7.0
5	Jane basin	1580	441	389	749	10.5	11.5	9.9
6	northwestern	1756	803	269	685	10.7	5.7	6.3
7	Weddell sea	2455	1205	666	583	2.4	9.5	4.2
8		2386	1058	571	757	1.5	9.8	4.4
9	central	2872	1130	656	1085	1.4	8.2	7.8
10	Weddell sea	2531	923	780	827	1.1	6.1	6.1
11		2524	894	383	1248	1.5	1.2	4.7
12	southeastern	3136	1481	522	1132	1.4	6.4	6.4
13	Weddell sea	2405	1298	392	715	1.2	4.4	4.1

m = meters, m/my = meters per one million years, ms = milliseconds, red = minimum values, blue = maximum values.

Pre-glacial: Seismic stratigraphic units WS-S1, WS-S2 and WS-S3 shown in Fig. 6 and 7.

Transitional: unit WS-S4 and Glacial: units WS-S5, WS-S6 and WS-S7.

Uncertainty in sediment thickness ~30 ms, equating to 50 m for the upper and 70 m for the lower sediments.

Uncertainty in interval velocity estimates from refraction data ~0.1 km/s and ~0.3 cm/ky for sedimentation rates.

The interpreted seismic stratigraphy (Figs. 5B and 6B) at these points were drawn on the time-diagram and vertically stretched so that the basement age, as well as the ages of the upper two units obtained from the boreholes (Fig. 3), matched the time-scale. The relative time span for the deposition of each unit was estimated by projecting the first and last occurrence of each unit back into the time scale (colour bars, Fig. 8). Each colour matches the corresponding seismic stratigraphic unit in the representative sections. The age range for each unit was used in combination with the sediment thickness estimates (Fig. 7) to deduce the sedimentation rates (Fig. 9).

4. Observations, results and interpretation

4.1. Basement ages

The compiled magnetic spreading anomaly isochron map (Fig. 2; Table 2; online Supplement 1) constrained the basement ages as follows: Weddell Sea basin, 142.8–19.2 Ma (M17o–C6m); southwest Scotia Sea basin, 30.9–10.5 Ma (C12m–C5n.2 m); Powell Basin, 29.7–21.1 Ma (C11n.1o–C6AAo) and Jane basin, 17.4–14.4 Ma (C5Dn–C5ADn). The oldest magnetic anomalies occur in the southeast (Explora Escarpment), becoming younger towards the northwest part of the basin, near the Antarctic Peninsula. The lateral spreading age range for the Weddell Sea basement implies that sediments in contact with the basement should be younger than 124 Ma in the southwest or 14 Ma in the northwestern Weddell Sea. The magnetic isochrons crossing the WS–SS transect constrained the basement ages for the 13 selected points used to construct the age model (thin red lines in Fig. 2; red drop down lines in Figs. 5 and 6; listed ages below the 13 points in Fig. 8).

4.2. Borehole correlation

The WS–SS seismic transect seismic data matched the key stratigraphic boundaries in ODP leg 113 sites 693, 694 and 697 well (Fig. 2). The upper part of WS-S3 was constrained to an Eocene age (site 693), WS-S4 Oligocene to Miocene (site 693), WS-S5 late to middle Miocene (all sites), and WS-S6 and WS-S7 constrained to Pliocene and Pleistocene respectively for all sites (Fig. 2). Through the seismic tie lines, our interpreted units WS-S2 to WS-S7 correlated well to units identified in the SHALDRIL boreholes as well (Fig. 10).

4.3. Seismic characterization and horizon stratigraphy

Through the borehole stratigraphy (Fig. 3) and the reference type-section (Fig. 4), we traced continuous horizons across adjacent profiles along the ~3300 km transect to produce a seamless correlation and a new stratigraphy (Figs. 5B and 6B). Two stratigraphic nomenclature models are proposed: The first is the nomenclature for the Weddell Sea, using the prefix WS and appended with “S” for seismic stratigraphic unit (units WS-S1 to WS-S7) and “u” to indicate the base reflection or horizon also referred to as an unconformity or discontinuity (WS-u1 to WS-u7 in Figs. 5B and 6B).

The second nomenclature is suggested for circum-Antarctic correlation of the pre-glacial to glacial components (PG, T and FG, numbered from bottom to top in Fig. 4). The second system allows the interpretation of additional units that can still be grouped under the appropriate PG, T or FG component for the construction of cross-regional isopach grids, irrespective of the regional stratigraphy.

The acoustic basement topography near the Antarctic Peninsula is mostly rugged, ridges occur and some seamounts break through to

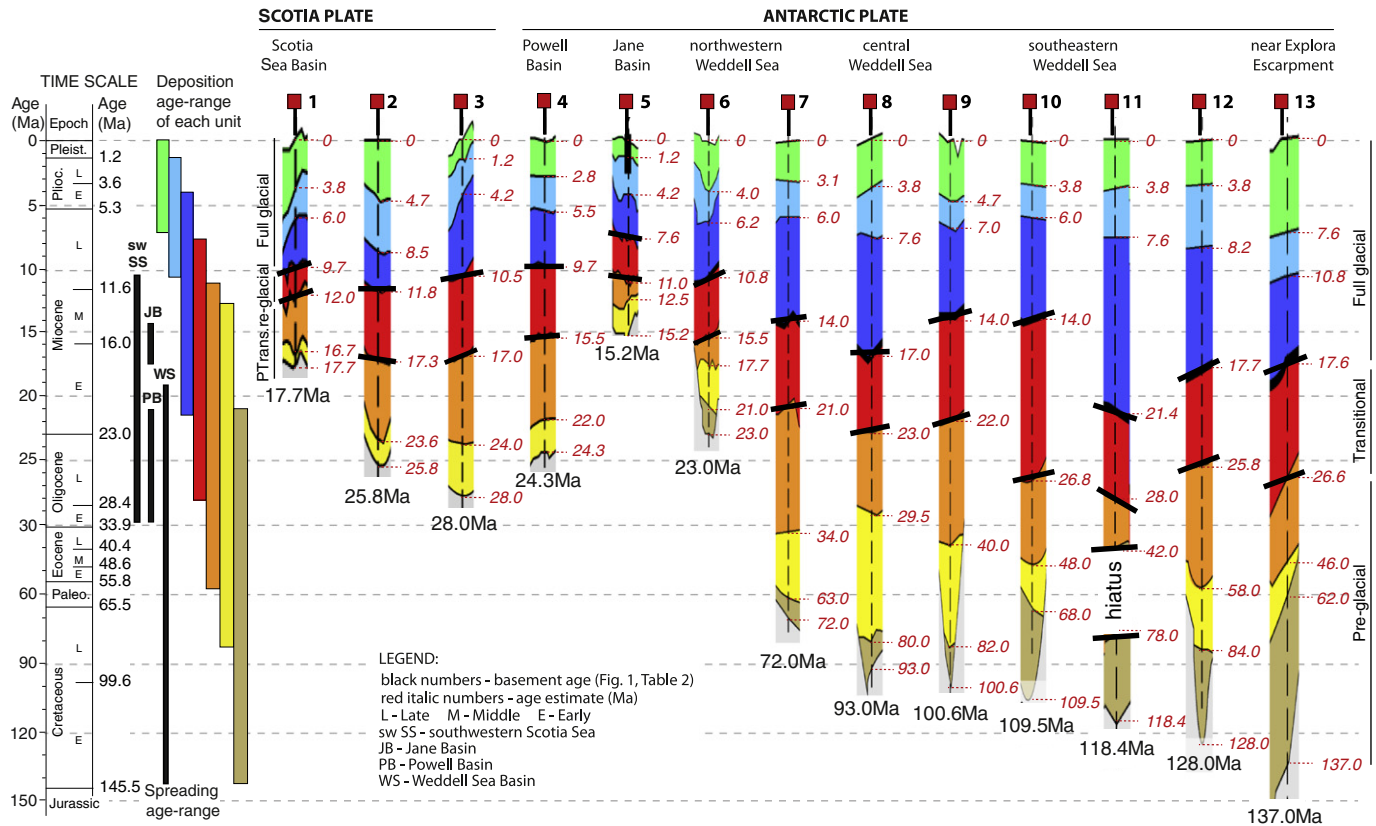


Fig. 8. Age model and associated sediment deposition along the WS-SS seismic transect. From left to right: Time scale of Epochs and boundary ages modified after Gradstein et al. (2004); Black bars = age-range obtained from the magnetic spreading anomaly isochron compilation (Fig. 2) for each basin. Colour bars = age-range of the deposition for each unit identified in the seismic data (Figs. 5 and 6), deduced from the first and last occurrence of each unit in the 13 scaled sections to the right, stratigraphy annotated. The tentative age for each horizon is annotated in red and read off from the time scale on the left. Basement ages at each point are annotated below. Thick black lines in the sections indicate the lower (uPG-T) and upper (uT-FG) boundaries of the pre-glacial to full glacial transitional unit. The vertical scale of the type sections represents time and not sediment thickness.

the seafloor (e.g. profiles SCAN04-17, M31 and M05 in Fig. 5A; north-western most part of profile BAS845-15, Fig. 6A). The Weddell Sea basement topography is less rugged with smaller valleys, but lies more or less on the same average level. In the absence of deep boreholes, the interpretation of basement is based on the seismic reflection

data. For clarity, faults were not interpreted. Our resulting acoustic basement horizon (WS-u1) compares well with the refraction data and derived crustal model of Rogenhagen and Jokat (2002).

The seismic reflectivity of units WS-S1 till WS-S7 (Figs. 5A and 6A) match those of each unit described in the type section (Fig. 4) very

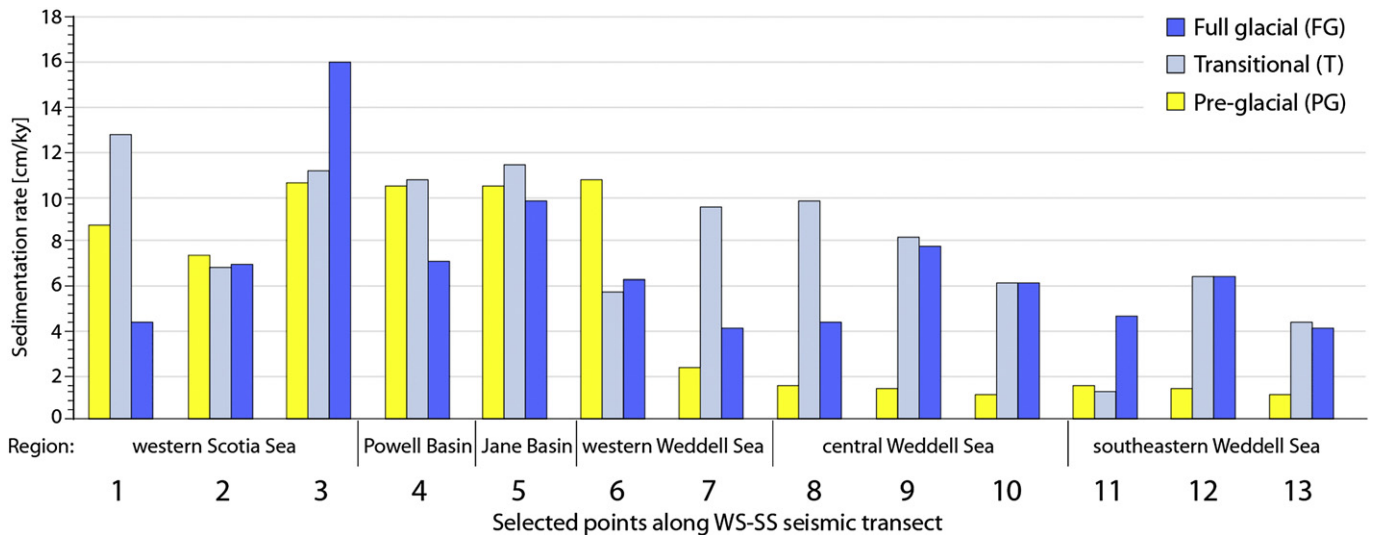


Fig. 9. Sedimentation rates for the pre-glacial (PG), transitional (T) and full glacial (FG) regimes at the 13 selected points along the WS-SS seismic transect (for location see Fig. 7A). Calculations are based on the sediment thickness in Fig. 7 and online Supplement 4, the interpreted seismic reflection data (Figs. 5 and 6) and the hypothetical age model in Fig. 8. Rates are given in cm/ky and listed in Table 4 and online Supplement 5.

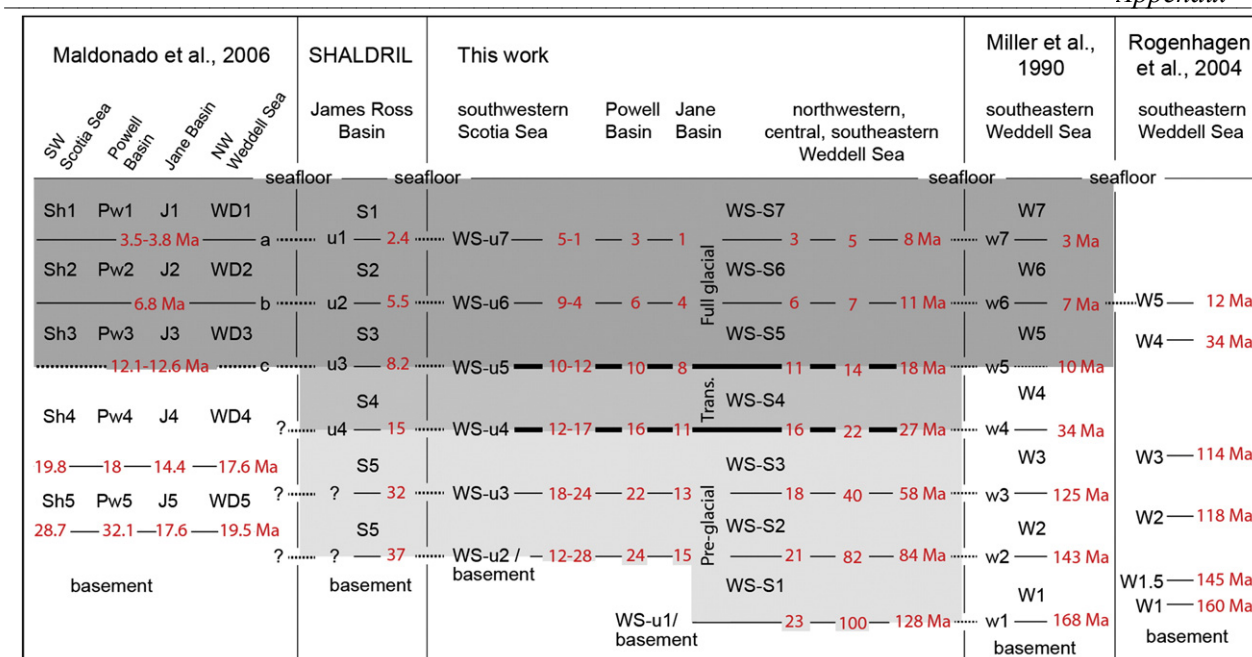


Fig. 10. Seismic stratigraphy correlation chart linking seismic units and horizons from this paper, to previous studies in the Weddell Sea and Scotia Sea. Thin black lines = mapped horizons in all studies; thick black lines = lower boundary of the proposed transitional and full glacial units, this paper; Dashed lines = correlated seismic horizons according to matching reflectors; red numbers = ages of the horizons, showing the lateral variation in age across the basins. Light grey = pre-glacial units; Medium grey = transitional units; Dark grey = full glacial units. SHALDRIL refers to Anderson (2006), Smith and Anderson (2010, 2011), Anderson and Wellner (2011), and Bohaty et al. (2011).

well and show negligible lateral variation between the northwestern and southeastern Weddell Sea, or the smaller Jane and Powell Basins. All units are laterally continuous and well stratified with reflectors that are mostly coherent, horizontal and undisturbed, and easy to trace over long distances. Layering is parallel to the seafloor except in the middle of the Weddell Sea basin where the older, lower amplitude units appear to form a mound. The mound is especially recognisable to the Southeast of borehole 694 in the seismic image (Fig. 6A).

The PG sequence WS-S1, WS-S2 and WS-S3, is bounded by reflector WS-u1 below and reflector WS-u4 above (Fig. 6A; online Supplement 3). WS-u4 or uPG-T marks a prominent change in seismic facies from low amplitude, more transparent, laterally discontinuous reflectors in the sequence below, to more continuous, higher amplitude, parallel reflections in the sequence above (Figs. 5A and 6A; online Supplements 2 and 3).

The T sequence consists of one seismic unit, WS-S4 and is bounded by reflector WS-u4 below and WS-u5 above, alternately referred to as horizons uPG-T and uT-FG (Figs. 5 and 6). Although thinner seismic units can be distinguished within WS-S4, the seismic facies characteristics are similar and grouped as one unit here. WS-u5 was picked as the top boundary horizon for this sequence because in the seismic data we see the lower reflective T-unit package below this reflection, rapidly transitioning into a sequence of high amplitude, closely spaced, horizontal reflections above (Fig. 6A). It is a thick strong high amplitude reflection that could easily be traced across the basin and merge with several unconformities above, especially near the flanks of the basin (Fig. 6A and 11; online Supplement 3). We interpreted these seismic characteristics to represent the first sedimentary sequences transported down-slope and onto the abyssal plain via the first ice sheet advancements to the outer shelf.

The FG sequence consists of three seismic units, WS-S5, -S6 and -S7 and is bounded by horizon WS-u5, the T to FG period unconformity (uT-FG) below, and the seafloor reflection above (Fig. 6). We assume the change in seismic facies and more complex internal structures (e.g. drifts) represent change in depositional processes. Hence we

interpret the sharp transition to represent the onset of the full glacial regime processes and transition to a modern polar ice sheet, consistent with observations around the Antarctic Peninsula (e.g. Diviacco et al., 2006; Rebesco et al., 2006; Rebesco and Camerlenghi, 2008).

The initial FG unit (WS-S5 or FG-1), drapes over this pre-glacial and transitional sequences mound and fills the basin low in the southeastern Weddell Sea (observed from point 10 to 13, Fig. 6). Thinner units WS-S6 and WS-S7 were deposited on the smoothed bathymetry as two horizontal bands of high amplitude finely laminated reflectors.

4.4. Sediment thicknesses

The lateral variations in sediment thickness are described for each unit in the Weddell Sea basin, from bottom to top and old to young, referring to Figs. 5 to 7 and online Supplement 4:

WS-S1 is absent in the Scotia Sea, Jane and Powell Basins, but continuous throughout the Weddell Sea basin (WSB). It increases in thickness from 282 m in the northwest (point 6, Fig. 7) to 545 m in the southeast at point 13.

WS-S2 ranges from 273 to 640 m in the Scotia Sea (points 1–3), 395 m in the Powell Basin (point 4) and 247 m in the Jane basin (point 5). An interesting trend is seen in the Weddell Sea basin, where WS-S2 is thickest in the centre (474 m at point 9 to 302 m at point 7) and thinner on both flanks (266 m at point 6 and 285–293 m at points 12 and 13, Fig. 7). Notably WS-S2 is absent at point 11.

WS-S3 is continuous along the entire transect and becomes thicker from the northwest to the southeast: 224 m thick at point 1 and thickening to 532 m at point 3 in the Scotia Sea, 524 m in the Powell basin, thinnest in the Jane basin (139 m) and ranges from 255 to 778 m (points 6 to 12, Fig. 7) in the Weddell Sea basin.

Collectively, WS-S1, WS-S2 and WS-S3 comprise the pre-glacial (PG) sequence, which ranges in total thickness from 441 to 1481 m (Table 4). A westward thickening of PG sediments was expected in the Weddell Sea basin, but instead we found a higher mound in the

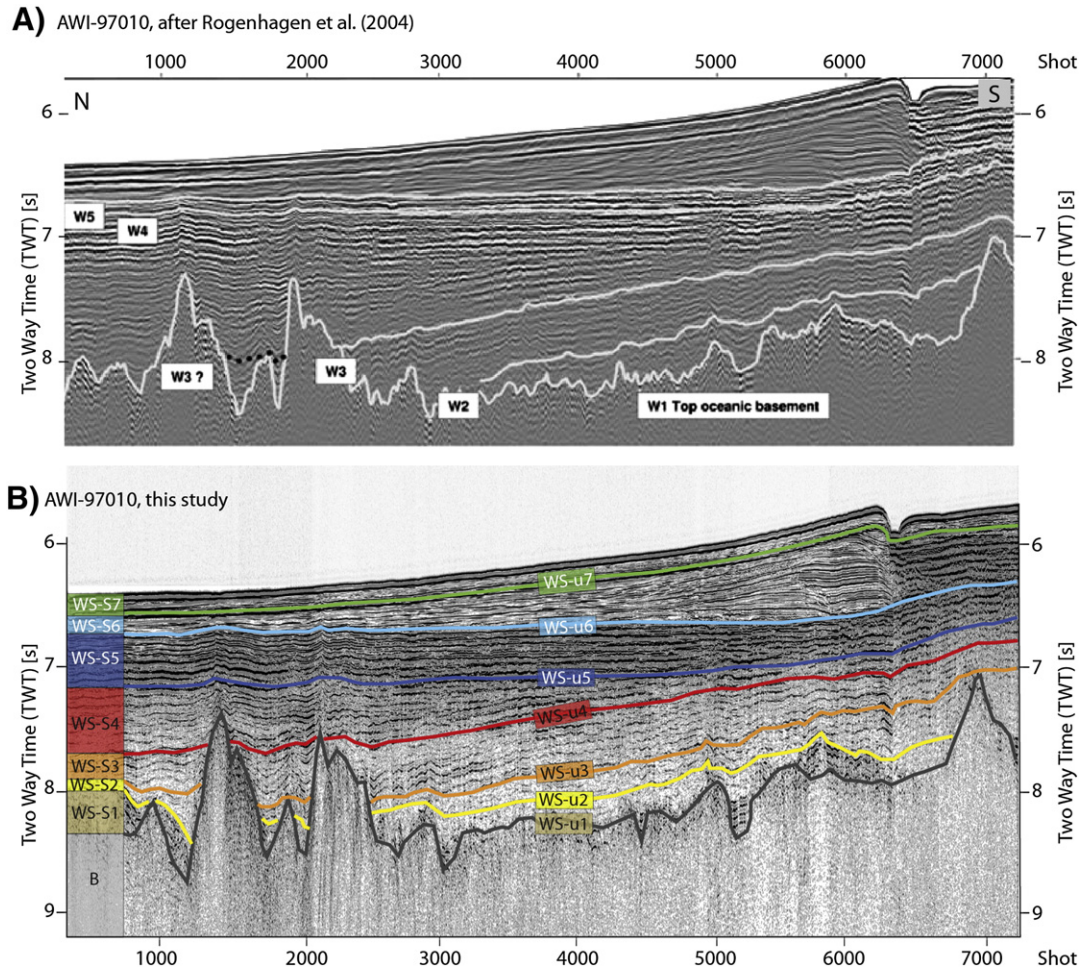


Fig. 11. Interpretation of multichannel seismic line AWI-97006 in time domain comparing the horizon stratigraphy of Rogenhagen et al. (2004) in (A) with the new Weddell Sea seismic units identified in the WS–SS transect (B). See Fig. 2 for location. Note the difference between W4 and our WS–u5, both horizons were interpreted to represent the full glacial onset. W4 was replaced with WS–u5 because of a large scale unconformity mapped between shots 4000–6000. Similarly WS–u4 was newly interpreted based on the unconformity between shots 2000–4000 and ~7.5 s TWT. The lower units were also subdivided and the basement interpreted below prominent reflectors just above, e.g. at shots 5000–6000 and ~8 s TWT.

middle (between points 7 and 10 in Fig. 6B) flanked by a deeper basin in the southeast (points 10 to 13 in Fig. 6B) and a thicker part near the continental slope at the Explora Escarpment.

WS–S4 or the transitional unit (T–1) varies in thickness throughout the Scotia Sea and Weddell Sea (red band in Figs. 6 and 7). The thinnest part is observed at point 6 (267 m) and the thickest part at point 10 (780 m) in the northwestern Weddell Sea (Table 4). WS–S4 seems to have partly filled in the palaeo basin low in the southeast (points 7 to 13) and thins over the mound.

WS–S5 is the most prominent and the first full glacial sequence (dark blue unit in Figs. 5B and 6B). It is laterally massive, thick and continuous. Similar to WS–S1 to WS–S4, WS–S5 thickens towards the Antarctic Peninsula shelf in the Scotia Sea (185–851 m from points 1 to 3). The thickness of WS–S5 is relatively constant in the northwestern Weddell Sea (280–398 m), but thickens to 974 m in the southeastern Weddell Sea (point 11) and filled the remaining palaeo basin low (points 9 to 13 in Fig. 7, online Supplement 5). WS–S5 seemed to mostly smooth out the Weddell Sea pre-glacial to transitional mound-and-flanking basin palaeotopography.

WS–S6 is 122–208 m thick across the Weddell Sea and 140–560 m thick in the Scotia Sea, following the same trend as units WS–S2 to WS–S5. The thickest parts occur in the centre of the Weddell Sea where it drapes over the mound (point 9, 209 m) and at either flank near the shelf (186 m at point 13 and 170 m at point 5; Fig. 7; online

Supplement 4). WS–S7 is the thinnest unit in the entire sedimentary sequence and shows little lateral variation in sediment thickness between the Scotia Sea (103–273 m) and Weddell Sea basin (126–215 m). Units WS–S5, WS–S6 and WS–S7 comprise the fully developed glacial (FG) sequence, which ranges in total thickness from 428 to 1684 m in the Scotia Sea and 583–1248 m in the Weddell Sea (Table 4; Fig. 7).

The total sediment thickness in the Scotia Sea ranges from 1218 to 3762 m, and in the Weddell Sea from 1745 to 3123 m (Table 4). We estimate the deep-sea Weddell basin to have a minimum area of $\sim 1.3 \times 10^6$ km² and a maximum area of $\sim 1.5 \times 10^6$ km² (red outline in Fig. 1 inset). The shelf areas are not incorporated due to lack of data in front of the Filchner–Ronne Ice shelf. Taking an average sediment thickness of ~2.5 km (Table 4) a first order minimum estimate of the total sediment volume for Weddell deep-sea basin would be 3.3×10^6 km³ and a conservative maximum volume estimate 3.9×10^6 km³. Under the assumption that the pre-glacial to fully glacial units occur throughout the Weddell Sea basin, we use the average thickness of each component (PG = 923 m, T = 478 m, FG = 769 m; Table 4) and the minimum and maximum basin area to estimate sediment volumes. Minimum volumes are: PG = 1.2×10^6 km³, T = 0.6×10^6 km³ and FG = 1.0×10^6 km³ and the conservative maximum volumes: PG = 1.4×10^6 km³, T = 0.7×10^6 km³ and FG = 1.2×10^6 km³.

4.5. Age model

In our age model Weddell Sea basement age is estimated at 137 Ma in the southeastern part of the transect and becomes progressively younger (~23 Ma) towards the northwest (Fig. 8). WS-S1 has the largest age range of all the units. In the southeast near the Explora Escarpment it is 137–62 Ma at point 13 and ~23 Ma in the northwest (point 6 in Fig. 8). Units WS-S2 and WS-S3 both follow a similar trend as WS-S1 and become younger to the northwest as well (84.0–17.7 Ma and 58.0–15.5 Ma at points 13 to 6, Fig. 8). A hiatus of ~36 Ma occurs at point 11 where unit WS-S2 is absent, probably due to erosion. The lower boundary of the transitional unit (horizon WS-u4 or uPG-T) decreases in age from 26.8 Ma in the southeastern Weddell Sea (point 13 in Fig. 8) and to 15.5 Ma in the northwestern Weddell Sea (point 6), being slightly younger in the Jane basin (11 Ma). The uPG-T horizon shows lateral age variation in the Scotia Sea of 17.3–12.0 Ma, the oldest part near the Antarctic Peninsula and becoming younger to the northwest (points 1–3, Fig. 8).

The upper boundary of the transitional unit (horizon WS-u5 or uT-FG), interpreted to represent the advancing ice sheets grounding on the outer shelf for long periods in a full glacial regime, also youngs from southeast to northwest (17.7–10.8 Ma at points 13 to 6, Fig. 8). We observe an older outlier age of ~26.8 Ma at point 11 in the Weddell Sea basin and a younger age of ~7.6 Ma at point 5 in the Jane Basin. Horizon WS-u6 has a tentative age of ~10.6 Ma in the southeastern Weddell Sea basin (point 13) and becomes increasingly younger up to 6.0 Ma in the northwest (point 7, Fig. 8). The model age of ~7.6 Ma at point 11 for WS-u6 fits with the regional trend. Horizon WS-u7 shows a modelled lateral age variation of ~3.8–1.2 Ma (points 1 to 4, Fig. 8).

4.6. Sedimentation rates

The age model was used in combination with the derived sediment thickness estimates (Fig. 7; Table 4) to deduce sedimentation rates for the pre-glacial, transitional and full glacial components of the deep-sea sediment archive in the Weddell Sea basin (Table 4; Fig. 9). Since there are uncertainties in our age model due to the absence of borehole age-control, we only comment the sedimentation rate trends. The pre-glacial sedimentation rates at points 4–6 in the Powell Basin, Jane Basin and northwestern Weddell Sea are the highest (10–11 cm/ky, Table 4; yellow bars in Fig. 9) and almost an order of magnitude higher than the rates in the central Weddell Sea (1.1–1.6 cm/ky). Although the Weddell Sea pre-glacial units are the thickest (894–1481 m), the sedimentation rates are the lowest.

The transitional sedimentation rates range from 1 to 10 cm/ky in the Weddell Sea and 7–13 cm/ky in the Scotia Sea (Table 4; middle bars in Fig. 9) and are almost an order of magnitude higher than the pre-glacial rates. An anomalous transitional sedimentation rate of 1.2 cm/ky occurs at point 11, the same place where the hiatus and eroded WS-S2 unit are observed (Fig. 8). In the central and northwestern Weddell Sea the transitional sedimentation rates are amongst the highest (8–10 cm/ky). Higher transitional sedimentation rates occur on the flanks of the Weddell Sea basin as expected (points 7–9 and 12; Fig. 9; Table 4) since it is closer to sediment supply from land.

The full glacial sedimentation rates are the highest at points 3 and 5 in the Scotia Sea and Jane Basin (~16 cm/ky and 10 cm/ky) and at points 9 and 11 in the Weddell Sea (~7–8 cm/ky, Fig. 9; Table 4).

5. Discussion

The new basin-wide seismic stratigraphy and assignment of seismic units to PG, T or FG components rest on the basic premise that glacial sediment input and transport is recorded in the seismic strata. Based on our age model, the seven identified horizons increase in age from the southeastern to the northwestern Weddell Sea. This result is different from local scale studies where a uniform age for

each horizon is often assumed (Miller et al., 1990; Rogenhagen et al., 2004; Maldonado et al., 2006). For the pre-glacial units this lateral-increase-in-age trend can be ascribed to sediments being deposited synchronous to seafloor spreading and formation of the Weddell Sea basin. However, in the transitional and full glacial units it is presumed to represent the lateral increase in sediment supply and consequential increase in down-slope and along-slope sediment transport processes. Such increases are often related to ice sheet advance and intensification of bottom currents. We compare our findings to previous work and discuss our observations in the context of implications for understanding the bottom water ocean circulation changes and ice sheet development in the pre-glacial to glacial climate transition.

5.1. Pre-glacial (PG) regime

Previous seismic stratigraphy work in the Scotia Sea, the Powell and Jane Basins, and in the northwestern Weddell Sea identified two pre-glacial seismic units assigned to Oligocene–early Miocene age (e.g. Sh5, Sh4; Pw5, Pw4; J5, J4; WD5, WD4 in Fig. 10). We identified additional prominent horizontal reflections in the central Weddell Sea (profile BAS645–15, Fig. 6) and upon tracing them as well as boundary horizon WS-u4 into the northwestern Weddell Sea, Powell and Jane Basins and southern Scotia Sea, found that they mismatched this previous work (Fig. 10). We consequently re-divided the PG seismic sequence into three units instead of the previous two, labelled bottom up as WS-S1, WS-S2 and WS-S3 (Figs. 6 and 10). These boundary horizons of these units (WS-u1, WS-u2, WS-u3) were traced farther into the southeastern Weddell Sea and matched all horizons in the seismic stratigraphy of Miller et al., 1990 (Fig. 10), but disagree with seismic stratigraphy model of Rogenhagen et al. (2004). Contrary to Rogenhagen et al. (2004), we re-interpret the basement reflector WS-u1 up to ~0.5 s deeper, below the series of strong horizontal reflectors directly above basement (Figs. 10 and 11). This was done because in our opinion these could either be older consolidated sediments or lava flows, especially considering that the thickest part lies near the Explora Escarpment.

Horizons WS-u2 and WS-u3 matched the seismic stratigraphy of SHALDRIL and Maldonado et al. (2006) in the northwestern Weddell Sea (Fig. 10). These two horizons were farther traced across the central Weddell Sea and into the southeastern part of the basin, where it mismatched horizons W2 and W3 in Rogenhagen et al. (2004) and we interpreted at different positions based the cross-basin correlation in continuous data and on observed unconformities (Figs. 10 and 11).

The PG horizons all show a lateral variation in age in the southern Scotia Sea, Jane and Powell Basins, northwestern and southeastern Weddell Sea (Fig. 10) and our age range compares well to previous tentative age estimates (Figs. 8 and 10; Maldonado et al., 2006; Miller et al., 1990). The PG ages in the northwestern Weddell Sea (Figs. 8 and 10) are consistent with late Oligocene pre-glacial strata (~28.4–23.3 Ma) drilled in SHALDRIL Hole 3C (Bohaty et al., 2011; Fig. 3).

The southeastern Weddell Sea basement is the oldest (up to ~145 Ma, M17; Fig. 1; Table 2) and nearest to the shelf at Dronning Maud Land. We would therefore expect to find the thickest sediments and highest sedimentation rates on the slope near this continental margin. Instead, we found a ~1130 m thick mound in the centre of the Weddell Sea basin on much younger basement (93–45 Ma, Figs. 1 and 6; Tables 2 and 4). The depositional geometry on both the northwestern and southeastern flanks of the mound has a basin shape (Figs. 6 and 12A). If the basin-like depressions were due to differential compaction, the reflectors would be offset or curved in the seismic image, but this is not observed. It also leaves the thinner units (<790 m) to the east of the mound and the partial absence of unit WS-S2 at point 11 unaccounted for.

We consider alternative processes that may cause high sediment transport to the deep-sea. A typical mechanism is ice rafting and ice

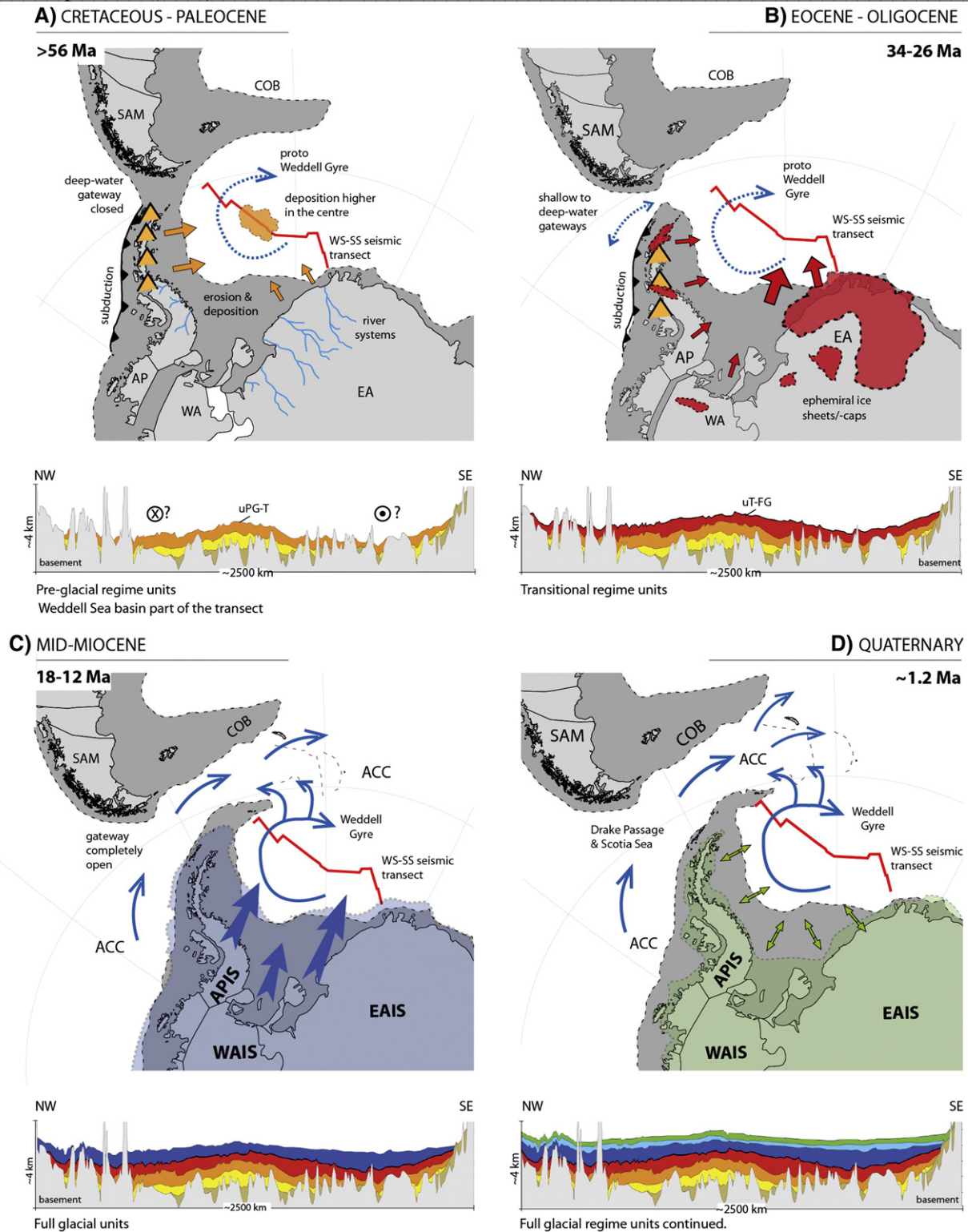


Fig. 12. Model showing the role of plate-tectonic motion, pre-glacial sedimentation, ice sheet development and ocean circulation in the greater Weddell Sea region, since the Cretaceous. Rivers, mountains, ice caps, ice sheet boundaries and the WS-SS transect are schematic interpretations. Diagrams below represent Weddell Sea Basin part of the transect. Plate reconstruction adapted from GPlates (Boyd et al., 2011) and associated sediment deposition for each regime, is illustrated in the diagram below. (A) Pre-glacial regime. COB = continent ocean boundary, SAM = South American plate, AP = Antarctic Peninsula, WA = West Antarctica, EA = East Antarctica. Orange triangles = mountain building in the Antarctic Peninsula, subsequent erosion and deep-sea deposition (orange arrows). Blue dashed line = the proto Weddell Sea Gyre, red line = Weddell Sea part of the WS-SS seismic transect, orange cloud = higher sediment deposition of PG-units near the centre. (B) Transitional regime. Red polygons = ice caps and smaller ice sheet development on the highlands of EA, the northern tip of the AP and WA. Red arrows indicate high sediment supply. (C) Full glacial regime. Transparent blue polygon = EAIS, WAIS and APIS, fully developed and grounded on the continental shelf; Thick blue arrows = high volume of sediment transport; Weddell Gyre and ACC = fully developed Antarctic Circum-polar Current (simplified after Livermore et al. (2007)). (D) Full glacial regime cont. Green arrows = smaller ice sheet advance and retreat cycles whilst ice sheets (transparent green polygon) still remain grounded on the outer shelf.

sheets pushing sediments onto the slope and rise as they ground on the outer shelf. However, given the warm climate and ice minimum conditions (Zachos et al., 2001) inferred for the Cretaceous–Eocene pre-glacial seismic sequence, mass sediment transport due to expanding ice sheets becomes an unlikely process and we have to consider other explanations. High bio-productivity and mortality could cause high pelagic fall-out and could account for high sediment supply in the deep-sea, but fail to explain the mound and basin-like depressions. Tectonic uplift and an underlying basement high or low are also excluded because, although the Weddell Sea basement is highly variable and uneven (Fig. 6) when averaged, it remains on a similar level.

Thinner units (<790 m) to the east of the mound (Fig. 6 and 12A), the partial absence of unit WS-S2 and the anomalously low transitional sedimentation rate of 1.2 cm/ky at point 11 (Figs. 6 and 8), collectively allow the interpretation that bottom current erosion may have caused this mound-basin depositional geometry. Such bottom currents could have been caused by down-slope sediment influx from the Crary Fan (Kuvaas and Kristoffersen, 1991; Bart et al., 1999; Michels et al., 2001, 2002) or a Cretaceous–Eocene proto-Weddell Gyre that build the mound in the centre whilst eroding the flanks asymmetrically. We consider it unlikely that the Crary Fan down-slope current could solely account for the mound-basin geometry for the following reasons: Michels et al. (2001, 2002) observed combined contourite–turbidite sedimentation patterns at the western and southeastern Weddell Sea margin (south of 70°S) for the transitional (W4) and full glacial sequences (their regional unconformity W5). Pre-glacial sediments were not considered in their study. Of the three identified main Crary Fan down-slope channels, each about 2–5 km wide, two could perhaps be interpreted in the WS–SS transect between points 8 and 9 (black arrows Fig. 6). However, these are at least two orders of magnitude smaller than the basin-wide features observed in the transect, unpronounced and constrained to uppermost the Pliocene–present day layers. Additionally the WS–SS transect is more than 500 km (or 5°) north from the slope and Crary Fan extent (Kuvaas and Kristoffersen, 1991; Bart et al., 1999; Michels et al., 2001, 2002). We thus favour the proposed proto-Weddell Gyre hypothesis as the most likely dominant process responsible for the depositional geometry.

The fact that the depression is deeper and the units thinner on the southeastern flank than on the northwestern flank, may be consistent with the up-current side and hence with a clockwise circulation (Fig. 12A). To our knowledge a proto-Weddell Gyre has not been proposed before, but Eocene–Oligocene proto-Antarctic Bottom Water and Weddell Sea Deep Water masses has been inferred for pre-glacial regimes at Maud Rise, from $\delta^{18}\text{O}$, mineral and grain analyses in ODP leg 113 site 690 (Diester-Haass et al., 1996).

Contourites were used to determine bottom current direction around the Antarctic Peninsula for transitional and full glacial deposits (e.g. Maldonado et al., 2005; Uenzelmann-Neben, 2006). Although typical contourite drift structures are not clearly observed in the WS–SS transect seismic data, the seismic profiles are too sparse to exclude their existence in the pre-glacial central Weddell deep-sea units. Further analyses of the two parallel transects (A and C in Fig. 1) are ongoing and might shed more light on the proto-gyre circulation direction. The driving force of the proto-gyre circulation remains unclear as well. The ACC is not fully developed because South America was still connected to Antarctica with shallow water gateways (Fig. 12A; Livermore et al., 2007), but Weddell Bottom Water could have formed due to sea ice. Either way, the mound feature is prominent enough that it warrants future investigation.

5.2. Transitional (T) regime

The base reflector of the transitional unit, WS-u5, was traced from the northwestern Weddell Sea into the Jane Basin, Powell Basin

and the Scotia Sea, where it exactly matched with horizon “c” of Maldonado et al. (2006; Fig. 10). Based on seismic facies changes and downlap terminations, they postulated that horizon “c” represents an erosional surface signalling the incursion of bottom water exchange between the Scotia and Weddell Sea and coeval to the Mi4 glaciation. WS-u5 and WS-u4 partially correlates to S3 (~8 Ma) in the SHALDRIL boreholes identified as the start of the PG to FG transitional sequence at the Antarctic Peninsula (Fig. 3; Smith and Anderson, 2010, 2011; Bohaty et al., 2011).

Our model age of ~17.6 Ma (point 13 in Fig. 8) is also consistent with the ODP leg 113 site 693 borehole age of early mid-Miocene–Late Miocene of 16–11 Ma (Figs. 3 and 10). Tracing WS-u5 into the southeastern Weddell Sea it matched horizon w5 of Miller et al. (1990) but mismatched the W4 marker horizon (Rogenhagen et al., 2004) that represents the onset of the FG regime in the deep-sea (Figs. 10 and 11). We re-interpret W4 of Rogenhagen et al. (2004) in the southeastern Weddell Sea and place it ~0.75 s deeper (WS-u5, dark blue line in Fig. 11).

Which depositional processes active in the Eocene–Oligocene transitional climate associated with high sediment transport may have formed this WS-S4 unit? Previous seismic stratigraphy studies postulated that ephemeral ice caps and small ice sheets formed on high elevations in the West Antarctica, with the EAIS periodically grounding on parts the outer shelf and increasing sediment supply to the deep-sea (e.g. Miller et al., 1990; Oszko, 1997; red polygons and arrows in Fig. 12B). Isolated gravel and terrigenous sand grains in ODP leg 113 site 689 and 690 at Maud Rise, offshore north of Dronning Maud Land, provided evidence for a grounded Eocene EAIS since ~45.5 Ma, probably with a more temperate rather than polar character (e.g. Ehrmann and Mackensen, 1992).

If it is the case that only the EAIS grounded during the Eocene–Oligocene, the highest sediment supply would presumably be in front of the Crary Fan and on the slope and rise of the southeastern Weddell Sea near the Explora Escarpment (Fig. 1), with little or no ice sheet related sediment supply at the Antarctic Peninsula. The effect would be transitional deposits that are thicker in the southeast than in the northwestern part of the Weddell Sea basin and the Antarctic Peninsula. On the contrary, we observe that unit WS-S4 is thickest in the northwestern Weddell Sea (<806 m), 400–600 m thick in the central and northeastern Weddell Sea and thinnest over the peak of the mound (~383 m; Fig. 7; Table 4; online Supplement 5). WS-S4 drapes over the mound and partly fills in the basin depressions to either side, whilst being continuous along the entire WS–SS transect and probably basin-wide (Fig. 6; online Supplement 3).

It is likely that bottom current processes could have redistributed sediments from the southeastern EAIS source region to the central and northwestern Weddell Sea, thus maintaining the eroded basin geometry to the east of the mound. The transitional unit displays no along-slope drift or contourite structures but was interpreted as a sheeted drift. Bottom current processes alone cannot account for the WS-S4 geometry. The continuous occurrence and thicker WS-S4 deposits in the northwestern Weddell Sea can also be explained by along-slope sediment supply from the proto-Weddell Gyre circulation, down-slope supply by an advancing ephemeral EAIS, and from advancing ice sheets in the North–West i.e. WAIS and the southern APIS.

SHALDRIL boreholes and seismic records on the southern margin of the Joinville Plateau show glacial marine sedimentary processes dominated sedimentation since the late Oligocene and a phased APIS expansion from south to north across the Peninsula in the late Miocene (e.g. Smith and Anderson, 2010, 2011; Bohaty et al., 2011) or Oligocene (Davies et al., 2012). High transitional sedimentation rates around the Antarctic Peninsula (11 cm/ky) and northwestern Weddell Sea (6–10 cm/ky; Fig. 9; Table 4) and the age variation of the initial ice grounding boundary horizon, uPG-T (27–16 Ma; WS-u4 in Fig. 10) across the Weddell Sea, allow the interpretation that the southern

part of the APIS probably already grounded in the early Miocene or even Oligocene, and the WAIS in the Oligocene. Sampling, drilling and multichannel seismic reflection data analyses of Drift 7 on the Pacific margin of the Peninsula, suggest down-slope transport as a result of the growth of the Antarctic Peninsula ice sheet in the Early Miocene (~15 Ma and 9.5 Ma; Uenzelmann-Neben, 2006). This early Miocene/Oligocene APIS and Oligocene WAIS expansion is not adequately reproduced by palaeoclimate models that suggested a late Miocene–early Pliocene APIS grounding (7.94–5.12 Ma, Bart et al., 2005; Pollard and DeConto, 2009; Table 1), but consistent with the SHALDRIL findings (Anderson et al., 2011).

5.3. Full glacial (FG) regime

In the Scotia Sea, Jane Basin, Powell Basin and northwestern Weddell Sea, seismic horizons WS-u5, -u6 and -u7 identified in this study match the horizons “c”, “b” and “a” of Maldonado et al. (2006; Fig. 10). Our interpreted horizons show a lateral age variation contrasting the uniform ages assigned in Maldonado et al. (2006; Fig. 10). Seismic units WS-S5, WS-S6 and WS-S7, listed from old to young, consistently matched the upper three units in the southern Scotia Sea (Sh3–Sh1), Powell Basin (Pw3–Pw1), Jane Basin (J3–J1) and northwestern Weddell Sea (WD3–WD1) mapped in previous studies (Fig. 10). Horizon WS-u6’s age of ~5.5 Ma in the Powell Basin (Figs. 8 and 10) is in broad agreement with the base-age of S2 (~5.5 Ma) dated in the nearby SHALDRIL cores, even though the latter lies on the shelf (Fig. 10; Smith and Anderson, 2010; Bohaty et al., 2011). WS-u7 is correlated to reflector “a” in Maldonado et al. (2006) dated in their study at 3.5–3.8 Ma from ODP leg 113 site 695–697 (see Fig. 2 for borehole locations). Our age range 3.8–1.2 Ma is also in good agreement to the base-age of S1 (2.4 Ma) in the SHALDRIL cores (Fig. 10; Smith and Anderson, 2010; Bohaty et al., 2011).

In the southeastern Weddell Sea, horizons WS-u6 and WS-u7 matched horizons w6 and w7 of Miller et al. (1990), dated at late Miocene (~7 Ma) and late Pliocene (~3 Ma) in ODP leg 113 sites 692 and 693 (Figs. 2C and 10). Horizon WS-u6 is correlated with horizon W5 of Rogenhagen et al. (2004) and our tentative model age of 10.8–8.2 Ma for the southeastern Weddell Sea broadly agrees with their older extrapolated age of ~12 Ma (Figs. 10 and 11). Horizon WS-u7 was absent in the Rogenhagen et al. (2004) model and is newly interpreted on the AWI-97 profiles (Figs. 6 and 11; Table 3) to match horizons traced from ODP leg 113 site 694 (Fig. 3).

Taking into account the geometry, lateral variation in sediment thickness and sedimentation rates of the transitional unit along the WS–SS transect, we infer from our observations which depositional processes in the Miocene–Quaternary may have played a role in the deposition of these units. WS-S5 filled the basin lows on either side of the inferred mound and levelled the basin bathymetry (dark blue unit, Figs. 6 and 12C). If the mound formed in response to an assumed proto-Weddell Gyre that intensified in the Miocene glacial regime, it poses the question of why the full-glacial units do not reflect mound geometry as well.

Reason for this change in geometry could be that the Weddell Gyre erosion capacity changed due to the development of the ACC (Table 1; Fig. 12C) or that the glacial/ice sheet till particles became too large to be transported by bottom currents over long distances. Sediments created by glacial process would have larger grain sizes, thus be heavier and require more energy to transport than pelagic fall-out. We consider it most likely that sedimentation rates were much higher than the erosion rate due to increased sediment supply and deposition to the deep-sea. Even after full glacial conditions were developed on the continent, there were still significant volumes of fine sediments being produced and deposited around the continent. It is generally observed that sedimentation rates increased during the early phases of glaciation, which is expected.

ODP Site 697 in Jane Basin reported a sedimentation rate of 4.4 cm/ky for the upper 200 m, increasing down core to 10 cm/ky for the interval of 250–300 m (Barker et al., 1988; Gersonde et al., 1990; Ramsay and Baldauf, 1990). Our estimated rate of 9.9 cm/ky for the full glacial unit (~749 m thick) in the Jane Basin compares extremely well to the ODP rates and to 10 cm/ky reported in Maldonado et al. (2006).

Sediment transport by expanding ice sheets is the most probable process capable of rapidly eroding sediments on land and the continental shelf, transporting it to the outer shelf and as the ice sheets grounded, pushed massive volumes of sediments over the edge in a bulldoze effect. Such increased supply to the deep-sea would balance the gyre or bottom current erosion and result in a smoothed out basin geometry. An alternative interpretation, although speculative, is that the proto-Weddell Gyre was constrained during its initial development to the margins of the basin and flowed mostly as a density nepheloid layer. The particles that escaped from this nepheloid layer were deposited in the central basin plain.

ODP leg 113 site 694 lies in the central Weddell Sea and on profile BAS845–15 of the WS–SS transect (Fig. 2). The matched seismic stratigraphy of this borehole and our transect (Fig. 3), constrained unit WS-S5 and reflectors WS-u5, WS-u6 to middle–late Miocene age in our age model (Fig. 8). The borehole log also reported glacial turbidite units and present evidence of deep-sea glacial sediment transport during this time, implying that grounded ice sheets were already present in the Miocene that drained into the Weddell Sea basin (Fig. 12C). Miocene continental scale ice sheets in Antarctica were also documented in other borehole and seismic reflection data (e.g. Barker et al., 1988; Miller et al., 1990; Zachos et al., 2001; Maldonado et al., 2005, 2006; Leitchenkov et al., 2008; Anderson et al., 2011; Escutia et al., 2011).

Units WS-S6 and WS-S7 were deposited in the Pliocene–Pleistocene (Fig. 3) and have an estimated average thickness of 158 m and 165 m, respectively across the Weddell Sea basin (Fig. 7; online Supplements 4 and 5). Even though these units are ascribed to the same glacial driven depositional processes as the on average 542 m thick WS-S5 unit below, they appear much thinner (Fig. 6B). One possibility could be that the initial full glacial ice sheet advancements and retreats already eroded most of the terrigenous and shelf sediments, which were created by the river systems and other erosional processes in the pre-glacial and transitional regimes. Hence resulting in lower sediment supply due to established ice sheets and bedrock erosion and smaller interglacial cycles (Fig. 12D).

6. Conclusions

The interpretation of the deep-sea sedimentary record along the ~3300 km WS–SS seismic transect contribute to our understanding of the Cretaceous to Quaternary evolution of the Antarctic ice sheets in the Weddell Sea basin. The main contributions are summarised in the following conclusions:

1. We developed a new seismic horizon stratigraphy for the Weddell Sea and southern Scotia Sea using boundary conditions from various datasets. Lower units (WS-S1, WS-S2, WS-S3 and WS-S4) were newly interpreted or re-interpreted. The upper 3 units (WS-S5, WS-S6 and WS-S7) are consistent with local scale studies.
2. The pre-glacial (WS-u1 to WS-u4), transitional (WS-u4 to WS-u5) and full glacial (WS-u5 to seafloor) boundary horizons were identified in the Weddell Sea basin and traced into the Jane and Powell Basins and southern Scotia Sea. The proposed seismic unit divisions are consistent with localized seismic stratigraphy studies around Antarctica in the Bellingshausen Sea (e.g. Scheuer et al., 2006), Wilkes Land (e.g. Escutia et al., 2011) East Antarctica (Leitchenkov et al., 2007), Scotia Sea and Antarctic Peninsula basins (Maldonado et al., 2006) and Weddell Sea (Miller et al., 1990), but disagrees with the stratigraphy of Rogenhagen et al. (2004).

3. Average values for the complete pre-glacial sequence in the Weddell Sea (excluding Jane and Powell Basins): sediment thickness = 1100 m, sedimentation rate = 2.7 cm/ky, volume = 1.3×10^6 km²; the transitional sequence: sediment thickness = 530 m, sedimentation rate = 6.4 cm/ky, volume = 0.7×10^6 km³ and; the complete full glacial sequence: sediment thickness = 880 m, sedimentation rate = 5.5 cm/ky, volume = 1.1×10^6 km³.
4. In the pre-glacial sequence (WS-S1, WS-S2 and WS-S3), a deposition mound-and-eroded-flank basin geometry lateral variation in sediment thickness, and sedimentation rates calculated from published interval velocity data support a Cretaceous proto-Weddell Gyre hypothesis. A deeper depression on the east of the mound, ascribed to higher erosion hints at a probable clockwise circulation, but in the absence of clear drift structures an anti-clockwise circulation cannot be excluded.
5. The transitional unit (WS-S4 or T-1) is interpreted to represent high sediment supply through accelerated down-slope mass sediment transport deposits such as turbidites, considered indicative of advancing ice sheets grounding on the outer shelf. The cross-basin occurrence and lateral age variation of this unit (~27 Ma in the southeastern Weddell Sea to ~11 Ma in the northwest) imply initial Oligocene grounding of the WAIS and initial early Miocene grounding of the APIS.
6. In the full glacial sequence, the up to 975 m thick WS-S5 unit is continuous and fills the depressions on either side of the mound-and-eroded-flank topography of the pre-glacial and transitional regimes. WS-S5 represents increased deep-sea sediment deposition due to amplified downslope sediment supply in response to advancing ice sheets permanently grounding on the outer shelf. The lateral continuity and age of this unit (~18–6 Ma from southeast to northwest) implies concurrent advancement and grounding of the EAIS, WAIS and APIS during the late to early Miocene.
7. The even distribution of the full glacial sequence along the transect suggests that early ice sheet/ice caps/glaciers must have transported sediments not only from the Ronne–Filchner outflow system but also from the Antarctic Peninsula. This is consistent with Smith and Anderson (2010) and implies expansion of the southern APIS to the outer shelf, earlier than the Pleistocene predicted in palaeoclimate models (e.g. Pollard and DeConto, 2009).
8. The younger glacial units WS-S6 and WS-S7 reflect decreased sediment supply to the basin, which is consistent with a reduction in sediment supply following the establishment of a polar glacial regime.

Our Weddell Sea basin seismic stratigraphy rests on the assumption that changes in the observed seismic pattern represent pre-glacial, transitional and full glacial sequences. The presented age model has been derived from all available age information, geophysical and stratigraphic data. The greatest uncertainties lie in the velocity model and estimated horizon ages. Even so, we consider these results a best estimate for deriving a working hypothesis although the lateral horizon ages within the sedimentary column are only constrained by secondary information. The identification of pre-glacial to glacial components in the deep-sea sediment archive enabled an initial quantification of sediment volumes and thicknesses and rates, which are useful to constrain future palaeobathymetry and palaeotopography reconstructions.

Supplementary data to this article can be found online at <http://dx.doi.org/10.1016/j.margeo.2012.11.004>.

Acknowledgements

YMM and AM thank the “Ministerio de Ciencia e Innovación” of Spain for support through the FPI programme and CGL2004-05646/ANT, CTM2008-06386-CO2/ANT and CTM2011-30241-CO2-01 projects. The study benefited greatly from a three-month research visit of YMM

to the Alfred Wegener Institute. We thank M. Rebesco and J. Anderson for their thorough evaluation and reviews of this paper. Colleagues J. Grützner, C. Läderach, M. Mieth and G. Uenzelmann-Neben are sincerely thanked for fruitful discussions that improved the manuscript significantly. This project has been funded through the Priority Program 1158 ‘Antarctic Research’ of the Deutsche Forschungsgemeinschaft under project number GO 724/10-1 (AL and KG) and contributes to the Circum-Antarctic Stratigraphy and Palaeobathymetry project (CASP), a Scientific Committee on Antarctic Research – Antarctic Climate Evolution (SCAR-ACE) working group. In memory to Peter Barker who passed away this year (25.06.2012), for his contributions as Principal Investigator on RRS Discovery Cruise 154 which collected line BAS845-15 line, the critical link in the WS-SS transect, and as Co-Chief Scientist on ODP Leg 113, which provided most of the available age control.

References

- Amante, C., Eakins, B.W., 2009. ETOPO1 1 Arc-Minute Global Relief Model: Procedures, Data Sources and Analysis. NOAA Technical Memorandum NESDIS NGDC-24. (19 pp.).
- Anderson, J.B., 1999. Antarctic Marine Geology. Cambridge University Press, Cambridge, (289 pp.).
- Anderson, J.B. (Ed.), 2006. SHALDRIL II Cruise Report (<http://shaldril.rice.edu/>, 369 pp.).
- Anderson, J.B., Wellner, J.S. (Eds.), 2011. Tectonic, Climatic, and Cryospheric Evolution of the Antarctic Peninsula. Geopress, American Geophysical Union, Washington DC, USA. <http://dx.doi.org/10.1029/SP063> (218 pp.).
- Anderson, J.B., Warny, S., Askin, R., Wellner, J., Bohaty, S., Smith, T., 2011. Cenozoic cryosphere expansion and the demise of Antarctica’s last refugium. Proceedings of the National Academy of Science 108, 11299–11726.
- Barker, P.F., 2001. Scotia Sea regional tectonic evolution: implications for mantle flow and palaeocirculation. Earth-Science Reviews 55, 1–39.
- Barker, P.F., Thomas, E., 2004. Origin, signature and palaeoclimate influence of the Antarctic Circumpolar Current. Earth-Science Reviews 55, 1–39. <http://dx.doi.org/10.1016/j.earscirev.2003.10.003>.
- Barker, P.F., Kennett, J.P., et al., 1988. Proceedings of the Ocean Drilling Program, Scientific Results Leg 113. Ocean Drilling Program, College Station, TX. <http://dx.doi.org/10.2973/odp.proc.ir.113.1988>. (774 pp.).
- Barker, P.F., Dalziel, I.W.D., Storey, B.C., 1991. Tectonic development of the Scotia Arc region. Tingey, R.J. Žed., Geology of Antarctica. Oxford Univ. Press, Oxford, In: pp. 215–248.
- Bart, P.J., De Batist, M., Jokat, W., 1999. Interglacial collapse of Cray trough-mouth Fan, Weddell Sea, Antarctica: implications for Antarctic glacial history. Journal of Sedimentary Research 69 (6), 1276–1289. <http://dx.doi.org/10.1306/D4268B5D-2B26-11D7-8648000102C1865D>.
- Bart, P.J., Egan, D., Warny, S.A., 2005. Direct constraints on Antarctic Peninsula Ice Sheet grounding events between 5.12 and 7.94 Ma. Journal of Geophysical Research 110, F04008. <http://dx.doi.org/10.1029/2004JF000254>.
- BAS, 1985. Tectonic map of Scotia Arc, sheet 3, scale 1:3,000,000. British Antarctic Survey, Cambridge.
- Bentley, M.J., Fogwill, C.J., Le Brocq, A.M., Hubbard, A.L., Sugden, D.E., Dunai, T.J., Freeman, S.P.H.T., 2010. Deglacial history of the West Antarctic Ice Sheet in the Weddell Sea embayment: constraints on past ice volume change. Geology 38 (5), 411–414.
- Berner, R.A., Kothavala, Z., 2001. GEOCARB III: A revised model of atmospheric CO₂ over Phanerozoic time. American Journal of Science 304, 397–437.
- Bohaty, S.M., Kulhanek, D.K., Wise Jr., S.W., Jemison, K., Warny, S., Sjunneskog, C., 2011. Age Assessment of Eocene-Pliocene Drill Cores Recovered During the SHALDRIL II Expedition, Antarctic Peninsula. In: Anderson, J.B., Wellner, J.S. (Eds.), Tectonic, Climatic, and Cryospheric Evolution of the Antarctic Peninsula. Special Publication, 63. American Geophysical Union, pp. 63–113. <http://dx.doi.org/10.1029/2010SP001049>.
- Bohoyo, F., 2004. Fragmentación continental y desarrollo de cuencas oceánicas en el sector meridional del Arco de Scotia, Antártida. Ph. D Thesis, University of Granada, Granada, 252 pp.
- Bohoyo, F., Galindo-Zaldívar, J., Maldonado, A., Schreider, A.A., Suriñach, E., 2002. Basin development subsequent to ridge-trench collision: the Jane Basin, Antarctica. Marine Geophysical Research 23, 413–421. <http://dx.doi.org/10.1023/B:MARI.0000018194.18098.0d>.
- Bohoyo, F., Galindo-Zaldívar, J., Jabaloy, A., Maldonado, A., Rodríguez-Fernández, J., Schreider, A., Suriñach, E., 2007. Extensional deformation and development of deep basins associated with the sinistral transcurrent fault zone of the Scotia–Antarctic plate boundary. Geological Society, London, Special Publications 290, 203–217. <http://dx.doi.org/10.1144/SP290.6>.
- Boyd, J., Müller, R., Gurnis, M., Torsvik, T., Clark, J., Turner, M., Ivey-Law, H., Watson, R., Cannon, J., 2011. Next-generation plate-tectonic reconstructions using GPlates. In: Keller, G., Bar, C. (Eds.), Geoinformatics: Cyber infrastructure for the Solid Earth Sciences. Cambridge University Press, pp. 95–114.
- Brown, B., Gaina, C., Müller, R.D., 2006. Circum-Antarctic palaeobathymetry. Palaeogeography, Palaeoclimatology, Palaeoecology 231, 158–168. <http://dx.doi.org/10.1016/j.palaeo.2005.07.033>.

- Busetti, M., Zanolla, C., Marchetti, A., 2000. Geological structure of the South Orkney microcontinent. *Terra Antarctica* 8 (2), 71–78.
- Cande, S.C., Kent, D.V., 1995. Revised calibration of the geomagnetic polarity timescale for the Late Cretaceous and Cenozoic. *Journal of Geophysical Research* 100 (B4), 6093–6095.
- Coren, F., Geccone, G., Lodolo, E., Zanolla, C., Zitellini, N., Bonazzi, C., Centonze, J., 1997. Morphology, seismic structure and tectonic development of the Powell Basin, Antarctica. *Journal of the Geological Society* 154, 849–862.
- Coxall, H.K., Wilson, P.A., P'alihe, H., Lear, C.H., Backman, J., 2005. Rapid stepwise onset of Antarctic glaciation and deeper calcite compensation in the Pacific Ocean. *Nature* 433, 53–57. <http://dx.doi.org/10.1038/nature03135>.
- Davies, B.J., Hambrey, M.J., Smellie, J.L., Crrivick, J.L., Glasser, N.F., 2012. Antarctic Peninsula ice sheet evolution during the Cenozoic era. *Quaternary Science Reviews* 31, 30–66. <http://dx.doi.org/10.1016/j.quascirev.2011.10.012>.
- DeConto, R.M., Pollard, D., 2003. Rapid Cenozoic glaciation of Antarctica induced by declining atmospheric CO₂. *Nature* 421, 245–249. <http://dx.doi.org/10.1038/nature01290>.
- DeSantis, L., Brancolini, G., Donda, F., 2003. Seismo-stratigraphic analysis of the Wilkes Land continental margin (East Antarctica): influence of glacially driven processes on the Cenozoic deposition. *Deep Sea Research Part II: Topical Studies in Oceanography* 50 (8–9), 1563–1594. [http://dx.doi.org/10.1016/S0967-0645\(03\)00079-1](http://dx.doi.org/10.1016/S0967-0645(03)00079-1).
- Diester-Haass, L., Robert, C., Chamley, H., 1996. The Eocene-Oligocene preglacial–glacial transition in the Atlantic sector of the Southern Ocean (ODP Site 690). *Marine Geology* 31, 123–149 (SSDI 0025-3227 (95)00174-3).
- Dingle, R.V., Lavelle, M., 1998. Late Cretaceous–Cenozoic climatic variations of the northern Antarctic Peninsula: new geo-chemical evidence and review. *Palaeogeography, Palaeoclimatology, Palaeoecology* 141, 215–232. [http://dx.doi.org/10.1016/S0031-0182\(98\)00056-X](http://dx.doi.org/10.1016/S0031-0182(98)00056-X).
- Diviacco, P., Rebesco, M., Camerlenghi, A., 2006. Late Pliocene mega debris flow deposit and related fluid escapes identified on the Antarctic Peninsula continental margin by seismic reflection data analysis. *Marine Geophysical Research* 27 (2), 109–128. <http://dx.doi.org/10.1007/s11001-005-3136-8>.
- Eagles, G., 2010. The age and origin of the central Scotia Sea. *Geophysical Journal International* 183 (2), 587–600. <http://dx.doi.org/10.1111/j.1365-246X.2010.04781.x>.
- Eagles, G., Livermore, R.A., 2002. Opening history of Powell Basin, Antarctic Peninsula. *Marine Geology* 195–205. [http://dx.doi.org/10.1016/S0025-3227\(02\)00191-3](http://dx.doi.org/10.1016/S0025-3227(02)00191-3).
- Eagles, G., Livermore, R.A., Fairhead, J.D., Morris, P., 2005. Tectonic evolution of the west Scotia Sea. *Journal of Geophysical Research* 110, B02401. <http://dx.doi.org/10.1029/JB2004003154>.
- Eagles, G., Livermore, R.A., Morris, P., 2006. Small basins in the Scotia Sea: the Eocene Drake Passage gateway. *Earth and Planetary Science Letters* 242, 343–353. <http://dx.doi.org/10.1016/j.epsl.2005.11.060>.
- Escutia, C., Brinkhuis, H., Klaus, A., the Expedition 318 Scientists, 2011. Proceedings IODP leg 318. Integrated Ocean Drilling Program Management International, Inc., Tokyo. <http://dx.doi.org/10.2204/iodp.proc.318.2011>.
- Ferris, J.K., Vaughan, A.P.M., Storey, B.C., 2000. Relics of a complex triple junction in the Weddell Sea embayment, Antarctica. *Earth and Planetary Science Letters* 178, 215–230.
- Galindo-Zaldívar, J., Bohoyo, F., Maldonado, A., Schreider, A., Surinách, E., Vázquez, J.T., 2006. Propagating rift during the opening of a small oceanic basin: the Protector Basin (Scotia Arc, Antarctica). *Earth and Planetary Science Letters* 241, 398–412. <http://dx.doi.org/10.1016/j.epsl.2005.11.056>.
- Gersonde, R., Burckle, L.H., 1990. Neogene diatom biostratigraphy of ODP Leg 113, Weddell Sea (Antarctic Ocean). In: Barker, P.F., Kennett, J.P. (Eds.), *Proceedings of the Ocean Drilling Program Science Results*, pp. 761–789. College Station, TX.
- Ghidella, M., La Brecque, J., 1997. The Jurassic conjugate margins of the Weddell Sea: considerations based on magnetic, gravity and paleobathymetry data. In: Ricci, C. (Ed.), *The Antarctic region: Geological Evolution and Processes*. Terra Antarctica Publication, pp. 441–451.
- Ghidella, M.E., Yáñez, G., LaBrecque, J.L., 2002. Revised tectonic implications for the magnetic anomalies of the western Weddell Sea. *Tectonophysics* 347, 65–86. [http://dx.doi.org/10.1016/S0040-1951\(01\)00238-4](http://dx.doi.org/10.1016/S0040-1951(01)00238-4).
- Gradstein, F.M., Agterberg, F.P., Ogg, J.G., Hardenbol, J., van Veen, P., Thierry, T., Huang, Z., 1994. A Mesozoic time scale. *Journal of Geophysical Research* 99 (B12), 24051–24074.
- Gradstein, F.M., Ogg, J.G., Smith, A.G., Bleeker, W., Lourens, L.J., 2004. A new Geologic Time Scale, with special reference to Precambrian and Neogene. *Episodes* 27, 83–100.
- Haq, B.U., Schutter, S.R., 2008. A chronology of Paleozoic sea-level changes. *Science* 322 (5898), 64–68. <http://dx.doi.org/10.1126/science.1161648>.
- Hayes, D.E., La Brecque, J.L., 1991. Sediment isopachs: circum-Antarctic to 30°S. In: Hayes, D.E. (Ed.), *Marine Geological and Geophysical Atlas of the Circum-Antarctic to 30°S*. Antarctic Research Series, 54. American Geophysical Union, Washington, D. C., pp. 29–35.
- Hayes, D.E., Zhang, C., Weissel, R.A., 2009. Modeling Paleobathymetry in the Southern Ocean. *EOS, Transactions of the American Geophysical Union* 90 (19), 165–172.
- Hinz, K., 1981. A hypothesis of terrestrial catastrophes - Wedges of verythick oceanward dipping layers beneath passive continental margins - Their origin and paleoenvironmental significance. *Geologisches Jahrbuch* E22, 3–28.
- Hinz, K., Krause, W., 1982. The continental margin of Queen Maud Land/Antarctica: seismic sequences, structural elements and geological development. *Geologisches Jahrbuch* E23, 17–41.
- Hinz, K., Kristoffersen, Y., 1987. Antarctica, recent advances in the understanding of the continental shelf. *Geologisches Jahrbuch* E37, 3–54.
- Hunter, R.J., Johnson, A.C., Aleshkova, N.D., 1996. Aeromagnetic data from the southern Weddell Sea embayment and adjacent areas: Synthesis and interpretation. In: Storey, B.C., King, E.C., Livermore, R.A. (Eds.), *Weddell Sea Tectonics and Gondwana Break-up: Geological Society Special Publication*, 108, pp. 143–154 (London).
- Jamieson, S.S.R., Sugden, D.E., Hulton, N.R.J., 2010. The evolution of the subglacial landscape of Antarctica. *Earth and Planetary Science Letters* 293, 1–27. <http://dx.doi.org/10.1016/j.epsl.2010.02.012>.
- Jokat, W., Hübscher, C., Meyer, U., Oszko, L., Schöne, T., Versteeg, W., Miller, H., 1996. The continental margin off East Antarctica between 10°W and 30°W. In: Storey, B., King, E.C., Livermore, R.A. (Eds.), *Weddell Sea Tectonics and Gondwana Break-up: Geological Society Special Publication*, 108, pp. 129–141 (London).
- Jokat, W., Boebel, T., König, M., Meyer, U., 2003. Timing and geometry of early Gondwana breakup. *Journal of Geophysical Research* 108 (B9), 2428. <http://dx.doi.org/10.1029/2002JB001802>.
- Kent, T.R., Gradstein, F.M., 1986. A Jurassic to recent chronology. In: Vogt, P.R., Tucholke, B.E. (Eds.), *The Geology of North America, Volume M. The Western North Atlantic Region*, Geological Society of America.
- Kennett, J.P., Houtz, R.E., Andrews, P.B., Edwards, A.R., Gostin, V.A., Hajos, M., Hampton, M., Jenkins, D.G., Margolis, S.V., Ovenshine, A.T., Perch-Nielsen, K., 1975. Cenozoic paleoceanography in the southwest Pacific Ocean, Antarctic glaciation, and the development of the circum-Antarctic current. In: Kennett, J.P., Houtz, R.E. (Eds.), *Initial Report DSDP 29*. US Government Printing Office, Washington, pp. 1155–1169.
- König, M., Jokat, W., 2006. The Mesozoic breakup of the Weddell Sea. *Journal of Geophysical Research* 111 (B12102). <http://dx.doi.org/10.1029/2005JB004035>.
- Kovacs, L.C., Morris, P., Brozena, J., Tikku, A., 2002. Seafloor spreading in the Weddell Sea from magnetic and gravity data. *Tectonophysics* 347, 43–64. [http://dx.doi.org/10.1016/S0040-1951\(01\)00237-2](http://dx.doi.org/10.1016/S0040-1951(01)00237-2).
- Kristoffersen, Y., Haugland, K., 1986. Geophysical evidence for East Antarctic plate boundary in the Weddell Sea. *Nature* 322, 538–541. <http://dx.doi.org/10.1038/322538a0>.
- Kuvaas, B., Kristoffersen, Y., 1991. The Cray Fan: a trough-mouth fan on the Weddell Sea Continental Margin, Antarctica. *Marine Geology* 97, 345–362.
- LaBrecque, J.L., Ghidella, M.E., 1997. Bathymetry, depth to magnetic basement, and sediment thickness estimates from aerogeophysical data over the western Weddell Sea. *Journal of Geophysical Research* 102, 7929–7945. <http://dx.doi.org/10.1029/96JB01264>.
- LaBrecque, J.L., Cande, S., Bell, R., Raymond, C., Brozena, J., Keller, M., Parra, J.C., Yáñez, G., 1986. Aerogeophysical survey yields new data in the Weddell Sea. *Antarctic Journal Review* 21, 69–71.
- Larter, R.D., Barker, P.F., 1989. Seismic stratigraphy of the Antarctic Peninsula Pacific margin: a record of Pliocene–Pleistocene ice volume and paleoclimate. *Geology* 17, 731–734. [http://dx.doi.org/10.1130/0091-7613\(1989\)017<0731:SSOTAP>2.3.CO;2](http://dx.doi.org/10.1130/0091-7613(1989)017<0731:SSOTAP>2.3.CO;2).
- Larter, R.D., Cunningham, A.P., 1993. The depositional pattern and distribution of glacial–interglacial sequences on the Antarctic Peninsula Pacific margin. *Marine Geology* 109, 203–219. [http://dx.doi.org/10.1016/0025-3227\(93\)90061-Y](http://dx.doi.org/10.1016/0025-3227(93)90061-Y).
- Laske, G., Masters, G., 1997. A global digital map of sediment thickness. *EOS, Transactions American Geophysical Union* 78 (46), F483 (Fall Meeting Supplement).
- Lawver, L.A., Gahagan, L.M., 1998. Opening of Drake Passage and its impact on Cenozoic ocean circulation. In: Crowley, T.J., Burke, K.C. (Eds.), *Tectonic Boundary Conditions for Climate Reconstructions*. Oxford Monographs on Geology and Geophysics. Oxford University Press, Oxford, pp. 212–223.
- Lawver, L.A., Gahagan, L., 2003. Evolution of Cenozoic Seaways in the circum-Antarctic region. *Palaeogeography, Palaeoclimatology, Palaeoecology* 198, 11–37. [http://dx.doi.org/10.1016/S0031-0182\(03\)00392-4](http://dx.doi.org/10.1016/S0031-0182(03)00392-4).
- Le Brocq, A.M., Payne, A.J., Vieli, A., 2010. An improved Antarctic dataset for high resolution numerical ice sheet models (ALBMAP v1). *Earth System Science Data Discussions* 3, 195–230. <http://dx.doi.org/10.5194/essdd-3-195-2010> (www.earth-syst-sci-data-discuss.net/3/195/2010/).
- Lear, C.H., Bailey, T.R., Pearson, P.N., Coxall, H.K., Rosenthal, Y., 2008. Cooling and ice growth across the Eocene–Oligocene transition. *Geology* 36, 251–254. <http://dx.doi.org/10.1130/G24584A.1>.
- Leitchenkov, G.L., Guseva, Y.B., Gandyukhin, V.V., 2007. Cenozoic environmental changes along the East Antarctic continental margin inferred from regional seismic stratigraphy. In: Cooper, A.K., Raymond, C.R. (Eds.), *Antarctica: A Keystone in a Changing World—Online Proceedings of the 10th ISAES: USGS Open-File Report 2007-1047*, Short Research Paper 005. <http://dx.doi.org/10.3133/of2007-1047.srp005>.
- Leitchenkov, G., Guseva, J., Gandyukhin, V., Grikurov, G., Kristoffersen, Y., Sand, M., Golynsky, A., Aleshkova, N., 2008. Crustal structure and tectonic provinces of the Riiser-Larsen Sea are (East Antarctica): results of Geophysical studies. *Marine Geophysical Research* 29, 135–158. <http://dx.doi.org/10.1007/s11011-008-9051-z>.
- Lindeque, A., Martos, Y.M., Gohl, K., Maldonado, A., 2012. Seafloor Spreading Magnetic Anomaly Isochron Map Compilation for the Weddell Sea and Scotia Sea. <http://dx.doi.org/10.1594/PANGAEA.777453> (www.pangea.de).
- Livermore, R.A., Hunter, R.J., 1996. Mesozoic seafloor spreading in the southern Weddell Sea. In: Storey, B., King, E.C., Livermore, R.A. (Eds.), *Weddell Sea Tectonics and Gondwana Break-up: Geological Society Special Publication*, 108, pp. 227–241 (London).
- Livermore, R.A., Balanyá, J.C., Maldonado, A., Martínez, J.M., Rodríguez-Fernández, J., Sanz de Galdeano, C., Galindo-Zaldívar, J., Jabaloy, A., Barnolas, A., Somoza, L., Hernández, J., Surinách, E., Víseras, C., 2000. Autopsy on a dead spreading centre: the Phoenix Ridge, Drake Passage, Antarctica. *Geology* 18, 607–610. [http://dx.doi.org/10.1130/0091-7613\(2000\)28<607:AOADSC>2.0.CO;2](http://dx.doi.org/10.1130/0091-7613(2000)28<607:AOADSC>2.0.CO;2).
- Livermore, R., Nankivell, A., Eagles, G., Morris, P., 2005. Paleogene opening of Drake Passage. *Earth and Planetary Science Letters* 236, 459–470. <http://dx.doi.org/10.1016/j.epsl.2005.03.027>.
- Livermore, R.A., Hillenbrand, C.-D., Meredith, M., Eagles, G., 2007. Drake Passage and Cenozoic climate: an open and shut case? *Geochemistry, Geophysics, Geosystems* 8, Q01005. <http://dx.doi.org/10.1029/2005GC001224>.

- Lodolo, E., Coren, F., Schreider, A.A., Ceccone, G., 1998. Geophysical evidence of a relict oceanic crust in the southwestern Scotia Sea. *Marine Geophysical Research* 19, 439–450. <http://dx.doi.org/10.1023/A:1004355707951>.
- Lodolo, E., Civile, D., Vuan, A., Tassone, A., Geletti, R., 2010. The Scotia–Antarctica plate boundary from 35°W to 45°W. *Earth and Planetary Science Letters* 293, 200–215. <http://dx.doi.org/10.1016/j.epsl.2009.12.045>.
- Lythe, M.B., Vaughan, G.D., the BEDMAP Consortium, 2001. BEDMAP: a new ice thickness and subglacial topographic model of Antarctica. *Journal of Geophysical Research* 106, 11335–11351. <http://dx.doi.org/10.1029/2000JB900449>.
- Maldonado, A., Aldaya, F., Balanya, J.C., Galindo-Zaldívar, J., Livermore, R.A., Monsen, F.M., Rodríguez-Fernández, J., Roussanov, M., Sanz de Galdeano, C., Surin, E., Viseras, C., 1993. Tectonics and paleoceanography in the northern sector of the Antarctic Peninsula: preliminary results of HESANT1992/93 cruise with the B/O HESPERIDES. *Scientia Marina* 57 (1), 79–89.
- Maldonado, A., Zitellini, N., Leitchenkov, G., Balanya, J.C., Coren, F., Galindo-Zaldívar, J., Lodolo, E., Jabaloy, A., Zanol, C., Rodríguez-Fernández, J., Vinnikovskaya, O., 1998. Small ocean basin development along the Scotia–Antarctica plate boundary and in the northern Weddell Sea. *Tectonophysics* 296, 371–402.
- Maldonado, A., Balanya, J.C., Barnolas, A., Galindo-Zaldívar, J., Hernández, J., Jabaloy, A., Livermore, R., Martínez-Martínez, J.M., Rodríguez-Fernández, J., Sanz de Galdeano, C., Somoza, L., Suriñach, E., Viseras, C., 2000. Tectonics of an extinct ridge-transform intersection, Drake Passage (Antarctica). *Marine Geophysical Research* 21, 43–68. <http://dx.doi.org/10.1023/A:1004762311398>.
- Maldonado, A., Barnolas, A., Bohoyo, F., Galindo-Zaldívar, J., Hernández-Molina, J., Lobo, F., Rodríguez-Fernández, J., Somoza, L., Vázquez, J.T., 2003. Contourite deposits in the central Scotia Sea: the importance of the Antarctic Circumpolar Current and Weddell Gyre flows. *Palaeogeography, Palaeoclimatology, Palaeoecology* 198, 187–221. [http://dx.doi.org/10.1016/S0031-0182\(03\)00401-2](http://dx.doi.org/10.1016/S0031-0182(03)00401-2).
- Maldonado, A., Barnolas, A., Bohoyo, F., Escutia, C., Galindo-Zaldívar, J., Hernández-Molina, F.J., Jabaloy, A., Lobo, F.J., Nelson, C.H., Rodríguez-Fernández, J., Somoza, L., Vázquez, J.T., 2005. Miocene to recent contourite drifts development in the northern Weddell Sea (Antarctica). *Global Planet Change* 45, 99–129.
- Maldonado, A., Bohoyo, F., Galindo-Zaldívar, J., Hernández-Molina, F.J., Jabaloy, A., Lobo, F.J., Rodríguez-Fernández, J., Suriñach, E., Vázquez, J.T., 2006. Ocean basins near the Scotia–Antarctic plate boundary: influence of tectonics and paleoceanography on the Cenozoic deposits. *Marine Geophysical Research* 27, 83–107. <http://dx.doi.org/10.1007/s11001-006-9003-4>.
- Maldonado, A., Bohoyo, F., Galindo-Zaldívar, J., Hernández-Molina, F.J., Lobo, F.J., Shreyder, A.A., Suriñach, E., 2007. Early opening of Drake Passage: regional seismic stratigraphy and paleoceanographic implications, in Antarctica: A Keystone in a Changing World. Extended Abstract EA57, online Proceedings of the 10th International Symposium on Antarctic Sciences (ISAES). In: Cooper, A.K., Raymond, C.R., et al. (Eds.), USGS Open-File Report (<http://pubs.usgs.gov/of/2007/1047/ea/of2007-1047ea057.pdf>).
- Michels, K.H., Rogenhagen, J., Kuhn, G., 2001. Recognition of contour-current influence in mixed contourite–turbidite sequences of the western Weddell Sea, Antarctica. *Marine Geophysical Research* 22, 465–485. <http://dx.doi.org/10.1023/A:1016303817273>.
- Michels, K.H., Kuhn, G., Hillenbrand, C.-D., Diekmann, B., Fütterer, D.K., Grobe, H., Uenzelmann-Neben, G., 2002. The southern Weddell Sea: combined contourite–turbidite sedimentation at the southeastern margin of the Weddell Gyre. In: Stow, D.A.V., Pudsey, C., Howe, J.C., Faugères, J.-C., Viana, A.R. (Eds.), *Geological Society of London, Memoirs*, 22, pp. 305–323. <http://dx.doi.org/10.1144/GSLMEM.2002.022.01.32>.
- Miller, H., Henriot, J.P., Kaul, N., Moons, A., 1990. A fine-scale stratigraphy of the eastern margin of the Weddell Sea. In: Bleil, U., Thiede, J. (Eds.), *Geological History of the Polar Oceans: Arctic Versus Antarctic*. Kluwer Academic Publishers, pp. 131–161.
- Miller, K.G., Wright, J.D., Katz, M.E., Browning, J.V., Cramer, B.S., Wade, B.S., Mizintseva, S.F., 2008. A view of Antarctic ice-sheet evolution from sea-level and deep-sea isotope changes during the Late Cretaceous–Cenozoic. In: Cooper, A.K., Barrett, P.J., Stagg, H., Storey, B., Stump, E., Wise, W., the 10th ISAES editorial team (Eds.), *Proceedings of the 10th International Symposium on Antarctic Earth Sciences*. The National Academies Press, Washington, DC. <http://dx.doi.org/10.3133/of2007-1047.kp06>.
- Nankivell, A.P., 1997. Tectonic evolution of the Southern Ocean. PhD thesis, Oxford University.
- Oszko, L., 1997. Tectonic structures and glaciomarine sedimentation in the South-Eastern Weddell Sea from seismic reflection data. *Berichte zur Polarforschung (Reports on Polar Research)*, 222. Alfred Wegener Institut für Polar und Meeresforschung, Bremerhaven, Germany. PhD thesis, University of Bremen. hdl:10013/epic.12931.
- Pagani, M., Zachos, J., Freeman, K.H., Tiplle, B., Bohaty, S., 2005. Marked decline in atmospheric carbon dioxide concentrations during the Paleogene. *Science* 309 (5734), 600–603. <http://dx.doi.org/10.1126/science.1110063>.
- Pollard, D., DeConto, R.M., 2009. Modelling West Antarctic ice sheet growth and collapse through the past five million years. *Nature* 458, 320–323. <http://dx.doi.org/10.1038/nature07809>.
- Pritchard, H.D., Arthern, R.J., Vaughan, D.G., Edwards, 2009. Extensive dynamic thinning on the margins of the Greenland and Antarctic ice sheets. *Nature* 461, 971–975. <http://dx.doi.org/10.1038/nature08471>.
- Ramsay, A.T.S., Baldauf, J.G., 1990. A reassessment of the Southern Ocean biochronology. *Memoirs of the Geological Society of America* 18, 1–122.
- Rebesco, M., Camerlenghi, A., 2008. Late Pliocene margin development and mega debris flow deposits on the Antarctic continental margins: evidence of the onset of the modern Antarctic Ice Sheet? *Palaeogeography, Palaeoclimatology, Palaeoecology* 260, 149–167.
- Rebesco, M., Camerlenghi, A., Geletti, R., Canals, M., 2006. Margin architecture reveals the transition to the modern Antarctic ice sheet ca. 3 Ma. *Geology* 34, 301–304. <http://dx.doi.org/10.1130/G22000.1>.
- Rignot, E.J., Bamber, J.L., van den Broeke, M.R., Davis, C., Li, Y., van de Berg, W., van Meijgaard, 2008. Recent Antarctic ice mass loss from radar interferometry and regional climate modelling. *Nature Geoscience* 1. <http://dx.doi.org/10.1038/ngeo102>.
- Ritzmann, O., 1998. Refraktionsseismische Untersuchungen am Kontinentalrand der Ostantarktis. Diploma thesis (unpublished), Rheinische Friedrich-Wilhelms Universität, Bonn.
- Rogenhagen, J., Jokat, W., 2000. The sedimentary structure in the western Weddell Sea. *Marine Geology* 168, 45–60. [http://dx.doi.org/10.1016/S0025-3227\(00\)00048-7](http://dx.doi.org/10.1016/S0025-3227(00)00048-7).
- Rogenhagen, J., Jokat, W., 2002. Origin of the gravity ridges and Anomaly-T in the southern Weddell Sea. In: Gamble, J.A., Skinner, D.N.B., Henrys, S. (Eds.), *Antarctica at the Close of a Millennium, Proceedings of the 8th International Symposium on Antarctic Earth Sciences*. Royal Society of New Zealand, Wellington, pp. 227–231.
- Rogenhagen, J., Jokat, W., Hinz, K., Kristoffersen, Y., 2004. Improved seismic stratigraphy of the Mesozoic Weddell Sea. *Marine Geophysical Researches* 25, 265–282. <http://dx.doi.org/10.1007/s11001-005-1335-y>.
- Scher, H.D., Martin, E.E., 2006. Timing and climatic consequences of the opening of Drake Passage. *Science* 312, 428–430.
- Scheuer, C., Gohl, K., Eagles, G., 2006. Gridded isopach maps from the South Pacific and their use in interpreting the sedimentation history of the West Antarctic continental margin. *Geochemistry, Geophysics, Geosystems* 7, Q11015. <http://dx.doi.org/10.1029/2006GC001315>.
- Smith, R.T., Anderson, J.B., 2010. Ice-sheet evolution in James Ross basin, Weddell Sea margin of the Antarctic Peninsula: the seismic stratigraphic record. *Geological Society of America Bulletin* 122 (5/6), 830–842. <http://dx.doi.org/10.1130/B26486.1>.
- Smith, R.T., Anderson, J.B., 2011. Seismic stratigraphy of the Joinville Plateau: implications for regional climate evolution. In: Anderson, J.B., Wellner, J.S. (Eds.), *Tectonic, Climatic, and Cryospheric Evolution of the Antarctic Peninsula*. Geopress, American Geophysical Union, Washington DC, USA, pp. 51–61. <http://dx.doi.org/10.1029/2010SP000980>.
- Smith, W.H.F., Sandwell, D.T., 1997. Global seafloor topography from satellite altimetry and ship depth soundings. *Science* 277, 1957–1962.
- Suriñach, E., Galindo-Zaldívar, J., Maldonado, A., Livermore, R., 1997. Large amplitude magnetic anomalies in the northern sector of the Powell Basin, NE Antarctic Peninsula. *Marine Geophysical Research* 19, 65–80. <http://dx.doi.org/10.1023/A:1004240931967>.
- Tripathi, A.K., Roberts, C.D., Eagle, R.A., 2009. Coupling of CO₂ and ice sheet stability over major climate transitions of the last 20 million years. *Science* 326, 1394–1397. <http://dx.doi.org/10.1016/j.gca.2011.01.018>.
- Tripathi, A.K., Roberts, C.D., Eagle, R.A., Li, G., 2011. A 20 million year record of planktic foraminiferal B/Ca ratios: systematics and uncertainties in pCO₂ reconstructions. *Geochimica et Cosmochimica Acta* 75 (10), 2582–2610. <http://dx.doi.org/10.1016/j.gca.2011.01.018>.
- Uenzelmann-Neben, G., 2006. Depositional patterns at Drift 7, Antarctic Peninsula: along-slope versus down-slope sediment transport as indicators for oceanic currents and climatic conditions. *Marine Geology* 233, 49–62. <http://dx.doi.org/10.1016/j.margeo.2006.08.008>.
- Wardell, N., Childs, J.R., Cooper, A.K., 2007. Advances through collaboration: sharing seismic reflection data via the Antarctic Seismic Data Library System for Cooperative Research (SDLS). In: Cooper, A.K., Raymond, C.R. (Eds.), *Antarctica: A Keystone in a Changing World—Online Proceedings of the 10th ISAES: USGS Open-File Report 2007-1047, Short Research Paper 001*. <http://dx.doi.org/10.3133/of2007-1047.srp001> (4 pp.).
- Wilson, D.S., Jamieson, S.S.R., Barrett, P.J., Leitchenkov, G., Gohl, K., Larter, R.D., 2011. Antarctic topography at the Eocene–Oligocene boundary. *Palaeogeography, Palaeoclimatology, Palaeoecology*. <http://dx.doi.org/10.1016/j.palaeo.2011.05.028>.
- Zachos, J.C., Kump, L.R., 2005. Carbon cycle feedbacks and the initiation of Antarctic glaciation in the earliest Oligocene. *Global and Planetary Change* 47, 51–66. <http://dx.doi.org/10.1016/j.gloplacha.2005.01.001>.
- Zachos, J., Pagani, M., Sloan, L., Thomas, E., Billups, K., 2001. Trends, rhythms, and aberrations in global climate 65 Ma to present. *Science* 292/5517, 686–693. <http://dx.doi.org/10.1126/science.1059412>.

**MARINE
GEOLOGY**

Initial Phase of the West Scotia Mid-Oceanic Ridge Opening

Al. A. Schreider^a, A. A. Schreider^b, J. Galindo-Zaldivar^c, A. Maldonado^d, and Y. Martos-Martin^d

^a *Open Joint-Stock Company, NIIGazekonomika, Moscow, Russia*

^b *Shirshov Institute of Oceanology, Russian Academy of Sciences, Moscow, Russia*

E-mail: aschr@ocean.ru

^c *University of Granada, Spain*

^d *Andalusia Institute of Earth Sciences, Granada, Spain*

Received December 29, 2010; in final form, September 8, 2011

Abstract—The first map illustrating the position of anomaly 12 extending in the NE–SW direction (25°) in the eastern peripheral part of the West Scotia Ridge is presented. Calculations of the paleomagnetic anomalies show that the spreading initiated in the period corresponding to Chron C12r (31.116–33.266 Ma ago). Chron C11r (30.217–30.627 Ma ago) was marked by a 200 km northwestward jump of the spreading axis. The calculation of the Euler poles and the rotation angles made it possible to reconstruct the zone of the initial breakup between South America and the Antarctic Peninsula along the western periphery of the continental Terror Rise.

DOI: 10.1134/S0001437012040091

INTRODUCTION

The formation of the Scotia Sea played the leading role in the destruction of the continental bridge between South America and Antarctica. Inasmuch as no deep-sea holes have yet been drilled in the Scotia Sea, the complex geological–geophysical interpretation of the data on the anomalous magnetic field represents the main tool for the study of this process.

Intense geological–geophysical investigations in the western Scotia Sea have been in progress since the mid-20th century [1–3, 5–9, 11, 12, 15, 18, 19, 22–25, 28, 29]. They revealed the abandoned West Scotia mid-oceanic ridge in the area with coordinates of 54 to 60° S and 41 to 67° W. In the bottom topography, the ridge is reflected in a horst-shaped rise over 500 km wide with highly differentiated relief. The ridge's crest towers up to 2 km above the surface of the adjacent abyssal plains of the Yagan and Ona basins in the northwest and southeast, respectively. The ridge is bordered by the Shackleton Fracture Zone in the west and by the southern peripheral part of the North Scotia Ridge in the east.

The ridge's axis corresponds to a high-amplitude (200–500 nT) magnetic anomaly up to 50 km wide. In the southeast and northwest, it joins magnetic anomalies with amplitudes of 100–300 nT and wave lengths of 20–40 km displaced along several transform faults for a few tens of kilometers. It should be noted that all the researchers emphasize the scarcity of factual data, which prevents the reliable discrimination between the younger and older paleomagnetic anomalies.

The complex analysis of the geophysical database developed by the authors of this work may be of help

for reconstructing the paleogeodynamics at the initial stage of the Drake Passage's opening. The database contains primarily available data on the anomalous magnetic field, including original data obtained recently by the Spanish R/V *Hesperides*. Of greatest importance is the geochronology of the bottom in the peripheral areas of the Ona Basin, which is discussed in these works. It should be noted that we use the latest scale of the linear magnetic anomalies in [20].

PECULIAR FEATURES OF THE BOTTOM SPREADING

The authors of [6, 10] were the first to identify linear magnetic anomalies in the Drake Passage east of the Shackleton Fracture Zone. According to their data, anomaly C8 is the oldest one, which means that the spreading initiated approximately 26 Ma ago and terminated around 6 Ma ago. Subsequently, this interpretation was multiply specified.

It was shown that the West Scotia mid-oceanic ridge and the adjacent basins are marked by a system of linear magnetic anomalies C3–C8 [1, 10–12, 28]. The authors of [21] proposed two alternative models for interpreting these anomalies. The first of them describes the observed undulations of the magnetic field by model anomalies C6C–C12 and the second one, by anomalies C4–C6. The authors themselves gave preference to the second model, according to which the spreading episode was dated back to 9–20 Ma.

At the same time, other investigations revealed a system of anomalies up to C10 in the southeastern part of the West Scotia Ridge and in the Ona and Yagan basins [1, 18, 24]. The geomagnetic investigations

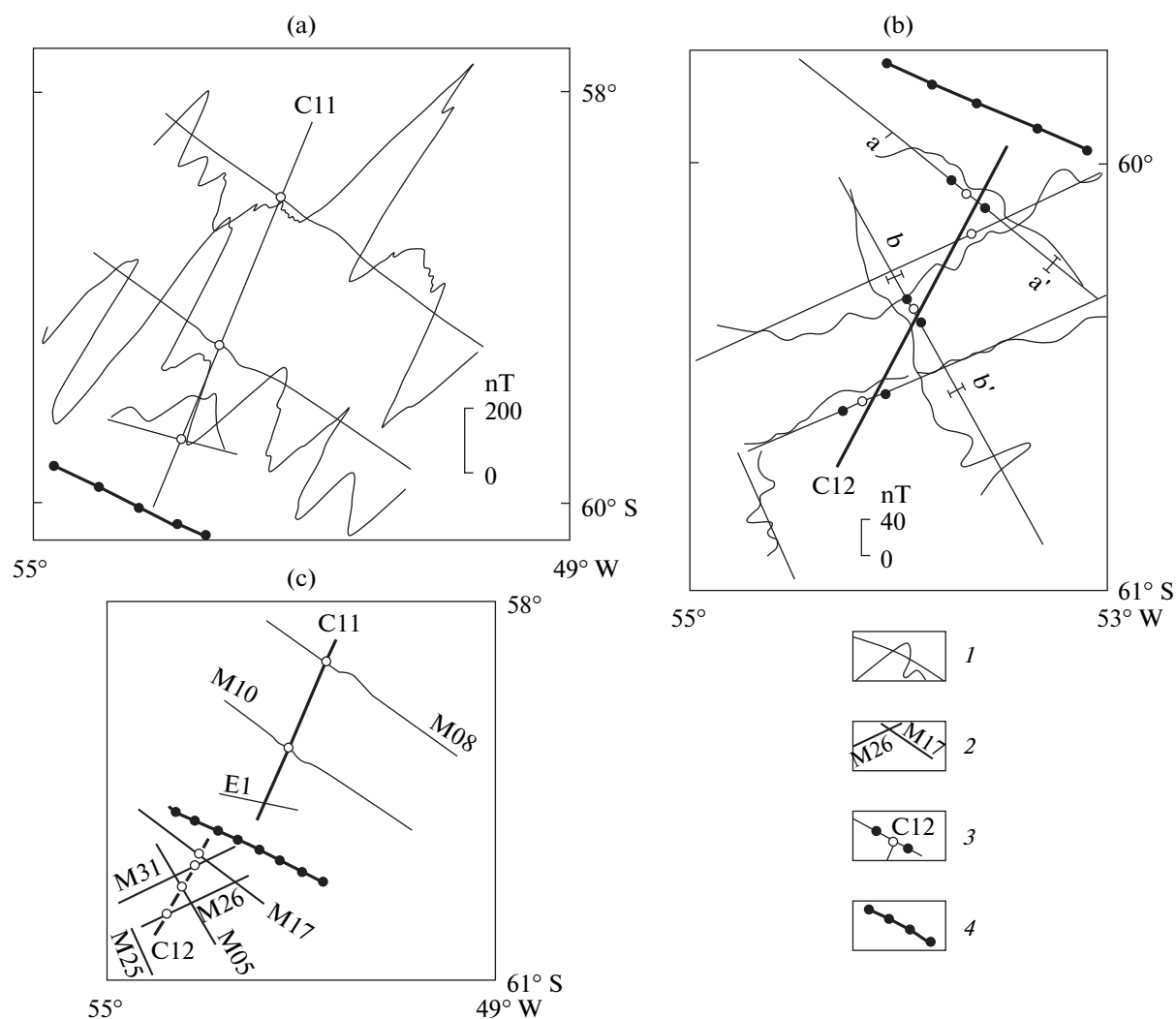


Fig. 1. The anomalous magnetic field along profiles M08, M10, and E1 (a) and M05, M17, M25, M26, and M31 (b) of the R/V *Hesperides*. The figure illustrates the correlation of the linear magnetic anomaly through the area (c) and its identification as C12 consistently with the modeling results in Fig. 2. The spatial position of its axis corresponds to the line of the initial breakup of the continental crust in the western peripheral part of the Terror Rise.

(1) plot of the anomalous magnetic field along the observation profiles; (2) observation profiles of the R/V *Hesperides*; (3) position of the axis of linear magnetic anomaly C12 and the oldest boundaries of Chron C12n; (4) position of the newly revealed transform fracture; segments a–a and b–b are as in Fig. 2.

conducted during Spanish research expeditions on the R/V *Hesperides* in 1992–1993 and 2004 (the SCAN expedition) yielded new data on the anomalous magnetic field in the southeastern part of the Ona Basin. For example, two additional undulations of the magnetic field are defined along the southwestern piedmonts of the Terror Rise in a small basin filled with sediments and underlain by the acoustic basement at depths exceeding 2 km. The joint areal analysis of the magnetic anomalies along profiles E1, M05, M08, M10, M17, M26, and M31 of the R/V *Hesperides* (Fig. 1) revealed their linear patterns with a NE–SW strike at an angle of $25 \pm 3^\circ$. If these undulations are of spreading origin, they may be interpreted in the context of the plate tectonics.

The linear magnetic anomalies were modeled with the assumption that the upper surface of the magnetoactive inversion layer corresponds to the surface of the crystalline basement and that the lower surface of this layer accepted to be 0.5 km thick is conformable with the basement's surface. The magnetization was accepted to be 2 A/m. The angular parameters of the magnetization vector were taken consistently with the parameters of the field of the earth's axis-symmetrical dipole, and the parameters of the present-day magnetic field correspond to the parameters of the DGRF field of the surveyed epoch.

The modeled geomagnetic data obtained by the Spanish expeditions allowed Chron C11r to be identified (Fig. 2). This provides grounds for considering the

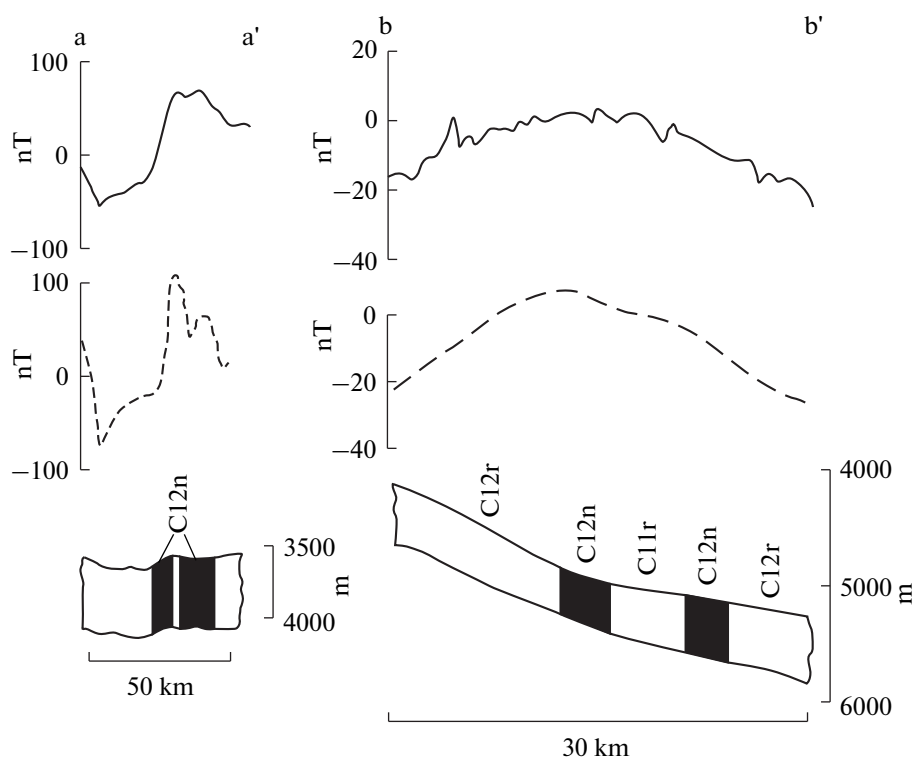


Fig. 2. Observed (solid line) and theoretical (dashed line) magnetic anomalies in the model of the bottom spreading along profiles *a-a* and *b-b* (the position of which is shown in Fig. 1). The calculation parameters of the theoretical magnetic anomalies are as in [15].

undulations of the anomalous magnetic field in the above-mentioned small basin at the base of the Terror Rise as corresponding to two symmetrically arranged chrons C12n and C12r [4, 13, 14, 16, 17, 27]. The episode of bottom spreading in this local basin occurred in the period of chrons C11r–C12r (30.2–33.2 Ma ago) with the spreading rate being equal approximately to 1 cm/year. The thorough analysis of these data points to the existence of a tectonic fracture that displaces the axis of linear magnetic anomaly C12 for a distance of approximately 30 km (Fig. 1).

It should be emphasized that anomaly C12 is indistinguishable at profile M25, which crosses the peripheral part of the Elephant Island block, which reflects the position of the southern boundary of the bottom spreading zone. Let us note that the results of the independent investigations in [26] yielded similar estimates for the onset of the spreading regime in the Scotia Sea (32 ± 2 Ma ago).

As was mentioned, according to the modeling, the abandoned paleospreading axis coincides with the reversely magnetized portion of new oceanic crust corresponding to Chron C12n located between two normally magnetized blocks (C12n), which are contiguous with two reversely magnetized blocks (C12r). The Euler poles and rotation angles were calculated for segments of Chron C12r(y). The pole position with coordinates of 19.8° S and 36° W and a rotation angle

module of 0.70° was used for reconstructing the mutual positions of the lower part of the basin's western slope and its counterpart contoured by the isohypse of 4 km on the eastern continental slope of the Terror Rise (map in [4]). The last map was compiled by combining the data from the electronic bottom topography map and on the thicknesses of the sedimentary cover. The isopach map of the Scotia Sea illustrates only the general (i.e., the most important) features of the sedimentary cover while lacking details. Nevertheless, it provides a certain idea of the sediment distribution through the region. It demonstrates that the thickness of the sediments is maximal in the south-eastern part of the region, where it amounts to 700–800 m. In the northwestern direction, it decreases to values of approximately 200 m.

The available data on the sedimentary cover were used for compiling the first electronic schematic map of the acoustic basement's surface for the western Scotia Sea, which is preliminary (taking into consideration the aforesaid about the isopach map) and illustrates only its most significant features [4]. The basement's surface in the axial part of the West Scotia paleospreading ridge is located at a depth of approximately 2 km. Toward the Yagan and Ona basins, it dips to 4 km in the west and >4.5 km in the east. In areas of the ridge's displacement by transform faults, the basement's surface dips locally to >5 km. It should be

noted that the compiled schematic map distinctly reveals some peculiar features of the transform faults while providing additional data on their positions and configurations, which were previously known only from the bottom topography.

The analysis of the calculated positions of the Euler pole shows that the slope areas corresponding to segments of chrons C12r(y) are relatively consistent with each other, which indicates that the western slope of the local basin is continental in origin, being formerly an element of the Terror Rise. In such a situation, the analyzed local basin should be underlain by the continental crust developed between the continental blocks separated during the initial stage of spreading in the peripheral part of the West Scotia mid-oceanic paleoridge. According to [15], the Terror Rise initially joined the Terro del Fuego area.

DISCUSSION

The new data provided grounds for the substantial revision of the available views on the configuration of the spreading paleoaxis during the initial phase of the bottom spreading in the West Scotia paleospreading ridge. According to these data, the spreading in the Drake Passage area presumably initiated during Chron C12r (31.1–33.2 Ma ago) and was in progress until Chron C11r (30.2–30.6 Ma ago) with rates of approximately 1 cm/year. The spatial position of the axis of linear magnetic anomaly C12 corresponds to the line of the initial continental crust's breakup in the western peripheral part of the Terror Rise.

The initial stage of the spreading in the West Scotia mid-oceanic paleoridge was accompanied by the breakup along the periphery of the Terror Rise and the separation of the continental block from the latter to form a narrow basin underlain by the oceanic crust bordered by continental blocks. Subsequently, the spreading axis jumped in the northwestern direction and the former axis was abandoned. This second phase of spreading was marked by the eventual separation of the Terror Rise from the Terro del Fuego massif.

CONCLUSIONS

Thus, the obtained new data reveal that the initial stage of the bottom's spreading in the Drake Passage area initiated along a spreading paleoaxis extending in the NE–SW direction (25°) in the western peripheral part of the Terror Rise during Chron C12r (31.116–33.266 Ma ago). They allowed the spatial position for the axis of the initial continental crust breakup to be established as well. Precisely, this episode of bottom spreading in the Drake Passage marks the beginning of the disintegration of the continental bridge between South America and Antarctica. This first phase terminated with a 200-km northwestward jump of the spreading axis during Chron C11r (slightly after 30.626 Ma ago) and the onset of the second stage of

the Drake Passage's opening. The disintegration of the continental bridge in the period of 31.116 to 33.266 Ma ago stimulated the formation of the Circum-Antarctic Current between the Pacific and Atlantic oceans marking the beginning of Antarctica's isolation in the studied region. This resulted, in turn, in the formation of new climatic conditions in the South Ocean.

ACKNOWLEDGMENTS

This work was supported by the Russian Foundation for Basic Research, project nos. 11-05-93981 INIS_a and 08-05-00138.

REFERENCES

1. *Atlas. Geological-Geophysical Atlas of the Atlantic Ocean* (GUGK, Moscow, 1990) [in Russian].
2. A. V. Zhivago, "Morphological Structure of the Bottom of the Southwestern Atlantic and Scotia Sea," *Trudy IO AN RAN*, **126**, 137–171 (1990).
3. G. B. Udintsev, G. V. Shenke, T. Shene, et al., "On the Bottom Structure of the Scotia Sea, Western Antarctic," *Doklady RAN*, **371**, No. 2, 243–247 (2000).
4. A. A. Shreider, Al. A. Shreider, G. L. Kashintsev, et al., "Peculiarities of Kinematics of the Mid-Oceanic West Scotia Ridge," *Okeanologiya*, **51**, No. 1, 175–187 (2011).
5. P. Barker, "A Spreading Center in the East Scotia Sea," *Earth and Planet. Sci. Lett.*, **15**, 123–132 (1972).
6. P. Barker, "The Cenozoic Subduction History of the Pacific Margin of the Antarctic Peninsula: Ridge Crest-Trench Interactions," *J. Geol. Soc. London*, **139**, 787–801 (1982).
7. P. Barker, "Scotia Sea Regional Tectonic Evolution: Implications for Mantle Flow and Paleocirculation," *Earth Science Reviews*, **55**, 1–39 (2001).
8. P. Barker and J. Burrell, "The Opening of Drake Passage," *Mar. Geol.*, **25**, 15–34 (1997).
9. P. Barker and I. Dalziel, in *Geodynamics of the Eastern Pacific Region, Caribbean and Scotia Arcs, Geodynamic Series* Vol. 9, 137–170 (1983).
10. P. F. Barker, I. Dalziel, and B. C. Storey, in *The Geology of Antarctica* (Oxford Science Publications, 1991) pp. 215–248.
11. P. Barker and I. Hill, "Back-Arc Extension in the Scotia Sea," *Phil. Trans. Royal Soc. London*, **300**, 249–262 (1981).
12. P. Barker and L. Lawver, "South American-Antarctic Plate Motion Over the Past 50 Myr, and the Evolution of the South American-Antarctic Ridge," *Geophys. J.*, **94**, 377–386 (1988).
13. F. Bohoyo, J. Galindo-Zaldivar, A. Jabaloy, et al., "Extensional Deformation and Development of Deep Basins Associated with the Transcurrent Fault Zone of the Scotia-Antarctic Plate Boundary," *Geol. Soc. Lond. Spec. Publ.*, **290**, 203–217 (2007a).
14. F. Bohoyo, J. Galindo-Zaldivar, A. Jabaloy, et al., "Desarrollo de Cuencas Extensionales Profundas con la Zona de Falla Transcurrente del Limite de Placas

- Scotia – Anarctica,” *Revista de la Sociedad Geologica de Espana*, **20**, Nos. 1–2, 89–103 (2007b).
- 1 15. G. Eagles, R. Livermore, D. Fairhead, and P. Morris, “Tectonic Evolution of the West Scotia Sea,” *J. Geophys. Res.*, **110**, 19 (2005).
 - 2 16. J. Galindo-Zaldívar, F. Bohoyo, and A. Maldonado, in *XXX Scientific Committee on Antarctic Research, Abstracts, St. Petersburg*, 67 (2008).
 - 3 17. J. Galindo-Zaldívar, A. Maldonado, J. Rodríguez-Fernández, et al., in *International Polar Year Science Conference, Abstracts, Oslo* No. EA10.1-2.3, 1 (2003).
 - 4 18. R. Geletti, E. Lodolo, A. Schreider, and A. Polonia, “Seismic Structure and Tectonics of the Shackleton Fracture Zone (Drake Passage, Scotia Sea),” *Mar. Geophys. Res.*, **26**, 17–28 (2005).
 19. M. Ghiglione, D. Yagupsky, M. Ghidella, and V. Ramos, “Continental Stretching Preceding the Opening of the Drake Passage: Evidence from Tierra del Fuego,” *Geology*, **36**, 643–646 (2008).
 20. F. Gradstein, J. Ogg, A. Smith, et al., *A Geologic Time Scale 2004* (Cam. Univ. Press, 2006).
 21. I. Hill and P. Barker, “Evidence for Miocene Back-Arc Spreading in the Scotia Sea,” *Geophys. J. R. Astr. Soc.*, **63**, 427–440 (1980).
 22. Y. Lagabrielle, Y. Goddard, Y. Donnadiou, et al., “The Tectonic History of Drake Passage and Its Possible Impacts on Global Climate,” *Earth and Planet. Sci. Lett.*, **279**, 197–211 (2009).
 23. E. Lodolo, D. Civile, A. Vuan, et al., “The Scotia–Antarctica Plate Boundary from 35° W to 45° W,” *Earth Planet. Sci. Lett.*, **293**, 200–215 (2010).
 24. E. Lodolo, F. Coren, A. A. Schreider, and G. Geccone, “Geophysical Evidence of a Relict Oceanic Crust in the Southwestern Scotia Sea,” *Mar. Geophys. Res.*, **19**, 439–450 (1998).
 25. E. Lodolo, F. Donda, and A. Tassone, “Western Scotia Sea Margins: Improved Constraints on the Opening of the Drake Passage,” *J. Geophys. Res.*, **111**, No. B06101, 14 (2006).
 26. M. Maffione, F. Speranza, C. Faccenna, and E. Rossetto, “Paleomagnetic Evidence for a Pre-Early Eocene Bending of the Patagonian Orocline (Tierra del Fuego, Argentina): Paleogeographic and Tectonic Implications,” *Earth and Planet. Sci. Lett.*, **289**, 273–286 (2010).
 27. A. Maldonado, F. Bohoyo, J. Galindo-Zaldívar, et al., 2 in *The 10th International Symposium on Antarctic Earth Sciences (August 26 to September 1, 2007)* (Univ. Calif., Santa Barbara, 2007). <http://isaes2007.geol.ucsb.edu>.
 28. *Tectonic Map of the Scotia Arc 1 : 3 000 000* (British Antarctic Survey, Cambridge, 1985).
 29. C. Thomas, R. Livermore, and F. Politz, “Motion of the Scotia Sea Plates,” *Geoph. J. Int.*, **155**, 789–804 (2003).

SPELL: 1. Livermore, 2. Bohoyo, 3. Fernández, 4. Lodolo

Furrows in the southern Scan Basin, Antarctica: interplay between tectonic and oceanographic influences

Francisco José Lobo · Francisco Javier Hernández-Molina · Fernando Bohoyo ·
Jesús Galindo-Zaldívar · Andrés Maldonado · Yasmína Martos ·
José Rodríguez-Fernández · Luis Somoza · Juan Tomás Vázquez

Received: 7 October 2010 / Accepted: 2 June 2011 / Published online: 14 June 2011
© Springer-Verlag 2011

Abstract Multibeam echosounder data and TOPAS seismic reflection profiles collected during the AntPac 1997, Scan 2004, and Scan 2008 cruises aboard the RV Hespérides reveal a host of surficial geomorphological features as yet poorly investigated in the Scan Basin, south-central Scotia Sea. This area represents one of the deep gateways between the Weddell Sea and the Scotia Sea, since it enables the northward flow of a branch of the Weddell Sea Deep Water

(WSDW). Analysis of the data identifies numerous elongated depressions interpreted as furrows in the southernmost sector of the basin. These furrows show two main trends, i.e., either N–NNW parallel to, or NE oblique to regional bathymetric contours. These trends plausibly reflect a tectonic influence on the bottom-flow distribution, conditioned by a set of recent, conjugate strike-slip faults that developed on the seafloor under dominant NNE–SSW compression and orthogonal extension. The furrows exhibit distinct geomorphological patterns at either side of the basin, which can be related to west–east asymmetry in the WSDW flow direction. Consistent with existing knowledge of regional WSDW dynamics, northward WSDW overflows would be channeled along the western part of the basin at higher bottom-current velocities, thereby generating more erosional-type furrows that are straighter, more elongated, and have more abrupt sidewalls than their eastern counterparts. In contrast, weaker southward WSDW would flow along the eastern part of the basin, resulting in more depositional-type furrows that are more curved, less elongated, and have gentler sidewalls.

Responsible guest editor: M. Rebesco

F. J. Lobo (✉) · J. Galindo-Zaldívar · A. Maldonado · Y. Martos ·
J. Rodríguez-Fernández
Instituto Andaluz de Ciencias de la Tierra,
CSIC-Universidad de Granada, Facultad de Ciencias,
Avenida de Fuentenueva s/n,
18002 Granada, Spain
e-mail: pacolobo@ugr.es

F. J. Hernández-Molina
Departamento de Geociencias Marinas y Ordenación
del Territorio, Universidad de Vigo,
36200 Vigo, Pontevedra, Spain

F. Bohoyo · L. Somoza
Instituto Geológico y Minero de España,
Ríos Rosas 23,
28003 Madrid, Spain

J. Galindo-Zaldívar
Departamento de Geodinámica, Universidad de Granada,
Facultad de Ciencias,
Avenida de Fuentenueva s/n,
18002 Granada, Spain

J. T. Vázquez
Centro Oceanográfico de Málaga,
Instituto Español de Oceanografía,
Puerto Pesquero s/n,
29640 Fuengirola, Málaga, Spain

Introduction

In contrast to relatively well-known large-scale contourite deposits such as elongate drifts and contourite sheets, knowledge of channel-related and confined drifts is more limited (Faugères and Stow 1993; Stow et al. 2002). Such examples as have been reported to date are generally from pelagic environments associated with various types of topographic constriction such as deep channels or gateways, which tend to cause an increase in flow velocity (Faugères and Stow 2008). Consequently, the interconnection of marine basins by deep gateways favors the

development of channel-related drifts, and of both erosional and depositional features (Hernández-Molina et al. 2008a).

Deep-water mass circulation generates both depositional and erosional features depending on the bottom-current velocity (Stow et al. 2009). The correct identification and interpretation of genetic and evolutionary patterns of erosional features are important for improving the understanding of oceanographic circulation and related processes under dominant erosional regimes in contourite systems (García et al. 2009). Furrows are relatively large-scale elongated features (widths between tens of meters and a few kilometers, and lengths between hundreds of meters and tens of kilometers) found in erosional contourite environments, with a wide range of types classified according to scale, morphology, isolated or clustered occurrence, fine-grained versus coarse-grained nature, and water depth at their edges (Stow et al. 2009). Their trend can be parallel, slightly oblique to the current, or modified by local topography, and they may occur in clusters, with separations of tens to hundreds of meters (e.g., see side-scan sonar images in Masson 2001 and Masson et al. 2004 for characteristic plan-view pattern of furrows, and Fig. 2 of Flood and Hollister 1980 for characteristic cross-view pattern of furrows). They are characterized by erosional incision into the seafloor on the order of meters, as evidenced by the presence of truncated layered reflections along their flanks (e.g., García et al. 2009; Sayago-Gil et al. 2010). They are regarded as high-velocity bedforms, with flow velocities ranging from tens of decimeters to meters per second according to the seafloor lithology (Stow et al. 2009).

The most detailed furrow descriptions have been provided for the western Atlantic continental rise, where their genesis has been linked to the establishment of secondary helical circulation in benthic boundary layers within deep thermohaline currents flowing along the regional bathymetric contours (Lonsdale and Spiess 1977; Embley et al. 1980; Flood 1983, 1994). In slope- and channel-related settings, erosional furrows commonly occur in areas with fine, cohesive sediments associated with small detached flow filaments separated from the main current as a result of topographic effects (Howe et al. 1997; Cunningham et al. 2002; Habgood et al. 2003; Hanquiez et al. 2007; García et al. 2009). In other physiographic settings, their formation has been associated to the action of impinging water mass flows affected by gravity processes (Habgood et al. 2003; Mulder et al. 2003; Hanquiez et al. 2007). In addition, some recent studies have established a genetic link between pockmark occurrence related to gas escape and subsequent furrow formation by bottom-current erosion (León et al. 2010; Kilhams et al. 2011, this volume).

The Scotia–Antarctic plate boundary is characterized by a complex array of continental blocks and oceanic basins

(Galindo-Zaldívar et al. 2002; Bohoyo 2004; Lodolo et al. 2010). Within this plate boundary, the Bruce Passage represents one of the main deep gateways between the Weddell Sea and the Scotia Sea (Fig. 1). North of this gateway, the Scan Basin is laterally bounded by the Bruce Bank to the west and the Discovery Bank to the east, which both comprise extended continental crust. This is a key area to trace the northward path of water masses emanating from the Weddell Sea (Figs. 1, 2), their interaction with the seafloor of the Scan Basin having generated a huge northward-migrating contourite fan coeval with a compressional regime (Hernández-Molina et al. 2007).

The aim of the present study is to elucidate the relative contributions of recent tectonics and regional oceanographic conditions to the generation and evolution of deep-water furrows identified in the proximal part of the sedimentary record of the Scan Basin.

Geological setting

The Scotia–Antarctica plate boundary, concentrated along the South Scotia Ridge, consists of a complex array of continental blocks that show evidence of tectonic activity related to the present-day sinistral transcurrent motion (Balanyá et al. 1999; Bohoyo et al. 2007). Several interconnected small oceanic basins bounded by extended continental blocks are recognized in the southern Scotia Sea (from west to east: the Ona, Protector, Dove, and Scan basins) and the northern Weddell Sea (the Powell and Jane basins), in the vicinity of the Scotia–Antarctica plate boundary (Fig. 2a). All these basins developed as a result of spreading in the Scotia Arc, and subduction of the Weddell Sea and Southern Atlantic oceanic crusts below several fragments of an eastward- and southward-migrating trench (Bohoyo et al. 2002, 2007; Bohoyo 2004; Galindo-Zaldívar et al. 2006; Maldonado et al. 2006; Lodolo et al. 2010). The opening of gateways connecting these basins occurred around the middle Miocene (Maldonado et al. 2003). The present-day sinistral transcurrent regime, with local compressional deformation, was in place once (1) all basins in the southern Scotia Sea were completely opened (10–12 Ma; Galindo-Zaldívar et al. 2006), (2) oceanic spreading in the East Scotia Ridge started at least 15 Ma (chron 5B; Larter et al. 2003), and (3) spreading in the West Scotia Ridge ceased 6 Ma ago (chron 3A; Maldonado et al. 2000).

The Scan Basin is a small, NE-trending oceanic basin of triangular shape located in the central sector of the southern Scotia Sea northeast of the Bruce Passage, this being the main connection between the Weddell and Scotia seas through the Jane Basin. The Scan Basin increases in width northward from 40 to 150 km, and it is ca. 250 km in length

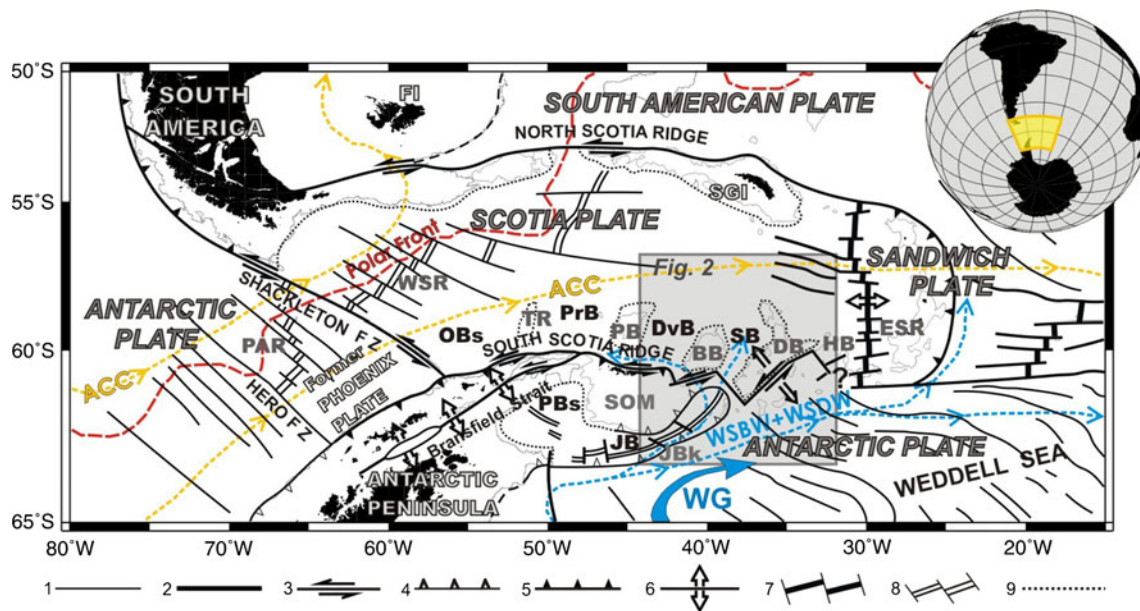


Fig. 1 Geological and oceanographic setting of the study area within the Scotia Arc (modified from Bohoyo et al. 2007): 1 inactive fracture zone, 2 active fracture zone, 3 transform or transcurrent fault, 4 inactive subduction zone or reverse fault, 5 active subduction zone, 6 rift, 7 active spreading axis, 8 inactive spreading axis, 9 continental–oceanic crustal boundary; *PAR* Phoenix–Antarctic Ridge, *BB* Bruce Bank, *DB* Discovery Bank, *DvB* Dove Basin, *ESR* East Scotia Ridge,

FI Falkland Islands, *FZ* fracture zone, *HB* Herdman Bank, *JBk* Jane Bank, *JB* Jane Basin, *OBs* Ona Basin, *PB* Pirie Bank, *PBs* Powell Basin, *PrB* Protector Basin, *SB* Scan Basin, *SGI* South Georgia Island, *SOM* South Orkney Microcontinent, *TR* Terror Rise, *WSR* West Scotia Ridge; *ACC* Antarctic Circumpolar Current, *WG* Weddell Gyre, *WSBW* Weddell Sea Bottom Water, *WSDW* Weddell Sea Deep Water. Polar Front position from Anderson et al. (2009)

(Fig. 2a). Basin morphology and orientation suggest that WNW–ESE oceanic spreading or continental crustal stretching have taken place, separating the Bruce Bank from the Discovery Bank (Hernández-Molina et al. 2007). A complex tectonic structure comprising topographic highs and troughs represents the plate boundary that separates the Scan Basin, through the Bruce Passage, from the northeastern prolongation of both the South Orkney Microcontinent and the Jane Basin (Hernández-Molina et al. 2007).

Oceanographic setting and sedimentary products

Two main deep-water masses occur in the region: the Circumpolar Deep Water (CDW), which flows mostly eastward along the Scotia Sea with the Antarctic Circumpolar Current (ACC), and the Antarctic Bottom Water composed of the Weddell Sea Bottom Water (WSBW) and the Weddell Sea Deep Water (WSDW; Naveira Garabato et al. 2002a; Carter et al. 2009; Fig. 2b). The WSBW is the deepest water mass and is bathymetrically constrained to circulating within the Weddell Sea. The WSDW, located above the WSBW, also flows within the Weddell Gyre, mainly along the northwestern Weddell Sea (Antarctic Peninsula slope). Farther northeast, the WSDW subdivides into two main cores. One core is channeled through the

Jane Basin and overflows into the Scotia Sea beyond the South Orkney Microcontinent, through the Orkney, Bruce, and Discovery passages (Fig. 2b). The other core moves around the South Sandwich Trench, flowing northward and exiting into the South Atlantic (Naveira Garabato et al. 2002a, b; Fig. 2b).

The general modern oceanographic regime was set up once (1) a deep-water pathway was established in the Drake Passage when the Scotia Arc started to develop, (2) gaps opened between the continental arc fragments to the east of the Scotia Sea, enabling complete, full-ocean-depth ACC development, and (3) gaps opened in the South Scotia Ridge, enabling the WSDW to escape from the Weddell Gyre into the Scotia Sea, and then to flow westward (Hernández-Molina et al. 2007). Those initial incursions of the WSDW into the Scotia Sea are estimated to have occurred in the middle Miocene (Maldonado et al. 2003, 2006).

Since the middle Miocene, regional sedimentary processes have been dominated by the effects of bottom-current circulation, as the northward transfer of deep-water flows from the Weddell Sea to the Scotia Sea has generated a complex array of contouritic deposits and erosional features. A large northward-migrating contouritic fan that developed after the opening of the Bruce Passage has been documented in the Scan Basin (Hernández-Molina et al. 2007, 2008a; Fig. 2a); this fan shows widespread erosional

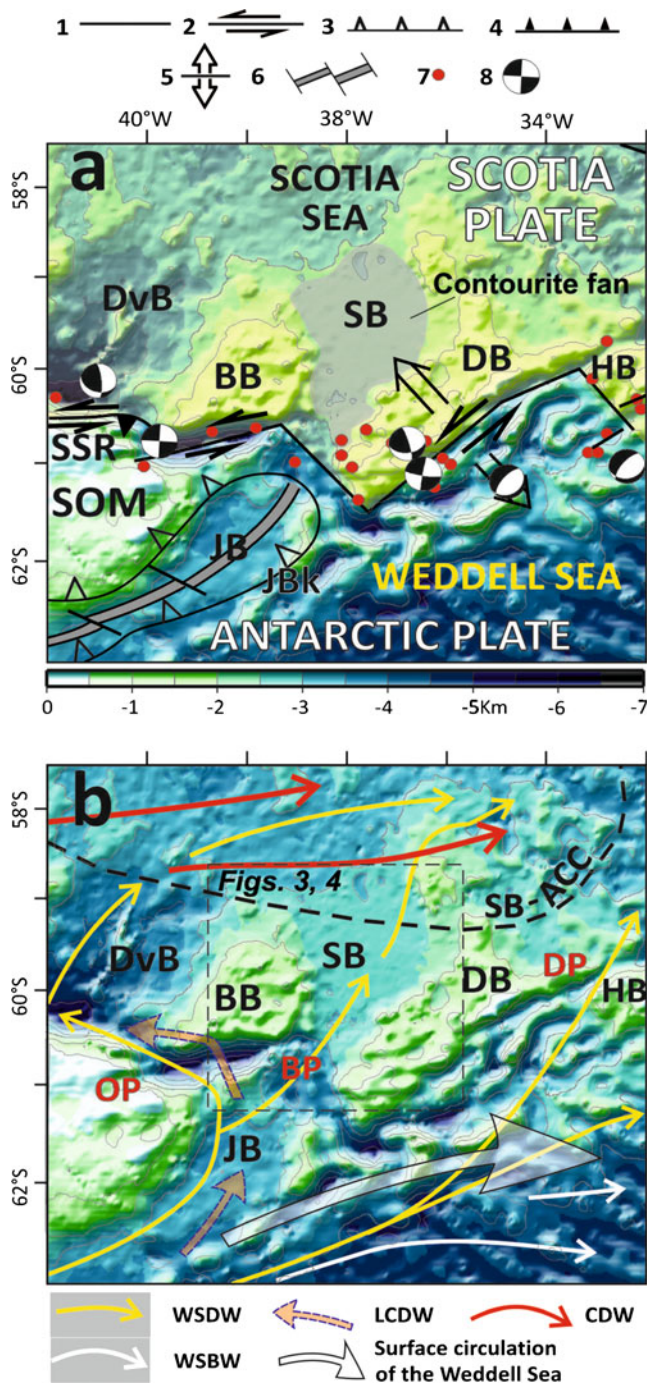


Fig. 2 Location of Scan Basin, showing its geological setting (a) and regional deep-water mass circulation (b): 1 transform fault, 2 active transcurrent fault, 3 inactive subduction zone, 4 active subduction zone, 5 active extensional zone, 6 inactive spreading centre, 7 earthquake, 8 focal mechanism; BB Bruce Bank, BP Bruce Passage, DB Discovery Bank, DP Discovery Passage, DvB Dove Basin, HB Herdman Bank, JB Jane Basin, JBk Jane Bank, SB Scan Basin, SOM South Orkney Microcontinent, OP Orkney Passage, SSR South Scotia Ridge, PP Philip Passage; CDW Circumpolar Deep Water, LCDW Lower Circumpolar Deep Water (from the Weddell Sea), WSBW Weddell Sea Bottom Water, WSDW Weddell Sea Deep Water; dashed square location of Figs. 3 and 4

features, suggesting intensified activity of the WSDW (Hernández-Molina et al. 2007; see their Figs. 3 and 4 for the large-scale seismic stratigraphy of the contouritic fan in the Scan Basin). Toward the central Scotia Sea, the interaction between the WSDW and the CDW has generated a large variety of depositional and erosional features in the distal part of the contourite fan (see Fig. 8 of Maldonado et al. 2003 for both depositional and erosional morphologies occurring in the distal part of the contourite fan).

Materials and methods

The database for this study comprises multibeam echosounder records and very high-resolution seismic reflection profiles run with a TOPAS (topographic parametric sonar) system in the Scan Basin (Fig. 3). These data were collected onboard the RV Hespérides during the AntPac 1997, Scan 2004, and Scan 2008 oceanographic cruises.

Swath bathymetric data were obtained with a SIMRAD EM 12 system on the 1997 cruise, and with a SIMRAD EM 120 system on the more recent cruises. This multibeam echosounder was set at an operating frequency of 12 kHz and a swath aperture of 120°, obtaining a seafloor coverage of about 3.5 times the water depth. Multibeam files were post-processed with NEPTUNE™ and CARIS™ softwares. The resulting bathymetric grids were displayed with the aid of ArcGIS™ software.

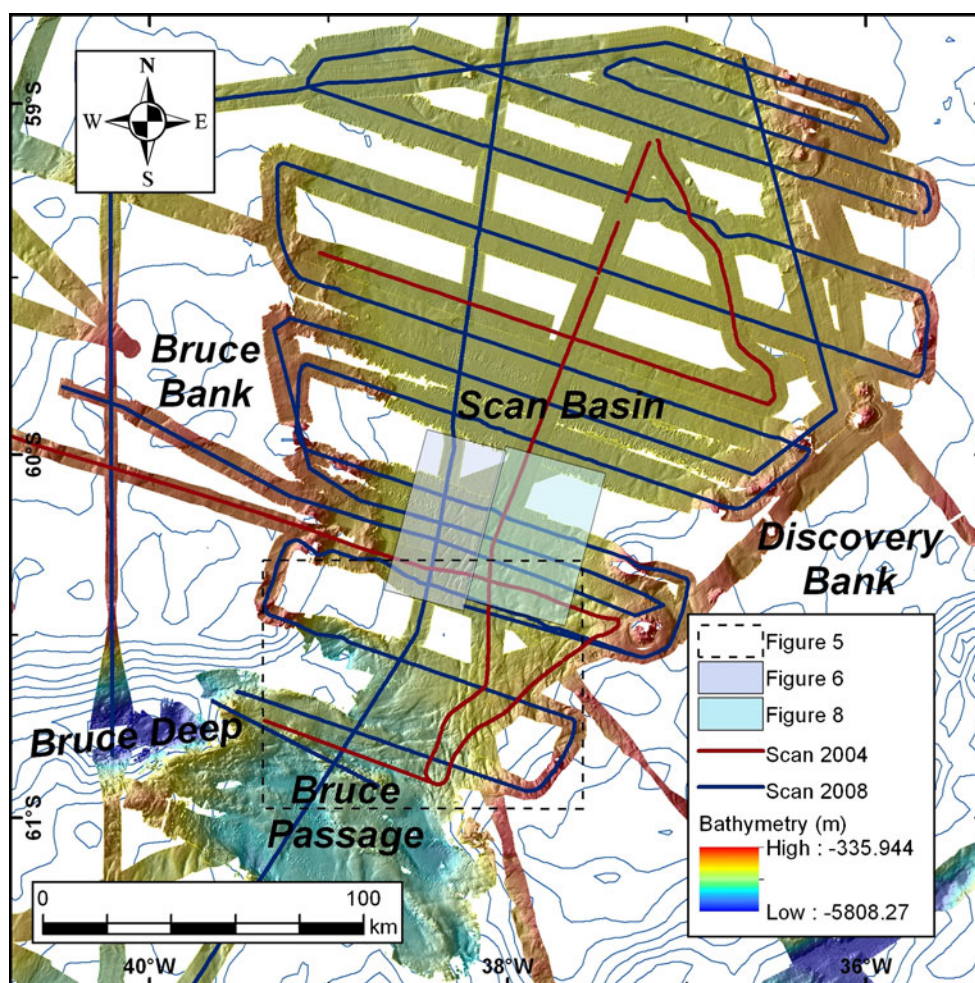
Seismic profiles were acquired using a TOPAS PS 18 system, operating with a primary frequency of 18 kHz and up to 30 kW power. Interfering seismic pulses generate a low-frequency secondary signal. Data acquisition was executed in high-penetration (chirp) mode by modulating two wave trains with initial and final frequencies of 1.5 and 5 kHz, respectively. Shot interval was between 5 to 7 s, recording length was about 400 ms, and sample frequency was 16 kHz. The acquired signal was post-processed (filters, bottom tracking, time variable gain, swell filter, stacking, muting, and delay correction) by using TOPAS™ and Radepro™ softwares. The resulting SEG-Y files were imported into Kingdom Suite™ software for interpretation. For descriptive purposes, vertical scales of seismic profiles are provided in two-way travel time below the seafloor and in water depth above the seafloor, using a conversion velocity of 1,500 m/s.

Results

Distribution of geomorphological features

The Scan Basin is irregularly shaped, widening to the north. The western boundary is N–S aligned, whereas the eastern boundary changes its orientation northward from NE to NNW

Fig. 3 Location of database used in this study, including multibeam bathymetry and parametric echosounder (TOPAS) profiles. Multibeam bathymetric data extend from the tops of the Bruce and Discovery banks (less than 300 m water depth) to water depths greater than 5,800 m in the Bruce Passage. *Dashed rectangle* Location of Fig. 5, *colored rectangles* locations of Figs. 6 and 8



(Figs. 2 and 4). Its maximum E–W extension occurs at about 59°30'S, where it reaches about 150 km. The southern ENE-trending boundary of the basin is the transition between layered strata attributed to contourite deposition to the north, and an irregular sea bottom in the Bruce Passage to the south, which is essentially free of sediment. The Scan Basin opens and merges with the Scotia Sea to the north (Fig. 4).

Morphological interpretation has revealed that the southern part of the basin close to the Bruce Passage is covered by numerous furrows, these being the focus of this study. To the north, the seafloor becomes featureless in the central basin, whereas toward the basin margins, scattered channel-like features still prevail. A contourite moat (channel trending parallel to the slope genetically linked to mounded drifts, according to Hernández-Molina et al. 2008b) occurs in the eastern basin, close to the base of the Discovery Bank. In the northern basin, major erosional features include several contourite moats (Fig. 4).

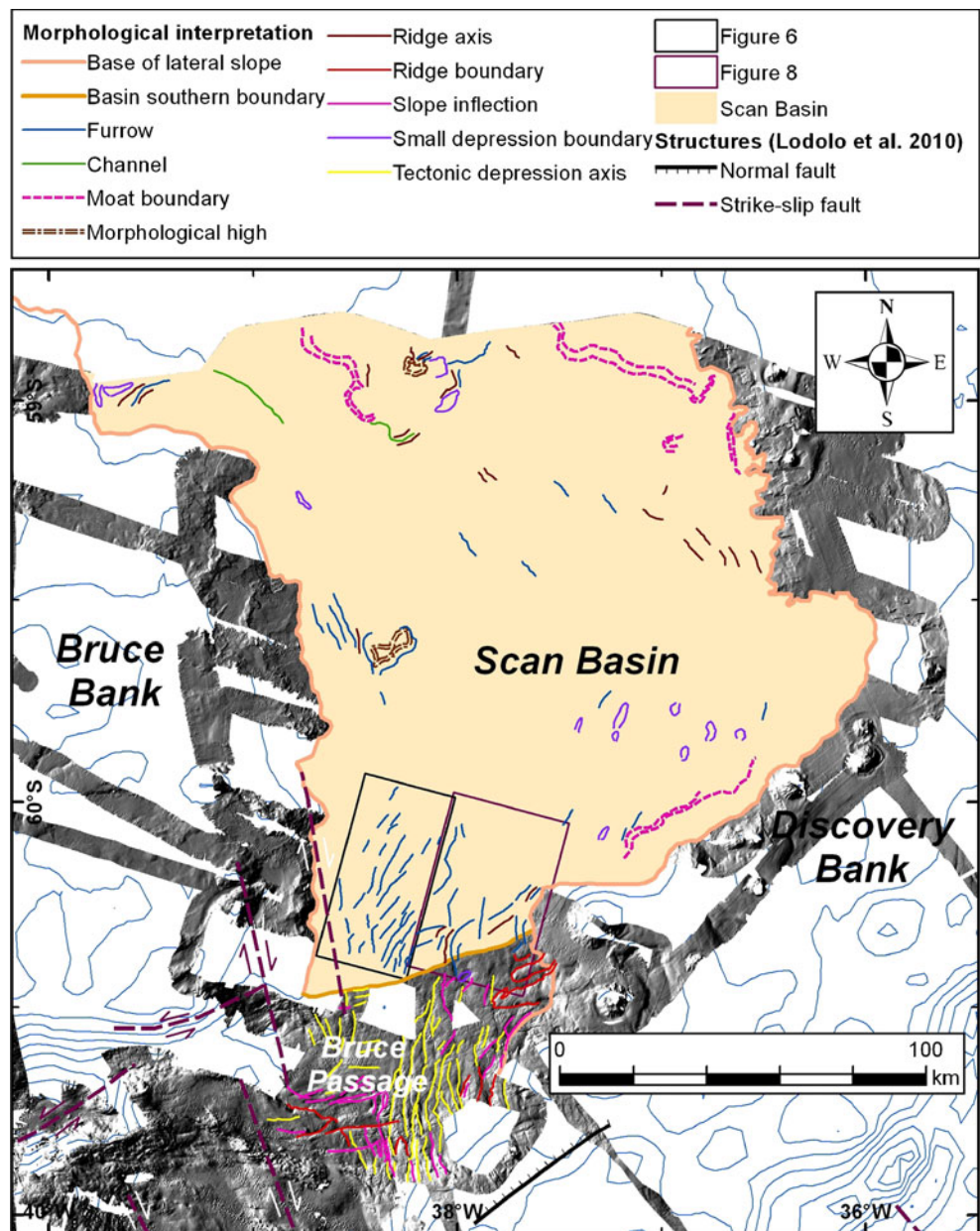
South of the Scan Basin, the Bruce Passage has a disrupted seafloor controlled by a west-dipping slope that establishes the eastern passage boundary (Fig. 5). This slope has a staircase profile, as it is dissected by numerous

N–S lineations that in plan view appear as elongate depressions. Northeast of this irregular slope, there are several ENE–WSW ridges very close to the southern basin boundary. West of the irregular slope, the deepest part of the passage has variously orientated lineations, but ENE–WSW slope inflections and ridges prevail. In addition, other sets of features such as slope inflections and/or elongate depressions show NNW to N trends. A steep slope constitutes the western passage boundary (Fig. 5).

Furrows in the southwestern Scan Basin

Abundant straight, elongate furrows are common in the southwestern Scan Basin, in water depths between 2,700 and 3,200 m (Fig. 6). The furrows have two trends: NE, and N to NNW, but the vast majority trend NE in this sector of the basin (Fig. 6). Most are less than 8 km in length, although three anomalously long furrows extend laterally for 12–18 km. In general, these long furrows show NNE trends to the south, changing to NE trends to the north. NE-trending furrows are very narrow (0.9–1.4 km wide) to the south, and slightly wider to the north (1.5–2 km). Plan-view

Fig. 4 Geomorphological interpretation of key surficial features identified on the seafloor of the Scan Basin, including nearby structures reported by Lodolo et al. (2010). Rectangles Locations of Figs. 6 and 8



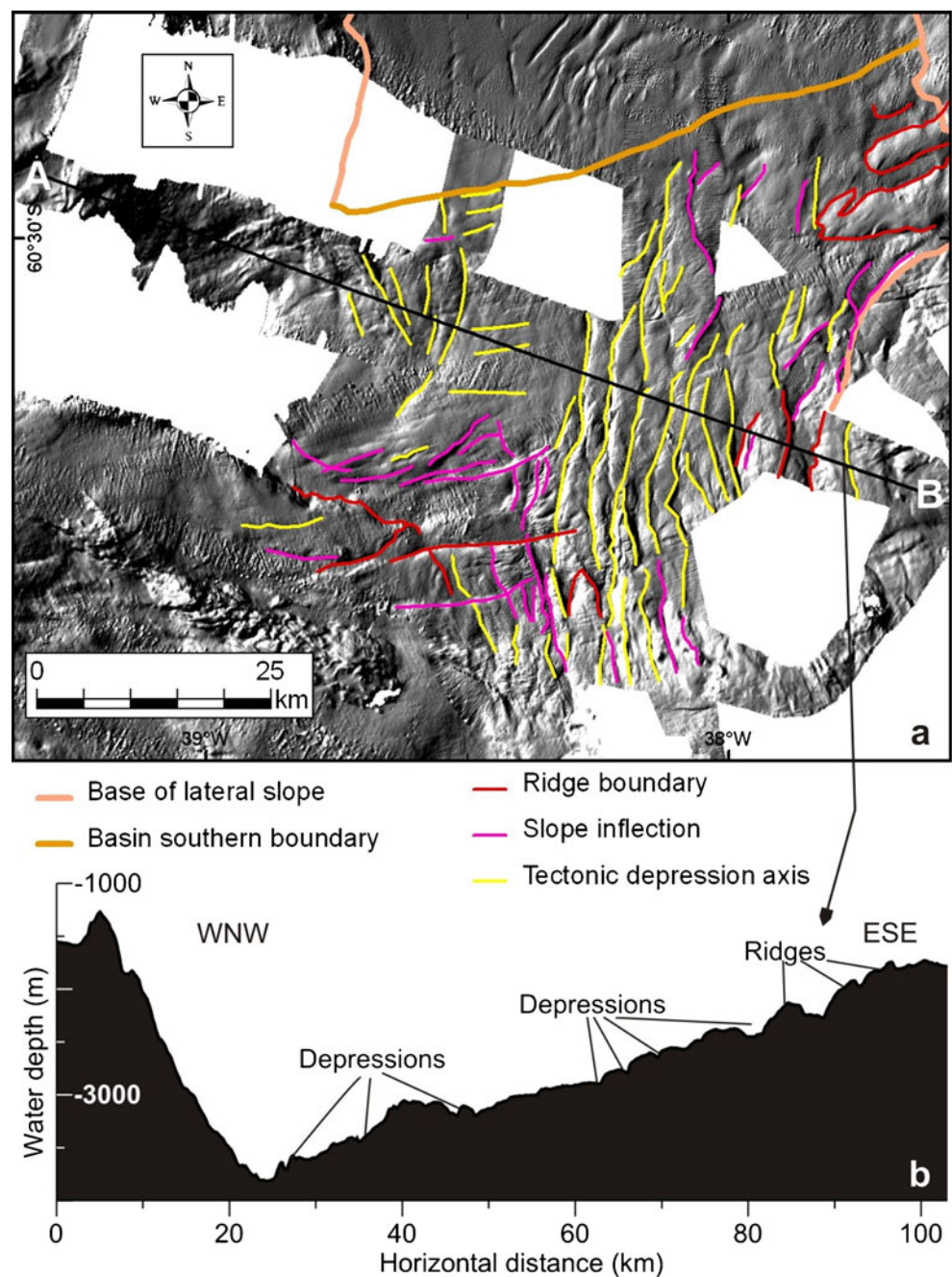
aspect ratios (i.e., relationship between furrow length and width, or elongation) of 3–5 are common. NE-trending furrows tend to be V-shaped in cross-section, with abrupt walls ($>6^\circ$) and deep incision on the order of tens of meters. Most of the furrows show higher western than eastern walls. The western walls are 20–40 m (26.5–53 ms) in height, whereas the eastern walls are usually <20 m (26.5 ms) high. Close to the boundary of the southernmost basin, several NE-trending furrows have the greatest depths; they are 55–60 m (73–80 ms) high at the western walls, and 40–45 m (53–60 ms) high at the eastern walls (Figs. 6, 7). Some of the eastern walls of these deep furrows are very steep ($>10^\circ$), indicating erosional truncation of adjacent layered strata (Fig. 7).

Furrows trending N to NNW occur in shallower water, paralleling the lateral slope. They are usually short (lengths <4 km), although two are longer than 8 km. They are very narrow, with widths of ca. 1 km or less (Fig. 6), and plan-view aspect ratios of 3 to more than 10. In cross-section they are V-shaped, with small depths along the axis (<10 m, or 13 ms) and wall gradients $<10^\circ$ (Figs. 6, 7a). Subsurface stratigraphy shows layered, sub-horizontal strata with moderate to high reflectivity and local reflection offset (Fig. 7a).

Furrows in the southeastern Scan Basin

In the southeastern Scan Basin, several furrows are identified at water depths between 2,900 and 3,100 m, immediately east

Fig. 5 Surficial geomorphology of the Bruce Passage: **a** multibeam bathymetry and interpretation of the most significant seafloor lineations; **b** representative physiographic profile across the Bruce Passage



of the main furrow occurrences and north of the N–S lineations covering the eastern slope of the Bruce Passage. In contrast to the furrows located to the west, these furrows are less straight and often arcuate (Fig. 8). In addition, they are not as common as furrows in the westernmost section.

Furrows in the southeastern Scan Basin show two main trends: N and NE, with local intersections between these directions. N-trending furrows are relatively straight; however, NE-trending furrows change to ENE trends to the north, delineating arcuate patterns. Locally, some of the furrows are bounded by bathymetric highs or ridges. Both N- and NE-trending furrows extend laterally for several kilometers

(>5 km) and are 1.5–4 km wide. Plan-view aspect ratios tend to be low (1.5–4; Fig. 8). The furrows are characterized by broad U-shaped profiles or by flat bottoms with gentle walls (up to 5°) underlain by stratified, laterally continuous reflections. The channel bottoms exhibit maximum depths of several tens of meters (up to 70 m, or 93 ms) along the central axis and underlying horizontal strata (Fig. 9a).

To the north, the longest furrow (at least 22 km long) is in the middle part of the basin and has an en-echelon pattern, as the furrow changes trend from NE to NNW (Fig. 8). Measured widths range between 2 and 3 km. Cross-sectional profiles exhibit relatively gentle walls only

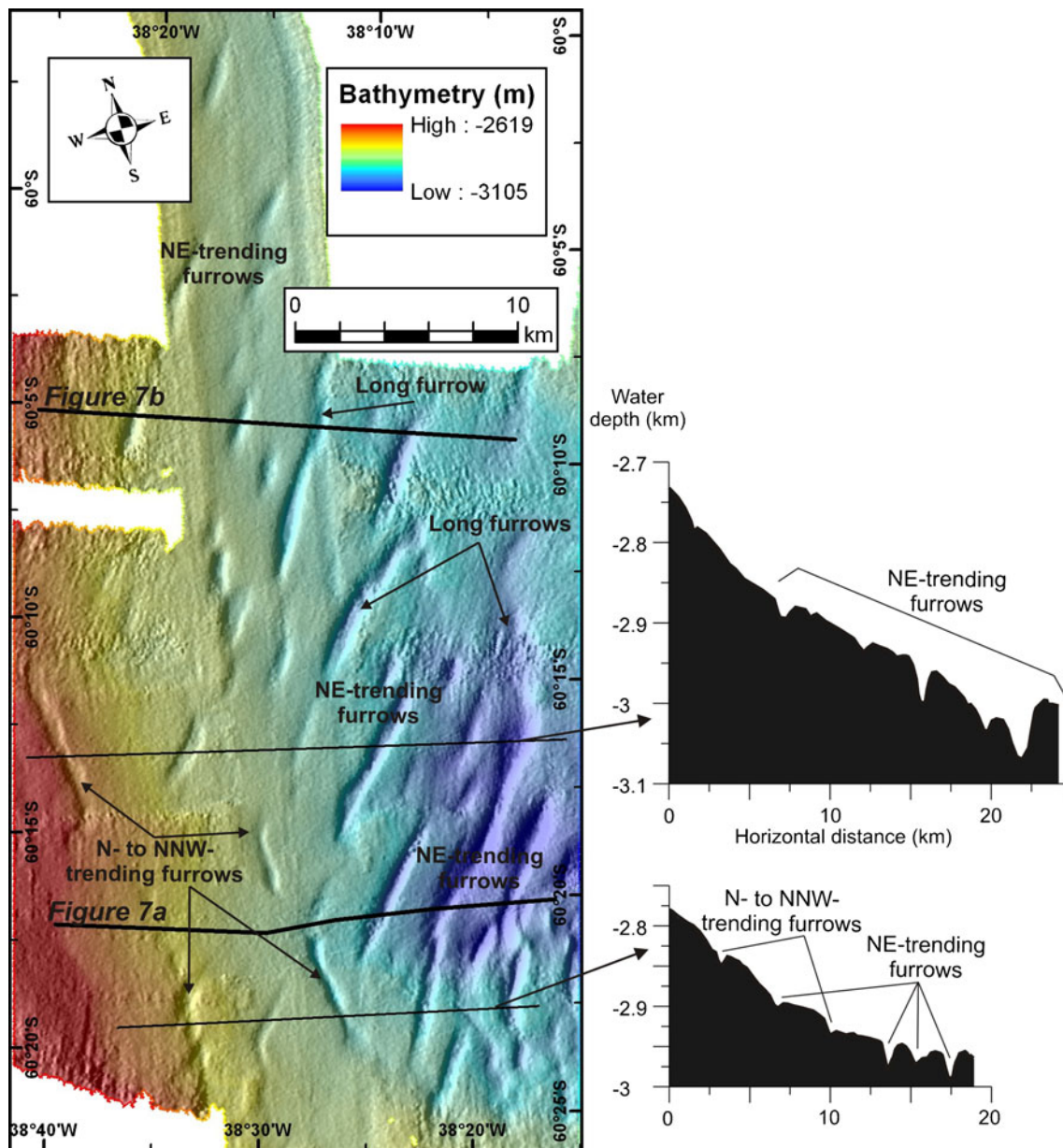


Fig. 6 Detailed multibeam bathymetric view (hill shade illuminated from the northwest) of furrows in the southwestern Scan Basin (see location in Figs. 3 and 4), with two physiographic profiles depicting their cross-view morphology. Two main sets of furrows are recognized.

Those occurring in shallower water trend N to NNW, paralleling the western boundary of the basin. The most abundant furrows are in deeper water, and trend mainly NE. *Thick black lines* Locations of TOPAS profiles shown in Fig. 7

locally exceeding 5° and a flat bottom along the furrow axis, with maximum depths of 30–40 m (40–53 ms). Sub-bottom stratigraphy shows reflections paralleling the seafloor morphology, with sediment infilling the furrow axis (Fig. 9b).

Discussion

Furrows in the study area are considerably wider and deeper than the large furrows described from the North Atlantic continental rise, which have widths of tens of

meters, lengths of hundreds of meters, and depths of a few meters (Lonsdale and Spiess 1977; Embley et al. 1980; Flood 1994). The origin of those furrows has been linked to purely oceanographic processes involving, for example, threads of unidirectional bottom currents generated by secondary helical circulation (Embley et al. 1980), and separated by broad bands of much lower velocity (Lonsdale and Spiess 1977). Thus, they are expected to occur in deep areas affected by bottom currents, where they would trend parallel to the direction of flow (Lonsdale and Spiess 1977; Flood 1983).

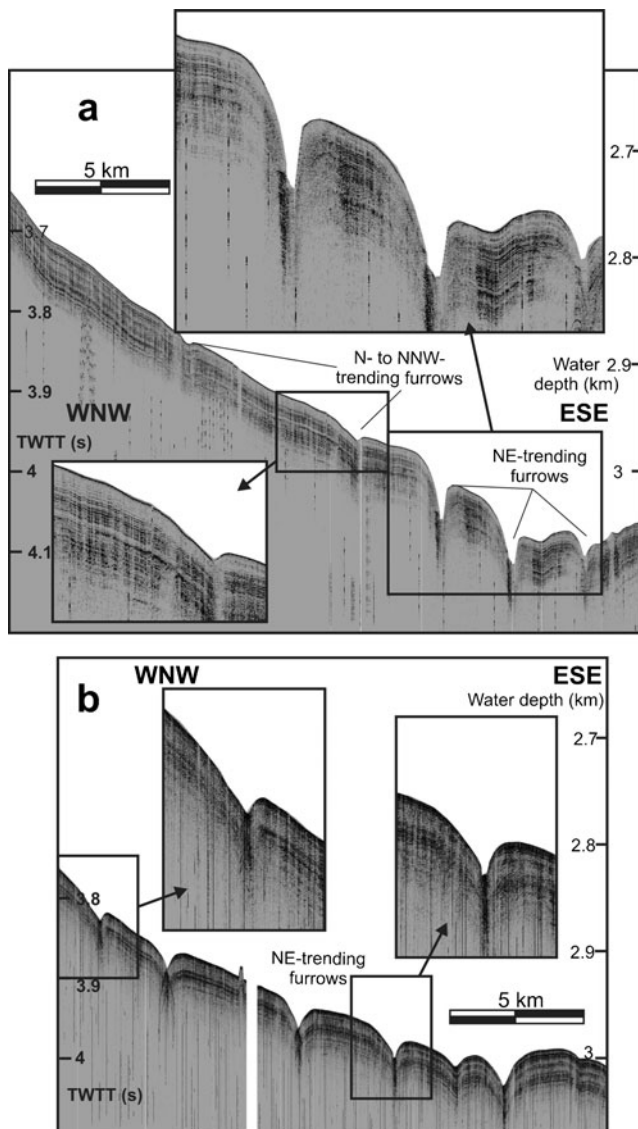


Fig. 7 TOPAS seismic profiles collected in the southwestern Scan Basin (see locations in Fig. 6): **a** TOPAS profile to the south, revealing both N- to NNW-trending furrows in shallower water, and NE-trending furrows in deeper water; **b** TOPAS profile to the north, where NE-trending furrows show steep V-shaped profiles. Vertical scales are in water depths (m) above and two-way travel time (TWTT, s) below the seafloor. Vertical exaggeration is 40×

In contrast, Scan Basin furrows are much more similar in size to furrows reported in deep channels such as the Western Falkland Trough (Howe et al. 1997; Cunningham et al. 2002) or the Faeroe-Shetland Channel (Masson 2001). In those settings, furrows cut down tens of meters (up to 130 m deep) and extend for tens of kilometers (up to 40 km long). These dimensions are considerably larger than for the North Atlantic rise furrows; this fact has been related to the existence of specific types of structural control. In the Western Falkland Trough, for example, furrows with dimensions similar to those of the present study area have

been interpreted as being controlled partially by the underlying geology, as either pre-existing scarps or outcropping bedrock that were subsequently modified by strong along-slope currents (Howe et al. 1997). In addition, the existence of long (tens of kilometers), highly linear furrows in the Faeroe-Shetland Channel and the Gulf of Cádiz suggests an underlying structural control (Masson 2001; León et al. 2010).

Origin of the furrows: tectonic imprint

In the study area, the considerable lengths of the furrows, as well as the dominantly straight patterns, are consistent with some kind of structural control (Fig. 10), as documented in other channel-related contourite environments (Howe et al. 1997; Masson 2001). In addition, there are two well-defined furrow trends. The one is roughly parallel to bathymetric contours (N to NNW); however, there is also a pervasive oblique trend (NE). Under pure oceanographic control, one would expect the linear features to be parallel or slightly oblique to the regional contours, as evidenced in other settings with furrow occurrence (Lonsdale and Spiess 1977; Howe et al. 1997). This parallel-to-contour pattern results from the dominant control of directionally stable, steady bottom currents (Flood 1983; Masson 2001).

Moreover, furrow orientation agrees with the regional stress field and with tectonic features associated to the nearby plate boundary. Earthquake focal mechanisms provide evidence of regional NE–SW to NNE–SSW compression in the Scotia Arc (Pelayo and Wiens 1989; Galindo-Zaldívar et al. 1996). In addition, the stress field of the Scan Basin is dominated by coeval WNW–ESE orthogonal extension associated with the development of two conjugate sets of strike-slip faults trending N to NNW and NE. The recent fault system is more strongly developed in the southern Scan Basin, toward the present-day Scotia–Antarctic plate boundary (Fig. 2a). Furthermore, the deformation of young sediments confirms the recent age of this stress field.

The Scotia–Antarctic plate boundary at the South Scotia Ridge is considered to be a sinistral transcurrent zone, which is assumed to have become active after the opening of the small basins in the southern Scotia Sea (BAS 1985; Galindo-Zaldívar et al. 1996; Bohoyo et al. 2007). The plate boundary has an en-echelon geometric arrangement east of the South Orkney Microcontinent (Bohoyo 2004; Lodolo et al. 2010), with a dominance of purely transcurrent sinistral faults with ENE to NNE trends (Bohoyo et al. 2007). Those segments are separated by a NNW-trending release zone formed by a system of right-lateral, strike-slip faults, which possibly accommodates the differential movements between blocks (Lodolo et al. 2010; Figs. 2a, 5). Those two main

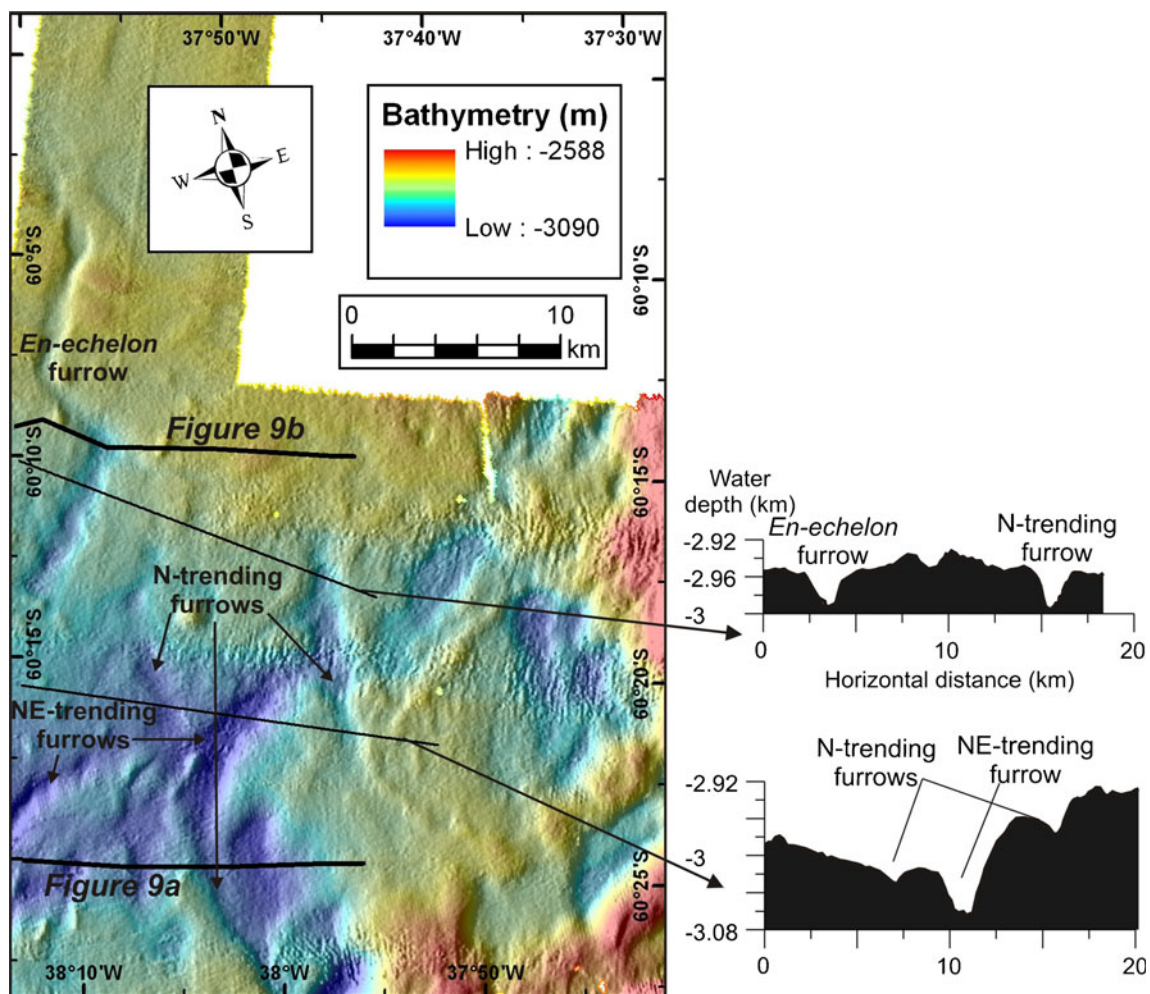


Fig. 8 Detailed multibeam bathymetric view (hill shade illuminated from the northwest) of furrows in the southeastern Scan Basin (see location in Figs. 3 and 4), with two physiographic profiles depicting

their cross-view morphology. The furrows generally trend N and NE. To the northwest, a long furrow shows an en-echelon pattern. *Thick black lines* Locations of TOPAS profiles shown in Fig. 9

trends are consistent with the lineations observed in the Bruce Passage, which also have two preferred orientations (Figs. 4, 5).

Based on this evidence, it is suggested that the orientation of the system of furrows has been controlled by a system of conjugate faults that developed under the dominant sinistral transruction along the South Scotia Ridge, related to the Scotia–Antarctic plate boundary (Fig. 10). The NNE–SSW maximum compression direction is inferred by the acute angle between the two sets of lineations representing the recent strike-slip fault system. Moreover, there is coeval WNW–ESE orthogonal extension. Although pure strike-slip faults do not produce reliefs, they generally have associated minor dip-slip components that contribute to generating small fault scarps that would interact with bottom currents to develop the observed straight furrows. In addition, fault-related breccias are more easily eroded by the

intense bottom flows than the surrounding undeformed sediments, thereby enhancing the geomorphological features of the faults.

Furrow modification by oceanographic forcing

Although the two main furrow trends are observed at both sides of the basin (suggesting a tectonic imprint), there are distinct morphological differences between western and eastern furrows in the study area (Figs. 6, 8): notably, (1) western furrows are very straight, in contrast to eastern furrows characterized by bends; (2) western furrows are narrower (ca. 1 km wide) than eastern furrows (widths of 2–4 km are common); (3) western furrows are more elongated (plan-view aspect ratios from 3 to more than 10) than eastern furrows (plan-view aspect ratios <4); (4) in cross-section, western furrows mostly show abrupt (>10°) V-shaped profiles, whereas eastern furrows typically show

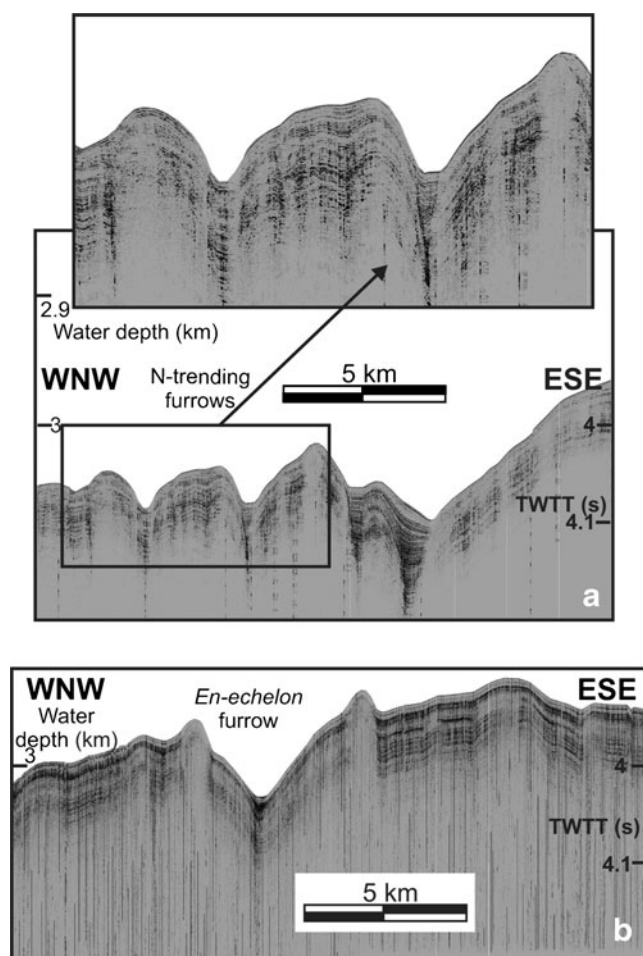


Fig. 9 TOPAS seismic profiles collected in the southeastern Scan Basin (see locations in Fig. 8): **a** TOPAS profile to the south, revealing N-trending furrows with wide, U-shaped cross-sections with some sediment infilling; **b** TOPAS profile to the north, showing the morphology and subsurface layering of the en-echelon furrow. Vertical scales are in water depths (m) above and two-way travel time (TWTT, s) below the seafloor. Vertical exaggeration is 40×

U-shaped profiles, or flat bottoms with gentler walls ($<5^\circ$); (5) western furrows show local truncations indicating signs of erosion; in contrast, eastern furrows tend to develop flat bottoms, indicating sediment ponding.

Those west–east geomorphological differences are interpreted in terms of variable WSDW overflow at the South Scotia Ridge through narrow passages between the Weddell Sea and the Scotia Sea (Naveira Garabato et al. 2002a), including the Bruce Passage located to the south of the study area (Gordon et al. 2001; Naveira Garabato et al. 2002b). In those passages, a west–east asymmetry in the flow direction has been detected (Fig. 10). There is a clear pattern of northward flow at the western side of each passage, contrasting with a southward flow along the eastern sides. The largest velocities are observed along the western sides (in the case of the Bruce Passage, flow velocities of about 10 cm/s have been recorded over the

western flank), i.e., northward flows are more vigorous and extensive than southward flows. As a consequence, there is a net northward export of WSDW (Naveira Garabato et al. 2002b).

The observed asymmetry of the flow through the Bruce Passage and the local erosional interaction of the WSDW with the seafloor would explain the contrasting furrow morphological patterns identified in the study area. Thus, the higher-velocity northward WSDW overflow along the western side of the passage would mainly influence western furrows in the Scan Basin, forming secondary bottom-current filaments and branches when interacting with local seafloor irregularities (such as faults) and producing more straight, elongated, abrupt, and erosional lineations. In contrast, the less intense southward WSDW flow would be focused along the eastern side, with less influence on the furrows; indeed, eastern furrows are less straight and elongated, with gentler walls and dominant signs of deposition rather than erosion (Fig. 10).

Once the furrows were generated by the interaction of the WSDW overflow with local tectonic lineations, they could have stabilized secondary circulation cells and acted as conduits, and this could have led to further differentiation, as documented in other areas of furrow occurrence (Tucholke 1979). As a final consequence, by inhibiting sedimentation particularly along the western basin margin, the bottom current (in this case, the WSDW) would have preserved the tectonic fabric, such as reported for the Western Falkland Trough (Cunningham et al. 2002).

Conclusions

Elongated, kilometric-scale furrows cover the southern part of the Scan Basin, one of the main present-day gateways between the Weddell Sea and the Scotia Sea close to the Scotia–Antarctic plate boundary. Their existence is consistent with a dominance of erosional processes generated by overflows of the Weddell Sea Deep Water, although they show contrasting patterns on either side of the basin. In the southwestern part they are straight, narrow, and have steep V-shaped profiles with local signs of erosion; in the southeastern part of the basin, they show arcuate patterns, are wider, and tend to develop symmetric U-shaped depositional profiles or flat bottoms with gentler walls.

Considerable evidence supports a complex genesis of furrows, with an enhanced influence of recent tectonics. Furrows in the southern Scan Basin show two main trends (N to NNW and NE) parallel and oblique to regional contours and arranged at an oblique angle, which is consistent with the regional NNE–SSW compression and

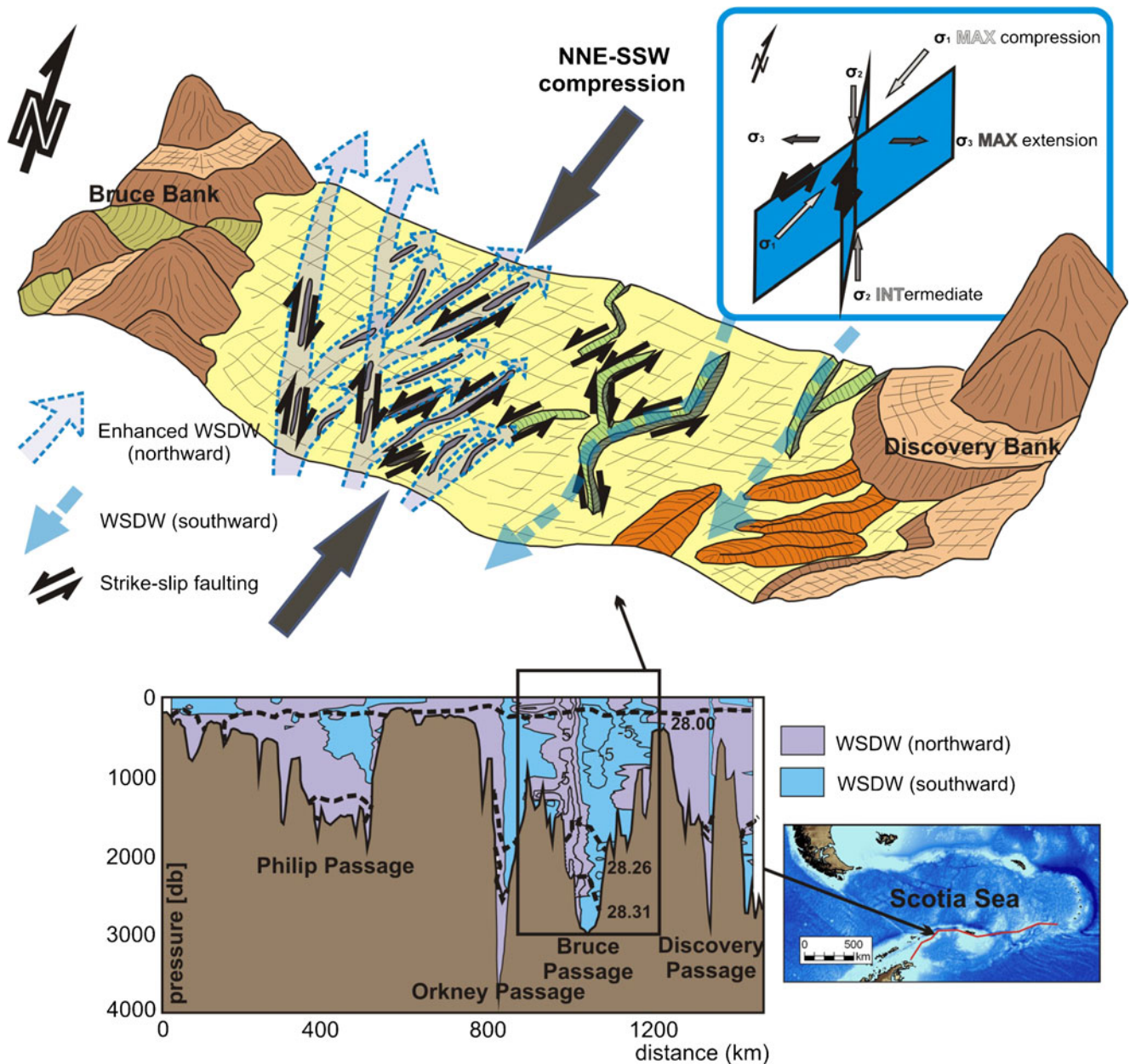


Fig. 10 Interpretative block diagram showing the main controlling factors for furrow occurrence in the southern part of the Scan Basin. The dominant NNE–SSW compressive regime is likely responsible for the generation of sets of conjugate strike-slip faults. Lateral differentiation between furrows is attributed to the reported west–east asymmetry in the flow direction across the Bruce Passage, as

northward WSDW overflow passes along the western margin, whereas southward WSDW flows along the eastern margin. A transect along the South Scotia Ridge with the vertical distribution of the cross-track velocity component is shown (modified from Naveira Garabato et al. 2002b). The contour interval (5 cm/s) is detailed in the Bruce Passage. *Dashed lines* Isopycnic water mass boundaries

the orthogonal extension associated to the transcurrent regime of the Scotia–Antarctic plate boundary along the South Scotia Ridge. It is proposed that the origin of such erosional features is related to the interaction of the WSDW overflow with seafloor irregularities linked to a system of strike-slip conjugate faults in the proximity of the plate boundary. The west–east morphologic distinction may be related to a west–east asymmetry in the flow direction

through the Bruce Passage (immediately south of the study area). More vigorous northward WSDW overflow along the western side would produce more straight, elongated, abrupt and erosional lineations in the southwestern part of the Scan Basin. In contrast, a weaker southward WSDW would flow along the eastern side of the basin and produce less straight and elongated furrows associated with more gentle, depositional profiles.

Acknowledgements This work was executed in the framework of the project CGL2004-05646/ANT of the Antarctic Spanish Program and it is also related to the projects CTM2008-06386-C02/ANT (POL2006.13836.C03.01) and CTM 2008-06399-C04/MAR (CONTOURIBER Project). The English style of the manuscript was thoroughly reviewed by Christine Laurin. Susana Diez (CSIC-UTM, Barcelona) and Marcellí Farrán (CSIC-CMIMA, Barcelona) provided very useful advice for reprocessing multibeam bathymetric data and TOPAS profiles, respectively. Michele Rebesco (guest editor) and two anonymous reviewers made very extensive and helpful comments that significantly improved the original version of the manuscript.

References

- Anderson RF, Ali S, Bradtmiller LI, Nielsen SHH, Fleisher MQ, Anderson BE, Burckle LH (2009) Wind-driven upwelling in the Southern Ocean and the deglacial rise in atmospheric CO₂. *Science* 323:1443–1448
- Balanyá JC, Galindo-Zaldívar J, Jabaloy A, Leitchenkov G, Maldonado A, Rodríguez-Fernández J, Vinnikovskaya O (1999) Structure of the South Powell Ridge (NE Antarctic Peninsula): new clues for changing tectonic regimes near the Scotia/Antarctica Plate boundary. *Geo-Mar Lett* 18(3):215–224. doi:10.1007/s003670050071
- BAS (1985) Tectonic map of the Scotia Arc. 1:3 000 000. British Antarctic Survey, Cambridge
- Bohoyo F (2004) Fragmentación continental y desarrollo de cuencas oceánicas en el sector meridional del Arco de Scotia, Antártida. PhD Thesis, University of Granada
- Bohoyo F, Galindo-Zaldívar J, Maldonado A, Schreider AA, Suriñach E (2002) Basin development subsequent to ridge-trench collision: the Jane Basin, Antarctica. *Mar Geophys Res* 23:413–421
- Bohoyo F, Galindo-Zaldívar J, Jabaloy A, Maldonado A, Rodríguez-Fernández J, Schreider A, Suriñach E (2007) Extensional deformation and development of deep basins associated with the sinistral transcurrent fault zone of the Scotia Antarctic plate boundary. *Geol Soc Lond Spec Publ* 290:203–217
- Carter L, McCave IN, Williams MJM (2009) Circulation and water masses of the Southern Ocean: a review. In: Florindo F, Siegert M (eds) *Antarctic climate evolution. Developments in Earth and Environmental Sciences*, vol 8. Elsevier, Amsterdam, pp 85–114
- Cunningham AP, Howe JA, Barker PF (2002) Contourite sedimentation in the Falkland Trough, western South Atlantic. *Geol Soc Lond Mem* 22:337–352
- Embley RW, Hoose PJ, Lonsdale P, Mayer L, Tucholke BE (1980) Furrowed mud waves on the western Bermuda Rise. *Geol Soc Am Bull* 91:731–740
- Faugères JC, Stow DAV (1993) Bottom-current-controlled sedimentation: a synthesis of the contourite problem. *Sedim Geol* 82:287–297
- Faugères JC, Stow DAV (2008) Contourite drifts: nature, evolution and facies. In: Rebesco M, Camerlenghi A (eds) *Contourites*. Elsevier, Amsterdam, pp 259–288
- Flood RD (1983) Classification of sedimentary furrows and a model for furrow initiation and evolution. *Geol Soc Am Bull* 94:630–639
- Flood RD (1994) Abyssal bedforms as indicators of changing bottom current flow: examples from the U.S. East Coast continental rise. *Paleoceanography* 9:1049–1060
- Flood RD, Hollister CD (1980) Submersible studies of deep-sea furrows and transverse ripples in cohesive sediments. *Mar Geol* 36:M1–M9
- Galindo-Zaldívar J, Jabaloy A, Maldonado A, Sanz de Galdeano C (1996) Continental fragmentation along the South Scotia Ridge transcurrent plate boundary (NE Antarctic Peninsula). *Tectonophysics* 242:275–301
- Galindo-Zaldívar J, Balanyá JC, Bohoyo F, Jabaloy A, Maldonado A, Martínez-Martínez JM, Rodríguez-Fernández J, Suriñach E (2002) Active crustal fragmentation along the Scotia-Antarctic plate boundary east of the South Orkney Microcontinent (Antarctica). *Earth Planet Sci Lett* 204:33–46
- Galindo-Zaldívar J, Bohoyo F, Maldonado A, Schreider A, Suriñach E, Vázquez JT (2006) Propagating rift during the opening of a small oceanic basin: the Protector Basin (Scotia Arc, Antarctica). *Earth Planet Sci Lett* 241:398–412
- García M, Hernández-Molina FJ, Llave E, Stow DAV, León R, Fernández-Puga MC, Díaz del Río V, Somoza L (2009) Contourite erosive features caused by the Mediterranean Outflow Water in the Gulf of Cadiz: quaternary tectonic and oceanographic implications. *Mar Geol* 257:24–40
- Gordon AL, Visbeck M, Huber B (2001) Export of Weddell Sea deep and bottom water. *J Geophys Res* 106:9005–9017
- Habgood EL, Kenyon NH, Masson DG, Akhmetzhanov A, Weaver PPE, Gardner J, Mulder T (2003) Deep-water sediment wave fields, bottom current sand channels and gravity flow channel-lobe systems: Gulf of Cadiz, NE Atlantic. *Sedimentology* 50:483–510
- Hanquiez V, Mulder T, Lecroart P, Gonthier E, Marchès E, Voisset M (2007) High resolution seafloor images in the Gulf of Cadiz, Iberian margin. *Mar Geol* 28:42–59
- Hernández-Molina FJ, Bohoyo F, Naveira Garabato A, Galindo-Zaldívar J, Lobo FJ, Maldonado A, Rodríguez-Fernández J, Somoza L, Stow DAV, Vázquez JT (2007) The Scan Basin evolution: oceanographic consequences of the deep connection between the Weddell and Scotia Seas (Antarctica). In: Cooper A, Raymond C, ISAES Editorial Team (eds) *Antarctica: a keystone in a changing world*. Online Proc 10th Int Symp Antarctic Earth Sciences, Santa Barbara. US Geol Surv Open-File Rep 2007-1047, Ext Abstr 086
- Hernández-Molina FJ, Maldonado A, Stow DAV (2008a) Abyssal plain contourites. In: Rebesco M, Camerlenghi A (eds) *Contourites*. Elsevier, Amsterdam, pp 347–378
- Hernández-Molina FJ, Llave E, Stow DAV (2008b) Continental slope contourites. In: Rebesco M, Camerlenghi A (eds) *Contourites*. Elsevier, Amsterdam, pp 379–408
- Howe JA, Pudsey CJ, Cunningham AP (1997) Pliocene-Holocene contourite deposition under the Antarctic Circumpolar Current, western Falkland Trough, south Atlantic Ocean. *Mar Geol* 138:27–50
- Kilham B, McArthur A, Huuse M, Ita E, Hartley A (2011) Enigmatic large-scale furrows of Miocene to Pliocene age from the central North Sea: current-scoured pockmarks? *Geo-Mar Lett* (in press). doi:10.1007/s00367-011-0235-1
- Larter RD, Vanneste LE, Morris P, Smythe DK (2003) Structure and tectonic evolution of the South Sandwich arc. In: Larter RD, Leat PT (eds) *Intra-oceanic subduction systems: tectonic and magmatic processes*. *Geol Soc Lond Spec Publ* 219:255–284
- León R, Somoza L, Medialdea T, Hernández-Molina FJ, Vázquez JT, Díaz-del-Río V, González FJ (2010) Pockmarks, collapses and blind valleys in the Gulf of Cádiz. *Geo-Mar Lett* 30(3/4):231–247. doi:10.1007/s00367-009-0169-z
- Lodolo E, Civile D, Vuan A, Tassone A, Geletti R (2010) The Scotia-Antarctica plate boundary from 35°W to 45°W. *Earth Planet Sci Lett* 293:200–215
- Lonsdale P, Spiess FN (1977) Abyssal bedforms explored with a deeply towed instrument package. *Mar Geol* 23:57–75
- Maldonado A, Balanyá JC, Barnolas A, Galindo-Zaldívar J, Hernández J, Jabaloy A, Livermore R, Martínez-Martínez JM, Rodríguez-Fernández J, Sanz de Galdeano C, Somoza L, Suriñach E, Viseras C (2000) Tectonics of an extinct ridge-transform intersection, Drake Passage (Antarctica). *Mar Geophys Res* 21:43–68

- Maldonado A, Barnolas A, Bohoyo F, Galindo-Zaldívar J, Hernández-Molina J, Lobo F, Rodríguez-Fernández J, Somoza L, Vázquez JT (2003) Contourite deposits in the central Scotia Sea: the importance of the Antarctic Circumpolar Current and the Weddell Gyre flows. *Palaeogeogr Palaeoclimatol Palaeoecol* 198:187–221
- Maldonado A, Bohoyo F, Galindo-Zaldívar J, Hernández-Molina J, Jabaloy A, Lobo F, Rodríguez-Fernández J, Suriñach E, Vázquez J (2006) Ocean basins near the Scotia–Antarctic plate boundary: influence of tectonics and paleoceanography on the Cenozoic deposits. *Mar Geophys Res* 27:83–107
- Masson DG (2001) Sedimentary processes shaping the eastern slope of the Faeroe-Shetland Channel. *Cont Shelf Res* 21:825–857
- Masson DG, Wynn RB, Bett BJ (2004) Sedimentary environment of the Faroe–Shetland and Faroe Bank Channels, north-east Atlantic, and the use of bedforms as indicators of bottom current velocity in the deep ocean. *Sedimentology* 51:1207–1241
- Mulder T, Voisset M, Lecroart P, Le Drezen E, Gonthier E, Hanquiez V, Faugères JC, Habgood E, Hernandez-Molina FJ, Estrada F, Llave-Barranco E, Poirier D, Gorini C, Fuchey Y, Voelker A, Freitas P, Lobo Sanchez F, Fernandez LM, Kenyon NH, Morel J (2003) The Gulf of Cadiz: an unstable giant contourite levee. *Geo-Mar Lett* 23(1):7–18. doi:10.1007/s00367-003-0119-0
- Naveira Garabato AC, Heywood KJ, Stevens DP (2002a) Modification and pathways of Southern Ocean Deep Waters in the Scotia Sea. *Deep-Sea Res I* 49:681–705
- Naveira Garabato AC, McDonagh EL, Stevens DP, Heywood KJ, Sanders RJ (2002b) On the export of Antarctic bottom water from the Weddell Sea. *Deep-Sea Res II* 49:4715–4742
- Pelayo AM, Wiens DA (1989) Seismotectonics and relative plate motions in the Scotia Sea Region. *J Geophys Res* 94:7293–7320
- Sayago-Gil M, Long D, Hitchen K, Díaz-del-Río V, Fernández-Salas LM, Durán-Muñoz P (2010) Evidence for current-controlled morphology along the western slope of Hatton Bank (Rockall Plateau, NE Atlantic Ocean). *Geo-Mar Lett* 30(2):99–111. doi:10.1007/s00367-009-0163-5
- Stow DAV, Faugères JC, Howe JA, Pudsey CJ, Viana AR (2002) Bottom currents, contourites and deep-sea sediment drifts: current state-of-the-art. *Geol Soc Lond Mem* 22:7–20
- Stow DAV, Hernández-Molina FJ, Llave E, Sayago M, Díaz del Río V, Branson A (2009) Bedform-velocity matrix: the estimation of bottom current velocity from bedform observations. *Geology* 37:327–330
- Tucholke BE (1979) Furrows and focussed echoes on the Blake Outer Ridge. *Mar Geol* 31:M13–M20

